Maria Augusta Neto · Ana Amaro
Luis Roseiro · José Cirne
Rogério Leal

Engineering Computation of Structures: The Finite Element Method

Springer

Engineering Computation of Structures: The Finite Element Method

Maria Augusta Neto • Ana Amaro • Luis Roseiro
José Cirne • Rogério Leal

Engineering Computation of Structures: The Finite Element Method

Springer

Maria Augusta Neto
CEMUC - Centre for Mechanical Engineering
University of Coimbra
Coimbra, Portugal

Ana Amaro
CEMUC - Centre for Mechanical Engineering
University of Coimbra
Coimbra, Portugal

Luis Roseiro
Department of Mechanical Engineering
Polytechnic Institute of Coimbra
Coimbra, Portugal

José Cirne
Department of Mechanical Engineering
University of Coimbra
Coimbra, Portugal

Rogério Leal
Department of Mechanical Engineering
University of Coimbra
Coimbra, Portugal

Additional material to this book can be downloaded from http://extras.springer.com.

ISBN 978-3-319-17709-0 ISBN 978-3-319-17710-6 (eBook)
DOI 10.1007/978-3-319-17710-6

Library of Congress Control Number: 2015940757

Springer Cham Heidelberg New York Dordrecht London

Printed on acid-free paper

Springer International Publishing AG Switzerland is part of Springer Science+Business Media (www.springer.com)

Preface

The finite element method (FEM) has become an indispensable design tool in modelling and simulation of several engineering systems, and, therefore, the number of finite element computer programs that are now available to engineers is remarkable. All fields of engineering are facing great challenges in developing advanced systems that would contribute in solving problems affecting our life. Due to this fact, engineers must go through a very meticulous process of modelling, simulation, visualization, analysis, designing, prototyping, testing, and, finally, fabrication/construction. With modelling skills, the engineer gathers the physical and mathematical understanding of a problem, so the engineer combines with mathematics. Moreover, engineers with modelling and simulation skills must be able to analyze mathematically the finite element method.

This book provides unified and detailed course material on the FEM for engineers and students to solve primarily linear problems in mechanical engineering, with the main focus on static and dynamic structural problems. The purpose of the book is to contribute to the reader's understanding of the concepts, theories, and techniques used in the FEM. Fundamental and classical theories are introduced in a straightforward manner. Recent state-of-the-art treatment of engineering problems in designing and analyzing structural systems, including dynamic problems, is also discussed. Case studies are provided to implement the theory, the methodology, and techniques of the FEM. A text with significant concepts, theories, and modelling techniques, like the content in this book, helps engineers to use a commercial FEM software package in a professional and conscientious manner.

The FEM was originally developed to solve the stress field in continuum mechanics problems. Therefore, it seems appropriate to begin with the elasticity basic concepts and the classical theories of stressed materials and, only after, apply the relationship between forces, displacements, stresses, and strains on the process of modelling, simulating, and designing engineered technical systems. For this reason, the first chapter of this book is devoted to the mechanics of solids and structures by presenting the important basic principles. The derivation of key governing equations for 3D mathematical models is explained by means of drawings illustrating all the field variables and the relationships between them. Equations

for various types of mathematical models, such as 2D and 1D models, are then obtained from the general equations for 3D mathematical models. From our teaching practices, the method of introducing the general 3D equations before approaching other structural components provides students a fundamental background that helps the process of learning the equations of additional mathematical models.

Practice without theory is blind, but theory without practice is sterile. Therefore, the readers of this book are encouraged to discover, within the finite element method, the proper relationship between theory and practice. During the last half century, a huge number of techniques have been developed in the area of the FEM, but very few of them are often used in engineering practice. This book does not want to be exhaustive in theories but be informative enough for the main useful techniques. All the finite element theories presented are applied explicitly in case studies. Most of them are presented sequentially, making it easier for readers to follow, and are discussed in a manner that clarifies concepts of the FEM.

A chapter-by-chapter description of the book is given below.

Chapter 1: Describes the important relationships associated with the elasticity basic concepts and the classical mathematical models for solids and structures. Important field variables of solid mechanics are introduced, and the dynamic equations of these variables are derived. Mathematical models for 2D and 3D solids, trusses, Euler beams, Timoshenko beams, frames, and plates are covered in a concise manner.

Chapter 2: The general finite element procedure is introduced and Hamilton's principle is used to establish the general forms of finite element equations. Concept of strong and weak solutions of a system equation of motion is discussed. Construction of shape functions for interpolation of field variables is described and their mathematical properties are also discussed. The finite element equations are discussed for static, eigenvalue analysis, as well as transient analyses.

Chapter 3: Describes the procedure used to obtain finite element matrices for truss structures. The procedures to obtain shape functions, the strain matrix, local and global coordinate systems, and the assembly of global finite element system equations are described. Very straightforward examples are used to demonstrate a complete and detailed finite element procedure to compute numerical solutions, emphasizing the differences between exact and numerical procedures.

Chapter 4: Extends the finite element procedure to the analysis of beam structures. Shape functions and finite element matrices are described for the Euler-Bernoulli beam. Examples to demonstrate the application of the finite element procedure into modal and transient analyzes are presented. Finite element matrices for frame structures are formulated by combining matrices of truss and beam elements. 3D beam formulation is described emphasizing the transformation of element matrices between the local and global coordinate systems. An example is given to demonstrate the use of 3D beams to solve practical engineering problems.

Chapter 5: Presents the finite element equations for the stress analysis of 2D structures under plane stress and plane strain conditions. Finite element matrices for 2D solids are derived, namely, the matrices of linear triangular elements. Concepts of isoparametric and superparametric representation are described and used to formulate linear and quadratic triangular finite elements. Linear and quadratic rectangular elements are derived in detail. Important considerations and requirements for the accuracy of the analysis results and the convergence of a numerical solution are introduced. An example of steel bracket is used to study the accuracy and convergence of different mathematical models selected: Euler-Bernoulli and Timoshenko beam theories and plane stress mathematical model.

Chapter 6: Describes the procedure used to obtain finite element matrices for plate and shell structures. Matrices for thin rectangular plate elements, which are based on Kirchhoff assumptions, are derived, and the continuity requirements for their shape functions are covered. Matrices for thick rectangular plate elements, following the Reissner-Mindlin plate theory, are derived in detail. Discussion on the boundary conditions used at both theories for modelling physical situations is presented. A flat shell element is formulated by combining a rectangular plate element and a rectangular 2D solid plane stress element. Meanwhile a general nine-node shell finite element is also formulated. The difference between flat and general shell elements is discussed on the Scordelis-Lo cylindrical roof benchmark problem, using the ADINA program.

Chapter 7: Finite element matrices for 3D solids are developed. Tetrahedron and hexahedron elements are formulated in detail and the volume coordinates are described within the process. Higher-order finite elements are also formulated, and an example of using 3D solids elements for a dental implant modelling is presented.

Chapter 8: Presents a discussion on some modelling techniques for the stress analyses of solids and structures. Mesh symmetry, rigid elements and constraint equations, mesh compatibility, modelling of offsets, supports, and connections between elements with different mathematical bases are all covered. Advanced modelling of laminated composite materials is also presented.

Most of the content in the book was selected from excellent existing books on the FEM (listed in the References), with a special contribution from the K-J Bathe books. This author has been making fundamental contributions to the finite element development and was the founder of ADINA R&D, Inc. which developed the program used for solving the practical examples presented at the book. The ADINA is also used in the practical lectures of two FEM courses taught by the authors in the University of Coimbra.

The mentor on the use of ADINA program for instruction in the University of Coimbra is, unfortunately, no longer with us, having passed away in 2010. Authors would like to pay tribute to Professor Nuno Ferreira Rilo for the excellent work he has done in spreading the teachings of FEM using this program.

Since FEM is well documented in many existing books, the information within this book was limited to the necessary minimum required for the use of commercial FEM software packages in a professional and conscientious manner. Readers seeking more advanced theoretical background are advised to refer to books such as those by K-J B.

Coimbra, Portugal

Maria Augusta Neto
Ana Amaro
Luis Roseiro
José Cirne
Rogério Leal

Contents

Chapter 1
Mechanics of Solids and Structures

Solid and structural mechanics deal with the elasticity basic concepts and the classical theories of stressed materials. Mechanical components and structures are under a stress condition if they are subjected to external loads or forces. The relationship between stresses and strains, displacements and forces, stresses and forces are of main importance in the process of modeling, simulating and designing engineered technical systems. This chapter describes the important relationships associated with the elasticity basic concepts and the classical mathematical models for solids and structures. Important field variables of solid mechanics are introduced, and the dynamic equations of these variables are derived. Mathematical models for 2D and 3D solids, trusses, Euler-beams, Timoshenko-beams, frames and plates are covered in a concise manner.

1.1 Equations for 3D Mathematical Models

1.1.1 3D Kinematics and Strains

For simplicity reasons a point on a cartesian coordinate system will have coordinates denoted by x_1, x_2, x_3 and, similarly, the displacements will be denoted by u_1, u_2, u_3. This notation allows representing coordinates and displacements of a point by x_i and u_i, respectively, where the range of index i is of 1, 2, 3 for three-dimensional applications. Figure 1.1 shows a continuous three-dimensional elastic body with a volume Ω and a surface Γ. The surface of the solid is divided into two types of surfaces: a surface at which the external forces are prescribed, denoted by Γ_t; and a surface at which the displacements are prescribed, denoted by Γ_u. The body can also be loaded by volume or body forces denoted by $\mathbf{f}_b$ and surface forces denoted by $\mathbf{f}_s$.

M.A. Neto et al., *Engineering Computation of Structures: The Finite Element Method*, DOI 10.1007/978-3-319-17710-6_1

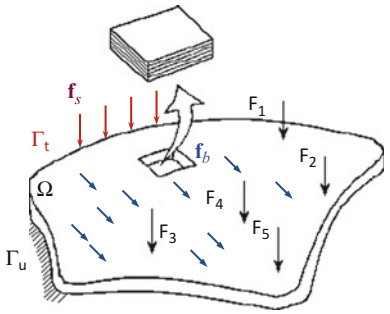

Fig. 1.1 Solid body with forces applied within the volume body and on the surface of the body [1]

The kinematics deal with a continuous displacement field u_i, thus the displacement field of a point is defined by three displacement components u, v and w in the direction of the three coordinate axes x_1, x_2, x_3

$$\mathbf{u} = \begin{bmatrix} u_1(x_1,\ x_2,\ x_3) \\ u_2(x_1,\ x_2,\ x_3) \\ u_3(x_1,\ x_2,\ x_3) \end{bmatrix} \tag{1.1}$$

Strain tensor ε_{ij} at any point in the body satisfies the following strain-displacement relations:

$$\varepsilon_{ij} = \frac{1}{2}\left(\frac{\partial u_i}{\partial x_j} + \frac{\partial u_j}{\partial x_i}\right) \tag{1.2}$$

and, therefore, the components of strain can be obtained from the derivatives of the displacements as follows:

$$\begin{aligned} &\varepsilon_{11} = \frac{\partial u_1}{\partial x_1};\ \varepsilon_{22} = \frac{\partial u_2}{\partial x_2};\ \varepsilon_{33} = \frac{\partial u_3}{\partial x_3} \\ &\gamma_{12} = 2\varepsilon_{12} = \frac{\partial u_1}{\partial x_2} + \frac{\partial u_2}{\partial x_1}; \\ &\gamma_{13} = 2\varepsilon_{13} = \frac{\partial u_1}{\partial x_3} + \frac{\partial u_3}{\partial x_1};\ \gamma_{23} = 2\varepsilon_{23} = \frac{\partial u_2}{\partial x_3} + \frac{\partial u_3}{\partial x_2} \end{aligned} \tag{1.3}$$

The relations presented on the last equation can be rewritten in the following matrix form

$$\boldsymbol{\varepsilon} = \mathbf{L}\,\mathbf{u} \tag{1.4}$$

where $\boldsymbol{\varepsilon}$ is the strain vector, and as the form

$$\boldsymbol{\varepsilon}^T = \begin{bmatrix} \varepsilon_{11} & \varepsilon_{22} & \varepsilon_{33} & \gamma_{23} & \gamma_{13} & \gamma_{12} \end{bmatrix} \tag{1.5}$$

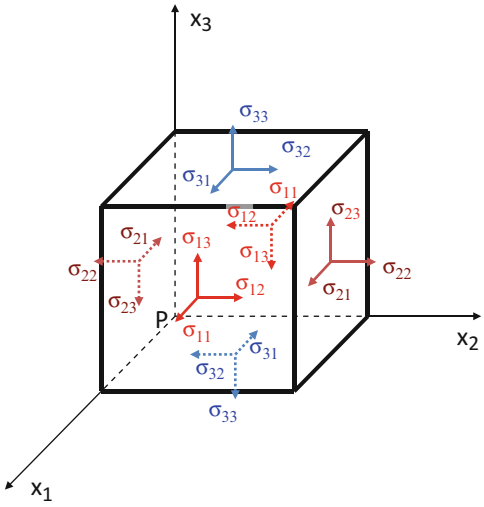

Fig. 1.2 Stress components at a point in a solid [1]

u is the displacement vector defined on Eq. (1.1), and **L** is a matrix of differential operators obtained from Eq. (1.3)

$$\mathbf{L} = \begin{bmatrix} \partial/\partial x_1 & 0 & 0 \\ 0 & \partial/\partial x_2 & 0 \\ 0 & 0 & \partial/\partial x_3 \\ 0 & \partial/\partial x_3 & \partial/\partial x_2 \\ \partial/\partial x_3 & 0 & \partial/\partial x_1 \\ \partial/\partial x_2 & \partial/\partial x_1 & 0 \end{bmatrix} \tag{1.6}$$

1.1.2 Stress and Constitutive Equations

The state of stress of any point in the body can be represented in an infinitely small cubic volume as shown in Fig. 1.2. On each cube surfaces there will be a normal component and two tangential components of stress. The normal component is designated as normal stress and the tangential components are named as shear stresses.

The notation convention for the subscript is that the first letter represents the index axis that is normal to the surface on which the stress is acting and, the second letter represents the index axis direction of the stress. The components of the stresses that are presented are all positive. Thus, the state of stress of a point is completely defined with the knowledge of nine stress components, σ_{ij}. Nevertheless, by taking moments of forces about the central axes of the cube at equilibrium state, it is

possible to verify that $\sigma_{12} = \sigma_{21}$; $\sigma_{13} = \sigma_{31}$; $\sigma_{23} = \sigma_{23}$. Therefore, in practice the state of stress of a point is completely defined with the knowledge of six stress components. These stresses are often written in a vector of

$$\sigma^T = \left[\sigma_{11}\ \sigma_{22}\ \sigma_{33}\ \sigma_{23}\ \sigma_{13}\ \sigma_{12}\right] \tag{1.7}$$

At any point in the body, the relationship between the stress and strain is defined by the constitutive equation of the material and, it is commonly called Hooke's law. The generalized Hooke's law for general anisotropic materials can be written in the following matrix form

$$\boldsymbol{\sigma} = \mathbf{c}\,\boldsymbol{\varepsilon} \tag{1.8}$$

where $\mathbf{c}$ is a matrix of material constants and is named stiffness material matrix. The constitutive equation can be written explicitly as

$$\begin{bmatrix} \sigma_{11} \\ \sigma_{22} \\ \sigma_{33} \\ \sigma_{23} \\ \sigma_{13} \\ \sigma_{12} \end{bmatrix} = \begin{bmatrix} c_{11} & c_{12} & c_{13} & c_{14} & c_{15} & c_{16} \\ & c_{22} & c_{23} & c_{24} & c_{25} & c_{26} \\ & & c_{33} & c_{34} & c_{35} & c_{36} \\ & sy & & c_{44} & c_{45} & c_{46} \\ & & & & c_{55} & c_{56} \\ & & & & & c_{66} \end{bmatrix} \begin{bmatrix} \varepsilon_{11} \\ \varepsilon_{22} \\ \varepsilon_{33} \\ 2\varepsilon_{23} \\ 2\varepsilon_{13} \\ 2\varepsilon_{12} \end{bmatrix} \tag{1.9}$$

Due to the stress and strain tensors symmetry, the stiffness material matrix is also symmetric, which mean that $\mathbf{c}$ matrix is completely defined with the knowledge of 21 independent material constants. However, for isotropic materials the stiffness material matrix can be reduce to

$$\mathbf{c} = \begin{bmatrix} c_{11} & c_{12} & c_{12} & 0 & 0 & 0 \\ & c_{11} & c_{12} & 0 & 0 & 0 \\ & & c_{11} & 0 & 0 & 0 \\ & sy & & (c_{11} - c_{12})/2 & 0 & 0 \\ & & & & (c_{11} - c_{12})/2 & 0 \\ & & & & & (c_{11} - c_{12})/2 \end{bmatrix} \tag{1.10}$$

with

$$c_{11} = \frac{E(1-\upsilon)}{(1-2\upsilon)(1+\upsilon)};\ c_{12} = \frac{E\upsilon}{(1-2\upsilon)(1+\upsilon)};\ G = \frac{c_{11} - c_{12}}{2} \tag{1.11}$$

where E, υ and G are Young's modulus, Poisson's ratio and the shear modulus of the material, respectively. Among these three constants there are only two independent constants: the Young's modulus and the Poisson's ratio.

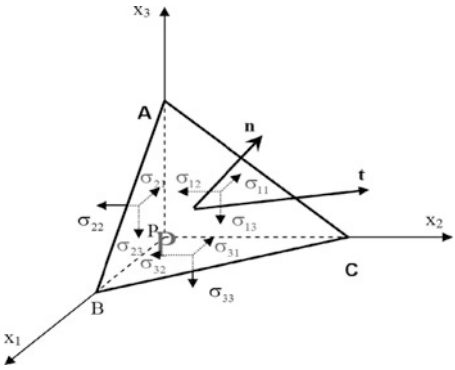

Fig. 1.3 Stress components at a small tetrahedron [1]

1.1.3 Cauchy's Equation

Assume that stress components are known and that an oblique plane cuts the infinitely small cubic volume, presented in Fig. 1.2, in such a way that is possible to extract the infinitely small tetrahedron volume presented in Fig. 1.3. The surface ABC is a face of the tetrahedron volume and is also part of the oblique cut plane, which the outwards normal n point towards the removed part of the infinitely small cubic volume. The geometric relations among the areas of the tetrahedron faces can be defined as,

$$\begin{aligned} \langle ABP \rangle &= \langle ABC \rangle \cos(\mathbf{n}, x_2) = A\, n_2 \\ \langle BCP \rangle &= \langle ABC \rangle \cos(\mathbf{n}, x_3) = A\, n_3 \\ \langle APC \rangle &= \langle ABC \rangle \cos(\mathbf{n}, x_1) = A\, n_1 \end{aligned} \tag{1.12}$$

and, taking in account that the tetrahedron must be in equilibrium, is possible to establish the equilibrium of forces in all directions and, particularly, through direction x_1 as

$$t_1 A - \sigma_{11} A\, n_1 - \sigma_{21} A\, n_2 - \sigma_{31} A\, n_3 + \frac{1}{3} A\, h\, b_1 = 0 \tag{1.13}$$

where it is assumed that volume forces are applied at the centroid of tetrahedron volume and the distance between point P and the face ABC is h. Simplification of Eq. (1.13) leads to

$$t_1 = \sigma_{11} n_1 + \sigma_{21} n_2 + \sigma_{31} n_3 \tag{1.14}$$

Using the same procedure, over directions x_1 and x_2, is possible to establish

$$\begin{aligned} t_2 &= \sigma_{12} n_1 + \sigma_{22} n_2 + \sigma_{32} n_3 \\ t_3 &= \sigma_{13} n_1 + \sigma_{23} n_2 + \sigma_{33} n_3 \end{aligned} \tag{1.15}$$

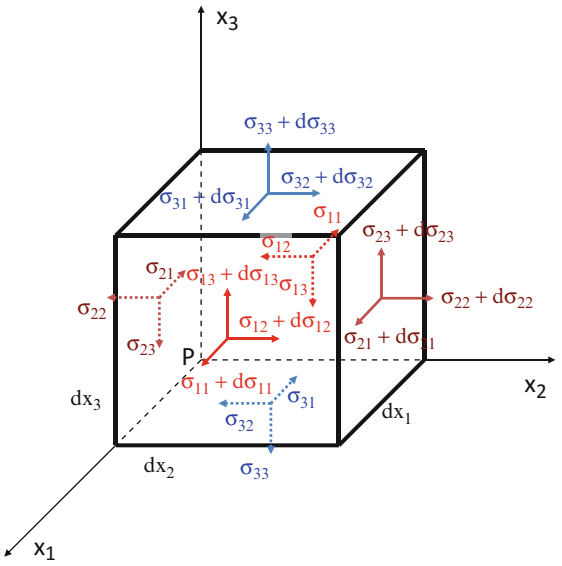

Fig. 1.4 Stress in a infinitely small block [1]

Equations (1.14) and (1.15) are represented in a matrix forma as

$$\mathbf{t} = \boldsymbol{\sigma}\ \mathbf{n} \tag{1.16}$$

where t is the stress vector over face ABC.

1.1.4 Dynamic Equilibrium Equations

The stress distribution in a body at dynamic equilibrium must be compatible with the overall motion of the body. To formulate equilibrium equations is also necessary to consider an infinitely small cube, as shown in Fig. 1.4. In general, the stresses are not uniform and they vary from one point to another in a continuum way. Thus, even that the infinitely small cube is constructed using parallel cutting planes at the body and, therefore, their normal match, the Cartesian components of stress on neighbor points vary of intensity. Nevertheless, if the points on opposite sides are close enough, is possible to consider that the variation of tension between them is continuous, linear and defined as

$$d\sigma_{ij} = \frac{\partial \sigma_{ij}}{\partial x_k} dx_k \tag{1.17}$$

Because the body is in dynamic equilibrium it is necessary to account the inertial forces of the infinitely small cube. So, the equilibrium of forces in the x_1 direction gives [1]

$$(\sigma_{11} + d\sigma_{11})\, dx_2 dx_3 - \sigma_{11} dx_2 dx_3 + (\sigma_{21} + d\sigma_{21})\, dx_1 dx_3 - \sigma_{12} dx_1 dx_3 + (\sigma_{31} + d\sigma_{31})\, dx_2 dx_1 - \sigma_{31} dx_2 dx_1 + b_1 dx_1 dx_2 dx_3 = \underbrace{\rho \ddot{u}_1 dx_1 dx_2 dx_3}_{inertial\ force} \quad (1.18)$$

After accounting the Eq. (1.17) into Eq. (1.18), assuming also the symmetry of stress tensor and making some simplifications, the latter equation can be written as

$$\frac{\partial \sigma_{11}}{\partial x_1} + \frac{\partial \sigma_{21}}{\partial x_2} + \frac{\partial \sigma_{31}}{\partial x_3} + b_1 = \rho \ddot{u}_1 \quad (1.19)$$

where $\ddot{u}_i$ represents the second derivatives of i displacement field with respect time.

Similarly, the equilibrium of forces in the x_2 and x_3 directions leads to other two equilibrium equations, written as

$$\frac{\partial \sigma_{12}}{\partial x_1} + \frac{\partial \sigma_{22}}{\partial x_2} + \frac{\partial \sigma_{32}}{\partial x_3} + b_2 = \rho \ddot{u}_2 \quad (1.20)$$

$$\frac{\partial \sigma_{13}}{\partial x_1} + \frac{\partial \sigma_{23}}{\partial x_2} + \frac{\partial \sigma_{33}}{\partial x_3} + b_3 = \rho \ddot{u}_3 \quad (1.21)$$

The equilibrium equations can be written in a matrix form, as

$$\mathbf{L}^T \boldsymbol{\sigma} + \mathbf{f}_b = \rho \ddot{\mathbf{u}} \quad (1.22)$$

Using Eqs. (1.22), (1.8) and (1.4) is possible to write equilibrium equations in terms of the displacement field, as

$$\mathbf{L}^T \mathbf{c}\, \mathbf{L}\, \mathbf{u} + \mathbf{f}_b = \rho \ddot{\mathbf{u}} \quad (1.23)$$

Equation 1.23 is the general form of the dynamic equilibrium equation written in a matrix form. Nevertheless, if loads applied on the body are not time dependent, the time variation of displacements is zero and the body should be in static equilibrium. Thus, the static equilibrium equations can be obtained from Eq. (1.23) by setting the right hand side of this equation equal to zero, leading to

$$\mathbf{L}^T \mathbf{c}\, \mathbf{L}\, \mathbf{u} + \mathbf{f}_b = \mathbf{0} \quad (1.24)$$

1.2 Equations for 2D Mathematical Models

If a structure has one of its dimensions much smaller than the other two, the analysis of such structure can be simplified using 2D geometric models. Mathematically speaking, this procedure try to remove one of the three coordinates, usually the x_3, assuming that all variables of the problem are independent of this coordinate [2].

There are primarily two types of 2D mathematical models: those that are in plane stress or strain conditions and those that are in bending conditions.

1.2.1 Plane Stress and Strain Conditions

Structures for which plane stress conditions can be assumed are structures whose thickness in the x_3 direction is very small when compared with dimensions in the x_1 and x_2 directions. External forces are applied on the x_1-x_2 plane and, because the structure is thin in the x_3 direction, $(h/L \ll 1)$, the assumption that variations of the stress components with x_3 is uniform and that will be functions of the x_1 and x_2 directions $\sigma(x_1, x_2)$ is valid. Moreover, because the structure in the x_3 direction is under a stress free condition, the micro-equilibrium of any structural point is achieved by removing the three x_3 stress components, see Fig. 1.5, which means that the transverse stresses are negligible. Therefore, in practice, the state of stress at any point in a plane stress condition is completely defined with the knowledge of three stress components. These stresses are often written in a vector form as

$$\boldsymbol{\sigma}^T = \left[\sigma_{11} \ \sigma_{22} \ \sigma_{12} \right] \tag{1.25}$$

The strain components at any point in a plane stress condition, for isotropic materials, may be obtained from the reverse form of Eqs. (1.9) and (1.10), by setting to zero all the three x_3 stress components, leading to

$$\begin{bmatrix} \varepsilon_{11} \\ \varepsilon_{22} \\ \varepsilon_{33} \\ \gamma_{23} \\ \gamma_{13} \\ \gamma_{12} \end{bmatrix} = \frac{1}{E} \begin{bmatrix} 1 & -\nu & -\nu & 0 & 0 & 0 \\ -\nu & 1 & -\nu & 0 & 0 & 0 \\ -\nu & -\nu & 1 & 0 & 0 & 0 \\ 0 & 0 & 0 & 2(1+\nu) & 0 & 0 \\ 0 & 0 & 0 & 0 & 2(1+\nu) & 0 \\ 0 & 0 & 0 & 0 & 0 & 2(1+\nu) \end{bmatrix} \begin{bmatrix} \sigma_{11} \\ \sigma_{22} \\ 0 \\ 0 \\ 0 \\ \sigma_{12} \end{bmatrix} \tag{1.26}$$

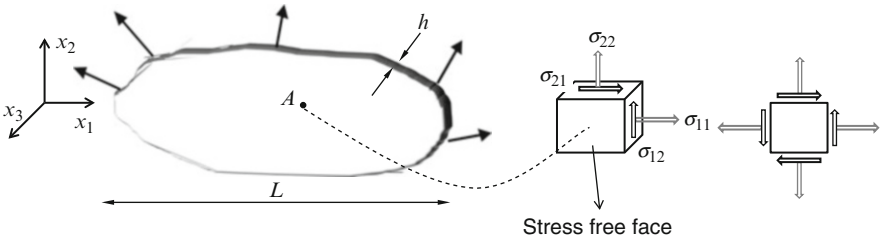

Fig. 1.5 Structure in a plane stress conditions

From Eq. (1.26) is possible to verify that the condition $\sigma_{33} = 0$ leads to the transverse normal strain given by

$$\varepsilon_{33} = -\frac{\nu}{E}(\sigma_{11} + \sigma_{22}) \tag{1.27}$$

and the condition $\sigma_{23} = \sigma_{13} = 0$, leads to zero shear strains, i.e.,

$$\gamma_{13} = \gamma_{23} = 0 \tag{1.28}$$

Structures for which plane strain conditions can be assumed are structures whose dimension in the x_3 direction is very large when compared with dimensions in the x_1 and x_2 directions. The applied forces act in the x_1-x_2 plane and do not vary in the x_3 direction, i.e. loads are uniformly distributed with respect to the large dimension and act perpendicular to it. Some important practical applications of this strain state appear in the analysis of dams, tunnels, and other geotechnical works, see Fig. 1.6. Moreover, the cross-section that is defined in the x_1-x_2 plane do not vary with the x_3 direction and, therefore, it can be taken as a representative cell.

For a structure in plane strain conditions, the strains in the x_3 direction ($\varepsilon_{33}, \varepsilon_{13}, \gamma_{23}$) are negligible and strains are often written in a vector form as

$$\boldsymbol{\varepsilon}^T = \begin{bmatrix} \varepsilon_{11} & \varepsilon_{22} & \gamma_{12} \end{bmatrix} \tag{1.29}$$

The stress components at any point in a plane strain condition may be obtained from the reverse form of Eq. (1.9), with $\mathbf{c}$ given by Eq. (1.10), and setting to zero all the three x_3 strain components.

1.2.1.1 Kinematic and Strain Relationships

The kinematics for plane stress or plane strain problems does not account for the displacement component w in the direction of coordinate x_3. Thus, the displacement vector has the form

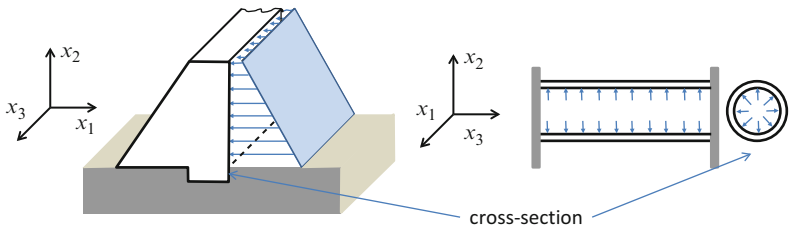

Fig. 1.6 Structure in a plane strain conditions

$$\mathbf{u} = \begin{bmatrix} u_1(x_1,\ x_2) \\ u_2(x_1,\ x_2) \end{bmatrix} \tag{1.30}$$

and, therefore, the components of strain can be obtained from the derivatives of the displacements as follows:

$$\varepsilon_{11} = \frac{\partial u_1}{\partial x_1};\ \varepsilon_{22} = \frac{\partial u_2}{\partial x_2};\ \gamma_{12} = \frac{\partial u_1}{\partial x_2} + \frac{\partial u_2}{\partial x_1} \tag{1.31}$$

The relations presented on the last equation can be rewritten in the following matrix form

$$\boldsymbol{\varepsilon} = \mathbf{L}\,\mathbf{u} \tag{1.32}$$

where $\boldsymbol{\varepsilon}$ is the strain vector defined on Eq. (1.29), $\mathbf{u}$ is the displacement vector defined in Eq. (1.30) and $\mathbf{L}$ is a matrix of differential operators obtained from Eq. (1.31)

$$\mathbf{L} = \begin{bmatrix} \partial/\partial x_1 & 0 \\ 0 & \partial/\partial x_2 \\ \partial/\partial x_2 & \partial/\partial x_1 \end{bmatrix} \tag{1.33}$$

1.2.1.2 Constitutive Equations

The generalized Hooke's law for general isotropic materials can be written in the form of Eq. (1.8), where $\mathbf{c}$ is the stiffness matrix for isotropic materials defined on Eq. (1.10). To obtain the equivalent law for plane stress conditions, the Eq. (1.26) may be rewritten in a more compact form as

$$\begin{bmatrix} \varepsilon_{11} \\ \varepsilon_{22} \\ \gamma_{12} \end{bmatrix} = \frac{1}{E} \begin{bmatrix} 1 & -\upsilon & 0 \\ -\upsilon & 1 & 0 \\ 0 & 0 & 2(1+\nu) \end{bmatrix} \begin{bmatrix} \sigma_{11} \\ \sigma_{22} \\ \sigma_{12} \end{bmatrix} \tag{1.34}$$

where ε_{33} is defined by Eq. (1.27), now inverting Eq. (1.34) yields

$$\begin{bmatrix} \sigma_{11} \\ \sigma_{22} \\ \sigma_{12} \end{bmatrix} = \frac{E}{(1-\upsilon^2)} \begin{bmatrix} 1 & \upsilon & 0 \\ \upsilon & 1 & 0 \\ 0 & 0 & (1-\upsilon)/2 \end{bmatrix} \begin{bmatrix} \varepsilon_{11} \\ \varepsilon_{22} \\ \gamma_{12} \end{bmatrix} \tag{1.35}$$

Equation 1.35 is the constitutive equation for isotropic materials under plane stress conditions.

For isotropic materials in plane strain conditions, the equalities $\varepsilon_{33} = \varepsilon_{13} = \varepsilon_{23} = 0$ are imposed in Eq. (1.9), leading to

$$\begin{bmatrix} \sigma_{11} \\ \sigma_{22} \\ \sigma_{12} \end{bmatrix} = \frac{E\,(1-\upsilon)}{(1+\upsilon)\,(1-2\upsilon)} \times \begin{bmatrix} 1 & \upsilon/\,(1-\upsilon) & 0 \\ \upsilon/\,(1-\upsilon) & 1 & 0 \\ 0 & 0 & (1-2\upsilon)\,/\,(2\,(1-\upsilon)) \end{bmatrix} \begin{bmatrix} \varepsilon_{11} \\ \varepsilon_{22} \\ 2\varepsilon_{12} \end{bmatrix} \tag{1.36}$$

with

$$\sigma_{33} = \frac{E\upsilon}{(1-2\upsilon)\,(1+\upsilon)}(\varepsilon_{11} + \varepsilon_{22}) \tag{1.37}$$

1.2.1.3 Dynamic Equilibrium Equations

The dynamic equilibrium equations for problems in plane stress and strain conditions can be obtained from Eqs. (1.19) and (1.20) by removing the terms related to the x_3 coordinate, as

$$\frac{\partial \sigma_{11}}{\partial x_1} + \frac{\partial \sigma_{21}}{\partial x_2} + b_1 = \rho \ddot{u}_1 \tag{1.38}$$

$$\frac{\partial \sigma_{12}}{\partial x_1} + \frac{\partial \sigma_{22}}{\partial x_2} + b_2 = \rho \ddot{u}_2 \tag{1.39}$$

The condensed matrix form of Eqs. (1.38) and (1.39) is given by

$$\mathbf{L}^T \boldsymbol{\sigma} + \mathbf{f}_b = \rho \ddot{\mathbf{u}} \tag{1.40}$$

where $\mathbf{L}$ is a matrix of differential operators defined in Eq. (1.33), $\mathbf{u}$ is the displacement vector defined in Eq. (1.30) and $\ddot{\mathbf{u}}$ is the acceleration vector.

For static problems, the right hand side of Eq. (1.40) is removed, and the static equilibrium equations can be written as

$$\mathbf{L}^T \boldsymbol{\sigma} + \mathbf{f}_b = \mathbf{0} \tag{1.41}$$

Notice that Eq. (1.40) has the same form of Eq. (1.22), the only difference resides in the dimensions of matrices and vectors involved.

1.2.2 Bending Conditions

The geometrical feature of structures under bending conditions is similar to those under plane stress, that is, thickness in the x_3 direction is very small when compared

with dimensions in the x_1 and x_2 directions. Nevertheless, external forces are applied perpendicularly to its geometrical plane and, therefore, they will experience bending resulting deflection in the normal direction. These kinds of structures are named plates. Examples of plate structures are wings of aircrafts, wind turbine blades, roof of houses, solar panels and etc. The main characteristic of plate stresses is that the stress σ_{33} is assumed to be zero.

From the kinematic point of view there are several theories for analyzing deflection in plate structures. Nevertheless, these theories can be basically grouped into major categories: theory for thin plates and theory for thick plates. Thin plate theory is often called Classical Plate Theory or Kirchhoff plate theory while the more simple thick plate theory is called First Order Shear Deformation Theory or Reissner-Mindlin theory.

1.2.2.1 Classic Plate Theory

Derivation of the classical plate model starts from some kinematic assumptions which were originally made by Kirchhoff. The Kirchhoff assumptions are [3]:

- The transverse normal is infinitely rigid along its own direction;
- The transverse normal of the plate remains straight during deformation;
- The transverse normal remains normal to the reference surface of the plate during deformation.

The first Kirchhoff assumption implies that every material point that shares the same transverse normal will move rigidly along the transverse direction, which also implies that the transverse displacement of every material point of the plate with the same in-plane location remains the same. Therefore, the transverse displacement of the plate can be described as

$$u_3(x_1, x_2, x_3) = w(x_1, x_2) \tag{1.42}$$

The second Kirchhoff assumption implies that the in-plane displacement field of the plate is, almost linear in terms of x_3 coordinate, defined by

$$u_1(x_1, x_2, x_3) = x_3 \phi_2(x_1, x_2) \tag{1.43}$$

$$u_2(x_1, x_2, x_3) = -x_3 \phi_1(x_1, x_2) \tag{1.44}$$

The physical meaning of the in-plane rigid rotations ϕ_1 and ϕ_2 of the transversal normal is explained by the sketch presented in Fig. 1.7, in which a set of unit vectors $\mathbf{e}_i$ $(i = 1, 2, 3)$ associated with coordinates x_i $(i = 1, 2, 3)$ were introduced to facilitate the derivation of plate models. This reference frame is attached at a point of the plate structure such that $\mathbf{e}_3$ is along the transverse normal, $\mathbf{e}_1$ and $\mathbf{e}_2$ define the

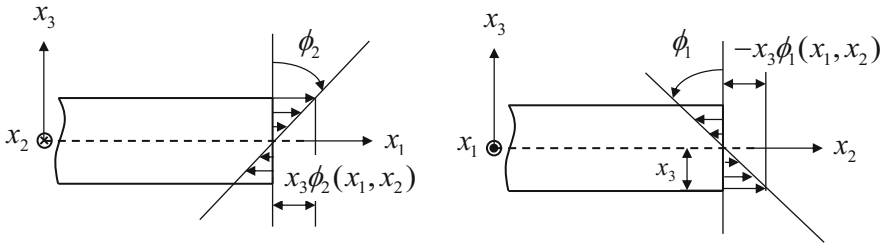

Fig. 1.7 Representation of the in-plane displacement field

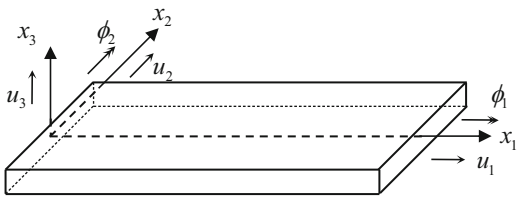

Fig. 1.8 Sign convention for plate displacement and rotations

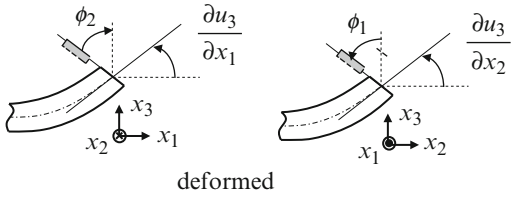

Fig. 1.9 Plate reference surface slope and transverse normal rotations of the Kirchhoff theory

plate reference surface. The sign conventions for the displacements and rotations are presented in Fig. 1.8.

Note that because the rigid body rotations of the transverse normal are positive when they rotate around the positive side of axes, the negative sign in Eq. (1.44) is to assure that a positive x_3 value and a positive value of ϕ_1 rotation will create a negative in-plane displacement along x_2 direction.

The third Kirchhoff assumptions implies that rotations of the transverse normal must be obtained from the partial derivatives of the reference surface as presented at Fig. 1.9 and defined by

$$\phi_1 = \frac{\partial w}{\partial x_2}; \quad \phi_2 = -\frac{\partial w}{\partial x_1} \tag{1.45}$$

Note that the minus sign in the second Eq. (1.45) is due to the sign convention presented in Fig. 1.8. Substituting Eq. (1.45) into Eqs. (1.43) and (1.44) is possible to eliminate the variables ϕ_1 and ϕ_2 from the in-plane displacement field. Thus, the Kirchhoff displacement field for a plate-like structure is written as

$$u_1(x_1, x_2, x_3) = -x_3 \frac{\partial w}{\partial x_1} \tag{1.46}$$

$$u_2(x_1, x_2, x_3) = -x_3 \frac{\partial w}{\partial x_2} \tag{1.47}$$

$$u_3(x_1, x_2, x_3) = w(x_1, x_2) \tag{1.48}$$

The displacement field presented in Eqs. (1.46), (1.47) and (1.48) assume that the in-plane displacements of any material point at the plate reference surface are null and, of any material point placed above or below the reference surface are defined in order to assure that the surface transverse normal, at this material point, remains normal to the deformed plate reference surface. So the Kirchhoff assumptions can be viewed as constraining the plate structure in such a way that physical deformation must behave according to these assumptions. Physically, we might not be able to apply such constraints and, therefore, the mathematical model is stiffer than the original structure leading to displacements that are generally smaller than those obtained from the 3D theory.

Stress and Strain

Substituting the Kirchhoff displacement field in Eq. (1.2) is possible to obtain the 3D strain field as

$$\varepsilon_{11} = -x_3 \frac{\partial^2 w}{\partial x_1^2};\ \varepsilon_{22} = -x_3 \frac{\partial^2 w}{\partial x_2^2};\ 2\varepsilon_{12} = -2x_3 \frac{\partial^2 w}{\partial x_1 \partial x_2}; \tag{1.49}$$

$$\varepsilon_{13} = \varepsilon_{23} = \varepsilon_{33} = 0 \tag{1.50}$$

The relations presented in Eq. (1.49) can be rewritten in the following matrix form

$$\boldsymbol{\varepsilon} = -x_3 \mathbf{L}\, w \tag{1.51}$$

where $\boldsymbol{\varepsilon}$ is the strain vector defined on Eq. (1.29) and $\mathbf{L}$ is a matrix of differential operators given by

$$\mathbf{L} = \begin{bmatrix} \partial^2/\partial x_1^2 \\ \partial^2/\partial x_2^2 \\ 2\partial^2/(\partial x_1 \partial x_2) \end{bmatrix} \tag{1.52}$$

The null value of ε_{33} strain is a direct consequence of the first Kirchhoff assumption, which implies that no strain exist in the transverse direction, while the null value of transverse shear strains, ε_{13} and ε_{23}, is a direct consequence of the third Kirchhoff assumption. In fact, the 90° angle between transverse normal line and the reference surface, before deformation, only can remain at 90° after deformation if the transverse shear strains are zero.

Once the strain field is known, the stress field in the plate structure may be obtained from the generalized 3D Hooke's law for isotropic materials, leading to

$$\begin{bmatrix} \sigma_{11} \\ \sigma_{22} \\ \sigma_{12} \end{bmatrix} = \begin{bmatrix} \lambda + 2G & \lambda & 0 \\ \lambda & \lambda + 2G & 0 \\ 0 & 0 & G \end{bmatrix} \begin{bmatrix} \varepsilon_{11} \\ \varepsilon_{22} \\ 2\varepsilon_{12} \end{bmatrix} \tag{1.53}$$

$$\sigma_{33} = \lambda \left(\varepsilon_{11} + \varepsilon_{22} \right); \; \sigma_{13} = \sigma_{23} = 0 \tag{1.54}$$

where $\lambda = \upsilon E / \left[(1 + \upsilon) (1 - 2\upsilon) \right]$ and $G = E / \left[2 (1 + \upsilon) \right]$ is the shear modulus. Note that Eqs. (1.36) and (1.53) as well as Eqs. (1.37) and (1.54) are equivalents. Although this stress field naturally flows from the generalized Hooke's law and the strain field in Eqs. (1.49) and (1.50), it does not agree very well with the experimental measurements [3]. This drawback can be overcome by assuming additional assumptions regarding the stress field. Thus, since the thickness of the plate is much smaller than the in-plane dimension of the plate is possible to assume that $\sigma_{33} = 0$. Nevertheless, the stress assumption $\sigma_{i3} = 0$ corresponds to the plane stress condition in which the strain ε_{33} is defined as

$$\varepsilon_{33} = \frac{\upsilon}{\upsilon - 1} \left(\varepsilon_{11} + \varepsilon_{22} \right) \tag{1.55}$$

Meanwhile, Eq. (1.55) directly contradicts the ε_{33} strain value presented in Eq. (1.50) that was obtained using the Kirchhoff assumptions, except when $\upsilon = 0$, which in general is not true.

Using the transverse normal strain given in Eq. (1.55) and the additional strain measurements in Eq. (1.49) into the generalized Hooke's law, will lead to the following stress field

$$\begin{bmatrix} \sigma_{11} \\ \sigma_{22} \\ \sigma_{12} \end{bmatrix} = \frac{E}{(1 - \upsilon^2)} \begin{bmatrix} 1 & \upsilon & 0 \\ \upsilon & 1 & 0 \\ 0 & 0 & (1 - \upsilon)/2 \end{bmatrix} \begin{bmatrix} \varepsilon_{11} \\ \varepsilon_{22} \\ 2\varepsilon_{12} \end{bmatrix} \tag{1.56}$$

$$\sigma_{13} = \sigma_{23} = \sigma_{33} = 0 \tag{1.57}$$

Clearly the above stress field corresponds to the constitutive law for the case of a plate under plane stress conditions, which means that the stress field in Eqs. (1.56) and (1.57) conflicts with the stress field obtained using the Kirchhoff assumptions, Eqs. (1.53) and (1.54). These contradictions can be partially justified by the fact that we need to rely on the Kirchhoff assumptions to obtain a simple expression of the 3D kinematics in terms of 2D kinematics and we also use the assumption that the plate is under plane stress conditions, so that the results can better agree with reality [3]. Finally, the stresses can be obtained by substituting Eq. (1.51) into Eq. (1.56)

$$\boldsymbol{\sigma} = -x_3 \, \mathbf{c} \, \mathbf{L} \, w \tag{1.58}$$

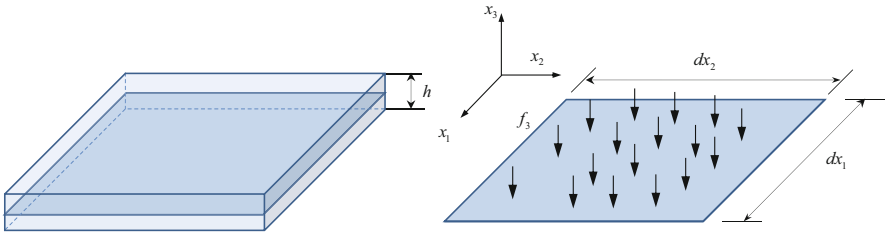

Fig. 1.10 Dimensions of an isolated plate cell

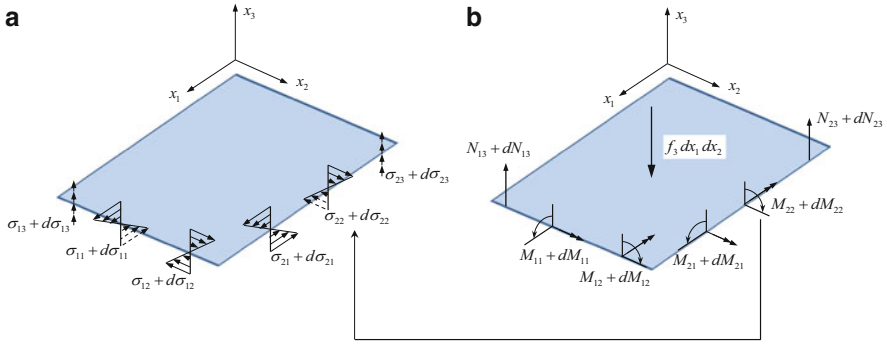

Fig. 1.11 Isolated plate cell and representation of: (**a**) stresses; (**b**) shear forces and moments

Notice that in Eq. (1.58) the **c** matrix is defined according the constitutive law for plane stress conditions.

Moments and Shear Forces

In order to evaluate the resultant forces and moments acting in a plate it is necessary to integrate the several stresses through the plate thickness. Figure 1.10 shows a small representative cell with dimensions $dx_1 \times dx_2$ from a plate of thickness h. The plate is submitted to external forces, here denoted by f_3, and inertial force proportional to the material density. Figure 1.11a shows the distributed normal and shear stresses in two faces of the representative cell. Notice that the two remaining faces will also have distributed normal and shear stresses, in such a way that the variation term $\left(d\sigma_{ij};\ i,j = 1,2\right)$ is removed and their sense is opposite to the senses depicted on the opposite face.

The moments $M_{ij};\ i,j = 1,2$ result from the distributed stresses $\sigma_{ij};\ i,j = 1,2$ and the transverse shear stress resultants $N_{i3};\ i = 1,2$ result from the distributed shear stresses $\sigma_{i3};\ i = 1,2$. Although the transversal shear stresses $\sigma_{i3};\ i = 1,2$ vanish due to the third Kirchhoff assumption and the Hooke's law, such stress values are not zero and, they are needed to balance the vertical load on the plate, which is the primary load mechanism. Nevertheless, is possible to obtain $N_{i3};\ i = 1,2$ from the equilibrium considerations and from these values estimate $\sigma_{i3};\ i = 1,2$ [3]. For instance, assuming that the transverse shear stresses have a uniform variation

through the plate thickness, $\sigma_{i3} = N_{i3}/h;\ i = 1, 2$. Another way to the estimate transverse shear stresses is through 3D equilibrium equations and the knowledge of in-plane stresses $\sigma_{ij};\ i, j = 1, 2$.

The classical plate resultants are defined as follows:

$$\mathbf{M} = \begin{bmatrix} M_{11} \\ M_{22} \\ M_{12} \end{bmatrix} = \int_{-\frac{h}{2}}^{\frac{h}{2}} x_3 \begin{bmatrix} \sigma_{11} \\ \sigma_{22} \\ \sigma_{12} \end{bmatrix} dx_3 = \int_{-\frac{h}{2}}^{\frac{h}{2}} x_3\ \boldsymbol{\sigma}\ dx_3 \tag{1.59}$$

Using the relation (1.58) into Eq. (1.59) leads to

$$\mathbf{M} = -\int_{-\frac{h}{2}}^{\frac{h}{2}} x_3^2\ \mathbf{c}\ \mathbf{L}\ w\ dx_3 = -\frac{h^3}{12}\mathbf{c}\ \mathbf{L}\ w \tag{1.60}$$

where $\mathbf{c}$ has the same form for plane stress conditions, defined by Eq. (1.56), and $\mathbf{L}$ is the differential operator matrix given by Eq. (1.52).

Dynamic Equilibrium Equations

To derive dynamic equilibrium equations for the classical plate model, it is necessary to consider the equilibrium of the differential plate element presented in Fig. 1.11. So, considering the equilibrium in the x_3 direction, and noting that $d(\bullet) = (\partial(\bullet)/\partial x_i)\, dx_i\ \ (i = 1, 2)$, is possible to write

$$\left(\frac{\partial N_{13}}{\partial x_1} dx_1\right) dx_2 + \left(\frac{\partial N_{23}}{\partial x_2} dx_2\right) dx_1 + (f_3 - \rho h \ddot{w})\, dx_1 dx_2 = 0 \tag{1.61}$$

or

$$\frac{\partial N_{13}}{\partial x_1} + \frac{\partial N_{23}}{\partial x_2} + f_3 = \rho h \ddot{w} \tag{1.62}$$

Equilibrium also implies that the summation of moments along all the directions should vanish. Thus, considering the moment equilibrium with respect to the x_1 axes and neglecting the second order small terms, gives

$$N_{23} = \frac{\partial M_{12}}{\partial x_1} + \frac{\partial M_{22}}{\partial x_2} \tag{1.63}$$

and summing the moments about to the x_2 axis, yields

$$N_{13} = \frac{\partial M_{11}}{\partial x_1} + \frac{\partial M_{21}}{\partial x_2} \tag{1.64}$$

In which the relation $M_{12} = M_{21}$ is used.

To obtain the dynamic equilibrium equations for plates, the relation presented in Eq. (1.60) is used in Eqs. (1.63) and (1.64) after which the resulting values of N_{13} and N_{23} are substituted into Eq. (1.62), leading to

$$D\left(\frac{\partial^4 w}{\partial x_1^4}+2\frac{\partial^4 w}{\partial x_1^2\partial x_2^2}+\frac{\partial^4 w}{\partial x_2^4}\right)+\rho h\ddot{w}=f_3 \tag{1.65}$$

where $D = Eh^3/\left(12\left(1-\upsilon^2\right)\right)$ is known as the bending stiffness of a plate. The static equilibrium equation for plates may be obtained from Eq. (1.65) by dropping the inertial term

$$D\left(\frac{\partial^4 w}{\partial x_1^4}+2\frac{\partial^4 w}{\partial x_1^2\partial x_2^2}+\frac{\partial^4 w}{\partial x_2^4}\right)=f_3 \tag{1.66}$$

Equation 1.66 is the basic equation of Kirchhoff plate bending theory which is a biharmonic partial differential equation for the transverse displacement that can be written in a more compact form as

$$\nabla^4 w=\frac{f_3}{D} \tag{1.67}$$

1.2.2.2 Reissner-Mindlin Plate Theory

The Reissner-Mindlin plate theory may be obtained from the Kirchhoff theory by removing the third Kirchhoff assumption, which implies that the transverse normal remains straight during deformation, but it not necessarily remains normal to the reference surface, as shown in Fig. 1.12. Therefore, under such assumptions the displacement field of the First order Shear Deformation Theory is written in the form of Eqs. (1.42), (1.43) and (1.44). Nevertheless, the relations on Eq. (1.45) are no longer valid and, ϕ_1 and ϕ_2 are, respectively, the positive rotations about x_1 and x_2 axes of the normal to the reference surface and they are treated as independent variables.

Because the Reissner-Mindlin plate model has one less assumption, it is expected that displacements obtained by this model will be larger than those obtained using the classical plate model based on the Kirchhoff assumptions. Nevertheless, this assumption is only valid for plates in which shear deformation and rotary inertia effects are important.

Stress and Strain

Substituting the Reissner-Mindlin displacement field in Eq. (1.2) is possible to obtain the 3D strain field as

$$\varepsilon_{11}=x_3\frac{\partial\phi_2}{\partial x_1};\ \varepsilon_{22}=-x_3\frac{\partial\phi_1}{\partial x_2};\ \gamma_{12}=x_3\left(\frac{\partial\phi_2}{\partial x_2}-\frac{\partial\phi_1}{\partial x_1}\right); \tag{1.68}$$

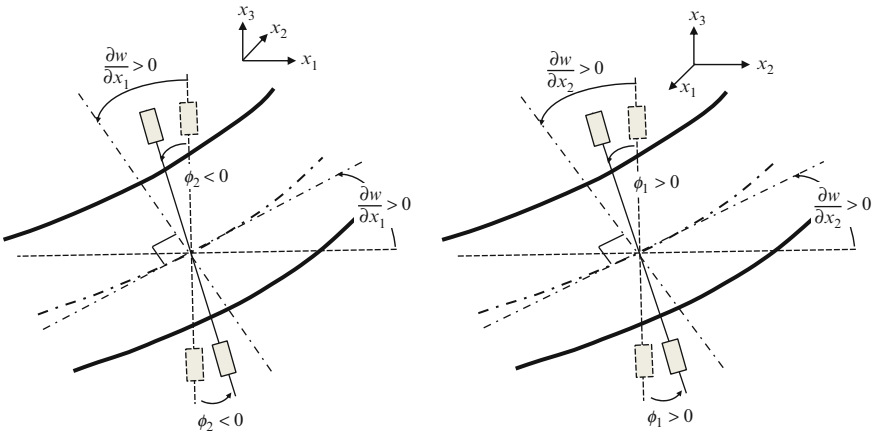

Fig. 1.12 Plate reference surface slope and transverse normal rotations of the Reissner-Mindlin theory

$$\gamma_{13} = \phi_2 + \frac{\partial w}{\partial x_1};\ \gamma_{23} = -\phi_1 + \frac{\partial w}{\partial x_2};\ \varepsilon_{33} = 0 \tag{1.69}$$

The relations presented in Eqs. (1.68) and (1.69) may be separated into bending (in-plane) and transverse shear groups. So, Eq. (1.68) can be rewritten in the following matrix form

$$\boldsymbol{\varepsilon}_b = -x_3 \mathbf{L}\, \boldsymbol{\theta} \tag{1.70}$$

where

$$\boldsymbol{\varepsilon}_b^T = \begin{bmatrix} \varepsilon_{11} & \varepsilon_{22} & \gamma_{12} \end{bmatrix} \tag{1.71}$$

$$\mathbf{L} = \begin{bmatrix} 0 & -\partial/\partial x_1 \\ \partial/\partial x_2 & 0 \\ \partial/\partial x_1 & -\partial/\partial x_2 \end{bmatrix} \tag{1.72}$$

$$\boldsymbol{\theta}^T = \begin{bmatrix} \phi_1 & \phi_2 \end{bmatrix} \tag{1.73}$$

and the transverse shear strains can be written as

$$\boldsymbol{\varepsilon}_s = \begin{bmatrix} \gamma_{13} \\ \gamma_{23} \end{bmatrix} = \begin{bmatrix} \phi_2 + \dfrac{\partial w}{\partial x_1} \\ -\phi_1 + \dfrac{\partial w}{\partial x_2} \end{bmatrix} \tag{1.74}$$

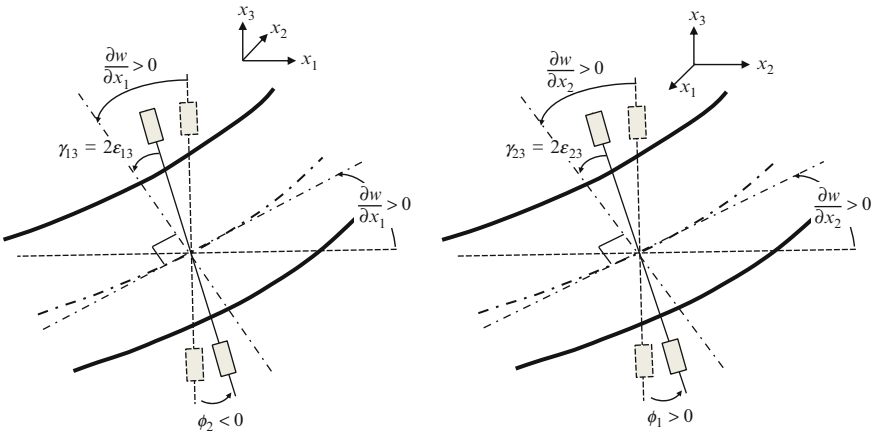

Fig. 1.13 Transverse shear strains of the Reissner-Mindlin plate theory

In Eq. (1.74) is possible to see that transverse shear strains are independent of the plate thickness, and they are exactly equal to the additional rotations of the normal to the reference surface after deformation, as shown in Fig. 1.13. Nevertheless, if the transverse shear strains are negligible, $\varepsilon_{13} = 0$, $\varepsilon_{23} = 0$, the above equation will lead to

$$\phi_1 = \frac{\partial w}{\partial x_2} \tag{1.75}$$

$$\phi_2 = -\frac{\partial w}{\partial x_1} \tag{1.76}$$

and we are in face of the Kirchhoff theory.

The stress relations may also be separated into bending (in-plane) and transverse shear groups. Using the in-plane strains given in Eq. (1.70) into the generalized Hooke's law for the case of a plate under plane stress conditions, will lead to the following stress field

$$\boldsymbol{\sigma}_b = -x_3\, \mathbf{c}_b\, \boldsymbol{\varepsilon}_b = -x_3\, \mathbf{c}_b\, \mathbf{L}\, \boldsymbol{\theta} \tag{1.77}$$

where $\mathbf{c}_b$ still has the same form for plane stress conditions. The transverse shear stress relates to the transverse shear strain in the form

$$\boldsymbol{\sigma}_s = \begin{bmatrix} \sigma_{13} \\ \sigma_{23} \end{bmatrix} = \begin{bmatrix} G & 0 \\ 0 & G \end{bmatrix} \begin{bmatrix} \gamma_{13} \\ \gamma_{23} \end{bmatrix} = \mathbf{c}_s \boldsymbol{\varepsilon}_s \tag{1.78}$$

where G is the shear modulus. Since transverse shear strains are independent of the plate thickness, which mean that are constant through the plate thickness, it follows that the transverse shear stresses also have a constant distribution through the plate thickness. However, in plates the transverse shear stress varies at least quadratically through the plate thickness. The discrepancy between both states of stress is often corrected by computing the transverse shear correction coefficient, k_s, the factor is computed such that the strain energy due to the transverse shear stresses equals the strain energy due to the true transverse shear stresses predicted by the three-dimensional elasticity theory [4,5]. A parameter value of 5/6 has been extensively used for the case of homogeneous rectangular beams and plates made of isotropic materials. Thus, Eq. (1.78) is modified as

$$\boldsymbol{\sigma}_s = k_s \, \mathbf{c}_s \boldsymbol{\varepsilon}_s \tag{1.79}$$

Moments and Shear Forces

The resultant forces and moments acting in a Reissner-Mindlin plate can also be similarly obtained as that of a classical plate. Nevertheless, at this time the transverse shear resultant forces are defined as

$$\mathbf{N} = \begin{bmatrix} N_{13} \\ N_{23} \end{bmatrix} = \int_{-\frac{h}{2}}^{\frac{h}{2}} \begin{bmatrix} \sigma_{13} \\ \sigma_{23} \end{bmatrix} dx_3 = \int_{-\frac{h}{2}}^{\frac{h}{2}} \boldsymbol{\sigma}_s \, dx_3 = h \, k_s \, \mathbf{c}_s \boldsymbol{\varepsilon}_s = \mathbf{D}_s \boldsymbol{\varepsilon}_s \tag{1.80}$$

Using the relation (1.77) into Eq. (1.59), the resultant moments are defined as

$$\mathbf{M} = -\int_{-\frac{h}{2}}^{\frac{h}{2}} x_3^2 \, \mathbf{c}_b \, \boldsymbol{\varepsilon}_b \, dx_3 = -\frac{h^3}{12} \mathbf{c}_b \, \boldsymbol{\varepsilon}_b = \mathbf{D}_b \, \boldsymbol{\varepsilon}_b \tag{1.81}$$

The constitutive relations in Eqs. (1.80) and (1.81) can be rewritten in the following matrix form

$$\begin{bmatrix} \mathbf{M} \\ \mathbf{N} \end{bmatrix} = \begin{bmatrix} \mathbf{D}_b & \mathbf{0} \\ \mathbf{0} & \mathbf{D}_s \end{bmatrix} \begin{bmatrix} \boldsymbol{\varepsilon}_b \\ \boldsymbol{\varepsilon}_s \end{bmatrix} \tag{1.82}$$

where $\mathbf{D}_b$ is the bending stiffness matrix and $\mathbf{D}_s$ is shear stiffness matrix.

The equilibrium equations for a Reissner-Mindlin plate can also be similarly obtained as that of a classical plate. For the purpose of this notes the above concepts of the Reissner-Mindlin plate will be sufficient and, therefore, the equilibrium equations will not be shown.

1.3 Equations for 1D Mathematical Models

If a structure has one of its dimensions much larger than the other two, the analysis of such structure can be simplified using 1D geometric models. Mathematically speaking, this procedure try to remove two of the three coordinates, usually x_2 and x_3, assuming that all variables of the problem are independent of these coordinates. The axis of the structure is defined along that longer dimension, and a cross-section normal to this axis is assumed to smoothly vary along the span of the structure [6]. There are primarily three types of 1D mathematical models: trusses, shafts and beams. The main difference among those models is related to the kind of load at which they are subjected.

1.3.1 Equations for Truss Members

Derivation of the classical truss model starts from some kinematic assumptions which are [3]:

- The truss cross-section is infinitely rigid in its own plane, remaining plane after deformation;
- Loads can only be applied axially.

Experimental observations show that these assumptions are reasonable for slender structures. When one or more of these conditions are not met, the classical truss model derived based on these assumptions may be inaccurate. To help the discussion of the mathematical implication of these assumptions, consider a set of Cartesian axes attached at the geometric center of the truss cross-section, such that x_1 is along the axis of the truss, and x_2 and x_3 define the plane of the cross-section. The displacement of an arbitrary point of the truss in the x_1, x_2 and x_3 directions are defined by $u_1(x_i)$, $u_2(x_i)$ and $u_3(x_i)$ $(i = 1, 2, 3)$, respectively.

The first assumption implies that the displacement of any material point in the cross-sectional plane solely consists of three rigid body translations $u(x_1)$, $v(x_1)$ and $w(x_1)$. The second assumption implies that the only rigid body translation that is different of zero is the axial displacement, as depicted in Fig. 1.14. So the displacement field for a truss-like structure may be write as

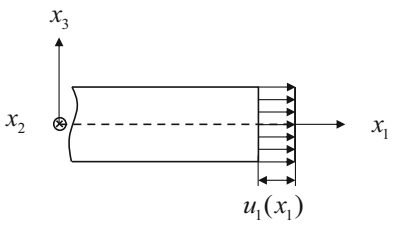

Fig. 1.14 Axial displacement of a truss structure

$$u_1(x_1, x_2, x_3) = u(x_1);\ u_2(x_1, x_2, x_3) = 0;\ u_3(x_1, x_2, x_3) = 0 \tag{1.83}$$

Notice that the truss structure may be loaded with concentrated and distributed axial loads, the distributed load is denoted by $p_1(x_1)$ and the concentrated load is denoted by P_1.

Strain, Stress and Axial Force

Substituting the displacement field showed at Eq. (1.83) into Eq. (1.2) is possible to obtain the 3D strain field as,

$$\varepsilon_{11} = \frac{du}{\partial x_1};\ \varepsilon_{22} = 0;\ \varepsilon_{33} = 0;\ \gamma_{12} = 0;\ \gamma_{13} = 0;\ \gamma_{23} = 0; \tag{1.84}$$

Using the generalized 3D Hooke's law for homogeneous and isotropic material and the strain field in Eq. (1.84) is possible to define the stress field as

$$\sigma_{11} = (\lambda + 2G)\frac{du}{dx_1};\ \sigma_{22} = \sigma_{33} = \lambda\frac{du}{dx_1};\ \sigma_{12} = \sigma_{13} = \sigma_{23} = 0 \tag{1.85}$$

where λ and G are defined after Eq. (1.54). Although this stress field naturally flows from the generalized Hooke's law and from the strain field in Eq. (1.84), it does not agree very well with the experimental measurements [3]. This drawback can be overcome by assuming additional assumptions regarding the stress field. Thus, since the dimension of the cross-section of the truss is much smaller that the length of the truss, is possible to assume that $\sigma_{22} = \sigma_{33} \approx 0$ when compared to σ_{11} this assumption clearly conflicts with the stress field presented in Eq. (1.85). The reason is that the first assumption of the classical truss model clearly violates the reality. In fact, it is well known that when the truss is deformed the cross-section will deform in its own plane due to Poisson's effect. For this reason the previous assumption used to obtaining kinematics is overruled and, instead, the following assumptions for the stress field is assumed

$$\sigma_{11} = E\frac{du}{dx_1};\ \sigma_{22} = \sigma_{33} = \sigma_{12} = \sigma_{13} = \sigma_{23} = 0 \tag{1.86}$$

Because $\sigma_{22} = \sigma_{33} = 0$, from the Hooke's law it follows that $\varepsilon_{22} = \varepsilon_{33} = -\upsilon/E\ \varepsilon_{11}$ and, this relation contradicts with the strain field in Eq. (1.84) except when $\upsilon = 0$, which in general is not true. Nevertheless, these contradictions can be partially justified by the fact that to obtain a simple expression of the 3D kinematics in terms of the 1D kinematics same simplification assumptions are used and that the stress on Eq. (1.86) can also better agree with reality.

The resultant of axial force that is acting in the truss is defined as

$$F_{11} = \int_A \sigma_{11}\, dA = \int_A E\varepsilon_{11}\, dA = S_{11}\frac{du}{dx_1} \tag{1.87}$$

with

$$S_{11} = \int_A E \, dA \tag{1.88}$$

Equation (1.88) is used to compute the truss axial stiffness.

Dynamic Equilibrium Equations
Dynamic equilibrium equations for the classical truss model may be obtained by eliminating the x_2 and x_3 dimension terms from Eq. (1.19). Thus, the dynamic equilibrium equation for a truss structure is

$$\frac{\partial \sigma_{11}}{\partial x_1} + b_1 = \rho \ddot{u}_1 \tag{1.89}$$

Substituting Eq. (1.86) into Eq. (1.89) will lead to the governing equations for elastic and homogeneous trusses as follows

$$E\frac{d^2u}{dx_1^2} + b_1 = \rho \ddot{u}_1 \tag{1.90}$$

For bars of constant cross-sectional properties, with an area A, the integration of Eq. (1.90) over the cross-sectional domain will lead to

$$EA\frac{d^2u}{dx_1^2} + b_1 A = \rho A \ddot{u}_1 \tag{1.91}$$

Denoting the external force applied in the axial direction of the bar by $p_1 = b_1 A$ and eliminating the inertial term in Eq. (1.91), the static equilibrium equation for trusses can be written as

$$EA\frac{d^2u}{dx_1^2} + p_1 = 0 \tag{1.92}$$

Equation 1.92 is the basic equation of trusses structures which is a second order differential equation for the axial displacement.

1.3.2 Equations for Shaft Members

Derivation of the shaft model starts from some kinematic based on Saint Venant assumptions [3]:

- The shape and size of the cross section in its own plane are preserved, which implies that each cross section rotates like a rigid body;

- The cross section does not remain plane after deformation but warp proportionally to the rate of twist;
- The rate of twist is uniform along the beam, which implies that the twist angle is a linear function of the beam axis.

Using the first assumption of Saint Venant, is possible to conclude that the in-plane displacement due to the twist angle $\phi_1(x_1)$ can be described as

$$u_1(x_1, x_2, x_3) = 0;\ u_2(x_1, x_2, x_3) = -x_3\phi_1;\ u_3(x_1, x_2, x_3) = x_2\phi_1 \tag{1.93}$$

The second assumption of Saint Venant simplification states that the axial displacement field will be proportional to the twist rate $k_1 = d\phi_1/dx_1$ and has an arbitrary variation over the cross-section that can be described by the unknown warping functions $\psi(x_2, x_3)$ such that

$$u_1(x_1, x_2, x_3) = \psi(x_2, x_3)\, k_1 \tag{1.94}$$

It deserves to be noted that the twist rate is constant according to the third assumption. Figure 1.15 shows the deformation of a square shaft under torsion, is possible to see that the original plane of the cross section have warped out.

Usually, the warping function $\psi(x_2, x_3)$ is solved separately over the cross-sectional domain according to the elasticity theory and, it is governed by Eq. (1.95) at all points of the cross-section.

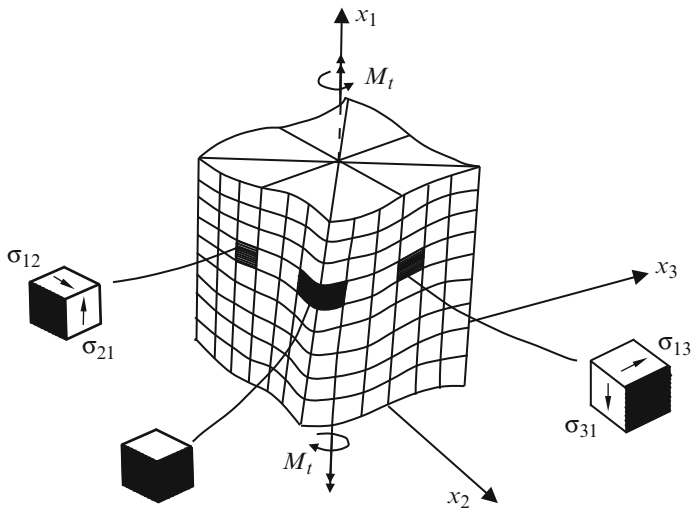

Fig. 1.15 Deformation of a square shaft in torsion

$$\frac{\partial^2 \psi\left(x_2, x_3\right)}{\partial x_2^2}+\frac{\partial^2 \psi\left(x_2, x_3\right)}{\partial x_3^2}=0 \tag{1.95}$$

Notice that for isotropic and homogeneous shafts with circular cross-section the warping function vanishes and the displacement field is described by Eq. (1.93).

Strain, Stress and Torsional Moment

Substituting the displacement field showed at Eqs. (1.93) and (1.94) into Eq. (1.2) is possible to obtain the 3D strain field as,

$$\varepsilon_{11}=\varepsilon_{22}=\varepsilon_{33}=\varepsilon_{23}=0;\ \gamma_{12}=\left(\frac{\partial \psi}{\partial x_2}-x_3\right) k_1;\ \gamma_{13}=\left(\frac{\partial \psi}{\partial x_3}+x_2\right) k_1 \tag{1.96}$$

It worth to point here that expressing the twist rate, $k_1\left(x_1\right)$, as a function of x_1 is a direct violation of the third Saint Venant assumption.

Using the generalized 3D Hooke's law for homogeneous and isotropic material and the strain field in Eq. (1.96) is possible to define the stress field as

$$\sigma_{11}=\sigma_{22}=\sigma_{33}=0;\ \sigma_{12}=2G\varepsilon_{12};\ \sigma_{13}=2G\varepsilon_{13};\ \sigma_{23}=0 \tag{1.97}$$

The resultant of torsion moment that is acting in the shaft is defined as

$$M_{11}=\int_A \left(x_2\sigma_{13}-x_3\sigma_{12}\right) dA=\int_A G\left(x_2\gamma_{13}-x_3\gamma_{12}\right)\ dA \tag{1.98}$$

Substituting the strain field showed at Eq. (1.96) into Eq. (1.98), is possible to describe the torsion moment as

$$M_{11}=\int_A G\left(x_2^2+x_3^2+x_2\frac{\partial \psi}{\partial x_3}-x_3\frac{\partial \psi}{\partial x_2}\right)\ k_1\ dA \tag{1.99}$$

and noting that $k_1\left(x_1\right)=d\phi_1/dx_1$ is constant over the cross-sectional area, Eq. (1.99) may be written as

$$M_{11}=S_{22}\frac{d\phi_1}{dx} \tag{1.100}$$

where S_{22} is the torsional stiffness defined by

$$S_{22}=\int_A \left(x_2^2+x_3^2+x_2\frac{\partial \psi}{\partial x_3}-x_3\frac{\partial \psi}{\partial x_2}\right)\ dA \tag{1.101}$$

For isotropic and homogeneous shafts with circular cross-section the warping function vanishes and Eq. (1.101) leads to the polar moment of inertia of the cross-section. For other cross-section geometries S_{22} is less than the polar moment of inertia of the cross-section and, therefore, to compute the torsional stiffness it is necessary to evaluate Eq. (1.101). Nevertheless, for the case of isotropic and homogeneous shafts with rectangular cross-section the value of torsional stiffness is computed using a torsional correction factor, k, which means that Eq. (1.100) will have the form

$$M_{11} = G\, kJ \frac{d\phi_1}{dx} \tag{1.102}$$

where

$$J = \int_A \left(x_2^2 + x_3^2\right)\, dA \tag{1.103}$$

and the torsional correction factor is defined according relations presented at Table 1.1.

For the case of isotropic and homogeneous shafts with arbitrary cross-section different values of the torsional correction stiffness should be used [7].

Static Equilibrium Equation

To derive dynamic equilibrium equations for the shaft model, it is necessary to consider the equilibrium of the differential element presented in Fig. 1.16.

Summing all the moments in the axial direction yields the following equation

Table 1.1 Torsional correction factor for rectangular cross-sections [2]

a/b	1	1.5	1.75	2	2.5	3	4	6	8
k	0.141	0.196	0.214	0.229	0.249	0.263	0.281	0.299	0.307

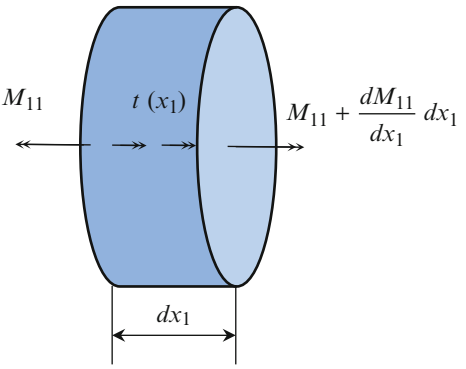

Fig. 1.16 Infinitesimal element of a shaft

$$-M_{11} + M_{11} + \frac{dM_{11}}{dx_1} dx_1 + t(x_1)\, dx_1 = 0 \tag{1.104}$$

Last equation can be rearranged in the form,

$$\frac{dM_{11}}{dx_1} = -t(x_1) \tag{1.105}$$

and, substituting the resultant moment showed at Eq. (1.100) into Eq. (1.105), is possible to obtain the shaft dynamic equilibrium equation as

$$\frac{d}{dx_1}\left(S_{22}\frac{d\phi_1}{dx_1}\right) = -t(x_1) \tag{1.106}$$

Equation 1.106 is the basic equation of shaft structures and is a second order differential equation.

1.3.3 Equations for Classic Beams

Beam structures are geometrically similar to truss members, the difference is that the forces applied on a beam structure are perpendicular to the axis of the beam while on a truss members are parallel to the truss axis. Therefore, a beam member experience bending. There are several theories for analyzing beam structures, which can be basically divided into two main groups: theory for thin beams and theory for thick beams. The thin beam theory is also commonly called Euler-Bernoulli beam model while the simplest thick beam theory is called Timoshenko beam model. In Euler-Bernoulli beam theory shear deformations are neglected, and plane sections remain plane and normal to the longitudinal axis during deformation. In the Timoshenko beam theory, plane sections still remain plane during deformation but not necessarily normal to the longitudinal beam axis. The angular difference between the plane section that might remain normal to the longitudinal axis and the plane section rotation is the shear deformation. However, experimental observations have been show that Euler-Bernoulli assumptions are reasonable for slender structures made of isotropic materials, as the case of the structures analyzed herein and, therefore, this text focuses on the Euler-Bernoulli theory.

Euler-Bernoulli Assumptions
Derivation of the classical beam model starts from some kinematic assumptions which are [3]:

- The beam cross-section is infinitely rigid in its own plane;
- The beam cross-section remains plane after deformation;
- Lines that are straight and perpendicular to the geometrical beam axis remain straight and perpendicular during deformation.

Consider a set of Cartesian axes attached at the geometric center of the beam cross-section, such that x_1 is along the axis of the beam, x_2 and x_3 define the plane of the beam cross-section. The displacement of an arbitrary point of the beam in the x_1, x_2 and x_3 directions are defined by $u_1(x_i)$, $u_2(x_i)$ and $u_3(x_i)$ $(i = 1,2,3)$, respectively. The complete 3D displacement field of a beam-like structure implied by the Euler-Bernoulli assumptions is defined as

$$u_1(x_1, x_2, x_3) = -x_2 \frac{dv(x_1)}{dx_1} - x_3 \frac{dw(x_1)}{dx_1} \tag{1.107}$$

$$u_2(x_1, x_2, x_3) = v(x_1) \tag{1.108}$$

$$u_3(x_1, x_2, x_3) = w(x_1) \tag{1.109}$$

The first Euler-Bernoulli assumption implies that the displacement field of any material point in the cross-section plane will consist of two translations $v(x_1)$ and $w(x_1)$, as represented at Fig. 1.17.

The second Euler-Bernoulli assumption implies that the displacement field of any material point in the cross-section plane with coordinates $(x_2 \neq 0, x_3 \neq 0)$, has an axial displacement $-x_2\phi_3 + x_3\phi_2$, as depicted in Fig. 1.17. Notice, that because the sign convention represented in Fig. 1.17 the term $x_2\phi_3$ has a negative sign. In this way, is assured that a positive value of rotation ϕ_3 will create a negative axial displacement for a positive x_2.

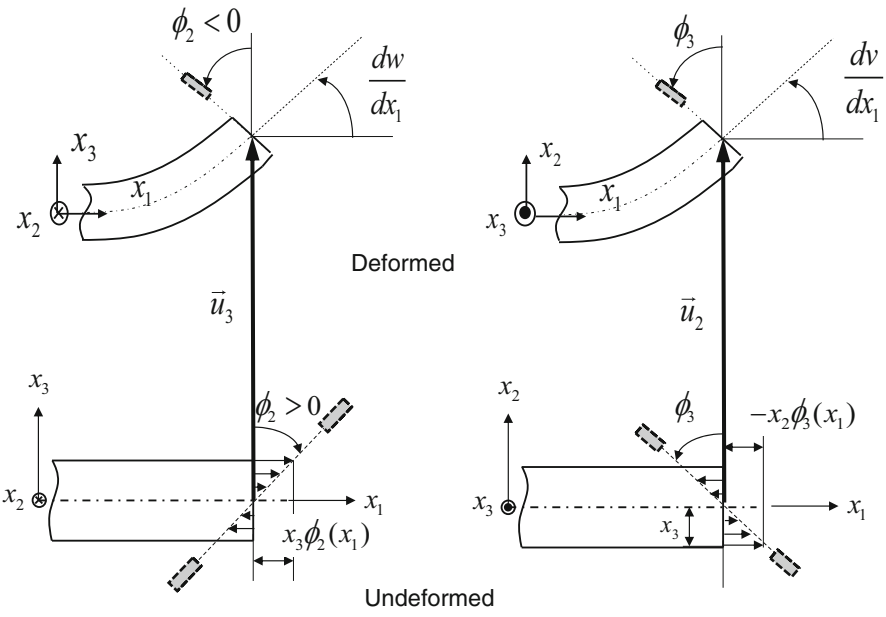

Fig. 1.17 Representation of the Euler-Bernoulli 3D displacement

The third Euler-Bernoulli assumption implies that the rotation of the cross-section beam must be equal to the slope of the beam axis, as depicted in Fig. 1.17.

$$\phi_3 = \frac{\partial v}{\partial x_1}; \;\; \phi_2 = -\frac{\partial w}{\partial x_1} \tag{1.110}$$

The minus sign on the second equation is a consequence of the sign conventions. Because of the Euler-Bernoulli assumptions, the mathematical model of the beam structure is stiffer than the original beam. Thus, the displacement field obtained using this mathematical model will be smaller than that obtained using the 3D elasticity theory.

Strain, Stress and Bending Moments

Substituting the displacement field showed at Eqs. (1.107), (1.108) and (1.109) into Eq. (1.2) is possible to obtain the 3D strain field as,

$$\varepsilon_{11} = -x_2 \frac{d^2 v}{dx_1^2} - x_3 \frac{d^2 w}{dx_1^2} \;\; \varepsilon_{22} = \varepsilon_{33} = \varepsilon_{23} = \varepsilon_{12} = \varepsilon_{13} = 0 \tag{1.111}$$

Denoting the curvatures $d^2v/dx_1^2, -d^2w/dx_1^2$ about the axes x_2 and x_3, respectively, by $k_3(x_1)$ and $k_2(x_1)$ is possible to express the axial strain variation in the form

$$\varepsilon_{11}(x_1, x_2, x_3) = x_3 k_2(x_1) - x_2 k_3(x_1) \tag{1.112}$$

Using the generalized 3D Hooke's law for homogeneous and isotropic material and the strain field in Eq. (1.111) is possible to define the stress field as

$$\sigma_{11} = (\lambda + 2G)\,\varepsilon_{11}; \;\; \sigma_{22} = \sigma_{33} = \lambda \varepsilon_{11}; \;\; \sigma_{12} = \sigma_{13} = \sigma_{23} = 0 \tag{1.113}$$

Although this stress field naturally flows from the generalized Hooke's law and the strain field in Eq. (1.101), it does not agree very well with the experimental measurements [3]. This drawback can be overcome by assuming additional assumptions regarding the stress field. Thus, since the dimension of the cross-section of the beam is much smaller that the length of the beam, is possible to assume that $\sigma_{22} = \sigma_{33} \approx 0$ when compared to σ_{11}, this assumption clearly conflicts with the stress field presented in Eq. (1.113). The reason is that the first assumption of the classical beam model clearly violates the reality. In fact, is well known that when the beam is deformed the cross-section will deform in its own plane due to Poisson's effect. For this reason the previous assumption used to obtaining kinematics is overruled and, instead, the following assumptions for the stress field is assumed

$$\sigma_{11} = E\varepsilon_{11}; \;\; \sigma_{22} = \sigma_{33} = \sigma_{12} = \sigma_{13} = \sigma_{23} = 0 \tag{1.114}$$

Because $\sigma_{22} = \sigma_{33} = 0$ from the Hooke's law it follows that $\varepsilon_{22} = \varepsilon_{33} = -\upsilon/E\ \varepsilon_{11}$ and, this relation contradicts with the strain field in Eq. (1.111) except when $\upsilon = 0$, which in general is not true. Nevertheless, these contradictions can be partially justified by the fact that to obtain a simple expression of the 3D kinematics in terms of the 1D kinematics same simplification assumptions are used and that the stress on Eq. (1.114) can also better agree with reality.

The resultant of axial force and bending moments that are acting in the beam are defined as

$$F_{11} = \int_A \sigma_{11} dA = \int_A E\,(x_3 k_2 - x_2 k_3)\, dA = S_{13} k_2 + S_{14} k_3 \tag{1.115}$$

$$M_{22} = \int_A x_3 \sigma_{11} dA = \int_A x_3 E\,(x_3 k_2 - x_2 k_3)\, dA = S_{33} k_2 + S_{34} k_3 \tag{1.116}$$

$$M_{33} = -\int_A x_2 \sigma_{11} dA = \int_A x_2 E\,(x_3 k_2 - x_2 k_3)\, dA = S_{34} k_2 + S_{44} k_3 \tag{1.117}$$

with

$$\begin{aligned} &S_{13} = \int_A E\, x_3\, dA;\ S_{14} = -\int_A E\, x_2\, dA;\ S_{33} = \int_A E\, x_3^2\, dA; \\ &S_{34} = -\int_A E\, x_2 x_3\, dA;\ S_{44} = \int_A E\, x_2^2\, dA \end{aligned} \tag{1.118}$$

These quantities are called beam stiffness.

Dynamic Equilibrium Equations

To derive dynamic equilibrium equations for the beam model, it is necessary to consider the equilibrium of the differential elements presented in Fig. 1.18.

The summation of forces along the axis x_2 that are presented in the first sketch of Fig. 1.18 gives the transverse force equilibrium equation in this direction in the

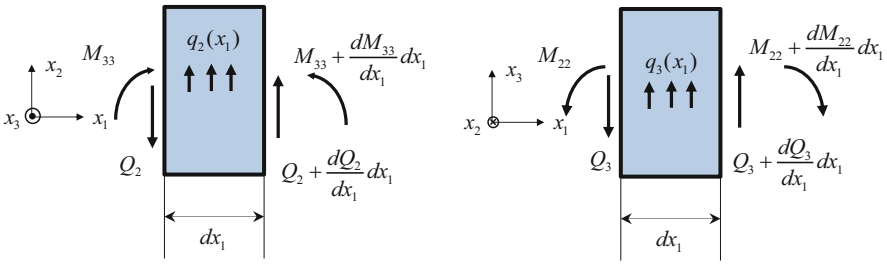

Fig. 1.18 Free body diagram for transverse shear forces and bending moments

form

$$\frac{dQ_2}{dx_1} = -q_2(x_1) + \rho A\ddot{v} \tag{1.119}$$

While the summation of the moments about an axis parallel to x_3 yields

$$-M_{33} + M_{33} + \frac{dM_{33}}{dx_1}dx_1 + Q_2 dx_1 - \frac{1}{2}(q_2 - \rho A\ddot{v})(dx_1)^2 = 0 \tag{1.120}$$

And neglecting the second order term leads to

$$\frac{dM_{33}}{dx_1} = -Q_2 \tag{1.121}$$

Similarly, summing the forces along the axis x_3 that are presented in the second sketch of Fig. 1.18, gives the transverse force equilibrium equation in this direction in the form

$$\frac{dQ_3}{dx_1} = -q_3(x_1) + \rho A\ddot{w} \tag{1.122}$$

and the summation of the moments about an axis parallel to x_2 yields

$$\frac{dM_{22}}{dx_1} = Q_3 \tag{1.123}$$

In order to remove shear forces Q_2 and Q_3 from Eqs. (1.121) and (1.123), respectively, is possible to take the derivative of these equations leading to

$$\frac{d^2M_{33}}{dx_1^2} = -\frac{dQ_2}{dx_1} \tag{1.124}$$

$$\frac{d^2M_{22}}{dx_1^2} = \frac{dQ_3}{dx_1} \tag{1.125}$$

and, now, substituting the right hand side of Eqs. (1.124) and (1.125) by the right hand side of equations (1.119) and (1.122), respectively, leads to

$$\frac{d^2M_{33}}{dx_1^2} = q_2(x_1) - \rho A\ddot{v} \tag{1.126}$$

$$\frac{d^2M_{22}}{dx_1^2} = -q_3(x_1) + \rho A\ddot{w} \tag{1.127}$$

The dynamic equilibrium equations for beams can be obtained by substituting Eqs. (1.116) and (1.117) into Eqs. (1.127) and (1.126), respectively:

$$\frac{d^2}{dx_1^2}\left(-S_{34}\frac{d^2w}{dx_1^2}+S_{44}\frac{d^2v}{dx_1^2}\right)=q_2\left(x_1\right)-\rho A\ddot{v} \tag{1.128}$$

$$\frac{d^2}{dx_1^2}\left(S_{33}\frac{d^2w}{dx_1^2}-S_{34}\frac{d^2v}{dx_1^2}\right)=q_3\left(x_1\right)-\rho A\ddot{w} \tag{1.129}$$

Notice that in Eqs. (1.128) and (1.129) the bending deformations in two directions are still coupled if the cross bending stiffness S_{34} is not zero. Nevertheless, if the coordinate system orientation is coincident with the principal axes of inertia of the cross-section then the cross bending stiffness is zero. Under such conditions Eqs. (1.128) and (1.129) assume the form

$$\frac{d^2}{dx_1^2}\left(\overline{S}_{44}\frac{d^2v}{dx_1^2}\right)=q_2\left(x_1\right)-\rho A\ddot{v} \tag{1.130}$$

$$\frac{d^2}{dx_1^2}\left(\overline{S}_{33}\frac{d^2w}{dx_1^2}\right)=q_3\left(x_1\right)-\rho A\ddot{w} \tag{1.131}$$

with

$$\overline{S}_{33}=\frac{S_{44}+S_{33}}{2}-H;\ \overline{S}_{44}=\frac{S_{44}+S_{33}}{2}+H;\ H=\sqrt{\frac{\left(S_{44}-S_{33}\right)^2}{4}+S_{34}^2} \tag{1.132}$$

The static equilibrium equations for beams can be obtained by dropping the dynamic terms on Eqs. (1.130) and (1.131), as

$$\frac{d^2}{dx_1^2}\left(\overline{S}_{44}\frac{d^2v}{dx_1^2}\right)=q_2\left(x_1\right) \tag{1.133}$$

$$\frac{d^2}{dx_1^2}\left(\overline{S}_{33}\frac{d^2w}{dx_1^2}\right)=q_3\left(x_1\right) \tag{1.134}$$

1.3.4 Equations for 3D Beams

The 3D beam models can deal with extension, torsion and bending in two transverse directions. The mathematical model is based in Euler-Bernoulli and Saint Venant assumptions. So combining the displacement expressions in Eqs. (1.83), (1.93), (1.94) and (1.107), (1.108) and (1.109) yields

$$u_1(x_1, x_2, x_3) = u(x_1) - x_3 \frac{dw(x_1)}{dx_1} - x_2 \frac{dv(x_1)}{dx_1} + \psi(x_2, x_3) k_1 \tag{1.135}$$

$$u_2(x_1, x_2, x_3) = v(x_1) - x_3 \phi_1(x_1) \tag{1.136}$$

$$u_3(x_1, x_2, x_3) = w(x_1) + x_2 \phi_1(x_1) \tag{1.137}$$

The complete 3D displacement field of the beam is expressed in terms of three sectional displacements $u(x_1), v(x_1), w(x_1)$ and one sectional rotation $\phi(x_1)$ associated with the centroid of the beam cross section.

Stress, Strain and Bending Moments

Substituting the displacement field showed at Eqs. (1.135), (1.136) and (1.137) into Eq. (1.2) is possible to obtain the 3D strain field as,

$$\varepsilon_{11} = \frac{du}{dx_1} - x_2 \frac{d^2 v}{dx_1^2} - x_3 \frac{d^2 w}{dx_1^2} \tag{1.138}$$

$$\varepsilon_{22} = \varepsilon_{33} = \gamma_{23} = 0 \tag{1.139}$$

$$\gamma_{12} = \left(\frac{\partial \psi}{\partial x_2} - x_3 \right) k_1; \quad \gamma_{13} = \left(\frac{\partial \psi}{\partial x_3} + x_2 \right) k_1 \tag{1.140}$$

Using the following notation:

$$\varepsilon_{11}^0 = \frac{du}{dx_1}; \; k_1(x_1) = \frac{d\phi_1}{dx_1}; \; k_2(x_1) = -\frac{d^2 w}{dx_1^2}; \; k_3(x_1) = \frac{d^2 v}{dx_1^2} \tag{1.141}$$

where ε_{11}^0 is the axial strain, k_1 is the twist rate, k_2 and k_3 are defined after Eq. (1.111), the axial strain distribution ε_{11} can be expressed as

$$\varepsilon_{11}(x_1, x_2, x_3) = \varepsilon_{11}^0(x_1) + x_3 k_2(x_1) - x_2 k_3(x_1) \tag{1.142}$$

The expressions in Eq. (1.141) can be considered as the 1D beam strain-displacement relations for classical 3D beam models.

The beam stress field can be obtained using the strain field in Eqs. (1.138), (1.139) and (1.140) into the generalized 3D Hooke's law. For instance, for an isotropic material yields

$$\begin{aligned} &\sigma_{11} = (\lambda + 2G) \varepsilon_{11}; \; \sigma_{22} = \sigma_{33} = \lambda \varepsilon_{11}; \; \sigma_{12} = G \gamma_{12}; \\ &\sigma_{13} = G \gamma_{13}; \; \sigma_{23} = 0 \end{aligned} \tag{1.143}$$

As seen before, introducing the following assumption:

$$\sigma_{22} = \sigma_{33} = 0 \tag{1.144}$$

The ending stress field can be written as

$$\begin{aligned} &\sigma_{11} = E\varepsilon_{11};\ \sigma_{12} = G\gamma_{12};\ \sigma_{13} = G\gamma_{13};\\ &\sigma_{22} = \sigma_{33} = \sigma_{23} = 0 \end{aligned} \tag{1.145}$$

The resultant of forces and moments that are acting in the beam are defined as

$$F_{11} = \int_A E\left(\varepsilon_{11}^0 + x_3k_2 - x_2k_3\right) dA = S_{11}\varepsilon_{11}^0 + S_{13}k_2 + s_{14}k_3 \tag{1.146}$$

$$M_{11} = \int_A G\left(x_2^2 + x_3^2 + x_2\frac{\partial\psi}{\partial x_3} - x_3\frac{\partial\psi}{\partial x_2}\right) k_1\, dA = S_{22}k_1 \tag{1.147}$$

$$M_{22} = \int_A x_3\sigma_{11}dA = \int_A x_3E\left(\varepsilon_{11}^0 + x_3k_2 - x_2k_3\right) dA = S_{13}\varepsilon_{11}^0 + S_{33}k_2 + S_{34}k_3 \tag{1.148}$$

$$M_{33} = -\int_A x_2\sigma_{11}dA = \int_A x_2E\left(\varepsilon_{11}^0 + x_3k_2 - x_2k_3\right) dA = S_{14}\varepsilon_{11}^0 + S_{34}k_2 + S_{44}k_3 \tag{1.149}$$

with

$$S_{11} = \int_A E\, dA \tag{1.150}$$

and with S_{13}, S_{14}, S_{22}, S_{34} and S_{44} defined by Eqs. (1.101) and (1.118).

Equations (1.146), (1.147), (1.148) and (1.149) can be written in a matrix form

$$\begin{bmatrix} F_{11} \\ M_{11} \\ M_{22} \\ M_{33} \end{bmatrix} = \begin{bmatrix} S_{11} & 0 & S_{13} & S_{14} \\ 0 & S_{22} & 0 & 0 \\ S_{13} & 0 & S_{33} & S_{34} \\ S_{14} & 0 & S_{34} & S_{44} \end{bmatrix} \begin{bmatrix} \varepsilon_{11}^0 \\ k_1 \\ k_2 \\ k_3 \end{bmatrix} \tag{1.151}$$

The matrix in equation 1.151 is called classical beam stiffness, in which S_{11} is the extension stiffness, S_{13} and S_{14} are the extension-bending coupling stiffness, S_{22} is the torsional stiffness, S_{33} and S_{44} are the bending stiffness and S_{34} is the cross bending stiffness. Due to the Saint Venant assumptions and to the fact that the beam is made of isotropic material, the entries on the second row and second column of the matrix in Eq. (1.150) are all zero except to the diagonal term, which means that the torsional behavior is decoupled from extension and bending.

Entries on the first row and first column of the matrix in Eq. (1.151) are not all zero, which means that extension and bending behavior are not decoupled. Nevertheless, because derivations presented on Sect. 1.3.3 were obtained using

a beam coordinate system that is located at the centroid of the cross section of the beam, S_{13} and S_{14} are zero. In fact, it is possible to decouple extension and bending by choosing the origin of the coordinate system in such a way that when an axial force is applied at this point no bending deformation will appear. Such point is called centroid of the cross section of the beam. Under this condition all the previous formulations remains the same, and the constitutive relations will have the form

$$\begin{bmatrix} F_{11} \\ M_{11} \\ M_{22} \\ M_{33} \end{bmatrix} = \begin{bmatrix} S_{11} & 0 & 0 & 0 \\ 0 & S_{22} & 0 & 0 \\ 0 & 0 & S_{33} & S_{34} \\ 0 & 0 & S_{34} & S_{44} \end{bmatrix} \begin{bmatrix} \varepsilon_{11}^0 \\ k_1 \\ k_2 \\ k_3 \end{bmatrix} \tag{1.152}$$

Notice that the bending deformations in two directions are still coupled, the cross bending stiffness S_{34} is not zero. Nevertheless, assuming that the orientation of the beam coordinate system is coincident with the principal axes of inertia of the cross-section, then the cross bending stiffness is zero. Under such conditions, Eq. (1.152) will have the form

$$\begin{bmatrix} F_{11} \\ M_{11} \\ M_{22} \\ M_{33} \end{bmatrix} = \begin{bmatrix} S_{11} & 0 & 0 & 0 \\ 0 & S_{22} & 0 & 0 \\ 0 & 0 & \overline{S}_{33} & 0 \\ 0 & 0 & 0 & \overline{S}_{44} \end{bmatrix} \begin{bmatrix} \varepsilon_{11}^0 \\ k_1 \\ k_2 \\ k_3 \end{bmatrix} \tag{1.153}$$

$\overline{S}_{33}$ and $\overline{S}_{44}$ are called principle bending stiffnesses and are defined in Eq. (1.132)

Static Equilibrium Equations

The static equilibrium equations for the 3D beam model can be obtained by combining Eqs. (1.92), (1.106), (1.133) and (1.134) yields

$$\frac{\partial}{\partial x_1}\left(S_{11}\frac{du}{dx_1}\right) + p_1 = 0 \tag{1.154}$$

$$\frac{d}{dx_1}\left(S_{22}\frac{d\phi_1}{dx_1}\right) = -t\,(x_1) \tag{1.155}$$

$$\frac{d^2}{dx_1^2}\left(\overline{S}_{33}\frac{d^2w}{dx_1^2}\right) = q_3\,(x_1) \tag{1.156}$$

$$\frac{d^2}{dx_1^2}\left(\overline{S}_{44}\frac{d^2v}{dx_1^2}\right) = q_2\,(x_1) \tag{1.157}$$

These equations are in the form of four uncoupled differential equations in terms of four beam variables, u, v, w and ϕ_1. The equations are of second order in the axial displacement and in the twist beam, and fourth order in the transverse displacements v and w. The solution of these equations can only be obtained if boundary conditions

are defined and, these boundary conditions, can be derived based on equilibrium considerations using free body diagrams at the boundary points.

1.3.5 Equations for Timoshenko Beams

Considering the Euler-Bernoulli beam theory, already discussed briefly in previous section, the shear deformations are neglected. While this classic beam theory may be quite adequate for thin to moderate beam structures made of isotropic material, many thick beam structures and advanced thin beam structures made of composite material require the shear effect account.

Composite materials consist of a combination of materials that are mixed together to achieve specific structural properties. The individual materials do not dissolve or merge completely in the composite, but they act together as one. Normally, the components can be physically identified as they interface with one another. The properties of the composite material are superior to the properties of the individual materials from which it is constructed. In fact, in this kind of material, even when the transverse stresses are small when compared to the normal or to the in-plane shear stresses, they can still can induce failures of composite in the transverse directions. Thus, the transverse stress is not always neglected in composite analyses.

So, in this section, a discussion of an alternative approach to formulating beam structures will be presented. The base of this theory includes the effect of shear deformations by retaining the assumption that the plane section originally normal to the neutral axis remains plane but rotates by an amount ϕ, equal to the rotation of the neutral axis, dw/dx, minus the shear strain γ, as depicted in Fig. 1.13. The total rotation of the cross section is given, as

$$\begin{aligned} \phi_2 &= \frac{d\,w}{d\,x_1} - \gamma_{13} \\ \phi_3 &= \frac{d\,v}{d\,x_1} + \gamma_{12} \end{aligned} \tag{1.158}$$

The complete 3D displacement field of a beam-like structure implied by the Timoshenko assumptions is defined as

$$u_1\,(x_1, x_2, x_3) = x_3\phi_2 - x_2\phi_3 \tag{1.159}$$

$$u_2\,(x_1, x_2, x_3) = v\,(x_1) \tag{1.160}$$

$$u_3\,(x_1, x_2, x_3) = w\,(x_1) \tag{1.161}$$

Where the rotations of the cross sections ϕ_2 and ϕ_3 are positives about the axes x_2 and x_3, respectively.

Strain, Stress and Bending Moments
Substituting the displacement field showed at Eqs. (1.159), (1.160) and (1.161) into Eq. (1.2) is possible to obtain the 3D strain field as,

$$\begin{aligned} \varepsilon_{11} &= x_3 \frac{d\phi_2}{dx_1} - x_2 \frac{d\phi_3}{dx_1} \\ \varepsilon_{22} &= \varepsilon_{33} = \varepsilon_{23} = 0 \\ 2\varepsilon_{12} &= -\phi_3 + \frac{dv}{dx} \\ 2\varepsilon_{13} &= \phi_2 + \frac{dw}{dx} \end{aligned} \tag{1.162}$$

Denoting $d\phi_2/dx$, $d\phi_3/dx$ by $k_2^{'}(x_1)$ and $k_3^{'}(x_1)$, respectively, is possible to express the axial strain variation in the form

$$\varepsilon_{11}\left(x_1, x_2, x_3\right) = x_3 k_2'\left(x_1\right) - x_2 k_3'\left(x_1\right) \tag{1.163}$$

Using the generalized 3D Hooke's law for homogeneous and isotropic material and the strain field in Eq. (1.101) is possible to define the stress field as

$$\begin{aligned} l\sigma_{11} &= (\lambda + 2G)\ \varepsilon_{11} \\ \sigma_{22} &= \sigma_{33} = \lambda \varepsilon_{11}; \\ \sigma_{23} &= 0 \\ \sigma_{13} &= G\gamma_{13} \\ \sigma_{12} &= G\gamma_{12} \end{aligned} \tag{1.164}$$

As in the case of Bernoulli beam theory, although this stress field naturally flows from the generalized Hooke's law and the strain field in Eq. (1.162), the first relation of Eq. (1.164) does not agree very well with the experimental measurements. This drawback can be overcome by assuming additional assumptions regarding the stress field. Thus, since the dimension of the cross-section of the beam is much smaller that the length of the beam, is possible to assume that $\sigma_{22} = \sigma_{33} \approx 0$ when compared to σ_{11}, but this assumption clearly conflicts with the stress field presented in Eq. (1.164). For this reason the previous assumption used to obtaining kinematics is overruled and, instead, the following assumptions for the stress field is assumed

$$\begin{aligned} \sigma_{11} &= E\varepsilon_{11} \\ \sigma_{22} &= \sigma_{33} = \sigma_{23} = 0 \\ \sigma_{13} &= G\gamma_{13} \\ \sigma_{12} &= G\gamma_{12} \end{aligned} \tag{1.165}$$

The resultant forces and bending moments that are acting in the beam are defined as

$$F_{11} = \int_A \sigma_{11} dA = \int_A E\left(x_3 k_2' - x_2 k_3'\right) dA = S_{11} k_2' + S_{12} k_3' \tag{1.166}$$

$$M_{22} = \int_A \left(x_3 \sigma_{11}\right) dA = \int_A x_3 E\left(x_3 k_2' - x_2 k_3'\right) dA = S_{21} k_2' + S_{22} k_3' \tag{1.167}$$

$$M_{33} = -\int_A x_2 \sigma_{11} dA = -\int_A x_2 E\left(x_3 k_2' - x_2 k_3'\right) dA = S_{31} k_2' + S_{32} k_3' \tag{1.168}$$

$$F_{13} = \int_A \sigma_{13} dA = \int_A G\left(2\varepsilon_{13}\right) dA = S_{43} k_{13}' \tag{1.169}$$

$$F_{12} = \int_A \sigma_{12} dA = \int_A G\left(2\varepsilon_{12}\right) dA = S_{54} k_{12}' \tag{1.170}$$

$$M_{11} = \int_A \left(x_2 \sigma_{13} - x_3 \sigma_{12}\right) dA = \int_A x_2 G\left(2\varepsilon_{13}\right) dA - \int_A x_3 G\left(2\varepsilon_{12}\right) dA = S_{63} k_{13}' + S_{64} k_{12}' \tag{1.171}$$

with

$$\begin{aligned}
S_{11} &= \int_A E\, x_3\, dA; \quad S_{12} = -\int_A E\, x_2\, dA; \\
S_{21} &= \int_A E\, x_3^2\, dA; \quad S_{22} = -\int_A E\, x_2 x_3\, dA; \\
S_{31} &= S_{22}; \quad S_{32} = \int_A E\, x_2^2\, dA; \\
S_{43} &= \int_A G\, dA; \quad S_{54} = S_{43}; \\
S_{63} &= \int_A G\, x_2\, dA; \quad S_{64} = -\int_A G\, x_3\, dA
\end{aligned} \tag{1.172}$$

Equations (1.166), (1.167), (1.168), (1.169), (1.170) and (1.171) can be written in a matrix form as

$$\begin{bmatrix} F_{11} \\ M_{22} \\ M_{33} \\ F_{13} \\ F_{12} \\ M_{11} \end{bmatrix} = \begin{bmatrix} S_{11} & S_{12} & 0 & 0 \\ S_{21} & S_{22} & 0 & 0 \\ S_{31} & S_{32} & 0 & 0 \\ 0 & 0 & S_{43} & 0 \\ 0 & 0 & 0 & S_{54} \\ 0 & 0 & S_{63} & S_{64} \end{bmatrix} \begin{bmatrix} k_2' \\ k_3' \\ k_{13}' \\ k_{12}' \end{bmatrix} \tag{1.173}$$

Assuming that the origin of the beam coordinate system is located at the centroid of the cross section and its orientation is coincident with the principal axes of inertia of the cross-section, all the previous formulations remains the same and, the constitutive relations will have the form

$$\begin{bmatrix} M_{22} \\ M_{33} \\ F_{13} \\ F_{12} \end{bmatrix} = \begin{bmatrix} \overline{S}_{21} & 0 & 0 & 0 \\ 0 & \overline{S}_{32} & 0 & 0 \\ 0 & 0 & S_{43} & 0 \\ 0 & 0 & 0 & S_{54} \end{bmatrix} \begin{bmatrix} k_2' \\ k_3' \\ k_{13}' \\ k_{12}' \end{bmatrix} \tag{1.174}$$

$\overline{S}_{21}$ and $\overline{S}_{32}$ are called principle bending stiffnesses and may be defined according Eq. (1.132).

Timoshenko Equilibrium Equations

Assuming that Eqs. (1.156) and (1.157) can be written in a general form as

$$\frac{d^2}{dx^2}\left(S\frac{d\phi}{dx}\right) = q(x) \tag{1.175}$$

where ϕ is either defined by Eq. (1.158), for the case of Timoshenko theory, or by dw/dx, for the Euler-Bernoulli theory. So, using Eq. (1.158) into Eq. (1.175), the Timoshenko differential equation in the plane x_1x_3 is written as

$$\frac{d^2}{dx_1}\left[\overline{S}_{33}\frac{d}{dx_1}\left(\frac{dw}{dx_1} - \gamma_{13}\right)\right] = q_3\,(x_1) \tag{1.176}$$

The static equilibrium Eq. (1.176) is now accounting for the shear term γ. The Timoshenko theory assumes that shear strain is constant over the cross section. In reality, the shear stress and strain are not uniform over the cross section, so a shear coefficient, k_s, is introduced as a correction factor, allowing the non-uniform shear strain to be expressed as a constant. So, if the cross section area of the beam is A and, the shear strain γ in Eq. (1.158) is an equivalent constant strain on a corresponding shear area A_s [8]

$$\tau = \frac{Q}{A_s};\ \gamma = \frac{\tau}{G};\ k_s = \frac{A_s}{A} \tag{1.177}$$

Where Q is the shear force. The value of the shear coefficient depends on the shape of the beam cross sections and was originally introduced by Timoshenko [9]. Bathe [8] have presented a simple procedure based on the condition that when the shear force Q acts on the shear area A_s, the constant shear stress defined in Eq. (1.176) must yield the same shear strain energy as the correct shearing stress acting on the cross sectional area A. For rectangular cross sectional beams the value of 5/6 is obtained.

Using the shear coefficient in Eq. (1.177), the average shear strain is defined as

$$\gamma = \frac{Q}{k_s AG} \tag{1.178}$$

Using the latter relation in Eq. (1.158), is possible to rewrite Eq. (1.176) as

$$\frac{d^2}{dx_1}\left[\overline{S}_{33}\frac{d}{dx_1}\left(\frac{dw}{dx_1} - \frac{Q_{13}}{k_s AG}\right)\right] = q_3\,(x_1) \tag{1.179}$$

Using a similar procedure, is possible to obtain the Timoshenko differential equation in the plane x_1x_2, which can be written as

$$\frac{d^2}{dx_1}\left[\overline{S}_{44}\frac{d}{dx_1}\left(\frac{dv}{dx_1} - \frac{Q_{12}}{k_s AG}\right)\right] = q_2\,(x_1) \tag{1.180}$$

Equations (1.179) and (1.180) are of fourth order in the transverse displacements v and w. The solution of these equations can only be obtained if boundary conditions are defined. Note that boundary conditions can be derived from equilibrium considerations by using free body diagrams at the boundary points.

References

1. Leal RP (2004) Folhas de apoio de Mecânica dos Sólidos. Departamento de Engenharia Mecânicam, Universidade de Coimbra, Coimbra, Portugal
2. Rekach VG (1978) Static theory of thin walled space structures. Mir Publisher, Moscow
3. Yu W (2012) Three-ways to derive the Euler-Bernoulli-Saint Venant beam theory. iMechanica
4. Wang CM, Reddy JN, Lee KH (2000) Shear deformable beams and plates: relationships with classical solutions. Elsevier Science, Amsterdam/New York
5. Popescu B, Hodges DH (2000) On asymptotically correct Timoshenko-like anisotropic beam theory. Int J Solids Struct 37(3):535–558. doi:10.1016/S0020-7683(99)00020-7
6. Bauchau OA, Craig JI (2009) Euler-Bernoulli beam theory. In: Bauchau OA, Craig JI (eds) Structural analysis, vol 163, Solid mechanics and its applications. Springer, Dordrecht, pp 173–221. doi:10.1007/978-90-481-2516-6_5
7. Wagner W, Gruttmann F, Sprenger W (2001) A finite element formulation for the simulation of propagating delaminations in layered composite structures. Int J Numer Method Eng 51(11):1337–1359. doi:10.1002/nme.210
8. Bathe K-J (1996) Finite element procedures. Prentice Hall, Princeton, New Jersey
9. Timoshenko SP (1921) On the correction factor for shear of the differential equation for transverse vibrations of bars of uniform cross-section. Philos Mag 744

Chapter 2
Introduction to Finite Element Method

As discussed in Chap. 1, mechanic problems are governed by a set of partial differential equations that are valid in a certain domain and they needed to be solved for evaluating the stress condition of mechanical components. Although analytic methods can be employed to solve linear problems involving partial differential equations, its use to analyze complex structures may be a difficult or, even, an impossible task. Thus, in this chapter, Hamilton's principle, which one of the most powerful energy principle, is introduced for the FEM formulation of problems of mechanics of solids and structures. The approach adopted in this chapter is to directly work out the dynamic system equations, after which the static dynamic equations can be easily obtained by simply dropping out the dynamic terms

2.1 Strong and Weak Formulations

Strong formulations lead to strong solutions in the sense that they require strong continuity in the field variables. For instance, the partial differential equations developed in the previous chapter are strong forms of the system equations of motion for structural mechanical systems. Strong solutions of these field variables need to be differentiable up to an order that assure the correctness of the partial differential equations. Thus, exact solutions of a strong form of the system equations are usually very difficult to obtain for complex engineering systems. Thus, alternative approximation and numerical methods may be used.

The accuracy of both alternative methods relies on the ability to develop accurate function approximations. In the approximation methods a trial function is defined by a single expression valid throughout the whole domain, while in the numerical finite element method the domain is divided into a number of non-overlapping subdomains and then the approximation is constructed in a piecewise manner over each subdomain. If the subdomains have a relatively simple shape and if the trial

M.A. Neto et al., *Engineering Computation of Structures: The Finite Element Method*, DOI 10.1007/978-3-319-17710-6_2

functions definition is repeatable over these subdomains, is possible to deal with assembled regions of complex shapes quite readily. The piecewise definition of trial or shape functions means that discontinuities in the approximating function or in its derivatives will occur [1].

A weak form of the system equations can be based on an energy principle. The energy principle can be categorized as a special form of the variational principle which is particularly suited for problems of the mechanics of solids and structures [2, 3]. The weak form is often expressed in a mathematical integral that requires a weaker continuity on the field variables than strong formulations. Moreover, formulations based on weak form usually produce a set of discretized system equations that are easy to solve and that give accurate approximations, especially for problems of complex geometry. The finite element method is a typical example of successfully using weak form formulations that leads to a set of well-behaved algebraic system equations, if the problem domain is properly divided.

2.2 Hamilton's Principle

To derive the discretized form of the dynamic system equations the Hamilton's variational principle will be used. The mathematical form of this principle is stated as [4, 5]

$$\delta \int_{t_1}^{t_2} (T - U + W)\, dt = 0 \tag{2.1}$$

where t_1 and t_2 are the initial and finial times of the analysis, respectively. T is the total kinetic energy, U represents the potential energy of the flexible structure and W the potential of the applied forces that are acting in the body. This principle states simply that for a deformable mechanical system in which the response is time-dependent, the evolution of the real configuration (path) is defined by the admissible function that makes the functional at Eq. (2.1) stationary. An admissible function must satisfy the compatibility equations, the kinematic boundary conditions and constraints at the initial and final times.

As time unfolds, the motion of the deformable system travels a curve in the configuration space called the true path. A different path, known as the varied path, results from imagining the system as moving through configuration space by a slightly different path defined by the virtual displacement $\delta\mathbf{u}$. Of all the possible paths through configuration space, Eq. (2.1) consider only those that coincide with the true path at times t_1 and t_2, and it follows that $\delta\mathbf{u} = \mathbf{0}$ at those two times [6].

The kinetic energy associated with a flexible body that has volume Ω is given as [7]

$$T = \frac{1}{2}\int_{\Omega} \dot{\mathbf{u}}\ \rho\ \dot{\mathbf{u}}\ d\Omega \tag{2.2}$$

being $\dot{\mathbf{u}}$ the velocity vector and ρ the mass density.

The total potential energy of a deformable structure is given as

$$U = \frac{1}{2}\int_{\Omega} \left(\boldsymbol{\varepsilon}^T\ \mathbf{c}\ \boldsymbol{\varepsilon}\right) d\Omega \tag{2.3}$$

where $\boldsymbol{\varepsilon}$ are the elastic strains and $\mathbf{c}$ is the stiffness material matrix.

The total work W done by the external mechanical loading is given by Tzou [8] as

$$W = \int_{\Omega} \mathbf{u}^T \mathbf{f}_b\ d\Omega + \int_{\Gamma_s} \mathbf{u}^T \mathbf{f}_s\ d\Gamma_s + \sum_i \mathbf{u}_i^T \mathbf{f}_i^c \tag{2.4}$$

in which $\mathbf{u}$ is the displacement field, $\mathbf{f}_b$ is the body load vector, $\mathbf{f}_s$ is the surface load vector and $\mathbf{f}_i^c$ is the i*th* concentrated load vector. Substituting Eqs. (2.2), (2.3), and (2.4) into Eq. (2.1) and computing its variation yields to the following variational statement:

$$\left[\int_{\Omega} \delta\mathbf{u}^T \rho\dot{\mathbf{u}}\ d\Omega\right]_{t_1}^{t_2} - \int_{t_1}^{t_2} \left[\int_{\Omega} \left(\delta\mathbf{u}^T\rho\ddot{\mathbf{u}} - \delta\boldsymbol{\varepsilon}^T\mathbf{c}\ \boldsymbol{\varepsilon} + \delta\mathbf{u}^T\mathbf{f}_b\right)\ d\Omega + \int_{\Gamma_s} \delta\mathbf{u}^T\mathbf{f}_s\ d\Gamma_s + \sum_i \delta\mathbf{u}^T\mathbf{f}_i^c\right] dt = 0 \tag{2.5}$$

The computation of variation is only in $\mathbf{u}$ and its derivatives, which means that the space and time parameters denoted by x_i and t are not affected by the variation. Notice that where the system information is prescribed its variation must be zero. In fact, if the configuration of the system is prescribed then the variation must necessarily be zero because otherwise any change in the original configuration would result in a different problem [6]. Thus, imposing the usual constraint of no variation at the time endpoints implies that $\delta\mathbf{u}\,(t_1) = \mathbf{0}$ and $\delta\mathbf{u}\,(t_2) = \mathbf{0}$ and Eq. (2.5) yields to

$$\int_{t_1}^{t_2} \left[\int_{\Omega} \left(\delta\mathbf{u}^T\rho\ddot{\mathbf{u}} - \delta\boldsymbol{\varepsilon}^T\mathbf{c}\ \boldsymbol{\varepsilon} + \delta\mathbf{u}^T\mathbf{f}_b\right)\ d\Omega + \int_{\Gamma_s} \delta\mathbf{u}^T\mathbf{f}_s\ d\Gamma_s + \sum_i \delta\mathbf{u}^T\mathbf{f}_i^c\right] dt = 0 \tag{2.6}$$

Because the strain field is related to displacement field, in Eq. (2.6), the unknowns are the mechanical displacements. The solution of these unknowns will be obtained numerically using the finite element method.

2.3 Finite Element Method

The standard FEM procedure can be summarized into three main steps: domain discretization, displacement approximation and finite element equations.

2.3.1 Domain Discretization

The domain discretization is often called domain meshing and it consists on the division of the original domain into n finite elements. With the computer advent this task has been used to develop user-friendly pre and postprocessor programs for numerical simulations in science and engineering, namely GID Pré/Post Processor [9], Femap [10] etc. These pre/post processors are especially useful for complex geometries, as the case of a two-dimensional geometry problem presented at Fig. 2.1.

The meshing technique requires unique numbers for all the finite elements and nodes that define the structural domain. A finite element is composed of nodes and of edges; the finite element shape is defined by connecting its nodes in a pre-defined consistent way to create the element connectivity. The continuity of the mesh is assured by the connectivity among nodes. To form the entire domain of the problem is possible to think in the process of building a puzzle where the puzzle pieces (finite elements) have numbered vertices (nodes). Thus, that one empty part of the puzzle can be occupied by a puzzle piece it is necessary that numbers associated with their vertices are coinciding with the numbers of the vertices that define the outline available. A finite element mesh can be constructed using different types of finite elements as long as they are compatible on the connection regions.

The finite element mesh quality can have a large influence on the accuracy of a simulation based on the solution of partial differential equations [11]. But what, exactly, is mesh quality? As far as the authors are aware, the only available definition is proposed by Knupp:

> Mesh quality concerns the characteristics of a mesh that permit a particular partial differential equation simulation to be efficiently performed, with fidelity to the underlying physics, and with the accuracy required for the problem.

In fact, this definition is true because the same mesh can lead to different accuracies as different calculations are performed, i.e., one mesh which give

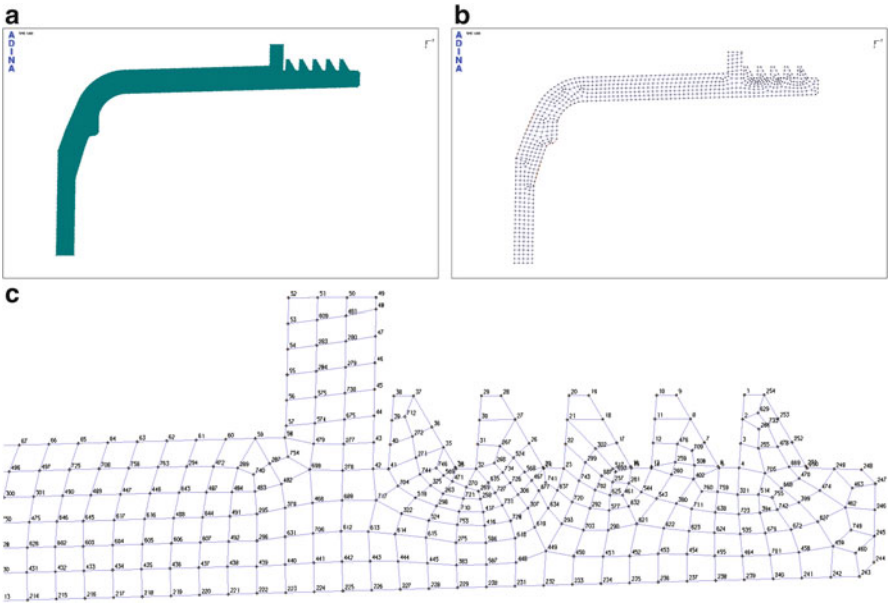

Fig. 2.1 Example of a surface mesh: (**a**) surface geometry; (**b**) surface meshed; (**c**) zoom of elements and nodes numbering

accurate static results does not assure accurate dynamic results. On the other hand, the mesh should not blur the simulation, i.e., finite elements with inverted normal can cause a loss of fidelity or even cause the simulation halt prematurely. Moreover, the mesh should not contribute to ill-conditioning of the system matrix that needed to be solved and, simultaneously, should reduce both global and local errors. Meanwhile, generally speaking, a finer mesh yields accurate results but increases the computational cost. Thus, the mesh is usually not uniform and, finer meshes are used at the areas in which the displacement gradient is larger or at areas in which a critical accuracy is required.

2.3.2 Displacement Approximation

In order to formulate FEM equations form general finite elements, it is convenient to use a local coordinate system in which the limits of variation of each coordinate are related to the position of the basis point of the local system and to the geometrical limits of the finite element. In Fig. 2.2 is possible to see two different locations for the local coordinate system; Fig. 2.2a shows the typical placement of a local coordinate system for 1D meshes and Fig. 2.2b shows the placement of a local

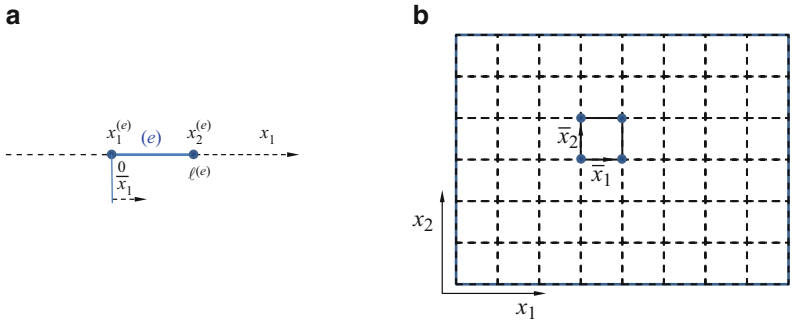

Fig. 2.2 Local and global coordinate systems: (**a**) 1D mesh; (**b**) 2D mesh

coordinate system for a 2D mesh. Thus, a finite element mesh has a number of local coordinate systems that is equal to the number of finite elements within the mesh.

Using the element local coordinate system is possible to interpolate the displacement within the finite element by a polynomial function that must verify the boundary conditions at the element nodes and, in the end, the displacement within the finite element can be interpolated as

$$\tilde{\mathbf{u}}\left(\bar{x}_1, \bar{x}_2, \bar{x}_3\right) = \overline{\mathbf{N}}\left(\bar{x}_1, \bar{x}_2, \bar{x}_3\right)\ \bar{\mathbf{u}} \tag{2.7}$$

where the superscript $(\tilde{\bullet})$ stands for approximation and $\bar{\mathbf{u}}$ is the nodal displacement associated with the finite element. Note that for notation simplicity, in this section, the superscript (e) , which is associated with the finite element number, is omitted in all vectors and matrices. Vector $\bar{\mathbf{u}}$ is the first quantity that the analyst wants to evaluate, and can be written as

$$\bar{\mathbf{u}} = \begin{bmatrix} \bar{\mathbf{u}}_1 \\ \bar{\mathbf{u}}_2 \\ \vdots \\ \bar{\mathbf{u}}_n \end{bmatrix} \tag{2.8}$$

where n is the number of element nodes and $\bar{\mathbf{u}}_i$ contains the degrees of freedom associated with node i of the finite element. For 3D mathematical models vectors $\bar{\mathbf{u}}_i$ have the form

$$\bar{\mathbf{u}}_i = \begin{bmatrix} u_i\left(\bar{x}_1, \bar{x}_2, \bar{x}_3\right) \\ v_i\left(\bar{x}_1, \bar{x}_2, \bar{x}_3\right) \\ w_i\left(\bar{x}_1, \bar{x}_2, \bar{x}_3\right) \end{bmatrix} \begin{array}{l} \rightarrow \text{displacement in the } \bar{\mathrm{x}}_1\text{-direction} \\ \rightarrow \text{displacement in the } \bar{\mathrm{x}}_2\text{-direction} \\ \rightarrow \text{displacement in the } \bar{\mathrm{x}}_3\text{-direction} \end{array} \tag{2.9}$$

For 2D or 1D mathematical models vectors $\bar{\mathbf{u}}_i$ can also consist of rotations. Moreover, for transformation simplicity, nodal rotations should be placed after nodal displacements following the sequential axes $\bar{x}_1, \bar{x}_2$ and $\bar{x}_3$. Thus, at Eq. (2.7), the dimension of vector $\bar{\mathbf{u}}$ is defined as $n \times m$, being m the number of degrees of freedom at one node.

Matrix $\overline{\mathbf{N}}$ in Eq. (2.7) contains the interpolation functions for the nodes of the finite element. These functions are called shape functions, and they predefine the shape of the displacement variations with respect to the element coordinates. The general form of this matrix is

$$\begin{gathered}\overline{\mathbf{N}}\left(\bar{x}_1, \bar{x}_2, \bar{x}_3\right) = \left[\overline{\mathbf{N}}_1\left(\bar{x}_1, \bar{x}_2, \bar{x}_3\right) \overline{\mathbf{N}}_2\left(\bar{x}_1, \bar{x}_2, \bar{x}_3\right) \ldots \overline{\mathbf{N}}_n\left(\bar{x}_1, \bar{x}_2, \bar{x}_3\right)\right] \\ \downarrow \qquad \downarrow \qquad \ldots \qquad \downarrow \\ \textit{for node } 1 \quad \textit{for node } 2 \quad \ldots \quad \textit{for node } n\end{gathered} \tag{2.10}$$

where $\overline{\mathbf{N}}_i$ is a sub-matrix containing the shape functions associated with the i nodal degrees of freedom. The n sub-matrices can be arranged as

$$\overline{\mathbf{N}}_i = \begin{bmatrix} N_1 & 0 & 0 & 0 \\ 0 & N_2 & 0 & 0 \\ 0 & 0 & \ddots & 0 \\ 0 & 0 & 0 & N_n \end{bmatrix}_i \tag{2.11}$$

in Eq. (2.11), N_j represents the shape function associated with the jth degree of freedom at the ith element node.

Shape functions are obtained using the standard procedure presented in the next section. Meanwhile, for the ith element node is not guaranteed that $N_1 = N_2 = \cdots = N_n$ it will depend on the element formulation.

2.3.3 *Procedure to Define Shape Function*

Consider that local coordinates of the ith element node are denoted by vector $\bar{\mathbf{x}}_i$: for 1D problems $\bar{\mathbf{x}}_i = \{\bar{x}_1\}_i$, for 2D problems $\bar{\mathbf{x}}_i^T = \left[\bar{x}_1 \ \bar{x}_2\right]_i$ and for 3D problems $\bar{\mathbf{x}}_i^T = \left[\bar{x}_1 \ \bar{x}_2 \ \bar{x}_3\right]_i$. To create the interpolation function of each displacement component of a finite element, it is required that the number of shape function equals, at least, the number of nodes. Some exceptions to the previous rule are for instance: 1D finite elements based on the Euler-Bernoulli theory and 2D finite elements based on the Classical theory. For now, consider the explanation of the standard procedure to obtain the shape functions of one displacement component only. This procedure is applicable in a straightforward form to the remaining components. First the function that approximate the displacement component $u_h\left(\bar{\mathbf{x}}\right)$ is created in the form of a linear combination of monomials $\phi_i\left(\bar{\mathbf{x}}\right)$ and coefficients a_i, i.e.

$$u_h\left(\bar{\mathbf{x}}\right) = \sum_{i=1}^{n} \phi_i\left(\bar{\mathbf{x}}\right) a_i = \mathbf{\Phi}^T \mathbf{a} \quad (i = 1, \cdots, n) \tag{2.12}$$

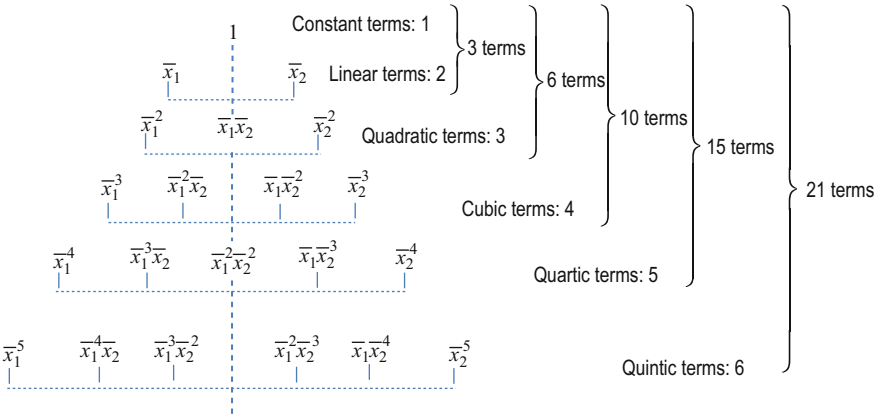

Fig. 2.3 Pascal triangle of monomials for 2D cases

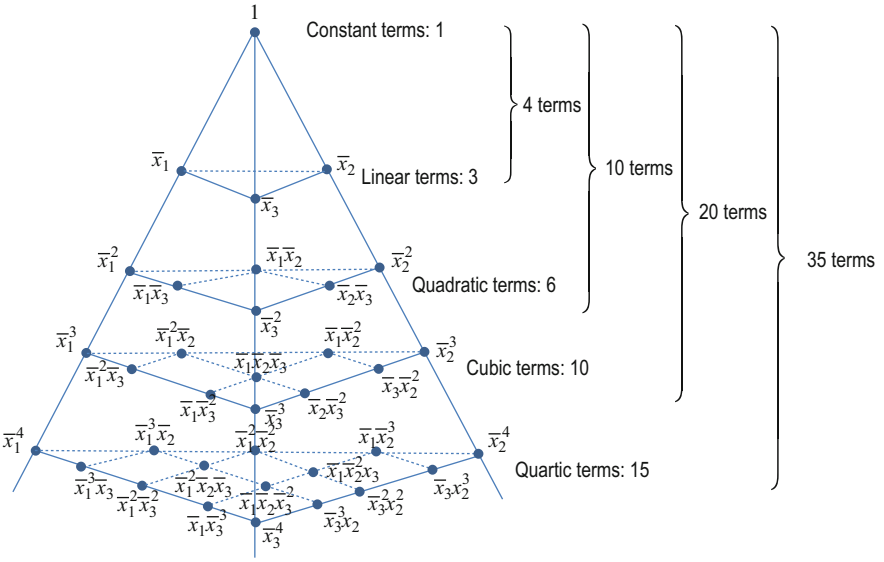

Fig. 2.4 Pascal pyramid of monomials for 3D cases

Note that a_i is the coefficient for the monomial known $\phi_i(\bar{\mathbf{x}})$ and needs to be computed. In fact, $\phi_i(\bar{\mathbf{x}})$ in Eq. (2.12) represent a set of selected monomials:

- For 1D problems are built with n terms of one-dimensional monomials;
- For 2D problems are built with n terms of the Pascal's triangle shown in Fig. 2.3
- For 3D problems are built with n terms of the Pascal's pyramid shown in Fig. 2.4

A basis of complete order of p in 1D cases can be obtained by following the first edge of the Pascal's triangle presented in Fig. 2.3 and it has de form

$$\mathbf{\Phi}^T(\bar{x}_1) = \left[\, 1\ \bar{x}_1\ \bar{x}_1^2\ \bar{x}_1^3\ \bar{x}_1^4\ \bar{x}_1^5\ \ldots\ \bar{x}_1^p \,\right] \tag{2.13}$$

For 2D cases a basis of complete order p it will group all the members of a Pascal triangle in which the vertices of the base edge are associated with monomials x_1^p and x_2^p, and it has the form

$$\mathbf{\Phi}^T(\bar{x}_1, \bar{x}_2) = \left[\, 1\ \bar{x}_1\ \bar{x}_2\ \bar{x}_1\bar{x}_2\ \bar{x}_1^2\ \bar{x}_2^2\ \ldots\ \bar{x}_1^p\ \bar{x}_2^p \,\right] \tag{2.14}$$

For 3D cases a basis of complete order p it will group all the members of a Pascal pyramid, Fig. 2.4, in which the vertices of the base triangle are associated with monomials x_1^p, x_2^p and x_3^p, and it has the form

$$\mathbf{\Phi}^T(\bar{x}_1, \bar{x}_2, \bar{x}_3) = \left[\, 1\ \bar{x}_1\ \bar{x}_2\ \bar{x}_3\ \bar{x}_1\bar{x}_2\ \bar{x}_1\bar{x}_3\ \bar{x}_2\bar{x}_3\ \bar{x}_1^2\ \bar{x}_2^2\ \bar{x}_3^2\ \ldots\ \bar{x}_1^p\ \bar{x}_2^p\ \bar{x}_3^p \,\right] \tag{2.15}$$

The coefficients a_i in Eq. (2.12) can be computed by applying the displacement boundary conditions of the finite element at the n nodes, i. e. the displacement at each finite element node equals the displacement that is calculated using Eq. (2.12). So, at node i boundary condition has the form

$$u_i^h = \mathbf{\Phi}\left(\bar{\mathbf{x}}_i\right)\mathbf{a} \tag{2.16}$$

where u_i^h represents the nodal value of u^h at position $\bar{\mathbf{x}}_i$. Repeating this equation for all the remaining nodes, the final system of equations can be written in the following matrix form

$$\bar{\mathbf{u}} = \mathbf{C}\,\mathbf{a} \tag{2.17}$$

vector $\bar{\mathbf{u}}$ is defined in Eqs. (2.8) and (2.9). Nevertheless, the vector in Eq. (2.9) has only one component and matrix $\mathbf{C}$ is given by

$$\mathbf{C} = \begin{bmatrix} \phi_1(\bar{\mathbf{x}}_1) & \phi_2(\bar{\mathbf{x}}_1) & \cdots & \phi_n(\bar{\mathbf{x}}_1) \\ \phi_1(\bar{\mathbf{x}}_2) & \phi_2(\bar{\mathbf{x}}_2) & \cdots & \phi_n(\bar{\mathbf{x}}_2) \\ \vdots & \vdots & \ddots & \vdots \\ \phi_1(\bar{\mathbf{x}}_n) & \phi_2(\bar{\mathbf{x}}_n) & \cdots & \phi_n(\bar{\mathbf{x}}_n) \end{bmatrix} \tag{2.18}$$

Note that Eq. (2.18) is a matrix with algebraic values for instance, for two dimensional polynomials is possible to write

$$\mathbf{C} = \begin{bmatrix} 1 & (\bar{x}_1)_1 & (\bar{x}_2)_1 & (\bar{x}_1)_1(\bar{x}_2)_1 & \cdots & \left(\bar{x}_1^p\right)_1 & \left(\bar{x}_2^p\right)_1 \\ 1 & (\bar{x}_1)_2 & (\bar{x}_2)_2 & (\bar{x}_1)_2(\bar{x}_2)_2 & \cdots & \left(\bar{x}_1^p\right)_2 & \left(\bar{x}_2^p\right)_2 \\ \vdots & \vdots & \vdots & \vdots & \vdots & \vdots & \vdots \\ 1 & (\bar{x}_1)_n & (\bar{x}_2)_n & (\bar{x}_1)_n(\bar{x}_2)_n & \cdots & \left(\bar{x}_1^p\right)_n & \left(\bar{x}_2^p\right)_n \end{bmatrix} \tag{2.19}$$

where $\left(\bar{x}_j\right)_i$ represents the jth coordinate of ith element node. Assuming that the inverse of matrix $\mathbf{C}$ in Eq. (2.19) exists, Eq. (2.17) can be used to evaluate the coefficient vector $\mathbf{a}$, as

$$\mathbf{a} = \mathbf{C}^{-1}\bar{\mathbf{u}} \tag{2.20}$$

Using this information back in Eq. (2.12), is possible to write

$$u_h(\bar{\mathbf{x}}) = \boldsymbol{\Phi}^T \mathbf{C}^{-1} \bar{\mathbf{u}} = \overline{\mathbf{N}}\,\bar{\mathbf{u}} \tag{2.21}$$

where $\overline{\mathbf{N}}$ is a matrix of shape functions $N_i(\bar{\mathbf{x}})$ defined by

$$\overline{\mathbf{N}}(\bar{\mathbf{x}}) = \boldsymbol{\Phi}^T(\bar{\mathbf{x}})\ \mathbf{C}^{-1} = \left[\underbrace{\boldsymbol{\Phi}^T(\bar{\mathbf{x}})\,\mathbf{C}_1^{-1}}_{N_1(\bar{\mathbf{x}})}\ \underbrace{\boldsymbol{\Phi}^T(\bar{\mathbf{x}})\,\mathbf{C}_2^{-1}}_{N_2(\bar{\mathbf{x}})}\ \cdots\ \underbrace{\boldsymbol{\Phi}^T(\bar{\mathbf{x}})\,\mathbf{C}_n^{-1}}_{N_n(\bar{\mathbf{x}})}\right] \tag{2.22}$$

and, $\mathbf{C}_i^{-1}$ is the ith column of matrix $\mathbf{C}^{-1}$. Using the information presented in Eq. (2.22) is possible to write the relation:

$$N_i(\bar{\mathbf{x}}) = \boldsymbol{\Phi}^T(\bar{\mathbf{x}})\ \mathbf{C}_i^{-1} \tag{2.23}$$

In Eq. (2.23) it is assumed that inverse of matrix $\mathbf{C}$ exists, if is not the case the construction of shape functions will fail. The computation of matrix $\mathbf{C}^{-1}$ is dependent on basis function used and on the nodal distribution of the element [3]. Nevertheless, in this text, the elements that are discussed are those in which matrix $\mathbf{C}$ is invertible.

In the process of computing deformations associated with a finite element, derivatives of shape functions are needed and, since they have a polynomial form, they can be obtained very easily.

2.3.4 Characteristic of Shape Functions

Consistency

The consistency of shape functions, within the finite element, is closely linked to its polynomial order, i.e. it depends on the complete order of monomials $\phi_i(\bar{\mathbf{x}})$ used in Eq. (2.12). If the complete order of monomial represents a polynomial of order k, the element shape functions are called k-complete and are said to posses C^k consistency, if they are able to represent exactly all polynomial terms of order $\leq k$. Note that this requirement applies at the element level and involves all element shape functions.

The verification of this requirement can be done assuming a displacement-based finite element in which $k \leq n$, being n the number of nodes of the element. Hence, the element displacement in the $\bar{x}_1$ direction can be defined as

$$\tilde{u}\left(\overline{\mathbf{x}}\right) = \sum_{i=1}^{k} \phi_i\left(\overline{\mathbf{x}}\right) \alpha_i = \mathbf{\Phi}^T \boldsymbol{\alpha} \quad i = 1, \ldots, k \leq n \tag{2.24}$$

where $\phi_i\left(\overline{\mathbf{x}}\right)$ are monomials that are included in Eq. (2.16). In order to make $i = n$ in Eq. (2.24), is possible to rewrite this equation such that

$$\tilde{u}\left(\overline{\mathbf{x}}\right) = \sum_{i=1}^{n} \phi_i\left(\overline{\mathbf{x}}\right) a_i = \mathbf{\Phi}^T \mathbf{a} \quad i = 1, \ldots, n \tag{2.25}$$

where

$$a^T = [\alpha_1\, \alpha_2\, \cdots\, \alpha_k\, 0 \cdots 0] \tag{2.26}$$

and vector $\mathbf{\Phi}$ is updated in order to include all monomials terms of Eq. (2.16). The consistency requires that the displacement field in the $\overline{x}_1$ direction should be exactly represented for any values of α coefficients, so evaluating Eq. (2.25) in each finite element node, yields

$$\begin{aligned}
\overline{\mathbf{u}} &= \begin{bmatrix} u_1 \\ u_2 \\ \vdots \\ u_k \\ u_{k+1} \\ \vdots \\ u_n \end{bmatrix} \\
&= \begin{bmatrix}
\phi_1\left(\overline{\mathbf{x}}_1\right) & \phi_2\left(\overline{\mathbf{x}}_1\right) & \cdots & \phi_k\left(\overline{\mathbf{x}}_1\right) & \phi_{k+1}\left(\overline{\mathbf{x}}_1\right) & \cdots & \phi_n\left(\overline{\mathbf{x}}_1\right) \\
\phi_1\left(\overline{\mathbf{x}}_2\right) & \phi_2\left(\overline{\mathbf{x}}_2\right) & \cdots & \phi_k\left(\overline{\mathbf{x}}_2\right) & \phi_{k+1}\left(\overline{\mathbf{x}}_2\right) & \cdots & \phi_n\left(\overline{\mathbf{x}}_2\right) \\
\vdots & \vdots & \vdots & \vdots & \vdots & \vdots & \vdots \\
\phi_1\left(\overline{\mathbf{x}}_k\right) & \phi_2\left(\overline{\mathbf{x}}_k\right) & \cdots & \phi_k\left(\overline{\mathbf{x}}_k\right) & \phi_{k+1}\left(\overline{\mathbf{x}}_k\right) & \cdots & \phi_n\left(\overline{\mathbf{x}}_k\right) \\
\phi_1\left(\overline{\mathbf{x}}_{k+1}\right) & \phi_2\left(\overline{\mathbf{x}}_{k+1}\right) & \cdots & \phi_k\left(\overline{\mathbf{x}}_{k+1}\right) & \phi_{k+1}\left(\overline{\mathbf{x}}_{k+1}\right) & \cdots & \phi_n\left(\overline{\mathbf{x}}_{k+1}\right) \\
\vdots & \vdots & \vdots & \vdots & \vdots & \vdots & \vdots \\
\phi_1\left(\overline{\mathbf{x}}_n\right) & \phi_2\left(\overline{\mathbf{x}}_n\right) & \cdots & \phi_k\left(\overline{\mathbf{x}}_n\right) & \phi_{k+1}\left(\overline{\mathbf{x}}_n\right) & \cdots & \phi_n\left(\overline{\mathbf{x}}_n\right)
\end{bmatrix}
\begin{bmatrix} \alpha_1 \\ \alpha_2 \\ \\ \alpha_k \\ 0 \\ \\ 0 \end{bmatrix} = \mathbf{Ca}
\end{aligned} \tag{2.27}$$

To understand if the displacement field on Eq. (2.24) can be recover, Eq. (2.27) can be inserted into the displacement approximation (Eq. 2.21), what gives

$$u_h\left(\overline{\mathbf{x}}\right) = \mathbf{\Phi}^T\, \mathbf{C}^{-1}\, \overline{\mathbf{u}} = \mathbf{\Phi}^T\, \mathbf{C}^{-1}\mathbf{C}\, \mathbf{a} = \mathbf{\Phi}^T \mathbf{a} = \tilde{u}\left(\overline{\mathbf{x}}\right) \tag{2.28}$$

This is what is given in Eq. (2.24). This proves that any field given by Eq. (2.24) will be exactly reproduced at the element level if shape functions are used, as long as the given function is included in the approximation function used for constructing the shape functions [3].

Linear Independence
Shape functions are linearly independent. This property is justified by the fact that the approximation function in Eq. (2.24) is constructed with basic functions that are linearly-independent. Thus, because the shape functions are equivalent to the basis function in the function space, the shape functions are also linearly independent.

Kronecker Delta Properties
Shape functions have the property of the kroncker delta δ_{ij}, which is a function of two variables, defined as

$$N_i\left(\overline{\mathbf{x}}_j\right) = \delta_{ij} = \begin{cases} 1 & i = j \\ 0 & i \neq j \end{cases} \qquad i, j = 1, \ldots, n \tag{2.29}$$

Kronecker delta property of shape functions implies that the shape function N_i must equals the unity at node i and zero at remaining element nodes. To understand this, assume that the element displacement depends only from the displacement at node i and the displacement at this node is u_i. Therefore, the vector of element nodal displacement is

$$\overline{\mathbf{u}}^T = \left[0\ 0 \cdots u_i\ 0 \cdots\right] \tag{2.30}$$

Using this information into Eq. (2.21) and evaluating the displacement at node j, $\overline{\mathbf{x}}_j$, yields

$$\tilde{u}\left(\overline{\mathbf{x}}_j\right) = \sum_{k=1}^{n} N_k\left(\overline{\mathbf{x}}_j\right) u_k = N_i u_i \tag{2.31}$$

So, if $j = i$ Eq. (2.31) becomes

$$\tilde{u}\left(\overline{\mathbf{x}}_i\right) = N_i u_i \tag{2.32}$$

to assure that Eq. (2.32) equals the displacement at node i, u_i, it is necessary that

$$N_i = 1 \tag{2.33}$$

If $j \neq i$ the displacement computed by Eq. (2.21) must be zero, what yields

$$N_i u_i = 0 \tag{2.34}$$

Which requires

$$N_i\left(\overline{\mathbf{x}}_j\right) = 0 \tag{2.35}$$

Accordingly Eqs. (2.31) and (2.35) is possible to conclude that shape functions posses the Kronecker delta function property.

Unity Property
Shape functions verify the unity requirement:

$$\sum_{i=1}^{n} N_i\left(\overline{\mathbf{x}}\right) = 1 \tag{2.36}$$

This property is important to assure that the displacement approximation function is able of reproducing a constant displacement field or a rigid body motion over the finite element.

Assume that within the finite element the solution should be defined as

$$u\left(\overline{\mathbf{x}}\right) = c \tag{2.37}$$

Which means that in each element node the Eq. (2.37) must be verified and, therefore, the nodal displacements associated with the finite element are defines as

$$\overline{\mathbf{u}}^T = \left[\, c \; c \cdots c \,\right] \tag{2.38}$$

So, using Eq. (2.38) into Eq. (2.21) yields

$$u\left(\overline{\mathbf{x}}\right) = \sum_{i=1}^{n} N_i\left(\overline{\mathbf{x}}\right) u_i = c \sum_{i=1}^{n} N_i\left(\overline{\mathbf{x}}\right) \tag{2.39}$$

In order to assure that Eqs. (2.37) and (2.39) give the same value, equality (2.36) should be verified.

Linear Reproduction
If the first order monomial is included in the basis function, then shape functions construction must be able to represent a linear function, i.e.

$$\begin{cases} \sum_{i=1}^{n} N_i\left(\overline{\mathbf{x}}\right)\left(\overline{x}_1\right)_i = \overline{x}_1 \\ \sum_{i=1}^{n} N_i\left(\overline{\mathbf{x}}\right)\left(\overline{x}_2\right)_i = \overline{x}_2 \\ \sum_{i=1}^{n} N_i\left(\overline{\mathbf{x}}\right)\left(\overline{x}_3\right)_i = \overline{x}_3 \end{cases} \tag{2.40}$$

In Eq. (2.40) $\left(\overline{x}_j\right)_i$ represents the nodal value of the coordinates, $\overline{x}_j$.

Assume that within the exact finite element the displacement field in the $\bar{x}_1$ direction is a linear function of coordinate $\bar{x}_1$, defined as

$$u(\bar{\mathbf{x}}) = \bar{x}_1 \tag{2.41}$$

The exact nodal displacements associated with the finite element, in the $\bar{x}_1$ direction, are defines as

$$\bar{\mathbf{u}}^T = \left[(\bar{x}_1)_1 \ (\bar{x}_1)_2 \cdots (\bar{x}_1)_n \right] \tag{2.42}$$

Using Eq. (2.42) into Eq. (2.21) yields

$$u(\bar{\mathbf{x}}) = \sum_{i=1}^{n} N_i(\bar{\mathbf{x}}) (\bar{x}_1)_i \tag{2.43}$$

Thus, to assure that Eqs. (2.41) and (2.43) give the same value, equality (2.40) should be verified.?

2.3.5 *Finite Element Equations in Local Coordinate System*

Formulation of the finite element equations is based on the application of Hamilton's principle to each finite element in the analysis domain. So, it is necessary to create the discretized form of Eq. (2.6). To do that, is possible to start with the discretized form of each term that appears in Eq. (2.1) and then apply the Hamilton's principle.

By substituting Eq. (2.7) into Eq. (2.2), is possible to define the finite element kinetic energy as

$$T = \frac{1}{2}\int_{\Omega^e} \rho \dot{\mathbf{u}}^T \dot{\mathbf{u}} \, d\Omega^e = \frac{1}{2}\int_{\Omega^e} \rho \dot{\bar{\mathbf{u}}}^T \bar{\mathbf{N}}^T \bar{\mathbf{N}} \, \dot{\bar{\mathbf{u}}} \, d\Omega^e = \frac{1}{2}\dot{\bar{\mathbf{u}}}^T \left(\int_{\Omega^e} \rho \bar{\mathbf{N}}^T \bar{\mathbf{N}} \, d\Omega^e \right) \dot{\bar{\mathbf{u}}} \tag{2.44}$$

By denoting

$$\bar{\mathbf{m}} = \int_{\Omega^e} \rho \bar{\mathbf{N}}^T \bar{\mathbf{N}} \, d\Omega^e \tag{2.45}$$

That is named mass matrix of the finite element, Eq. (2.44) can be rewritten as

$$T = \frac{1}{2}\dot{\bar{\mathbf{u}}}^T \bar{\mathbf{m}} \, \dot{\bar{\mathbf{u}}} \tag{2.46}$$

The strain energy is expressed by Eq. (2.3) and, because the finite element strain field has not been defined, is important to use the differential operator $\mathbf{L}$ to write the element strain field as

$$\boldsymbol{\varepsilon} = \overline{\mathbf{L}}\mathbf{u} = \overline{\mathbf{L}}\overline{\mathbf{N}}\,\overline{\mathbf{u}} = \overline{\mathbf{B}}\,\overline{\mathbf{u}} \tag{2.47}$$

in which $\overline{\mathbf{B}}$ is called the strain matrix. By substituting Eq. (2.47) into Eq. (2.3) we have

$$U = \frac{1}{2}\int_{\Omega^e} \overline{\mathbf{u}}^T \overline{\mathbf{B}}^T \mathbf{c}\, \overline{\mathbf{B}}\,\overline{\mathbf{u}}\, d\Omega^e = \frac{1}{2}\overline{\mathbf{u}}^T \left(\int_{\Omega^e} \overline{\mathbf{B}}^T \mathbf{c}\, \overline{\mathbf{B}}\; d\Omega^e \right) \overline{\mathbf{u}} \tag{2.48}$$

By denoting

$$\overline{\mathbf{k}} = \int_{\Omega^e} \overline{\mathbf{B}}^T \mathbf{c}\, \overline{\mathbf{B}}\; d\Omega^e \tag{2.49}$$

That is named stiffness matrix of the finite element, Eq. (2.48) can be rewritten as

$$U = \frac{1}{2}\overline{\mathbf{u}}^T \overline{\mathbf{k}}\,\overline{\mathbf{u}} \tag{2.50}$$

Finally, to obtain the work done by the external mechanical loading, Eq. (2.7) is substituted into Eq. (2.4),

$$W = \int_{\Omega^e} \overline{\mathbf{u}}^T \overline{\mathbf{N}}^T \mathbf{f}_b\, d\Omega^e + \int_{\Gamma_s^e} \overline{\mathbf{u}}^T \overline{\mathbf{N}}^T \mathbf{f}_s\, d\Gamma_s^e + \sum_i \overline{\mathbf{u}}^T \overline{\mathbf{N}}^T \mathbf{f}_i^c = \overline{\mathbf{u}}^T \overline{\mathbf{f}} \tag{2.51}$$

with

$$\overline{\mathbf{f}} = \int_{\Omega^e} \overline{\mathbf{N}}^T \mathbf{f}_b\, d\Omega^e + \int_{\Gamma_s^e} \overline{\mathbf{N}}^T \mathbf{f}_s\, d\Gamma_s^e + \sum_i \overline{\mathbf{N}}^T \mathbf{f}_i^c = \overline{\mathbf{F}}_b + \overline{\mathbf{F}}_s + \overline{\mathbf{F}}_c \tag{2.52}$$

where $\overline{\mathbf{F}}_b$, $\overline{\mathbf{F}}_s$ and $\overline{\mathbf{F}}_c$ are the nodal forces acting on the nodes of the element and they can be added up to form the total nodal force vector $\overline{\mathbf{f}}$.

Substituting Eqs. (2.46), (2.50), and (2.51) into Eq. (2.1), leads to

$$\delta \int_{t_1}^{t_2} \left(\frac{1}{2}\dot{\overline{\mathbf{u}}}^T \overline{\mathbf{m}}\,\dot{\overline{\mathbf{u}}} - \frac{1}{2}\overline{\mathbf{u}}^T \overline{\mathbf{k}}\,\overline{\mathbf{u}} + \overline{\mathbf{u}}^T \overline{\mathbf{f}} \right) dt = 0 \tag{2.53}$$

and, because the variation and integration operators are interchangeable, is possible to write

$$\int_{t_1}^{t_2} \left(\delta\dot{\overline{\mathbf{u}}}^T \overline{\mathbf{m}}\,\dot{\overline{\mathbf{u}}} - \delta\overline{\mathbf{u}}^T \overline{\mathbf{k}}\,\overline{\mathbf{u}} + \delta\overline{\mathbf{u}}^T \overline{\mathbf{f}} \right) dt = 0 \tag{2.54}$$

The variation and the differentiation operators are also interchangeable, i.e.

$$\delta \dot{\bar{\mathbf{u}}}^T = \delta \left(\frac{d\, \bar{\mathbf{u}}^T}{dt} \right) = \frac{d}{dt} \left(\delta\, \bar{\mathbf{u}}^T \right) \tag{2.55}$$

and integrating the first term by parts on Eq. (2.54), we obtain

$$\int_{t_1}^{t_2} \left(\delta \dot{\bar{\mathbf{u}}}^T \bar{\mathbf{m}}\, \dot{\bar{\mathbf{u}}} \right) dt = \left[\delta \bar{\mathbf{u}}^T \bar{\mathbf{m}}\, \dot{\bar{\mathbf{u}}} \right]_{t_1}^{t_2} - \int_{t_1}^{t_2} \left(\delta \bar{\mathbf{u}}^T \bar{\mathbf{m}}\, \ddot{\bar{\mathbf{u}}} \right) dt = - \int_{t_1}^{t_2} \left(\delta \bar{\mathbf{u}}^T \bar{\mathbf{m}}\, \ddot{\bar{\mathbf{u}}} \right) dt \tag{2.56}$$

Note that in deriving Eq. (2.56), the condition $\delta \bar{\mathbf{u}} = 0$ at t_1 and t_2 have been used. Substituting Eq. (2.56) into Eq. (2.54), yields

$$\int_{t_1}^{t_2} \delta \bar{\mathbf{u}}^T \left(-\bar{\mathbf{m}}\, \ddot{\bar{\mathbf{u}}} - \bar{\mathbf{k}}\, \bar{\mathbf{u}} + \bar{\mathbf{f}} \right) dt = 0 \tag{2.57}$$

To assure that the integral in Eq. (2.57) is zero for any variation of displacements, $\delta \bar{\mathbf{u}}$, which cannot be zero in the time interval, the quantity in brackets has to vanish, i.e.

$$\bar{\mathbf{m}}\, \ddot{\bar{\mathbf{u}}} + \bar{\mathbf{k}}\, \bar{\mathbf{u}} = \bar{\mathbf{f}} \tag{2.58}$$

Equation (2.58) is the FEM equation for a finite element. $\bar{\mathbf{m}}$ and $\bar{\mathbf{k}}$ are the mass and stiffness matrices of the finite element and $\bar{\mathbf{f}}$ is the element force vector of the total external forces acting on the nodes of the finite element. All these element matrices and vectors are dependent on the shape functions used to approximate the element displacements.

2.3.6 *Coordinate Transformation of the Finite Element Equations*

In general, the domain of structures is divided into many finite elements and each of these finite elements may possess different local orientations. Nevertheless, to assemble all the element equations and form the global system equations, all the element equations must be written in the global coordinate system. Thus, a coordinate transformation has to be performed for each finite element.

This transformation gives the relationship between the displacement vector $\bar{\mathbf{u}}$ defined on the local coordinate system and the element displacement vector $\mathbf{u}$ defined on the global coordinate system, i.e.

$$\bar{\mathbf{u}} = \mathbf{T}\, \mathbf{u} \tag{2.59}$$

where $\mathbf{T}$ is the transformation matrix and it has different forms depending on the type of the finite element. The transformation matrix can also be applied to transform the force vector between the local and global coordinate systems:

$$\bar{\mathbf{f}} = \mathbf{T}\,\mathbf{f} \tag{2.60}$$

Substituting Eq. (2.59) into Eq. (2.58) leads to

$$\overline{\mathbf{m}}\,\mathbf{T}\,\ddot{\mathbf{u}} + \bar{\mathbf{k}}\,\mathbf{T}\,\mathbf{u} = \bar{\mathbf{f}} \tag{2.61}$$

Now multiplying at left both sides of Eq. (2.61) by $\mathbf{T}^T$, we get

$$\mathbf{T}^T\overline{\mathbf{m}}\,\mathbf{T}\,\ddot{\mathbf{u}} + \mathbf{T}^T\bar{\mathbf{k}}\,\mathbf{T}\,\mathbf{u} = \mathbf{T}^T\bar{\mathbf{f}} \tag{2.62}$$

By denoting

$$\mathbf{m} = \mathbf{T}^T\overline{\mathbf{m}}\,\mathbf{T};\;\; \mathbf{k} = \mathbf{T}^T\bar{\mathbf{k}}\,\mathbf{T} \tag{2.63}$$

Equation (2.62) can be rewritten as

$$\mathbf{m}\,\ddot{\mathbf{u}} + \mathbf{k}\,\mathbf{u} = \mathbf{f} \tag{2.64}$$

Equation (2.64) is the element equation based on the global coordinate system.

2.3.7 Global Finite Element Equations

Equation (2.64) is valid for each finite element of a structural domain, and the global finite element system equations are obtained by assembling together all equations on the form of Eq. (2.64) to obtain

$$\mathbf{M}\,\ddot{\mathbf{U}} + \mathbf{K}\,\mathbf{U} = \mathbf{F} \tag{2.65}$$

where $\mathbf{M}$ and $\mathbf{K}$ are the global mass and stiffness matrices, $\mathbf{U}$ is the vector of global displacements that contains displacements of the all nodes in the entire problem domain, and $\mathbf{F}$ is a vector that groups all the equivalent nodal forces. The assembly process consists on adding up the contributions of all elements connected at a node.

2.3.8 Imposing Boundary Conditions

Solutions of Eq. (2.65) can only be obtained if support conditions are defined, because the global stiffness matrix does not usually have a full rank and, therefore, it is non-negative definite or positive semi-definite. Physically, this means that if

external forces are applied to one unconstrained body, it will be able to move freely in the space and, therefore, rigid body motion is allowed. Moreover, the elastic displacements cannot be uniquely determined from Eq. (2.65). Thus, solutions of Eq. (2.65) are only possible for structural systems that have the rigid body motion remove. The number of rigid body movements that needs to be removed depends on the number of physical degrees of freedom that are included in the numerical model. For instance, when we solve a beam problem using a finite element with six degrees of freedom per node, three translations and three rotations, and loads do not include twist moments, the solution is possible only if twist rigid movements are removed at the numerical model.

Mathematically speaking, the constraints can be imposed by simply removing the rows and columns of Eq. (2.65) that correspond to the constrained nodal degrees of freedom. After a correct selection of constrained degrees of freedom, stiffness and mass matrices in Eq. (2.65) will be of full rank and, therefore, will be positive definite. Moreover, since both matrices are symmetric, the resultant system will have a system matrix that is symmetric positive definite.

2.4 FE Static Analysis

In static analysis the external forces are static, which means that no time variation exists. Thus, the elastic acceleration vector, $\ddot{\mathbf{U}}$, that appears in Eq. (2.65) will vanish and, the static system of equations takes the well known form

$$\mathbf{K}\,\mathbf{U} = \mathbf{F} \tag{2.66}$$

Solutions of Eq. (2.66) may be obtained by numerous methods and algorithms. Nevertheless, there are essentially two different classes of methods: direct solution techniques and iterative solution methods. For a direct solution of Eq. (2.66) a sequence of steps and operations are predetermined in an exact manner, whereas iteration is used an iterative solution method is employed [2]. For small systems, Gauss elimination and LU decomposition are often used and, for large systems the iterative methods can be much more effective. In fact, these and other methods are available in any library of a finite element program. By solving the Eq. (2.66) the displacements at the finite nodes are obtained and, the strain and stress in any element can be retrieved using Eqs. (2.47) and (1.8), respectively.

2.5 Eigenvalue Analysis

The solution of Eq. (2.65) may be obtained by using the so-called direct integration method. However, a particular solution of this equation is obtained by setting $\mathbf{F} = \mathbf{0}$, which means that the system is free of external force, then the discretized system equation becomes

$$\mathbf{M}\,\ddot{\mathbf{U}} + \mathbf{K}\,\mathbf{U} = \mathbf{0} \tag{2.67}$$

Equation (2.67) is associated with the called dynamic frequency analysis. The solution of this equation can be assumed as

$$\mathbf{U} = \mathbf{\Phi}\sin(\omega t) \tag{2.68}$$

where $\mathbf{\Phi}$ is a vector containing the amplitude of nodal displacements, ω is the frequency of vibration and t is the time. Substituting Eq. (2.68) into Eq. (2.67), is possible to obtain the generalized eigenproblem as

$$\mathbf{K}\,\mathbf{\Phi} = \omega^2\mathbf{M}\,\mathbf{\Phi} \tag{2.69}$$

or

$$(\mathbf{K} - \lambda\,\mathbf{M})\;\mathbf{\Phi} = \mathbf{0} \tag{2.70}$$

with

$$\lambda = \omega^2 \tag{2.71}$$

Equation (2.70) is called the eigenvalue equation, in which a non-zero solution for $\mathbf{\Phi}$ only exist if the determinate of the dynamic matrix vanish, i.e.

$$\det(\mathbf{K} - \lambda\,\mathbf{M}) = |\mathbf{K} - \lambda\,\mathbf{M}| = \mathbf{0} \tag{2.72}$$

Expansion of Eq. (2.72) will lead to a polynomial of λ of order equal to the dimension of the dynamic matrix $(\mathbf{K} - \lambda\,\mathbf{M})$. So, assuming that the dimension of the dynamic matrix is of N, the polynomial equation will have a maximum number of N roots, $\lambda_1, \lambda_2, \ldots, \lambda_N$, called eigenvalues. These values are related to the natural frequencies of the system by Eq. (2.71). The natural frequency is a very important characteristic of a structure; smaller frequencies have associated higher amplitudes of displacement and, therefore, are more dangerous. In fact, it has been found that if a structure is excited by a load with a frequency coincident with one of the structure's natural frequencies, the structure can undergo extremely violent vibration. Moreover, if this excitation prevail in time, it can leads to catastrophic failure of the structural system. Therefore, an eigenvalue analysis has to be performed in designing a structural system that is to be subjected to dynamic loadings.

By substituting an eigenvalue λ_i into Eq. (2.70) leads to

$$(\mathbf{K} - \lambda_i\,\mathbf{M})\;\mathbf{\Phi}_i = \mathbf{0} \tag{2.73}$$

which is a set of algebraic equations. The solution $\mathbf{\Phi}_i$ is called the ith eigenvector that corresponds to the vibration mode associated with the ith vibration frequency.

The vibration mode $\mathbf{\Phi}_i$ gives the shape of the structure when is vibrating at the frequency λ_i. Therefore, analysis of the eigenvalue equation also gives very important information on the possible shape of vibration experienced by the structure. Thus, this kind of analysis can also be used to identify the structure weakness; points with higher amplitude of displacement are weak points that can be structurally reinforced. Mathematically, eingenvectors can be used to construct a transformation basis allowing changing the generalized nodal displacements to generalized modal displacements. This technique is named mode superposition, and is specially indicated to solve Eq. (2.65) that will be discussed in the next section.

Because the mass matrix is symmetric positive definite and the stiffness matrix is also symmetric and either positive or positive semi-definite, the eigenvalues are all real or and either positive or zero. Usually, a zero eigenvalue is possible to obtain only if rigid body movements are allowed and, physically, the corresponding eigenvectors represent these rigid body movements without deformation associated. Moreover, it is possible that the system has coincident eigenvalues and, if there are m coincident eigenvalues, the eigenvalue is said to be of multiplicity of m. Meanwhile, for an eigenvalue of multiplicity m there are m linearly independent eigenvectors. This means that the so-called geometric multiplicity of this eigenvector is also m. For instance, a beam with a circular cross-section is expected to have, at least, two coincident eigenvalues that are associated with two similar shape vibrations in two orthogonal directions.

A great number of numerical methods for the effective computation of the eigenvalues and eigenvectors for an eigenvalue equations systems, as presented in Eqs. (2.72) and (2.73), have been developed. Intensive research has been conducted and many sophisticated algorithms are already available in computational libraries of finite element programs. The commonly used methods are [12]: jacobi's method, Given's method and householder's method, the bisection method, inverse iteration, QR method, subspace iteration, lanczo's method and etc.

Properties of Eigenvectors

The solution of a generalized eigenproblem in the form of Eq. (2.70) yields N eigenvalues $\lambda_1, \lambda_2, \ldots, \lambda_N$ and N corresponding eigenvectors $\mathbf{\Phi}_1, \mathbf{\Phi}_2, \ldots, \mathbf{\Phi}_N$. Each eigenpair $(\lambda_1, \mathbf{\Phi}_1)$ satisfies Eq. (2.73), i.e.

$$\mathbf{K}\mathbf{\Phi}_i = \lambda_i \, \mathbf{M}\mathbf{\Phi}_i \tag{2.74}$$

Equation (2.74) says that if we establish a vector $\lambda_i \mathbf{M}\mathbf{\Phi}_i$ and use it as a load vector $\mathbf{F}$ in the equation $\mathbf{KU} = \mathbf{F}$, then $\mathbf{U} = \mathbf{\Phi}_i$ [2]. Equation (2.74) also shows that an eigenvector is defined only within a multiple of itself, i.e., the relation is also valid

$$\mathbf{K}\,(\alpha\mathbf{\Phi}_i) = \lambda_i \, \mathbf{M}\,(\alpha\mathbf{\Phi}_i) \tag{2.75}$$

where α is a nonzero constant. Equation (2.75) states that if $\mathbf{\Phi}_i$ is an eigenvector then $\alpha\mathbf{\Phi}_i$ is also an eigenvector and, therefore, is possible to say that an eigenvector is

only defined by its direction in the N dimensional space considered. So, in structural mechanics eigenvectors $\mathbf{\Phi}_i$ satisfy Eq. (2.74) and also the relation $\mathbf{\Phi}_i^T \mathbf{M} \mathbf{\Phi}_i = 1$, which fixes the lengths of eigenvectors.

An important relation that eigenvectors should satisfy is the so-called M-orthonormality, i.e.

$$\mathbf{\Phi}_i^T \mathbf{M} \mathbf{\Phi}_j = \delta_{ij}; \quad i,j = 1, \ldots, N \tag{2.76}$$

where δ_{ij} is the Kronecker delta symbol. Premultiplying Eq. (2.74) by $\mathbf{\Phi}_j^T$ and, using the condition at Eq. (2.76), yields

$$\begin{cases} \mathbf{\Phi}_i^T \mathbf{K} \mathbf{\Phi}_j = \lambda_i \; j = i \\ \mathbf{\Phi}_i^T \mathbf{K} \mathbf{\Phi}_j = 0 \; j \neq i \end{cases} \tag{2.77}$$

which means that eigenvectors are also **K**-orthogonal.

2.6 Transient Analysis

The transient analysis of a structural system should be performed whenever the system is subjected to transient excitation. A transient excitation is a time dependent solicitation that is exerted on the structure, which leads to a structural response that is also time dependent. The discrete governing equation system for such a structure is given by Eq. (2.65). However, when the displacements of a flexible body are time dependent several sets of forces play a role on its response. Among these, forces that oppose the motion due to the frictional resistance are related in a nonlinear way with the relative velocity of body points. The structural damping results from material hysteresis and it can be approximated by a proportional damping [13]. Thus, it should be mentioned that the general system equation for a structure with structural damping can be written as

$$\mathbf{M}\,\ddot{\mathbf{U}} + \mathbf{C}\,\dot{\mathbf{U}} + \mathbf{K}\,\mathbf{U} = \mathbf{F} \tag{2.78}$$

where $\dot{\mathbf{U}}$ is the vector of generalized velocity components and **C** is the matrix of damping coefficients that can be determined experimentally.

The finite element damping matrix is often expressed as a linear combination of the stiffness and mass matrices, and is the so-called proportional damping [14], as

$$\mathbf{C} = \alpha \mathbf{K} + \beta \mathbf{M} \tag{2.79}$$

where, for the purpose of Eq. (2.79), α and β are the stiffness and mass proportional damping constants respectively. These parameters can be determined experimentally [15]. However, denoting the damping ratio by ξ the damping constants may be obtained as fractions of the critical damping for a given frequency as [16]

$$\xi_i = \frac{1}{2}\left(\alpha\omega_i + \frac{\beta}{\omega_i}\right) \tag{2.80}$$

Denoting, two fractions of the critical damping ratio by ξ_1 and ξ_2 at two different frequencies ω_1 and ω_2, solving the Eq. (2.80) for the damping constants, are obtained as

$$\begin{aligned} \alpha &= 2\left(\xi_2\omega_2 - \xi_1\omega_1\right) / \left(\omega_2^2 - \omega_1^2\right) \\ \beta &= 2\omega_1\omega_2\left(\xi_1\omega_2 - \xi_2\omega_1\right) / \left(\omega_2^2 - \omega_1^2\right) \end{aligned} \tag{2.81}$$

Mathematically, Eq. (2.78) represents a system of linear differential equations of second order and, in principle, the solution can be obtained by standard procedures suitable for the solution of differential equations with constant coefficients [2]. However, the procedures available for the solution of general systems of differential equations can become very expensive if the order of the system matrices is large, unless specific advantage is taken of the special characteristics of the coefficient matrices, **K**, **C** and **M**. The procedures that will be presented are divided into methods of solution: direct integration and mode superposition. The choice for one method or the other is determined only by their numerical effectiveness.

2.6.1 Direct Integration Methods

In direct integration methods, the Eq. (2.78) is integrated using a numerical step-by-step procedure. The term direct is used to emphasize that before the numerical integration no transformation of Eq. (2.78) is carried out. First, direct numerical integration is based on the solution of Eq. (2.78) only in a set of discrete time intervals Δt. This means that time domain is also discretized in a number of time steps N_t, in which the solution is obtained. Secondly, direct numerical integration is also based in the idea that variations of displacements, velocities and accelerations within each time interval Δt are assumed. In fact, it is the assumption on the variation of displacements, velocities and accelerations within each time interval that determines the accuracy, stability and cost of the solution procedure [2]. Let's assume that the domain time is T, which is subdivided into N_t equal time intervals Δt (i.e. $\Delta t = T_t/N_t$), and the integration scheme employed establishes an approximate solution at times $\Delta t,\ 2\Delta t,\ 3\Delta t, \ldots, t, t + \Delta t, \ldots,\ T$. Because an algorithm calculates the solution at the next required time, $t + \Delta t$, from the solution at the previous times, let assume that solutions are known at $0, \Delta t, 2\Delta t, \ldots, t$ times.

There are two main types of direct integration method: explicit and implicit. In explicit methods the solution of the displacement at time $t + \Delta t$ are obtained by using Eq. (2.78) at time t. On the other hand, implicit integrations methods evaluate displacements at time $t + \Delta t$ by using Eq. (2.78) at time $t + \Delta t$.

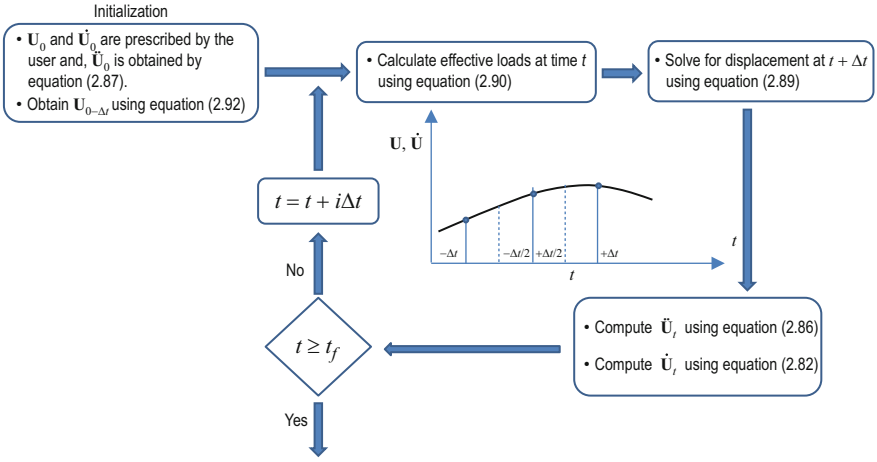

Fig. 2.5 Solution procedure for the central difference algorithm

Central Difference Algorithm

The finite difference equations may be explained with the help of Fig. 2.5, in which the black curve represents the function that is being approximated. The first approximation is associated with the computation of the first derivative of U, defined as

$$\dot{\mathbf{U}}_t = \frac{\mathbf{U}_{t+\Delta t} - \mathbf{U}_{t-\Delta t}}{2\Delta t} \Rightarrow \mathbf{U}_{t+\Delta t} = 2\Delta t\, \dot{\mathbf{U}}_t + \mathbf{U}_{t-\Delta t} \tag{2.82}$$

To find the second derivative, first look at the first derivatives at the half intervals

$$\dot{\mathbf{U}}_{t-\Delta t/2} = \frac{\mathbf{U}_t - \mathbf{U}_{t-\Delta t}}{\Delta t} \tag{2.83}$$

$$\dot{\mathbf{U}}_{t+\Delta t/2} = \frac{\mathbf{U}_{t+\Delta t} - \mathbf{U}_t}{\Delta t} \tag{2.84}$$

The slope between these two points then is:

$$\ddot{\mathbf{U}}_t = \frac{\dot{\mathbf{U}}_{t+\Delta t/2} - \dot{\mathbf{U}}_{t-\Delta t/2}}{\Delta t} \tag{2.85}$$

Substituting Eqs. (2.83) and (2.84) into Eq. (2.85) yields

$$\ddot{\mathbf{U}}_t = \frac{1}{2(\Delta t)^2} \left(\mathbf{U}_{t+\Delta t} - 2\mathbf{U}_t + \mathbf{U}_{t-\Delta t}\right) \tag{2.86}$$

Now, to evaluate the displacement solution at time $t + \Delta t$, let consider Eq. (2.78) written at time t, i.e.

$$\mathbf{M}\,\ddot{\mathbf{U}}_t + \mathbf{C}\,\dot{\mathbf{U}}_t + \mathbf{K}\,\mathbf{U}_t = \mathbf{F}_t \tag{2.87}$$

So, substituting the relations for $\ddot{\mathbf{U}}_t$ and $\dot{\mathbf{U}}_t$ in Eqs. (2.86) and (2.82), respectively, into Eq. (2.87), yields

$$\left(\frac{1}{\Delta t^2}\mathbf{M} + \frac{1}{2\Delta t}\mathbf{C}\right)\mathbf{U}_{t+\Delta t} = \mathbf{F}_t - \left(\mathbf{K} - \frac{2}{\Delta t^2}\mathbf{M}\right)\mathbf{U}_t - \left(\frac{1}{\Delta t^2}\mathbf{M} - \frac{1}{2\Delta t}\mathbf{C}\right)\mathbf{U}_{t-\Delta t} \tag{2.88}$$

For which is possible to solve for $\mathbf{U}_{t+\Delta t}$.

Equation (2.88) is only effective if for each time step the computation can be performed very efficiently. For this reason, the method is largely applied only when a lumped mass matrix can be used and velocity-dependent damping can be neglected [2]. In that case, Eq. (2.88) reduces to

$$\left(\frac{1}{\Delta t^2}\mathbf{M}\right)\mathbf{U}_{t+\Delta t} = \widehat{\mathbf{F}}_t \tag{2.89}$$

where

$$\widehat{\mathbf{F}}_t = \mathbf{F}_t - \left(\mathbf{K} - \frac{2}{\Delta t^2}\mathbf{M}\right)\mathbf{U}_t - \left(\frac{1}{\Delta t^2}\mathbf{M} - \frac{1}{2\Delta t}\mathbf{C}\right)\mathbf{U}_{t-\Delta t} \tag{2.90}$$

If the mass matrix is diagonal, the system of Eq. (2.89) can be solved without factorizing the system matrix, i.e. only matrix multiplications are required to define the right-hand-side, $\widehat{\mathbf{F}}_t$, and the displacement components are obtained by

$$(U_{t+\Delta t})_i = \left(\widehat{F}_t\right)_i \left(\frac{\Delta t^2}{M_{ii}}\right);\ \ i = 1, \ldots, N \tag{2.91}$$

The time step procedure, referred to Fig. 2.5, starts at instant $t = 0$, in which initial conditions $\mathbf{U}_0$ and $\dot{\mathbf{U}}_0$ are known, and the accelerations $\ddot{\mathbf{U}}_0$ are computed using Eq. (2.87). Nevertheless, to evaluate $\mathbf{U}_{0+\Delta t}$ by Eq. (2.89) the vector $\widehat{\mathbf{F}}_0$ must be defined, using $\mathbf{U}_{0-\Delta t}$, in Eq. (2.90). So, eliminating $\mathbf{U}_{t+\Delta t}$ from Eqs. (2.82) and (2.86), leads to

$$\mathbf{U}_{0-\Delta t} = \mathbf{U}_0 - \Delta t\,\dot{\mathbf{U}}_0 + \frac{\Delta t^2}{2}\ddot{\mathbf{U}}_0 \ <?pag?> \tag{2.92}$$

Equation (2.92) is used to define a special starting point and, therefore, the solution it will be stronger influenced by the initial estimation of displacements. Thus, generally, in the solution procedure a relatively small time step size must be used.

The central difference method is conditionally stable; this means that if the time step Δt is larger than a critical value Δt_{cr}, the computed solution will become unstable and might grow without limit. The critical value can be calculated from the mass and stiffness properties of the numerical model [2], i.e.

$$\Delta t \leq \Delta t_c \cong \frac{T_n}{\Pi} = \frac{2}{\omega_n} \tag{2.93}$$

where T_n is the smallest period of the numerical model, in which the dimension of the finite element model is assumed to be n. The period T_n can be calculated solving Eq. (2.70), and considering the higher frequency ω_n available in finite element model. The time steps used in the explicit methods are typically 100–1,000 times smaller than those used with implicit methods [3].

The central difference method is most effective when low-order elements are employed. Hence quadratic 3-D solid and shell elements are not allowed. In the ADINA program the time step can be specified by the user, or calculated automatically [17]. When the user specifies the time, the program does not perform any stability checking. It is the user's responsibility to ensure that an appropriate stable time step is selected. Nevertheless, when automatic time step calculation is selected, the time step entry is only used to determine the number of nominal time steps and the frequency of output results. The stable time step is used instead of the value set by the user unless this value is smaller.

The Wilson θ Algorithm

The Wilson method is an extension of the linear acceleration method and the acceleration is assumed to be liner from time t to time $t + \theta\Delta t$, where $\theta \geq 1.0$ [2]. Obviously, when $\theta = 1.0$ the method reduces to the linear acceleration scheme, but for unconditional stability teat must be higher or equal to 1.37, and usually value of 1.4 is used. The increase in time is denoted by τ, with $0 < \tau \leq \theta\Delta t$, then in the time interval $[t;\ t + \tau]$ it is assumed that

$$\ddot{\mathbf{U}}_{t+\tau} = \ddot{\mathbf{U}}_t + \frac{\tau}{\theta\Delta t}\Delta\ddot{\mathbf{U}} \tag{2.94}$$

Integrating Eq. (2.94) in τ, assuming $\tau = 0$, for time t, and $\tau = \theta\Delta t$, to time $t + \tau$, leads to the velocities equation

$$\int_0^\tau \ddot{\mathbf{U}}_{t+\tau}\, d\tau = \ddot{\mathbf{U}}_t \int_0^\tau d\tau + \frac{\Delta\ddot{\mathbf{U}}}{\theta\Delta t}\int_0^\tau \tau\, d\tau \tag{2.95}$$

$$\dot{\mathbf{U}}_{t+\tau} - \dot{\mathbf{U}}_t = \ddot{\mathbf{U}}_t\tau + \frac{\tau^2}{2\theta\Delta t}\Delta\ddot{\mathbf{U}} \tag{2.96}$$

and, integrating Eq. (2.96)

$$\mathbf{U}_{t+\tau} = \mathbf{U}_t + \dot{\mathbf{U}}_t\tau + \frac{1}{2}\ddot{\mathbf{U}}_t\tau^2 + \frac{\tau^3}{6\theta\Delta t}\Delta\ddot{\mathbf{U}} \tag{2.97}$$

In the upper limit of the time interval, $\tau = \theta\Delta t$, the following equalities are applied

$$\begin{aligned}\ddot{\mathbf{U}}_{t+\theta\Delta t} - \ddot{\mathbf{U}}_t &= \Delta\ddot{\mathbf{U}} \\ \dot{\mathbf{U}}_{t+\theta\Delta t} - \dot{\mathbf{U}}_t &= \Delta\dot{\mathbf{U}} \\ \mathbf{U}_{t+\theta\Delta t} - \mathbf{U}_t &= \Delta\mathbf{U}\end{aligned} \tag{2.98}$$

Using the relations in Eq. (2.98) into Eqs. (2.96) and (2.97) is possible to obtain

$$\dot{\mathbf{U}}_{t+\theta\Delta t} = \dot{\mathbf{U}}_t + \frac{\theta\Delta t}{2}\left(\ddot{\mathbf{U}}_{t+\theta\Delta t} + \ddot{\mathbf{U}}_t\right) \tag{2.99}$$

$$\mathbf{U}_{t+\theta\Delta t} = \mathbf{U}_t + \theta\Delta t\,\dot{\mathbf{U}}_t + \frac{(\theta\Delta t)^2}{6}\left(\ddot{\mathbf{U}}_{t+\theta\Delta t} + 2\ddot{\mathbf{U}}_t\right) \tag{2.100}$$

Equation (2.100) can be used to solve for $\ddot{\mathbf{U}}_{t+\theta\Delta t}$, leading to

$$\ddot{\mathbf{U}}_{t+\theta\Delta t} = \frac{6}{(\theta\Delta t)^2}\left(\mathbf{U}_{t+\theta\Delta t} - \mathbf{U}_t\right) - \frac{6}{(\theta\Delta t)}\dot{\mathbf{U}}_t - 2\ddot{\mathbf{U}}_t \tag{2.101}$$

and, substituting Eq. (2.101) into (2.99) we obtain

$$\dot{\mathbf{U}}_{t+\theta\Delta t} = \frac{3}{\theta\Delta t}\left(\mathbf{U}_{t+\theta\Delta t} - \mathbf{U}_t\right) - 2\dot{\mathbf{U}}_t - \frac{\theta\Delta t}{2}\ddot{\mathbf{U}}_t \tag{2.102}$$

To obtain the solution for the displacements, velocities and accelerations at time $t + \Delta t$, the equilibrium Eq. (2.78) is written at time $t + \theta\Delta t$, as

$$\mathbf{M}\,\ddot{\mathbf{U}}_{t+\theta\Delta t} + \mathbf{C}\,\dot{\mathbf{U}}_{t+\theta\Delta t} + \mathbf{K}\,\mathbf{U}_{t+\theta\Delta t} = \tilde{\mathbf{F}}_{t+\theta\Delta t} \tag{2.103}$$

Notice that in the last equation load vector at time $t+\theta\Delta t$ is linearly extrapolated as

$$\tilde{\mathbf{F}}_{t+\theta\Delta t} = \mathbf{F}_t + \theta\left(\mathbf{F}_{t+\theta\Delta t} - \mathbf{F}_t\right) \tag{2.104}$$

substituting Eqs. (2.101) and (2.102) into Eq. (2.103), we obtain [2]

$$\widehat{\mathbf{K}}\mathbf{U}_{t+\theta\Delta t} = \widehat{\mathbf{F}}_{t+\theta\Delta t} \tag{2.105}$$

where

$$\widehat{\mathbf{K}} = \mathbf{K} + \frac{6}{(\theta\Delta t)^2}\mathbf{M} + \frac{3}{\theta\Delta t}\mathbf{C} \tag{2.106}$$

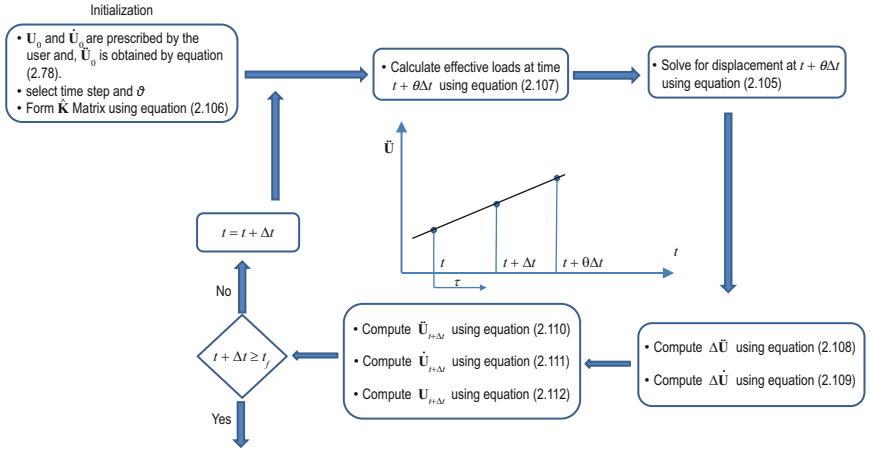

Fig. 2.6 Solution procedure for Wilson-θ algorithm

$$\widehat{\mathbf{F}}_{t+\theta\Delta t} = \tilde{\mathbf{F}}_{t+\theta\Delta t} + \mathbf{M}\left(\frac{6}{(\theta\Delta t)^2}\mathbf{U}_t + \frac{12}{(\theta\Delta t)^2}\dot{\mathbf{U}}_t + 2\ddot{\mathbf{U}}_t\right) + \mathbf{C}\left(\frac{3}{(\theta\Delta t)^2}\mathbf{U}_t + 2\dot{\mathbf{U}}_t + \frac{\theta\Delta t}{2}\ddot{\mathbf{U}}_t\right) \tag{2.107}$$

The complete integration algorithm used within the integration is presented in Fig. 2.6. From the solution of Eq. (2.105) is possible to evaluate the increment on acceleration and velocity by Eqs. (2.101) and (2.102), respectively, as

$$\Delta\ddot{\mathbf{U}} = \ddot{\mathbf{U}}_{t+\theta\Delta\Delta t} - \ddot{\mathbf{U}}_t = \frac{6}{(\theta\Delta t)^2}\left(\mathbf{U}_{t+\theta\Delta t} - \mathbf{U}_t\right) - \frac{6}{(\theta\Delta t)}\dot{\mathbf{U}}_t - 3\ddot{\mathbf{U}}_t \tag{2.108}$$

$$\Delta\dot{\mathbf{U}} = \dot{\mathbf{U}}_{t+\theta\Delta t} - \dot{\mathbf{U}}_t = \frac{3}{\theta\Delta t}\left(\mathbf{U}_{t+\theta\Delta t} - \mathbf{U}_t\right) - 3\dot{\mathbf{U}}_t - \frac{\theta\Delta t}{2}\ddot{\mathbf{U}}_t \tag{2.109}$$

Finally, the accelerations, velocities and displacements for the next time, $t + \Delta t$ are obtained by setting $\tau = \Delta t$ in Eqs. (2.94), (2.96), and (2.97), respectively, leading to

$$\ddot{\mathbf{U}}_{t+\Delta t} = \ddot{\mathbf{U}}_t + \frac{1}{\theta}\Delta\ddot{\mathbf{U}} \tag{2.110}$$

$$\dot{\mathbf{U}}_{t+\Delta t} = \dot{\mathbf{U}}_t + \ddot{\mathbf{U}}_t\Delta t + \frac{\Delta t}{2\theta}\Delta\ddot{\mathbf{U}} \tag{2.111}$$

$$\mathbf{U}_{t+\Delta t} = \mathbf{U}_t + \dot{\mathbf{U}}_t\Delta t + \frac{1}{2}\ddot{\mathbf{U}}_t\Delta t^2 + \frac{\Delta t^2}{6\theta}\Delta\ddot{\mathbf{U}} \tag{2.112}$$

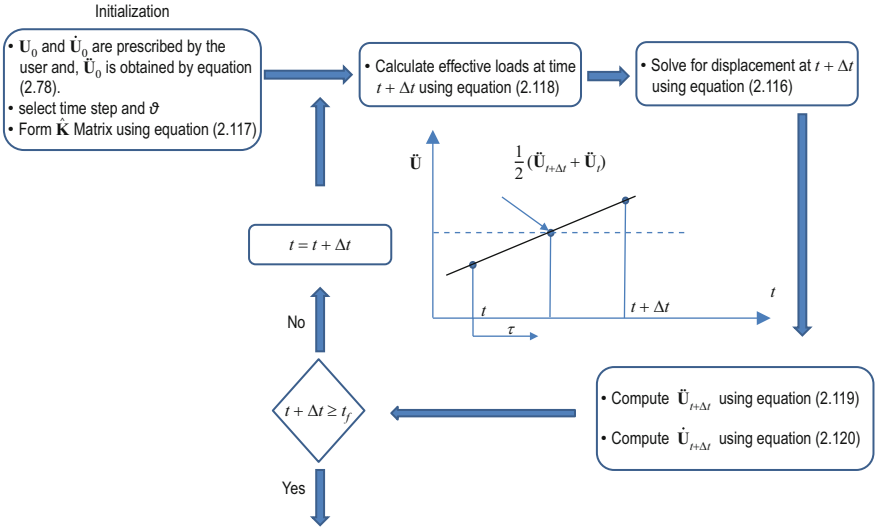

Fig. 2.7 Solution procedure for Newmark algorithm

Because Eqs. (2.110), (2.111), and (2.112) are expressed only in terms of the same quantities at time t, no special starting procedure is needed in the Wilson-θ algorithm. Nevertheless, when big time steps are used, the numerical results obtained by the Wilson-θ algorithm may lead to wrong solutions. This happens because the method suffers from the so-called numerical damping effect, which is characterized by a decrease of displacements, velocities and accelerations that is higher than that observed when structural damping is accounted for.

The Newmark Algorithm

The complete algorithm using the Newmark integration scheme is presented in Fig. 2.7. The Newmark integration scheme is also based on the linear acceleration method and in the following assumptions [2]:

$$\dot{\mathbf{U}}_{t+\Delta t} = \dot{\mathbf{U}}_t + \left[(1-\delta)\,\ddot{\mathbf{U}}_t + \delta\ddot{\mathbf{U}}_{t+\Delta t}\right]\Delta t \tag{2.113}$$

$$\mathbf{U}_{t+\Delta t} = \mathbf{U}_t + \dot{\mathbf{U}}_t\,\Delta t + \left[\left(\frac{1}{2}-\alpha\right)\ddot{\mathbf{U}}_t + \alpha\ddot{\mathbf{U}}_{t+\Delta t}\right]\Delta t^2 \tag{2.114}$$

where α and δ are parameters that can be computed to obtain integration accuracy and stability. When $\delta = 0.5$ and $\alpha = 1/6$ relations (2.113) and (2.114) are coincident with expressions of the linear acceleration method, which is also obtained setting teat equal to one in the Wilson θ method.

Newmark proposed an unconditionally stable scheme, which correspond to the constant-average-acceleration method, in which the values $\delta = 0.5$ and $\alpha = 1/4$

are used. Because it is also an implicit method, the solution of the displacements, velocities and accelerations at time $t + \Delta t$ are obtained writing the equilibrium Eq. (2.78) at this time, i.e.

$$\mathbf{M}\,\ddot{\mathbf{U}}_{t+\Delta t} + \mathbf{C}\,\dot{\mathbf{U}}_{t+\Delta t} + \mathbf{K}\,\mathbf{U}_{t+\Delta t} = \mathbf{F}_{t+\Delta t} \tag{2.115}$$

To write Eq. (2.115) in terms of $\mathbf{U}_{t+\theta\Delta t}$ only; first Eq. (2.114) is used to solve for $\ddot{\mathbf{U}}_{t+\theta\Delta t}$, and then substituting the resulting expression of $\ddot{\mathbf{U}}_{t+\theta\Delta t}$ into Eq. (2.113) leads to expressions of $\ddot{\mathbf{U}}_{t+\theta\Delta t}$ and $\dot{\mathbf{U}}_{t+\theta\Delta t}$ in terms of the unknown displacements $\mathbf{U}_{t+\theta\Delta t}$ only. These two finally relations are substituted into Eq. (2.115) leading to

$$\widehat{\mathbf{K}}\mathbf{U}_{t+\Delta t} = \widehat{\mathbf{F}}_{t+\Delta t} \tag{2.116}$$

where

$$\widehat{\mathbf{K}} = \mathbf{K} + \frac{1}{\alpha\Delta t^2}\mathbf{M} + \frac{\delta}{\alpha\Delta t}\mathbf{C} \tag{2.117}$$

$$\begin{aligned}\widehat{\mathbf{F}}_{t+\Delta t} =& \mathbf{F}_{t+\Delta t} + \mathbf{M}\left(\frac{1}{\alpha\Delta t^2}\mathbf{U}_t + \frac{1}{\alpha\Delta t}\dot{\mathbf{U}}_t + \left(\frac{1}{2\alpha} - 1\right)\ddot{\mathbf{U}}_t\right) \\ &+ \mathbf{C}\left(\frac{\delta}{\alpha\Delta t}\mathbf{U}_t + \left(\frac{1}{\alpha} - 1\right)\dot{\mathbf{U}}_t + \frac{\Delta t}{2}\left(\frac{\delta}{\alpha} - 2\right)\ddot{\mathbf{U}}_t\right)\end{aligned} \tag{2.118}$$

To calculate accelerations and velocities at time $t + \Delta t$ Eqs. (2.113) and (2.114) are used, which leads to

$$\ddot{\mathbf{U}}_{t+\Delta t} = \frac{1}{\alpha\Delta t^2}\left(\mathbf{U}_{t+\Delta t} - \mathbf{U}_t\right) - \frac{1}{\alpha\Delta t}\dot{\mathbf{U}}_t - \left(\frac{1}{2\alpha} - 1\right)\ddot{\mathbf{U}}_t \tag{2.119}$$

$$\dot{\mathbf{U}}_{t+\Delta t} = \dot{\mathbf{U}}_t + \left[(1-\delta)\ \ddot{\mathbf{U}}_t + \delta\ \ddot{\mathbf{U}}_{t+\Delta t}\right]\Delta t \tag{2.120}$$

There is a close relationship between the computer implementation of the Newmark method and the Wilson method, so is quite easily to create a computer program that accepts both methods. Moreover, it can be showed that the Newmark is in general stable when the following constraints are satisfied:

$$\delta \geq 0.5 \tag{2.121}$$

$$\alpha \geq \frac{(\delta + 0.5)^2}{4} \tag{2.122}$$

when the parameter δ is smaller than 0.5 an effect of negative numerical damping is observed.

2.6.2 Mode Superposition Method

The Figs. 2.6 and 2.7 summarize implicit direct integration schemes, in which is possible to see that if a diagonal mass matrix and no damping are assumed, the number of operations for one time step are somewhat larger than $2nm_k$. Where n and m_k are the order and the half-bandwith of the stiffness matrix considered. Notice, that an advantage of the finite element analysis is that the global stiffness matrix is not only symmetric and positive definite but also banded; i.e., $k_{ij} = 0$ for $j > i + m_k$, where m_k is the half-bandwidth of the system. The fact that in finite element analysis all nonzero elements are clustered around the diagonal of the system matrices greatly reduces the total number of operations and the high-speed storage required in the equation solution. Nevertheless, the $2nm_k$ operations are required for the solution of the system equations in each time step [2]. Furthermore, if a consistent mass matrix is used or a damping matrix is included in the analysis, an additional number of operations proportional to nm_k is required per time step. Therefore, neglecting the operations for the initial calculations, a total number of about $\alpha nm_k s$ operations is required in the complete integration, where α depends on the characteristics of the matries used and s is the number of time steps.

Hence, the number of operations required in a direct integration procedure is directly proportional to the order of the stiffness matrix and to the number of time steps. Thus, implicit direct integration can be expected to be effective only when the response for a relatively short duration is required. If the integration must be carried out for many time steps, it may be advantageous to first transform the equilibrium equations, Eq. (2.78), into a form in which the step-by-step solution is less costly.

Modal Transformation

Thus, an alternative way of solving the equilibrium equations is using the so-called modal analysis technique in which the following transformation is used

$$\mathbf{U}\,(\bar{x}_i, t) = \mathbf{\Phi}\,(\bar{x}_i)\ \mathbf{x}(t);\quad i = 1, 2, 3 \tag{2.123}$$

where $\mathbf{\Phi}$ is a $n \times n$ square matrix and $\mathbf{x}(t)$ is a time-dependent vector of order n. The transformation matrix $\mathbf{\Phi}$ will have to be determined and the components of vector $\mathbf{x}(t)$ are referred as generalized displacements. Substituting relation (2.123) into Eq. (2.78) and premultiplying by $\mathbf{\Phi}^T$, leads to

$$\widehat{\mathbf{M}}\,\ddot{\mathbf{x}}(t) + \widehat{\mathbf{C}}\,\dot{\mathbf{x}}(t) + \widehat{\mathbf{K}}\,\mathbf{x}(t) = \widehat{\mathbf{F}} \tag{2.124}$$

where

$$\widehat{\mathbf{M}} = \mathbf{\Phi}^T\mathbf{M}\,\mathbf{\Phi};\quad \widehat{\mathbf{C}} = \mathbf{\Phi}^T\mathbf{C}\,\mathbf{\Phi};\quad \widehat{\mathbf{K}} = \mathbf{\Phi}^T\mathbf{K}\,\mathbf{\Phi};\quad \widehat{\mathbf{F}} = \mathbf{\Phi}^T\mathbf{F} \tag{2.125}$$

The objective of the transformation is to obtain new stiffness, mass and damping matrices $\widehat{\mathbf{K}}$, $\widehat{\mathbf{M}}$ and $\widehat{\mathbf{C}}$ with a smaller bandwidth than the original system matrices and, therefore, matrix $\mathbf{\Phi}$ should be selected accordingly. In addition, matrix $\mathbf{\Phi}$ must be non-singular in order to have a unique relation (2.123). In fact, in theory, there can be many different transformation matrices that would reduce the bandwidth of the system matrices. However, an effective transformation matrix is established using the displacement solutions of the free-vibration equilibrium equations with damping neglected, which is defined by Eq. (2.67) and, leads to the solution of the generalized eigenproblem in Eq. (2.69). So, let's assume that matrix $\mathbf{\Phi}$ is composed by the n eigenvectors $\mathbf{\Phi}$ that form the solution of Eq. (2.69). Moreover, let's defining a diagonal matrix $\boldsymbol{\lambda}$, which stores the eigenvalues λ_i on its diagonal, i.e.

$$\mathbf{\Phi} = \left[\mathbf{\Phi}_1\ \mathbf{\Phi}_2\ \ldots\ \mathbf{\Phi}_n\right]; \qquad \boldsymbol{\lambda} = \begin{bmatrix} \lambda_1 & 0 & 0 & 0 \\ 0 & \lambda_2 & 0 & 0 \\ 0 & 0 & \ddots & 0 \\ 0 & 0 & 0 & \lambda_n \end{bmatrix} \tag{2.126}$$

and, since the eigenvectors satisfy the so-called $\mathbf{M}$-orthonormality, the following relations are valid

$$\widehat{\mathbf{M}} = \mathbf{\Phi}^T \mathbf{M}\ \mathbf{\Phi} = \mathbf{I}; \quad \widehat{\mathbf{K}} = \mathbf{\Phi}^T \mathbf{K}\ \mathbf{\Phi} = \boldsymbol{\lambda} \tag{2.127}$$

Using matrix $\mathbf{\Phi}$ defined in Eq. (2.126) into Eq. (2.123) allow to describe the nodal displacements of the flexible body by a weighted sum of its modes of vibration.

Substituting relations Eqs. (2.126) and (2.127) into Eq. (2.124), we obtain equilibrium equations that correspond to the modal generalized to the modal generalized displacements

$$\ddot{\mathbf{x}}(t) + \widehat{\mathbf{C}}\ \dot{\mathbf{x}}(t) + \boldsymbol{\lambda}\ \mathbf{x}(t) = \widehat{\mathbf{F}} \tag{2.128}$$

The initial conditions on $\mathbf{x}(t)$ are obtained using (2.123) and the $\mathbf{M}$-orthonormality of $\mathbf{\Phi}$, i.e., at initial time we get

$$\mathbf{x}\,(t=0) = \mathbf{\Phi}^T \mathbf{M}\ \mathbf{U}_0; \quad \dot{\mathbf{x}}\,(t=0) = \mathbf{\Phi}^T \mathbf{M}\ \dot{\mathbf{U}}_0 \tag{2.129}$$

The Eq. (2.128) show that if a damping matrix is not included in the analysis, the finite element equilibrium equations are decoupled.

Modal Analysis Without Damping Effect

Since, the derivation of the damping matrix cannot be carried out explicitly and, therefore, the damping effects can be included only approximately, in many cases damping effects are neglected.

So, if velocity-dependent damping effects are not included in the analysis, Eq. (2.128) reduces to

$$\ddot{\mathbf{x}}(t) + \boldsymbol{\lambda}\ \mathbf{x}(t) = \widehat{\mathbf{F}} \tag{2.130}$$

Equation (2.130) represents a system of n individual equations of the form

$$x_i(t) + \lambda_i x_i(t) = \widehat{f}_i(t);\quad \widehat{f}_i(t) = \boldsymbol{\Phi}_i^T \mathbf{F}(t);\quad i = 1, 2, \ldots, n \tag{2.131}$$

with

$$\begin{aligned} x_i|_{,t=0} &= \boldsymbol{\Phi}_i^T \mathbf{M}\ \mathbf{U}_0 \\ \dot{x}_i|_{,t=0} &= \boldsymbol{\Phi}_i^T \mathbf{M}\ \dot{\mathbf{U}}_0 \end{aligned} \tag{2.132}$$

Notice that each *i*th equation in Eq. (2.131) is the equilibrium equation of a single degree of freedom system with unit mass and stiffness λ_i, which solution can be obtained using the integration algorithms presented previously. Nevertheless, for the complete response, the solution of all *n* equations in Eq. (2.131) must be calculated and then the finite element nodal point displacements are obtained by superposition of the response in each modal degree of freedom, i.e.

$$\mathbf{U}(t) = \sum_{i=1}^{n} \boldsymbol{\Phi}_i x_i(t) \tag{2.133}$$

Notice that if time integration methods used on the direct integration procedures are the same used in the direct integration and in the solution of Eq. (2.131), the solutions obtained using both procedures are identical. In fact, the only difference between a mode superposition and a direct integration analysis is that prior to the time integration, a change of basis is carried out by Eq. (2.123) and, since mathematically the same space is spanned by the *n* eigenvectors as by the *n* nodal points, the same solution must be obtained in both analyses. The choice of whether to use direct integration or mode superposition will therefore decided by considerations of effectiveness only [2]. This aspect is related with the fact that frequently only a small fraction of the total number of decoupled equations, Eq. (2.131), needs to be considered in order to obtain a good approximate solution to the exact solution.

Actually, it will be the frequency content of the loading that determines whether the *i*th equation in Eq. (2.131), which is associated the *i*th frequency of system vibration, will contribute significantly to the response **U**(t). To clarify this idea, let's consider a one degree of freedom system with the following equilibrium equation

$$\ddot{x}(t) + w^2 x(t) = A \sin(\widehat{w}t) \tag{2.134}$$

where A and $\hat{w}$ are the amplitude and the frequency of excitation. The solution of Eq. (2.134) to the initial conditions $x(0) = 0$ and $\dot{x}(0) = 0$, can be written as [2]

$$x(t) = D\ x_{stat} + x_{trans} \tag{2.135}$$

with

$$D = \frac{1}{1-(\widehat{w}/w)^2}; \quad x_{stat} = \frac{A}{w^2}\sin(\widehat{w}t); \quad x_{trans} = \left(\frac{1}{w} - \frac{A\widehat{w}/w^3}{1-(\widehat{w}/w)^2}\right)\sin(wt) \tag{2.136}$$

where D is the dynamic load factor, x_{stat} is the steady state response of the system and x_{trans} is the transient response. The dynamic load factor grows to infinite when $\widehat{w} = w$, indicating resonance.

Equation (2.135) shows that the complete response of a single degree of freedom system is the sum of two contributions [2]:

- A dynamic response defined by multiplying the steady state response by a dynamic load factor;
- An additional dynamic response which can be called the transient response.

Notice that these observations may be applied in the analysis of a multiple degrees of freedom system, since the complete response of these systems is obtained as a superposition of the response measured in each modal degree of freedom (as presented in Eq. (2.133)) and, secondly, loads can be represented in a Fourier decomposition as a sum of harmonic sine and cosine contributions. Figure 2.8 shows the variation of the dynamic load factor as a function of quotient $\hat{w}/w$, in which is possible to observe that no damping is used and, therefore, resonance appears to the unity value of this quotient. Moreover, is possible to recognize that in the modes for which the relation $\hat{w}/w$ is large the dynamic load factor is negligible, while for modes in which the relation $\hat{w}/w$ is close to zero the dynamic load factor is significant and the static response is measured for this case. These behavior may be justified by the fact that when loads vary rapidly the system is not able to follow this variation whereas a slow load variation allows to systems track almost statically this variation. Therefore, in the analysis of a multiple degree of freedom system, the response associated with the frequencies of the system that are much larger than the highest frequencies contained in the loads is simply a small static response.

Frequently, only the first p equilibrium equations in Eq. (2.131) need to be included in the analysis, in order to obtain a good approximate solution. This means that the response in Eq. (2.123) is obtained by summing the contribution of the first p modes only, i.e.

$$\mathbf{U}^p(t) = \sum_{i=1}^{p} \mathbf{\Phi}_i x_i(t); \quad p \leq n \tag{2.137}$$

where $\mathbf{U}^p$ approximate the exact solution $\mathbf{U}$ of (2.123). Hence, is primarily because of the fact that in a mode superposition analysis only a few modes may need to be considered that the mode superposition procedure can be much more effective than direct integration [2]. However, it also follows that the effectiveness of mode superposition depends on the number of modes that need to be included in the

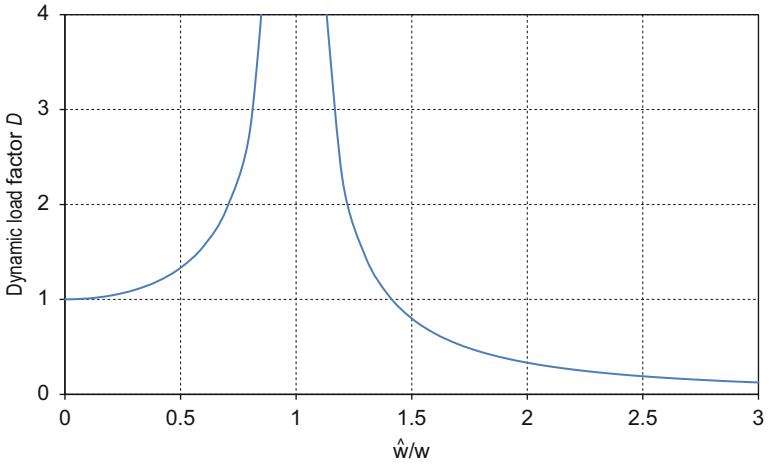

Fig. 2.8 Dynamic load factor

analysis. In general, the kind of structure considered and the spatial distribution and the frequency content of the loading determine the number of modes to be used.

Frequently, is true that only the first p equilibrium equations in Eq. (2.131) need to be included in the analysis, but it should always be kept in mind that an approximate solution of Eq. (2.124) is sought. Meaning that if not enough modes are considered, the solution of latter equation is not hundred percent correct. So an indication of the accuracy of analysis at any time t can be obtained evaluating an error measure ε^p, such as [2]

$$\varepsilon^p(t) = \frac{\left\| \mathbf{F}(t) - \left(\mathbf{M}\ddot{\mathbf{U}}^p(t) + \mathbf{K}\mathbf{U}^p(t) \right) \right\|}{\|\mathbf{F}\|_2} \tag{2.138}$$

where the condition $\|\mathbf{F}\|_2 \neq 0$ is assumed. If a good approximate solution has been obtained, the error in Eq. (2.138) will be small at any time t. If not, a possible error is due to not including enough modes in the analysis. The error in Eq. (2.138) determines how well equilibrium is satisfied and is a measure of how much the nodal point loads are not balanced by inertia and elastic nodal point forces. Alternatively, ε^p can be seen as a measure of the part of the external load vector that has not be included in the mode superposition analysis [2]. Since is possible to evaluate

$$\Delta\mathbf{F} = \mathbf{F} - \sum_{i=1}^{p} \widehat{f}_i \, (\mathbf{M}\boldsymbol{\Phi}_i) \tag{2.139}$$

Where $\widehat{f}_i$ is defined in Eq. (2.131) and is evaluated at each correction step. Assuming a properly modeled problem, the response to the load vector defined in Eq. (2.139) should be at most a static response. Therefore, a good correction $\Delta\mathbf{U}$ to the solution

$\mathbf{U}^p$ can be obtained from

$$\mathbf{K}\Delta\mathbf{U} = \Delta\mathbf{F} \tag{2.140}$$

The solution of Eq. (2.140) is called the static correction.

Modal Analysis Including Damping
Considering the analysis of systems in which the damping effect is included, the mode superposition analysis is particularly effective if it is assumed that damping is proportional, in that case the following relation is valid

$$\begin{cases} c\boldsymbol{\Phi}_i^T\mathbf{C}\boldsymbol{\Phi}_j = 2\omega_i\xi_i;\ j = i \\ \boldsymbol{\Phi}_i^T\mathbf{C}\boldsymbol{\Phi}_j = 0; \qquad j \neq i \end{cases} \tag{2.141}$$

where ξ_i is the damping ratio associated with the ith frequency. Equation (2.141) states that the eigenvectors $\boldsymbol{\Phi}_i$ are also **C**-orthogonal. The assumption of Eq. (2.141) means that the total damping in the structure is accounted as the sum of individual damping in each mode. The damping ratio on one mode could be experimentally evaluated, for example, by imposing initial conditions that excite the structure on that mode only (say $\mathbf{U}_0 = \boldsymbol{\Phi}_i$) and measuring the amplitude decay during the experimental vibration.

Substituting Eq. (2.141) into Eq. (2.128), is possible to reduce Eq. (2.128) to a system of n individual equations of the form

$$x_i(t) + 2\omega_i\xi_i\dot{x}_i(t) + \lambda_i x_i(t) = \widehat{f}_i(t);\quad \widehat{f}_i(t) = \boldsymbol{\Phi}_i^T\mathbf{F}(t);\quad i = 1, 2, \ldots, n \tag{2.142}$$

the initial conditions on $x_i(t)$ have already been defined in Eq. (2.132). Once more, is possible to constant that Eq. (2.139) represent the equilibrium equation governing the motion of the single degree of freedom system considered in Eq. (2.131) with the additional term related with damping ratio ξ_i. The solution procedure of Eq. (2.142) is the same as in the case when damping is neglected, except that the response in each mode is obtained by a different equation.

Nevertheless, as in the case of using direct step-by-step integration procedures, it can be numerically more efficient to evaluate matrix **C** explicitly and, then substituted into Eq. (2.141) yielding to damping ratios ξ_i. If two damping ratios can be assumed, the Rayleigh damping defined by Eq. (2.79) can be used, where α and β can determined from the two given ratios as defined by Eq. (2.81). However, it may be well that the damping ratios are known for many more than two frequencies. In that case two average values, say $\overline{\xi}_1$ and $\overline{\xi}_2$, are used to evaluate α and β [2].

2.6.3 Practical Considerations

Effective solutions of dynamic problems require an appropriate selection of time integration scheme and, because this choice depends on the finite element idealiza-

tion of the physical problem to be analyzed, the choice of an integration scheme and the finite element model are closely related and must be considered together.

The selection of an appropriate finite element model for structural dynamic analysis requires the concept that only the lowest vibration modes of a physical system are being excited by the external load vector. So, assuming that the Fourier analysis of a dynamic external load includes only frequencies below w_l, the finite element model should at most represent accurately the frequencies of the system that are below the cutoff frequency $w_{co} = 4 \times w_l$ [2]. In fact, in Fig. 2.8 it can be seen that for values of $\widehat{w}/w \ (= w_l/w_{co})$ smaller than 0.25 an almost static response is measured and is this response is directly included in the direct integration step-by-step dynamic response calculations. Moreover, in Eq. (2.136) is possible to observe that the static displacement response in the highest frequencies is small, thus when the static response is small it may well be expedient to use $w_{co} = w_l$ [2].

The complete procedure for the modeling of a structural vibration problem is therefore [2]:

- Identify the significantly frequencies contained in the loading, even that those frequencies change as a function of time, consider that that the highest significant frequency contained in the loading be w_l.
- Chose a finite element model that can accurately represent all frequencies up to about $w_{co} = 4 \times w_l$.
- Perform the direct integration analysis using a time step that should equal about $\frac{1}{20}T_{co}$, where $T_{co} = 2\pi/w_{co}$.

If the later step is performed by mode superposition method, then the cutoff frequency would be the highest frequency to be included in the solution.

References

1. Zienkiewicz OC, Morgan K (1983) Finite elements and approximation. Wiley, New York
2. Bathe K-J (1996) Finite element procedures. Prentice Hall, Englewood Cliffs
3. Liu GR, Quek SS (2003) The finite element method: a practical course. Butterworth-Heinemann, Amsterdam
4. Hwang WS, Park HC (1993) Finite element modeling of piezoelectric sensors and actuators. AIAA J 31:930–937
5. Neto MA, Leal RP, Yu W (2012) A triangular finite element with drilling degrees of freedom for static and dynamic analysis of smart laminated structures. Comput Struct 108–109:61–74. doi:10.1016/j.compstruc.2012.02.014
6. Baddour N (2007) Hamilton's principle for the derivation of equations of motion. http://www.academia.edu/164428/Hamiltons_Principle_for_the_Derivation_of_Equations_of_Motion
7. Wang SY (2004) A finite element model for the static and dynamic analysis of a piezoelectric bimorph. Int J Solids Struct 41(15):4075–4096. doi:10.1016/j.ijsolstr.2004.02.058
8. Tzou HS (1993) Piezoelectric shells. In: Solid mechanics and its applications. Kluwer Academic Publishers, Dordrecht
9. GID Manual de Utilización C (2014) http://www.gidhome.com/home
10. Femap SPs (2014) http://www.plm.automation.siemens.com/en_us/products/femap/
11. Knupp PM (2007) Remarks on mesh quality. Paper presented at the 45th AIAA aerospace sciences meeting and exhibit, Reno, 7–10 Jan 2007

12. Lee N-S, Bathe K-J (1993) Effects of element distortions on the performance of isoparametric elements. Int J Numer Methods Eng 36(20):3553–3576. doi:10.1002/nme.1620362009
13. Zienkiewicz OC, Taylor RL (2000) The finite element method. Butterworth-Heinemann, Boston
14. Cook RD, Malkus DS, Plesha ME (1989) Concepts and applications of finite elements analysis. Willey, New York
15. Chapra SC, Canalae RP (2010) Numerical methods for engineers. McGraw-Hill, Boca Raton
16. Craig RR (1981) Structural dynamics: an introduction to computer methods. Wiley, New York
17. ADINA R & D I (2014) User's manual. R&D Inc., Boston

Chapter 3
Finite Element Method for Trusses

A truss is a structural element that is designed to support only axial forces, therefore it deforms only in its axial direction. The cross-section of the bar can have arbitrary geometry, but its dimensions should be much smaller than the bar length. Finite element developments for truss members will be performed in this chapter. The simplest and most widely used finite element for truss structures is the well-known truss or bar finite element with two nodal points. Such kind of finite elements are applicable for analysis of skeletal type of truss structural systems both in two-dimensional and three-dimensional space. Basic concepts, procedures and formulations can also be found in a great number of existing books [1–3]. In skeletal structures consisting of truss members, the truss elements are linked by pins or hinges, without any friction, so there are only forces that transmitted among bars, which means that no moments are transmitted. In the presentation of this concept it will be assumed that truss elements have uniform cross-section. These concepts can be easily extended to treat bars with varying cross-section. Moreover, from the mechanical viewpoint, there is no reason to use bars with a varying cross-section since the force in a bar is uniform.

3.1 FE Matrices and Vectors of Trusses

3.1.1 Degrees of Freedom Identification

The application of the finite element method involves dividing the domain into subdomains with features and loading that are simple to treat. In the case of a structure consisting of trusses or bar elements, let's consider that each structural element has constant elastic properties and uniform cross-section. Moreover, let's assume that each of these structural elements is bounded by two nodes ($n = 2$).

M.A. Neto et al., *Engineering Computation of Structures: The Finite Element Method*, DOI 10.1007/978-3-319-17710-6_3

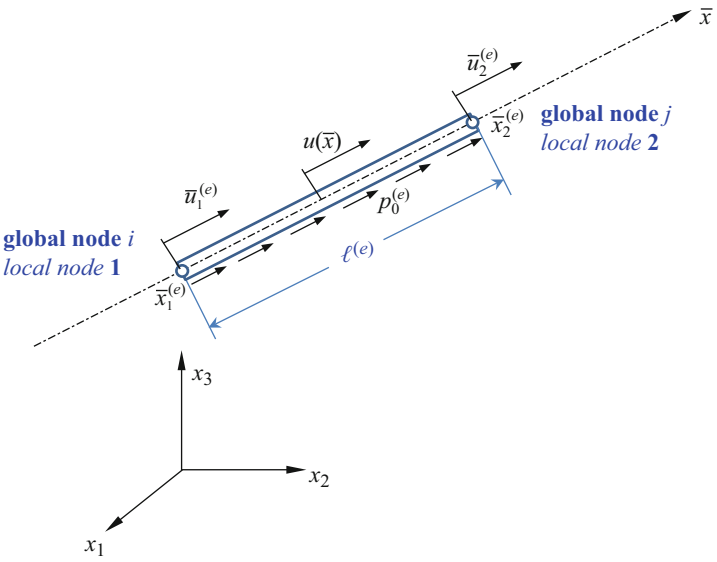

Fig. 3.1 Truss finite element with two degrees of freedom

Consider the bar divided into m finite elements from which the element (e) is highlighted, as presented in Fig. 3.1, the extreme points of this element are called nodal points and are identified by their coordinate $\bar{x}_1^{(e)}$ and $\bar{x}_2^{(e)}$ along the local axis $\bar{x}$, which is coincident with the bar axis and has the origin at the first node.

Due to the axial loading, there is only one degree of freedom at each node that is the axial displacement. Therefore, there is a total of two DOFs for the finite element.

3.1.2 FE Approximation of the Displacement

Taking in account the FEM discussed in the previous chapter, the displacement within a finite element should be written in the form

$$\tilde{u}\left(\bar{x}\right) = \overline{\mathbf{N}}\left(\bar{x}\right)\bar{\mathbf{u}} \tag{3.1}$$

where $\tilde{u}$ is the axial approximation within the finite element (e), $\overline{\mathbf{N}}$ is a matrix of shape functions with the inherent properties described in Chap. 2 and $\bar{\mathbf{u}}$ is the vector of finite element displacements, defined as

$$\bar{\mathbf{u}} = \begin{bmatrix} \bar{u}_1 \\ \bar{u}_2 \end{bmatrix} \tag{3.2}$$

Construction of shape functions, to the truss element, follows the standard procedure described in Sect. 2.3.3. Thus, because there are only two DOFs, i.e. only two unknowns, a complete basis of order $p = 1$ can be given in a general form

$$\tilde{u}(\bar{x}) = a_0 + a_1\bar{x} = \underbrace{\begin{bmatrix} 1 & \bar{x} \end{bmatrix}}_{\mathbf{\Phi}^T} \underbrace{\begin{bmatrix} a_0 \\ a_1 \end{bmatrix}}_{\mathbf{a}} = \mathbf{\Phi}^T\mathbf{a} \tag{3.3}$$

where $\bar{x}_1^{(e)} \leq \bar{x} \leq \bar{x}_2^{(e)}$. Note that the polynomial order of the basis function depends on to the number of nodes and degrees of freedom per node that are used to approximate the displacement $\tilde{u}$. Because of the consistency property of shape functions discussed in Sect. 2.3.4, polynomial basis function should be of a complete order. If a polynomial basis of the kth order is skipped, the shape function constructed will only be able to ensure consistency until (k-1)th order, regardless of how many higher orders of monomials are included in the basis [4]. Due to the fact that the finite element (e) is connected to the neighbor's finite elements by its nodes, the solution given by Eq. (3.3) can be admissible only if the support conditions in the nodal points are verified, i.e. the displacements of nodal points should be

$$\begin{aligned} \tilde{u}(\bar{x} = 0) &= u_1 \\ \tilde{u}(\bar{x} = \ell) &= u_2 \end{aligned} \tag{3.4}$$

Using Eq. (3.3), we have

$$\underbrace{\begin{bmatrix} \bar{u}_1 \\ \bar{u}_2 \end{bmatrix}}_{\bar{\mathbf{u}}} = \underbrace{\begin{bmatrix} 1 & 0 \\ 1 & \ell \end{bmatrix}}_{\mathbf{C}} \underbrace{\begin{bmatrix} a_0 \\ a_1 \end{bmatrix}}_{\mathbf{a}} \tag{3.5}$$

Solving Eq. (3.5) for parameters $\mathbf{a}$, leads to

$$\underbrace{\begin{bmatrix} a_0 \\ a_1 \end{bmatrix}}_{\mathbf{a}} = \underbrace{\begin{bmatrix} 1 & 0 \\ -1/\ell & 1/\ell \end{bmatrix}}_{\mathbf{C}^{-1}} \underbrace{\begin{bmatrix} u_1 \\ u_2 \end{bmatrix}}_{\bar{\mathbf{u}}} \tag{3.6}$$

Substituting Eq. (3.6) into Eq. (3.3), leads to

$$\tilde{u}(\bar{x}) = \mathbf{\Phi}^T \mathbf{a} = \underbrace{\begin{bmatrix} 1 & \bar{x} \end{bmatrix}}_{\mathbf{\Phi}^T} \underbrace{\begin{bmatrix} 1 & 0 \\ -1/\ell & 1/\ell \end{bmatrix}}_{\mathbf{C}^{-1}} \underbrace{\begin{bmatrix} u_1 \\ u_2 \end{bmatrix}}_{\bar{\mathbf{u}}} = \underbrace{\begin{bmatrix} \underbrace{1-\bar{x}/\ell}_{N_1(\bar{x})} & \underbrace{\bar{x}/\ell}_{N_2(\bar{x})} \end{bmatrix}}_{\overline{\mathbf{N}}(\bar{x})} \underbrace{\begin{bmatrix} u_1 \\ u_2 \end{bmatrix}}_{\bar{\mathbf{u}}} = \overline{\mathbf{N}}(\bar{x})\,\bar{\mathbf{u}} \tag{3.7}$$

In Eq. (3.7) is possible to see the shape functions for the finite element truss. Thus, the shape matrix is then obtained as

$$\overline{\mathbf{N}}(\bar{x}) = \begin{bmatrix} N_1(\bar{x}) & N_2(\bar{x}) \end{bmatrix} \tag{3.8}$$

where the shape functions for a truss element can be written as

$$N_1(\bar{x}) = 1 - \frac{\bar{x}}{\ell} \tag{3.9}$$

$$N_2(\bar{x}) = \frac{\bar{x}}{\ell} \tag{3.10}$$

We obtain two shape functions because the number of DOFs of the finite element is also of two. Figure 3.2 shows the graphical representation of Eqs. (3.9) and (3.10).

From Fig. 3.2, it is clear that function N_i gives the shape of the contribution of the ith degree of freedom to the displacement approximation within the finite element. Moreover, the maximum contribution is verified at the node where the ith degree of freedom is located, where its value is the unity. In this case, the shape functions vary linearly across the element and, therefore, are called linear shape functions. Substituting Eqs. (3.9), (3.10), into Eq. (3.7), leads to

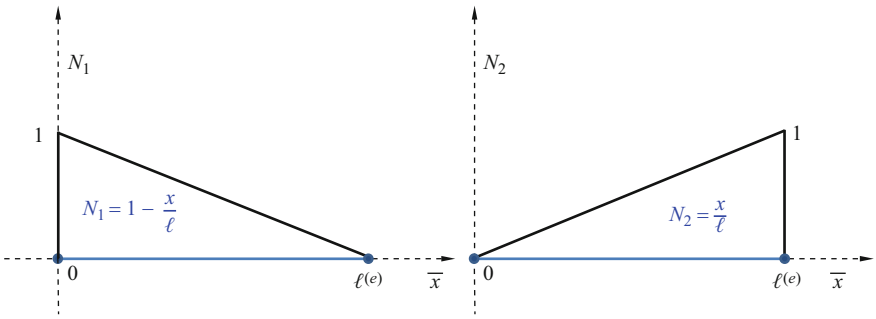

Fig. 3.2 Linear shape function for the truss finite element with two degrees of freedom

$$\tilde{u}\left(\overline{x}\right) = N_1\left(\overline{x}\right) + N_2\left(\overline{x}\right) = u_1 + \left(u_2 - u_1\right)\frac{\overline{x}}{\ell} \tag{3.11}$$

Equation (3.11) clearly states that the displacement within the finite element varies linearly.

3.1.3 FE Approximation of Strain

The approximation of the element displacements allows the evaluation of other quantities, namely element strains and stresses. As discussed in Chap. 1 within Sect. 1.3.1, in a truss there are only one strain and stress components. The corresponding strain can be obtained as

$$\tilde{\varepsilon}_{11}\left(\overline{x}\right) = \frac{d\tilde{u}\left(\overline{x}\right)}{d\overline{x}} = \frac{u_2 - u_1}{\ell} \tag{3.12}$$

Equation (3.12) results from the direct differentiation of Eq. (3.11) with respect to $\overline{x}$. This equation shows that strain is constant over the finite element.

Meanwhile, in the previous chapter it was showed that the stiffness matrix is obtained using the finite element strain matrix, **B**. In the case of a truss finite element, this can be easily done. Thus, Eq. (3.12) can be re-written in a matrix form as

$$\tilde{\varepsilon}_{11}\left(\overline{x}\right) = \frac{d\tilde{u}\left(\overline{x}\right)}{d\overline{x}} = L\,\overline{\mathbf{N}}\,\overline{\mathbf{u}} = \overline{\mathbf{B}}\,\overline{\mathbf{u}} \tag{3.13}$$

where the strain matrix $\overline{\mathbf{B}}$ has the following form

$$\overline{\mathbf{B}} = L\overline{\mathbf{N}} = \frac{d}{d\overline{x}}\left[\,1 - \tfrac{\overline{x}}{\ell}\;\; \tfrac{\overline{x}}{\ell}\,\right] = \frac{1}{\ell}\left[\,-1\;\; 1\,\right] \tag{3.14}$$

3.1.4 Element Matrices in Local Coordinate System

The stiffness matrix for truss finite elements can be obtained using Eq. (2.49) from the previous chapter, leading to

$$\overline{\mathbf{k}} = \int_{\Omega^e} \overline{\mathbf{B}}^T \mathbf{c}\,\overline{\mathbf{B}}\,d\Omega^e = A\int_0^{\ell} \begin{bmatrix} -\frac{1}{\ell} \\ \frac{1}{\ell} \end{bmatrix} E \left[\,-\tfrac{1}{\ell}\;\; \tfrac{1}{\ell}\,\right] d\overline{x} = \frac{AE}{\ell}\begin{bmatrix} 1 & -1 \\ -1 & 1 \end{bmatrix} \tag{3.15}$$

where A is the cross-section area of the truss finite element. Note that for the one-dimensional truss structure, the material constant matrix **c** reduce to elastic modulus, E, see Eq. (1.86) in Sect. 1.3.1 of Chap. 1. Because the stiffness matrix on Eq. (3.15) is symmetric, during the finite element computation, only half of the terms in the matrix need to be evaluated and stored.

The mass matrix for the truss elements can be obtained using Eqs. (3.8) and (2.45):

$$\overline{\mathbf{m}} = \int_{\Omega^e} \rho \overline{\mathbf{N}}^T \overline{\mathbf{N}} \, d\Omega^e = A\rho \int_0^{\ell} \begin{bmatrix} 1 - \frac{\bar{x}}{\ell} \\ \frac{\bar{x}}{\ell} \end{bmatrix} \begin{bmatrix} 1 - \frac{\bar{x}}{\ell} & \frac{\bar{x}}{\ell} \end{bmatrix} d\bar{x}$$

$$= A\rho \int_0^{\ell} \begin{bmatrix} \left(1 - \frac{\bar{x}}{\ell}\right)^2 & \left(1 - \frac{\bar{x}}{\ell}\right)\frac{\bar{x}}{\ell} \\ \left(1 - \frac{\bar{x}}{\ell}\right)\frac{\bar{x}}{\ell} & \left(\frac{\bar{x}}{\ell}\right)^2 \end{bmatrix} d\bar{x} = \frac{A\rho\ell}{6} \begin{bmatrix} 2 & 1 \\ 1 & 2 \end{bmatrix} \tag{3.16}$$

The mass matrix is found to be also symmetrical.

The nodal force vector for truss elements can be obtained using Eqs. (3.8) and (2.52), assuming that the element is loaded by a constant distributed force p_0 along the $\bar{x}$- axis, and two concentrated forces f_{c1} and f_{c2} at two nodes 1 and 2, respectively. Thus, the total nodal force vector becomes

$$\bar{\mathbf{f}} = \int_{\Omega^e} \overline{\mathbf{N}}^T \mathbf{f}_b \, d\Omega^e + \sum_{i=1}^{2} \overline{\mathbf{N}}^T \mathbf{f}_i^c = p_0 \int_0^{\ell} \begin{bmatrix} 1 - \frac{\bar{x}}{\ell} \\ \frac{\bar{x}}{\ell} \end{bmatrix} d\bar{x} + \begin{bmatrix} N_1 \, (\bar{x} = 0) f_{c1} \\ N_2 \, (\bar{x} = \ell) f_{c2} \end{bmatrix}$$

$$= \frac{p_0 \ell}{2} \begin{bmatrix} 1 \\ 1 \end{bmatrix} + \begin{bmatrix} f_{c1} \\ f_{c2} \end{bmatrix} \tag{3.17}$$

3.1.5 Element Matrices in the Global Coordinate System

Element matrices presented before are formulated in the local coordinate system, in which the $\bar{x}$-axis coincides with the axis of the finite element bar. Nevertheless, in practical problems there are many bars with a different orientation with respect to the reference coordinate system and, therefore, to assemble all the element matrices is strictly necessary to define these matrices in only one coordinate system that is the global coordinate system. Thus a coordinate system transformation has to be performed for each finite element to formulate its element matrices on the global coordinate system.

3D Trusses

Let's assume that local nodes 1 and 2 of the finite element correspond to the global nodes i and j, respectively, as shown in Fig. 3.3. The local displacement at each finite element node may be projected into the global coordinate system $(x_i;\ i = 1, 2, 3)$ leading to global displacement components $\left(u_j^{(e)};\ j = 1, 2, \ldots, 6\right)$. The global displacement at one node in space should have three components in the x_1, x_2 and x_3 directions, and should be numbered sequentially.

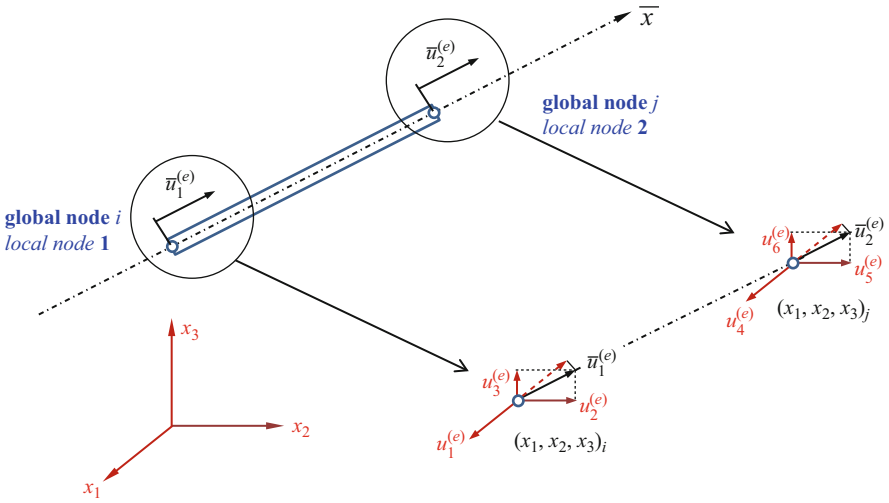

Fig. 3.3 Local and global coordinate systems in the truss finite element

The coordinate transformation gives the relationship between the nodal displacement vector $\bar{\mathbf{u}}$ based on the local coordinate system and the nodal displacement vector $\mathbf{u}$, for the same finite element, based on the global coordinate system $(x_i;\ i = 1, 2, 3)$

$$\bar{\mathbf{u}} = \mathbf{T}\,\mathbf{u} \tag{3.18}$$

with

$$\mathbf{u} = \begin{bmatrix} u_1^{(e)} \\ u_2^{(e)} \\ u_3^{(e)} \\ u_4^{(e)} \\ u_5^{(e)} \\ u_6^{(e)} \end{bmatrix} \tag{3.19}$$

and $\mathbf{T}$ is the transformation matrix for the truss element, given by

$$\mathbf{T} = \begin{bmatrix} l_{ij} & m_{ij} & n_{ij} & 0 & 0 & 0 \\ & & & l_{ij} & m_{ij} & n_{ij} \end{bmatrix} \tag{3.20}$$

where

$$\begin{aligned} l_{ij} &= \cos(\bar{x}, x_1) = \frac{(x_1)_j - (x_1)_i}{\ell} \\ m_{ij} &= \cos(\bar{x}, x_2) = \frac{(x_2)_j - (x_2)_i}{\ell} \\ n_{ij} &= \cos(\bar{x}, x_3) = \frac{(x_3)_j - (x_3)_i}{\ell} \end{aligned} \tag{3.21}$$

are the direction cosines of the axial axis and ℓ is the element length, which can be computed using the element global coordinates of the two nodes, by

$$\ell = \left[\left(x_{1_j} - x_{1_i} \right)^2 + \left(x_{2_j} - x_{2_i} \right)^2 + \left(x_{3_j} - x_{3_i} \right)^2 \right]^{1/2} \tag{3.22}$$

The transformation matrix preserves the length of the displacement vector and, therefore, it is an orthogonal matrix, i.e.

$$\mathbf{T}\mathbf{T}^T = \mathbf{I} \tag{3.23}$$

where $\mathbf{I}$ is an identity matrix of dimension 2×2. The transformation matrix for a truss element transforms a vector of dimension 6×1, which is defined in the global coordinate system, into the correspondent vector of dimension 2×1 defined in the local coordinate system.

Substituting Eqs. (3.15) and (3.18) into Eq. (2.63) yields

$$\mathbf{k} = \mathbf{T}^T \overline{\mathbf{k}}\, \mathbf{T} = \frac{AE}{\ell} \left[\begin{array}{ccc:ccc} l_{ij}^2 & l_{ij}m_{ij} & l_{ij}n_{ij} & -l_{ij}^2 & -l_{ij}m_{ij} & -l_{ij}n_{ij} \\ l_{ij}m_{ij} & m_{ij}^2 & m_{ij}n_{ij} & -l_{ij}m_{ij} & -m_{ij}^2 & -m_{ij}n_{ij} \\ l_{ij}n_{ij} & m_{ij}n_{ij} & n_{ij}^2 & -l_{ij}n_{ij} & -m_{ij}n_{ij} & -n_{ij}^2 \\ \cdots & \cdots & \cdots & \cdots & \cdots & \cdots \\ -l_{ij}^2 & -l_{ij}m_{ij} & -l_{ij}n_{ij} & l_{ij}^2 & l_{ij}m_{ij} & l_{ij}n_{ij} \\ -l_{ij}m_{ij} & -m_{ij}^2 & -m_{ij}n_{ij} & l_{ij}m_{ij} & m_{ij}^2 & m_{ij}n_{ij} \\ -l_{ij}n_{ij} & -m_{ij}n_{ij} & -n_{ij}^2 & l_{ij}n_{ij} & m_{ij}n_{ij} & n_{ij}^2 \end{array} \right] \tag{3.24}$$

Taking into account the second formulation of equation (2.63), and Eqs. (3.16) and (3.18), becomes

$$\mathbf{m} = \mathbf{T}^T \overline{\mathbf{m}}\, \mathbf{T} = \frac{A\rho\ell}{6} \left[\begin{array}{ccc:ccc} 2l_{ij}^2 & 2l_{ij}m_{ij} & 2l_{ij}n_{ij} & l_{ij}^2 & l_{ij}m_{ij} & l_{ij}n_{ij} \\ 2l_{ij}m_{ij} & 2m_{ij}^2 & 2m_{ij}n_{ij} & l_{ij}m_{ij} & m_{ij}^2 & m_{ij}n_{ij} \\ 2l_{ij}n_{ij} & 2m_{ij}n_{ij} & 2n_{ij}^2 & l_{ij}n_{ij} & m_{ij}n_{ij} & n_{ij}^2 \\ \cdots & \cdots & \cdots & \cdots & \cdots & \cdots \\ l_{ij}^2 & l_{ij}m_{ij} & l_{ij}n_{ij} & 2l_{ij}^2 & 2l_{ij}m_{ij} & 2l_{ij}n_{ij} \\ l_{ij}m_{ij} & m_{ij}^2 & m_{ij}n_{ij} & 2l_{ij}m_{ij} & 2m_{ij}^2 & 2m_{ij}n_{ij} \\ l_{ij}n_{ij} & m_{ij}n_{ij} & n_{ij}^2 & 2l_{ij}n_{ij} & 2m_{ij}n_{ij} & 2n_{ij}^2 \end{array} \right] \tag{3.25}$$

Note that the coordinate transformation preserves the symmetrical properties of stiffness and mass matrices. The transformation matrix is applied also for the forces given in Eq. (3.17) and the right hand side of Eq. (2.62), i.e.

$$\mathbf{f} = \mathbf{T}^T\bar{\mathbf{f}} = \frac{p_0\ell}{2}\begin{bmatrix} l_{ij} \\ m_{ij} \\ n_{ij} \\ l_{ij} \\ m_{ij} \\ n_{ij} \end{bmatrix} + \begin{bmatrix} l_{ij}f_{c1} \\ m_{ij}f_{c1} \\ n_{ij}f_{c1} \\ l_{ij}f_{c2} \\ m_{ij}f_{c2} \\ n_{ij}f_{c2} \end{bmatrix} \tag{3.26}$$

Both element stiffness and mass matrices have a dimension of 6×6 in the three-dimensional space and the force vector have a dimension of 6×1, because the finite element in the global coordinate system has a total of six DOFs.

2D Trusses

A planar truss is a structure in which all the structural components are represented in the same plane. All the formulations of coordinate transformation can be obtained from the counterpart of those for spatial trusses by simply removing the rows and/or columns corresponding to the axe that is not included in the plane of the truss structure. Assuming that the planar truss is defined in the global x_1x_2 plane, we need to remove the rows and/or columns corresponding the x_3 axis and, therefore, the displacement at the first local node should have only two components in the x_1 and x_2 directions.

The coordinate transformation, which gives the relation between vectors $\bar{\mathbf{u}}$ and $\mathbf{u}$, has the same form as Eq. (3.19).

$$\mathbf{u} = \begin{bmatrix} u_1^{(e)} \\ u_2^{(e)} \\ u_3^{(e)} \\ u_4^{(e)} \end{bmatrix} \tag{3.27}$$

The transformation matrix $\mathbf{T}$ is given by

$$\mathbf{T} = \begin{bmatrix} l_{ij} & m_{ij} & 0 & 0 \\ 0 & 0 & l_{ij} & m_{ij} \end{bmatrix} \tag{3.28}$$

and the force vector in the global coordinate system is

$$\mathbf{f} = \mathbf{T}^T\bar{\mathbf{f}} = \frac{p_0\ell}{2}\begin{bmatrix} l_{ij} \\ m_{ij} \\ l_{ij} \\ m_{ij} \end{bmatrix} + \begin{bmatrix} l_{ij}f_{c1} \\ m_{ij}f_{c1} \\ l_{ij}f_{c2} \\ m_{ij}f_{c2} \end{bmatrix} \tag{3.29}$$

All the equations of a planar truss have a similar form to the corresponding equations for a space truss. The main difference of the stiffness and mass matrices is related with their dimension:

$$\mathbf{k} = \mathbf{T}^T \overline{\mathbf{k}}\, \mathbf{T} = \frac{AE}{\ell} \begin{bmatrix} l_{ij}^2 & l_{ij}m_{ij} & -l_{ij}^2 & -l_{ij}m_{ij} \\ l_{ij}m_{ij} & m_{ij}^2 & -l_{ij}m_{ij} & -m_{ij}^2 \\ -l_{ij}^2 & -l_{ij}m_{ij} & l_{ij}^2 & l_{ij}m_{ij} \\ -l_{ij}m_{ij} & -m_{ij}^2 & l_{ij}m_{ij} & m_{ij}^2 \end{bmatrix} \tag{3.30}$$

$$\mathbf{m} = \mathbf{T}^T \overline{\mathbf{m}}\, \mathbf{T} = \frac{A\rho\ell}{6} \begin{bmatrix} 2l_{ij}^2 & 2l_{ij}m_{ij} & l_{ij}^2 & l_{ij}m_{ij} \\ 2l_{ij}m_{ij} & 2m_{ij}^2 & l_{ij}m_{ij} & m_{ij}^2 \\ l_{ij}^2 & l_{ij}m_{ij} & 2l_{ij}^2 & 2l_{ij}m_{ij} \\ l_{ij}m_{ij} & m_{ij}^2 & 2l_{ij}m_{ij} & 2m_{ij}^2 \end{bmatrix} \tag{3.31}$$

Note that Eq. (3.30) can be obtained from Eq. (3.24), and that Eq. (3.31) can be obtained (3.25) by removing third and sixth rows and columns.

3.1.6 Global Truss Equations

The discretized form of the global system equations is obtained by assembling the contributions of all elements connected at the several nodes of the truss structure. This assemblage process leads to Eq. (2.65) of Chap. 2, which solution can only be obtained if boundary conditions are define. In fact, the stiffness matrix in Eq. (2.65) is usually singular, because forces are applied to one unconstrained structure and rigid body motion is allowed.

In practice, truss structures are supported somehow by ground or by a main structure at a certain nodes. When a node is fixed some or all displacements must be zero. The boundary conditions can be imposed numerically in Eq. (2.65) by cancelling the corresponding rows and columns in the system of equations. Meanwhile, this equation can be solved leading to the knowledge of displacement, velocity and acceleration at all nodes. Moreover, the displacements at any position other than the nodal positions can be also obtained using interpolation over finite elements by the shape functions.

3.1.7 Recovering Stress and Strain

The strain in any truss element can be recovered using the element deformation matrix, as

$$\varepsilon_{11} = \overline{\mathbf{B}}\overline{\mathbf{u}} = \overline{\mathbf{B}}\, \mathbf{T}\, \mathbf{u} \tag{3.32}$$

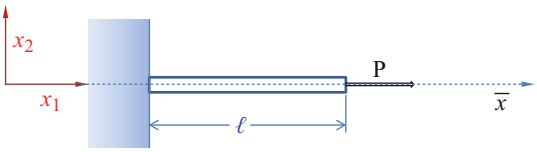

Fig. 3.4 Clamped bar under a static load

and the element stress can also be recovered using the Hooke's law defined in Eq. (1.86) of Chap. 1, as

$$\sigma_{11} = E\overline{\mathbf{B}}\overline{\mathbf{u}} = E\,\overline{\mathbf{B}}\,\mathbf{T}\,\mathbf{u} \tag{3.33}$$

Note that the quantities defined at Eqs. (3.32) and (3.33) are defined in the element local coordinate system.

3.1.8 First Discussion Example

Since until now we only talk about the linear truss finite element, let's consider the simplest application of a truss structure: a uniform bar subject to a concentrate axial force.

Example 3.1: A Uniform Bar Subjected to an Axial Force
The bar has a uniform cross-section area, denoted by A and it is fixed at one end and is loaded at the free end by a horizontal load of P, as shown in Fig. 3.4. The material of the bar is isotropic with Young's modulus E.

Exact Solutions
The exact solution can be obtained from the strong formulation of a bar structure, namely from the governing Eq. (1.92), of Chap. 1. Since the bar is free of body forces, the equation can now be written as

$$\frac{\partial^2 u}{\partial \overline{x}^2} = 0 \tag{3.34}$$

The general solution of Eq. (3.34) can be obtained very easily as

$$u\,(\overline{x}) = c_0 + c_1\overline{x} \tag{3.35}$$

where c_0 and c_1 are unknown constants that can be determined from the boundary conditions. Since the displacement at the fixed end is known, the displacement boundary condition is

$$u\,(\overline{x} = 0) = 0 \tag{3.36}$$

and, therefore, Eq. (3.36) leads to $c_0 = 0$. To compute c_1 is necessary to use the natural boundary condition, which is related with the stress at the free end of bar, and can be computed using Eq. (1.86) as

$$\sigma_{11}|_{\bar{x}=\ell} = E \left. \frac{\partial u}{\partial \bar{x}} \right|_{\bar{x}=\ell} \tag{3.37}$$

and, simultaneously, from classical mechanics it can be evaluated as

$$\sigma_{11}|_{\bar{x}=\ell} = \frac{\mathrm{P}}{A} \tag{3.38}$$

So, the boundary condition at the free end of bar is obtained equating Eqs. (3.37) and (3.38), as

$$E \left. \frac{\partial u}{\partial \bar{x}} \right|_{\bar{x}=\ell} = \frac{\mathrm{P}}{A} \tag{3.39}$$

leading to

$$c_1 = \frac{\mathrm{P}}{EA} \tag{3.40}$$

Substituting $c_0 = 0$ and Eq. (3.40) into Eq. (3.35), the solution of the displacement of the bar is written as

$$u(\bar{x}) = \frac{\mathrm{P}}{EA} \bar{x} \tag{3.41}$$

and the displacement at the free end is given by

$$u(\bar{x} = \ell) = \frac{\mathrm{P}\ell}{EA} \tag{3.42}$$

Numerical Solution

To evaluate the numerical solution by the finite element method it is necessary to perform the discretization of the bar. Using one finite element, the bar finite element model is represented as shown in Fig. 3.5.

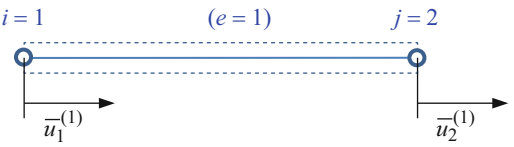

Fig. 3.5 A bar modeled by one finite element

The element stiffness matrix is defined in local coordinate system by Eq. (3.15), and there is no need to perform coordinate transformation, as the local and global coordinate systems are parallel. Moreover, since the number of elements at the bar finite element is only one, there is also no need to perform assembly. Thus, the finite element equations becomes

$$\frac{AE}{\ell}\begin{bmatrix} 1 & -1 \\ -1 & 1 \end{bmatrix}\begin{bmatrix} u_1^{(1)} \\ u_2^{(1)} \end{bmatrix} = \begin{bmatrix} F_1 \\ F_2 \end{bmatrix} \tag{3.43}$$

The right hand side of Eq. (3.43) has the load vector, since there is only one concentrated load P applied in the global node $j = 2$, the component F_2 is equal to P and F_1 is the reaction force applied at node $i = 1$ that is unknown.

Note that in Eq. (3.43) the stiffness is a singular matrix, which means that its determinate is zero, and therefore its inverse does not exist. Thus, to solve Eq. (3.43) it is necessary to impose boundary conditions. Since the displacement at node i is known, the easy way of imposing this boundary condition is to simply remove the first row and the first column of Eq. (3.43),

$$u_2^{(1)} = \frac{\mathrm{P}\ell}{AE} \tag{3.44}$$

Comparing Eq. (3.44) with Eq. (3.42) is possible to conclude that both solutions are coincident. The displacement variation within the finite element can be obtained by substituting $u_1^{(1)} = 0$ and Eq. (3.44) into Eq. (3.7):

$$\tilde{u}(\bar{x}) = \begin{bmatrix} 1 - \frac{\bar{x}}{\ell} & \frac{\bar{x}}{\ell} \end{bmatrix}\begin{bmatrix} u_1^1 \\ u_2^1 \end{bmatrix} = \begin{bmatrix} 1 - \frac{\bar{x}}{\ell} & \frac{\bar{x}}{\ell} \end{bmatrix}\begin{bmatrix} 0 \\ (\mathrm{P}\ell)/(EA) \end{bmatrix} = \frac{\mathrm{P}}{EA}\bar{x} \tag{3.45}$$

Equation (3.45) is also exactly the same as the exact solution presented in Eq. (3.41). Using the identity matrix for the transformation matrix on Eqs. (3.32) and (3.33) is possible to obtain the stress in the bar, as

$$\tilde{\sigma}_{11} = E\begin{bmatrix} -\frac{1}{\ell} & \frac{1}{\ell} \end{bmatrix}\begin{bmatrix} 0 \\ u_2^1 \end{bmatrix} = \frac{\mathrm{P}}{A} \tag{3.46}$$

This is also exactly the same as the exact solution presented in Eq. (3.38).

Final Discussion

Usually, solutions obtained by the FEM are only approximations of the exact solutions. Nevertheless, in this example the exact solution is also obtained by using the finite element method. In fact, the finite element method can lead to the exact solution of problems, whenever the order of finite element shape functions is equal to the order of the exact solution of displacement. Therefore, the exact solution of the problem is included in the assumed displacement function that is used to form the shape functions. Hence this example allow to confirm the reproduction property

of the FEM that if the exact solution can be formed by the basis function used to construct the FEM shape function, the FEM always produce the exact solution. Making use of this property, one may try to add basis functions that form the exact solution or part of the exact solution to achieve better accuracy in the numerical solution [4].

In complex problems exact solutions are difficult to obtain and, usually, they cannot be written in the form of a combination of monomials. Thus, the finite element solution based on the use of polynomial shape functions will not reproduce the exact one. So, a main question arises: *how is possible to ensure that the FEM can produce a good approximation of the solution of a complex problem?* The answer may be sought in the convergence property of finite element method: a numerical solution converges to the exact solution that is continuous at arbitrary accuracy, when the element size becomes infinitely small and, as long as, the complete linear polynomial basis is included in the basis that is used to form the finite element shape functions. In fact, using the local Taylor expansion of a continuous function $u(x)$, a continuous displacement in the vicinity of point x_i can always be approximated using the equation

$$u(x) = u(x_i) + \left.\frac{\partial u}{\partial x}\right|_i (x - x_i) + o\left(h^2\right) \tag{3.47}$$

where h is the characteristic size related to $(x - x_i)$ or to the finite element size and $o(h^2)$ represents a second order error.

Note that if an accuracy of $o(h^1)$ is used, means that the second term of the right hand side of Eq. (3.47) is not included and, therefore, a constant value is used to reproduce function $u(x)$. However, in a finite element model the definition of a constant displacement within each finite element of the model will possibly not be continuous between elements, unless the entire displacement field is constant, which is only possible for a rigid movement that is not included in equations of motion. Thus, to guarantee the convergence of a continuous function its local Taylor expansion must be a complete polynomial up to at least the first order. The Taylor expansion up to the order of p can be given as

$$u(x) = u(x_i) + \left.\frac{\partial u}{\partial x}\right|_i (x - x_i) + \frac{1}{2!}\left.\frac{\partial^2 u}{\partial x^2}\right|_i (x - x_i)^2 + \cdots + \frac{1}{p!}\left.\frac{\partial^p u}{\partial x^p}\right|_i (x - x_i)^p + o\left(h^{p+1}\right) \tag{3.48}$$

The error in Eq. (3.48) is of the order $o\left(h^{p+1}\right)$ and, therefore, the order of the rate of convergence is of the same order. For linear finite elements p is equal to one, and the rate of convergence for the displacement is therefore of $o(h^2)$. In terms of a finite element model, this implies that if the mesh element size is reduced to half, $(h = h/2)$, the error associated with the displacement results will be reduced by a rate of one quarter.

Using this mathematical concept is possible to say that for problems whose exact solutions are of a polynomial type, the FEM is able to reproduce the exact solution

using a minimum number of elements, as long as the complete order of the basis functions incorporate the order of the exact solution. For complex problems whose exact solutions are of a very high polynomial order or even a non-polynomial type, is up to the technical finite element analyst to select the mesh density that leads to the best desired accuracy of the FEM results. A great number of finite element programs allow to the user select between the so-called h – adaptivity and p – adaptivity analyses. Conventionally, h is used to represent the characteristic size of the mesh while p is used to represent the order of the polynomial basis function. So, h – adaptivity analysis uses finer finite element meshes and p – adaptivity analysis uses a higher order of shape functions to achieve the desired accuracy of the FEM results.

3.2 FE Matrices and Vectors for High Order Truss Elements

For truss structures loaded by body forces distributed in the truss axial direction, the exact solutions are no longer linear and higher order finite elements must be used for more accurate analysis. The procedure for developing such higher one-dimensional finite elements is the same as for the linear elements. The only difference is the number of nodes per element and, therefore, the order of the shape functions.

In order to simplify the derivation of all matrices and vectors of higher order finite elements a translation of coordinates is used. So, usually, the natural coordinates η are used instead of the local coordinates $\bar{x}$. Figure 3.6 shows the position of the origin of the natural coordinates, which is located at the midpoint of the one-dimensional element.

The coordinate transformation presented on Fig. 3.6 is described as

$$\begin{array}{ll} \bar{x} = g(\eta) = \frac{\ell}{2}(\eta + 1); & \eta = h(\bar{x}) = \frac{2\bar{x}}{\ell} - 1 \\ d\bar{x} = \frac{\ell}{2} d\eta; & d\eta = \frac{2}{\ell} d\bar{x} \end{array} \tag{3.49}$$

In the natural coordinate system, the element is defined in the range of $-1 \leq \eta \leq 1$. The shape function of a higher finite element can be obtained from the so-called Lagrange polynomials

$$N_k(\eta) = l_k^n(\eta) \tag{3.50}$$

where l_k^n is the well-known Lagrange basis polynomials

$$l_k^n = \prod_{\substack{i=1 \\ i \neq k}}^{n} \frac{(\eta - \eta_i)}{(\eta_k - \eta_i)} = \frac{(\eta - \eta_1)(\eta - \eta_2) \cdots (\eta - \eta_{k-1})(\eta - \eta_{k+1}) \cdots (\eta - \eta_n)}{(\eta_k - \eta_1)(\eta_k - \eta_2) \cdots (\eta_k - \eta_{k-1})(\eta_k - \eta_{k+1}) \cdots (\eta_k - \eta_n)} \tag{3.51}$$

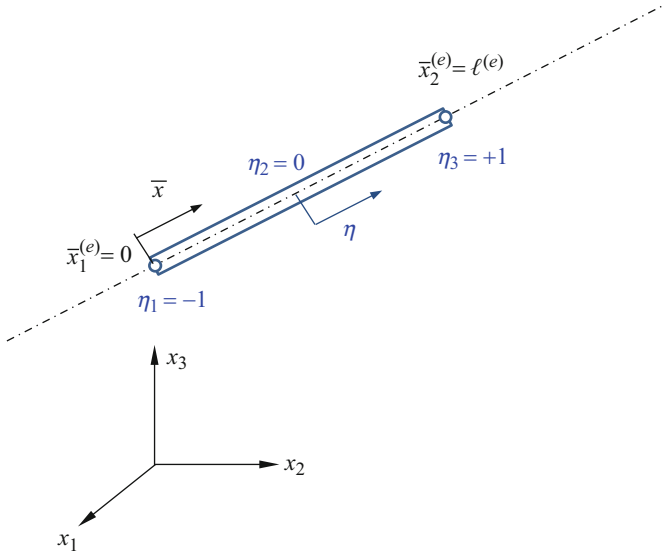

Fig. 3.6 Local and natural coordinates in one-dimensional finite elements

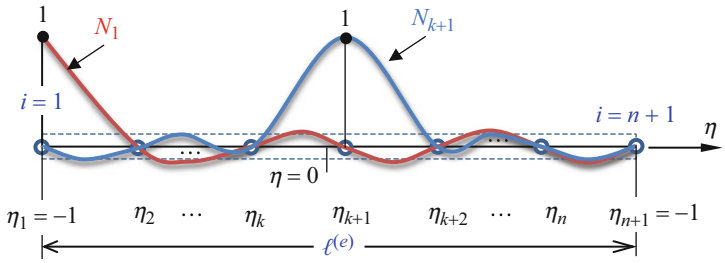

Fig. 3.7 One-dimensional element of nth order with $(n + 1)$ nodes

From Eq. (3.51) it is clear that

$$N_k(\eta) = \begin{cases} 1 \text{ at node } k \text{ where } \eta = \eta_k \\ 0 \text{ at other nodes} \end{cases} . \tag{3.52}$$

Therefore, the high order shape functions defined by Eq. (3.50) have the delta function property. Figure 3.7 shows the first and the $(k + 1)$ th shape functions of an element of nth order with $(n + 1)$ nodes.

Using Eq. (3.51), the quadratic one-dimensional element with three nodes, shown in Fig. 3.8, can be obtained explicitly as

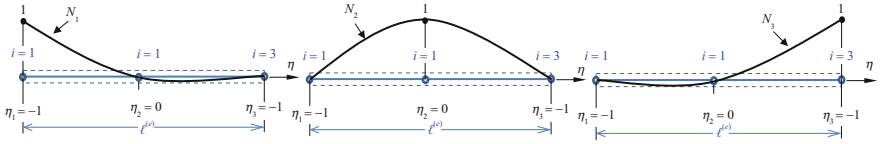

Fig. 3.8 Shape functions of the one-dimensional element of second order

$$\begin{aligned} N_1(\eta) &= \tfrac{\eta}{2}(\eta - 1) \\ N_2(\eta) &= \left(1 - \eta^2\right) \\ N_3(\eta) &= \tfrac{\eta}{2}(\eta + 1) \end{aligned} \tag{3.53}$$

Meanwhile, the stiffness matrix is obtained using the finite element strain matrix $\mathbf{B}$. In the case of a finite element truss that is described by the natural coordinates, the Eq. (3.12) should be re-written as

$$\tilde{\varepsilon}_{11}(\bar{x} = g(\eta)) = \frac{d\tilde{u}(g(\eta))}{d\bar{x}} = \frac{d\tilde{u}(g(\eta))}{d\eta}\frac{d\eta}{d\bar{x}} = L\,\overline{\mathbf{N}}(\eta)\;\overline{\mathbf{u}} = \overline{\mathbf{B}}(\eta)\;\overline{\mathbf{u}} \tag{3.54}$$

where the strain matrix $\overline{\mathbf{B}}(\eta)$ has the form

$$\overline{\mathbf{B}}(\eta) = L\overline{\mathbf{N}} = \frac{d}{d\eta}\left[\tfrac{\eta}{2}(\eta-1)\;\left(1-\eta^2\right)\;\tfrac{\eta}{2}(\eta+1)\right]\frac{d\eta}{d\bar{x}} = \left[\eta - \tfrac{1}{2}\;-2\eta\;\eta + \tfrac{1}{2}\right]\frac{2}{\ell} \tag{3.55}$$

The stiffness matrix for truss finite elements can be obtained using Eq. (2.49) from the previous chapter, leading to

$$\begin{aligned} \overline{\mathbf{k}} &= \int_{\Omega^e} \overline{\mathbf{B}}^T \mathbf{c}\,\overline{\mathbf{B}}\,d\Omega^e = A\int_0^{\ell} \overline{\mathbf{B}}^T(\eta)\,E\,\overline{\mathbf{B}}(\eta)\;d\bar{x} = AE\int_{h(0)=-1}^{h(\ell)=1} \overline{\mathbf{B}}^T(\eta)\,\overline{\mathbf{B}}(\eta)\;\tfrac{\ell}{2}d\eta \\ &= \tfrac{EA}{3\ell}\begin{bmatrix} 7 & -8 & 1 \\ -8 & 16 & -8 \\ 1 & -8 & 7 \end{bmatrix} \end{aligned} \tag{3.56}$$

where A is the cross-section area. Note that for the one-dimensional truss structure, the material constant matrix $\mathbf{c}$ reduce to elastic modulus, E, see Eq. (1.86) in Sect. 1.3.1 of Chap. 1.

The mass matrix for the truss elements can be obtained using Eqs. (3.53) and (2.45) as

$$\overline{\mathbf{m}} = \int_{\Omega^e} \rho \overline{\mathbf{N}}^T \overline{\mathbf{N}}\, d\Omega^e = A\rho \int_0^{\ell} \overline{\mathbf{N}}^T \overline{\mathbf{N}}\, d\overline{x} = A\rho \int_{-1}^{1} \overline{\mathbf{N}}^T \overline{\mathbf{N}} \frac{\ell}{2} d\eta$$

$$= \frac{A\rho\ell}{2} \int_{-1}^{1} \begin{bmatrix} \frac{\eta}{2}(\eta-1) \\ (1-\eta^2) \\ \frac{\eta}{2}(\eta+1) \end{bmatrix} \begin{bmatrix} \frac{\eta}{2}(\eta-1) & (1-\eta^2) & \frac{\eta}{2}(\eta+1) \end{bmatrix} d\eta$$

$$= \frac{A\rho\ell}{8} \int_{-1}^{1} \begin{bmatrix} \eta^4 - 2\eta^3 + \eta^2 & 2(-\eta^4 + \eta^3 + \eta^2 - \eta) & \eta^4 - \eta^2 \\ 2(-\eta^4 + \eta^3 + \eta^2 - \eta) & 4(\eta^4 - 2\eta^2 + 1) & 2(-\eta^4 - \eta^3 + \eta^2 + \eta) \\ \eta^4 - \eta^2 & 2(-\eta^4 - \eta^3 + \eta^2 + \eta) & \eta^4 + 2\eta^3 + \eta^2 \end{bmatrix} d\eta$$

$$= \frac{A\rho\ell}{30} \begin{bmatrix} 4 & 2 & -1 \\ 2 & 16 & 2 \\ -1 & 2 & 4 \end{bmatrix} \tag{3.57}$$

The mass matrix is found to be also symmetrical.

The nodal force vector for truss elements can be obtained using Eqs. (3.53) and (2.52), assuming that the element is loaded by a constant distributed force p_0 along the $\overline{x}$-axis, and no concentrated forces are applied. Thus, the total nodal force vector becomes

$$\bar{\mathbf{f}} = \int_{\Omega^e} \overline{\mathbf{N}}^T \mathbf{f}_b\, d\Omega^e = p_0 \int_0^{\ell} \begin{bmatrix} \frac{\eta}{2}(\eta-1) \\ (1-\eta^2) \\ \frac{\eta}{2}(\eta+1) \end{bmatrix} d\overline{x}$$

$$= \frac{p_0\ell}{2} \int_{-1}^{1} \begin{bmatrix} \frac{\eta}{2}(\eta-1) \\ (1-\eta^2) \\ \frac{\eta}{2}(\eta+1) \end{bmatrix} d\eta = \frac{p_0\ell}{6} \begin{bmatrix} 1 \\ 4 \\ 1 \end{bmatrix} \tag{3.58}$$

3.2.1 Numerical Integration

The integration of the components of all element vectors and/or matrices can be carried out analytically, as in the previous section. Nevertheless, in the development of complex finite elements this can be a difficult task. So, in order to have an adequate tool for the integration of element quantities that are hardly integrable analytically, numerical integration is introduced and examined for a truss example. By means of numerical integration, it is possible to integrate arbitrary functions in an approximate way. The essential advantages of numerical integration are summarized as follows:

- Simplification of the integration;
- Integration of analytically non-integrable functions;
- Selective subintegration for elimination of defects from the element formulation.

In opposition to these advantages there are actually some limitation, namely: the generation of element matrices and vectors is numerically costly and in some cases, the element matrices and vectors are integrated inexactly.

Within the framework of numerical integration, the so-called Gauss-Legendre quadrature is well established. Using the Gauss-Legendre quadrature is possible to replace the analytical integration of a function $f(\eta)$ over the domain space $\eta \in [-1,\ 1]$ by the weighted sum

$$\int_{-1}^{1} f(\eta)\ d\eta = \sum_{i=1}^{n} f(\eta_i)\,\omega_i \tag{3.59}$$

where ω_i represent the weight coefficients to the function values at the locations η_i and n is the number of integration points, or the so-called Gauss points. Polynomials with the degree (p)

$$p \leq 2n - 1 \tag{3.60}$$

can be integrated exactly by Gauss-Legendre quadrature, higher-order polynomials and other functions can be integrated only approximately. The Gauss-Legendre quadrature is summarize in Table 3.1.

To define the necessary integration order for the exact integration of the element quantities as such stiffness, mass and load vector it is necessary to account for the integrand function. For instance, to numerically integrate the component $\bar{k}_{11}$ in Eq. (3.56) will have

$$\bar{k}_{11} = \frac{2EA}{\ell}\int_{-1}^{1} \frac{dN_1}{d\eta}\frac{dN_1}{d\eta}d\eta = \frac{2EA}{\ell}\int_{-1}^{1}\left(\eta - \frac{1}{2}\right)\left(\eta - \frac{1}{2}\right)d\eta = \frac{2EA}{\ell}\int_{-1}^{1} f(\eta)\,d\eta \tag{3.61}$$

Because the function that needs to be integrated is a second order polynomial $(n = 2)$, the number of points that should be used to evaluate exactly the numerical integration of $\bar{k}_{11}$ is of two $(n = 2 \leq 2 \times (p = 2) - 1)$. Thus, using a Gauss-Legendre table is possible to select the information presented in Table 3.2 and use it as follows

$$\int_{-1}^{1} f(\eta)\ d\eta = \sum_{i=1}^{2} f(\eta_i)\,\omega_i = \left(\eta_1 - \frac{1}{2}\right)^2 w_1 + \left(\eta_2 - \frac{1}{2}\right)^2 w_2 = 1.166667 \tag{3.62}$$

Table 3.1 Gauss points and weight factors of the Gauss-Legendre quadrature

(p)	$(2p-1)$	$f(\eta_i)$	(η_i)	Weight (w_i)
1	1	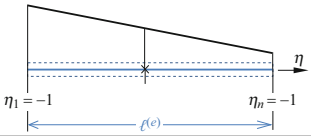	0.0	2.0
2	3	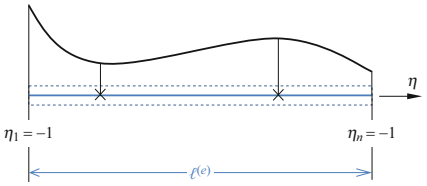	$\eta_1 = -1/\sqrt{3}$	1.0
			$\eta_2 = 1/\sqrt{3}$	1.0
3	5	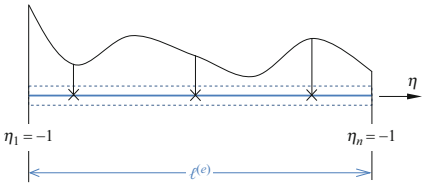	$\eta_1 = -\sqrt{3/5}$	$w_1 = 5/9$
			$\eta_2 = 0$	$w_2 = 8/9$
			$\eta_3 = \sqrt{3/5}$	$w_3 = 5/9$
4	7	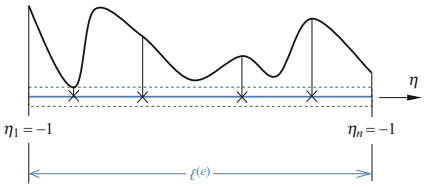	$\eta_1 = -0.86114$	$w_1 = 0.34785$
			$\eta_2 = -0.33998$	$w_2 = 0.65241$
			$\eta_3 = 0.33998$	$w_3 = 0.65241$
			$\eta_4 = 0.86114$	$w_4 = 0.34785$

Table 3.2 Two Gauss points and respective weights

Number of points (p)	Coordinate of points ($\pm\eta_i$)	Weight (w_i)
2	0.577350269	1.0

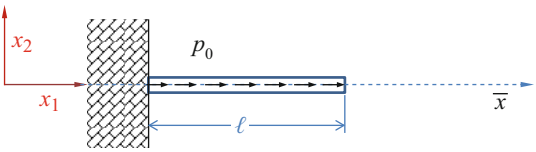

Fig. 3.9 Clamped bar loaded by a constant body force distributed in the truss axial direction

and, substituting Eq. (3.62) into Eq. (3.61), yields

$$\overline{k}_{11} = \frac{2EA}{\ell}\int_{-1}^{1} f(\eta)\, d\eta = \frac{2EA}{\ell} \times 1.166667 = 2.333333\frac{EA}{\ell} = \frac{7EA}{3\ell} \tag{3.63}$$

The solution in Eq. (3.63) is the same presented at Eq. (3.56).

3.2.2 Second Discussion Example

Consider the simplest application of a truss structure: a uniform bar subjected to a constant distributed axial force.

Example 3.2: A Uniform Bar Subjected to a Constant Force Distributed Axially
The bar has a uniform cross-section area, denoted by A and, it is fixed at one end and loaded by a constant body force distributed in the truss axial direction, as shown in Fig. 3.9. The material of the bar is isotropic with Young's modulus E.

Exact Solutions
The exact solution can be obtained from the strong formulation of a bar structure, namely from the governing Eq. (1.92), of Chap. 1. Since the bar is loaded by constant body forces, the equation can now be written as

$$EA\frac{\partial^2 u}{\partial \overline{x}^2} = -p_0 \tag{3.64}$$

The general solution of Eq. (3.34) can be obtained by performing two integrations, leading to

$$u(\overline{x}) = -\frac{p_0}{2EA}\overline{x}^2 + c_1\overline{x} + c_2 \tag{3.65}$$

where c_1 and c_2 are unknown constants that can be determined by the boundary conditions. Since, the displacement at the fixed end is known, the displacement

boundary condition for this case is defined by Eq. (3.36), and, therefore, leads to $c_2 = 0$. To compute the c_1 is necessary to use the natural boundary condition, which is defined by Eq. (3.37), and from classical mechanics it is clear that at the free end, the bar is free of stress. So, the boundary condition at the free end is obtained by setting Eq. (3.37) equal to zero, i.e.

$$E \left. \frac{\partial u}{\partial \bar{x}} \right|_{\bar{x}=\ell} = 0 \tag{3.66}$$

leading to

$$c_1 = \frac{p_0 \ell}{EA} \tag{3.67}$$

Substituting this value and $c_2 = 0$ into Eq. (3.65), the solution of the displacement of the bar is written as

$$u(\bar{x}) = \frac{p_0}{2EA} \bar{x} (2\ell - \bar{x}) \tag{3.68}$$

and the displacement at the free end is given by

$$u(\bar{x}) = \frac{p_0 \ell^2}{2EA} \tag{3.69}$$

Numerical Solution

To evaluate the numerical solution by the finite element method it is necessary to perform the discretization of the bar. Using one second order finite element, the bar finite element model is represented as shown in Fig. 3.10.

The element stiffness matrix is defined in local coordinate system by Eq. (3.56), and there is no need to perform coordinate transformation, as the local and global coordinate systems are parallel. The total nodal force vector is defined by Eq. (3.58). Moreover, since the number of elements at the bar is only one, there is also no need to perform assembly. Thus, the finite element equations becomes

$$\frac{EA}{3\ell} \begin{bmatrix} 7 & -8 & 1 \\ -8 & 16 & -8 \\ 1 & -8 & 7 \end{bmatrix} \begin{bmatrix} u_1^{(1)} \\ u_2^{(1)} \\ u_3^{(1)} \end{bmatrix} = \frac{p_0 \ell}{6} \begin{bmatrix} 1 \\ 4 \\ 1 \end{bmatrix} \tag{3.70}$$

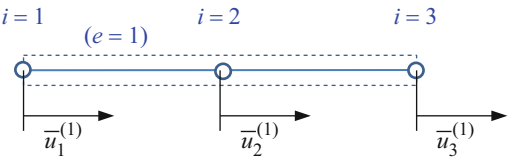

Fig. 3.10 A bar modeled by one second order finite element

To solve Eq. (3.70) it is necessary to impose boundary conditions. Since the displacement at node 1 is known, the easy way of imposing this boundary condition is to simply remove the first row and the first column of Eq. (3.70), leading to

$$\frac{EA}{3\ell}\begin{bmatrix} 16 & -8 \\ -8 & 7 \end{bmatrix}\begin{bmatrix} u_2^{(1)} \\ u_3^{(1)} \end{bmatrix} = \frac{p_0\ell}{6}\begin{bmatrix} 4 \\ 1 \end{bmatrix} \tag{3.71}$$

Equation (3.71) can be solved by inverting the system matrix, leading to

$$\begin{bmatrix} u_2^{(1)} \\ u_3^{(1)} \end{bmatrix} = \frac{3p_0\ell^2}{6EA}\begin{bmatrix} 0.146 & 0.167 \\ 0.167 & 0.333 \end{bmatrix}\begin{bmatrix} 4 \\ 1 \end{bmatrix} = \frac{p_0\ell^2}{2EA}\begin{bmatrix} 0.75 \\ 1 \end{bmatrix} = \frac{p_0\ell^2}{2EA}\begin{bmatrix} 3/4 \\ 1 \end{bmatrix} \tag{3.72}$$

From Eq. (3.72) is possible to see that the axial displacement at the free end, $u_3^{(1)}$, is coincident with the solution presented in (3.69). The displacement variation within the finite element can be obtained by substituting $u_1^{(1)} = 0$ and Eq. (3.72) into Eq. (3.1)

$$\tilde{u}(\eta) = \frac{p_0\ell^2}{2EA}\left[\frac{\eta}{2}(\eta-1)\ \left(1-\eta^2\right)\ \frac{\eta}{2}(\eta+1)\right]\begin{bmatrix} 0 \\ 3/4 \\ 1 \end{bmatrix} = \frac{p_0\ell^2}{4EA}\left(-\frac{\eta^2}{2}+\eta+\frac{3}{2}\right) \tag{3.73}$$

In order to compare Eq. (3.73) with the exact solution presented in Eq. (3.68), the coordinate transformation described by $h(\bar{x})$, at Eq. (3.49), can be substituted into Eq. (3.73), i.e.

$$\tilde{u}(h(\bar{x})) = \frac{p_0\ell^2}{4EA}\left(-\frac{h(\bar{x})^2}{2}+h(\bar{x})+\frac{3}{2}\right) = \frac{p_0}{2EA}\bar{x}(2\ell-\bar{x}) \tag{3.74}$$

Equation (3.74) is also exactly the same as the exact solution presented in Eq. (3.68), when $\bar{x} = \ell$.

Final Discussion

In this example, the exact solution of the displacement field is the second order polynomial presented in Eq. (3.68). So, to achieve the same results by the use of the finite-element method was necessary to assure that the order of the finite element shape functions used within the discretization procedure is equal to the order of the exact solution of displacement. Therefore, in this way, the exact solution of the problem is included in the assumed displacement function.

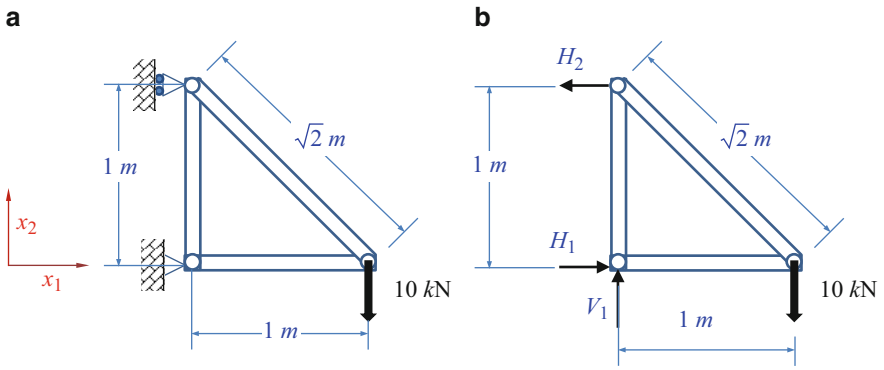

Fig. 3.11 Truss structure with three bars: (**a**) support conditions; (**b**) body free diagram

3.2.3 Third Discussion Example

Example 3.3: Truss Structure Subjected to a Vertical Load
Consider the plane truss structure shown in Fig. 3.11. The structure is a planar structure made with three truss members and a vertical downward force of 10 kN is applied at the free vertex.

Exact Solutions
To evaluate the exact solution of the truss element forces is possible to use method of sections [5]. In this method is important to find the values of the reaction forces. Thus, Fig. 3.11b shows the loading diagram and contains the reaction forces from the supports. Since there is a pin joint it will have two reaction forces H_1 and V_1, one in the x_1 direction and the other in the x_2 direction, respectively. At the other support there is a roller joint and hence we have only a reaction force in the x_1 direction, H_2. To evaluate the reaction forces we can use equilibrium equations from static, in which force and moment balance can be written as

$$\begin{cases} H_1 - H_2 = 0 \\ V_1 - 10000 = 0 \\ H_2 \times 1 - 10000 \times 1 = 0 \end{cases} \iff \begin{cases} H_1 = 10000 \\ V_1 = 10000 \\ H_2 = 10000 \end{cases} \tag{3.75}$$

To use the analytical sections method is necessary to introduce a single straight line cutting through the members whose force must be calculated. However, this method has a limit in that the cutting line can pass through a maximum of only three members of the truss structure, if these three bars are not concurrent in the same point. This restriction is because this method uses the force balances in both axes direction and the moment balance, which gives a maximum of three equations to find a maximum of three unknown truss element forces through which this cut is made. So, performing a cut on the loading vertex, as presented on Fig. 3.12, is possible to write the following equations, as

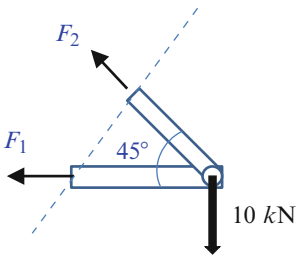

Fig. 3.12 Cut through the load vertex of the truss structure

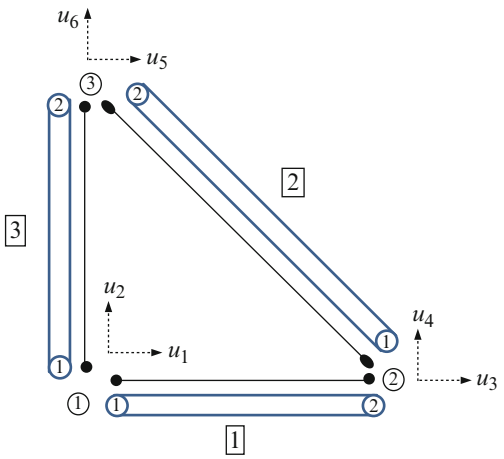

Fig. 3.13 Global and local numbering for the three-element truss

$$\begin{cases} F_2 \sin 45^0 - 10000 = 0 \\ F_2 \cos 45^0 + F_1 = 0 \end{cases} \iff \begin{cases} F_2 = 14.142 \text{ K N} \\ F_1 = -10 \quad \text{K N} \end{cases} \tag{3.76}$$

Performing a similar cut on the others vertexes, is possible to conclude that the vertical bar has an axial force of 10 kN.

Numerical Solution

In the process of solving numerically this problem is important to perform the discretization, which comprises numbering the finite elements and nodes. Thus, Fig. 3.13 shows the numerical model of the truss structure. Since each node can, in general, move in two directions, there are $3 \times 2 = 6$ degrees of freedom in the problem. However, in the local coordinate system of each finite element there is only one degree of freedom in each node. Table 3.3 shows the dimensions and material properties of the truss members.

The computation of element matrices implies the knowledge of the transformation matrix for each finite element. Thus, knowing the coordinates of finite element nodes in the global coordinate system is possible to use Eq. (3.21) to evaluate the finite element direction cosines, as presented in Table 3.4. Moreover, since

Table 3.3 Dimensions and mechanical properties of the truss members

Number of element	Cross-sectional area $[m^2]$	Length $[m]$	Young's modulus [GPa]
1	0.01	1	70
2	0.01	$\sqrt{2}$	70
3	0.01	1	70

Table 3.4 Global coordinates of nodes and direction cosines of elements

Number of element	Number of global node corresponding to		Coordinates in global coordinate system		Direction cosines	
	First element node (i)	Second element node (j)	$(x_1, x_2)_i$	$(x_1, x_2)_j$	l_{ij}	m_{ij}
1	1	2	$(0,0)_1$	$(1,0)_2$	1	0
2	2	3	$(1,0)_2$	$(0,1)_3$	$-1/\sqrt{2}$	$1/\sqrt{2}$
3	1	3	$(0,0)_1$	$(0,1)_3$	0	1

this problem is a planar problem, there is no need to compute the component n_{ij}. Note that because is a static problem, the element mass matrices don't need to be computed.

The element stiffness matrices are defined in the global coordinate system through Eq. (3.30),

$$\mathbf{k}^{(1)} = \frac{10^{-3} \times \left(70 \times 10^9\right)}{1.0} \begin{bmatrix} 1 & 0 & -1 & 0 \\ 0 & 0 & 0 & 0 \\ -1 & 0 & 1 & 0 \\ 0 & 0 & 0 & 0 \end{bmatrix} = \begin{bmatrix} 7 & 0 & -7 & 0 \\ 0 & 0 & 0 & 0 \\ -7 & 0 & 7 & 0 \\ 0 & 0 & 0 & 0 \end{bmatrix} \times 10^8 \left[\mathbf{N}m^{-1}\right] \tag{3.77}$$

$$\mathbf{k}^{(2)} = \frac{10^{-3} \times \left(70 \times 10^9\right)}{\sqrt{2}} \begin{bmatrix} 1/2 & -1/2 & -1/2 & 1/2 \\ -1/2 & 1/2 & 1/2 & -1/2 \\ -1/2 & 1/2 & 1/2 & -1/2 \\ 1/2 & -1/2 & -1/2 & 1/2 \end{bmatrix}$$

$$= \begin{bmatrix} 1 & -1 & -1 & 1 \\ -1 & 1 & 1 & -1 \\ -1 & 1 & 1 & -1 \\ 1 & -1 & -1 & 1 \end{bmatrix} \frac{7}{2\sqrt{2}} \times 10^8 \left[\mathbf{N}m^{-1}\right] \tag{3.78}$$

$$\mathbf{k}^{(3)} = \frac{10^{-3} \times \left(70 \times 10^9\right)}{1.0} \begin{bmatrix} 0 & 0 & 0 & 0 \\ 0 & 1 & 0 & -1 \\ 0 & 0 & 0 & 0 \\ 0 & -1 & 0 & 1 \end{bmatrix} = \begin{bmatrix} 0 & 0 & 0 & 0 \\ 0 & 7 & 0 & -7 \\ 0 & 0 & 0 & 0 \\ 0 & -7 & 0 & 7 \end{bmatrix} \times 10^8 \left[\mathbf{N}m^{-1}\right] \tag{3.79}$$

The next step after getting the element matrices will be to assemble the element matrices into a global finite element matrix. Since the total degrees of freedom in the structure is six, the global stiffness matrix will be a 6×6 matrix. The assembly process assures that the global stiffness of each node has the contribution of all elements that share the node. For example, looking at Table 3.4, it can be seen that elements one and three contribute to the stiffness associated with the degrees of freedom at node one, first and second global degrees of freedom. So, by adding the contributions from the individual element matrices into the respective positions in the global matrix, according the element connectivity's, the global matrix can be obtained. In fact, each one of the local degrees of freedom can be matched to one global degrees of freedom. By inspection of Fig. 3.13 and of Table 3.4, is possible to form the Table 3.5 that maps local to global numbers.

Using this table, it can be seen for instance that the third degree of freedom for the third element is the fifth degree of freedom in the global numbering system, and the fourth degree of freedom corresponds to the sixth global degree of freedom. Hence, the value in the third row and fourth column of the element stiffness matrix of the third element, denoted by $k_{34}^{(3)}$, should be added into the position in the fifth row and sixth column of the 6×6 global stiffness matrix, which can be written as

$$k_{34}^{(3)} \rightarrow k_{56} \tag{3.80}$$

Each one of the 16 positions of the element stiffness matrix of the three elements must be added into the global matrix according the mapping showed on Table 3.5. This gives the following results:

$$\mathbf{K} = \begin{bmatrix} k_{11}^{(1)} + k_{11}^{(3)} & k_{12}^{(1)} + k_{12}^{(3)} & k_{13}^{(1)} & k_{14}^{(1)} & k_{13}^{(3)} & k_{14}^{(3)} \\ k_{21}^{(1)} + k_{21}^{(3)} & k_{22}^{(1)} + k_{22}^{(3)} & k_{23}^{(1)} & k_{24}^{(1)} & k_{23}^{(3)} & k_{24}^{(3)} \\ k_{31}^{(1)} & k_{32}^{(1)} & k_{33}^{(1)} + k_{11}^{(2)} & k_{34}^{(1)} + k_{12}^{(2)} & k_{13}^{(2)} & k_{14}^{(2)} \\ k_{41}^{(1)} & k_{42}^{(1)} & k_{43}^{(1)} + k_{21}^{(2)} & k_{44}^{(1)} + k_{22}^{(2)} & k_{23}^{(2)} & k_{24}^{(2)} \\ k_{31}^{(3)} & k_{32}^{(3)} & k_{31}^{(2)} & k_{32}^{(2)} & k_{33}^{(2)} + k_{33}^{(3)} & k_{34}^{(2)} + k_{34}^{(3)} \\ k_{41}^{(3)} & k_{42}^{(3)} & k_{41}^{(2)} & k_{42}^{(2)} & k_{43}^{(2)} + k_{43}^{(3)} & k_{44}^{(2)} + k_{44}^{(3)} \end{bmatrix} \tag{3.81}$$

Table 3.5 Finite element code table

Number of element	First local degree of freedom	Second local degree of freedom	Third local degree of freedom	Fourth local degree of freedom
1	1	2	3	4
2	3	4	5	6
3	1	2	5	6

This matrix pre-multiplies the vector of nodal displacements according to Eq. (2.65) to yield the vector of externally applied nodal forces. The full system equations, can be written as

$$10^8 \times \begin{bmatrix} 7 & 0 & -7 & 0 & 0 & 0 \\ 0 & 7 & 0 & 0 & 0 & -7 \\ -7 & 0 & 7+\frac{7}{2\sqrt{2}} & -\frac{7}{2\sqrt{2}} & -\frac{7}{2\sqrt{2}} & \frac{7}{2\sqrt{2}} \\ 0 & 0 & -\frac{7}{2\sqrt{2}} & \frac{7}{2\sqrt{2}} & \frac{7}{2\sqrt{2}} & -\frac{7}{2\sqrt{2}} \\ 0 & 0 & -\frac{7}{2\sqrt{2}} & \frac{7}{2\sqrt{2}} & \frac{7}{2\sqrt{2}} & -\frac{7}{2\sqrt{2}} \\ 0 & -7 & \frac{7}{2\sqrt{2}} & -\frac{7}{2\sqrt{2}} & -\frac{7}{2\sqrt{2}} & \frac{7}{2\sqrt{2}}+7 \end{bmatrix} \begin{bmatrix} u_1 \\ u_2 \\ u_3 \\ u_4 \\ u_5 \\ u_6 \end{bmatrix} = \begin{bmatrix} 0 \\ 0 \\ 0 \\ -10000 \\ 0 \\ 0 \end{bmatrix} \tag{3.82}$$

Note that the only force component of the right hand side of Eq. (3.82) that is different of zero is the fourth component, which is defined as the force value that is applied at the node two in the opposite direction of the fourth unknown displacement.

The solution of Eq. (3.82) is not possible to obtain, because the system matrix is singular. Thus, to solve Eq. (3.82) is essential take in account the boundary conditions of the problem. In fact, this matrix can be reduced after applying boundary conditions, i.e. global displacements u_1, u_2 and u_5 are all known and their values are

$$u_1 = u_2 = u_5 = 0 \tag{3.83}$$

This implies that the first, second and the fifth rows, and also the correspondent columns, will have no effect on the solution of the matrix equation. Hence, the corresponding rows and columns can be removed

$$\mathbf{K} = 10^8 \times \left[\begin{array}{cc|cc|cc} 7 & 0 & -7 & 0 & 0 & 0 \\ 0 & 7 & 0 & 0 & 0 & -7 \\ \hline -7 & 0 & 7+\frac{7}{2\sqrt{2}} & -\frac{7}{2\sqrt{2}} & -\frac{7}{2\sqrt{2}} & \frac{7}{2\sqrt{2}} \\ 0 & 0 & -\frac{7}{2\sqrt{2}} & \frac{7}{2\sqrt{2}} & \frac{7}{2\sqrt{2}} & -\frac{7}{2\sqrt{2}} \\ \hline 0 & 0 & -\frac{7}{2\sqrt{2}} & \frac{7}{2\sqrt{2}} & \frac{7}{2\sqrt{2}} & -\frac{7}{2\sqrt{2}} \\ 0 & -7 & \frac{7}{2\sqrt{2}} & -\frac{7}{2\sqrt{2}} & -\frac{7}{2\sqrt{2}} & \frac{7}{2\sqrt{2}}+7 \end{array}\right] \tag{3.84}$$

The condensed global matrix is a 3×3 matrix, given as follows:

$$\mathbf{K} = 10^8 \times \begin{bmatrix} 7 + \frac{7}{2\sqrt{2}} & -\frac{7}{2\sqrt{2}} & \frac{7}{2\sqrt{2}} \\ -\frac{7}{2\sqrt{2}} & \frac{7}{2\sqrt{2}} & -\frac{7}{2\sqrt{2}} \\ \frac{7}{2\sqrt{2}} & -\frac{7}{2\sqrt{2}} & \frac{7}{2\sqrt{2}} + 7 \end{bmatrix} \tag{3.85}$$

It can easily be confirmed that this condensed stiffness matrix is semi-positive defined. Thus, the constrained global finite element equation is written as

$$10^8 \times \begin{bmatrix} 7 + \frac{7}{2\sqrt{2}} & -\frac{7}{2\sqrt{2}} & \frac{7}{2\sqrt{2}} \\ -\frac{7}{2\sqrt{2}} & \frac{7}{2\sqrt{2}} & -\frac{7}{2\sqrt{2}} \\ \frac{7}{2\sqrt{2}} & -\frac{7}{2\sqrt{2}} & \frac{7}{2\sqrt{2}} + 7 \end{bmatrix} \begin{bmatrix} u_3 \\ u_4 \\ u_6 \end{bmatrix} = \begin{bmatrix} 0 \\ -10000 \\ 0 \end{bmatrix} \tag{3.86}$$

The final step would be to solve Eq. (3.86) to obtain the unknown displacements. For that, is possible to use direct or iterative solution methods, but since this equation only involves three unknowns is also possible to obtain the solution manually. To this end, we obtain

$$\begin{aligned} u_3 &= -1.429 \times 10^{-5} m \\ u_4 &= -6.898 \times 10^{-5} m \\ u_6 &= -1.429 \times 10^{-5} m \end{aligned} \tag{3.87}$$

To obtain the stresses in the elements the Eq. (3.33) is used as follows:

$$\sigma_{11}^{(1)} = E(\mathbf{BTu})^{(1)} = 70 \times 10^9 \begin{bmatrix} -1 & 1 \end{bmatrix} \begin{bmatrix} 1 & 0 & 0 & 0 \\ 0 & 0 & 1 & 0 \end{bmatrix} \begin{bmatrix} u_1 = 0 \\ u_2 = 0 \\ u_3 = -1.429 \\ u_4 = -6.898 \end{bmatrix} \times 10^{-5}$$

$$= -1.0\, M\text{Pa} \tag{3.88}$$

$$\sigma_{11}^{(2)} = E(\mathbf{BTu})^{(2)} = 70 \times 10^9 \begin{bmatrix} -\frac{1}{\sqrt{2}} & \frac{1}{\sqrt{2}} \end{bmatrix} \begin{bmatrix} -\frac{1}{\sqrt{2}} & \frac{1}{\sqrt{2}} & 0 & 0 \\ 0 & 0 & -\frac{1}{\sqrt{2}} & \frac{1}{\sqrt{2}} \end{bmatrix} \begin{bmatrix} u_3 = -1.429 \\ u_4 = -6.898 \\ u_5 = 0 \\ u_6 = -1.429 \end{bmatrix}$$

$$\times 10^{-5} = 1.4\, M\text{Pa} \tag{3.89}$$

$$\sigma_{11}^{(3)} = E(\mathbf{BTu})^{(3)} = 70 \times 10^9 \begin{bmatrix} -1 & 1 \end{bmatrix} \begin{bmatrix} 0 & 1 & 0 & 0 \\ 0 & 0 & 0 & 1 \end{bmatrix} \begin{bmatrix} u_1 = 0 \\ u_2 = 0 \\ u_5 = 0 \\ u_6 = -1.429 \end{bmatrix} \times 10^{-5}$$

$$= -1.0\ M\text{Pa} \tag{3.90}$$

Note that in Eqs. (3.88), (3.89) and (3.90) the vector of the global element degrees of freedom can be defined from the rows of Table 3.4. The element axial forces can be obtained from the classical relations, as

$$\begin{aligned} \mathrm{P}^{(1)} &= \sigma_{11}^{(1)} A^{(1)} = -10000\ \mathrm{N} \\ \mathrm{P}^{(2)} &= \sigma_{11}^{(2)} A^{(2)} = 14142\ \mathrm{N} \\ \mathrm{P}^{(3)} &= \sigma_{11}^{(3)} A^{(3)} = -10000\ \mathrm{N} \end{aligned} \tag{3.91}$$

Moreover, using those equations that were eliminated in Eq. (3.84) is possible to write

$$\begin{aligned} &\Big[7 \times (u_1 = 0) + 0 \times (u_2 = 0) - 7 \times \left(u_3 = -1.429 \times 10^{-5}\right) + 0 \times \left(u_4 = -6.898 \times 10^{-5}\right) \\ &\quad + 0 \times (u_5 = 0) + 0 \times \left(u_6 = -1.429 \times 10^{-5}\right) \Big] \times 10^8 = F_1 \\ &\Big[0 \times (u_1 = 0) + 7 \times (u_2 = 0) + 0 \times \left(u_3 = -1.429 \times 10^{-5}\right) + 0 \times \left(u_4 = -6.898 \times 10^{-5}\right) \\ &\quad + 0 \times (u_5 = 0) - 7 \times \left(u_6 = -1.429 \times 10^{-5}\right) \Big] \times 10^8 = F_2 \\ &\Big[0 \times (u_1 = 0) + 0 \times (u_2 = 0) - \frac{7}{2\sqrt{2}} \times \left(u_3 = -1.429 \times 10^{-5}\right) + \frac{7}{2\sqrt{2}} \\ &\quad \times \left(u_4 = -6.898 \times 10^{-5}\right) + \frac{7}{2\sqrt{2}} \times (u_5 = 0) - \frac{7}{2\sqrt{2}} \times \left(u_6 = -1.429 \times 10^{-5}\right) \Big] \times 10^8 = F_5 \end{aligned} \tag{3.92}$$

leading to

$$\begin{aligned} H_1 &= F_1 \approx 10000 \\ V_1 &= F_2 \approx 10000 \\ H_2 &= F_5 \approx -10000 \end{aligned} \tag{3.93}$$

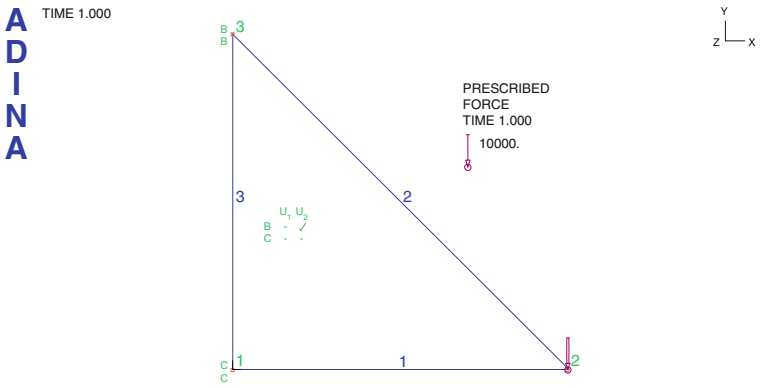

Fig. 3.14 Finite element mesh, loading, and boundary conditions of the three-element truss

Equations (3.91) and (3.92) give the reaction values. The numerical solution presented here can be compared with that computed by the finite element program ADINA [6]. In this program the truss structure is meshed by two-nodal truss finite elements with two degrees of freedom per node. The skeletal model of the truss structure is showed in Fig. 3.14.

The ADINA program plot the boundary conditions using capital letters: B, the only displacement constrained is that in the x-axes direction; C the displacement of nodal point 1 is constrained in both axes directions. Using the ADINA input file, the finite element equations are solved and the results are presented in Fig. 3.15. A deformation plot showing how the truss actually deforms under the specified loading is shown in Fig. 3.15a, in which is also presented the contour plot of the displacement magnitude. The magnitude of the deformation is magnified 10 % as the truly deformation is much smaller for viewing purposes. Figure 3.15b, c present the contour plot of the displacement in the x and y directions, while Fig. 3.15d, e present the contour plot of the axial stresses and axial forces, respectively. Finally, Fig. 3.15f shows the vector direction of the reaction forces.

Comparing the numerical results computed manually with those computed by ADINA program it can be seen that are coincident. Moreover, in engineering practice, problems can be of a much larger scale and, the unknowns or the number of degree of freedom will be higher. Therefore, numerical methods, or so-called solvers for solving the finite element equations have to be used. Typical real life engineering problems might involve hundreds of thousands, and even millions, of degrees of freedom. Many kinds of such solvers are routinely available in math or numerical libraries in computer systems [4].

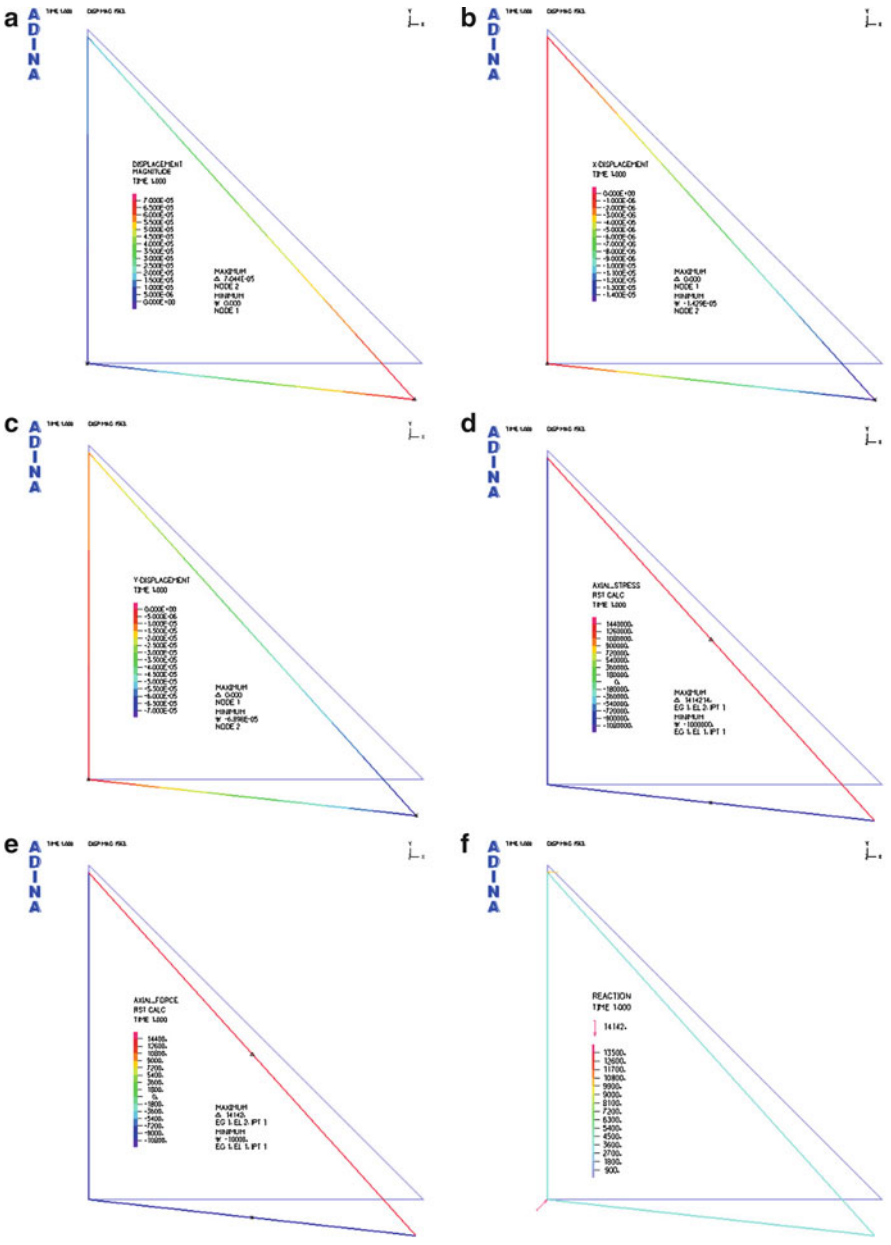

Fig. 3.15 ADINA numerical solution: (**a**) displacement magnitude; (**b**) x displacement; (**c**) y displacement; (**d**) axial stress; (**e**) axial force; (**f**) reactions magnitude

3.3 Review Questions

1. Consider the bar in Fig. 3.16. The bar has a variable cross-section area, denoted by A and, it is fixed at one end and loaded by a constant body force distributed in the truss axial direction, as shown. The material of the bar is isotropic with Young's modulus E.

   (a) Solve for the exact displacement response of the structure.
   (b) Using Eq. (3.15) compute the element stiffness matrix.
   (c) Using Eq. (3.16) compute the element mass matrix
   (d) Using the information of questions b and c, compute the maximum value of axial displacement and compare with the solution of question a.

2. How many degrees of freedom does a two-node 2D truss finite element has in its local coordinate system, and in the global coordinate system? If there are some differences, justify the answer.
3. How many degrees of freedom does a two-node 3D truss finite element has in its local coordinate system, and in the global coordinate system? justify.
4. Using a finite element program, work out the reaction forces of the truss structure shown in Fig. 3.17. All the truss members are of the same material (E = 210 GPa) and with the same cross-sectional area of 0.000314 m^2.

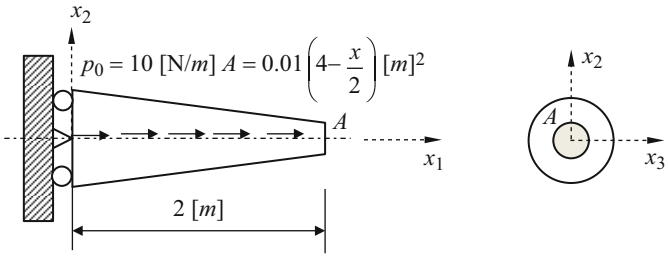

Fig. 3.16 Truss structure with a non-uniform cross-section area

Fig. 3.17 Truss structure

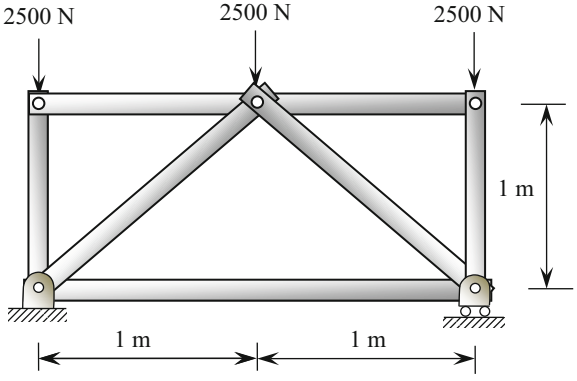

References

1. Bathe K-J (1996) Finite element procedures. Prentice Hall, Englewood Cliffs
2. Zienkiewicz OC, Morgan K (1983) Finite elements and approximation. Wiley, New York
3. Zienkiewicz OC, Taylor RL (2000) The finite element method. Butterworth-Heinemann, Woburn
4. Liu GR, Quek SS (2003) The finite element method: A practical course. Butterworth-Heinemann, Burlington
5. Timoshenko SP, Young DH (1965) Theory of structures. McGraw-Hill, Tokyo
6. ADINA R & D I (2014) User's manual. R & D Inc., Boston

Chapter 4
Finite Element Method for Beams

A beam is a structural member whose geometry is very similar to the geometry of a bar. It is also geometrically a bar of an arbitrary cross-section, by bar it is meant that one of the dimensions is considerably larger than the other two, whose primary function is to support transverse loading. The main difference between the beam and the truss is the type of load that they support. In fact, beams are the most common type of structural component, especially in civil and mechanical engineering. A beam resists to transverse loads mainly through a bending action and, the bending is responsible for compressive longitudinal stresses in one side of the beam and tensile stress on the other beam side. These two regions are separated by the neutral axis in which the stress is zero. The combination of tensile and compressive stresses produces an internal bending moment. Finite element equations for beam-like structures are developed in this chapter.

4.1 FE Matrices and Vectors of Beams

In beam structures, the beams are linked by welding, so forces and moments are transmitted among beams. The basic concepts, procedures and formulations can also be found in a great number of existing books [1–4]. In this presentation it will be assumed that beam elements have uniform cross-section. In fact, if a beam has a varying cross-section it can be divided into shorter elements where each one can be seen as a beam with a uniform cross-section. Nevertheless, the finite element matrices for varying cross-section geometry can also be developed easily using the concepts before introduced. The beam elements presented in this chapter are based on the Euler-Bernoulli theory that is applicable to thin beams made of isotropic material.

M.A. Neto et al., *Engineering Computation of Structures: The Finite Element Method*, DOI 10.1007/978-3-319-17710-6_4

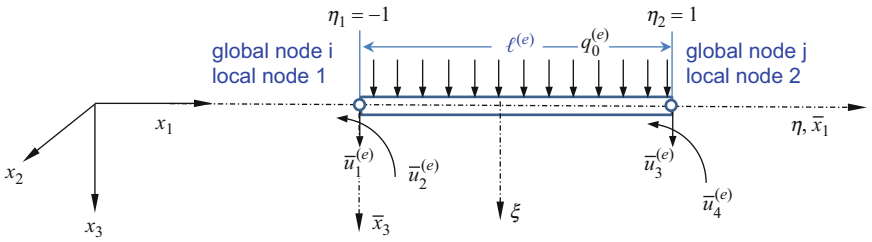

Fig. 4.1 Beam finite element with four degrees of freedom

4.1.1 Degrees of Freedom Identification

A plane beam resists primarily to transverse loading on a preferred longitudinal plane. Thus, in a planar beam the finite element has two degrees of freedom per node at its local coordinate system: displacement in the transverse direction and rotation around the axis normal to the beam plane. The application of the finite element method involves dividing the domain into subdomains with features and loading simple to treat. In the case of a structure consisting of beam elements, let consider that each structural element has constant elastic properties and uniform cross-section. Moreover, let's assume that each of these structural elements is bounded by two nodes ($n = 2$). Therefore, each beam finite element has a total of four degrees of freedom, as shown in Fig. 4.1.

Consider the beam divided into m finite elements from which the element (e) is highlighted, as presented in Fig. 4.1, the extreme points of this element are called nodal points and are identified by their coordinate η_1 and η_2 along the local axis η, which is coincident with the beam axis and has the origin at the middle section of the beam. Note that often is more convenient to develop the shape functions using the natural coordinate system than using the local coordinate system, $\bar{x}$. The relationship between both coordinate systems is presented at Chap. 3 on Eq. (3.49).

4.1.2 FE Approximation of the Displacement

Taking in account the FEM discussed in the previous chapter, the finite element displacement should be written in the form

$$\tilde{w}(\eta) = \overline{\mathbf{N}}(\eta)\,\overline{\mathbf{u}} \tag{4.1}$$

where $\tilde{w}$ is the axial approximation within the finite element (e), $\overline{\mathbf{N}}$ is the matrix of shape functions with the inherent properties described in Chap. 2 and $\bar{\mathbf{u}}$ is the vector of finite element displacements, defined as

$$\overline{\mathbf{u}} = \begin{bmatrix} \overline{u}_1 \\ \overline{u}_2 \\ \overline{u}_3 \\ \overline{u}_4 \end{bmatrix} \tag{4.2}$$

For construction the shape functions to the beam element, the standard procedure described in Sect. 2.3.3 is followed. Since there are four DOFs, i.e. four unknowns, a complete basis of order $p = 3$ can be given in a general form

$$\tilde{w}(\eta) = a_0 + a_1\eta + a_2\eta^2 + a_3\eta^3 = \underbrace{\begin{bmatrix} 1 & \eta & \eta^2 & \eta^3 \end{bmatrix}}_{\mathbf{\Phi}^T} \underbrace{\begin{bmatrix} a_0 \\ a_1 \\ a_2 \\ a_3 \end{bmatrix}}_{\mathbf{a}} = \mathbf{\Phi}^T\mathbf{a} \tag{4.3}$$

where $-1 \leq \eta \leq 1$, $\mathbf{\Phi}$ is the vector of basis function and $\mathbf{a}$ is the vector of unknowns parameters, as discussed in Chaps. 2 and 3. Note that because the second and the fourth degrees of freedom of the finite element represent the rotations of the beam cross-sections at the first and the second nodes, respectively, it is important to evaluate the differential of Eq. (4.3), as following:

$$\frac{\partial w}{\partial \overline{x}} = \frac{\partial w}{\partial \eta}\frac{\partial \eta}{\partial \overline{x}} = \frac{2}{\ell}\frac{\partial w}{\partial \eta} = \frac{2}{\ell}\left(a_1 + 2a_2\eta + 3a_3\eta^2\right) \tag{4.4}$$

In fact, Euler-Bernoulli theory states that both displacement and rotations must be continuous over the entire domain: within finite elements and in particular between elements. The shape functions that meet this requirement are said to have C^1 continuity. The requirement of the continuity of shape functions within each finite element can be trivially achieved, since these functions are interpolated through polynomial functions that are C^∞ continuous. The inter-element continuity is obtained by matching nodal displacements and rotations with adjacent elements. The physical reason of C^1 continuity is illustrated in Fig. 4.2, where the displacement is grossly exaggerated for better visibility.

As discussed previously, due to the fact that the finite element (e) is connected to the neighbor's finite elements by its nodes, the solution given by Eq. (4.3) is

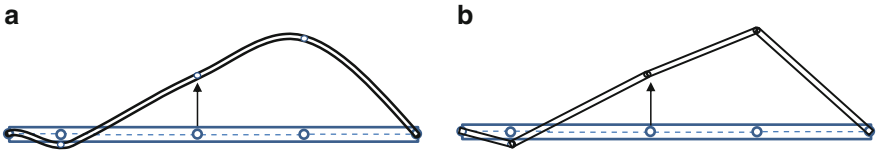

Fig. 4.2 Amplification of the deformation of a beam discretized with four elements: (**a**) Cubic deflection elements; (**b**) linear deflection elements. The linear version maintains only C^0 continuity, leading to material gaps and interpenetration at nodes

admissible only if the support conditions in the nodal points are verified, i.e. the displacements of nodal points should be

$$\textit{first node} \begin{cases} \tilde{w}(\eta_1 = -1) = \overline{u}_1 \\ \dfrac{\partial \tilde{w}(\eta_1 = -1)}{\partial \overline{x}} = \overline{u}_2 \end{cases} \tag{4.5}$$

$$\textit{second node} \begin{cases} \tilde{w}(\eta_1 = 1) = \overline{u}_3 \\ \dfrac{\partial \tilde{w}}{\partial \overline{x}}(\eta_1 = 1) = \overline{u}_4 \end{cases} \tag{4.6}$$

Using Eqs. (4.3) and (4.4) to establish the relations on Eqs. (4.5) and (4.6), gives

$$\underbrace{\begin{bmatrix} \overline{u}_1 \\ \overline{u}_2 \\ \overline{u}_3 \\ \overline{u}_4 \end{bmatrix}}_{\overline{\mathbf{u}}} = \underbrace{\begin{bmatrix} 1 & -1 & 1 & -1 \\ 0 & 2/\ell & -4/\ell & 6/\ell \\ 1 & 1 & 1 & 1 \\ 0 & 2/\ell & 4/\ell & 6/\ell \end{bmatrix}}_{\mathbf{C}} \underbrace{\begin{bmatrix} a_0 \\ a_1 \\ a_2 \\ a_3 \end{bmatrix}}_{\mathbf{a}} \tag{4.7}$$

Solving Eq. (4.7) for parameters $\mathbf{a}$, leads to

$$\underbrace{\begin{bmatrix} a_0 \\ a_1 \\ a_2 \\ a_3 \end{bmatrix}}_{\mathbf{a}} = \frac{1}{4} \underbrace{\begin{bmatrix} 2 & \ell & 2 & -\ell \\ -3 & -\ell & 3 & -\ell \\ 0 & -\ell & 0 & \ell \\ 1 & \ell & -1 & \ell \end{bmatrix}}_{\mathbf{C}^{-1}} \underbrace{\begin{bmatrix} \overline{u}_1 \\ \overline{u}_2 \\ \overline{u}_3 \\ \overline{u}_4 \end{bmatrix}}_{\overline{\mathbf{u}}} \tag{4.8}$$

Substituting the above equation into Eq. (4.3), leads to

$$\tilde{w}(\eta) = \mathbf{\Phi}^T \mathbf{a} = \mathbf{\Phi}^T \mathbf{C}^{-1} \overline{\mathbf{u}} = \overline{\mathbf{N}}(\eta)\, \overline{\mathbf{u}} \tag{4.9}$$

where $\overline{\mathbf{N}}$ is a matrix of shape functions defined as

$$\overline{\mathbf{N}}(\eta) = \begin{bmatrix} N_1(\eta) & N_2(\eta) & N_3(\eta) & N_4(\eta) \end{bmatrix} \tag{4.10}$$

where the shape functions are written as

$$\begin{aligned} N_1(\eta) &= \frac{1}{4}\left(2 - 3\eta + \eta^3\right) \\ N_2(\eta) &= \frac{\ell}{8}\left(1 - \eta - \eta^2 + \eta^3\right) \\ N_3(\eta) &= \frac{1}{4}\left(2 + 3\eta - \eta^3\right) \\ N_4(\eta) &= \frac{\ell}{8}\left(-1 - \eta + \eta^2 + \eta^3\right) \end{aligned} \tag{4.11}$$

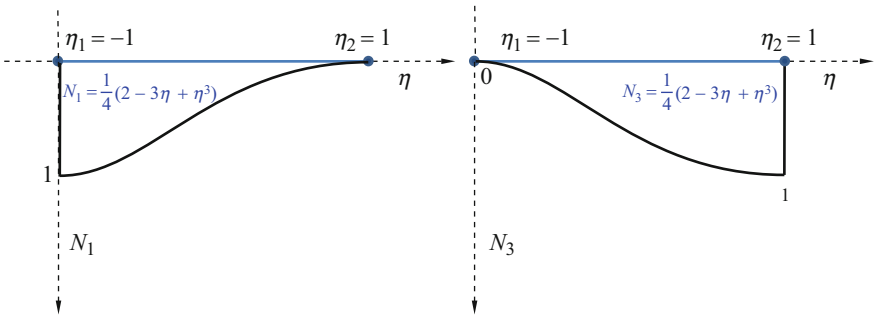

Fig. 4.3 Cubic displacement shape functions of a plane beam element

and their derivatives are

$$\begin{aligned} N_{1_\eta}(\eta) &= \frac{1}{4}\left(-3 + 3\eta^2\right) \\ N_{2_\eta}(\eta) &= \frac{\ell}{8}\left(-1 - 2\eta + 3\eta^2\right) \\ N_{3_\eta}(\eta) &= \frac{1}{4}\left(3 - 3\eta^2\right) \\ N_{4_\eta}(\eta) &= \frac{\ell}{8}\left(-1 + 2\eta + 3\eta^2\right) \end{aligned} \tag{4.12}$$

It can be easily confirmed that the two translational shapes functions N_1 and N_3 verify the conditions defined by Eqs. (2.29) and (2.36), which graphical representation is presented in Fig. 4.3. It can be easily confirmed that both rotational shapes functions N_2 and N_4 don't satisfy Eqs. (2.29) and (2.36). This is because these two shape functions are related to the rotational degrees of freedom and, therefore, they should verify that their derivative with respect $\bar{x}$ satisfy Eq. (2.29), i.e.

$$\begin{aligned} N_{1_{\bar{x}}}(\eta) &= N_{1_\eta}(\eta) \times \frac{2}{\ell} = \frac{1}{4}\left(-3 + 3\eta^2\right) \times \frac{2}{\ell} \\ N_{2_{\bar{x}}}(\eta) &= N_{2_\eta}(\eta) \times \frac{2}{\ell} = \frac{\ell}{8}\left(-1 - 2\eta + 3\eta^2\right) \times \frac{2}{\ell} \\ N_{3_{\bar{x}}}(\eta) &= N_{3_\eta}(\eta) \times \frac{2}{\ell} = \frac{1}{4}\left(3 - 3\eta^2\right) \times \frac{2}{\ell} \\ N_{4_{\bar{x}}}(\eta) &= N_{4_\eta}(\eta) \times \frac{2}{\ell} = \frac{\ell}{8}\left(-1 + 2\eta + 3\eta^2\right) \times \frac{2}{\ell} \end{aligned} \tag{4.13}$$

The graphical representation of $N_{2_{\bar{x}}}$ and $N_{4_{\bar{x}}}$ is presented in Fig. 4.4.

From Fig. 4.3, it is clear that functions N_i $(i = 1, 3)$ gives the shape of the contribution of the ith displacement degree of freedom to the displacement approximation

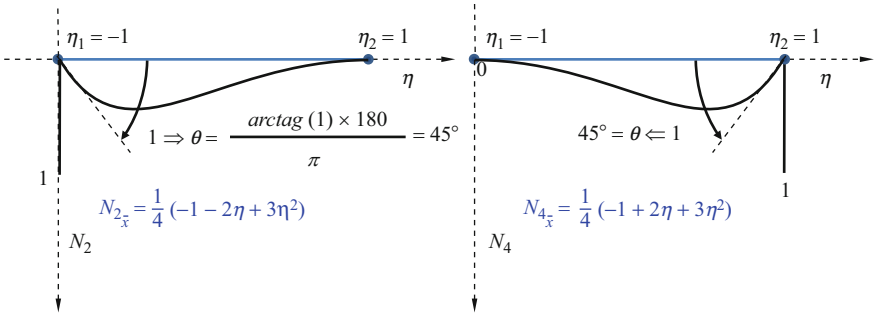

Fig. 4.4 Cubic rotational shape functions of a plane beam element

inside the finite element, while in the Fig. 4.4 N_i $(i = 2, 4)$ gives the shape of the contribution of the ith of rotational degrees of freedom to the element displacement approximation.

4.1.3 FE Approximation of Strain

As discussed in previous chapter, after computing shape functions is possible to obtain others quantities, namely the relationship between the strain and the deflection described in Eq. (1.111), as

$$\tilde{\varepsilon}_{11}(\bar{x}) = -\bar{x}_3 \frac{d^2\tilde{w}(\bar{x})}{d\bar{x}^2} = -\bar{x}_3 \frac{d\eta}{d\bar{x}} \times \frac{d\eta}{d\bar{x}} \times \frac{d^2\tilde{w}(\eta)}{d\eta^2} \tag{4.14}$$

In the previous chapter it was showed that the stiffness matrix is obtained using the finite element strain matrix **B**. In the case of a beam finite element, Eq. (4.15) can be re-written in a matrix form as

$$\tilde{\varepsilon}_{11}(\bar{x}) = -\frac{d\eta}{d\bar{x}} \times \frac{d\eta}{d\bar{x}} \times \frac{d^2\tilde{w}(\eta)}{d\eta^2} = -\frac{4\bar{x}_3}{\ell^2} \frac{d^2\overline{\mathbf{N}}}{d\eta^2}\,\overline{\mathbf{u}} = \overline{\mathbf{B}}\,\overline{\mathbf{u}} \tag{4.15}$$

where the strain matrix $\overline{\mathbf{B}}$ has the following form

$$\begin{aligned} \overline{\mathbf{B}} = L\overline{\mathbf{N}} &= -\frac{4\bar{x}_3}{\ell^2}\frac{d^2}{d\eta^2}\left[N_1(\eta)\;\; N_2(\eta)\;\; N_3(\eta)\;\; N_4(\eta)\right] \\ &= -\frac{\bar{x}_3}{\ell^2}\left[6\eta\;\ell\,(-1+3\eta)\;\; -6\eta\;\ell\,(1+3\eta)\right] \\ &= -\frac{\bar{x}_3}{\ell^2}\overline{\mathbf{N}}_{\eta\eta} \end{aligned} \tag{4.16}$$

4.1.4 Element Matrices in Local Coordinate System

The stiffness matrix for the beam finite element can be obtained substituting Eq. (4.16) into (2.49), leading to

$$\begin{aligned}\overline{\mathbf{k}} &= \int_{\Omega^e} \overline{\mathbf{B}}^T \mathbf{c}\, \overline{\mathbf{B}}\, d\Omega^e = E \int_A \frac{x_3^2}{\ell^4}\, dA \int_0^\ell \overline{\mathbf{N}}_{\eta\eta}^T\, \overline{\mathbf{N}}_{\eta\eta}\, d\bar{x} = \frac{E}{\ell^4} \int_A x_3^2\, dA \int_{-1}^1 \overline{\mathbf{N}}_{\eta\eta}^T\, \overline{\mathbf{N}}_{\eta\eta}\, \frac{\ell}{2} d\eta \\ &= \frac{E}{2\ell^3} \int_A x_3^2\, dA \int_{-1}^1 \overline{\mathbf{N}}_{\eta\eta}^T\, \overline{\mathbf{N}}_{\eta\eta}\, d\eta = \frac{EI}{2\ell^3} \int_{-1}^1 \overline{\mathbf{N}}_{\eta\eta}^T\, \overline{\mathbf{N}}_{\eta\eta}\, d\eta \\ &= \frac{EI}{\ell^3} \int_{-1}^1 \begin{bmatrix} N_{1_{\eta\eta}} N_{1_{\eta\eta}} & N_{1_{\eta\eta}} N_{2_{\eta\eta}} & N_{1_{\eta\eta}} N_{3_{\eta\eta}} & N_{1_{\eta\eta}} N_{4_{\eta\eta}} \\ & N_{2_{\eta\eta}} N_{2_{\eta\eta}} & N_{2_{\eta\eta}} N_{3_{\eta\eta}} & N_{2_{\eta\eta}} N_{4_{\eta\eta}} \\ & & N_{3_{\eta\eta}} N_{3_{\eta\eta}} & N_{3_{\eta\eta}} N_{4_{\eta\eta}} \\ \textit{sym.} & & & N_{4_{\eta\eta}} N_{4_{\eta\eta}} \end{bmatrix} d\eta \end{aligned} \tag{4.17}$$

where $I = \int_A x_3^2 dA$ is the second moment of area of the cross-section of the beam with respect to the x_2 axis. Evaluating the integrals in Eq. (4.17) leads to

$$\overline{\mathbf{k}} = \frac{EI}{\ell^3} \begin{bmatrix} 12 & 6\ell & -12 & 6\ell \\ & 4\ell^2 & -6\ell & 2\ell^2 \\ & & 12 & -6\ell \\ \textit{sym.} & & & 4\ell^2 \end{bmatrix} \tag{4.18}$$

To evaluate the mass matrix, Eqs. (4.10) and (4.11) are substituted into Eq. (2.45), leading to

$$\begin{aligned}\overline{\mathbf{m}} &= \int_{\Omega^e} \rho \overline{\mathbf{N}}^T \overline{\mathbf{N}}\, d\Omega^e = A\rho \int_0^\ell \overline{\mathbf{N}}^T \overline{\mathbf{N}}\, d\bar{x} = A\rho \int_{-1}^1 \overline{\mathbf{N}}^T \overline{\mathbf{N}}\, \frac{\ell}{2} d\eta \\ &= \frac{A\rho\ell}{2} \int_{-1}^1 \begin{bmatrix} N_1 N_1 & N_1 N_2 & N_1 N_3 & N_1 N_4 \\ & N_2 N_2 & N_2 N_3 & N_2 N_4 \\ & & N_3 N_3 & N_3 N_4 \\ \textit{sym.} & & & N_4 N_4 \end{bmatrix} d\eta \end{aligned} \tag{4.19}$$

where A is the area of the cross-section of the beam. Integrating the Eq. (4.19) the final element mass matrix is obtained

$$\overline{\mathbf{m}} = \frac{A\rho\ell}{420}\begin{bmatrix} 156 & 22\ell & 54 & -13\ell \\ & 4\ell^2 & 13\ell & -3\ell^2 \\ & & 156 & -22\ell \\ sym. & & & 4\ell^2 \end{bmatrix} \tag{4.20}$$

The nodal force vector for beam elements is obtained using Eqs. (4.11) and (2.52), assuming that the element is loaded by a constant distributed force q_0 along the $\bar{x}_3$-axis. The total nodal force vector becomes

$$\bar{\mathbf{f}} = \int_{\Omega^e} \overline{\mathbf{N}}^T \mathbf{f}_b \, d\Omega^e = q_0 \int_0^{\ell} \begin{bmatrix} N_1 \\ N_2 \\ N_3 \\ N_4 \end{bmatrix} d\bar{x} = q_0 \int_{-1}^{+1} \begin{bmatrix} N_1 \\ N_2 \\ N_3 \\ N_4 \end{bmatrix} \frac{\ell}{2} d\eta = \frac{q_0\ell}{2} \begin{bmatrix} 1 \\ \ell/6 \\ 1 \\ -\ell/6 \end{bmatrix} \tag{4.21}$$

Equation (4.21) shows that a uniform transverse load over a beam finite element can be replaced by two transverse node loads of value $(q_0\ell)/2$, as may be expected, and by two nodal moments of values $\pm\left(q_0\ell^2\right)/12$.

4.1.5 Element Matrices in the Global Coordinate System

Element matrices presented before are formulated in the local coordinate system, in which the local axis are parallel to the reference or global coordinate system. Thus a coordinate system transformation has not to be performed, since the transformation matrix is an identity matrix.

4.1.6 First Discussion Example

Example 4.1: A Cantilever Beam Subjected to a Downward Force
Consider the cantilever beam presented in Fig. 4.5. The beam is fixed at one end, and at the free end has a downward load of 1 kN. The cross-section of the beam is uniform and is also presented in Fig. 4.5. The beam is made of aluminium with an Young's modulus of 69 GPa and a Poisson's ratio of 0.33.

Exact Solutions
The exact solution can be obtained from the strong formulation of a beam structure, namely from the governing Eq. (1.156), of Chap. 1. Since the beam is free of body forces, the equation can now be written as

$$EI\frac{\partial^4 w}{\partial \bar{x}_1{}^4} = 0 \tag{4.22}$$

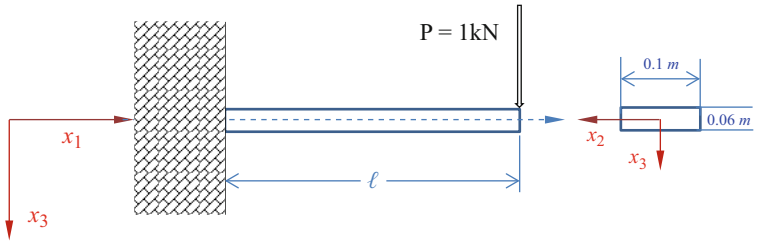

Fig. 4.5 Cantilever beam under a static load

The general solution of Eq. (4.22) is obtained after four integrations, as

$$w(\bar{x}) = c_0 + c_1\bar{x} + c_2\bar{x}^2 + c_3\bar{x}^3 \tag{4.23}$$

where c_i $(i = 0, 1, 2, 3)$ are unknown constants that can be determined by the boundary conditions. Since the displacement and the rotation at the fixed end are known, the displacement and rotation boundary conditions for this case are

$$w(\bar{x} = 0) = 0 \tag{4.24}$$

$$\left.\frac{\partial w}{\partial \bar{x}}\right|_{\bar{x}=0} = 0 \tag{4.25}$$

and, therefore, Eq. (4.24) leads to $c_0 = 0$, Eq. (4.25) leads to $c_1 = 0$. To compute c_2 and c_3 is necessary to use the natural boundary condition of beam structures. The natural boundary conditions are related with the transverse load and with the bending moment at the free end of beam, as

$$\left.\frac{\partial}{\partial \bar{x}}\left(-EI\frac{\partial^2 w}{\partial \bar{x}^2}\right)\right|_{\bar{x}=\ell} = P \Rightarrow c_3 = -\frac{P}{6EI} \tag{4.26}$$

$$\left.EI\frac{\partial^2 w}{\partial \bar{x}^2}\right|_{\bar{x}=\ell} = 0 \Rightarrow c_2 = -3c_3\ell = \frac{3P\ell}{6EI} \tag{4.27}$$

Substituting c_i $(i = 0, 1, 2, 3)$ into Eq. (4.23), the solution of the displacement of the beam is written as

$$w(\bar{x}) = \frac{\mathrm{P}\bar{x}^2}{6EI}(3\ell - \bar{x}) \tag{4.28}$$

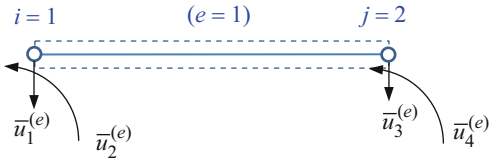

Fig. 4.6 A beam modeled by one finite element

and the displacement at the free end is given by

$$w\left(\overline{x}=\ell\right)=\frac{\mathrm{P}\ell^3}{3EI} \tag{4.29}$$

The second moment of area of the beam cross-section related with the x_2 is given by

$$I=\frac{bh^3}{12}=\frac{1}{12}0.1\times 0.06^3=1.8\times 10^{-6}m^4 \tag{4.30}$$

and, assuming a beam length of 0.5 m, using this information in Eq. (4.29), the displacement at the free end is of $3.355\times 10^{-4}m$. Moreover, the rotation of the cross-section at the free end is given by

$$\left.\frac{\partial w}{\partial \overline{x}}\right|_{\overline{x}=\ell}=\left.\left(\frac{P}{2EI}\overline{x}\left(2\ell-\overline{x}\right)\right)\right|_{\overline{x}=\ell}=\frac{P\ell^2}{2EI}=1.01\times 10^{-3}rad \tag{4.31}$$

Numerical Solution

To evaluate the numerical solution is necessary to perform the discretization of the beam. Using one finite element, the bar finite element model is represented in Fig. 4.6.

The element stiffness matrix is defined in local coordinate system by Eq. (4.18), and there is no need to perform coordinate transformation, since local and global coordinate systems are parallel. Moreover, as the number of elements at the bar finite element is only one, there is also no need to perform assembly. The finite element equations becomes

$$\frac{EI}{\ell^3}\begin{bmatrix}12 & 6\ell & -12 & 6\ell\\ 6\ell & 4\ell^2 & -6\ell & 2\ell^2\\ -12 & -6\ell & 12 & -6\ell\\ 6\ell & 2\ell^2 & -6\ell & 4\ell^2\end{bmatrix}\begin{bmatrix}u_1^1\\ u_2^1\\ u_3^1\\ u_4^1\end{bmatrix}=\begin{bmatrix}F_1\\ F_2\\ F_3\\ F_4\end{bmatrix} \tag{4.32}$$

The right hand side of Eq. (4.32) is related with the load vector components, since there is only one concentrated load P applied in the global node $j=2$, component F_3 is equal to P, F_1 and F_2 are reactions at the fixed end while F_4 is zero because there is no applied moment at node $j=2$.

To solve Eq. (4.32) it is necessary to impose boundary conditions. Since the displacement and the rotation at node i are zero, the easy way of imposing this boundary condition is to simply remove the first and the second rows and the first and the second columns of Eq. (4.32), leading to

$$\begin{bmatrix} 12 & -6\ell \\ -6\ell & 4\ell^2 \end{bmatrix} \begin{bmatrix} u_3^1 \\ u_4^1 \end{bmatrix} = \frac{\ell^3}{EI} \begin{bmatrix} P \\ 0 \end{bmatrix} \tag{4.33}$$

The matrix in Eq. (4.33) can be inverted leading to

$$\begin{bmatrix} u_3^1 \\ u_4^1 \end{bmatrix} = \frac{\ell}{12EI} \begin{bmatrix} 4\ell^2 & 6\ell \\ 6\ell & 12 \end{bmatrix} \begin{bmatrix} P \\ 0 \end{bmatrix} = \begin{bmatrix} \dfrac{\ell^3 P}{3EI} \\ \dfrac{\ell^2 P}{2EI} \end{bmatrix} \tag{4.34}$$

Comparing Eq. (4.34) with Eqs. (4.29) and (4.31) is possible to conclude that both solutions are coincident. After computing u_3^1 and u_4^1 they can be used back into the first two equations of Eq. (4.32) to obtain the reactions at node 1

$$\begin{aligned} F_1 = V_1 &= \frac{EI}{\ell^3} \left(-12 \times \frac{\ell^3 P}{3EI} + 6\ell \times \frac{\ell^2 P}{2EI} \right) \\ &= -P \text{ N} \end{aligned} \tag{4.35}$$

and

$$\begin{aligned} F_2 = M_1 &= \frac{EI}{\ell^3} \left(-6\ell \times \frac{\ell^3 P}{3EI} + 2\ell^2 \times \frac{\ell^2 P}{2EI} \right) \\ &= -P\ell \text{ N.m} \end{aligned} \tag{4.36}$$

These solutions agree with the analytical values provided by the Euler-Bernoulli Beam theory. Thus, the one-element idealization is enough for exactness. The reason is that the analytical deflection is cubic polynomial and it is included in the span of the element shape functions. This is also true if we were to calculate the deflection at any point within the finite element. For example, to calculate the deflection at the center of the beam, we can use the local coordinate or the natural coordinate system with $\eta = 0$, so substituting the values calculated at the nodes:

$$\tilde{w}(\eta) = \overline{\mathbf{N}}\Big|_{\eta=0} \overline{\mathbf{u}} = \begin{bmatrix} \frac{1}{2} & \frac{1}{16} & \frac{1}{2} & -\frac{1}{16} \end{bmatrix} \begin{bmatrix} 0 \\ 0 \\ \dfrac{\ell^3 P}{3EI} \\ \dfrac{\ell^2 P}{2EI} \end{bmatrix} = \frac{\ell^2 P}{EI} \left(\frac{\ell}{6} - \frac{1}{32} \right) \tag{4.37}$$

To evaluate the rotation at the center of the beam, the derivatives of the shape functions are used as follows:

$$\tilde{\theta}\Big|_{\eta=0} = \left(\frac{\partial \tilde{w}\,(\eta)}{\partial \bar{x}}\right)_{\eta=0} = \left(\frac{\partial \overline{\mathbf{N}}}{\partial \eta}\frac{\partial \eta}{\partial \bar{x}}\right)\Bigg|_{\eta=0} \bar{\mathbf{u}} = \left[-3\ -\frac{1}{4}\ 3\ -\frac{1}{4}\right]\begin{bmatrix} 0 \\ 0 \\ \dfrac{\ell^3 P}{3EI} \\ \dfrac{\ell^2 P}{2EI} \end{bmatrix} \tag{4.38}$$

$$= \frac{\ell^2 P}{EI}\left(\ell - \frac{1}{8}\right)$$

4.1.7 Second Discussion Example

Example 4.2: Modal Analysis of a Micro Transducer
This example has been presented by Liu and Quek [5] and it consists on the computation of the natural frequencies of a micro transducer. Figure 4.7 shows a micrograph of a micro polysilicon resonant micro-beam transducer. Resonant transducers allowing convert externally induced beam strain into a beam resonant frequency change. This change in resonant frequency is then typically detected by implanted piezoresistors or optical techniques. Such resonant transducers are used for measurements of pressure, acceleration, strain, vibration and so on. Technical systems that apply this technology are called electro-mechanical systems. Meanwhile, Micro-Electro-Mechanical Systems, or MEMS, is a technology that in its most general form can be defined as miniaturized mechanical and electro-mechanical elements that are made using the techniques of microfabrication. The critical physical dimensions of MEMS devices can vary from well below one micron on the lower end of the dimensional spectrum, all the way to several millimeters.

The principle of the resonant transducer actually lies in the clamped–clamped bridge on top of a membrane. This bridge is actually located at the center of the micrograph. Figure 4.8 shows a schematic side view of the bridge structure. The

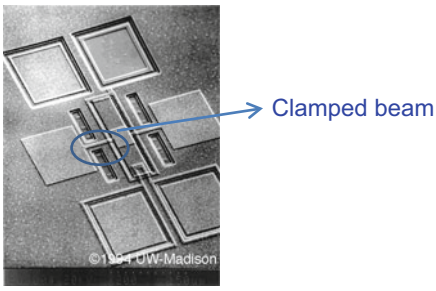

Fig. 4.7 Resonant micro-beam strain transducer [5]

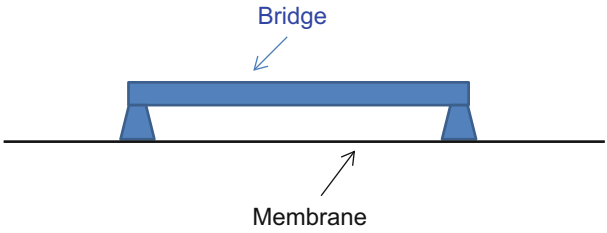

Fig. 4.8 Bridge in a micro resonant transducer [5]

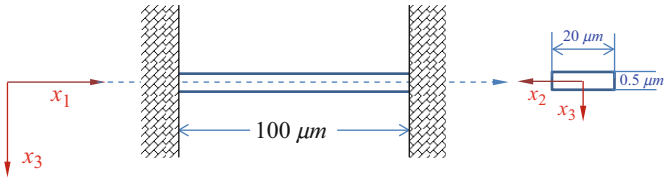

Fig. 4.9 Geometrical dimensions of a clamped-clamped bridge [5]

Table 4.1 Elastic properties of polysilicon

Young's Modulus, E	169 GPa	$0.169\ N(\mu m)^{-2}$
Poisson's ratio, ν	0.262	
Density, ρ	2,300 Kg/m^3	$2.3\times10^{-15} Kg/\mu m^3$

resonant frequency of the bridge is related to the force applied to it (between anchor points), its material properties, cross-sectional area and length. When the membrane deforms, for example, due to a change in pressure, the force applied to the bridge also changes, resulting in a variation in the resonant frequency of the bridge.

Thus, it is important to analyze the resonant frequency of this bridge structure in the design of the resonant transducer. The beam finite element in the software ADINA is used to solve the first three resonant frequencies of the bridge. The dimensions of the clamped–clamped bridge structure shown in Fig. 4.9 are used to model a bridge in a micro resonant transducer. The material properties of polysilicon, normally, used to make the resonant transducer, are shown in Table 4.1.

Note that ADINA input files does not mention the units of measurements that will be used. This implies that the units must be defined by the user and they should be consistent throughout the input file in all the information provided. For example, if the coordinate values of the nodes are in micrometers, the units for other values like the Young's modulus, density, forces and so on, must also undergo the necessary conversions in order to be consistent, before they are keyed into the preprocessor of ADINA. Note that in this case study, all the units are converted into micrometers to be consistent with the geometrical dimensions, as it can be seen from the values of Young's modulus and density that are shown in the third column of Table 4.1. This is the case for most finite element software, and many times, errors in analysis occur due to negligence in ensuring the units' consistency.

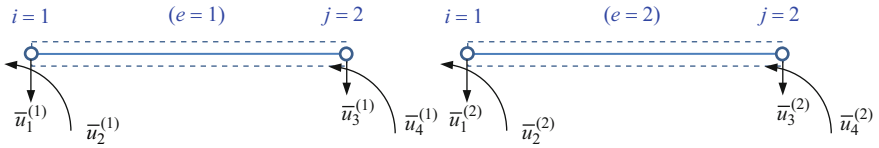

Fig. 4.10 A two finite elements model for the clamped-clamped beam

Table 4.2 Finite element code table for the beam

Number of element	First element degree of freedom	Second element degree of freedom	Third element degree of freedom	Fourth element degree of freedom
1	1	2	3	4
2	3	4	5	6

Numerical Solution

To evaluate the numerical solution is necessary to perform the discretization of the beam. Using two finite element, the beam finite element model is represented as shown in Fig. 4.10.

The element stiffness and mass matrices are defined in local coordinate system on Eqs. (4.18) and (4.19), respectively. Since the number of beam elements is of two and both elements have equal geometrical characteristics, the finite element matrices becomes

$$\mathbf{k}^{(1)} = \mathbf{k}^{(2)} = \frac{EI}{\ell^3}\begin{bmatrix} 12 & 6\ell & -12 & 6\ell \\ 6\ell & 4\ell^2 & -6\ell & 2\ell^2 \\ -12 & -6\ell & 12 & -6\ell \\ 6\ell & 2\ell^2 & -6\ell & 4\ell^2 \end{bmatrix} \tag{4.39}$$

$$\mathbf{m}^{(1)} = \mathbf{m}^{(1)} = \frac{A\rho\ell}{420}\begin{bmatrix} 156 & 22\ell & 54 & -13\ell \\ 22\ell & 4\ell^2 & 13\ell & -3\ell^2 \\ 54 & 13\ell & 156 & -22\ell \\ -13\ell & -3\ell^2 & -22\ell & 4\ell^2 \end{bmatrix} \tag{4.40}$$

The next step, after getting the element matrices, is to assemble the element matrices into global finite element matrices. Since the total degrees of freedom in the structure is six, the global stiffness matrix will be also a 6×6 matrix. The assembly process assures that the global stiffness and global mass of each node has the contribution of all elements that share the node. Table 4.2 shows the mapping of the local degrees of freedom to the global degrees of freedom.

So, using the concept explained in the Example 3.3 of Chap. 3, each of the 16 positions of the element stiffness and mass matrices of the two elements must be added into the global matrix according the mapping showed on Table 4.2. This gives the following results:

$$\mathbf{K} = \begin{bmatrix} k_{11}^{(1)} & k_{12}^{(1)} & k_{13}^{(1)} & k_{14}^{(1)} & 0 & 0 \\ k_{21}^{(1)} & k_{22}^{(1)} & k_{23}^{(1)} & k_{24}^{(1)} & 0 & 0 \\ k_{31}^{(1)} & k_{32}^{(1)} & k_{33}^{(1)} + k_{11}^{(2)} & k_{34}^{(1)} + k_{12}^{(2)} & k_{13}^{(2)} & k_{14}^{(2)} \\ k_{41}^{(1)} & k_{42}^{(1)} & k_{43}^{(1)} + k_{21}^{(2)} & k_{44}^{(1)} + k_{22}^{(2)} & k_{23}^{(2)} & k_{24}^{(2)} \\ 0 & 0 & k_{31}^{(2)} & k_{32}^{(2)} & k_{33}^{(2)} & k_{34}^{(2)} \\ 0 & 0 & k_{41}^{(2)} & k_{42}^{(2)} & k_{43}^{(2)} & k_{44}^{(2)} \end{bmatrix} \tag{4.41}$$

$$\mathbf{M} = \begin{bmatrix} m_{11}^{(1)} & m_{12}^{(1)} & m_{13}^{(1)} & m_{14}^{(1)} & 0 & 0 \\ m_{21}^{(1)} & m_{22}^{(1)} & m_{23}^{(1)} & m_{24}^{(1)} & 0 & 0 \\ m_{31}^{(1)} & m_{32}^{(1)} & m_{33}^{(1)} + m_{11}^{(2)} & m_{34}^{(1)} + m_{12}^{(2)} & m_{13}^{(2)} & m_{14}^{(2)} \\ m_{41}^{(1)} & m_{42}^{(1)} & m_{43}^{(1)} + m_{21}^{(2)} & m_{44}^{(1)} + m_{22}^{(2)} & m_{23}^{(2)} & m_{24}^{(2)} \\ 0 & 0 & m_{31}^{(2)} & m_{32}^{(2)} & m_{33}^{(2)} & m_{34}^{(2)} \\ 0 & 0 & m_{41}^{(2)} & m_{42}^{(2)} & m_{43}^{(2)} & m_{44}^{(2)} \end{bmatrix} \tag{4.42}$$

The equation of the problem is defined in Chap. 2 with equation number (2.70) and is called the eigenvalue equation, in which a non-zero solution for $\mathbf{\Phi}$ only exist if the determinate of the dynamic matrix vanish, i.e.

$$\det(\mathbf{K} - \lambda\ \mathbf{M}) = |\mathbf{K} - \lambda\ \mathbf{M}| = \mathbf{0} \tag{4.43}$$

where the dynamic matrix is defined as

$$\mathbf{D} = \begin{bmatrix} k_{11}^{(1)} - \lambda m_{11}^{(1)} & k_{12}^{(1)} - \lambda m_{12}^{(1)} & k_{13}^{(1)} - \lambda m_{13}^{(1)} & k_{14}^{(1)} - \lambda m_{14}^{(1)} & 0 & 0 \\ k_{21}^{(1)} - \lambda m_{21}^{(1)} & k_{22}^{(1)} - \lambda m_{22}^{(1)} & k_{23}^{(1)} - \lambda m_{23}^{(1)} & k_{24}^{(1)} - \lambda m_{24}^{(1)} & 0 & 0 \\ k_{31}^{(1)} - \lambda m_{31}^{(1)} & k_{32}^{(1)} - \lambda m_{32}^{(1)} & \left(k_{33}^{(1)} + k_{11}^{(2)}\right) - \lambda\left(m_{33}^{(1)} + m_{11}^{(2)}\right) & \left(k_{34}^{(1)} + k_{12}^{(2)}\right) - \lambda\left(m_{34}^{(1)} + m_{12}^{(2)}\right) & k_{13}^{(2)} - \lambda m_{13}^{(2)} & k_{14}^{(2)} - \lambda m_{14}^{(2)} \\ k_{41}^{(1)} - \lambda m_{41}^{(1)} & k_{42}^{(1)} - \lambda m_{42}^{(1)} & \left(k_{43}^{(1)} + k_{21}^{(2)}\right) - \lambda\left(m_{43}^{(1)} + m_{21}^{(2)}\right) & \left(k_{44}^{(1)} + k_{22}^{(2)}\right) - \lambda\left(m_{44}^{(1)} + m_{22}^{(2)}\right) & k_{23}^{(2)} - \lambda m_{23}^{(2)} & k_{24}^{(2)} - \lambda m_{24}^{(2)} \\ 0 & 0 & k_{31}^{(2)} - \lambda m_{31}^{(2)} & k_{32}^{(2)} - \lambda m_{32}^{(2)} & k_{33}^{(2)} - \lambda m_{33}^{(2)} & k_{34}^{(2)} - \lambda m_{34}^{(2)} \\ 0 & 0 & k_{41}^{(2)} - \lambda m_{41}^{(2)} & k_{42}^{(2)} - \lambda m_{42}^{(2)} & k_{43}^{(2)} - \lambda m_{43}^{(2)} & k_{44}^{(2)} - \lambda m_{44}^{(2)} \end{bmatrix} \tag{4.44}$$

The solution of Eq. (4.43) needs to account for the boundary conditions. Thus, in the process of solving Eq. (4.42), the matrix size can be reduced after applying boundary conditions, i.e. global displacements u_1, u_2, u_5 and u_6 are all known and their value is defined as

$$u_1 = u_2 = u_5 = u_6 = 0 \tag{4.45}$$

This means that the correspondent rows and columns have no effect on the solution of Eq. (4.42). Hence, we can simply remove the corresponding rows and columns from Eq. (4.43), and the condensed dynamic matrix is obtained as

$$\mathbf{D} = \begin{bmatrix} \left(k_{33}^{(1)} + k_{11}^{(2)}\right) - \lambda\left(m_{33}^{(1)} + m_{11}^{(2)}\right) & \left(k_{34}^{(1)} + k_{12}^{(2)}\right) - \lambda\left(m_{34}^{(1)} + m_{12}^{(2)}\right) \\ \left(k_{43}^{(1)} + k_{21}^{(2)}\right) - \lambda\left(m_{43}^{(1)} + m_{21}^{(2)}\right) & \left(k_{44}^{(1)} + k_{22}^{(2)}\right) - \lambda\left(m_{44}^{(1)} + m_{22}^{(2)}\right) \end{bmatrix}$$
$$= \begin{bmatrix} 6.76 \times 10^{-6} - \lambda \times 8.54 \times 10^{-13} & 0 \\ 0 & 5.633 \times 10^{-3} - \lambda \times 5.48 \times 10^{-11} \end{bmatrix} \tag{4.46}$$

and using Eqs. (4.45) and (4.42) is possible to define the characteristic polynomial of the eigenvalue problem, as

$$4.68 \times 10^{-23}\lambda^2 - 5.18 \times 10^{-15} + 3.81 \times 10^{-8} = 0 \tag{4.47}$$

The roots of Eq. (4.46) are $\lambda_1 = 7.913 \times 10^6$ and $\lambda_2 = 1.028 \times 10^8$, resulting in the natural frequencies of 477.0 Hz and of 1,614.1 Hz. The correspondent eigenvectors can be obtained by solving Eq. (2.73) for each eigenvalue. It is worth to mention that, as expected, the maximum number of natural frequencies given by this numerical model is of two. In fact even that the dimension of the dynamic matrix is of 6×6, the accounting for boundary conditions led to a smaller dimension of the dynamic matrix and, therefore, it is this final dimension that determines the maximum number of frequencies that can be numerically computed.

The same analysis can be performed in the ADINA program by selecting a Frequencies/Modes analysis. In this process, the first analysis will be performed by meshing the beam uniformly into two two-nodal beam elements, as shown in Fig. 4.10. After, refined uniform meshes of 10, 20, 40 and 60 elements will then be used to check the accuracy of the results obtained. This is a simplified way of performing the convergence test. Remember that usually the greater the number of elements, the greater the accuracy of results [2,5]. However, we can't simply use as many elements as possible all the time, since, there is usually a limit to the computer resources available. Hence, convergence tests are carried out to determine the optimum number of elements or nodes to be used for a certain problem.

All the frequencies obtained are presented in Table 4.3. Because the clamped–clamped beam structure is a simple problem, it is possible to evaluate the natural frequencies analytically. The results obtained from analytical calculations are also

Table 4.3 Frequencies of vibration of a clamped-clamped beam

	Natural frequencies [Hz]		
Number of beam elements	First	Second	Third
2	447.7	1,614.1	
10	440.57	1,214.69	2,382.87
20	440.56	1,214.39	2,380.67
40	440.56	1,214.37	2,380.53
60	440.56	1,214.37	2,380.53
Analytical	440.51	1,214.3	2,380.5

shown in Table 4.3 for comparison [5]. From the table, it can be seen that the finite element results give very good approximations of the clamped-clamped beam natural frequencies. Even with just two finite elements, the error of the first frequency is of about 1.63 %. Nevertheless, the third natural frequency is not possible to obtain with the first numerical model of the clamped-clamped beam. It can also be seen that as the number of elements increases, the finite element results gets closer and closer to the analytical calculations, and converges such that the results obtained for 40 and 60 elements show no difference up to the second decimal place. Moreover, for the first natural frequency the finite element results show no difference after 20 finite elements, which means that for the calculation of the first natural frequency is enough consider a numerical model with 20 finite elements. As expected, is possible to verify that in finite element analyses, the finer the mesh or the greater the number of elements used, the more accurate the results. However, more elements corresponds to the use of more computer resources and, therefore, a longer time of execution. Hence, it is advised to use the minimum number of elements which gives the results of desired accuracy.

The mode shapes can also be obtained through a modal analysis. Mode shapes can be considered as the way in which the structure vibrates at a particular natural frequency. It corresponds to the eigenvector of the finite element equation, just like the resonant frequencies corresponds to the eigenvalues of the finite element equation. Figures 4.11, 4.12 and 4.13 represent mode shapes obtained by plotting the z-eigenvector displacement components using 60 finite elements, and show how the clamped–clamped beam will vibrate at the natural frequencies.

Mode shapes can be important in some applications, where points of zero displacements, like the center of the beam in Fig. 4.12, need to be identified for the installation of some devices. For instance, for sensing capabilities is important to know where sensors may be placed to detect the desired vibration frequency. Thus, if a sensor is placed in the middle of beam span, it will be the right place to detect the first natural frequency.

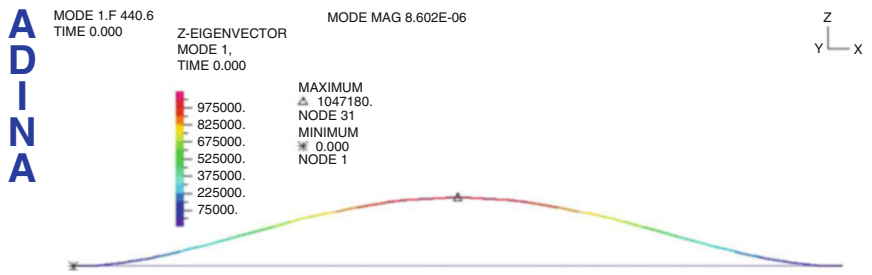

Fig. 4.11 First mode shape of the clamped-clamped beam using 60 finite elements

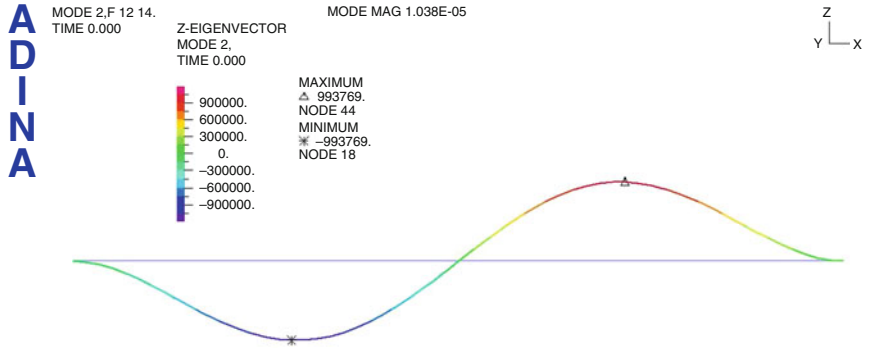

Fig. 4.12 Second mode shape of the clamped-clamped beam using 60 finite elements

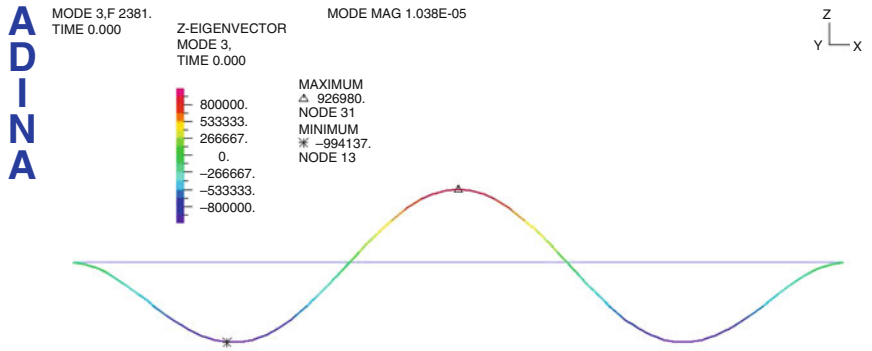

Fig. 4.13 Third mode shape of the clamped-clamped beam using 60 finite elements

Fig. 4.14 Geometry and load conditions of a rectangular beam

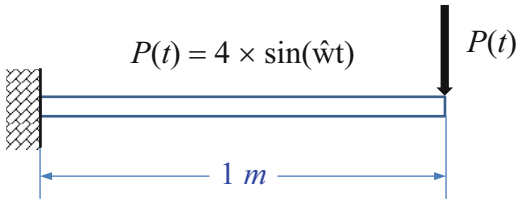

4.1.8 Third Discussion Example

Example 4.3: Transient Analysis of a Rectangular Beam
Consider the beam structure shown in Fig. 4.14. The structure is initially at rest and is subjected to a concentrated end load. The time history of the concentrated end load is also presented in Figure and the beam geometry and material properties are listed in Table 4.4.

The solution of this problem can be obtained using the concepts of transient analysis presented at Sect. 2.6 of Chap. 2. In order to apply either direct integration

Table 4.4 Beam geometry and material properties

Cross section area	0.0004 m^2
Young modulus	200 GPa
Density	7,800 kg/m^3

or mode superposition methods, is important knowing the load natural frequency and the beam natural frequencies. Supposing that the natural frequency of load is of 150 rad/s, the identification of natural frequencies and corresponding mode shapes can be achieved by means of eigenvalue analysis. The frequencies listed in Table 4.5 are calculated with discretization's using 20 and 40 equal-length elements. In this analysis we note that the 20-element model is stiffer than the 40-element model. In fact, after the fourth frequency, all frequency values given by the 20-element numerical model are higher than those given with the 40-element model.

The frequency of the external load lies between the first and second frequencies of both models. Using $4\times\widehat{w}$ as the cutoff frequency, it should be sufficient to include the response of two modes of vibration in the mode superposition technique, i.e. to use $p = 2$ in Eq. (2.137). However, for instructive purpose, let consider the response corresponding to $p = 1,\ 2,\ 3,\ 4$ and, because the first fourth frequencies are predicted well by the 20-element model, the response solution is obtained by this discretization. The modal solutions are obtained by numerical integration of Eq. (2.130) with a time step $\Delta t = 0.0002$, which is about $T_4/10$. For the direct integration with the Newmark method the solution is also obtained with the same time step. Nevertheless, for the central difference solution the time step needs to be sufficiently small for stability. For this reason, the time step can be evaluated using the highest frequency in the model, leading to $\Delta t_{crit} = 2/\omega_{40} = 0.471 \times 10^{-5}$. Therefore, in this academic example, the value $\Delta t = 0.25 \times 10^{-5}$ was used.

The results obtained at time 0.01 s are shown in Fig. 4.15 while the results obtained at ending time are shown in Fig. 4.16. The solution presented at Fig. 4.16 was obtained using only 210 time steps with the Newmark (NM) and mode superposition (MS) methods, but 16,800 time steps with the central difference method (CDM) were required. Figure 4.15 illustrate how the predicted response converges with increasing the number of modes included in the response prediction. The predicted response using two modes is almost the same as using three or four modes. Nevertheless, at instant 0.042 s, the predicted response is not sensitive to the number of modes, Fig. 4.16. Thus, between these two instants, the convergence behavior of the predicted response is different, which can be justified with the time history of external load, see Fig. 4.17. Notice that the instant 0.01 s is the moment at which the maximum magnitude of load is reached while time 0.042 s is the moment in which the external load is almost zero. Thus the tip displacement of beam for the 0.01 s instant is ten times greater than for 0.042 s and, because the first frequency of the numerical model is smaller than the external load frequency, the modal model with only one vibration mode is unable of reaching the true level of static displacement.

Moreover, if we consider the second frequency 643 rad/s, we have $\widehat{w}/w_2 = 0.23$ and from Fig. 2.8 it can be seen that this vibration mode can be important to

Table 4.5 Beam natural frequencies [rad/s]

Frequency number	20-element model	40-element model
1	102.77	102.77
2	643.01	643.00
3	1,795.94	1,795.89
4	3,506.71	3,506.33
5	5,770.59	5,768.88
6	8,573.77	8,568.23
7	11,901.30	11,886.70
8	15,737.40	15,704.00
9	20,066.10	19,998.00
10	24,871.70	24,745.00
11	30,139.50	29,919.80
12	35,854.90	35,497.00
13	42,002.90	41,450.40
14	48,565.20	47,753.80
15	55,515.50	54,381.50
16	62,807.70	61,307.70
17	70,350.10	68,507.60
18	77,940.20	75,956.60
19	85,094.10	83,630.70
20	90,684.10	91,506.60
21	123,063.00	99,560.90
22	130,162.00	107,770.00
23	139,835.00	116,112.00
24	151,064.00	124,560.00
25	163,435.00	133,090.00
26	176,796.00	141,674.00
27	191,101.00	150,282.00
28	206,345.00	158,878.00
29	222,542.00	167,423.00
30	239,695.00	175,870.00
31	257,782.00	184,162.00
32	276,724.00	192,233.00
33	296,351.00	200,002.00
34	316,358.00	207,371.00
35	336,250.00	214,223.00
36	355,295.00	220,423.00
37	372,495.00	225,819.00
38	386,588.00	230,249.00
39	396,097.00	233,554.00
40	424,338.00	235,599.00

evaluate a simple static response and that frequency can contribute to a small increase of response magnitude, notice that $A/w_2^2 = 9.67 \times 10^{-6}$. Nevertheless, considering the first frequency $\widehat{w}/w_1 = 1.5$, which means that dynamic factor load is close to the unity (resonance) and the response in this mode can contribute to

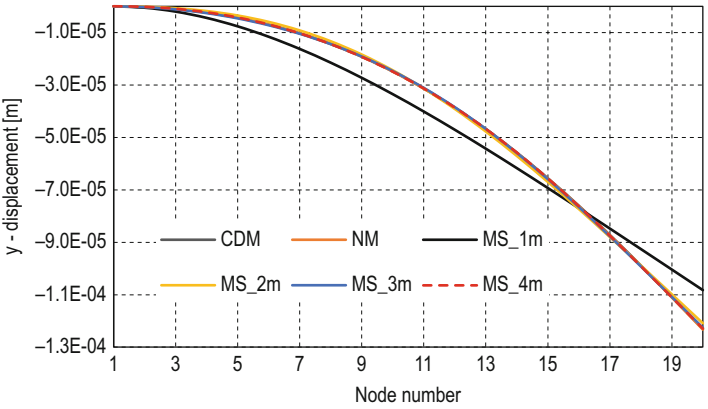

Fig. 4.15 Solution obtained at time 0.01 s

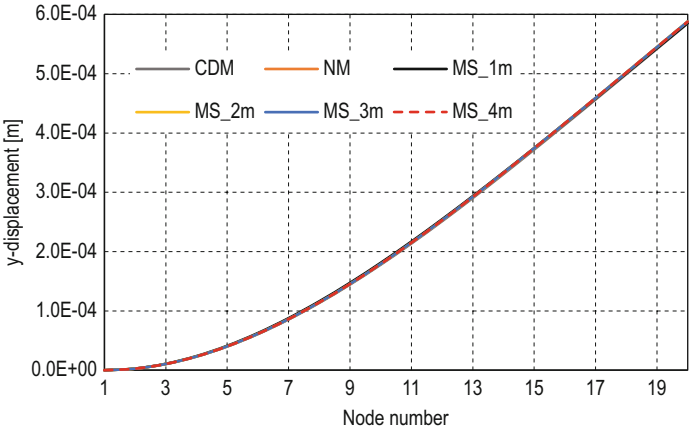

Fig. 4.16 Solution obtained at time 0.042 s

a significant increase of response magnitude, $A/w_1^2 = 3.78 \times 10^{-3}$. Therefore all natural frequencies, lower than frequencies of content load, should be included in the mode superposition analysis. This concept can be clarified if considering that the predicted results are obtained without the first frequency of the system, see Fig. 4.18. In this case neither of solutions is close to the correct.

4.2 FE Matrices and Vectors for Planar Beams (2-D Beams)

4.2.1 Degrees of Freedom Identification

A plan beam is used to model a straight bar of an arbitrary cross-section, which can deform not only in the axial direction but also in the transverse direction. Thus, in

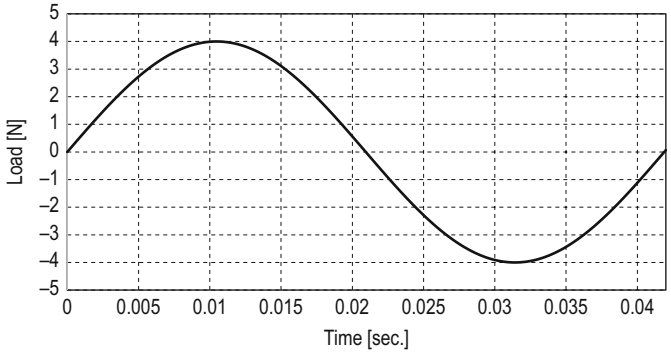

Fig. 4.17 Time history of the load

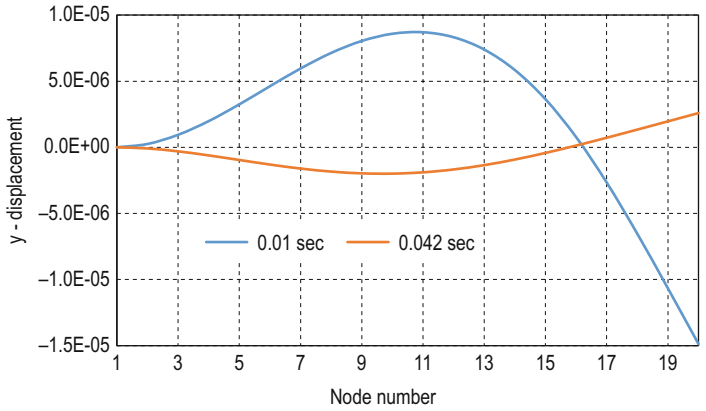

Fig. 4.18 Solution obtained using four frequencies without the first frequency of the system

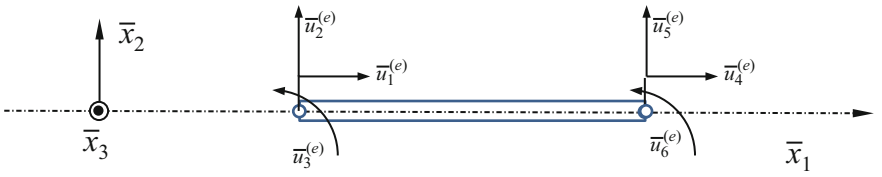

Fig. 4.19 Local and global coordinate systems in the 2-D beam element

a planar beam the finite element has three degrees of freedom per node at its local coordinate system: displacement in the axial and in the transverse directions and rotation about to the axis that is normal to the beam plane, as shown in Fig. 4.19.

4.2.2 *Local FE Matrices and Vectors for 2-D Beams*

The element matrices for a 2-D beam finite element can be formulated combining element matrices from truss and beam elements, without going through the detailed process of formulating shape functions. Thus the element displacement vector for a 2-D beam finite element can be written as

$$\overline{\mathbf{u}} = \begin{bmatrix} \overline{u}_1 \\ \overline{u}_2 \\ \overline{u}_3 \\ \overline{u}_4 \\ \overline{u}_5 \\ \overline{u}_6 \end{bmatrix} \tag{4.48}$$

Figure 4.20 shows the local degrees of freedom of the truss, beam and the 2-D beam finite elements. So, it can be seen that combining the truss and beam degrees of freedom will get the degrees of freedom to the 2-D beam finite element. Table 4.6 establishes the number degrees of freedom equivalence among finite elements.

Table 4.6 can be used to construct 2-D beam matrices and vectors, it is possible to see that the first degree of freedom for the 2-D beam element is also the first degree of freedom of the truss finite element, and that the fourth degree of freedom of the 2-D beam corresponds to the second degree of freedom of the truss finite element. Hence the value of the first row and the first column of the truss stiffness matrix in Eq. (3.15), denoted by k^t_{11}, should be placed into the position of the first row and first column of the 6×6 local 2-D beam stiffness matrix, i.e.

$$k^t_{11} \rightarrow k_{11};\ k^t_{22} \rightarrow k_{44};\ k^t_{12} \rightarrow k_{14};\ k^t_{21} \rightarrow k_{41} \tag{4.49}$$

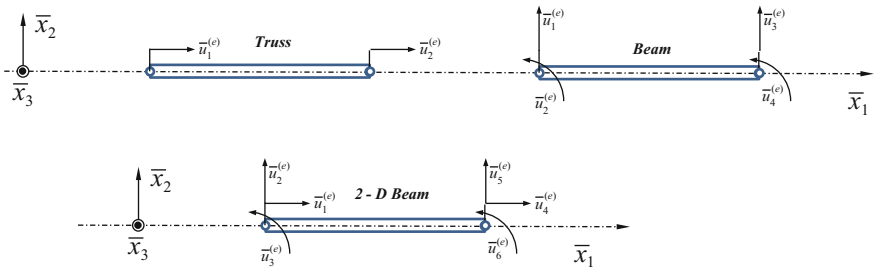

Fig. 4.20 Degrees of freedom in the local coordinate system of truss, beam and the 2-D beam element

Table 4.6 Equivalence of degrees of freedom

	Truss		Beam			
Degrees of freedom	1	2	1	2	3	4
2-D beam	1	4	2	3	5	6

and the 16 components of the beam stiffness matrix must be placed as follows:

$$\begin{aligned} k^b_{11} \rightarrow k_{22};\ k^b_{12} \rightarrow k_{23};\ k^b_{13} \rightarrow k_{25};\ k^b_{14} \rightarrow k_{16} \\ k^b_{22} \rightarrow k_{33};\ k^b_{23} \rightarrow k_{35};\ k^b_{24} \rightarrow k_{36} \\ k^b_{33} \rightarrow k_{55};\ k^b_{34} \rightarrow k_{56} \\ k^b_{44} \rightarrow k_{66} \end{aligned} \tag{4.50}$$

Notice that due to the symmetry of the beam stiffness, in Eq. (4.49) there are only ten components. So, the final 2-D beam stiffness can be written as

$$\overline{\mathbf{k}} = \begin{bmatrix} k^t_{11} & 0 & 0 & k^t_{12} & 0 & 0 \\ 0 & k^b_{11} & k^b_{12} & 0 & k^b_{13} & k^b_{14} \\ 0 & k^b_{21} & k^b_{22} & 0 & k^b_{23} & k^b_{24} \\ k^t_{21} & 0 & 0 & k^t_{22} & 0 & 0 \\ 0 & k^b_{31} & k^b_{32} & 0 & k^b_{33} & k^b_{34} \\ 0 & k^b_{41} & k^b_{42} & 0 & k^b_{43} & k^b_{44} \end{bmatrix} \tag{4.51}$$

Using the information from Eqs. (3.15) and (4.18) into Eq. (4.50) the stiffness matrix for the 2-D beam is obtained

$$\overline{\mathbf{k}} = \begin{bmatrix} \frac{AE}{\ell} & 0 & 0 & -\frac{AE}{\ell} & 0 & 0 \\ 0 & EI\frac{12}{\ell^3} & EI\frac{6}{\ell^2} & 0 & -EI\frac{12}{\ell^3} & EI\frac{6}{\ell^2} \\ 0 & EI\frac{6}{\ell^2} & EI\frac{4}{\ell} & 0 & -EI\frac{6}{\ell^2} & EI\frac{2}{\ell} \\ -\frac{AE}{\ell} & 0 & 0 & \frac{AE}{\ell} & 0 & 0 \\ 0 & -EI\frac{12}{\ell^3} & -EI\frac{6}{\ell^2} & 0 & EI\frac{12}{\ell^3} & -EI\frac{6}{\ell^2} \\ 0 & EI\frac{6}{\ell^2} & EI\frac{2}{\ell} & 0 & -EI\frac{6}{\ell^2} & EI\frac{4}{\ell} \end{bmatrix} \tag{4.52}$$

The element mass matrix of the 2-D beam element can also be obtained in the same way as the stiffness matrix, leading to

$$\overline{\mathbf{m}} = \begin{bmatrix} \frac{A\rho\ell}{3} & 0 & 0 & \frac{A\rho\ell}{6} & 0 & 0 \\ 0 & \frac{156}{420}A\rho\ell & \frac{22}{420}A\rho\ell^2 & 0 & \frac{54}{420}A\rho\ell & -\frac{13}{420}A\rho\ell^2 \\ 0 & \frac{22}{420}A\rho\ell^2 & \frac{4}{420}A\rho\ell^3 & 0 & \frac{13}{420}A\rho\ell^2 & -\frac{3}{420}A\rho\ell^3 \\ \frac{A\rho\ell}{6} & 0 & 0 & \frac{A\rho\ell}{3} & 0 & 0 \\ 0 & \frac{54}{420}A\rho\ell & \frac{13}{420}A\rho\ell^2 & 0 & \frac{156}{420}A\rho\ell & -\frac{22}{420}A\rho\ell^2 \\ 0 & -\frac{13}{420}A\rho\ell^2 & -\frac{3}{420}A\rho\ell^3 & 0 & -\frac{22}{420}A\rho\ell^2 & \frac{4}{420}A\rho\ell^3 \end{bmatrix} \tag{4.53}$$

The same procedure can be applied to the force vector as well. Thus the total nodal force vector becomes

$$\bar{\mathbf{f}} = \begin{bmatrix} \frac{p_0\ell}{2} + f_{c_x1} \\ \frac{q_0\ell}{2} + f_{c_y1} \\ \frac{q_0\ell^2}{12} + m_{c_z1} \\ \frac{p_0\ell}{2} + f_{c_x2} \\ \frac{q_0\ell}{2} + f_{c_y2} \\ -\frac{q_0\ell^2}{12} + m_{c_z2} \end{bmatrix} \tag{4.54}$$

4.2.3 Global FE Matrices and Vectors for 2-D Beams

Matrices formulated previously are for cases in which all structural elements of a mechanical system have an orientation that is parallel to the reference global system. Meanwhile, a real mechanical system comprises several structural elements of different orientations joined together. Thus, before the assemblage process, all the matrices must first be expressed in a common coordinate system, which is the global coordinate system. Moreover, the coordinate transformation process is the same described in Chap. 3 for truss structures.

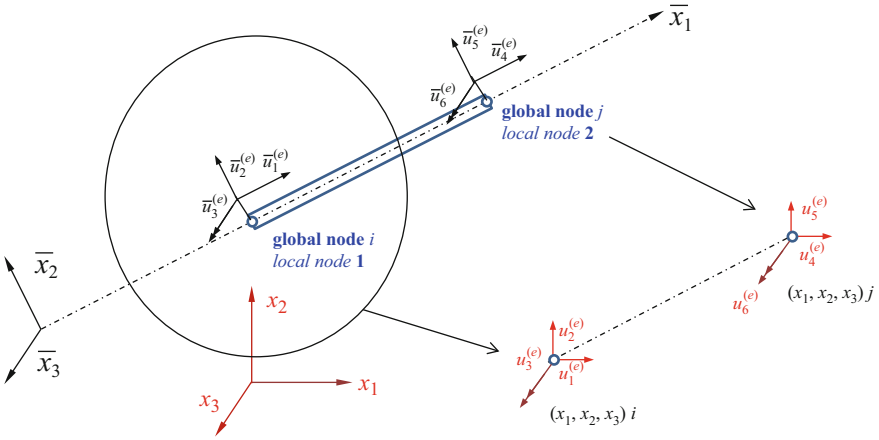

Fig. 4.21 Local and global coordinate systems in the 2-D beam element

Let's assume that local nodes 1 and 2 of the finite element correspond to the global nodes i and j, respectively. Furthermore, assume that the finite element is defined in the $x_1 - x_2$ plane. The local displacements and rotations at each finite element node may be projected into the global coordinate system $(x_i;\ i = 1, 2, 3)$ leading to global displacement components $\left(u_j^{(e)};\ j = 1, 2, 3\right)$, see Fig. 4.21. The global displacements at one node in space should also have two components in the x_1 and x_2 directions, and should be numbered sequentially, after which the global rotation will be also numbered sequentially.

The coordinate transformation gives the relationship between the nodal displacement vector $\bar{\mathbf{u}}$, based on the local coordinate system, and the nodal displacement vector $\mathbf{u}$, for the same finite element, based on the global coordinate system $(x_i;\ i = 1, 2, 3)$.

$$\bar{\mathbf{u}} = \mathbf{T}\,\mathbf{u} \tag{4.55}$$

with

$$\mathbf{u} = \begin{bmatrix} u_1^{(e)} \\ u_2^{(e)} \\ u_3^{(e)} \\ u_4^{(e)} \\ u_5^{(e)} \\ u_6^{(e)} \end{bmatrix} \tag{4.56}$$

and where $\mathbf{T}$ is the transformation matrix for the 2-D beam element

$$\mathbf{T} = \begin{bmatrix} \mathbf{R} & \mathbf{0} \\ \mathbf{0} & \mathbf{R} \end{bmatrix} \tag{4.57}$$

where $\mathbf{R}$ is the 3×3 transformation matrix from the local coordinate system to the global coordinate systems, which components are defined as

$$\mathbf{R} = \begin{bmatrix} \cos(\bar{x}_1, x_1) & \cos(\bar{x}_1, x_2) & \cos(\bar{x}_1, x_3) \\ \cos(\bar{x}_2, x_1) & \cos(\bar{x}_2, x_2) & \cos(\bar{x}_2, x_3) \\ \cos(\bar{x}_3, x_1) & \cos(\bar{x}_3, x_2) & \cos(\bar{x}_3, x_3) \end{bmatrix} = \begin{bmatrix} l_{11} & m_{12} & 0 \\ l_{21} & m_{22} & 0 \\ 0 & 0 & 1 \end{bmatrix} \tag{4.58}$$

Note that in Eq. (4.58) the third row and third column are easily computed, once the local $\bar{x}_3$ direction is coincident with the global x_3 direction. Assuming that the smaller angle between $\bar{x}_1$ and x_1 axes is denoted by α, is possible to write the components of matrix $\mathbf{R}$ as

$$l_{11} = \cos\alpha = \frac{(x_1)_j - (x_1)_i}{\ell}; \; m_{12} = \cos(90 - \alpha) = \sin\alpha = \frac{(x_2)_j - (x_2)_i}{\ell} \tag{4.59}$$

$$l_{21} = \cos(90 + \alpha) = -\sin\alpha = \frac{(x_2)_j - (x_2)_i}{\ell}; \; m_{22} = \cos\alpha = \frac{(x_1)_j - (x_1)_i}{\ell} \tag{4.60}$$

where the length of the element can be calculated by

$$\ell = \sqrt{\left((x_1)_j - (x_1)_i\right)^2 + \left((x_2)_j - (x_2)_i\right)^2} \tag{4.61}$$

Equation (4.55) simply state that the global displacement at each node is equal to the summation of all projections of the local displacements at each node into the several global axes. Thus, using the transformation matrix $\mathbf{T}$, the matrices for the 2-D beam element in the global coordinate system become

$$\mathbf{k} = \mathbf{T}^T \overline{\mathbf{k}}\, \mathbf{T} \tag{4.62}$$

$$\mathbf{m} = \mathbf{T}^T \overline{\mathbf{m}}\, \mathbf{T} \tag{4.63}$$

$$\mathbf{f} = \mathbf{T}^T \overline{\mathbf{f}} \tag{4.64}$$

Note that in these three equations there is no change in the dimension between the matrices and vectors in the local and global coordinate systems.

4.2.4 *Fourth Discussion Example*

Example 4.4: 2-D Structure Subjected to a Vertical Load
Consider the plane beam structure shown in Fig. 4.22. The structure is a planar structure made with three beam members and a vertical downward force of 10 kN is applied at the free vertex.

This structure is similar to the structure presented in Fig. 3.11, the only difference is that the elements are joined together by welding such that both forces and moments can be transmitted between members. Table 4.7 shows the dimensions and material properties of the beam members in the structure.

Modelling
In the process of solving numerically this problem is important to perform the discretization: numbering the finite elements and the nodes. The 2-D structure is meshed using two-nodal beam elements in the ADINA program. Note that in ADINA, as well as in many other software's, a general beam element is the 3-D beam element that will be formulated in the next section. Meanwhile, in ADINA is possible to select the element sub-type 2-D that has the same degrees of freedom of the 2-D beam element formulated in this section.

For the solution of the problem, 30 finite elements are used in the 2-D structure, as shown in Fig. 4.23. Like all finite element meshes, the connectivity at the nodes is very important because it provides the required connectivity among elements.

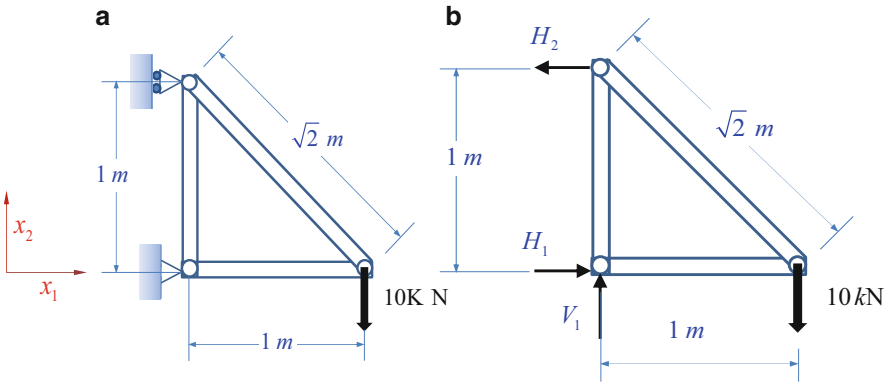

Fig. 4.22 Beam structure with three beams: (**a**) support conditions; (**b**) force reactions

Table 4.7 Dimensions and mechanical properties of the truss members

Number of element	Cross-sectional area [m^2]	Length [m^2]	Young's modulus [GPa]
1	0.1×0.01	1	70
2	0.1×0.01	$\sqrt{2}$	70
3	0.1×0.01	1	70

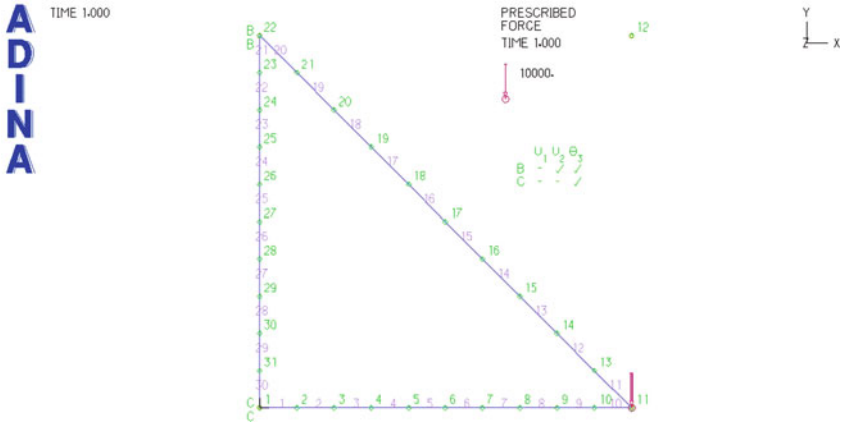

Fig. 4.23 Finite element mesh of a 2-D structure with representation of loading and boundary conditions used within the numerical model

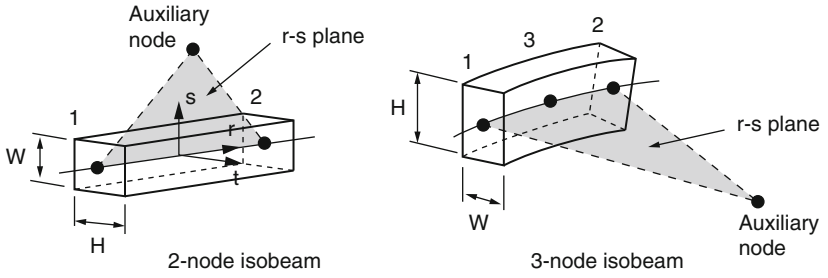

Fig. 4.24 Orientation of beam local axis in the ADINA [6]

In Fig. 4.23 letters B and C are used to represent the boundary conditions applied at nodes 22 and 1, respectively. Letter B is associated with a support that only restrains the displacement in the x direction while letter is associated with a support that fixes both displacements but left the rotation free. In Fig. 4.23 it can also be seen that the node 12 is not connected to the structure. This node appears because an auxiliary point was created and, therefore, the mesh procedure creates also a node in this position. Nevertheless, once this node has not mechanical properties associated, it will not be considered in the numerical analysis. The auxiliary point is needed because the cross section needs to be oriented within the x-y plane.

It is important to note the local $\bar{x}_2$ and $\bar{x}_3$ axes when specifying the dimensions of the cross sections. ADINA denotes the cross section beam axes by letters (t) and (s) and the r-axis is along the axial direction of the beam. The r-s plane is formed by the two end nodes, node i and j, of the beam and the auxiliary node. The width and height of a beam element are illustrated in Fig. 4.24.

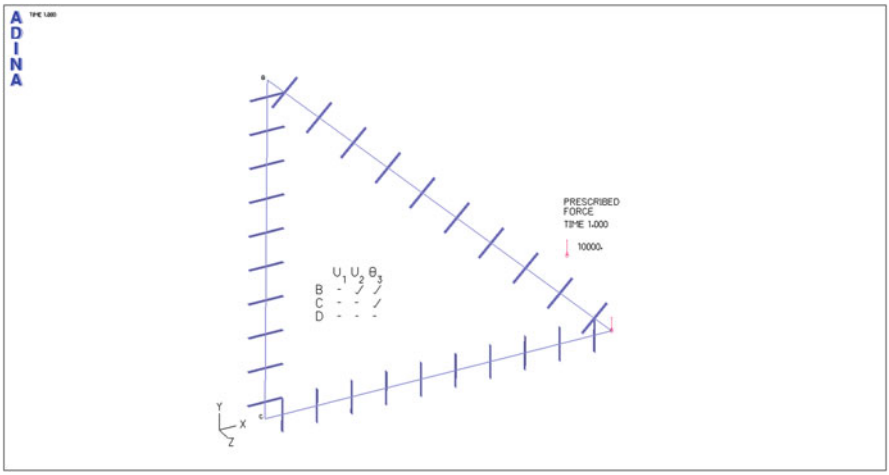

Fig. 4.25 Representation of the beam cross-section orientation in the ADINA program

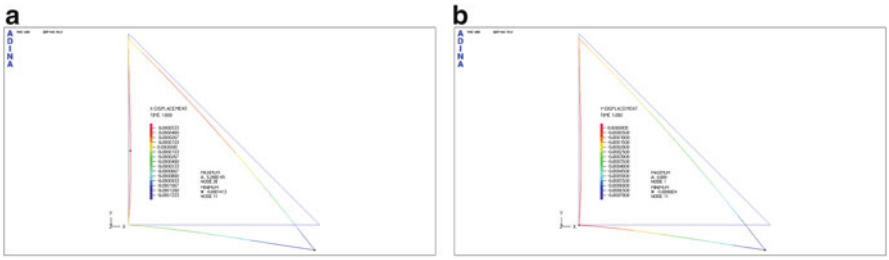

Fig. 4.26 Deformation plot of 2-D structure: (**a**) contour plot of the x displacement; (**b**) contour plot of the y displacement

Cross section orientations are plotted in Fig. 4.25. The ADINA program allows representing graphically the orientation of the element cross-section by changing mesh attributes.

Results and Discussion

Using the numerical model presented in Fig. 4.23, the finite element equation is solved by ADINA and a deformation plot showing how the 2-D beam actually deforms under the transversal load is shown in Fig. 4.26. The magnitude of the deformation is magnified 208 times, as the magnitude of the displacement is too small for viewing process. The maximum absolute value of x-displacement is of 0.1413 mm and the y-displacement is of 0.6824 mm, both displacements are located in the loading point.

Another important result obtainable from a numerical analysis would be the stresses that appear with this particular loading condition. However, because the beam bending stress depends on the point in which the evaluation needs to

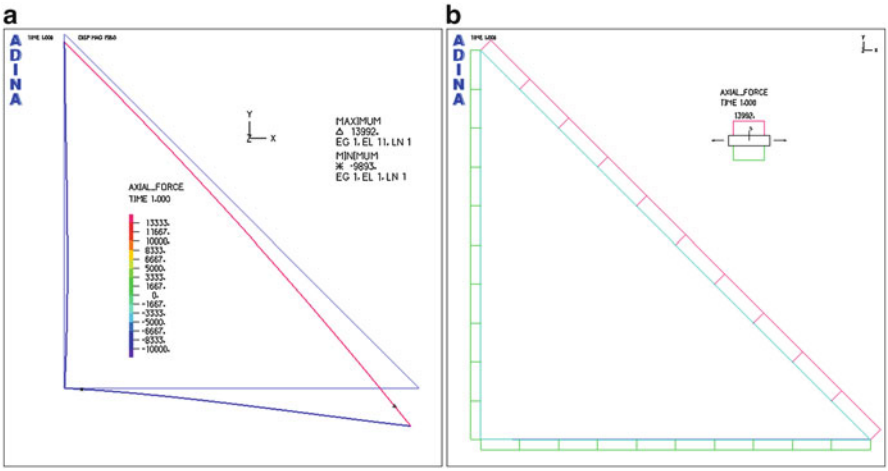

Fig. 4.27 Axial effort plot of 2-D structure: (**a**) contour plot; (**b**) element line plot

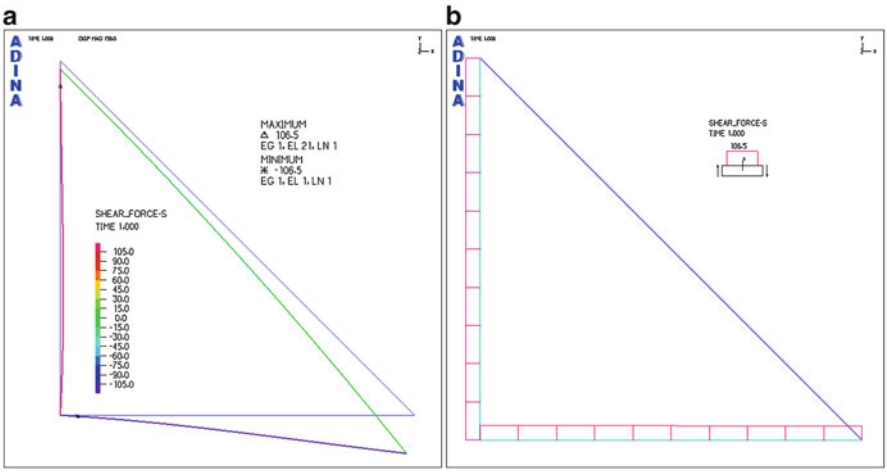

Fig. 4.28 Shear effort of 2-D structure: (**a**) contour plot; (**b**) element line plot

be performed, the ADINA does not account for the beam stress representation. Nevertheless, if the efforts are known, the stress can be computed from classic formulas of mechanics. Figures 4.27, 4.28 and 4.29 show the axial, shear and bending efforts calculated in the 2-D structure. These results can be used to obtain stresses at different points of the cross-section of the beams. From the results presented in Fig. 4.27 is possible to evaluate maximum and minimum axial stresses, i.e.

$$\sigma = \frac{13992}{0.1 \times 0.01} = 13.992\, MPa; \quad \sigma = -\frac{9893}{0.1 \times 0.01} = -9.893\, MPa \qquad (4.65)$$

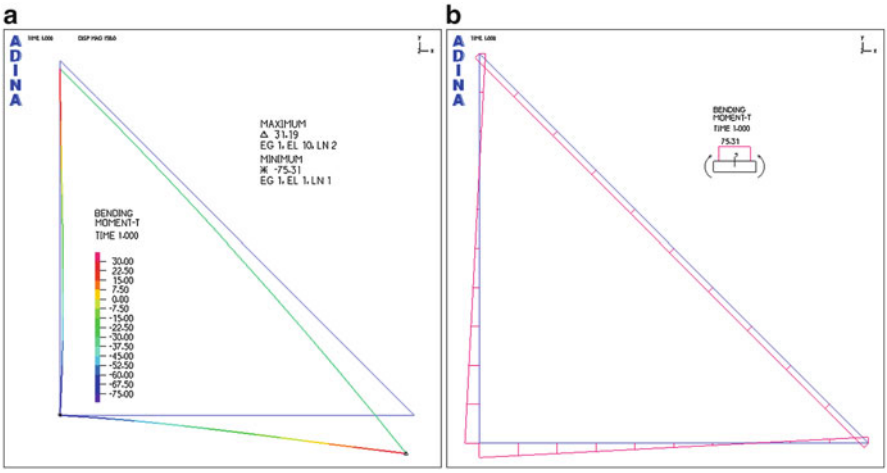

Fig. 4.29 Bending moment of 2-D structure: (**a**) contour plot; (**b**) element line plot

and the maximum bending stress at point C can be evaluated from Fig. 4.29 as

$$\sigma = \frac{75.31 \times 0.05}{\left(0.01 \times 0.1^3\right)/12} = 4.5186\, MPa \tag{4.66}$$

which means that the maximum combined normal stress at point C is defined as

$$\sigma = \frac{13992}{0.1 \times 0.01} + \frac{75.31 \times 0.05}{\left(0.01 \times 0.1^3\right)/12} = 18.5106\, MPa \tag{4.67}$$

4.3 FE Matrices and Vectors for 3-D Beams

A 3-D beam finite element is used to model a straight bar of an arbitrary cross-section, which can deform not only in the axial direction but also in the directions perpendicular to the axis of the bar. In this case the structure is able of carrying both axial and transverse forces, as well as moments. Therefore, a 3-D beam element is seen to have the properties of truss, beam and shaft elements. The 3-D element developed here is also known in many commercial software packages as the general beam element, or even simply the beam element. Commercial software packages usually offer both 2-D beam and 3-D beam elements, but 3-D beam structures are more often used in actual engineering applications. A three-dimensional spatial structure can practically take forces and moments of all directions. Hence, it can be considered to be the most general form of element with a one-dimensional geometry.

Fig. 4.30 Illustrative example of a space beam structure

Beam elements are applicable for the analysis of skeletal type systems of both planar beams (2-D beams) and space beams (3-D beams). A typical three-dimensional structure is shown in Fig. 4.30. Beam members in structure are joined together by welding so that both forces and moments can be transmitted between members.

In this book, it is assumed that the beam elements have a uniform cross sectional area. If a structure with varying cross-section is to be modeled using the formulation in this chapter, then it is advised that the structure should be divided into several elements with a constant cross-sectional area, so as to simulate the varying cross-section. Of course, if the variation in the cross-section is too severe for accurate approximation, the equations for a varying cross-sectional area should be formulated. This can be done, without much difficulty using the concepts and procedure given in this chapter. The basic concepts, procedures and formulations can also be found in many existing textbooks.

4.3.1 Degrees of Freedom Identification

Let's assume that local nodes 1 and 2 of the finite element correspond to the global nodes i and j, respectively, as shown in Fig. 4.31. The local displacements and rotations at each finite element node may be projected into the global

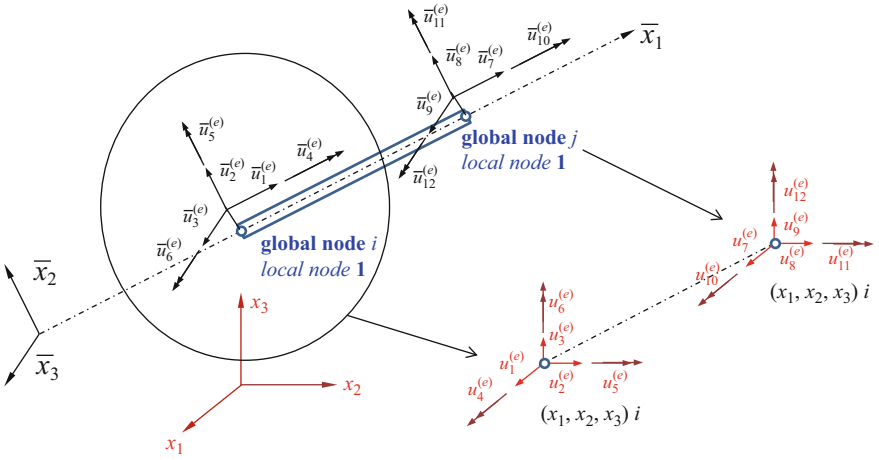

Fig. 4.31 Local and global coordinate systems in the 3-D beam element

coordinate system $(x_i;\ i = 1, 2, 3)$ leading to global displacement components $\left(u_j^{(e)};\ j = 1, 2, \ldots, 12\right)$. The global displacements at one node should have components in the x_1, x_2 and x_3 directions, and should be numbered sequentially, after which the global rotations will be also numbered sequentially. Therefore, for the element with two nodes represented in Fig. 4.31, there are 12 degrees of freedom.

The element displacement vector for a 3-D beam element in local coordinate system can be written as

$$\overline{\mathbf{u}} = \left[\, \overline{u}_1 \ \overline{u}_2 \ \overline{u}_3 \ \overline{u}_4 \ \overline{u}_5 \ \overline{u}_6 \ \overline{u}_7 \ \overline{u}_8 \ \overline{u}_9 \ \overline{u}_{10} \ \overline{u}_{11} \ \overline{u}_{12} \,\right]^T \tag{4.68}$$

4.3.2 *Local FE Matrices and Vectors for 3-D Beams*

The element matrices can be obtained by the process used previously to define the 2-D element matrices. So, combining the truss, shaft and beams degrees of freedom is possible to get the degrees of freedom of the 3-D beam finite element. Table 4.8 establishes the number degrees of freedom equivalence among finite elements. Notice that because the beam element can be on planes $x_1 - x_2$ and $x_1 - x_3$ the last two columns of Table 4.8 are related with the beam degrees of freedom on these planes. Moreover, I_y and I_z are the moment of inertia of the cross-section of the beam with respect to the x_2 and x_3 axes, respectively.

The development of a shaft finite element is very similar to the development of a truss finite element. The only difference is that the axial displacement is replaced by the angular rotation, and the axial force is replaced by torque. Thus, the stiffness matrix of a shaft finite element can be defined by Eq. (3.15) of Chap. 3 replacing the

Table 4.8 Equivalence of degrees of freedom for the 3-D beam

	Truss		Shaft		Beam $x_1 - x_2$ (I_z)				Beam $x_1 - x_3$ (I_y)			
Degrees of freedom	1	2	1	2	1	2	3	4	1	2	3	4
3-D beam	1	7	4	10	2	6	8	12	3	5	9	11

element tensile stiffness AE/ℓ by the torsional stiffness GJ/ℓ, where G is the shear modulus and J is the polar moment of inertia of the cross-section of the structure, i.e.

$$\overline{\mathbf{k}}^s = \frac{GJ}{\ell}\begin{bmatrix} 1 & -1 \\ -1 & 1 \end{bmatrix} \tag{4.69}$$

From Table 4.8 it can be seen that the value of the first row and the first column of the shaft stiffness matrix in Eq. (4.69), denoted by $\overline{k}^s_{11}$, should be placed into the position of the fourth row and fourth column of the 12×12 local 3-D beam stiffness matrix, i.e.

$$\overline{k}^s_{11} \rightarrow \overline{k}_{44};\ \overline{k}^s_{22} \rightarrow \overline{k}_{1010};\ \overline{k}^s_{12} \rightarrow \overline{k}_{410};\ \overline{k}^s_{21} \rightarrow k_{104} \tag{4.70}$$

and using the remaining information of Table 4.8, is possible to build the element stiffness as follows:

$$\overline{\mathbf{k}} =$$

$$\begin{bmatrix}
\frac{AE}{\ell} & 0 & 0 & 0 & 0 & 0 & -\frac{AE}{\ell} & 0 & 0 & 0 & 0 & 0 \\
0 & EI_z\frac{12}{\ell^3} & 0 & 0 & 0 & EI_z\frac{6}{\ell^2} & 0 & -EI_z\frac{12}{\ell^3} & 0 & 0 & 0 & EI_z\frac{6}{\ell^2} \\
0 & 0 & EI_y\frac{12}{\ell^3} & 0 & -EI_y\frac{6}{\ell^2} & 0 & 0 & 0 & -EI_y\frac{12}{\ell^3} & 0 & -EI_y\frac{6}{\ell^2} & 0 \\
0 & 0 & 0 & \frac{GJ}{\ell} & 0 & 0 & 0 & 0 & 0 & -\frac{GJ}{\ell} & 0 & 0 \\
0 & 0 & -EI_y\frac{6}{\ell^2} & 0 & EI_y\frac{4}{\ell} & 0 & 0 & 0 & -EI_y\frac{6}{\ell^2} & 0 & EI_y\frac{2}{\ell} & 0 \\
0 & EI_z\frac{6}{\ell^2} & 0 & 0 & 0 & EI_z\frac{4}{\ell} & 0 & -EI_z\frac{6}{\ell^2} & 0 & 0 & 0 & EI_z\frac{2}{\ell} \\
-\frac{AE}{\ell} & 0 & 0 & 0 & 0 & 0 & \frac{AE}{\ell} & 0 & 0 & 0 & 0 & 0 \\
0 & -EI_z\frac{12}{\ell^3} & 0 & 0 & 0 & -EI_z\frac{6}{\ell^2} & 0 & EI_z\frac{12}{\ell^3} & 0 & 0 & 0 & -EI_z\frac{6}{\ell^2} \\
0 & 0 & -EI_y\frac{12}{\ell^3} & 0 & -EI_y\frac{6}{\ell^2} & 0 & 0 & 0 & EI_y\frac{12}{\ell^3} & 0 & EI_y\frac{6}{\ell^2} & 0 \\
0 & 0 & 0 & -\frac{GJ}{\ell} & 0 & 0 & 0 & 0 & 0 & \frac{GJ}{\ell} & 0 & 0 \\
0 & 0 & -EI_y\frac{6}{\ell^2} & 0 & EI_y\frac{2}{\ell} & 0 & 0 & 0 & EI_y\frac{6}{\ell^2} & 0 & EI_y\frac{4}{\ell} & 0 \\
0 & EI_z\frac{6}{\ell^2} & 0 & 0 & 0 & EI_z\frac{2}{\ell} & 0 & -EI_z\frac{6}{\ell^2} & 0 & 0 & 0 & EI_z\frac{4}{\ell}
\end{bmatrix} \tag{4.71}$$

The same procedure is used to obtain the element mass matrix of the 3-D beam,

$$\overline{\mathbf{m}} =$$

$$\begin{bmatrix}
\frac{A\rho\ell}{3} & 0 & 0 & 0 & 0 & 0 & \frac{A\rho\ell}{6} & 0 & 0 & 0 & 0 & 0 \\
0 & \frac{156}{420}A\rho\ell & 0 & 0 & 0 & \frac{22}{420}A\rho\ell^2 & 0 & \frac{54}{420}A\rho\ell & 0 & 0 & 0 & -\frac{13}{420}A\rho\ell^2 \\
0 & 0 & \frac{156}{420}A\rho\ell & 0 & -\frac{22}{420}A\rho\ell^2 & 0 & 0 & 0 & \frac{54}{420}A\rho\ell & 0 & \frac{13}{420}A\rho\ell^2 & 0 \\
0 & 0 & 0 & \frac{35}{105}A\rho\ell r^2 & 0 & 0 & 0 & 0 & 0 & -\frac{35}{310}A\rho\ell r^2 & 0 & 0 \\
0 & 0 & -\frac{22}{420}A\rho\ell^2 & 0 & \frac{4}{420}A\rho\ell^3 & 0 & 0 & 0 & -\frac{13}{420}A\rho\ell^2 & 0 & -\frac{3}{420}A\rho\ell^3 & 0 \\
0 & \frac{22}{420}A\rho\ell^2 & 0 & 0 & 0 & \frac{4}{420}A\rho\ell^3 & 0 & \frac{13}{420}A\rho\ell^2 & 0 & 0 & 0 & -\frac{3}{420}A\rho\ell^3 \\
\frac{A\rho\ell}{6} & 0 & 0 & 0 & 0 & 0 & \frac{A\rho\ell}{3} & 0 & 0 & 0 & 0 & 0 \\
0 & \frac{54}{420}A\rho\ell & 0 & 0 & 0 & \frac{13}{420}A\rho\ell^2 & 0 & \frac{156}{420}A\rho\ell & 0 & 0 & 0 & -\frac{22}{420}A\rho\ell^2 \\
0 & 0 & \frac{54}{420}A\rho\ell & 0 & -\frac{13}{420}A\rho\ell^2 & 0 & 0 & 0 & \frac{156}{420}A\rho\ell & 0 & \frac{22}{420}A\rho\ell^2 & 0 \\
0 & 0 & 0 & -\frac{35}{310}A\rho\ell r^2 & 0 & 0 & 0 & 0 & 0 & \frac{35}{105}A\rho\ell r^2 & 0 & 0 \\
0 & 0 & \frac{13}{420}A\rho\ell^2 & 0 & -\frac{3}{420}A\rho\ell^3 & 0 & 0 & 0 & \frac{22}{420}A\rho\ell^2 & 0 & \frac{4}{420}A\rho\ell^3 & 0 \\
0 & -\frac{13}{420}A\rho\ell^2 & 0 & 0 & 0 & -\frac{3}{420}A\rho\ell^3 & 0 & -\frac{22}{420}A\rho\ell^2 & 0 & 0 & 0 & \frac{4}{420}A\rho\ell^3
\end{bmatrix} \tag{4.72}$$

where

$$r^2 = \frac{J}{A} \tag{4.73}$$

in which J is the polar moment of inertia of the cross-section of the beam with respect to the x_1 axis.

4.3.3 Global FE Matrices and Vectors for 3-D Beams

The transformation of the previous element matrices into the global coordinate system it is important, because is necessary accounting the several orientations of all local coordinate systems that are in a structure. The coordinate transformation gives the relationship between the nodal displacement vector $\bar{\mathbf{u}}$ based on the local coordinate system and the nodal displacement vector $\mathbf{u}$, for the same finite element, based on the global coordinate system ($x_i;\ i = 1, 2, 3$).

$$\overline{\mathbf{u}} = \mathbf{T}\,\mathbf{u} \tag{4.74}$$

with

$$\mathbf{u} = \begin{bmatrix} u_1 & u_2 & u_3 & u_4 & u_5 & u_6 & u_7 & u_8 & u_9 & u_{10} & u_{11} & u_{12} \end{bmatrix}^T \tag{4.75}$$

where $\mathbf{T}$ is the transformation matrix for the truss element, given by

$$\mathbf{T} = \begin{bmatrix} \mathbf{R} & \mathbf{0} & \mathbf{0} & \mathbf{0} \\ \mathbf{0} & \mathbf{R} & \mathbf{0} & \mathbf{0} \\ \mathbf{0} & \mathbf{0} & \mathbf{R} & \mathbf{0} \\ \mathbf{0} & \mathbf{0} & \mathbf{0} & \mathbf{R} \end{bmatrix} \tag{4.76}$$

and $\mathbf{R}$ is the 3×3 transformation matrix from the local coordinate system to the global coordinate systems, whose components are

$$\mathbf{R} = \begin{bmatrix} \cos(\bar{x}_1, x_1) & \cos(\bar{x}_1, x_2) & \cos(\bar{x}_1, x_3) \\ \cos(\bar{x}_2, x_1) & \cos(\bar{x}_2, x_2) & \cos(\bar{x}_2, x_3) \\ \cos(\bar{x}_3, x_1) & \cos(\bar{x}_3, x_2) & \cos(\bar{x}_3, x_3) \end{bmatrix} = \begin{bmatrix} l_{11} & m_{12} & n_{13} \\ l_{21} & m_{22} & n_{23} \\ l_{31} & m_{32} & n_{33} \end{bmatrix} \tag{4.77}$$

To evaluate the direction cosines, the three-dimensional orientation of the beam element need to be defined, as for the case of 2-D beams. The two nodes of the finite element are used to define the local $\bar{x}_1$ axis. However, the orientation of axes $\bar{x}_2$ and $\bar{x}_3$ can still rotate around the axis of the beam. To prevent this problem, one additional point in the local coordinate must be defined. ADINA program uses this auxiliary point to specify the cross-section dimensions of the beam, as point out in Fig. 4.24. This point can be selected according the desired orientation of the beam, but should never be selected at the local $\bar{x}_1$ axis. More details about the computation of these direction cosines can be view in the literature [5].

Using the transformation matrix, $\mathbf{T}$, the matrices for space finite elements in the global coordinate system can be obtained as

$$\mathbf{k} = \mathbf{T}^T \overline{\mathbf{k}}\, \mathbf{T} \tag{4.78}$$

$$\mathbf{m} = \mathbf{T}^T \overline{\mathbf{m}}\, \mathbf{T} \tag{4.79}$$

$$\mathbf{f} = \mathbf{T}^T \overline{\mathbf{f}} \tag{4.80}$$

4.3.4 Fifth Discussion Example

Example 4.5: 3D Structure
Consider the beam structure shown in Fig. 4.32. The structure is made with three beam members and two forces of 10 kN and 15 kN are applied at the free vertex. The structure dimensions are presented in the figure and the material has a Young's modulus of 210 GPa and a Poisson's ratio of 0.3.

Modelling
The 3-D structure is meshed using two-nodal beam elements in the ADINA program, 30 finite elements are used in the 3-D structure, as shown in Fig. 4.33. The letter B is used, once more, to represent the boundary conditions applied at nodes 11, 21 and 31. Letter B is associated with a support that restrains the displacement in the three axes directions and at node 1 it is represented the resultant load. As explained before in Fig. 4.24, ADINA denotes the cross section beam axes by letters (t) and (s) and the r-axis is along the axial direction of the beam. The r-s plane contains the two end nodes, node i and j, of the beam and the auxiliary node. Nevertheless, the s-axis may be defined using the global coordinates of a vector that is aligned with

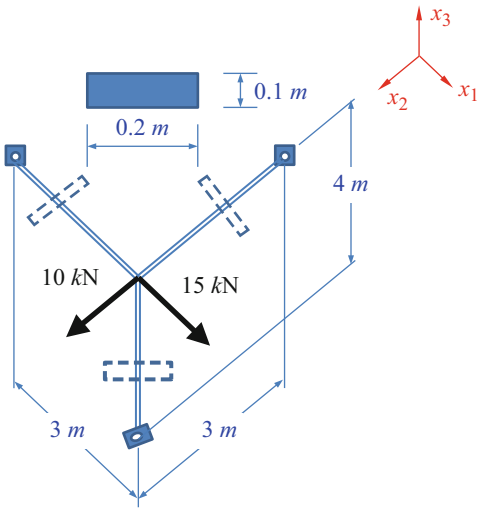

Fig. 4.32 A 3-D beam structure

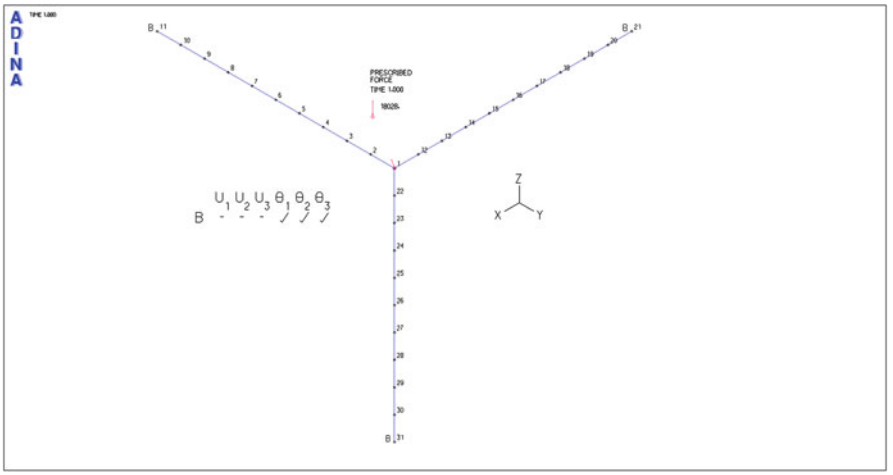

Fig. 4.33 Finite element mesh of a 3-D structure with representation of loading and boundary conditions used within the numerical model

the s-axis. Figure 4.34 shows the orientation of cross section for the three beams. The cross section orientation that is plotted in Fig. 4.34 was obtained using vector $\begin{bmatrix} 0 & 0 & 1 \end{bmatrix}^T$ for the generation of all elements that are in the $x-y$ plane and the vector $\begin{bmatrix} 1 & 1 & 0 \end{bmatrix}^T$ for the beam that is parallel to the z axis.

Results and Discussion

Using the numerical model presented in Fig. 4.33, the finite element equation is solved by ADINA and a deformation plot showing how the 3-d beam deforms under the load is presented in Fig. 4.35. The magnitude of the deformation is magnified

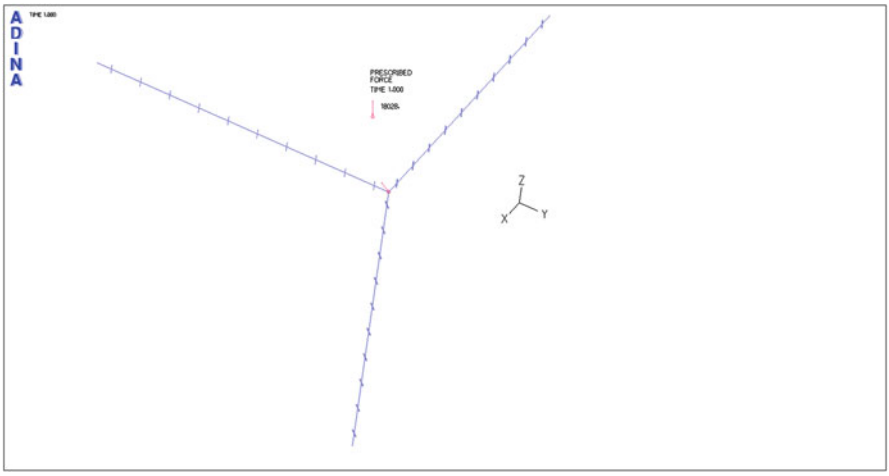

Fig. 4.34 Representation of the beam cross-section orientation in the ADINA program

40,000 times, because the magnitude of the displacement is too small for viewing process. The maximum absolute value of displacement is of 0.01286 mm and is located at the loading point.

Note that because the force of 15 kN is applied in the y direction, the y-displacement is higher than the x-axis displacement, but they have the same order. Another important result that could be obtained is the stress associated with this particular loading condition, as in the case of Example 4.3.

4.4 Discussion

In the formulation of the matrices for the previous 2-D and 3-D beam finite elements, the superposition of the truss, shaft and beam displacements has been used. This technique assumes that the axial effects are not coupled with the bending effects, meaning that axial forces applied on the finite element will not cause any bending deformation and the bending moments will not result in any axial displacement. These kind of assumptions are not valid for slander structures where buckling instability may arise. In practice, buckling is characterized by a sudden failure of a structural member subjected to high compressive stress, where the actual compressive stress at the point of failure is lower than the ultimate compressive stresses that the material is able of withstanding. For these kind of analysis it is necessary accounting for the axial-bending coupling effect, which leads to an additional matrix, called geometric stiffness matrix, dependent on the axial load. Moreover, the axial-bending coupling also appears in curved structures. Thus, in such cases, if the curvature is very large resulting in a significant coupling effect, a finer mesh should be used to provide the necessary accuracy.

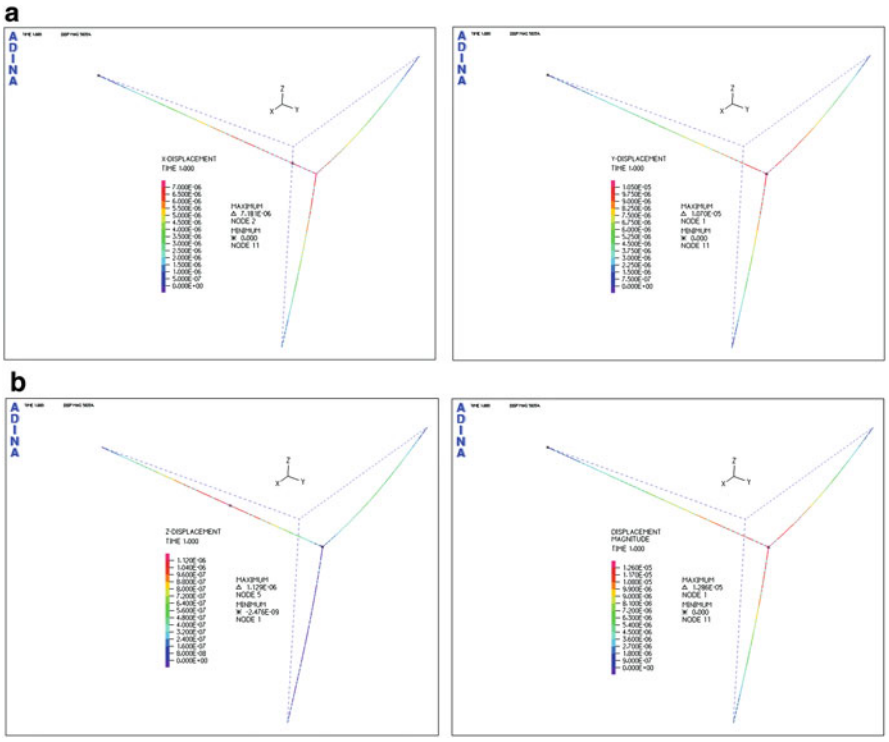

Fig. 4.35 Deformation plot of 2-D structure: (**a**) contour plot of the x displacement; (**b**) contour plot of the y displacement

All the beam elements formulated previously are on the so-called Euller-Bernoulli beam theory suitable for thin beams with a thickness to span ratio smaller than 1/20. For thick, or thin beams of large thickness to span ratio, the corresponding thick beams theories should be used to develop thick beams elements. The procedure of developing thick beams is very similar to that used to develop thick plates, which will be discussed later in Chap. 6.

4.5 Review Questions

1. Consider the beam in Fig. 4.36. The beam has a constant cross-section area, denoted by A, and it is fixed at one end and loaded by a distributed constant body force in the transversal direction, as shown. The material of the bar is isotropic with Young's modulus E.

   (a) Solve for the exact displacement response of the structure.
   (b) Using Eqs. (4.18) and (4.21) compute the maximum value of trans versal displacement and compare with the solution of question a.

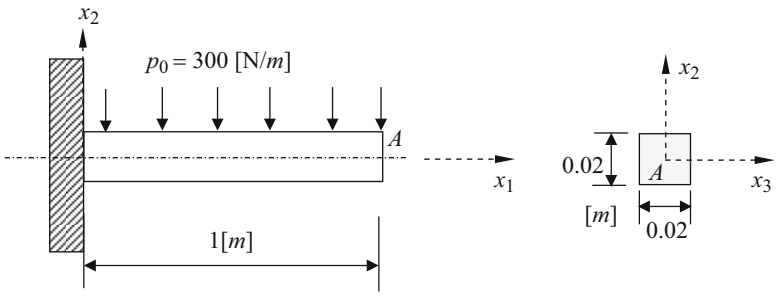

Fig. 4.36 Beam structure with a uniform cross-section

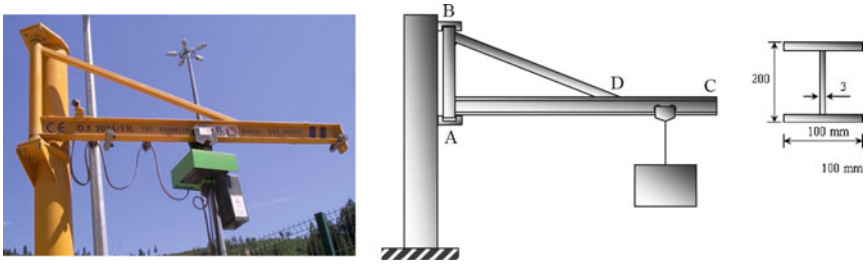

Fig. 4.37 Frame structure used for lifting loads

(c) Using Eqs. (4.18) and (4.20) compute the first two natural frequencies of beam.
(d) Assume that the structure, unloaded and in the undeformed stage, is subjected to an impact end load of 300 N. Perform a transient analysis for a time of 0.5 s. Show the time history of beam tip displacement.

2. How many degrees of freedom does a two-node 2D beams finite element has in its local coordinate system, and in the global coordinate system? Does rotational degrees of freedom undergo any trigonometric transformation?
3. Consider the structure in Fig. 4.37, used for lifting loads. All the structural components are of steel with a Young modulus of 210 GPa. The AB component is tubular and has an external diameter of 40 mm and a thickness of 3 mm, while the BD component is a square tube wit external dimensions of 10×10 mm^2 and thickness of 2 mm. The AC component is an I-beam, as shown, with a uniform thickness: AD length of 0.75 m; DC length of 0.25 m; AB length of 0.5 m. Compute maximum displacement and maximum stress.

References

1. Bathe K-J (1996) Finite element procedures. Prentice Hall, Englewood Cliffs
2. Zienkiewicz OC, Morgan K (1983) Finite elements and approximation. Wiley, New York

3. Zienkiewicz OC, Taylor RL (2000) The finite element method. Butterworth-Heinemann, Oxford/Boston
4. Reddy JN (1997) Mechanics of laminated composite plates and shells: theory and analysis. CRC Press, Boca Raton
5. Liu GR, Quek SS (2003) The finite element method: a practical course. Butterworth-Heinemann, Oxford
6. ADINA R & D I (2014) User's manual. R&D Inc., Boston

Chapter 5
Finite Element Method for Membranes (2-D Solids)

The development of finite element equations for the stress analysis of two dimensional structures subjected to external loads that are applied within their 2-D geometrical plane will be presented in this chapter. The basic concepts, procedures and formulations can also be found in many existing textbooks [1–4]. The element developed is called membrane or 2D solid element. The finite element solution will solve only the selected mathematical model and that all assumptions in this model will be reflected in the predicted response. Thus, the choice of an appropriate mathematical model is crucial and completely determines the insight into the physical problem that we can obtain by this kind of analysis.

5.1 Introduction

In engineering applications there are a great number of practical problems in which the analyst can idealize the use of bidimensional models and, as discussed in Chap. 1, there are several mathematical models that can be used to solve them. For instance, if there is a plate structure with a loading acting in the plane structure, as presented in Fig. 5.1a, the solution of stress and strain states can be obtained using 2D solid elements under plane stress conditions. Whereas to model the effect of the water pressure on a dam, as shown in Fig. 5.1b, there is a need of using 2D solid elements under plane strain conditions. Plane stress conditions are usually applied to structures that have a relatively small thickness when compared to its other dimensions, as the case of the structure presented in Fig. 5.1a. Whereas plane strain conditions are considered in situations in which the thickness of the structure is relatively large as compared to its other dimensions, and the loading is uniform along the thickness direction. In both conditions, the system equation can be

M.A. Neto et al., *Engineering Computation of Structures: The Finite Element Method*, DOI 10.1007/978-3-319-17710-6_5

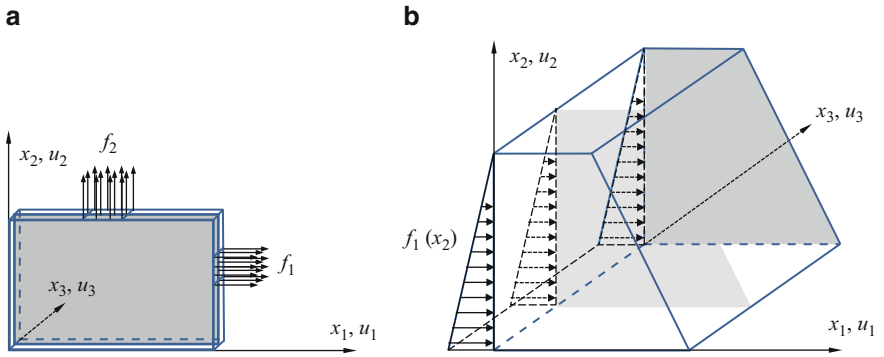

Fig. 5.1 Typical 2D problems in: (**a**) plane stress conditions; (**b**) plane strain conditions

drastically simplified, as showed in Chap. 1. Moreover, formulations of plane stress and plane strain conditions are very similar, the main difference is related with the material stiffness matrix. The geometrical shape of a 2D solid finite element can be triangular, rectangular or quadrilateral with straight or curved edges. The order of 2D solid elements can be determined by the order of the shape functions used within the displacement numerical approximations, as for the case of any other kind of finite element. A finite element is called linear if its shape functions are linear, quadratic if those functions are quadratic and are called high order if their shape functions are cubic or of an higher order. The edges of linear elements are straight while in quadratic elements they can be curved. In engineering practice, the most often used elements are linear. Quadratic finite elements are also used in situations that require high stress accuracy. Higher order elements have also been developed for specific problems, but they are less used. 2D solid elements can only deform in the plane where the geometrical model is defined, so let's assume that the geometrical model is defined in the $x_1 - x_2$ plane. For plane strain conditions the thickness of the true structure is not important and is, normally, treated as a unit quantity uniformly throughout the 2D model. However, for plane stress conditions, the thickness is an important parameter changing the stiffness and the stress level. Within this chapter it is assumed that all the structures have a uniform thickness h. Nevertheless, if the structure has a non uniform thickness, the numerical model may be created by dividing the original model into parts of uniform thickness, where in elements of uniform thickness can be used. Alternatively, formulation of elements with varying thickness can also be easily formulated. The equations of motion for 2D finite elements are more complex than those for the 1D finite elements, essentially, because of the higher dimension. Meanwhile, the procedure for developing these equations is very similar to that used at the 1D truss elements, with the following three-step procedure: (1) construction of the shape functions matrix; (2) formulation of the strain matrix; (3) calculation of the element matrices.

5.2 2D-Solid Linear Triangular Elements

The formulation of the linear triangular 2D-solid element is the simplest formulation among all the 2D solid elements, and is also the less accurate compared to linear quadrilateral elements. Nevertheless, linear triangular finite elements are a very useful element in the adaptivity of complex geometries. Moreover, triangular elements are normally used in the mesh of 2D models involving complex geometries with acute corners. In addition, the triangular configuration with the simplest topological feature makes it easier to develop meshing processors.

5.2.1 Degrees of Freedom Identification

Consider a 2D geometrical model of a rectangular structure in the $x_1 - x_2$ plane, shown schematically in Fig. 5.2, the 2D domain is divided in a proper manner into a number of triangular elements. In a mesh of linear triangular elements, each triangular element has three nodes and three straight edges. Consider now a triangular element of thickness h, shown in Fig. 5.3, the element nodes are numbered counter-clockwise. In the 2D solid finite elements the displacement field has two components (u_1, u_2) and hence each node has two degrees of freedom. Since a linear

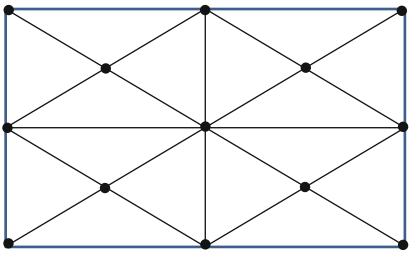

Fig. 5.2 Rectangular domain meshed with triangular elements

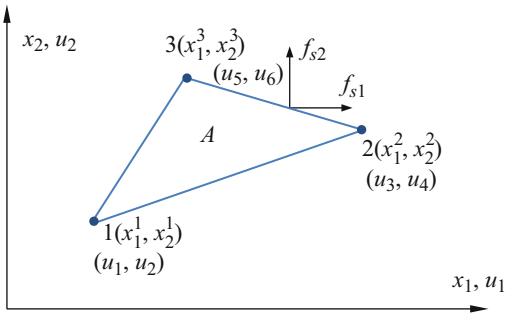

Fig. 5.3 A linear triangular finite element

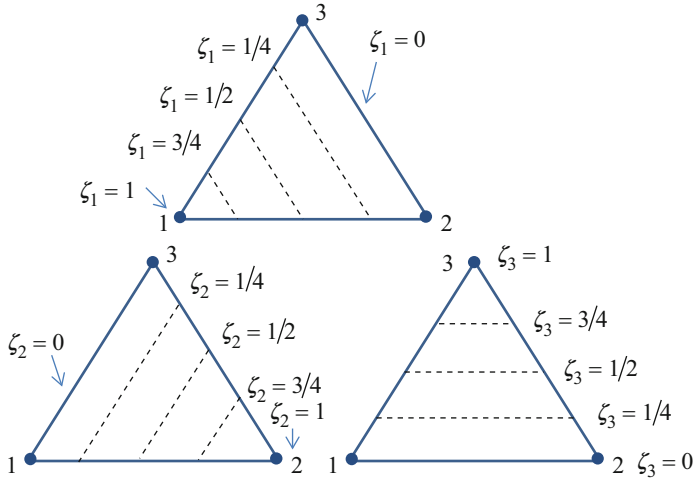

Fig. 5.4 Graphical representation of the triangular coordinates

triangular element has three nodes, the total number of degrees of freedom of a linear triangular finite element is six.

The vector of nodal displacements is arranged in the following order:

$$\mathbf{u} = \Big[\underbrace{u_1 \quad u_2}_{\substack{\textit{displacements} \\ \textit{at node } 1}} \quad \underbrace{u_3 \quad u_4}_{\substack{\textit{displacements} \\ \textit{at node } 2}} \quad \underbrace{u_5 \quad u_6}_{\substack{\textit{displacements} \\ \textit{at node } 3}} \Big]^T \tag{5.1}$$

The location of nodes is defined by their Cartesian coordinates (x_1^i, x_2^i) for $i = 1,2,3$, but they can also be located in terms of a triangular coordinate parametric system denoted by ζ_1, ζ_2 and ζ_3. In the literature these parameters have a great number of names: natural coordinates; area coordinates; barycentric coordinates; shape function coordinates; etc. in this chapter the name triangular coordinates is used to emphasize the close association with this particular geometry.

The equation $\zeta_i = cte$ represent a set of straight lines parallel to the side opposite to the ith corner, as shown in Fig. 5.4. The triangular sides are described by the triangular coordinates: $\zeta_3 = 0$ (side of nodes 1 and 2); $\zeta_1 = 0$ (side of nodes 2 and 3); $\zeta_2 = 0$ (side of nodes 3 and 1). Thus, the three corners have the following triangular coordinates: $1(1,0,0)$; $2(0,1,0)$; $3(0,0,1)$. The triangular coordinates are not independent because they verify the following relation:

$$\zeta_1 + \zeta_2 + \zeta_3 = 1 \tag{5.2}$$

The relation between Cartesian and triangular coordinates is defined as

$$\begin{aligned} x_1 &= x_1^1\zeta_1 + x_1^2\zeta_2 + x_1^3\zeta_3 \\ x_2 &= x_2^1\zeta_1 + x_2^2\zeta_2 + x_2^3\zeta_3 \end{aligned} \tag{5.3}$$

which means that Cartesian coordinates of any point within the finite element can be obtained from the knowledge of its triangular coordinates and the Cartesian coordinates of the element nodes. Equations (5.2) and (5.3) can be rewritten in a matrix form as

$$\begin{bmatrix} 1 \\ x_1 \\ x_2 \end{bmatrix} = \begin{bmatrix} 1 & 1 & 1 \\ x_1^1 & x_1^2 & x_1^3 \\ x_2^1 & x_2^2 & x_2^3 \end{bmatrix} \begin{bmatrix} \zeta_1 \\ \zeta_2 \\ \zeta_3 \end{bmatrix} \tag{5.4}$$

Assuming that element area is different of zero, Eq. (5.4) may be inverted as

$$\begin{aligned} \begin{bmatrix} \zeta_1 \\ \zeta_2 \\ \zeta_3 \end{bmatrix} &= \frac{1}{2A} \begin{bmatrix} x_1^2x_2^3 - x_1^3x_2^2 & x_2^2 - x_2^3 & x_1^3 - x_1^2 \\ x_1^3x_2^1 - x_1^1x_2^3 & x_2^3 - x_2^1 & x_1^1 - x_1^3 \\ x_1^1x_2^2 - x_1^2x_2^1 & x_2^1 - x_2^2 & x_1^2 - x_1^1 \end{bmatrix} \begin{bmatrix} 1 \\ x_1 \\ x_2 \end{bmatrix} \\ &= \frac{1}{2A} \begin{bmatrix} 2A_{23} & Y_{23} & X_{32} \\ 2A_{31} & Y_{31} & X_{13} \\ 2A_{12} & Y_{12} & X_{21} \end{bmatrix} \begin{bmatrix} 1 \\ x_1 \\ x_2 \end{bmatrix} \end{aligned} \tag{5.5}$$

with

$$\begin{aligned} X_{jk} = x_1^j - x_1^k;\ Y_{jk} = x_2^j - x_2^k;\ A_{jk} = x_1^j x_2^k - x_1^k x_2^j; \\ A = \left(x_1^2x_2^3 - x_1^3x_2^2\right) + \left(x_1^3x_2^1 - x_1^1x_2^3\right) + \left(x_1^1x_2^2 - x_1^2x_2^1\right) \end{aligned} \tag{5.6}$$

Where A is the triangle area, A_{jk} is the area subtended by corners j, k and the origin of the Cartesian system. When the origin of the Cartesian system is taken at the centroid of the triangle it follows that: $A_{23} = A_{31} = A_{12} = A/3$.

Equation (5.4) can be used to evaluate partial derivatives, as

$$\frac{\partial x_1}{\partial \zeta_i} = x_1^i;\ \frac{\partial x_2}{\partial \zeta_i} = x_2^i \tag{5.7}$$

While Eq. (5.5) can be used to evaluate the inverse partial derivative, as

$$\frac{\partial \zeta_i}{\partial x_1} = \frac{Y_{jk}}{2A};\ \frac{\partial \zeta_i}{\partial x_2} = \frac{X_{kj}}{2A} \tag{5.8}$$

Where j and k denote the sequential permutation of index i. For instance, if $i = 2$, then $j = 3$ and $k = 1$. Thus, the derivatives of a function $f(\zeta_1, \zeta_2, \zeta_3)$ with respect to variables x_1 and x_2 follows the application of the chain rule derivative, as

$$\begin{bmatrix} \dfrac{\partial f}{\partial x_1} \\ \dfrac{\partial f}{\partial x_2} \end{bmatrix} = \frac{1}{2A} \begin{bmatrix} Y_{23} & Y_{31} & Y_{12} \\ X_{23} & X_{31} & x_{12} \end{bmatrix} \begin{bmatrix} \dfrac{\partial f}{\partial \zeta_1} \\ \dfrac{\partial f}{\partial \zeta_2} \\ \dfrac{\partial f}{\partial \zeta_3} \end{bmatrix} = \mathbf{J}^{-1} \begin{bmatrix} \dfrac{\partial f}{\partial \zeta_1} \\ \dfrac{\partial f}{\partial \zeta_2} \\ \dfrac{\partial f}{\partial \zeta_3} \end{bmatrix} \tag{5.9}$$

5.2.2 FE Approximation of the Displacement

The displacement field $\tilde{\mathbf{u}}$ it will be a function of coordinates (x_1, x_2) and, the displacement at any point in the element, is expressed using the displacement at the nodes and the shape functions, i.e.

$$\tilde{\mathbf{u}}(x_1, x_2) = \mathbf{N}(x_1, x_2)\,\mathbf{u} \tag{5.10}$$

where $\mathbf{N}$ is the matrix of shape functions, defined as

$$\mathbf{N} = \begin{bmatrix} N_1 & 0 & N_2 & 0 & N_3 & 0 \\ 0 & N_1 & 0 & N_2 & 0 & N_3 \end{bmatrix} \tag{5.11}$$

in which N_i $(i = 1, 2, 3)$ are the shape functions corresponding to the three nodes of the triangular finite element. So, Eq. (5.10) can be written explicitly as

$$\begin{aligned} \tilde{u}_1(x_1, x_2) &= N_1(x_1, x_2)\,u_1 + N_2(x_1, x_2)\,u_3 + N_3(x_1, x_2)\,u_5 \\ \tilde{u}_2(x_1, x_2) &= N_1(x_1, x_2)\,u_2 + N_2(x_1, x_2)\,u_4 + N_3(x_1, x_2)\,u_6 \end{aligned} \tag{5.12}$$

Note that because the two components are independent from each other, each displacement component at any point is approximated by an interpolation from the correspondent nodal degrees of freedom using the shape functions. In the next section, the shape functions for triangular finite elements will be constructed using triangular coordinates.

5.2.3 Shape Functions for Triangular Elements

The procedure of determining the shape functions for triangular finite elements follows the standard procedure described in Sect. 2.3.3 of Chap. 2, by starting with an assumption of the displacements using polynomial basis functions with unknown constants. After which, these unknown constants are determined using the nodal displacements at the nodes of element.

Another alternative procedure and effective method for creating shape functions for triangular elements is to use the triangular coordinates. The use of these coordinates will immediately lead to the shape functions. That is, $N_i = \zeta_i$ for $i = 1, 2, 3$, and the displacement field at an arbitrary point $p(\zeta_1, \zeta_2, \zeta_3)$ is defined as

$$\begin{bmatrix} \tilde{u}_1(\zeta_1, \zeta_2, \zeta_3) \\ \tilde{u}_2(\zeta_1, \zeta_2, \zeta_3) \end{bmatrix} = \begin{bmatrix} \zeta_1 & 0 & \zeta_2 & 0 & \zeta_3 & 0 \\ 0 & \zeta_1 & 0 & \zeta_2 & 0 & \zeta_3 \end{bmatrix} \begin{bmatrix} u_1 \\ u_2 \\ u_3 \\ u_4 \\ u_5 \\ u_6 \end{bmatrix} = \mathbf{N}(\zeta_1, \zeta_2, \zeta_3)\,\mathbf{u} \tag{5.13}$$

5.2.4 FE Approximation of Strain

As discussed in previous chapter, after computing shape functions is possible to obtain others quantities, namely the relationship between the strain and the deflection described in Eq. (1.133) of Chap. 1, as the derivative of the displacement field with respect x_1 and x_2,

$$\begin{bmatrix} \tilde{\varepsilon}_{11} \\ \tilde{\varepsilon}_{22} \\ \tilde{\varepsilon}_{12} \end{bmatrix} = \begin{bmatrix} \partial/\partial x_1 & 0 \\ 0 & \partial/\partial x_2 \\ \partial/\partial x_2 & \partial/\partial x_1 \end{bmatrix} \begin{bmatrix} \tilde{u}_1 \\ \tilde{u}_2 \end{bmatrix} \tag{5.14}$$

Using the information in Eqs. (5.13) and (5.8) is possible to rewrite Eq. (5.14), as

$$\begin{aligned} \varepsilon_{11} &= \frac{\partial \zeta_1}{\partial x_1}u_1 + \frac{\partial \zeta_2}{\partial x_1}u_3 + \frac{\partial \zeta_3}{\partial x_1}u_5 = \frac{Y_{23}}{2A}u_1 + \frac{Y_{31}}{2A}u_3 + \frac{Y_{12}}{2A}u_5 \\ \varepsilon_{22} &= \frac{\partial \zeta_1}{\partial x_2}u_2 + \frac{\partial \zeta_2}{\partial x_2}u_4 + \frac{\partial \zeta_3}{\partial x_2}u_6 = \frac{X_{32}}{2A}u_2 + \frac{X_{13}}{2A}u_4 + \frac{X_{21}}{2A}u_6 \\ \varepsilon_{12} &= \frac{\partial \zeta_1}{\partial x_2}u_1 + \frac{\partial \zeta_2}{\partial x_2}u_3 + \frac{\partial \zeta_3}{\partial x_2}u_5 + \frac{\partial \zeta_1}{\partial x_1}u_2 + \frac{\partial \zeta_2}{\partial x_1}u_4 + \frac{\partial \zeta_3}{\partial x_1}u_6 \\ &= \frac{X_{32}}{2A}u_1 + \frac{X_{13}}{2A}u_3 + \frac{X_{21}}{2A}u_5 + \frac{Y_{23}}{2A}u_2 + \frac{Y_{31}}{2A}u_4 + \frac{Y_{12}}{2A}u_6 \end{aligned} \tag{5.15}$$

Or in a matrix form, as

$$\begin{bmatrix} \varepsilon_{11} \\ \varepsilon_{22} \\ \varepsilon_{12} \end{bmatrix} = \frac{1}{2A} \begin{bmatrix} Y_{23} & 0 & Y_{31} & 0 & Y_{12} & 0 \\ 0 & X_{32} & 0 & X_{13} & 0 & X_{21} \\ X_{32} & Y_{23} & X_{13} & Y_{31} & X_{21} & Y_{12} \end{bmatrix} \begin{bmatrix} u_1 \\ u_2 \\ u_3 \\ u_4 \\ u_5 \\ u_6 \end{bmatrix} \iff \boldsymbol{\varepsilon} = \mathbf{B}\mathbf{u} \tag{5.16}$$

where **B** is the strain-displacement matrix of the triangular finite element. Note that this matrix is constant over the element, thus the linear triangular elements are also referred to as a constant strain elements or constant stress elements. In practice, stress or strain varies across the structure, thus the use of coarse meshes of linear triangular elements will result in a rather inaccurate stress or strain distribution.

5.2.5 *Element Matrices*

The stiffness matrix for finite element can be obtained substituting Eq. (5.16) into (2.49) from the Chap. 2, leading to

$$\mathbf{k} = \int_{\Omega^e} \mathbf{B}^T \mathbf{c}\, \mathbf{B}\, d\Omega^e = \int_A \left(\int_0^h dx_3 \right) \mathbf{B}^T \mathbf{c}\, \mathbf{B}\, dA = \int_A h\, \mathbf{B}^T \mathbf{c}\, \mathbf{B}\, dA \tag{5.17}$$

where the material constant matrix **c** has been given by Eqs. (1.35) and (1.36) of Chap. 1, respectively, for the plane stress and plane strain problems. Since the strain matrix **B** is a constant matrix, as shown in Eq. (5.16), and the thickness of the element is assumed to be constant, the integration of Eq. (5.19) can be carried out very easily, which leads to

$$\mathbf{k} = h\, A\, \mathbf{B}^T \mathbf{c}\, \mathbf{B} \tag{5.18}$$

where A denotes the surface element area.

To evaluate the mass matrix, Eq. (5.13) is substituted into Eq. (2.45), leading to

$$\mathbf{m} = \int_{\Omega^e} \rho \overline{\mathbf{N}}^T \overline{\mathbf{N}}\, d\Omega^e = \int_A \int_0^h dx_3\, \rho \overline{\mathbf{N}}^T \overline{\mathbf{N}}\, dA = \int_A h\rho \overline{\mathbf{N}}^T \overline{\mathbf{N}}\, dA \tag{5.19}$$

For finite elements with a constant thickness and density, Eq. (5.19) yields

$$\mathbf{m} = h\rho \int_A \begin{bmatrix} N_1N_1 & 0 & N_1N_2 & 0 & N_1N_3 & 0 \\ 0 & N_1N_1 & 0 & N_1N_2 & 0 & N_1N_3 \\ N_2N_1 & 0 & N_2N_2 & 0 & N_2N_3 & 0 \\ 0 & N_2N_1 & 0 & N_2N_2 & 0 & N_2N_3 \\ N_3N_1 & 0 & N_3N_2 & 0 & N_3N_3 & 0 \\ 0 & N_3N_1 & 0 & N_3N_2 & 0 & N_3N_3 \end{bmatrix} dA \tag{5.20}$$

The integration of all the terms in the mass matrix can be carried out by simply using a mathematical formula developed by Eisenberg and Malvern [5]:

$$\int_A \zeta_1^m \zeta_2^n \zeta_3^p \, dA = \frac{m!\, n!\, p!}{(m+n+p+2)!} 2A \tag{5.21}$$

where $\zeta_i \ (i = 1, 2, 3)$ are the shape function of triangular elements. Therefore, the element mass matrix is defined as

$$\mathbf{m} = \frac{\rho h A}{12} \begin{bmatrix} 2 & 0 & 1 & 0 & 1 & 0 \\ 0 & 2 & 0 & 1 & 0 & 1 \\ 1 & 0 & 2 & 0 & 1 & 0 \\ 0 & 1 & 0 & 2 & 0 & 1 \\ 1 & 0 & 1 & 0 & 2 & 0 \\ 0 & 1 & 0 & 1 & 0 & 2 \end{bmatrix} \tag{5.22}$$

The nodal force vector for 2D solid elements can be obtained using Eqs. (2.51) and (2.52), assuming that the element is loaded by a constant distributed force $\mathbf{f}_s$ on the edge 2–3 as shown in Fig. 5.3, leads to the following equation

$$\mathbf{f} = \int_{\ell_{23}} \mathbf{N}_{2-3}^T \mathbf{f}_s \, d\ell = \int_{\ell_{2-3}} \begin{bmatrix} 0 & 0 \\ 0 & 0 \\ N_2 & 0 \\ 0 & N_2 \\ N_3 & 0 \\ 0 & N_3 \end{bmatrix} \begin{bmatrix} f_{s1} \\ f_{s2} \end{bmatrix} d\ell \tag{5.23}$$

where ℓ_{2-3} is the length of the edge 2–3. Because force $\mathbf{f}_s$ is constant within the element edge, the above equation becomes

$$\mathbf{f} = \frac{1}{2} \ell_{2-3} \begin{bmatrix} 0 \\ 0 \\ f_{s1} \\ f_{s2} \\ f_{s1} \\ f_{s2} \end{bmatrix} \tag{5.24}$$

The global finite element equation can be obtained by assembling the element matrices by summing up the contribution from all the adjacent elements at the shared nodes.

5.3 Isoparametric Representation

The procedure used in the last section, to formulate the element matrices of the linear triangle, can be extended to formulate quadrilateral elements as well as higher order triangles. Nevertheless, the use of this procedure encounters the following difficulties:

- The construction of shape functions that satisfy consistency requirements for higher order elements with curved boundaries becomes increasingly complicated.
- Integrals that appear in the expressions of the element stiffness matrix and consistent nodal force vector can no longer be evaluated in simple closed form.

These two drawbacks can be overcome through the concepts of isoparametric finite elements and numerical integration, respectively. In fact, the linear triangle presented in the previous section is also an isoparametric element although was not originally derived busing such concept. Nevertheless, the two key Eqs. (5.4) and (5.13) that define the triangle geometry and the displacement field, respectively, confirm the main idea of isoparametric elements, illustrated in Fig. 5.5.

In Fig. 5.5 is evident that if the order of shape functions is higher than one the geometry of the elements will no longer be straight. An alternative to the isoparametric concept is the superparametric representation of triangular elements as illustrated in Fig. 5.6. In this concept the triangular coordinates are used to define the element geometry while the displacement field is defined by the shape function, which in turn are expressed in terms of the triangular coordinates. For the linear triangular element, defined in the previous section, shape functions and triangular coordinates are coincident.

Meanwhile, if higher order triangular finite elements are developed using the procedure illustrated in Fig. 5.6, while keeping straight sides, only the displacement field is improved whereas the geometry remains the same. In this section, the concept of isoparametric representation is introduced for two dimensional elements.

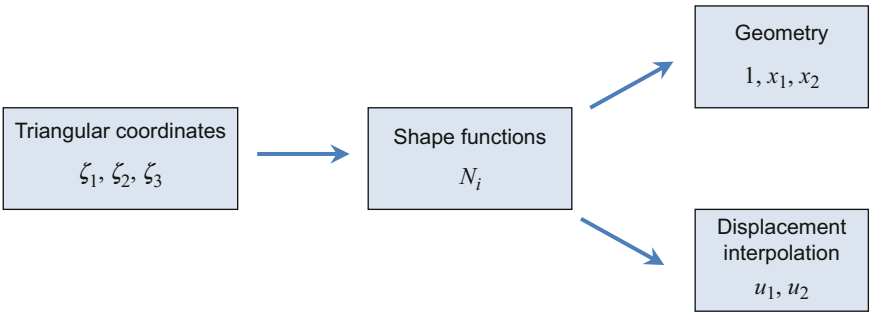

Fig. 5.5 Isoparametric representation of triangular finite elements

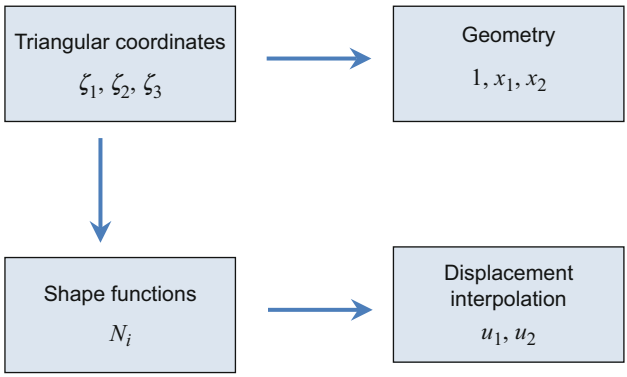

Fig. 5.6 Superparametric representation of triangular finite elements

5.3.1 Isoparametric Formulation

The procedure presented in Fig. 5.6 can be generalized to an arbitrary two-dimensional element with n nodes. In this context, two set of relations are required: one to define the element geometry and the other to approximate the element displacements, i.e.

$$1 = \sum_{i=1}^{n} N_i;\ x_1 = \sum_{i=1}^{n} N_i x_1^i;\ x_2 = \sum_{i=1}^{n} N_i x_2^i \tag{5.25}$$

$$u_1 = \sum_{i=1}^{n} N_i u_{(i-1)*k+1};\ u_2 = \sum_{i=1}^{n} N_i u_{(i-1)*k+2} \tag{5.26}$$

where Eq. (5.25) is the interpolation equation of element geometry and Eq. (5.26) is the interpolation equation for the displacement components. Note that in Eq. (5.26) the index k is the number of degrees of freedom per node, in 2D-solid finite elements is equal to two. Moreover, these two equations can be combined in a matrix form as

$$\begin{bmatrix} 1 \\ x_1 \\ x_2 \\ \tilde{u}_1 \\ \tilde{u}_2 \end{bmatrix} = \begin{bmatrix} 1 & 1 & \cdots & 1 \\ x_1^1 & x_1^2 & \cdots & x_1^n \\ x_2^1 & x_2^2 & \cdots & x_2^n \\ u_1 & u_{(2-1)*k+1} & \cdots & u_{(n-1)*k+1} \\ u_2 & u_{(2-1)*k+2} & \cdots & u_{(n-1)*k+2} \end{bmatrix} \begin{bmatrix} N_1 \\ N_2 \\ \vdots \\ N_n \end{bmatrix};\ k = 1, \ldots, df \tag{5.27}$$

In Eq. (5.27) is possible to include additional rows if more variables of the problem are interpolated by the same shape functions. For example, suppose that

the thickness h and the temperature field T are both interpolated from the n node values:

$$\begin{bmatrix} 1 \\ x_1 \\ x_2 \\ \tilde{u}_1 \\ \tilde{u}_2 \\ \tilde{h} \\ \tilde{T} \end{bmatrix} = \begin{bmatrix} 1 & 1 & \cdots & 1 \\ x_1^1 & x_1^2 & \cdots & x_1^n \\ x_2^1 & x_2^2 & \cdots & x_2^n \\ u_1 & u_{(2-1)*k+1} & \cdots & u_{(n-1)*k+1} \\ u_2 & u_{(2-1)*k+2} & \cdots & u_{(n-1)*k+2} \\ h_1 & h_2 & \cdots & h_n \\ T_1 & T_2 & \cdots & T_n \end{bmatrix} \begin{bmatrix} N_1 \\ N_2 \\ \vdots \\ N_n \end{bmatrix}; \; k = 1, \ldots, df \tag{5.28}$$

Comparing Eqs. (5.27) and (5.28) it can be seen that the vector of shape functions does not change.

5.3.2 *Isoparametric Formulation for Triangular Elements*

For the linear triangular element the shape functions are simple the triangular coordinates. Nevertheless, to developing higher order elements we make use of the triangular coordinates system. Figure 5.7 shows a general triangular element of order m, which means that for each triangular coordinate direction the number of nodes is of $m + 1$.

The node $i(I, J, K)$ presented in Fig. 5.7 is located at the Ith node in the ζ_1 direction, at the Jth node in the ζ_2 direction, and at the node Kth in the ζ_3 direction. From Fig. 5.7 it can also be confirmed that at any node the following relation is verified

$$I + J + K = m \tag{5.29}$$

Using this information is possible to write the shape functions in the form [6, 7]

$$N_i = L_I(\zeta_1) L_J(\zeta_2) L_K(\zeta_3) \tag{5.30}$$

Where L_I, L_J and L_K are the Lagrange polynomials, and can be written as

$$L_\beta(\zeta_\alpha) = \frac{(\zeta_\alpha - (\zeta_\alpha)_0)(\zeta_\alpha - (\zeta_\alpha)_1) \cdots (\zeta_\alpha - (\zeta_\alpha)_{\beta-1})}{((\zeta_\alpha)_\beta - (\zeta_\alpha)_0)((\zeta_\alpha)_\beta - (\zeta_\alpha)_1) \cdots ((\zeta_\alpha)_\beta - (\zeta_\alpha)_{\beta-1})} \tag{5.31}$$

where $\alpha = 1, 2, 3$ and $\beta = I, J, K$. For example, when $\alpha = 1$ and $\beta = I$ is possible to write

$$L_I(\zeta_1) = \frac{(\zeta_1 - (\zeta_1)_0)(\zeta_1 - (\zeta_1)_1) \cdots (\zeta_1 - (\zeta_1)_{I-1})}{((\zeta_1)_I - (\zeta_1)_0)((\zeta_1)_I - (\zeta_1)_1) \cdots ((\zeta_1)_I - (\zeta_1)_{I-1})} \tag{5.32}$$

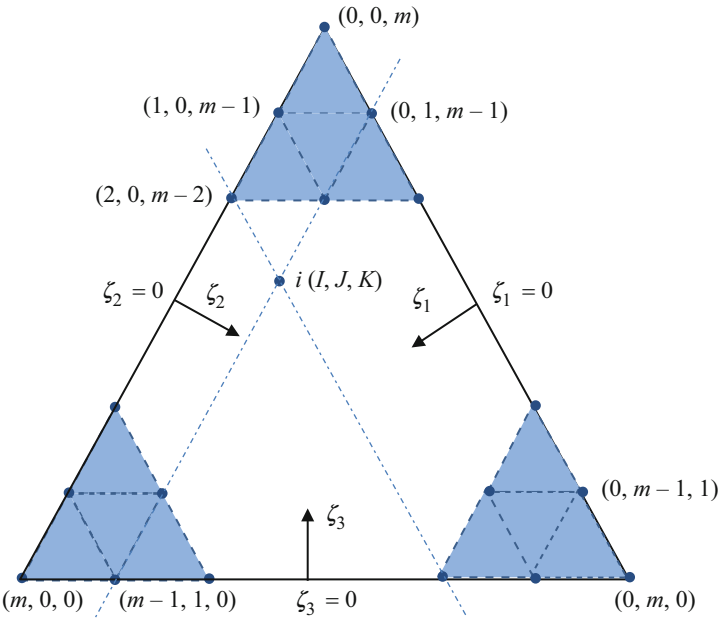

Fig. 5.7 A general triangular finite element of order m. The node $i(I, J, K)$ is located at the Ith node in the ζ_1 direction, at the Jth node in the ζ_2 direction, and at the node Kth in the ζ_3 direction [6]

The polynomial $L_I(\zeta_1)$ can be interpreted as the Ith basis polynomial of ζ_1 for constructing a polynomial interpolation of order I over I sample points.

Linear Triangle

The linear triangle studied in the Sect. 5.2 may be presented as an isoparametric representation element, as

$$\begin{bmatrix} 1 \\ x_1 \\ x_2 \\ \tilde{u}_1 \\ \tilde{u}_2 \end{bmatrix} = \begin{bmatrix} 1 & 1 & 1 \\ x_1^1 & x_1^2 & x_1^3 \\ x_2^1 & x_2^2 & x_2^3 \\ u_1 & u_{(2-1)*2+1} & u_{(3-1)*2+1} \\ u_2 & u_{(2-1)*2+2} & u_{(3-1)*2+2} \end{bmatrix} \begin{bmatrix} N_1 \\ N_2 \\ N_3 \end{bmatrix} = \begin{bmatrix} 1 & 1 & 1 \\ x_1^1 & x_1^2 & x_1^3 \\ x_2^1 & x_2^2 & x_2^3 \\ u_1 & u_3 & u_5 \\ u_2 & u_4 & u_6 \end{bmatrix} \begin{bmatrix} N_1 \\ N_2 \\ N_3 \end{bmatrix} \tag{5.33}$$

The shape functions are simply the triangular coordinates. In fact, the linear triangle is the only triangular element that is both superparametric and isoparametric.

Quadratic Triangle

Consider a quadratic triangular element shown in Fig. 5.8, the element has six nodes: three corner nodes and three mid-side nodes. The calculation of the first shape function can be considered by noting that the location of node 1 is described by the following coefficients

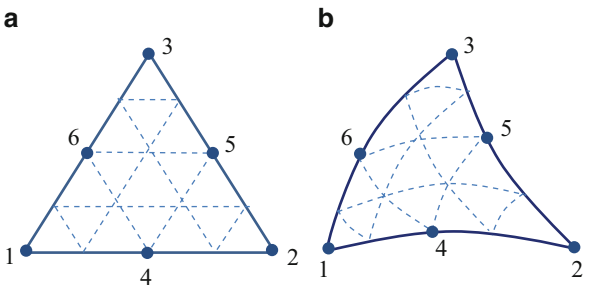

Fig. 5.8 (**a**) Superparametric representation of triangular element; (**b**) isoparametric representation of triangular element

$$I = 2;\ J = 0;\ K = 0 \tag{5.34}$$

So, using Eq. (5.30) is possible to write

$$N_1 = L_2(\zeta_1)\, L_0(\zeta_2)\, L_0(\zeta_3) \tag{5.35}$$

with

$$L_2(\zeta_1) = \frac{(\zeta_1 - (\zeta_1)_0)\,(\zeta_1 - (\zeta_1)_1)}{((\zeta_1)_2 - (\zeta_1)_0)\,((\zeta_1)_2 - (\zeta_1)_1)};\ L_0(\zeta_2) = 1;\ L_0(\zeta_3) = 1 \tag{5.36}$$

and

$$\begin{aligned} &(\zeta_1)_0 = 0 \ \text{ at nodes 2, 3 and 5} \\ &(\zeta_1)_1 = 0.5 \text{ at mid-side nodes 4 and 6} \\ &(\zeta_1)_2 = 1.0 \text{ at node 1} \end{aligned} \tag{5.37}$$

Note that in Eq. (5.36), $L_0(\zeta_i)\ \ i = 1, 2, 3$ are equal to the unity due to the fact that Lagrange basis of order 0 are always equal to the unity. Using Eqs. (5.36) and (5.37) into Eq. (5.35) is possible to write

$$N_1 = \frac{(\zeta_1 - (\zeta_1)_0)\,(\zeta_1 - (\zeta_1)_1)}{((\zeta_1)_2 - (\zeta_1)_0)\,((\zeta_1)_2 - (\zeta_1)_1)} = \frac{(\zeta_1 - 0)\,(\zeta_1 - 0.5)}{(1 - 0)\,(1 - 0.5)} = (2\zeta_1 - 1)\,\zeta_1 \tag{5.38}$$

For the other two corner nodes 2, 3 we have exactly the same quantity:

$$N_2 = L_0(\zeta_1)\, L_2(\zeta_2)\, L_0(\zeta_3) = (2\zeta_2 - 1)\,\zeta_2 \tag{5.39}$$

$$N_3 = L_0(\zeta_1)\, L_0(\zeta_2)\, L_2(\zeta_3) = (2\zeta_3 - 1)\,\zeta_3 \tag{5.40}$$

For the mid-side node 4 the coefficients I, J and K are defined as

$$I = 1;\ J = 1;\ K = 0 \tag{5.41}$$

So, using Eq. (5.30) is possible to write

$$N_4 = L_1(\zeta_1) L_1(\zeta_2) L_0(\zeta_3) \tag{5.42}$$

with

$$\begin{aligned} L_1(\zeta_1) &= \frac{(\zeta_1 - (\zeta_1)_0)}{((\zeta_1)_1 - (\zeta_1)_0)}; \\ L_1(\zeta_2) &= \frac{(\zeta_2 - (\zeta_2)_0)}{((\zeta_2)_1 - (\zeta_2)_0)}; \; L_0(\zeta_3) \end{aligned} \tag{5.43}$$

and

$$\begin{aligned} (\zeta_2)_0 &= 0 \;\; \text{at nodes 1, 3 and 6} \\ (\zeta_2)_1 &= 0.5 \text{ at mid-side nodes 4 and 5} \\ (\zeta_2)_2 &= 1.0 \text{ at node 2} \end{aligned} \tag{5.44}$$

Using Eqs. (5.43) and (5.44) into Eq. (5.42) is possible to write

$$N_4 = \frac{(\zeta_1 - (\zeta_1)_0)}{((\zeta_1)_1 - (\zeta_1)_0)} \frac{(\zeta_2 - (\zeta_2)_0)}{((\zeta_2)_1 - (\zeta_2)_0)} = 2\zeta_1 2\zeta_2 = 4\zeta_1\zeta_2 \tag{5.45}$$

For the other two mid-side nodes 5, 6 we have exactly the same quantity:

$$N_5 = L_0(\zeta_1) L_1(\zeta_2) L_1(\zeta_3) = 4\zeta_2\zeta_3 \tag{5.46}$$

$$N_6 = L_1(\zeta_1) L_0(\zeta_2) L_1(\zeta_3) = 4\zeta_1\zeta_3 \tag{5.47}$$

Sides of element may have parabolically curved geometry defined the location of the mid-nodes 4, 5 and 6. Thus, the triangular coordinates for a curved triangle are no longer straight lines, but they form a curvilinear system as can be observed in Fig. 5.8b. Moreover, using the same procedure is possible to develop cubic triangles. The cubic triangle has a total of ten nodes, which nine are located at the sides and the tenth node is an interior node.

5.3.3 Isoparametric Formulation for Rectangular Elements

Triangular elements are usually not preferred by many analysts nowadays, unless there are difficulties with the meshing and re-meshing of models of complex geometry [8]. The main reason is that triangular elements are usually less accurate than rectangular or quadrilateral elements. Moreover, the formulation of equations of rectangular elements is simpler than the formulation of equations for triangular elements. In fact, the shape functions of rectangular elements can be formulated easily due to their regularity within the rectangular shape of finite elements.

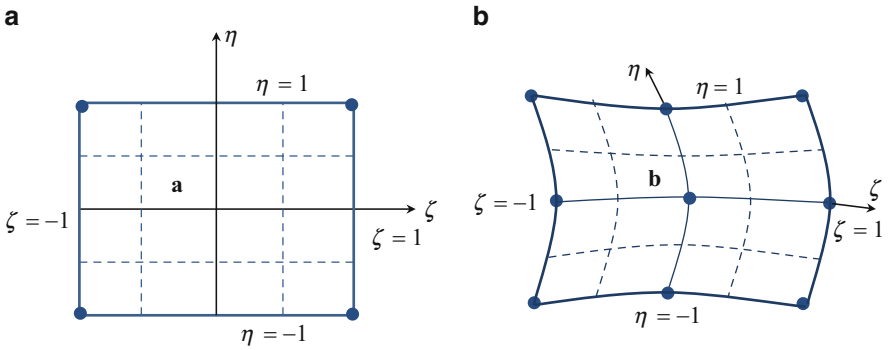

Fig. 5.9 Quadrilateral coordinates: (**a**) Straight sides; (**b**) curved sides

Fig. 5.10 Typical shape functions for Lagrangian elements [3]

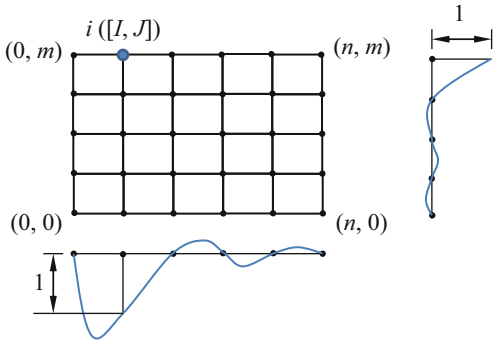

Before presenting examples of rectangular elements, the appropriate natural coordinate system for that geometry must be introduced. The natural coordinates for a rectangular element are ζ and η, which are illustrated in Fig. 5.9, for both straight sided and curved side rectangles. These are called quadrilateral coordinates and their variation range is within -1 and $+1$ taking the value zero over the quadrilateral medians. This particular variation facilitate the use of standard gauss integration formulas.

Due to the regularity of nodes along both the natural coordinate directions, the shape function of elements can be obtained by multiplying one-dimensional shape functions with respect to the ζ and η directions, using the Lagrange interpolations defined in Eq. (3.51) [3]. Thus, consider the element shown in Fig. 5.10 in which a series of nodes, external and internal, are placed on a regular grid. It is required to determine a shape function for the point indicated by the blue circle. Clearly, is the product of a fifth-order and a fourth-order polynomial. The fifth-order polynomial should have an unity value at all nodes of the second column, and zero elsewhere, while the fourth-order polynomial should have an unity value on the top row of nodes and zero elsewhere. This principle of shape construction satisfies all the inter-element continuity conditions and gives the unity at the nodal point concerned.

Thus in two dimensions, if we label the node i by its column and row numbers, I, J, we have

$$N_i = N_I^{1D}(\zeta)\, N_J^{1D}(\eta) = L_I^n(\zeta)\, L_J^m(\eta) \tag{5.48}$$

where L_k^n are polynomials in one dimension and are known as Lagrange polynomials, which can be written as

$$L_k^n(\zeta) = \prod_{\substack{i=1 \\ i \neq k}}^{n+1} \frac{(\zeta - \zeta_i)}{(\zeta_k - \zeta_i)} = \frac{(\zeta - \zeta_1)\cdots(\zeta - \zeta_{k-1})(\zeta - \zeta_{k+1})\cdots(\zeta - \zeta_n)(\zeta - \zeta_{n+1})}{(\zeta_k - \zeta_1)\cdots(\zeta_k - \zeta_{k-1})(\zeta_k - \zeta_{k+1})\cdots(\zeta_k - \zeta_n)(\zeta_k - \zeta_{n+1})} \tag{5.49}$$

The polynomial terms that are present in a situation where $n = m$ are presented on Fig. 5.11, which are based on the Pascal triangle. Is possible to verify that the number of polynomial terms used is larger than those needed for a complete expansion of order n.

Linear Rectangular Element

When linear rectangular elements are used, the domain is discretized into a number of rectangular elements with four nodes and four straight edges, as shown in Fig. 5.12a. The nodes in each element are numbered as 1, 2, 3 and 4 in a counterclockwise direction. Note also that, since each node has two DOFs, the total DOFs

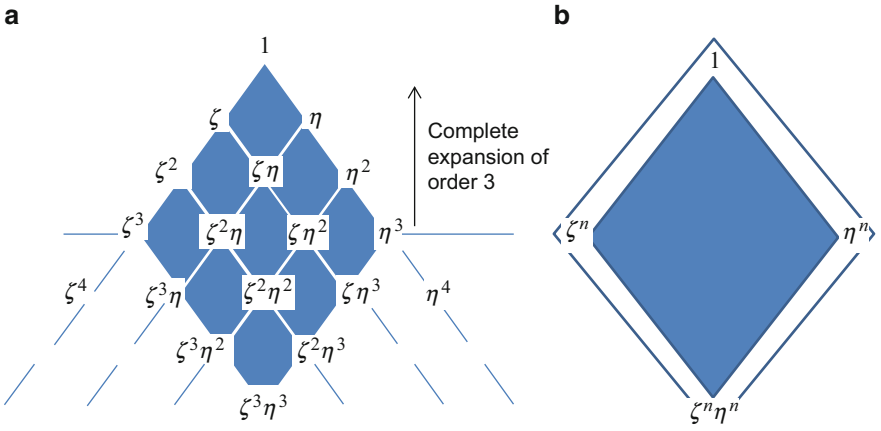

Fig. 5.11 Polynomial terms appearing in a complete Lagrange expansion of a polynomial of order: (**a**) three; (**b**) n [3]

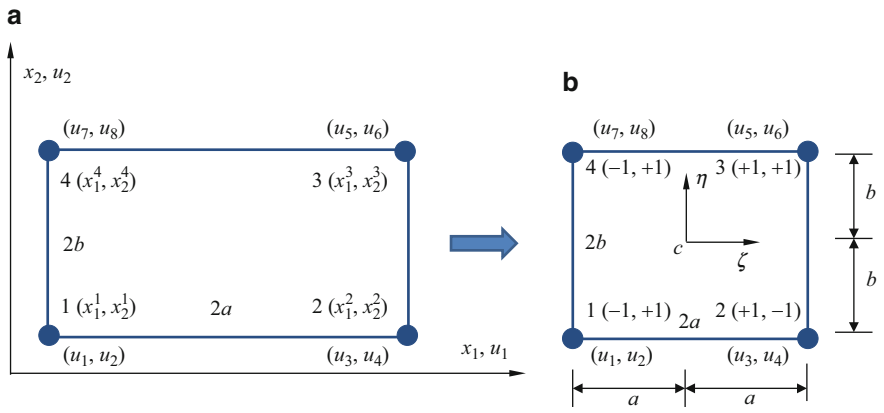

Fig. 5.12 Rectangular finite element and the coordinate system: (**a**) physical coordinates; (**b**) natural coordinates [6]

for a linear rectangular element would be eight. The dimension of the element is defined here as $2a \times 2b \times h$. Moreover, it will be convenient to use a normalized coordinate system, thus the natural coordinate system (ξ, η) with its origin located at the center of the rectangular element is defined, see Fig. 5.12b.

The relationship between the physical coordinate (x_1, x_2), Fig. 5.12a, and the local natural coordinate system (ξ, η), in Fig. 5.12b, is given by

$$\begin{aligned} \zeta &= \frac{x_1 - x_1^c}{a} \Rightarrow d\zeta = \frac{dx_1}{a} \\ \eta &= \frac{x_2 - x_2^c}{b} \Rightarrow d\eta = \frac{dx_2}{b} \end{aligned} \tag{5.50}$$

Equation (5.50) defines a very simple coordinate transformation between physical and natural coordinate systems for rectangular elements.

The linear rectangular finite element in Fig. 5.12b is the simplest member of the rectangular family. It is defined by

$$\begin{bmatrix} 1 \\ x_1 \\ x_2 \\ \tilde{u}_1 \\ \tilde{u}_2 \end{bmatrix} = \begin{bmatrix} 1 & 1 & 1 & 1 \\ x_1^1 & x_1^2 & x_1^3 & x_1^4 \\ x_2^1 & x_2^2 & x_2^3 & x_2^4 \\ u_1 & u_{(2-1)*2+1} & u_{(3-1)*2+1} & u_{(4-1)*2+1} \\ u_2 & u_{(2-1)*2+2} & u_{(3-1)*2+2} & u_{(4-1)*2+2} \end{bmatrix} \begin{bmatrix} N_1 \\ N_2 \\ N_3 \\ N_4 \end{bmatrix} \tag{5.51}$$

Using Eqs. (5.48) and (5.49), the shape functions of the four-node linear element shown in Fig. 5.12 can be given as

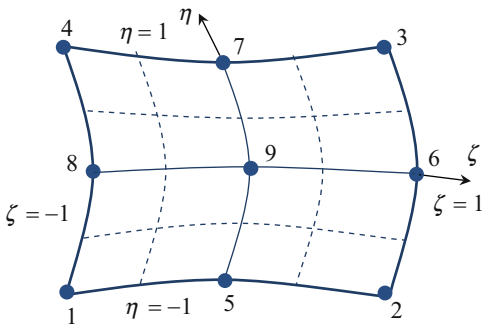

Fig. 5.13 The nine-node biquadratic quadrilateral finite element

$$
\begin{aligned}
N_1 &= N_1^{1D}(\zeta)\, N_1^{1D}(\eta) = L_1^1(\zeta)\, L_1^1(\eta) \\
&= \frac{(\zeta-\zeta_2)}{(\zeta_1-\zeta_2)}\frac{(\eta-\eta_2)}{(\eta_1-\eta_2)} = \frac{(\zeta-1)}{(-1-1)}\frac{(\eta-1)}{(-1-1)} = \frac{1}{4}(1-\zeta)(1-\eta) \\
N_2 &= N_2^{1D}(\zeta)\, N_1^{1D}(\eta) = L_2^1(\zeta)\, L_1^1(\eta) \\
&= \frac{(\zeta-\zeta_1)}{(\zeta_2-\zeta_1)}\frac{(\eta-\eta_2)}{(\eta_1-\eta_2)} = \frac{(\zeta+1)}{(1+1)}\frac{(\eta-1)}{(-1-1)} = \frac{1}{4}(1+\zeta)(1-\eta) \\
N_3 &= N_2^{1D}(\zeta)\, N_2^{1D}(\eta) = L_2^1(\zeta)\, L_2^1(\eta) \\
&= \frac{(\zeta-\zeta_1)}{(\zeta_2-\zeta_1)}\frac{(\eta-\eta_1)}{(\eta_2-\eta_1)} = \frac{(\zeta+1)}{(1+1)}\frac{(\eta+1)}{(1+1)} = \frac{1}{4}(1+\zeta)(1+\eta) \\
N_4 &= N_1^{1D}(\zeta)\, N_2^{1D}(\eta) = L_1^1(\zeta)\, L_2^1(\eta) \\
&= \frac{(\zeta-\zeta_2)}{(\zeta_1-\zeta_2)}\frac{(\eta-\eta_1)}{(\eta_2-\eta_1)} = \frac{(\zeta-1)}{(-1-1)}\frac{(\eta+1)}{(1+1)} = \frac{1}{4}(1-\zeta)(1+\eta)
\end{aligned}
\tag{5.52}
$$

These functions vary linearly on quadrilateral coordinate lines ($\zeta = \pm 1$) and ($\eta = \pm 1$) but are not linear polynomials as in the case of the three-node triangle. In fact, From Eq. (5.52), it can easily be seen that all the shape functions are formed using the same set of four basis functions:

$$1,\ \zeta,\ \eta,\ \zeta\eta \tag{5.53}$$

which are linearly-independent. The latest basis, in Eq. (5.53), is obtained as the product of two linear functions and because of that is called bilinear term.

Quadratic Rectangular Element

The nine node rectangular element shown in Fig. 5.13 is the next complete member of the quadrilateral family. It has eight external nodes and one internal node. This higher order rectangular finite element is the most widely used and it is defined by

$$\begin{bmatrix} 1 \\ x_1 \\ x_2 \\ \tilde{u}_1 \\ \tilde{u}_2 \end{bmatrix} = \begin{bmatrix} 1 & x_1^1 & x_2^1 & u_1 & u_2 \\ 1 & x_1^2 & x_2^2 & u_{(2-1)*2+1} & u_{(2-1)*2+2} \\ 1 & x_1^3 & x_2^3 & u_{(3-1)*2+1} & u_{(3-1)*2+2} \\ 1 & x_1^4 & x_2^4 & u_{(4-1)*2+1} & u_{(4-1)*2+2} \\ 1 & x_1^5 & x_2^5 & u_{(5-1)*2+1} & u_{(5-1)*2+2} \\ 1 & x_1^6 & x_2^6 & u_{(6-1)*2+1} & u_{(6-1)*2+2} \\ 1 & x_1^7 & x_2^7 & u_{(7-1)*2+1} & u_{(7-1)*2+2} \\ 1 & x_1^8 & x_2^8 & u_{(8-1)*2+1} & u_{(8-1)*2+2} \\ 1 & x_1^9 & x_2^9 & u_{(9-1)*2+1} & u_{(9-1)*2+2} \end{bmatrix}^T \begin{bmatrix} N_1 \\ N_2 \\ N_3 \\ \vdots \\ N_9 \end{bmatrix} \tag{5.54}$$

This element is often referred to as the Lagrangian quadrilateral in the finite element literature. Using Eqs. (5.48) and (5.49), the nine-node quadratic element shown in Fig. 5.13 can be completely defined by

$$\begin{aligned}
N_1 &= N_1^{1D}(\zeta) N_1^{1D}(\eta) = L_1^2(\zeta) L_1^2(\eta) = \tfrac{1}{4}\zeta(1-\zeta)\eta(1-\eta) \\
N_2 &= N_3^{1D}(\zeta) N_1^{1D}(\eta) = L_3^2(\zeta) L_1^2(\eta) = -\tfrac{1}{4}\zeta(1+\zeta)\eta(1-\eta) \\
N_3 &= N_3^{1D}(\zeta) N_3^{1D}(\eta) = L_3^2(\zeta) L_3^2(\eta) = \tfrac{1}{4}\zeta(1+\zeta)(1+\eta)\eta \\
N_4 &= N_1^{1D}(\zeta) N_3^{1D}(\eta) = L_1^2(\zeta) L_3^2(\eta) = -\tfrac{1}{4}\zeta(1-\zeta)(1+\eta)\eta \\
N_5 &= N_2^{1D}(\zeta) N_1^{1D}(\eta) = L_2^2(\zeta) L_1^2(\eta) = -\tfrac{1}{2}(1+\zeta)(1-\zeta)(1-\eta)\eta \\
N_6 &= N_3^{1D}(\zeta) N_2^{1D}(\eta) = L_3^2(\zeta) L_2^2(\eta) = \tfrac{1}{2}\zeta(1+\zeta)(1+\eta)(1-\eta) \\
N_7 &= N_2^{1D}(\zeta) N_3^{1D}(\eta) = L_3^2(\zeta) L_1^2(\eta) = \tfrac{1}{2}(1+\zeta)(1-\zeta)(1+\eta)\eta \\
N_8 &= N_1^{1D}(\zeta) N_2^{1D}(\eta) = L_1^2(\zeta) L_2^2(\eta) = -\tfrac{1}{2}\zeta(1-\zeta)(1-\eta)\eta \\
N_9 &= N_2^{1D}(\zeta) N_2^{1D}(\eta) = L_2^2(\zeta) L_2^2(\eta) = \left(1-\zeta^2\right)\left(1-\eta^2\right)
\end{aligned} \tag{5.55}$$

From Eq. (5.55) it can be seen that the shape functions are formed using a set of nine basis functions, defined as

$$1,\ \zeta,\ \eta,\ \zeta\eta,\ \zeta^2,\ \eta^2,\ \zeta^2\eta,\ \zeta\eta^2,\ \zeta^2\eta^2 \tag{5.56}$$

which are linearly independent. Moreover, because the basis functions in Eq. (5.56) also so contain the linear basis functions, these shape functions can also be expected to have linear field reproduction. The shape function associated with the internal node 9 is called a bubble function, because of its geometric shape. The procedure used for the nine-node element, can be also used to create any other Lagrange finite element of higher order.

Meanwhile, the Lagrange type of elements is not very widely used, due to the presence of the interior node. Figure 5.14 depicts a more widely used eight-node variant element called serendipity quadrilateral, in which the interior node is eliminated by kinematic constrains. The element in Fig. 5.14 has four corner nodes and four mid-side nodes. The shape functions in the natural coordinates for this quadratic rectangular element are given as [3]

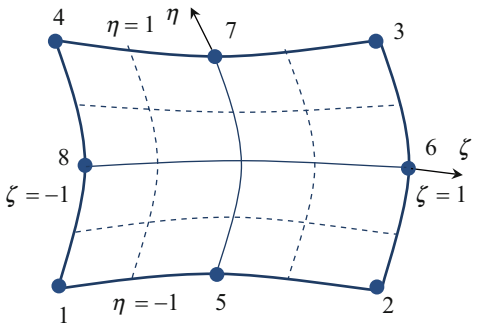

Fig. 5.14 The eight-node serendipity element

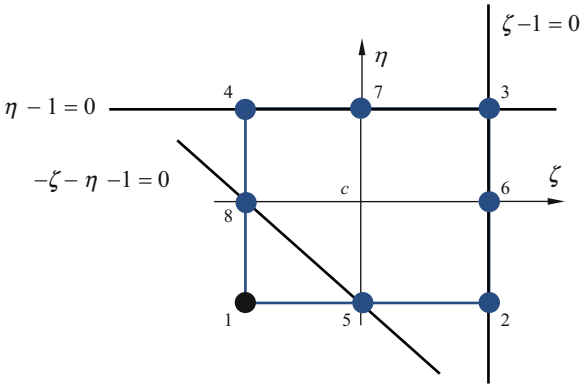

Fig. 5.15 Construction of the N_1 shape function of the eight-node serendipity element [6]

$$
\begin{aligned}
N_i &= \frac{1}{4}\left(1+\zeta_i\zeta\right)\left(1+\eta_i\eta\right)\left(\zeta_i\zeta+\eta_i\eta-1\right) \quad i=1,2,3,4\\
N_i &= \frac{1}{2}\left(1-\zeta^2\right)\left(1+\eta_i\eta\right) \qquad\qquad\qquad\quad i=5,7\\
N_i &= \frac{1}{4}\left(1+\zeta_i\zeta\right)\left(1-\eta^2\right) \qquad\qquad\qquad\quad i=6,8
\end{aligned}
\tag{5.57}
$$

Where (ζ_i, η_i) are the natural coordinates of node i, it is very easy to observe that the shape functions posses the delta function property. Shape functions are constructed by simple imposing the shape properties. For instance, for the corner node 1, where $\zeta_1 = -1$ and $\eta_1 = -1$, the shape function N_1 has to pass the following three lines as shown in Fig. 5.15.

Thus, to ensure that N_1 vanish at remote nodes it is necessary to assure that shape function contains the following functions:

$$
\begin{aligned}
&1-\zeta=0\\
&1-\eta=0\\
&-\zeta-\eta-1=0
\end{aligned}
\tag{5.58}
$$

and, therefore, N_1 can then immediately be written as

$$
N_1 = C\left(1-\zeta\right)\left(1-\eta\right)\left(-\zeta-\eta-1\right) \tag{5.59}
$$

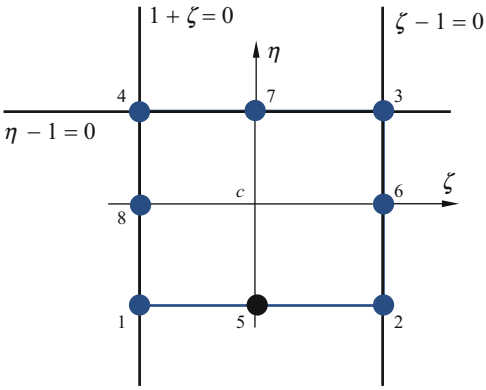

Fig. 5.16 Construction of the N_5 shape function of the eight-node serendipity element [6]

Where C is a constant that can be determined from the condition that it has to be unity value at node 1, which gives

$$C = \frac{1}{(1-(-1))\,(1-(-1))\,(-(-1)-(-1)-1)} = \frac{1}{4} \tag{5.60}$$

And, finally, the shape function N_1 can be written as

$$N_1 = \frac{1}{4}\,(1+\zeta_1\zeta)\,(1+\eta_1\eta)\,(\zeta_1\zeta+\eta_1\eta-1) \tag{5.61}$$

Which is the first equation of Eq. (5.57) when $i = 1$. Shape functions at all the other corner nodes can be constructed in exactly the same manner.

To construct the shape function number 5 it is necessary to enforce that this function must passes through the following three lines, as shown in Fig. 5.16.

$$\begin{aligned} 1-\zeta &= 0 \\ 1+\zeta &= 0 \\ 1-\eta &= 0 \end{aligned} \tag{5.62}$$

Thus, shape N_5 can be immediately be written as

$$N_5 = C\,(1+\zeta)\,(1-\zeta)\,(1-\eta) \tag{5.63}$$

Where C is a constant to be determined using the condition that is has to be unity at node 5, which gives

$$C = \frac{1}{(1+0)\,(1-0)\,(1-(-1))} = \frac{1}{2} \tag{5.64}$$

Finally

$$N_5 = \frac{1}{2}\left(1-\zeta^2\right)(1+\eta_5\eta) \tag{5.65}$$

Which is the second equation in Eq. (5.57) for $i = 5$.

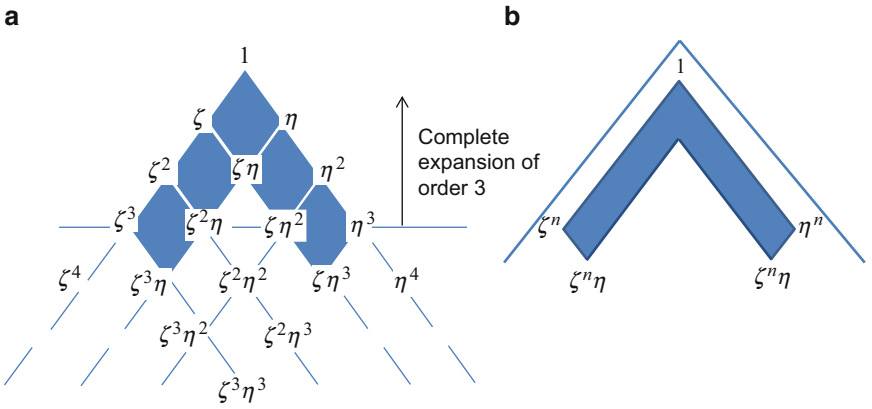

Fig. 5.17 Polynomial terms appearing in a serendipity-type expansion of a polynomial of order: (**a**) three; (**b**) n [3]

To obtain the shape function for nodes 6 and 8, which should be coincident with the third equation in Eq. (5.57) for $i = 6$ and $i = 8$, respectively. It can be easily seen that all the shape functions can be formed using the same set of basis functions

$$1,\ \zeta,\ \eta,\ \zeta\eta,\ \zeta^2,\ \eta^2,\ \zeta^2\eta,\ \zeta\eta^2 \tag{5.66}$$

With this mode of generating shape functions for this class of elements, it is immediately obvious that a fewer degrees of freedom are now necessary for a given complete polynomial expansion. In Fig. 5.17 it can be seen the serendipity-type expansion of a polynomial for a cubic element. However, the functions generated by nodes placed only along the edges will not generate complete polynomials beyond cubic order. For higher order it is necessary to supplement the expansion by internal nodes or by the use of nodeless variables which contain appropriate polynomial terms [3].

5.4 2D-Solid Quadrilateral Elements

As shown previously, the shape functions of rectangular finite elements can be easily generated, hence the formulation of the equations for rectangular elements is simpler compared to the triangular elements. Nevertheless, a rectangular element has a structured geometry and, therefore, is difficult to use it to perform a mesh discretization of a domain with an irregular geometry. A more general finite element would be the so-called quadrilateral element, which can have non parallel edges. But because a quadrilateral element may has an irregular shape, a question arise: how the numerical integration of the mass and stiffness matrices of quadrilateral elements is evaluated? Note that the Gauss integration scheme can only be applied on finite elements with a normalized geometry. Thus, the Gauss integration scheme requires

the map of a general quadrilateral into the rectangular normalized geometry. This mapping is assured using the isoparametric formulation of an element. Once the mapping is established, the rest of the finite element procedure is exactly the same as that used for formulating rectangular finite elements. So, the simple three-step procedure is applicable, and will be shown in the following sections.

5.4.1 FE Approximation of the Displacement

The displacement field within the element is expressed as an interpolation of the nodal displacement using shape functions. So, the displacement vector is assumed to have the form, i.e.,

$$\tilde{\mathbf{u}}(x_1, x_2) = \mathbf{N}(x_1, x_2)\,\mathbf{u} \tag{5.67}$$

Note that in Eq. (5.67) the shape function are dependent in the physical coordinates (x_1, x_2). Nevertheless, as it has been seen in the previous section, the use of natural coordinates will make the construction of the shape functions and the evaluation of the matrix integration very much easier. So the mapping between physical and natural coordinates is assured by Eq. (5.50). This kind of coordinate mapping technique is one of the most often used techniques in the FEM, and it is very powerful when used for developing elements of complex shapes.

The displacement vector $\mathbf{u}$, in Eq. (5.67), is assumed to have the form

$$\mathbf{u} = \begin{bmatrix} u_1 \\ u_2 \\ u_3 \\ u_4 \\ \vdots \\ u_{(n-1)*2+1} \\ u_{(n-1)*2+2} \end{bmatrix} \begin{matrix} \left.\begin{matrix} \\ \\ \end{matrix}\right\} \textit{displacements at node } 1 \\ \left.\begin{matrix} \\ \\ \end{matrix}\right\} \textit{displacements at node } 2 \\ \left.\begin{matrix} \\ \\ \end{matrix}\right\} \textit{displacements at node} \cdots \\ \left.\begin{matrix} \\ \\ \end{matrix}\right\} \textit{displacements at node } n \end{matrix} \tag{5.68}$$

and the matrix of shape functions has the form

$$\mathbf{N} = \begin{bmatrix} \underbrace{N_1}_{\textit{Node } 1} & \underbrace{0}_{} & \underbrace{N_2}_{\textit{Node } 2} & \underbrace{0}_{} & \underbrace{\cdots}_{\textit{Node} \cdots} & \underbrace{N_n}_{\textit{Node } n} \\ 0 & N_1 & 0 & N_2 & \cdots & N_n \end{bmatrix} \tag{5.69}$$

where the shape functions N_i $(i = 1, 2, \ldots, n)$ are the shape functions corresponding to the n nodes of the rectangular finite element. The shape functions for linear and quadratic finite elements are presented in Sect. 5.3.3.

5.4.2 FE Approximation of Strain

Using the same procedure as for the case of the triangular element, the strain matrix **B** would have the form

$$\mathbf{B} = \left[\mathbf{B}_1 \; \mathbf{B}_2 \cdots \mathbf{B}_n \right] \tag{5.70}$$

where $\mathbf{B}_i \, (i = 1, 2, \ldots, n)$ are the strain matrices corresponding to the n nodes of the rectangular finite element, i.e.

$$\mathbf{B}_i = \begin{bmatrix} \dfrac{\partial N_i}{\partial x_1} & 0 \\ 0 & \dfrac{\partial N_i}{\partial x_2} \\ \dfrac{\partial N_i}{\partial x_2} & \dfrac{\partial N_i}{\partial x_1} \end{bmatrix} \tag{5.71}$$

To evaluate such matrices a coordinate transformation is necessary and the derivatives with respect to x_1 and x_2 are given by the chain rule, as

$$\begin{aligned} \frac{\partial N_i}{\partial x_1} &= \frac{\partial N_i}{\partial \zeta}\frac{\partial \zeta}{\partial x_1} + \frac{\partial N_i}{\partial \eta}\frac{\partial \eta}{\partial x_1} \\ \frac{\partial N_i}{\partial x_2} &= \frac{\partial N_i}{\partial \zeta}\frac{\partial \zeta}{\partial x_2} + \frac{\partial N_i}{\partial \eta}\frac{\partial \eta}{\partial x_2} \end{aligned} \tag{5.72}$$

Equation (5.72) can be put in a matrix form as

$$\begin{bmatrix} \dfrac{\partial N_i}{\partial x_1} \\ \dfrac{\partial N_i}{\partial x_2} \end{bmatrix} = \begin{bmatrix} \dfrac{\partial \zeta}{\partial x_1} & \dfrac{\partial \eta}{\partial x_1} \\ \dfrac{\partial \zeta}{\partial x_2} & \dfrac{\partial \eta}{\partial x_2} \end{bmatrix} \begin{bmatrix} \dfrac{\partial N_i}{\partial \zeta} \\ \dfrac{\partial N_i}{\partial \eta} \end{bmatrix} = \mathbf{J}^{-1} \begin{bmatrix} \dfrac{\partial N_i}{\partial \zeta} \\ \dfrac{\partial N_i}{\partial \eta} \end{bmatrix} \tag{5.73}$$

where **J** is the Jacobian of the two-dimensional transformations that connect the differentials of (x_1, x_2) to those of (ζ, η) and vice-versa. So, using the chain rule:

$$\begin{aligned} \begin{bmatrix} dx_1 \\ dx_2 \end{bmatrix} &= \begin{bmatrix} \dfrac{\partial x_1}{\partial \zeta} & \dfrac{\partial x_1}{\partial \eta} \\ \dfrac{\partial x_2}{\partial \zeta} & \dfrac{\partial x_2}{\partial \eta} \end{bmatrix} \begin{bmatrix} d\zeta \\ d\eta \end{bmatrix} = \mathbf{J}^T \begin{bmatrix} d\zeta \\ d\eta \end{bmatrix}; \\ \begin{bmatrix} d\zeta \\ d\eta \end{bmatrix} &= \begin{bmatrix} \dfrac{\partial \zeta}{\partial x_1} & \dfrac{\partial \zeta}{\partial x_2} \\ \dfrac{\partial \eta}{\partial x_1} & \dfrac{\partial \eta}{\partial x_2} \end{bmatrix} \begin{bmatrix} dx_1 \\ dx_2 \end{bmatrix} = \mathbf{J}^{-T} \begin{bmatrix} dx_1 \\ dx_2 \end{bmatrix} \end{aligned} \tag{5.74}$$

To evaluate the entries of **J** at any rectangular location, let make use of the isoparametric formulation in Eq. (5.25), which is repeated here for convenience

$$x_1 = \sum_{i=1}^{n} x_1^i N_i(\zeta, \eta); \quad x_2 = \sum_{i=1}^{n} x_2^i N_i(\zeta, \eta); \tag{5.75}$$

Which can be differentiated with respect to the natural coordinates as,

$$\begin{aligned} \frac{\partial x_1}{\partial \zeta} &= \sum_{i=1}^{n} x_1^i \frac{\partial N_i(\zeta, \eta)}{\partial \zeta}; \quad \frac{\partial x_2}{\partial \zeta} = \sum_{i=1}^{n} x_2^i \frac{\partial N_i(\zeta, \eta)}{\partial \zeta} \\ \frac{\partial x_1}{\partial \eta} &= \sum_{i=1}^{n} x_1^i \frac{\partial N_i(\zeta, \eta)}{\partial \eta}; \quad \frac{\partial x_2}{\partial \eta} = \sum_{i=1}^{n} x_2^i \frac{\partial N_i(\zeta, \eta)}{\partial \eta} \end{aligned} \tag{5.76}$$

because the x_1^i and x_2^i do not depend on ζ and η. Equation (5.76) can be written in a matrix form, as

$$\mathbf{J} = \begin{bmatrix} \frac{\partial x_1}{\partial \xi} & \frac{\partial x_2}{\partial \xi} \\ \frac{\partial x_1}{\partial \eta} & \frac{\partial x_2}{\partial \eta} \end{bmatrix} = \begin{bmatrix} \frac{\partial N_1}{\partial \xi} & \frac{\partial N_2}{\partial \xi} & \cdots & \frac{\partial N_n}{\partial \xi} \\ \frac{\partial N_1}{\partial \eta} & \frac{\partial N_2}{\partial \eta} & \cdots & \frac{\partial N_n}{\partial \eta} \end{bmatrix} \begin{bmatrix} x_1^1 & x_2^1 \\ x_1^2 & x_2^2 \\ \vdots & \vdots \\ x_1^n & x_2^n \end{bmatrix} \tag{5.77}$$

After the computation of Eq. (5.77), the inverse of Jacobian is then obtained by numerically inverting this matrix, as

$$\mathbf{J}^{-1} = \frac{1}{J} \begin{bmatrix} J_{22} & -J_{12} \\ -J_{21} & J_{11} \end{bmatrix}; \quad J = J_{11}J_{22} - J_{12}J_{21} \tag{5.78}$$

where J denotes the determinant of Jacobean matrix.

Using Eq. (5.78) in Eq. (5.73) is possible to obtain the following relation

$$\begin{aligned} \frac{\partial N_i}{\partial x_1} &= \frac{J_{22}}{J}\frac{\partial N_i}{\partial \zeta} - \frac{J_{12}}{J}\frac{\partial N_i}{\partial \eta} \\ \frac{\partial N_i}{\partial x_2} &= -\frac{J_{21}}{J}\frac{\partial N_i}{\partial \zeta} + \frac{J_{11}}{J}\frac{\partial N_i}{\partial \eta} \end{aligned} \tag{5.79}$$

Which leads to the following $\mathbf{B}_i$ matrix

$$\mathbf{B}_i = \frac{1}{J} \begin{bmatrix} J_{22}\frac{\partial N_i}{\partial \zeta} - J_{12}\frac{\partial N_i}{\partial \eta} & 0 \\ 0 & -J_{21}\frac{\partial N_i}{\partial \zeta} + J_{11}\frac{\partial N_i}{\partial \eta} \\ -J_{21}\frac{\partial N_i}{\partial \zeta} + J_{11}\frac{\partial N_i}{\partial \eta} & J_{22}\frac{\partial N_i}{\partial \zeta} - J_{12}\frac{\partial N_i}{\partial \eta} \end{bmatrix} \tag{5.80}$$

Note that the strain matrix in Eq. (5.80) for a linear rectangular element is no longer a constant matrix, see the shape functions in Eq. (5.52). This implies that the strain and, therefore, the stress within the finite element is no longer constant.

5.4.3 *Element Matrices*

The stiffness matrix of a general 2D-solid finite element is given the Eq. (5.17), which is reproduced as

$$\mathbf{k} = \int_A h\, \mathbf{B}^T \mathbf{c}\, \mathbf{B}\, dA \tag{5.81}$$

In Eq. (5.81), **B** is the strain matrix that has been discussed previously, h is the thickness and, if it is variable, it can be interpolated via the shape functions. Meanwhile, to integrate Eq. (5.81) numerically by a two-dimensional product Gauss rule, is necessary to reduce it to the canonical form, as

$$\mathbf{k} = \int_{-1}^{+1}\int_{-1}^{+1} \mathbf{F}\,(\zeta, \eta)\, d\zeta d\eta \tag{5.82}$$

Note that for the case of natural coordinates (ζ, η), everything in Eq. (5.81) already fits this form, except the element of area dA.

To evaluate the area transformation, let consider the element with area OABC presented in Fig. 5.18, the area of this differential parallelogram can be computed as

$$\begin{aligned} dA = \overrightarrow{OB} \times \overrightarrow{OA} &= \begin{bmatrix} \frac{\partial x_1}{\partial \eta} d\eta \\ \frac{\partial x_2}{\partial \eta} d\eta \end{bmatrix} \times \begin{bmatrix} \frac{\partial x_1}{\partial \zeta} d\zeta \\ \frac{\partial x_2}{\partial \zeta} d\zeta \end{bmatrix} = \frac{\partial x_1}{\partial \zeta} d\zeta \frac{\partial x_2}{\partial \eta} d\eta - \frac{\partial x_1}{\partial \eta} d\eta \frac{\partial x_2}{\partial \zeta} d\zeta \\ &= \begin{vmatrix} \frac{\partial x_1}{\partial \zeta} & \frac{\partial x_1}{\partial \eta} \\ \frac{\partial x_2}{\partial \zeta} & \frac{\partial x_2}{\partial \eta} \end{vmatrix} d\zeta d\eta = J d\zeta d\eta \end{aligned} \tag{5.83}$$

From Eq. (5.83) is possible to see that J is a (non-constant) scaling factor that relates the area in the original geometry to an equivalent area in the normalized geometry. For a well-defined mapping, J must have the same sign at all points in the normalized geometry and small variations on all model. Moreover, highly distorted mappings have badly formed elements, meaning that J shows large variations. Thus, in Eq. (5.82) the matrix function $\mathbf{F}(\zeta, \eta)$ is written as

$$\mathbf{F}\,(\zeta, \eta) = h\mathbf{B}^T\mathbf{c}\mathbf{B}\, J \tag{5.84}$$

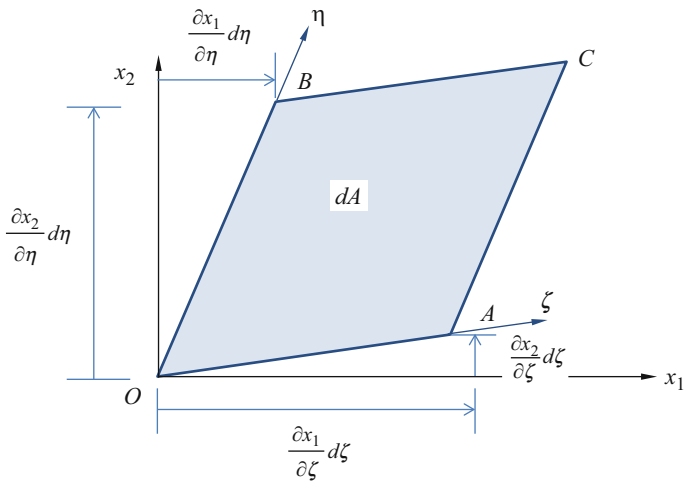

Fig. 5.18 Parallelogram geometry

Which leads to the following stiffness matrix

$$\mathbf{k} = \int_{-1}^{+1}\int_{-1}^{+1} \mathbf{B}^T \mathbf{c}\mathbf{B}\, hJ\, d\zeta d\eta \tag{5.85}$$

The material constant matrix **c** has been given by Eqs. (1.35) and (1.36), respectively, for plane stress and plane strain problems. Nevertheless, the evaluation of the integral in Eq. (5.85) would not be an easy task, since the strain matrix **B** is a function of natural coordinate. In practice, the numerical integration scheme is used to evaluate the integral. The Gauss integration scheme is a very simple and efficient procedure that performs numerical integral, and it is briefly outlined in the next section.

To obtain the element mass matrix, Eq. (5.67) is substituted into Eq. (2.45), leading to

$$\mathbf{m} = \int_{\Omega^e} \rho \overline{\mathbf{N}}^T \overline{\mathbf{N}}\, d\Omega^e = \int_A \int_0^h dx_3\, \rho \overline{\mathbf{N}}^T \overline{\mathbf{N}}\, dA = \int_A h\rho \overline{\mathbf{N}}^T \overline{\mathbf{N}}\, dA = \int_{-1}^{+1}\int_{-1}^{+1} h\rho J\, \overline{\mathbf{N}}^T \overline{\mathbf{N}}\, d\zeta d\eta \tag{5.86}$$

The evaluation of the integral in Eq. (5.86) can be carried out exactly. Nevertheless, in practice, this integral are calculated numerically, as the case of the stiffness matrix, using the gauss integration scheme.

5.4.4 Numerical Integration by Gauss Rules

Numerical integration is indispensable for practical evaluation of integrals over isoparametric element domains. The standard rule is based on the Gauss integration because such rules use a minimal number of points to achieve a desired level of accuracy. This efficiency is important to save computational effort, since a matrix product is evaluated at each simple point. The one dimensional rule has been defined in Sect. 3.2.1 of Chap. 3.

The simplest two-dimensional Gauss rules are called product rules. They are obtained by applying the one-dimensional rules to each independent variable. Thus, the Gauss integration is simple defined as

$$I = \int_{-1}^{+1}\int_{-1}^{+1} f(\zeta,\eta)\, d\zeta d\eta = \sum_{i=1}^{p_1}\sum_{j=1}^{p_2} w_i w_j f\left(\xi_i, \eta_j\right) \tag{5.87}$$

where p_1 and p_2 are the number of Gauss points in the ζ and η directions, respectively. Figure 5.19 shows the locations of the first four two-dimensional Gauss product rules in a square region.

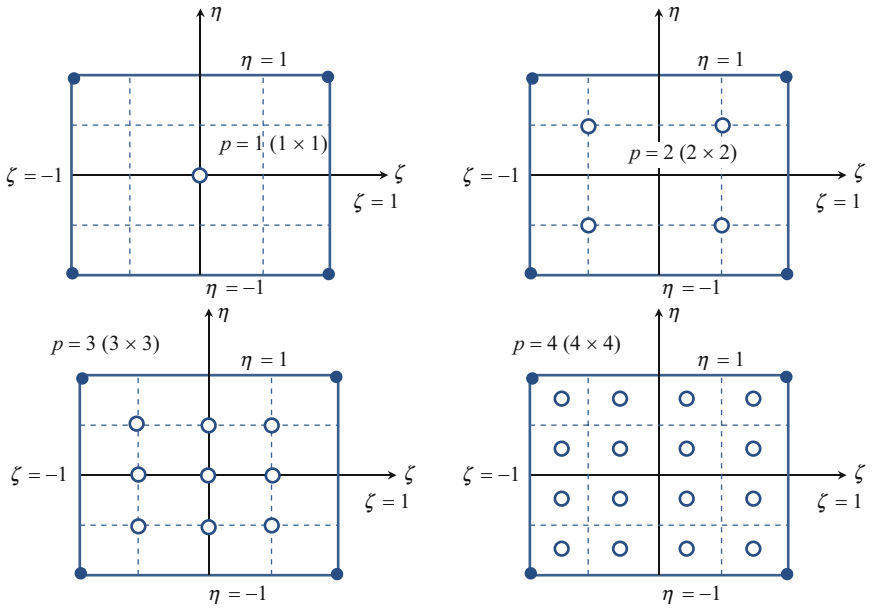

Fig. 5.19 The first four two-dimensional Gauss product rules for. The sample points are marked with circles filled the *white* color

Usually, the same number $p = p_1 = p_2$ is chosen if the shape functions are taken to be the same in both ζ and η directions. This is in fact the case for all rectangles presented here. The selection of appropriate number of integration points depends on the polynomial degree of the integrand. As a general rule, more points should be used for a higher order of elements. It is also noted that using a smaller number of Gauss points tends to counteract the over-stiff behavior associated with the displacement-based finite element method [8]. This over-stiff behavior of the displacement-based finite element method comes about primarily because of the use of the shape function. In fact, the displacement in an element is approximated using the shape functions and the nodal displacements. This implies that the deformation of the element is actually prescribed in the fashion of the shape function. This gives a constraint to the element, and thus the element behaves more stiffly than it should. It is often observed that higher order elements are usually softer than lower order ones. This is because the use of more nodes decreases the constraint on the element.

5.5 Convergence of Results

Once the finite element method is a numerical procedure for solving complex engineering problems there are some important considerations to the accuracy of the analysis results and the convergence of the numerical solution. Thus, in this section we analyze the requirement of a displacement-based finite element leading to monotonically convergent solutions.

5.5.1 Definition of Convergence

The procedure of reaching a finite element solution requires the idealization of an actual physical problem into a mathematical model and, after which, the use of a numerical method to get its numerical solution. Figure 5.20 summarize this concept [2].

Frequently, the difficulty in the implementation of Fig. 5.20 is associated with the definition of the differential equations of motion of the mathematical model, which in the analysis of complex problems may be unknown, such as the response prediction of a three-dimensional shell. Thus, in a practical analysis the finite element idealization of the physical problem is established directly. However, from the point of view of studding the convergence of the finite element solution with the number of finite elements used within the finite mesh, it is helpful to assume that a mathematical model is implied in the finite element representation of the physical problem. Hence, as the number of finite elements is increased, a proper finite element solution should converge to the analytical solution of the differential equations that govern the response of the mathematical model [2]. Nevertheless, if the differential equations of motion are not known and/or analytical solutions cannot

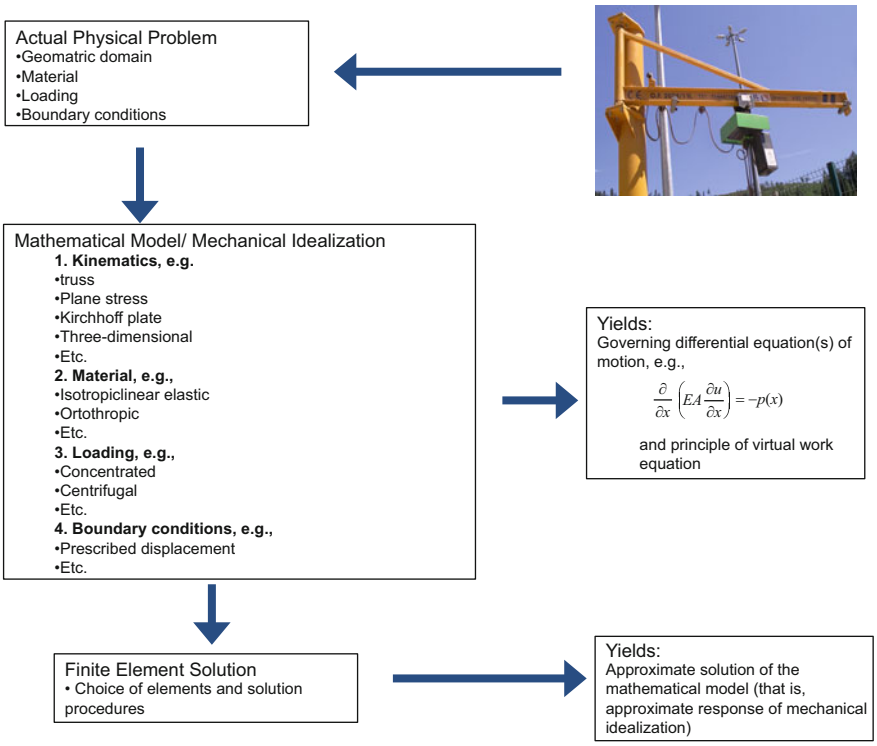

Fig. 5.20 Finite element solution procedure [2]

be obtained, the convergence of solution can be measured only on the fact that all the basic assumptions in the mathematical model must be satisfied at convergence.

The finite element solution is affected by different sources of errors: Round-off errors, which are a result of the finite precision of arithmetic's of the computer used; errors in the constitutive modeling are due to the linearization and the integration of the constitutive relations; errors in the calculation of the dynamic response are due to the errors that arise in the numerical integration of the equations of motion or to a deficient representation of the behavior of the technical system in a mode superposition analysis; errors in the iterative solution procedures, because convergence of the numerical solution is based on measurements on increments of the solution variables that are small but no zero. Nevertheless, in this section we will focus only in the finite errors that are due to the interpolation of the solution variables.

We recall that for the generality of static structural problems presented in Chap. 1, the exact solution of a mathematical model should be the displacement field that holds the solution of the following equation

$$L\,\mathbf{u} = \mathbf{f} \tag{5.88}$$

where L is differential operator, $\mathbf{u}$ is the exact displacement field and $\mathbf{f}$ represents loading functions. Assuming that the finite solution is represented by $\mathbf{u}_h$, this solution will allow to define the finite element space field given by the interpolation functions. Thus, is possible to define convergence to mean that

$$L\mathbf{u}_h \rightarrow L\mathbf{u} \text{ as } h \rightarrow 0 \tag{5.89}$$

Physically, this statement means that the strain energy calculated by the finite element solution converges to the exact strain energy of the mathematical model as the finite element mesh is refined. Depending on the specific displacement-based finite elements used in the numerical analysis, the finite solution may converge monotically or nonmonotonically to the exact solution as the number of finite elements is increased [2].

5.5.2 *Criteria for Monotonic Convergence*

Generally, if the elements are complete and the elements on the mesh are compatible, the monotonic convergence of a finite mesh is assured. The requirement of completeness of an element means that the displacement functions of the element must be able to represent the rigid body displacement and a constant strain rates. The requirement of compatibility means that all the element degrees of freedom within and across the element boundaries must be continuous [2]. Physically, compatibility ensures that no gaps occur between elements when the assemblage is loaded. For finite elements where only translational nodal degrees of freedom are defined, only continuity in the displacements must be preserved. However, when rotational degrees of freedom are also presented and if those are obtained by differentiation of the transverse displacement, as in the case of the formulation of Euler-Bernoulli beam elements and of the Kirchhoff plate bending elements, it is also necessary to satisfy the element continuity in the corresponding first displacement derivatives.

Rigid body displacements are those displacements in which the element is able to perform rigid body motion, meaning that no elastic stresses are being developed on it. In the case of 2D-solid elements, the element must be able to translate uniformly in both directions of its plane and to rotate about its normal without deforming; these three rigid modes are shown in Fig. 5.21.

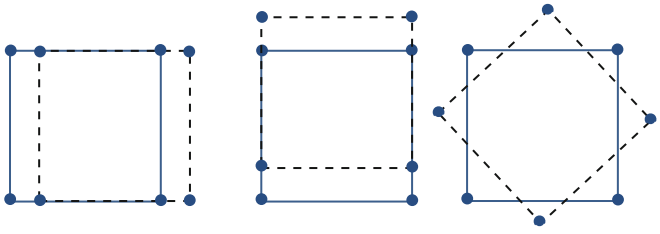

Fig. 5.21 Rigid body modes of a plane stress element [2]

The number of rigid body modes that an element must be able to undergo can usually be identified by inspection, but for complex finite elements the individual straining modes and rigid body modes are displayed effectively by representing the element stiffness matrix in the basis of eigenvectors [2]. Thus, solving the eigenproblem

$$\mathbf{k}\boldsymbol{\Phi}_i = \lambda_i \boldsymbol{\Phi}_i \tag{5.90}$$

Or

$$\mathbf{k}\boldsymbol{\Phi} = \boldsymbol{\Phi}\boldsymbol{\lambda} \tag{5.91}$$

where $\boldsymbol{\Phi}$ is a matrix storing the eigenvectors $\boldsymbol{\Phi}_i$ $(i = 1, \ldots, n)$ and $\boldsymbol{\lambda}$ is a diagonal matrix storing the corresponding eigenvalues. Using the eigenvector orthonormality property, is possible to evaluate the natural frequencies as

$$\boldsymbol{\Phi}^T \mathbf{k}\boldsymbol{\Phi} = \boldsymbol{\lambda} \tag{5.92}$$

Inspection of Eq. (5.92) may show clearly whether the rigid modes and what additional straining modes are present. Note that since the finite element analysis overestimate the stiffness, the smaller the element eigenvalues the more effective will be the element.

The necessity of an element is able to represent constant strain rates can be physically understood if we assume that more and more elements are used in the assemblage to represent the structure. Then, in the limit, as each element approaches a very small size, the strain in the each element approaches a constant value, and any complex variation of the strain within the structure can be effectively approximated.

As said before, the element compatibility is automatic ensured between truss and beam elements because they are linked only at nodes, but compatibility is also relatively easy to maintain two-dimensional plane strain, plane stresses and in three-dimensional analysis, since only translational degrees of freedom are used as nodal point variables. However, the requirements of compatibility are difficult to satisfy in plate bending analysis, and particularly in thin shell analysis if the rotations are derived from the transverse displacement. For this reason, much of the research work has been directed toward the development of plate and shell elements, in which the displacements and rotations are direct variables. So, whether a specific element is complete and compatible depends on the formulation used within its development and, each formulation need be analyzed individually [2].

5.6 Discussion Example

From the finite element solution procedure presented in Fig. 5.20, it is clear that the finite element solution will solve only the selected mathematical model and that all assumptions in this model will be reflected in the predicted response. Thus, the choice of an appropriate mathematical model is crucial and completely determines the insight into the physical problem that we can obtain by the analysis [2].

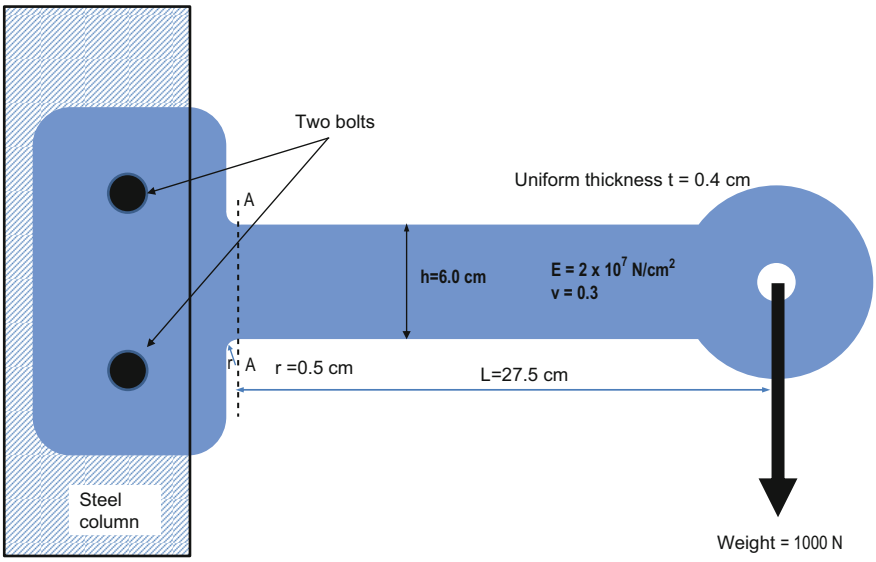

Fig. 5.22 Physical problem of a steel bracket [2]

In order to define the reliability and effectiveness of a chosen model we can think on a very comprehensive mathematical of the physical problem and measure the response of our selected model against the response of the comprehensive model. In this context, the selected mathematical model is efficient if yields the required response to a sufficient accuracy and at least cost and, is reliable if the response is known to be predicted within a selected level of accuracy. Let consider a simple example of bracket used to support a vertical load, as shown in Fig. 5.22 [2].

The bracket is screwed to a very thick steel column, the thick of the steel is larger than the thickness and the height of the bracket, meaning that the steel column can be assumed as a practically rigid structure. Thus, the bracket problem can be solved applying a rigid column boundary condition to it. Moreover, it is also assumed that the load is applied very slowly. The load condition is defined relatively to the largest natural period of the bracket; that is, the time span over which the load is increased from zero to its full value is much longer than the fundamental period of the bracket. So, this statement is translate to the mathematical approximation as a static analysis.

To evaluate the total moment at section AA and the deflection at the load application, see Fig. 5.22, is possible to consider beam mathematical models, leading to

$$\begin{aligned} \mathrm{M} &= \mathrm{P} \times \ell = 1000 \times 27.5 = 27500 \text{ Ncm} \\ \delta_1 &= \frac{P \times (\ell + r_n)^3}{3EI} = \frac{1000 \times (27.5 + 0.5)^3 \times 12}{3 \times 2 \times 10^7 \times 0.4 \times 6^3} = 0.0508 \text{ cm} \\ \delta_2 &= \delta_1 + \frac{P \times (\ell + r_n)}{5/6GA} = 0.0508 + \frac{1000 \times (27.5 + 0.5)}{0.833 \times 7692308 \times 0.4 \times 6} = 0.053 \text{ cm} \end{aligned} \tag{5.93}$$

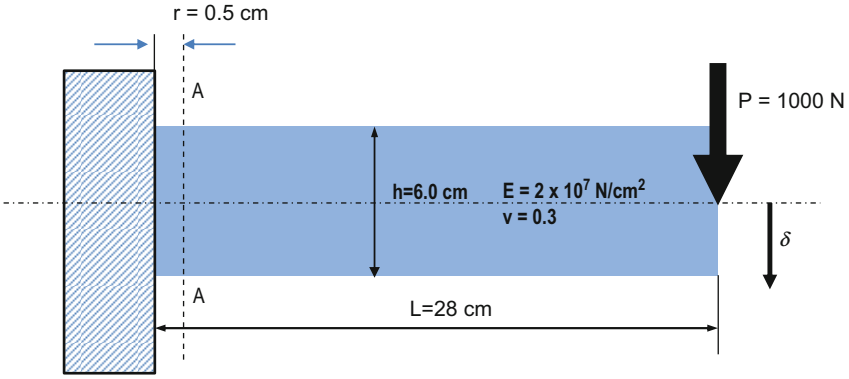

Fig. 5.23 Beam model of a steel bracket [2]

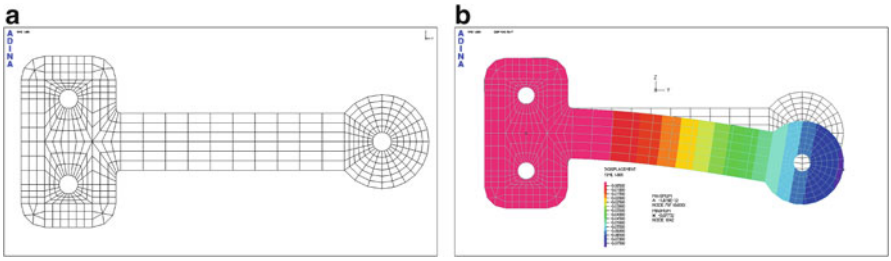

Fig. 5.24 (**a**) Mesh of nine-node elements used in finite element discretization; (**b**) displacement shape representation

where δ_1 is the solution based on the Euler-Beurnolli Beam theory while δ_2 is based on the Timoshenko beam theory, which takes the shear effect in account. The structural model used to evaluate the solutions presented in Eq. (5.93) is depicted in Fig. 5.23.

The reliability of this mathematical model can be assessed by the comparison of the solutions in Eq. (5.93) against with those available from a comprehensive mathematical model, which can be a fully three-dimensional representation of the full bracket. Although the three-dimensional comprehensive mathematical model could be a very comprehensive model, a linear elastic two-dimensional plane stress model will be used instead. In fact, this two-dimensional model can represent the geometry of the bracket more accurately than the beam model and assumes a two-dimensional stress distribution in the bracket. So, the bending moment at section AA and the deflection under the load calculated with this model can be expected to be quite close to those calculated with a three-dimensional model and, certainly this two-dimensional model represents a higher model against which we can measure the adequacy of the results given in Eq. (5.93) [2].

Figure 5.24a shows the finite element discretization used in the solution of the plane stress mathematical model. Notice that the bolt fastenings and the contact

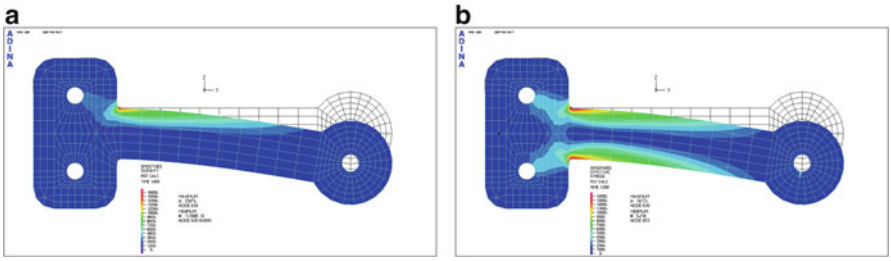

Fig. 5.25 (**a**) Maximum principal stress; (**b**) effective stress distribution

conditions between the steel column and the bracket are not accounted in the model and, also, the pin carrying the load is not modeled. Because the numerical model is based on plane stress conditions, the stress components σ_{33}, σ_{23} and σ_{13} are zero. The displacement was obtained assuming that circular lines delimiting the bolt area do not have displacement in the direction, while the point placed in the geometrical center of the support has no any displacement.

Figure 5.24b shows the deformed configuration obtained in the numerical model. The x_3 displacement at the point of load application is of 0.06417 cm. The maximum displacement of the beam model is considerably less than this value, meaning that the beam model is considerably more rigid than the plane stress model. In fact, in the beam model, the assumption that the support is completely rigid neglects any deformation between the beam and the bolts, which are not in agreement with the problem physics. Nevertheless, the same magnitude of the bending moment at section AA is predicted by both models.

Considering these results, is possible to say that the beam mathematical model is reliable if the required bending moment is to be predicted within 1 % and the displacement is to be predicted only within 20 % of accuracy [2]. Meanwhile, the maximum stress in the bracket cannot be predicted accurately by the simple mathematical beam model. The beam model totally neglects the stress increase due to the presence of fillets. Figure 5.25 shows the maximum principal stress near the fillet.

The important points that can be noted here are the following [2]:

- The selection of the mathematical model depends on the response that needs to be predicted;
- The most effective mathematical model is that one which delivers the answers to the questions in a reliable manner, i.e. within an acceptable error, with the least amount of computational effort;
- A finite element model can solve accurately only the chosen mathematical model and cannot predict any extra information that that contained in the model;
- The reliability of the chosen mathematical model requires the assessment of the results against the results obtained with a very-comprehensive mathematical model.

5.7 Review Questions

1. Why there is need of mapping a quadrilateral finite element into a normalized geometry? What is the shape of the normalized geometry?
2. What is the geometrical meaning of J in Eq. (5.84)?
3. Assuming that a linear quadrilateral has a constant thickness, how many Gauss points are required to evaluate the mass matrix and the stiffness matrices exactly?
4. Construct the shape function of a corner node, for the nine-node rectangular element.
5. Beside the number of nodes per element, what is the main difference between linear triangle and bilinear rectangular elements?
6. Using Eq. (5.76), compute the Jacobian matrix of the finite element shown in Fig. 5.26.
7. Compute the end displacement of the beam shown in Fig. 5.27. The beam is made of a material with Young's modulus of 200 GPa and is loaded with a triangular

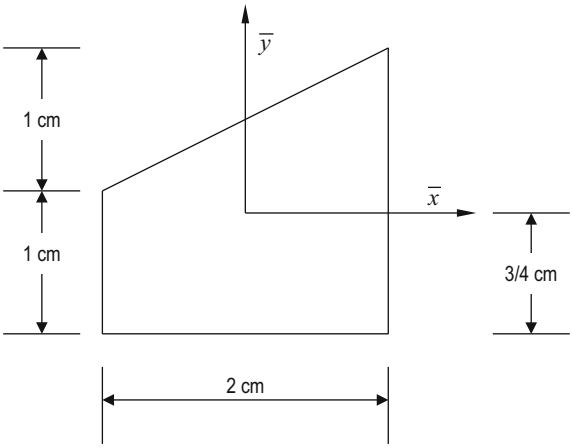

Fig. 5.26 One quadrilateral finite element

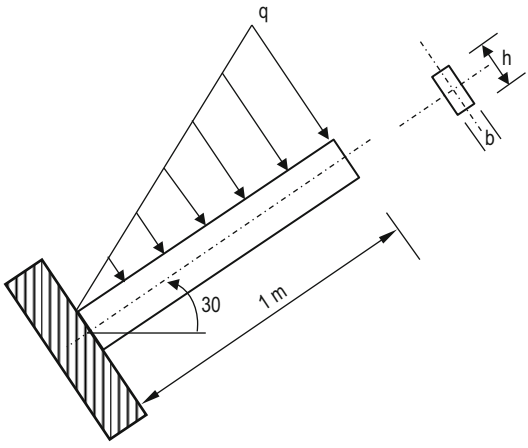

Fig. 5.27 Beam under a triangular load

distributed force, which maximum value is of 200 KPa. The beam has cross-section dimensions of 0.1×0.05 m^2.

References

1. Reddy JN (1993) Finite element method. Wiley, New York
2. Bathe K-J (1996) Finite element procedures. Prentice Hall, Englewood Cliffs
3. Zienkiewicz OC, Taylor RL (2000) The finite element method. Butterworth-Heinemann, Boston
4. Brenner S, Scott LR (2008) The mathematical theory of finite element method. Springer, New York
5. Eisenberg MA, Malvern LE (1973) On finite element integration in natural coordinates. Int J Nume Methods Eng 7:574–575
6. Argyris JH, Fried I, Scharpf DW (1968) The TET 20 and TEA 8 elements for the matrix displacement method. Aero J 72:618–625
7. Piltner R, Taylor RL (2000) Triangular finite elements with rotational degrees of freedom and enhanced strain modes. Comput Struct 75(4):361–368
8. Liu GR, Quek SS (2003) The finite element method: a practical course. Butterworth-Heinemann, Amsterdam/Burlington

Chapter 6
Finite Element Method for Plates/Shells

The development of finite element equations for the stress analysis of two dimensional structures subjected to external loads applied transversely to their 2-D geometrical plane will be presented in this chapter. The basic concepts, procedures and formulations can also be found in many existing textbooks [1–3]. The procedure followed in this chapter is to first develop the FE matrices for plate elements and, then, the FE matrices for flat shell elements are obtained by superimposing the matrices of plate elements and those of 2D solid plane stress elements developed in Chap. 5. Whereas for general shell finite elements the displacement and the geometry interpolations are obtained by considering also the isoparametric concept.

6.1 Introduction

As discussed in Chap. 1, a plate structure is geometrically similar to the structure of the 2D plane stress problem, but it usually carries only transversal loads that lead to bending deformation in the plate. For example, higher floors of a building are a typical plate structure that carries most of us every day, as are the wings of aircraft, which usually carry loads like the engines [4]. The plate structure can be schematically represented by its middle surface laying on the $x_1 - x_2$ plane, as shown in Fig. 6.1. The transverse loading on a plate produces deflection and rotation of the normals of the middle plane. The element developed to model such plate structures is known as plate element. The formulation of a plate element is very similar to the formulation of a 2D solid element, except for the process of deriving the strain matrix in which the theory of plates is used instead. Plates and shells are a particular form of a three-dimensional solid for which the thickness of such solids is very small when compared with other dimensions. There are a number of theories that govern the behavior of such structures, which are based on several assumptions that result in a series of approximations. The thin plate theory is based on the assumptions

M.A. Neto et al., *Engineering Computation of Structures: The Finite Element Method*, DOI 10.1007/978-3-319-17710-6_6

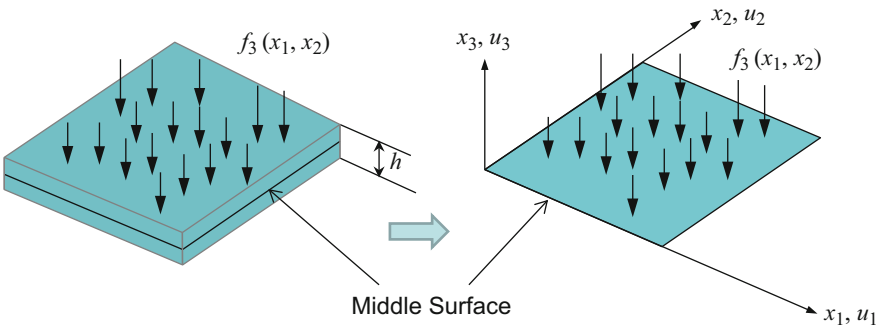

Fig. 6.1 A plate and its coordinates system

formalized by Kirchhoff in 1850. Later, in 1945, a relaxation of the Kirchhoff assumptions was made by Reissner and in a slightly different manner by Mindlin in 1951. These modified theories are called Reissner-Mindlin and they represent an extension of the field of application to the thick plates. Although the thick plate theory is simpler to implement in the finite element method, its analytical treatment presents more difficulties. In fact, in the thin plate theory it is possible to represent the state of deformation by the transversal displacement of the middle plane of the plate, see Eq. (1.49) of Chap. 1. Hence, this formulation introduces second derivatives of the transversal displacement in the strain definition and, therefore, in order to assure that the deformation is different of zero, it is necessary to impose continuity conditions between elements not only in the transversal displacement but also on its derivatives, which means that displacement approximations must have a C_1 continuity. Thus, to impose continuity at the interface of elements, it will always be necessary to use both displacement and first derivative of displacement in nodes.

Determination of suitable shape functions for C_1 continuities is more complex than those required for C_0 continuity. Indeed, as the complete slope continuity is required on the interfaces between several elements, the mathematical and computational difficulties involved rise significantly. However, it is relatively simple to obtain shape functions that preserve the continuity of displacement and they may violate its slope continuity among elements but, normally, not at the nodes where such continuity is imposed. These kind of functions are said to be non-conforming or incompatible shape functions. The shape functions for rectangular elements are the simplest to form for thin plates and therefore are introduced first.

6.2 Thin Plate Formulation

Following the Kirchhoff plate theory, see Chap. 1, the bending deformation will force the cross-section of the plate to rotate in the way shown in Fig. 6.2.

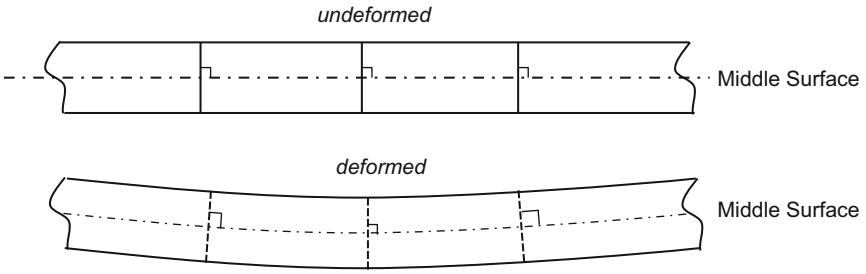

Fig. 6.2 A straight fibre that is perpendicular to the middle plane of the plate before deformation remain straight and normal to it after deformation

The displacement components for a thin plate are written as

$$\begin{aligned} u_1(x_1, x_2, x_3) &= -x_3 \frac{\partial w}{\partial x_1} \\ u_2(x_1, x_2, x_3) &= -x_3 \frac{\partial w}{\partial x_2} \\ u_3(x_1, x_2, x_3) &= w(x_1, x_2) \end{aligned} \tag{6.1}$$

And the strain-displacement relation are defined as

$$\boldsymbol{\varepsilon} = -x_3 \boldsymbol{\chi} \tag{6.2}$$

where $\boldsymbol{\chi}$ is the matrix that contains the changes in the curvature of the plate, given as

$$\boldsymbol{\chi} = \mathbf{L}w = \begin{bmatrix} \partial^2 w/\partial x_1^2 \\ \partial^2 w/\partial x_2^2 \\ 2\partial^2 w/(\partial x_1 \partial x_2) \end{bmatrix} \tag{6.3}$$

The potential energy expression for a thin plate element is

$$U = \frac{1}{2} \int_A \int_0^h \boldsymbol{\varepsilon}^T \mathbf{c}\, \boldsymbol{\varepsilon}\, dA\, dx_3 = \frac{1}{2} \int_A \frac{h^3}{12} \boldsymbol{\chi}^T \mathbf{c}\, \boldsymbol{\chi}\, dA \tag{6.4}$$

where the relation of Eq. (6.2) have been used in Eq. (6.4). The kinetic energy of the thin plate is given by

$$T = \frac{1}{2} \int_\Omega \rho \left(\dot{u}_1^2 + \dot{u}_2^2 + \dot{u}_3^2 \right) d\Omega \tag{6.5}$$

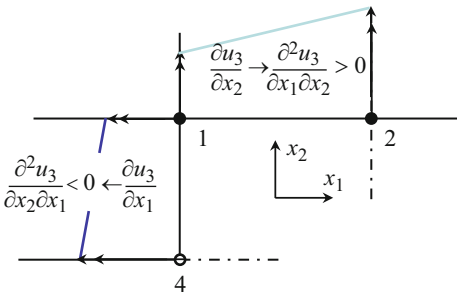

Fig. 6.3 Continuity requirements for the normal slopes [3]

Which is basically a sum of the contribution of three velocity components in the x_1, x_2 and x_3 directions of all the particles in the entire domain of the plate. Substituting Eq. (6.1) into Eq. (6.5) leads to

$$T = \frac{1}{2}\int_{\Omega} \rho \left(x_3^2 \left(\frac{\partial \dot{w}}{\partial x_1} \right)^2 + x_3^2 \left(\frac{\partial \dot{w}}{\partial x_2} \right)^2 + \dot{w}^2 \right) d\Omega = \frac{1}{2}\int_{\Omega} \dot{\tilde{\mathbf{u}}}^T \mathbf{H}\, \dot{\tilde{\mathbf{u}}}\, d\Omega \tag{6.6}$$

where

$$\dot{\tilde{\mathbf{u}}} = \left[\dot{w}(x_1, x_2) \quad \frac{\partial \dot{w}(x_1, x_2)}{\partial x_1} \quad \frac{\partial \dot{w}(x_1, x_2)}{\partial x_2} \right]^T \tag{6.7}$$

and

$$\mathbf{H} = \rho \begin{bmatrix} 1 & 0 & 0 \\ 0 & x_3^2 & 0 \\ 0 & 0 & x_3^2 \end{bmatrix} \tag{6.8}$$

6.2.1 Continuity Requirements for Shape Functions

The presence of second order derivatives at the strain representation in the formulation of thin plates indicates that C_1 continuity of the shape functions are required. To ensure the continuity of the displacement u_3 and of its normal slope, $\partial u_3/\partial n$, cross an interface line, it is necessary to have both u_3 and $\partial u_3/\partial n$ defined by values of nodal parameters along that interface. This continuity is difficult to achieve and reasons for this are given below [3].

Consider that the side 1–2 of a rectangular element is depicted at Fig. 6.3. The normal direction n is coincident with the x_2 direction and, it is necessary that u_3 and $\partial u_3/\partial x_2$ will be uniquely determined by values of u_3, $\partial u_3/\partial x_1$, $\partial u_3/\partial x_2$ at the nodes lying along this line. Thus, following the principles explained in Chap. 4, is possible to write approximation functions as

$$u_3 = w = a_0 + a_1 x_1 + a_2 x_2 + \cdots \tag{6.9}$$

and

$$\frac{\partial u_3}{\partial x_2} = b_0 + b_1 x_1 + b_2 x_2 + \cdots \tag{6.10}$$

The number of constants in each equation must allow determining a unique solution and they must be evaluated using the nodal degrees of freedom associated with the line. Thus, similarly to 1-D Euler-Bernoulli beam elements, if only two nodes are presented in a line, a cubic variation of u_3 in the x_1 direction should be permissible, since $u_3, \partial u_3/\partial x_1$ are specified at each node. But, because both 1–2 nodes have only one degree of freedom of $\partial u_3/\partial x_2$ at each node, or two-term in line 1–2, only a linear variation of $\partial u_3/\partial x_2$ would be permissible. A similar exercise could be performed along the side placed in the x_2 axis in which the continuity of function $\partial u_3/\partial x_1$, along this side, is granted by the nodal degrees of freedom at nodes 1 and 4 only.

So, along the side 1–2 the function $\partial u_3/\partial x_2$ depends only on the 1–2 nodal values of $\partial u_3/\partial x_2$ while along the side 1–4 the function $\partial u_3/\partial x_1$ depends only on the 1–4 nodal values of $\partial u_3/\partial x_1$. If the function $\partial u_3/\partial x_2$ is differentiated with respect to x_1, along the side 1–2, the subsequent function $\partial^2 u_3/\left(\partial x_1 \partial x_2\right)$ depends on nodal parameters of line 1–2 only, while the differentiation of function $\partial u_3/\partial x_1$ with respect to x_2, $\partial^2 u_3/\left(\partial x_2 \partial x_1\right)$, along the side 1–4, depends on the nodal parameters of line 1–4. For the case of arbitrary parameters of $\partial u_3/\partial x_2$ and $\partial u_3/\partial x_1$ at nodes 2 and 4, respectively, an inconsistency arises at the common node 1, as we cannot have there the necessary identity for continuous function:

$$\frac{\partial^2 u_3}{\partial x_1 \partial x_2} = \frac{\partial^2 u_3}{\partial x_2 \partial x_1} \tag{6.11}$$

Meaning that it is impossible to specify simple polynomial expressions for shape functions ensuring full compatibility when only $u_3, \partial u_3/\partial x_1, \partial u_3/\partial x_2$ are prescribed at corner nodes [3, 5]. Thus, if any functions satisfying the compatibility are found with three nodal variables, they must be such that at corner nodes these functions are not continuously differentiable and the cross-derivative is not unique.

A way of overcoming this difficulty would be to specify the cross-derivative as one of the nodal degrees of freedom. This, for an assembly of rectangular elements, is convenient and indeed permissible [3]. But, generally, the extension of this idea to the nodes at which a number of element interfaces are connected with different angles, see Fig. 6.4, is not permissible.

Here the continuity of cross-derivatives in several sets of orthogonal directions implies a specification of all second derivatives at a node. However, if the plate stiffness varies abruptly from one element to each other, this violates physical requirements. The difficulties of finding compatible displacement functions have led

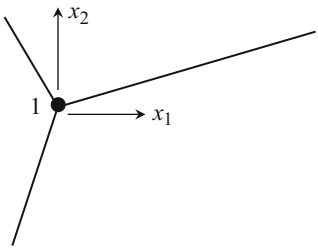

Fig. 6.4 Nodes where elements meet in arbitrary directions [3]

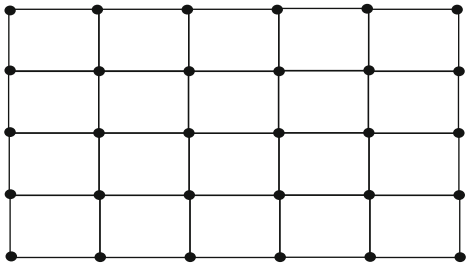

Fig. 6.5 2D domain of a plate meshed by rectangular elements

to many attempts of ignoring the complete slope continuity while still continuing with the other necessary criteria, lead to the appearing of several successful non-conforming elements.

6.2.2 Degrees of Freedom Identification

Consider a 2D geometrical model of a rectangular structure in the $x_1 - x_2$ plane, shown schematically in Fig. 6.5, the 2D domain is divided in a proper manner into a number of rectangular elements. In a mesh of rectangular elements, each element has four nodes and four straight edges. Consider now a rectangular element of thickness h, shown in Fig. 6.6, the element nodes are numbered counter-clockwise. At each node of the finite element the degrees of freedom are: displacement in the x_3 direction, u_{3_i}; the rotation about the x_1 axis, θ_{1_i}; the rotation about the x_2 axis, θ_{2_i} Hence each node has three degrees of freedom. Since a rectangular element has four nodes, the total number of degrees of freedom of a rectangular element with only corner nodes is of 12.

The vector of nodal displacements is arranged in the following order:

$$\mathbf{u} = \left[\mathbf{u}_1 \ \mathbf{u}_2 \ \mathbf{u}_3 \ \mathbf{u}_4 \right]^T \tag{6.12}$$

with

$$\mathbf{u}_i = \left[u_{3_i} \ \phi_{1_i} \ \phi_{2_i} \right]^T \tag{6.13}$$

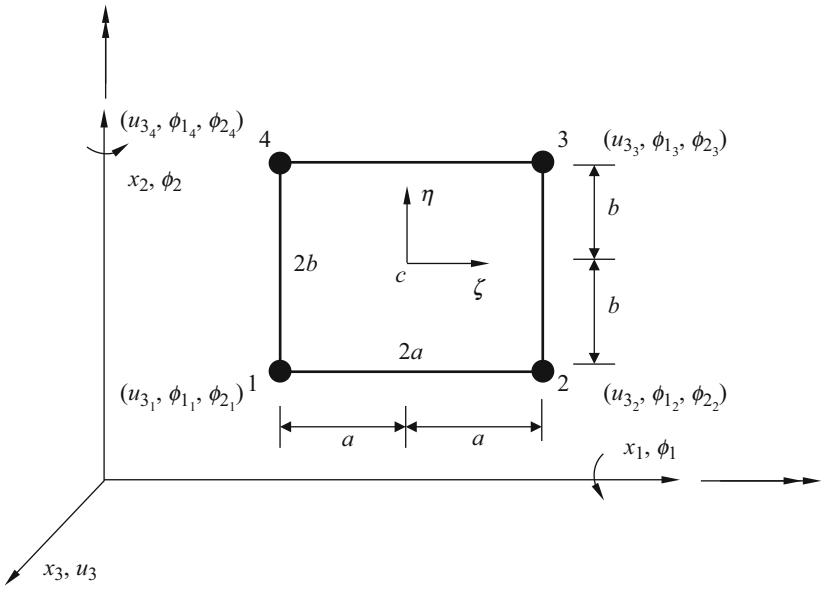

Fig. 6.6 Rectangular element in natural coordinates

Following the conventions of the first chapter, see Fig. 1.9, is possible to write the following relations:

$$\begin{bmatrix} \phi_1 \\ \phi_2 \end{bmatrix} = \begin{bmatrix} 0 & 1 \\ -1 & 0 \end{bmatrix} \begin{bmatrix} \dfrac{\partial w}{\partial x_1} \\ \dfrac{\partial w}{\partial x_2} \end{bmatrix} \tag{6.14}$$

The relation in Eq. (6.14) allow transformations needed for shells to be carried out in an easier manner.

6.2.3 FE Approximation of the Displacement

The displacement field $\tilde{u}_3$ is a function of coordinates (x_1, x_2). A convenient polynomial function, which can be used to define the shape functions, should have 12 parameters, since the number of DOFs is 12. Thus, this function is obtained by omitting certain terms of a complete fourth-order polynomial, as

$$\begin{aligned} \tilde{u}_3(x_1, x_2) =& \tilde{w} = a_1 + a_2 x_1 + a_3 x_2 + a_4 x_1^2 + a_5 x_1 x_2 + a_6 x_2^2 + a_7 x_1^3 \\ &+ a_8 x_1^2 x_2 + a_9 x_1 x_2^2 + a_{10} x_2^3 + a_{11} x_1^3 x_2 + a_{12} x_1 x_2^3 \\ =& \boldsymbol{\Phi}^T \mathbf{a} \end{aligned} \tag{6.15}$$

From the Fig. 5.11 is possible to see that in Eq. (6.15) the omitted terms are

$$x_1^4,\ x_1^2x_2^2,\ x_2^4 \tag{6.16}$$

The approximation in Eq. (6.15) has the main advantage of assuring that along any x_1 or x_2 constant lines the displacement $\tilde{u}_3$ has a cubic variation. The element sides are composed by lines. In each boundary line the degrees of freedom are the two end values of slopes and the two displacements, which allow defining uniquely a cubic variation of the displacement along these sides, see Sect. 6.2.1. As such degrees of freedom are common to adjacent elements the continuity of the transversal displacement will be imposed along any interface.

From Eq. (6.15), it can be observed that the gradient of the displacement in the direction normal to any boundary line varies in a cubic way. For instance, the values of the normal $\partial u_3/\partial x_2$ along a line on which x_1 is constant, is defined as

$$\frac{\partial \tilde{u}_3}{\partial x_2} = a_3 + a_5x_1 + 2a_6x_2 + a_8x_1^2 + 2a_9x_1x_2 + 3a_{10}x_2^2 + a_{11}x_1^3 + 3a_{12}x_1x_2^2 \tag{6.17}$$

Nevertheless, on such lines only two values of the normal slopes are defined and, therefore, the cubic approximation is not specified uniquely. Thus, in general, a discontinuity will occur and shape functions are said non-conforming.

6.2.4 Shape Functions

The procedure of determining the shape functions of finite elements follows the standard procedure described in Sect. 2.3.3 of Chap. 2, and begins with an assumption of the displacements, using polynomial basis functions with unknown constants. After, these unknown constants are determined using the nodal displacements at nodes of element.

In order to evaluate the vector **a** of parameters, presented Eq. (6.15), is necessary to write the 12 simultaneous equations linking the values of displacement and its slopes at the four nodes, i.e. [3]

$$\begin{aligned}
\tilde{w} = u_{3_i} &= a_1 + a_2x_1^i + a_3x_2^i + a_4\left(x_1^i\right)^2 \cdots \\
\frac{\partial \tilde{u}_3\left(x_1^i, x_2^i\right)}{\partial x_2} &= \phi_{1_i} = a_3 + a_5x_1^i + \cdots \qquad i = 1,2,3,4 \\
-\frac{\partial \tilde{u}_3\left(x_1^i, x_2^i\right)}{\partial x_1} &= \phi_{2_i} = -a_2 - 2a_4x_1^i + \cdots
\end{aligned} \tag{6.18}$$

Listing all 12 equations, they are written in a condensed matrix form, as

$$\mathbf{u} = \mathbf{C}\mathbf{a} \tag{6.19}$$

where $\mathbf{C}$ is a 12 by 12 matrix depending on the nodal coordinates and $\mathbf{a}$ is the vector of the 12 parameters. Inverting Eq. (6.19) leads to

$$\mathbf{a} = \mathbf{C}^{-1}\mathbf{u} \tag{6.20}$$

This inversion can be carried out by computer or algebraically [6]. Substituting Eq. (6.20) into Eq. (6.15) is possible to write the expression for the element displacement in a standard form as

$$\tilde{u}_3(x_1, x_2) \equiv \tilde{w}(x_1, x_2) = \mathbf{\Phi}^T\mathbf{C}^{-1}\mathbf{u} = \mathbf{N}\mathbf{u} \tag{6.21}$$

with

$$\mathbf{\Phi}^T = \left[\, 1 \; x_1 \; x_2 \; x_1^2 \; x_1x_2 \; x_2^2 \; x_1^3 \; x_1^2x_2 \; x_1x_2^2 \; x_2^3 \; x_1^3x_2 \; x_1x_2^3 \,\right] \tag{6.22}$$

An explicit form of the shape function $\mathbf{N}$ was derived by Melosh [7] and can be written in terms of natural coordinates, as

$$\mathbf{N} = \left[\, \mathbf{N}_1 \; \mathbf{N}_2 \; \mathbf{N}_3 \; \mathbf{N}_4 \,\right] \tag{6.23}$$

with

$$\mathbf{N}_i^T = \frac{1}{8}(1 + \zeta\zeta_i)(1 + \eta\eta_i)\begin{bmatrix} 2 + \zeta\zeta_i + \eta\eta_i - \zeta^2 - \eta^2 \\ b\eta_i\left(1 - \eta^2\right) \\ a\zeta_i\left(1 - \zeta^2\right) \end{bmatrix} \tag{6.24}$$

where (ζ_i, η_i) represent the natural coordinates associated with node i and (ζ, η) are the natural coordinates, which are related with the physical coordinates in Eq. (5.50).

6.2.5 *FE Approximation of Strain*

As discussed in previous chapter, after computing shape functions is possible to obtain other quantities, namely the relationship between the strain and the deflection described in Eq. (6.2), as [3]

$$\begin{bmatrix} \tilde{\varepsilon}_{11} \\ \tilde{\varepsilon}_{22} \\ \tilde{\varepsilon}_{12} \end{bmatrix} = -x_3 \begin{bmatrix} \partial^2 \tilde{w}/\partial x_1^2 \\ \partial^2 \tilde{w}/\partial x_2^2 \\ 2\partial^2 \tilde{w}/(\partial x_1 \partial x_2) \end{bmatrix}$$

$$= -x_3 \begin{bmatrix} 2a_4 + 6a_7 x_1 + 2a_8 x_2 + 6a_{11} x_1 x_2 \\ 2a_6 + 2a_9 x_1 + 6a_{10} x_2 + 6a_{12} x_1 x_2 \\ 2a_5 + 4a_8 x_1 + 4a_9 x_2 + 6a_{11} x_1^2 + 6a_{12} x_2^2 \end{bmatrix} = -x_3 \boldsymbol{\chi} \tag{6.25}$$

noting that the curvatures $\boldsymbol{\chi}$ in Eq. (6.25), can be written as

$$\boldsymbol{\chi} = \mathbf{L}w = \mathbf{Q}\mathbf{a} \tag{6.26}$$

with

$$\mathbf{Q} = \begin{bmatrix} 0 & 0 & 0 & 2 & 0 & 0 & 6x_1 & 2x_2 & 0 & 0 & 6x_1x_2 & 0 \\ 0 & 0 & 0 & 0 & 0 & 2 & 0 & 0 & 2x_1 & 6x_2 & 0 & 6x_1x_2 \\ 0 & 0 & 0 & 0 & 2 & 0 & 0 & 4x_1 & 4x_2 & 0 & 6x_1^2 & 6x_2^2 \end{bmatrix} \tag{6.27}$$

and substituting Eq. (6.20) into Eq. (6.26), we obtain

$$\boldsymbol{\chi} = \mathbf{Q}\mathbf{C}^{-1}\mathbf{u} = \mathbf{B}\mathbf{u} \tag{6.28}$$

Thus, substituting Eq. (6.28) into Eq. (6.25), is possible to write

$$\boldsymbol{\varepsilon} = -x_3 \mathbf{B}\mathbf{u} \tag{6.29}$$

where $\mathbf{B}$ is the strain-displacement matrix of the rectangular finite element.

6.2.6 *Element Matrices*

Standard procedures can now be used. So, the stiffness matrix for the finite element can be obtained substituting Eq. (6.29) into Eq. (2.49) of Chap. 2, leading to

$$\mathbf{k} = \int_{\Omega^e} x_3^2 \mathbf{B}^T \mathbf{c}\, \mathbf{B}\, d\Omega^e = \int_A \left(\int_0^h x_3^2 dx_3 \right) \mathbf{B}^T \mathbf{c}\, \mathbf{B}\, dA = \int_A \frac{h^3}{12}\, \mathbf{B}^T \mathbf{c}\, \mathbf{B}\, dA \tag{6.30}$$

where the material constant matrix $\mathbf{c}$ has been given by Eqs. (1.35) and (1.36) of Chap. 1, for plane stress problems. Since the strain matrix $\mathbf{B}$ is not a constant matrix, as shown in Eq. (6.27), and the thickness of the element is assumed constant, the integration of Eq. (6.30) can be carried out substituting Eq. (6.28) into Eq. (6.30), as

$$\mathbf{k} = \frac{h^3}{12}\mathbf{C}^{-T}\left(\int_A \mathbf{Q}^T\mathbf{c}\,\mathbf{Q}\,dA\right)\mathbf{C}^{-1} \tag{6.31}$$

where A denotes the surface element area. In Eq. (6.31), the terms not containing x_1 and x_2 were moved from the operation of integrating and, if matrix $\mathbf{c}$ is constant, the term within the integration sign can be multiplied out and integrated explicitly.

To evaluate the mass matrix, Eq. (6.21) is substituted into Eq. (6.7), leading to

$$\dot{\tilde{\mathbf{u}}} = \begin{bmatrix} \boldsymbol{\Phi}^T\mathbf{C}^{-1} = \mathbf{N} \\ \boldsymbol{\Phi}_{x_1}^T\mathbf{C}^{-1} = \mathbf{N}_{x_1} \\ \boldsymbol{\Phi}_{x_2}^T\mathbf{C}^{-1} = \mathbf{N}_{x_2} \end{bmatrix}\dot{\mathbf{u}} = \overline{\mathbf{N}}\,\dot{\mathbf{u}} \tag{6.32}$$

Now, substituting Eq. (6.32) into Eq. (6.6), we obtain

$$T = \frac{1}{2}\int_\Omega \dot{\tilde{\mathbf{u}}}^T\mathbf{H}\,\dot{\tilde{\mathbf{u}}}\,d\Omega = \frac{1}{2}\dot{\mathbf{u}}^T\left(\int_\Omega \overline{\mathbf{N}}^T\mathbf{H}\,\overline{\mathbf{N}}\,d\Omega\right)\dot{\mathbf{u}} = \frac{1}{2}\dot{\mathbf{u}}^T\mathbf{m}\,\dot{\mathbf{u}} \tag{6.33}$$

where $\mathbf{m}$ is the element mass defined as

$$\mathbf{m} = \int_{\Omega^e} \overline{\mathbf{N}}^T\mathbf{H}\,\overline{\mathbf{N}}\,d\Omega^e = \int_A \overline{\mathbf{N}}^T\left(\int_0^h \mathbf{H}\,dx_3\right)\overline{\mathbf{N}}\,dA = \int_A \overline{\mathbf{N}}^T\mathbf{I}\,\overline{\mathbf{N}}\,dA \tag{6.34}$$

with

$$\mathbf{I} = \rho\begin{bmatrix} h & 0 & 0 \\ 0 & \frac{h^3}{12} & 0 \\ 0 & 0 & \frac{h^3}{12} \end{bmatrix} \tag{6.35}$$

The integration of all the terms in the mass matrix can be carried out explicitly or by numerical integration. Nevertheless, to use numerical integration a coordinate transformation is necessary.

The nodal force vector can be obtained using Eqs. (2.51) and (2.52), assuming that the element is loaded by a constant distributed pressure f_p on the element area, as

$$\mathbf{f} = \int_A \mathbf{N}^T f_p\,dA = \begin{bmatrix} \mathbf{f}_1 \\ \mathbf{f}_2 \\ \mathbf{f}_3 \\ \mathbf{f}_4 \end{bmatrix} \tag{6.36}$$

with

$$\mathbf{f}_i = \frac{1}{12} f_p ab \begin{bmatrix} 3 \\ b \\ -a \end{bmatrix}; \; i = 1, 2, 3, 4 \tag{6.37}$$

where $\mathbf{f}_i$ is the nodal load vector for the uniform load defined by Zienkiewicz and Taylor [3].

6.2.7 Discussion

In the 1950s, the success of the Finite Element Method with membrane-type structural problems, open the path for its application to plate bending and shell problems. The first results using rectangular models were published by the late 1950s. Meanwhile, the construction of successful triangular elements to model plates and shells of arbitrary geometry proved being more difficult than expected and, their failures, led to a more complete understanding of the theoretical basis of FEM.

The major source of difficulties in the development of plate bending finite elements is associated with the stricter continuity requirements. As seen in Sect. 6.2.1, the aim of attaining normal slope inter-element compatibility, poses serious problems. The first successful rectangular plate bending element developed by Adini and Clough [8] has 12 degrees of freedom (DOF) and uses a complete third order polynomial expansion in x_1 and x_2, was presented in Sect. 6.2.2. It satisfies the transverse deflection continuity, but normal slope continuity is only maintained at the four corner points. Later in 1963, Melosh proposed another expansion of the approximation polynomial and, erroneously, stated that the element satisfies C_1 continuity [9]. The error was noted in a subsequent discussion [10]. The construction of fully compatible polynomial expansions of various orders for rectangular shapes was solved by Bogner et al. through Hermitian interpolation functions [11]. Later in an Addendum published as an Appendix to the 1966 Proceedings volume, they recognized the lack of the twist mode for dynamic analysis and, therefore, an additional degree of freedom: the twist curvature, was added at each corner. The resulting 16-DOF element is complete and compatible, and produced excellent results. More refined rectangular elements with 36 DOFs have been also developed using fifth order Hermite polynomials.

Flat triangular plate elements have a wider range of application than rectangular elements. However, the development of adequate kinematic expansions was not an easy problem and kept researchers busy for decades. The first fully compatible 9-DOF cubic triangle was constructed by a macro-element technique as described in [12]. After this element, several triangular finite elements were presented. Nevertheless, most of these elements proved to be excessively stiff, particularly for high aspect ratios. Thus, the research on displacement-assumed models starts

to focus on relaxing or abandoning the assumptions of Kirchhoff thin-plate theory. Relaxing these assumptions has produced elements based on the so-called discrete Kirchhoff theory [13, 14]. In this method the primary expansion is made for the plate rotations and, the rotations are linked to the nodal degrees of freedom by introduction the thin-plate normality conditions at selected boundary points. A clear and relatively simple account is given by Batoz et al. [15]. The most successful of these elements is the DKT (Discrete Kirchhoff Triangle), an explicit formulation has been presented by Batoz [16]. This element is also available in the ADINA program.

A more drastic step is based on the abandoning of the Kirchhoff theory in favor of the Reissner-Mindlin theory. The continuity requirements for the displacement assumption are lowered to C_0 and the transverse shear becomes an integral part of the formulation. Thus, Mindlin plate theory works better to thick plates than to the thin ones. In fact, the construction of robust C_0 triangular bending elements is delicate, as they are susceptible to 'shear locking' effects, in the thin-plate regime. Nevertheless, many structures may not be considered as thin plates, or rather their transverse shear strains cannot be ignored. Therefore, the Reissner-Mindlin plate theory is more suitable, and the elements developed based on this theory are more practical and useful. In the next section will only discuss the elements developed based on the Reissner-Mindlin plate theory.

6.3 Thick Plate Formulation

Following the Reissner-Mindlin plate theory, see Chap. 1, the bending deformation will force the cross-section of the plate to rotate in the way shown in Fig. 6.7. The displacement components for a thick plate are written as

$$u_1(x_1, x_2, x_3) = x_3\phi_2 \tag{6.38}$$

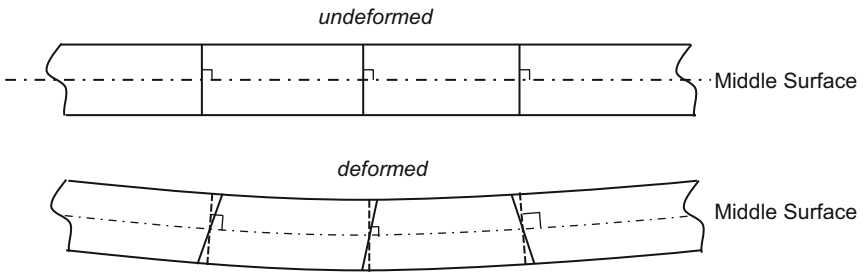

Fig. 6.7 A straight fibre that is perpendicular to the middle plane of the plate before deformation remains straight, but not normal to it, after deformation [4]

$$u_2(x_1, x_2, x_3) = -x_3\phi_1 \tag{6.39}$$

$$u_3(x_1, x_2, x_3) = w(x_1, x_2) \tag{6.40}$$

where ϕ_1 and ϕ_2 are the rotations of the plate fiber about the x_1 and x_2 axes, respectively. The in-plane or bending strains can be obtained as

$$\boldsymbol{\varepsilon}_b = -x_3\boldsymbol{\chi} \tag{6.41}$$

where $\boldsymbol{\chi}$ is the curvature, given as

$$\boldsymbol{\chi} = \mathbf{L}\boldsymbol{\theta} = \begin{bmatrix} -\dfrac{\partial\phi_2}{\partial x_1} \\ \dfrac{\partial\phi_1}{\partial x_2} \\ \dfrac{\partial\phi_1}{\partial x_1} - \dfrac{\partial\phi_2}{\partial x_2} \end{bmatrix} \tag{6.42}$$

where $\mathbf{L}$ is the differential operator defined in Eq. (1.72). The transverse shear strains are defined by Eq. (1.74).

The strain energy expression for a thick plate element is

$$U = \frac{1}{2}\int_A \int_0^h \boldsymbol{\varepsilon}_b^T \boldsymbol{\sigma}_b \, dA \, dx_3 + \frac{1}{2}\int_A \int_0^h \boldsymbol{\varepsilon}_s^T \boldsymbol{\sigma}_s \, dA \, dx_3 \tag{6.43}$$

The first term on the right-hand side of Eq. (6.43) is related with the bending stresses and strains, whereas the second term is for the transverse stresses and strains. σ_b is the bending stress that is related with the bending strain by Eq. (1.77), see Sect. 1.2.2.2 of Chap. 1. σ_s is the average shear stresses relating to the shear strain in the form

$$\boldsymbol{\sigma}_s = \begin{bmatrix} \sigma_{13} \\ \sigma_{23} \end{bmatrix} = k \begin{bmatrix} G & 0 \\ 0 & G \end{bmatrix} \begin{bmatrix} \gamma_{13} \\ \gamma_{23} \end{bmatrix} = k\, \mathbf{c}_s \boldsymbol{\varepsilon}_s \tag{6.44}$$

where G is the shear modulus and k is a constant that is usually taken to be 5/6, as explained in Sect. 1.2.2.2. So, substituting Eqs. (1.77) and (6.41) into Eq. (6.43), the strain energy can be re-written as

$$U = \frac{1}{2}\int_A \boldsymbol{\chi}^T \frac{h^3}{12} \mathbf{c}_b \boldsymbol{\chi} \, dA + \frac{1}{2}\int_A \boldsymbol{\varepsilon}_s^T hk \, \mathbf{c}_s \boldsymbol{\varepsilon}_s dA \tag{6.45}$$

The kinetic energy expression for a thick plate element is given by

$$T = \frac{1}{2}\int_{\Omega} \rho \left(\dot{u}_1^2 + \dot{u}_2^2 + \dot{u}_3^2\right) d\Omega \tag{6.46}$$

Substituting Eqs. (6.38), (6.39), and (6.40) into the above equation leads to

$$T = \frac{1}{2}\int_{A} \rho \left(h\,\dot{w}^2 + \frac{h^3}{12}\dot{\phi}_1^2 + \frac{h^3}{12}\dot{\phi}_2^2\right) dA = \frac{1}{2}\int_{A} \left(\dot{\mathbf{u}}^T \mathbf{I}\,\dot{\mathbf{u}}\right) dA \tag{6.47}$$

with

$$\dot{\mathbf{u}} = \begin{bmatrix} \dot{w} \\ \dot{\phi}_1 \\ \dot{\phi}_2 \end{bmatrix} \tag{6.48}$$

and I is the matrix defined in Eq. (6.35).

6.3.1 Shape Functions

In the Reissner-Mindlin plate theory the rotations ϕ_1 and ϕ_2 are defined independently of the transversal displacement w. Thus, the displacement and rotations can be interpolated separately with independent shape functions. Actually, the procedure of field variable interpolation is the same used at the 2D solid finite elements, except that the number of variables is three instead of two.

The approximation of displacement and rotations for a rectangular finite element with four corner nodes is given by

$$\tilde{w}\,(x_1, x_2) = \sum_{i=1}^{4} N_i w_i;\;\; \tilde{\phi}_1\,(x_1, x_2) = \sum_{i=1}^{4} N_i \phi_{1_i};\;\; \tilde{\phi}_2\,(x_1, x_2) = \sum_{i=1}^{4} N_i \phi_{2_i} \tag{6.49}$$

where the interpolation functions are the same as the four-node 2D Solid element in Chap. 5, i.e. Eq. (5.52). The elements constructed will be conforming elements, which means that all the field variables are continuous on the edges between elements. Eq. (6.49) can be re-written as

$$\tilde{\mathbf{u}} = \begin{bmatrix} \tilde{w} \\ \tilde{\phi}_1 \\ \tilde{\phi}_2 \end{bmatrix} = \mathbf{N}\mathbf{u} \tag{6.50}$$

where $\mathbf{u}$ is the generalized displacement vector for all the nodes in the element, which are arranged in the following order

$$\mathbf{u}^T = \left[\, w_1\;\phi_{1_1}\;\phi_{2_1}\;w_2\;\phi_{1_2}\;\phi_{2_2}\;w_3\;\phi_{1_3}\;\phi_{2_3}\;w_4\;\phi_{1_4}\;\phi_{2_4}\,\right] \tag{6.51}$$

and the shape matrix is defined as

$$\mathbf{N} = \begin{bmatrix} N_1 & 0 & 0 & N_2 & 0 & 0 & N_3 & 0 & 0 & N_4 & 0 & 0 \\ 0 & N_1 & 0 & 0 & N_2 & 0 & 0 & N_3 & 0 & 0 & N_4 & 0 \\ 0 & 0 & N_1 & 0 & 0 & N_2 & 0 & 0 & N_3 & 0 & 0 & N_4 \end{bmatrix} \tag{6.52}$$

6.3.2 FE Approximation of Strains

In thick plates the strain energy is composed by bending and transverse shear strains, see Eq. (6.45). The approximation of the bending strain in the finite element can be obtained substituting Eq. (6.50) into Eq. (6.41), as

$$\begin{bmatrix} \tilde{\varepsilon}_{11} \\ \tilde{\varepsilon}_{22} \\ \tilde{\varepsilon}_{12} \end{bmatrix} = -x_3 \begin{bmatrix} -\dfrac{\partial \phi_2}{\partial x_1} \\ \dfrac{\partial \phi_1}{\partial x_2} \\ \dfrac{\partial \phi_1}{\partial x_1} - \dfrac{\partial \phi_2}{\partial x_2} \end{bmatrix} = -x_3 \boldsymbol{\chi} = -x_3 \mathbf{B}_b \mathbf{u} \tag{6.53}$$

where $\mathbf{B}_b$ is the bending strain-displacement matrix, defined as

$$\mathbf{B}_b = \begin{bmatrix} \mathbf{B}_{b_1} & \mathbf{B}_{b_2} & \mathbf{B}_{b_3} & \mathbf{B}_{b_4} \end{bmatrix} \tag{6.54}$$

In which $\mathbf{B}_{b_i}$ has the form

$$\mathbf{B}_{b_i} = \begin{bmatrix} 0 & 0 & -\partial N_i/\partial x_1 \\ 0 & \partial N_i/\partial x_2 & 0 \\ 0 & \partial N_i/\partial x_1 & -\partial N_i/\partial x_2 \end{bmatrix} \tag{6.55}$$

and the derivatives of shape functions are obtained by Eqs. (5.73) and (5.78), leading to

$$\mathbf{B}_{b_i} = \frac{1}{J} \begin{bmatrix} 0 & 0 & -J_{22}\dfrac{\partial N_i}{\partial \zeta} + J_{12}\dfrac{\partial N_i}{\partial \eta} \\ 0 & -J_{21}\dfrac{\partial N_i}{\partial \zeta} + J_{11}\dfrac{\partial N_i}{\partial \eta} & 0 \\ 0 & J_{22}\dfrac{\partial N_i}{\partial \zeta} - J_{12}\dfrac{\partial N_i}{\partial \eta} & J_{21}\dfrac{\partial N_i}{\partial \zeta} - J_{11}\dfrac{\partial N_i}{\partial \eta} \end{bmatrix} \quad \mathbf{c}_b = -\frac{h^3}{12}\,\mathbf{c} \quad \mathbf{c}_{sh} = h\,\mathbf{c}_s \tag{6.56}$$

The approximation of the transverse shear strains in the finite element are obtained substituting Eq. (6.50) into Eq. (1.74), as

$$\tilde{\boldsymbol{\varepsilon}}_s = \begin{bmatrix} 2\tilde{\varepsilon}_{13} \\ 2\tilde{\varepsilon}_{23} \end{bmatrix} = \begin{bmatrix} \tilde{\phi}_2 + \dfrac{\partial \tilde{w}}{\partial x_1} \\ -\tilde{\phi}_1 + \dfrac{\partial \tilde{w}}{\partial x_2} \end{bmatrix} = \mathbf{B}_s \mathbf{u} \tag{6.57}$$

where $\mathbf{B}_s$ is the shear strain-displacement matrix, defined as

$$\mathbf{B}_s = \begin{bmatrix} \mathbf{B}_{s_1} & \mathbf{B}_{s_2} & \mathbf{B}_{s_3} & \mathbf{B}_{s_4} \end{bmatrix} \tag{6.58}$$

where $\mathbf{B}_{s_i}$ has the form

$$\mathbf{B}_{s_i} = \begin{bmatrix} \partial N_i/\partial x_1 & 0 & N_i \\ \partial N_i/\partial x_2 & -N_i & 0 \end{bmatrix} = \begin{bmatrix} \dfrac{1}{J}\left(J_{22}\dfrac{\partial N_i}{\partial \zeta} - J_{12}\dfrac{\partial N_i}{\partial \eta}\right) & 0 & N_i \\ \dfrac{1}{J}\left(-J_{21}\dfrac{\partial N_i}{\partial \zeta} + J_{11}\dfrac{\partial N_i}{\partial \eta}\right) & -N_i & 0 \end{bmatrix} \tag{6.59}$$

6.3.3 Element Matrices

The stiffness matrix of a general thick finite element is given by substituting Eqs. (6.53) and (6.57) into Eq. (6.45), from which we obtain

$$\mathbf{k} = \int_A \mathbf{B}_b^T \frac{h^3}{12} \mathbf{c}_b \mathbf{B}_b \, dA + \int_A \mathbf{B}_s^T hk \, \mathbf{c}_s \mathbf{B}_s dA = \mathbf{k}_b + \mathbf{k}_s \tag{6.60}$$

The integration of Eq. (6.60) can be evaluated analytically. However, in practices the gauss integration scheme is used to evaluate it numerically, being necessary to reduce it to the canonical form, as

$$\mathbf{k} = \int_{-1}^{+1} \int_{-1}^{+1} \mathbf{F}(\zeta, \eta) \, d\zeta d\eta \tag{6.61}$$

Note that for the case of natural coordinates (ζ, η), everything in Eq. (6.60) already fits this form, except the element of area dA. Nevertheless, as seen in Sect. 5.4.3, the transformation of the element area is defined by

$$dA = J \, d\zeta d\eta \tag{6.62}$$

leading to the following final expression

$$\mathbf{k} = \int_{-1}^{+1}\int_{-1}^{+1} \mathbf{B}_b^T \frac{h^3}{12} \mathbf{c}_b \mathbf{B}_b \, J \, d\zeta \, d\eta + \int_{-1}^{+1}\int_{-1}^{+1} \mathbf{B}_s^T hk \, \mathbf{c}_s \mathbf{B}_s \, J \, d\zeta \, d\eta = \mathbf{k}_b + \mathbf{k}_s \tag{6.63}$$

To obtain the element mass matrix, Eq. (6.50) is substituted into Eq. (6.47), leading to

$$\mathbf{m} = \int_A \mathbf{N}^T \mathbf{I} \, \mathbf{N} \, dA = \int_{-1}^{+1}\int_{-1}^{+1} \mathbf{N}^T \mathbf{I} \, \mathbf{N} \, J \, d\zeta d\eta \tag{6.64}$$

The evaluation of the integral in Eq. (6.64) can be carried out exactly. Nevertheless, in practice, this integral are calculated numerically, as the case of the stiffness matrix, using the gauss integration scheme.

To obtain the force vector, Eq. (6.50) is substituted into Eq. (2.52), leading to

$$\mathbf{f} = \int_A \mathbf{N}^T \begin{bmatrix} f_3 \\ 0 \\ 0 \end{bmatrix} dA \tag{6.65}$$

where it is assumed that the element is under a force per unit of surface, in the x_3 direction, of f_3. If the load that is constant, the above equation becomes

$$\mathbf{f}^T = \frac{4ab}{4} f_3 \begin{bmatrix} 1 & 0 & 0 & 1 & 0 & 0 & 1 & 0 & 0 & 1 & 0 & 0 \end{bmatrix} \tag{6.66}$$

Equation (6.66) gives the information that the distributed force is divided into four concentrated forces of one quarter of the total load.

6.3.4 Higher Order Elements

Rectangular thick plate finite elements of higher order can be formulated using the same procedure used to develop the previous linear rectangular thick plate finite element. Thus, for a rectangular thick finite element with n number of nodes, the displacement and rotations are approximated as

$$\tilde{w}\left(x_1, x_2\right) = \sum_{i=1}^{n} N_i w_i; \;\; \tilde{\phi}_1\left(x_1, x_2\right) = \sum_{i=1}^{n} N_i \phi_{1_i}; \;\; \tilde{\phi}_2\left(x_1, x_2\right) = \sum_{i=1}^{n} N_i \phi_{2_i} \tag{6.67}$$

where the shape function N_i is the same used to develop the corresponding 2D solid finite element.

6.3.5 Discussion

The simplicity of developing finite elements based on the Reissner-Mindlin theory makes it the mostly used to formulate thick plate elements. Nevertheless, the basic difficulty of this theory is that poor shear strains and stresses are predicted with Mindlin-based elements. These poor shear strain predictions result in a strong artificial stiffening of the elements as the thickness/length ratio decreases. This effect of shear locking is more pronounced for low-order elements and when elements are geometrically distorted, because the error in the shear stresses is then larger.

The shear locking can be observed in an isotropic plate with a small constant thickness, when subjected to concentrated node loads. Thus, assume that the global finite element equations for a plate under static loads is written as

$$(\mathbf{K}_b + \mathbf{K}_s)\,\mathbf{U} = \mathbf{F} \tag{6.68}$$

where $\mathbf{K}_b$ is the global bending stiffness matrix while $\mathbf{K}_s$ is the global shear stiffness matrix. In the case of isotropic plates under plane stress conditions, Eq. (6.68) can be re-written as [17]

$$\left(\frac{Eh^3}{12\,(1-\upsilon^2)}\widehat{\mathbf{K}}_b + Gh\,\widehat{\mathbf{K}}_s\right)\mathbf{U} = \mathbf{F} \tag{6.69}$$

where $\widehat{\mathbf{K}}_b$ is evaluated from $\mathbf{K}_b$ by evidencing common terms, see Eq. (1.35), and $\widehat{\mathbf{K}}_s$ is obtained from $\mathbf{K}_s$. Now, dividing Eq. (6.69) by $Eh^3/\left[12\left(1-\nu^2\right)\right]$ leads to

$$\left(\widehat{\mathbf{K}}_b + \alpha\,\widehat{\mathbf{K}}_s\right)\mathbf{U} = \frac{12\left(1-\upsilon^2\right)}{Eh^3}\mathbf{F} = \widehat{\mathbf{F}} \tag{6.70}$$

with

$$\alpha = \frac{12\left(1-\upsilon^2\right)G}{Eh^2} \tag{6.71}$$

For thin plates, the solution of Eq. (6.70) should be of the same order of the Kirchhoff solution, which means that the effect of $\widehat{\mathbf{K}}_s$ term in Eq. (6.70) should vanish. Nevertheless, observing Eq. (6.70) it can be seen that when $h \to 0$ the coefficient $\alpha \to \infty$ grows infinitely, which means that for thin plates the shear tem in Eq. (6.70) will gain significance relatively to the bending term, in such way that the bending contribution vanish. Thus, to $h \to 0$ the solution of Eq. (6.70) is basically given as

$$\widehat{\mathbf{K}}_s\mathbf{U} = \frac{1}{\alpha}\widehat{\mathbf{F}} = \mathbf{0} \tag{6.72}$$

Note that the trivial solution of Eq. (6.72) is the null solution, meaning that in the limit $\alpha \to \infty$ the solution of Eq. (6.72) will be stiffer than the solution based on the Kirchhoff theory. Moreover, the only way to get a solution of Eq. (6.72) different from the trivial one is making the shear stiffness matrix singular, which can be achieved by changing the number of Gauss points used for the numerical integration of stiffness matrices.

Numerical integration is indispensable for practical evaluation of integrals over isoparametric element domains. The standard rule is based on the Gauss integration because such rules use a minimal number of points to achieve a desired level of accuracy. The one dimensional rule has been defined in Sect. 3.2.1 of Chap. 3 while the two dimensional rule has been defined in Sect. 5.3.4 of Chap. 5. This efficiency is important to save computational effort, since a matrix product is evaluated at each sample point. Moreover, in practice, the choice of the numerical integration order is important because, first, the cost of analysis increases when higher-order of integration is employed and, secondly, using a different integration order, the results can be affected by a large amount [2].

Generally, all finite element matrices can be evaluated by numerical integration, and the appropriate integration order depends on the finite element matrix that is evaluated and on the specific formulation of the finite element that is being considered. The first observation in the selection of the order of the numerical integration is that, in theory, if a high enough order is used, all matrices will be evaluated very accurately. On the other hand, using a too low order of integration, leads to an inaccurate evaluation of matrices and the problem solution may not be possible [2]. In fact, if the order of numerical integration is too low, the matrix can have a larger number of zero eigenvalues than the number of physical rigid body modes. A simple example is the evaluation of the stiffness matrix of a three-node truss element, for which if one-point of Gauss numerical integration is used, the row and column corresponding to the degree of freedom at the midnode of the element are null vectors, leading to a structure of stiffness matrix that is singular. Hence, in general, the integration order should be higher than a certain limit. Meanwhile, as a general rule, the full numerical integration should always be used for displacement-based finite element formulation, where the definition of full numerical integration should be considered as the order that gives the exact matrices when the elements are geometrically undistorted [2]. Using this integration order for a geometrically distorted element will not yield the exactly integrated element matrices. However, the analysis is reliable because the numerical integration errors are acceptably small assuming of course reasonable geometric distortions.

Noting that the displacement formulation of finite element analysis yields a strain energy smaller than the exact strain energy of the mathematical/mechanical model being considered, the displacement results based on a displacement formulation are obtained with an overestimation of stiffness. Therefore, we may expect that without evaluating the displacement-based element stiffness matrices accurately, in the numerical integration, better solution results can be obtained. This expected behavior can only be effective if the error in the numerical integration is able to compensate the overestimation of the structural stiffness due to the finite

element discretization [2], in such case the procedure is named reduced integration. Moreover, additionally to the reduced integration order of all finite element matrices a selective integration may also be considered, in which case different strain terms (bending and shear strains) are integrated with different orders of integration. The key question as to whether a reduced and/or selectively integrated element can be recommended for practical use is: has the element formulation, using a specific integration procedure, been sufficiently tested an analyzed for its stability convergence? If tractable, a mathematical stability and convergence analysis is of course most desirable.

6.4 Shell Elements

A shell structure carries loads in all directions, and therefore undergoes bending and twisting, as well as in-plane deformation. Some common examples would be the dome-like design of the roof of a building with a large volume of space; or a building with special architectural requirements such as a church or mosque; or structures with a special functional requirement such as cylindrical and hemispherical water tanks; or lightweight structures like the fuselage of an aircraft, as shown in the work of Quek and Liu [4]. Shell elements have to be used for modelling such structures. The simplest, but widely used, way to obtain a shell element is to superimpose a plate bending stiffness and a plane stress membrane stiffness. In this way flat shell elements can be formulated easily by combining the 2D solid element, formulated in Chap. 5, and the plate element formulated in the previous section. The procedure for developing such an element is very similar to the short cut method used to formulate the 3-D beams elements using the truss and beam elements, as discussed in Chap. 5. Of course, the shell element can also be formulated using the usual method of defining shape functions, substituting into the constitutive equations, and thus obtaining the element matrices.

6.4.1 Flat Shell Finite Elements

Flat shell finite elements can be used to model components of shells and can also be employed to model general curved shells as an assemblage of flat elements. The curvature of the shell is then followed by changing the orientation of the shell elements in space. For very large curvatures of the shell a fine mesh of elements has to be used during the domain discretization. An alternative to this formulation is presented in the next section. In this section flat shell elements are developed and presented.

Similar to the 3-D beams, a flat shell finite element has six degrees of freedom per node: three translational displacements, one displacement in each x_1, x_2 and x_3 directions, and three rotational degrees of freedom with respect the x_1, x_2 and

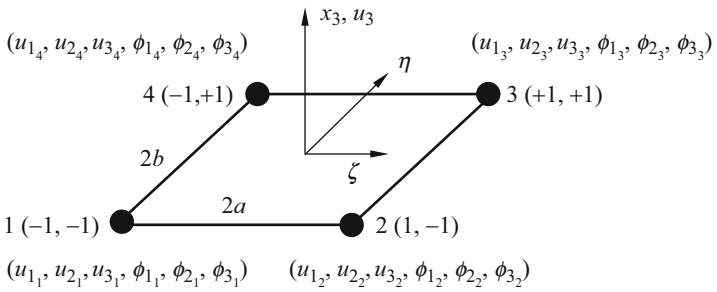

Fig. 6.8 Middle plane of a rectangular shell element

x_3 axes, respectively. Figure 6.8 shows the middle plane of a rectangular flat shell element and the degrees of freedom at the nodes.

The generalized displacement vector for the element can be written as

$$\mathbf{u}^T = \begin{bmatrix} \mathbf{u}_1 & \mathbf{u}_2 & \mathbf{u}_3 & \mathbf{u}_4 \end{bmatrix} \tag{6.73}$$

where $\mathbf{u}_i$ $(i = 1, 2, 3, 4)$ is the displacement vector at node i, defined as

$$\mathbf{u}_i = \begin{bmatrix} u_1 \\ u_2 \\ u_3 \\ \phi_1 \\ \phi_2 \\ \phi_3 \end{bmatrix}_i \tag{6.74}$$

The stiffness matrix of a 2D solid rectangular finite element is used for representing the membrane effects of the flat shell element. The corresponding flat shell degrees of freedom are the in plane displacements u_1 and u_2. So, the stiffness matrix associated with the membrane effect can be expressed in the following form:

$$\mathbf{k}^m = \begin{bmatrix} \mathbf{k}_{11}^m & \mathbf{k}_{12}^m & \mathbf{k}_{13}^m & \mathbf{k}_{14}^m \\ \mathbf{k}_{21}^m & \mathbf{k}_{22}^m & \mathbf{k}_{23}^m & \mathbf{k}_{24}^m \\ \mathbf{k}_{31}^m & \mathbf{k}_{32}^m & \mathbf{k}_{33}^m & \mathbf{k}_{34}^m \\ \mathbf{k}_{41}^m & \mathbf{k}_{42}^m & \mathbf{k}_{43}^m & \mathbf{k}_{44}^m \end{bmatrix} \tag{6.75}$$

In Eq. (6.75) the superscript m stands for the sub-matrices of the membrane matrix and each sub-matrix have a dimension of 2×2, since it corresponds to the two DOFs u_1 and u_2 at each node. Note that the matrix above is the same stiffness matrix of a four-noded 2D rectangular solid element, except that it is written in terms of sub-matrices according the nodes.

In a similar way, the stiffness matrix for a rectangular plate element is used for representing the bending effects of the flat shell element. The corresponding flat shell degrees of freedom are the plate displacements u_3 and ϕ_1, ϕ_2. So, the stiffness matrix associated with the bending effect can be expressed in the following form:

$$\mathbf{k}^b = \begin{bmatrix} \mathbf{k}_{11}^b & \mathbf{k}_{12}^b & \mathbf{k}_{13}^b & \mathbf{k}_{14}^b \\ \mathbf{k}_{21}^b & \mathbf{k}_{22}^b & \mathbf{k}_{23}^b & \mathbf{k}_{24}^b \\ \mathbf{k}_{31}^b & \mathbf{k}_{32}^b & \mathbf{k}_{33}^b & \mathbf{k}_{34}^b \\ \mathbf{k}_{41}^b & \mathbf{k}_{42}^b & \mathbf{k}_{43}^b & \mathbf{k}_{44}^b \end{bmatrix} \tag{6.76}$$

in Eq. (6.76) the superscript b stands for the sub-matrices of the bending matrix that includes the shear stiffness, as defined in Eq. (6.63), and each bending sub-matrix have a dimension of 3×3.

The stiffness matrix for the flat shell element in the local coordinate system can be formulated by combining sub-matrices of Eqs. (6.75) and (6.76) as follows:

$$\mathbf{k}_{ij}^s = \begin{bmatrix} \mathbf{k}_{ij}^m & \mathbf{0} & 0 \\ \mathbf{0} & \mathbf{k}_{ij}^b & 0 \\ 0 & 0 & 0 \end{bmatrix}; \ (i,j = 1, \ldots, 4) \tag{6.77}$$

leading to the following flat shell stiffness matrix:

$$\mathbf{k} = \begin{bmatrix} \mathbf{k}_{11}^s & \mathbf{k}_{12}^s & \mathbf{k}_{13}^s & \mathbf{k}_{14}^s \\ \mathbf{k}_{21}^s & \mathbf{k}_{22}^s & \mathbf{k}_{23}^s & \mathbf{k}_{24}^s \\ \mathbf{k}_{31}^s & \mathbf{k}_{32}^s & \mathbf{k}_{33}^s & \mathbf{k}_{34}^s \\ \mathbf{k}_{41}^s & \mathbf{k}_{42}^s & \mathbf{k}_{43}^s & \mathbf{k}_{44}^s \end{bmatrix} \tag{6.78}$$

Note that in Eq. (6.77), one additional row and one additional column of zero values is added to the assemblage of the sub-membrane and sub-bending stiffness matrices, which are related to the DOF ϕ_{3_i}. In fact, the process of formulating a flat shell element by superimposing the plate bending behavior and the plane stress behavior leads to a flat shell finite element with five degrees of freedom in the local coordinate system, as shown in Fig. 6.9, but since in shell analysis we deal with six degrees of freedom per node, an additional degree of freedom per node is added to the finite element.

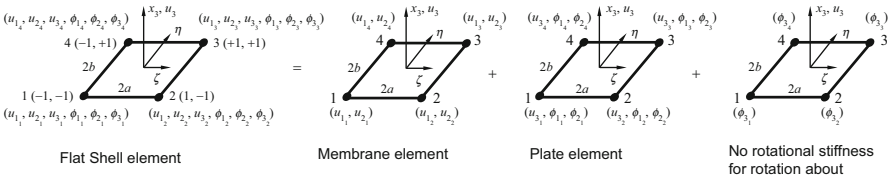

Fig. 6.9 Basic flat rectangular shell element with one additional degree of freedom at a node

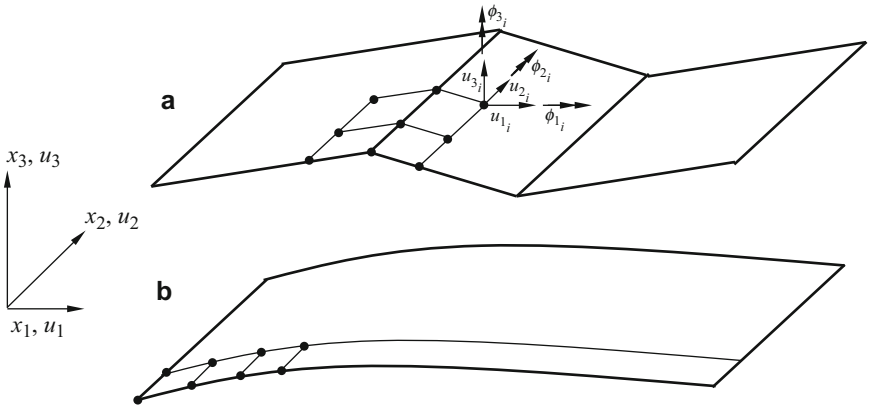

Fig. 6.10 Flat rectangular shell element within the analysis of: (**a**) folded plate structure; (**b**) slightly curved shell [2]

Nevertheless, the stiffness coefficients related with these additional degrees of freedom have been set equal to zero. The reason for doing so is that these degrees of freedom have not been included in the formulation of the finite element; thus the element rotation ϕ_3 at a node is not measured and does not contribute to the strain energy stored in the element. If these additional degrees of freedom are removed, the stiffness matrix would have a reduced dimension of 20×20 instead of the extended dimension of 24×24. However, using the extended matrix in Eq. (6.78) will make more convenient for transforming the matrix from the local coordinate system into the global coordinate system. The solution of a shell model can be obtained using the Eq. (6.78) as long as the elements surrounding a node are not coplanar. In Fig. 6.10 it can be seen that for the folded plate model and for the slightly curved shell this condition is not guaranteed in all the structure.

In these cases, the global stiffness matrix is singular or ill-conditioned because of the zero diagonal elements in Eq. (6.78) and, difficulties arise in solving the global equilibrium equations [2]. To overcome this problem it is possible to add a small stiffness coefficient corresponding to the ϕ_3 rotation, i.e., instead of Eq. (6.77) we can use

$$\widehat{\mathbf{k}}_{ij}^{s} = \begin{bmatrix} \mathbf{k}_{ij}^{m} & \mathbf{0} & 0 \\ \mathbf{0} & \mathbf{k}_{ij}^{b} & 0 \\ 0 & 0 & k \end{bmatrix}; \quad (i = j = 1, \ldots, 4) \tag{6.79}$$

where k is about one-thousandth of the smallest diagonal element of $\widehat{\mathbf{k}}_{ij}^{s}$ $(i = j)$. The stiffness coefficient k must be large enough to allow accurate solutions of the finite element system equilibrium equations and small enough to avoid affecting the system response significantly.

Similarly, the mass matrix for a rectangular flat shell element can be obtained in the same way as the stiffness matrix. Thus, the mass matrix for the 2D solid

element is used for accounting the membrane effects, which can be expressed in the following form using sub-matrices according to the nodes:

$$\mathbf{m}^m = \begin{bmatrix} \mathbf{m}_{11}^m & \mathbf{m}_{12}^m & \mathbf{m}_{13}^m & \mathbf{m}_{14}^m \\ \mathbf{m}_{21}^m & \mathbf{m}_{22}^m & \mathbf{m}_{23}^m & \mathbf{m}_{24}^m \\ \mathbf{m}_{31}^m & \mathbf{m}_{32}^m & \mathbf{m}_{33}^m & \mathbf{m}_{34}^m \\ \mathbf{m}_{41}^m & \mathbf{m}_{42}^m & \mathbf{m}_{43}^m & \mathbf{m}_{44}^m \end{bmatrix} \tag{6.80}$$

where each membrane sub-matrix has also a dimension of 2×2.

The mass matrix for a rectangular plate element is used for describing the shell bending effects. So, the bending mass matrix can also be expressed in the following form using sub-matrices according to the nodes:

$$\mathbf{m}^b = \begin{bmatrix} \mathbf{m}_{11}^b & \mathbf{m}_{12}^b & \mathbf{m}_{13}^b & \mathbf{m}_{14}^b \\ \mathbf{m}_{21}^b & \mathbf{m}_{22}^b & \mathbf{m}_{23}^b & \mathbf{m}_{24}^b \\ \mathbf{m}_{31}^b & \mathbf{m}_{32}^b & \mathbf{m}_{33}^b & \mathbf{m}_{34}^b \\ \mathbf{m}_{41}^b & \mathbf{m}_{42}^b & \mathbf{m}_{43}^b & \mathbf{m}_{44}^b \end{bmatrix} \tag{6.81}$$

where each bending sub-matrix has also a dimension of 3×3.

The mass matrix for the flat shell element in the local coordinate system can be formulated by combining the sub-matrices of Eqs. (6.80) and (6.81) as follows:

$$\mathbf{m}_{ij}^s = \begin{bmatrix} \mathbf{m}_{ij}^m & \mathbf{0} & 0 \\ \mathbf{0} & \mathbf{m}_{ij}^b & 0 \\ 0 & 0 & 0 \end{bmatrix}; \ (i,j = 1,\ldots,4) \tag{6.82}$$

leading to the following flat shell mass matrix:

$$\mathbf{m} = \begin{bmatrix} \mathbf{m}_{11}^s & \mathbf{m}_{12}^s & \mathbf{m}_{13}^s & \mathbf{m}_{14}^s \\ \mathbf{m}_{21}^s & \mathbf{m}_{22}^s & \mathbf{m}_{23}^s & \mathbf{m}_{24}^s \\ \mathbf{m}_{31}^s & \mathbf{m}_{32}^s & \mathbf{m}_{33}^s & \mathbf{m}_{34}^s \\ \mathbf{m}_{41}^s & \mathbf{m}_{42}^s & \mathbf{m}_{43}^s & \mathbf{m}_{44}^s \end{bmatrix} \tag{6.83}$$

Similarly, it is noted that the terms corresponding to the DOF ϕ_3 are zero for the same reasons as explained for the stiffness matrix.

6.4.2 Flat Shell Finite Elements in Global Coordinate System

The matrices for flat shell elements in the global coordinate system can be obtained by performing the following transformations:

$$\mathbf{K} = \mathbf{T}^T \mathbf{k}\, \mathbf{T} \tag{6.84}$$

$$\mathbf{M} = \mathbf{T}^T \mathbf{m}\, \mathbf{T} \tag{6.85}$$

$$\mathbf{F} = \mathbf{T}^T \mathbf{f} \tag{6.86}$$

Where $\mathbf{T}$ is the element transformation matrix, given by

$$\mathbf{T} = \begin{bmatrix} \mathbf{R} & \mathbf{0} & \mathbf{0} & \mathbf{0} \\ \mathbf{0} & \mathbf{R} & \mathbf{0} & \mathbf{0} \\ \mathbf{0} & \mathbf{0} & \mathbf{R} & \mathbf{0} \\ \mathbf{0} & \mathbf{0} & \mathbf{0} & \mathbf{R} \end{bmatrix}; \ \mathbf{R} = \begin{bmatrix} \mathbf{t} & \mathbf{0} \\ \mathbf{0} & \mathbf{t} \end{bmatrix} \tag{6.87}$$

where $\mathbf{R}$ is the transformation matrix for all six nodal degrees of freedom, three translations and three rotations, thus the $\mathbf{t}$ matrix is defined as

$$\mathbf{t} = \begin{bmatrix} l_1 & m_1 & n_1 \\ l_2 & m_2 & n_2 \\ l_3 & m_3 & n_3 \end{bmatrix} \tag{6.88}$$

where l_k, m_k and n_k $(k = 1, 2, 3)$ are direction cosines, which can be obtained in exactly the same way as described in Sect. 4.4.3. The difference is that there is no need to define the additional point 3, as there are already four nodes for the shell element. The local coordinates (ζ, η, x_3) can be conveniently defined under the global coordinate system using the four nodes of the flat shell element.

6.4.3 Discussion

The direct superposition of the matrices for 2D solid elements and plate elements are performed by assuming that the membrane effects are not coupled with the bending effects at the individual element level. This implies that membrane forces will not result in any bending deformation, and bending forces will not cause any in-plane displacement in the element. Nevertheless, for a shell structure in space, the membrane and bending effects are coupled globally, meaning that the membrane force at an element may result in bending deformations in the other elements, and the bending forces in an element may create in-plane displacements in other elements. These coupling effects are more significant for shell structures with a strong curvature. Therefore, for those structures, a finer element mesh should be used. Using the shell elements developed in this approach implies that the curved shell structure has to be meshed by piecewise flat elements. This simplification in geometry needs to be taken into account when evaluating the results obtained [4].

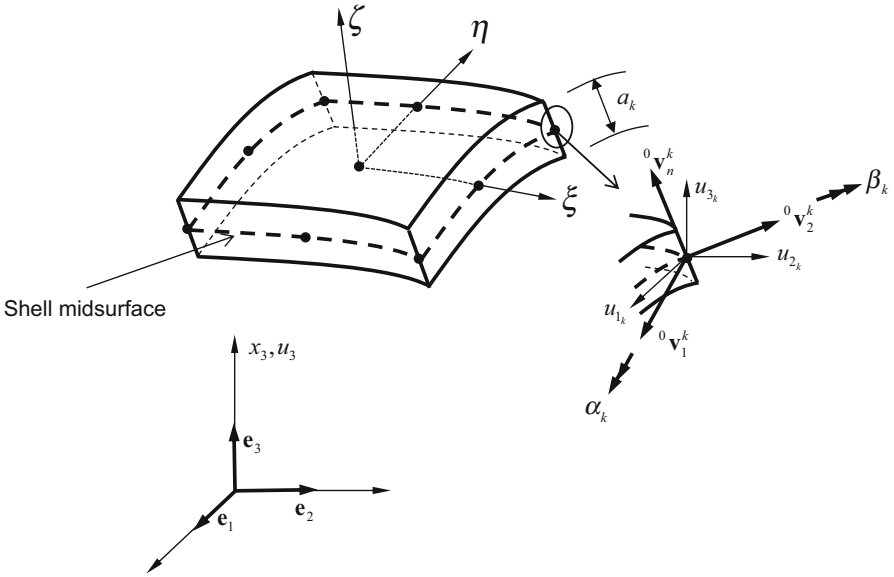

Fig. 6.11 Nine-node shell finite element and coordinate systems [2]

6.4.4 General Shell Finite Elements

General shell elements can be used to analyze very complex shell geometries and stress distributions. Nevertheless, as you might have guessed, it is going to be very mathematically painful.

The displacement interpolation is obtained by considering also the geometry interpolation, as for isoparametric elements. So, consider a general shell finite element with a variable number of nodes, q. In Fig. 6.11 is possible to see a shell finite element for which $q = 9$.

In which, ${}^0\mathbf{v}_n^k$ is a unit vector normal to the shell mid-surface in the t direction at nodal point k with the following direction cosines $\left({}^0\mathrm{v}_{n1}^k, {}^0\mathrm{v}_{n2}^k, {}^0\mathrm{v}_{n3}^k\right)$. Note that a left superscript is used to denote the configuration of the element; i.e., the superscript 0 denotes the element configuration before deformation while superscript 1 denotes the element configuration after deformation. So, using the natural coordinates (ξ, η, ζ), Cartesian coordinates of a point in the element with q nodes, before and after deformations can be given as [2].

$$
\begin{aligned}
{}^j x_1(\xi,\eta,\zeta) &= \sum_{k=1}^{q} N_k{}^j x_1^k + \zeta \sum_{k=1}^{q} \frac{a_k}{2} N_k{}^j \mathrm{v}_{n_1}^k \\
{}^j x_2(\xi,\eta,\zeta) &= \sum_{k=1}^{q} N_k{}^j x_2^k + \zeta \sum_{k=1}^{q} \frac{a_k}{2} N_k{}^j \mathrm{v}_{n_2}^k \qquad ; (j = 0, 1) \\
{}^j x_3(\xi,\eta,\zeta) &= \sum_{k=1}^{q} N_k{}^j x_3^k + \zeta \sum_{k=1}^{q} \frac{a_k}{2} N_k{}^j \mathrm{v}_{n_3}^k
\end{aligned}
\tag{6.89}
$$

Note that in Eq. (6.89) $N_k\,(\xi,\eta)$ are the two-dimensional Lagrange shape functions presented at Sect. 5.3.3. Moreover, the first term on the right hand-side of Eq. (6.89) represent the position of any point in the mid-surface (if $\zeta = 0$) while the second term allow to define the position of any point within the shell thickness. For an element with a variable thickness, the thickness at any point p of the element and the direction in which the thickness is measured are given as

$$\frac{a_p}{2}{}^0\mathbf{v}_n^p = \sum_k^q \frac{a_k}{2} N_k|_{p(\xi_p,\eta_p)}\,{}^0\mathbf{v}_n^k \tag{6.90}$$

The displacement components are defined as

$$\begin{aligned} u_1\,(\xi,\eta,\zeta) &= \sum_{k=1}^{q} N_k u_1^k + \zeta \sum_{k=1}^{q} \frac{a_k}{2} N_k \mathrm{v}_{n_1}^k \\ u_2\,(\xi,\eta,\zeta) &= \sum_{k=1}^{q} N_k u_2^k + \zeta \sum_{k=1}^{q} \frac{a_k}{2} N_k \mathrm{v}_{n_2}^k \\ u_3\,(\xi,\eta,\zeta) &= \sum_{k=1}^{q} N_k u_3^k + t \sum_{k=1}^{q} \frac{a_k}{2} N_k \mathrm{v}_{n_3}^k \end{aligned} \tag{6.91}$$

The first terms in the right hand-side of Eq. (6.91) are displacements in the mid-surface of the shell and, $\mathbf{v}_n^k$ stores the increments in the direction cosines of ${}^0\mathbf{v}_n^k$, i.e.

$$\mathbf{v}_n^k = {}^1\mathbf{v}_n^k - {}^0\mathbf{v}_n^k \tag{6.92}$$

However, the components of vector $\mathbf{v}_n^k$ can be expressed in terms of rotations at the nodal point k, (α_k, β_k). An efficient way for evaluating these rotations is to define two unity vectors ${}^0\mathbf{v}_1^k$ and ${}^0\mathbf{v}_2^k$ that should be orthogonal to ${}^0\mathbf{v}_n^k$; i.e.

$${}^0\mathbf{v}_1^k = \frac{\mathbf{e}_2 \times {}^0\mathbf{v}_n^k}{\left\|\mathbf{e}_2 \times {}^0\mathbf{v}_n^k\right\|} \tag{6.93}$$

where $\mathbf{e}_2$ is represented in Fig. 6.6 and, is an unit vector in the direction of the x_2-axis. Note that for the special case in which the vector ${}^0\mathbf{v}_n^k$ is parallel to $\mathbf{e}_2$, we may simply use ${}^0\mathbf{v}_1^k$ equal to $\mathbf{e}_3$. The vector ${}^0\mathbf{v}_2^k$ is obtained as

$${}^0\mathbf{v}_2^k = {}^0\mathbf{v}_n^k \times {}^0\mathbf{v}_1^k \tag{6.94}$$

Now, assuming that α_k and β_k are the rotations of the director vector ${}^0\mathbf{v}_n^k$ bout the vectors ${}^0\mathbf{v}_1^k$ and ${}^0\mathbf{v}_2^k$, respectively, and assuming that these rotations are small, is possible to write the following relation

$$\mathbf{v}_n^k = -{}^0\mathbf{v}_2^k \alpha_k + {}^0\mathbf{v}_1^k \beta_k \tag{6.95}$$

Substituting Eq. (6.95) into Eq. (6.91) leads to

$$\begin{aligned} u_1(\xi,\eta,\zeta) &= \sum_{k=1}^{q} N_k u_1^k + \zeta \sum_{k=1}^{q} \frac{a_k}{2} N_k \left(-{}^0\mathrm{v}_{2_1}^k \alpha_k + {}^0\mathrm{v}_{1_1}^k \beta_k\right) \\ u_2(\xi,\eta,\zeta) &= \sum_{k=1}^{q} N_k u_2^k + \zeta \sum_{k=1}^{q} \frac{a_k}{2} N_k \left(-{}^0\mathrm{v}_{2_2}^k \alpha_k + {}^0\mathrm{v}_{1_2}^k \beta_k\right) \\ u_3(\xi,\eta,\zeta) &= \sum_{k=1}^{q} N_k u_3^k + \zeta \sum_{k=1}^{q} \frac{a_k}{2} N_k \left(-{}^0\mathrm{v}_{2_3}^k \alpha_k + {}^0\mathrm{v}_{1_3}^k \beta_k\right) \end{aligned} \tag{6.96}$$

Equation (6.96) can be written in the standard finite element form, as

$$\tilde{\mathbf{u}}(\xi,\eta,\zeta) = \mathbf{N}\,\mathbf{u} \tag{6.97}$$

with

$$\mathbf{N}(\xi,\eta,\zeta) = \begin{bmatrix} N_1 & 0 & 0 & \zeta N_1 g_{1_1}^1 & \zeta N_1 g_{2_1}^1 & \cdots & N_q & 0 & 0 & \zeta N_q g_{1_1}^q & \zeta N_q g_{2_1}^q \\ 0 & N_1 & 0 & \zeta N_1 g_{1_2}^1 & \zeta N_1 g_{2_2}^1 & \cdots & 0 & N_q & 0 & \zeta N_q g_{1_2}^q & \zeta N_q g_{2_2}^q \\ 0 & 0 & N_1 & \zeta N_1 g_{1_3}^1 & \zeta N_1 g_{2_3}^1 & \cdots & 0 & 0 & N_q & \zeta N_q g_{1_3}^q & \zeta N_q g_{2_3}^q \end{bmatrix} \tag{6.98}$$

and

$$\mathbf{g}_1^k = -1/2 a_k {}^0\mathbf{v}_2^k; \;\; \mathbf{g}_2^k = 1/2 a_k {}^0\mathbf{v}_1^k \tag{6.99}$$

$$\mathbf{u}^T = \left[u_{1_1} \; u_{2_1} \; u_{3_1} \; \alpha_1 \; \beta_1 \cdots u_{1_q} \; u_{2_q} \; u_{3_q} \; \alpha_q \; \beta_q \right] \tag{6.100}$$

After the element displacement and coordinates definitions in Eqs. (6.96) and (6.89) is possible to proceed, as usual, to evaluate the element matrices of a displacement-based finite element.

To evaluate the strain-displacement matrix, it is necessary to evaluate the displacement derivatives, i.e. the derivatives of the first equation presented in Eq. (6.96) are defined as

$$\begin{bmatrix} \dfrac{\partial \tilde{u}_1}{\partial \xi} \\ \dfrac{\partial \tilde{u}_1}{\partial \eta} \\ \dfrac{\partial \tilde{u}_1}{\partial \zeta} \end{bmatrix} = \begin{bmatrix} \dfrac{\partial}{\partial r} \left[N_1 \; 0 \; 0 \; \zeta N_1 g_{1_1}^1 \; \zeta N_1 g_{2_1}^1 \cdots N_q \; 0 \; 0 \; \zeta N_q g_{1_1}^q \; \zeta N_q g_{2_1}^q \right] \\ \dfrac{\partial}{\partial s} \left[N_1 \; 0 \; 0 \; \zeta N_1 g_{1_1}^1 \; \zeta N_1 g_{2_1}^1 \cdots N_q \; 0 \; 0 \; \zeta N_q g_{1_1}^q \; \zeta N_q g_{2_1}^q \right] \\ \left[0 \; 0 \; 0 \; N_1 g_{1_1}^1 \;\; N_1 g_{2_1}^1 \cdots N_q \; 0 \; 0 \;\; N_q g_{1_1}^q \;\; N_q g_{2_1}^q \right] \end{bmatrix} \mathbf{u} \tag{6.101}$$

and the derivatives of the second and third equations are obtained in a similar way.

To evaluate the strain-displacement matrix in the form of Cartesian coordinates, it is necessary to evaluate the Jacobian of the three-dimensional transformations that connect the differentials of (x_1, x_2, x_3) to those of (ξ, η, ζ) and vice-versa, see Sect. 5.4.2.

$$\begin{bmatrix} dx_1 \\ dx_2 \\ dx_3 \end{bmatrix} = \begin{bmatrix} \frac{\partial x_1}{\partial \xi} & \frac{\partial x_1}{\partial \eta} & \frac{\partial x_1}{\partial \zeta} \\ \frac{\partial x_2}{\partial \xi} & \frac{\partial x_2}{\partial \eta} & \frac{\partial x_2}{\partial \zeta} \\ \frac{\partial x_3}{\partial \xi} & \frac{\partial x_3}{\partial \eta} & \frac{\partial x_3}{\partial \zeta} \end{bmatrix} \begin{bmatrix} d\xi \\ d\eta \\ d\zeta \end{bmatrix} = \mathbf{J}^T \begin{bmatrix} d\xi \\ d\eta \\ d\zeta \end{bmatrix} \tag{6.102}$$

$$\begin{bmatrix} d\xi \\ d\eta \\ d\zeta \end{bmatrix} = \begin{bmatrix} \frac{\partial \xi}{\partial x_1} & \frac{\partial \xi}{\partial x_2} & \frac{\partial \xi}{\partial x_3} \\ \frac{\partial \eta}{\partial x_1} & \frac{\partial \eta}{\partial x_2} & \frac{\partial \eta}{\partial x_3} \\ \frac{\partial \zeta}{\partial x_1} & \frac{\partial \zeta}{\partial x_2} & \frac{\partial \zeta}{\partial x_3} \end{bmatrix} \begin{bmatrix} dx_1 \\ dx_2 \\ dx_3 \end{bmatrix} = \mathbf{J}^{-T} \begin{bmatrix} dx_1 \\ dx_2 \\ dx_3 \end{bmatrix} \tag{6.103}$$

So, using the standard transformation, is possible to write

$$\begin{bmatrix} \frac{\partial \tilde{u}_1}{\partial x_1} \\ \frac{\partial \tilde{u}_1}{\partial x_2} \\ \frac{\partial \tilde{u}_1}{\partial x_3} \end{bmatrix} = \mathbf{J}^{-1} \begin{bmatrix} \frac{\partial \tilde{u}_1}{\partial \xi} \\ \frac{\partial \tilde{u}_1}{\partial \eta} \\ \frac{\partial \tilde{u}_1}{\partial \zeta} \end{bmatrix} \tag{6.104}$$

Substituting Eq. (6.101) into Eq. (6.104) we obtain

$$\begin{bmatrix} \frac{\partial \tilde{u}_1}{\partial x_1} \\ \frac{\partial \tilde{u}_1}{\partial x_2} \\ \frac{\partial \tilde{u}_1}{\partial x_3} \end{bmatrix} = \begin{bmatrix} \frac{\partial N_1}{\partial x_1} & 0 & 0 & g^1_{1_1} G^1_1 & g^1_{2_1} G^1_1 & \cdots & \frac{\partial N_q}{\partial x_1} & 0 & 0 & g^q_{1_1} G^q_1 & g^q_{2_1} G^q_1 \\ \frac{\partial N_1}{\partial x_2} & 0 & 0 & g^1_{1_1} G^1_2 & g^1_{2_1} G^1_2 & \cdots & \frac{\partial N_q}{\partial x_2} & 0 & 0 & g^q_{1_1} G^q_2 & g^q_{2_1} G^q_2 \\ \frac{\partial N_1}{\partial x_3} & 0 & 0 & g^1_{1_1} G^1_3 & g^1_{2_1} G^1_3 & \cdots & \frac{\partial N_q}{\partial x_3} & 0 & 0 & g^q_{1_1} G^q_3 & g^q_{2_1} G^q_3 \end{bmatrix} \mathbf{u} \tag{6.105}$$

with,

$$\begin{aligned} \frac{\partial N_i}{\partial x_1} &= J^{-1}_{11} \frac{\partial N_i}{\partial \xi} + J^{-1}_{12} \frac{\partial N_i}{\partial \eta} \\ \frac{\partial N_i}{\partial x_2} &= J^{-1}_{21} \frac{\partial N_i}{\partial \xi} + J^{-1}_{22} \frac{\partial N_i}{\partial \eta} \quad i = 1, \ldots, q \\ \frac{\partial N_i}{\partial x_3} &= J^{-1}_{31} \frac{\partial N_i}{\partial \xi} + J^{-1}_{32} \frac{\partial N_i}{\partial \eta} \end{aligned} \tag{6.106}$$

$$
\begin{aligned}
G_1^i &= t\left(J_{11}^{-1}\frac{\partial N_i}{\partial \xi} + J_{12}^{-1}\frac{\partial N_i}{\partial \eta}\right) + J_{13}^{-1}N_i \\
G_2^i &= t\left(J_{21}^{-1}\frac{\partial N_i}{\partial \xi} + J_{22}^{-1}\frac{\partial N_i}{\partial \eta}\right) + J_{23}^{-1}N_i \quad i = 1,\ldots,q \\
G_3^i &= t\left(J_{31}^{-1}\frac{\partial N_i}{\partial \xi} + J_{32}^{-1}\frac{\partial N_i}{\partial \eta}\right) + J_{33}^{-1}N_i
\end{aligned}
\tag{6.107}
$$

where J_{ij}^{-1} denotes the *(i,j)* component of tensor $\mathbf{J}^{-1}$. The derivatives of $\tilde{u}_2$ and $\tilde{u}_3$ are obtained in analogous manner.

Using displacement derivatives and the relations in Eq. (1.3) is possible to obtain the assemblage for the strain-displacement matrix of a general shell finite element. So, assuming that the rows in this matrix correspond to all six global Cartesian strain components, ε_{11}, ε_{22},, $2\varepsilon_{23}$ the entries in the strain matrix $\mathbf{B}$ are constructed in the usual way, but then the stress-strain law must contain the shell assumption that the stress normal to the shell surface is zero [2]. Thus, the constitutive relation in Eq. (1.10) is rewritten as

$$
\boldsymbol{\sigma} = \mathbf{c}_{sh}\,\boldsymbol{\varepsilon} \tag{6.108}
$$

where

$$
\mathbf{c}_{sh} = \mathbf{T}^T \frac{E}{1-\nu^2}
\begin{bmatrix}
1 & \nu & 0 & 0 & 0 & 0 \\
\nu & 1 & 0 & 0 & 0 & 0 \\
0 & 0 & 0 & 0 & 0 & 0 \\
0 & 0 & 0 & \frac{1-\nu}{2} & 0 & 0 \\
0 & 0 & 0 & 0 & k\frac{1-\nu}{2} & 0 \\
0 & 0 & 0 & 0 & 0 & k\frac{1-\nu}{2}
\end{bmatrix}
\mathbf{T} \tag{6.109}
$$

and $\mathbf{T}$ represents the matrix that transforms the stress-strain law from the natural coordinate system of the shell finite element to the global Cartesian coordinate system. The components of the matrix T are obtained from the direction cosines of the (r, s, t) coordinate axes measured in the global coordinate system, i.e.

$$
\mathbf{T} = \begin{bmatrix}
l_1^2 & m_1^2 & n_1^2 & m_1n_1 & n_1l_1 & l_1m_1 \\
l_2^2 & m_2^2 & n_2^2 & m_2n_2 & n_2l_2 & l_2m_2 \\
l_3^2 & m_3^2 & n_3^2 & m_3n_3 & n_3l_3 & l_3m_3 \\
2l_2l_3 & 2m_2m_3 & 2n_2n_3 & m_2n_3 + m_3n_2 & n_2l_3 + n_3l_2 & l_2m_3 + l_3m_2 \\
2l_1l_3 & 2m_1m_3 & 2n_1n_3 & m_3n_1 + m_1n_3 & n_3l_1 + n_1l_3 & l_3m_1 + l_1m_3 \\
2l_1l_2 & 2m_1m_2 & 2n_1n_2 & m_1n_2 + m_2n_1 & n_1l_2 + n_2l_1 & l_1m_2 + l_2m_1
\end{bmatrix} \tag{6.110}
$$

where

$$
\begin{aligned}
l_1 &= \cos(e_1, e_r) \; m_1 = \cos(e_2, e_r) \; n_1 = \cos(e_3, e_r) \\
l_2 &= \cos(e_1, e_s) \; m_2 = \cos(e_2, e_s) \; n_2 = \cos(e_3, e_s) \\
l_3 &= \cos(e_1, e_t) \; m_3 = \cos(e_2, e_t) \; n_3 = \cos(e_3, e_t)
\end{aligned}
\tag{6.111}
$$

For the analysis of a general shell the evaluation of **T** matrix must be performed at each integration point that is employed in the numerical integration of the stiffness matrix. However, in the case of special shells and, in particular, when a plate is analyzed, the transformations matrix and the stress-strain matrix needs only be evaluated at specific points and can be repetitively.

It is instructive to compare a general shell element formulation with a shell element formulation based on the superimposing the plate bending and membrane stress behaviors. To identity the main computational difference we may simply compare the strain-displacement matrices at Eqs. (6.56) and (6.59) with Eq. (6.105) which can be used to develop the shell strain-displacement matrix. In fact, in Eqs. (6.56) and (6.59) the coordinate ζ related with the shell thickness direction is not present, so these element matrices are calculated by integrating numerically in the $\xi - \eta$ element mid-planes, whereas in the general shell element stiffness calculation numerical integration is also performed in the ζ-direction.

6.4.5 *Boundary Conditions*

In plate finite elements based on the Reissner-Mindlin plate theory, the transverse displacement and the section rotations are treated as independent variables, whereas for plate finite elements based on the Kirchhoff plate theory the transverse displacement is the only independent variable. Thus, in the Kirchhoff plate theory all boundary conditions are written only in terms of the transverse displacement, while in the Reissner-Mindlin plate theory the boundary conditions are written in terms of transverse displacement and of the section rotations. Because the section rotations are used as additional kinematic variables, the Reissner-Mindlin plate theory allows to model more accurately the physical condition of a support.

Consider the support conditions at the edge of the thin structure shown in Fig. 6.12 [2]. If this structure were modeled employing Reissner-Mindlin plate theory, the boundary conditions are that the transverse displacement of all nodes located on the support line is restrained to zero but the section rotations are free. On the other hand, if this structure were modeled using the Kirchhoff plate theory, the transverse displacement and the rotation given by $\partial w/\partial x_1$ would both be zero and, therefore, the finite element model would have also to impose that all nodes located on the support line are not free to rotate about x_2 axis, ϕ_2. Hence, the edge conditions in Fig. 6.12 should consider the following correspondent finite element model:

For the Reissner-Mindlin plate theory-based elements:

On the support line

$$u_3 = w = 0; \quad \phi_1 \textit{ and } \phi_2 \textit{ are left free} \tag{6.112}$$

For the Kirchhoff plate theory-based elements:

$$u_3 = w = \phi_2 = 0; \quad \phi_1 \textit{ is left free} \tag{6.113}$$

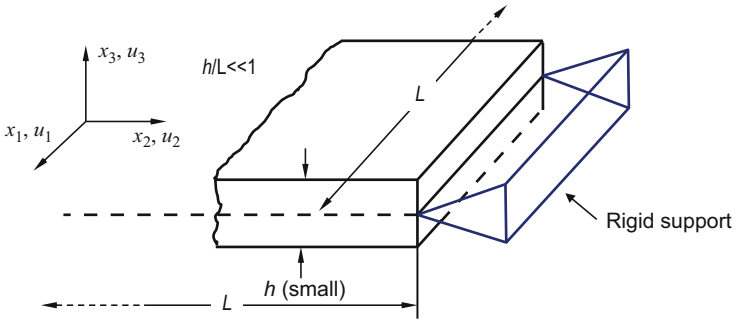

Fig. 6.12 Knife-edge support for thin structure [2]

where, in Eq. (6.113),

$$\phi_2 = -\frac{\partial w}{\partial x_1} \tag{6.114}$$

The boundary condition in Eq. (6.112) is referred as soft boundary condition for a simple support, whereas when ϕ_2 is also set to zero the boundary condition is of hard type. The plate is said clamped when the knife-edge support is also able to restrain the rotation ϕ_1. For this case, naturally, we have $w = \phi_1 = 0$ on the edge support, but regarding ϕ_2, an additional choice needs to be made: for a soft boundary condition ϕ_2 is left free while for a hard boundary condition ϕ_2 is set equal to zero. In practice, the soft boundary condition is used, but depending on the actual physical situation, the hard boundary condition may also be employed.

The important point is that when the Reissner-Mindlin plate theory-based elements are used, the boundary conditions on the transverse displacement and rotations are not necessarily the same as when Kirchhoff plate theory is being used and a choice needs to be made for modeling appropriately the actual physical situation. The same observation hold for the use of the shell elements presented earlier, for which the section rotations are also independent variables [2].

6.5 Discussion Example

This is a well known Scordelis-Lo cylindrical roof benchmark problem [18]. The problem consists of a cylindrical roof with rigid support conditions at edges $x = \pm L/2$ while lateral edges are free, see Fig. 6.13, the material is homogeneous and isotropic with $E = 3 \times 10^6$ psi and $\upsilon = 0$. The shell is assumed to deform under its own weight, i.e. load acts vertically down and not perpendicularly to the surface of the shell [19].

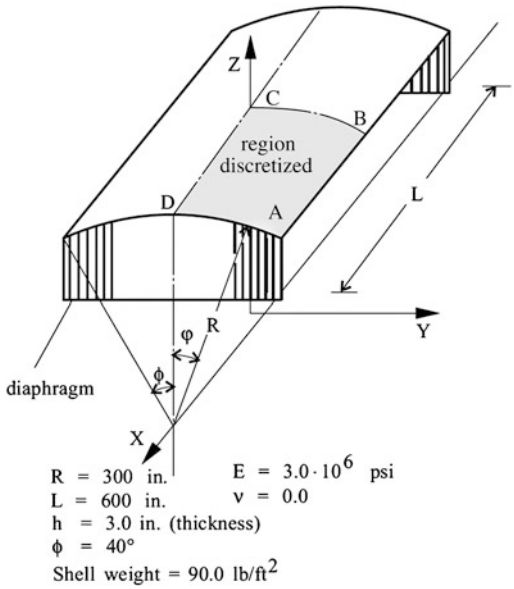

Fig. 6.13 Scordelis-Lo cylindrical roof benchmark problem [20]

Due to symmetry, only one quarter of the cylindrical shell roof needs to be considered. The shaded region in Fig. 6.13 is modeled using isoparametric shell elements. The symmetry boundary conditions are specified as follows:

$$u_1 = \phi_2 = \phi_3 = 0 \quad \textit{on side BC} \tag{6.115}$$

$$u_2 = \phi_1 = \phi_3 = 0 \quad \textit{on side CD} \tag{6.116}$$

The nodes corresponding to the side DA are fixed for translation in the x_2 and x_3 directions. The analytical shallow shell solution generally quoted for the vertical deflection at the center of the free edge, point B, is of -3.703 in. [21]. Nevertheless, a deep shell exact analytical solution quoted is of -3.6288 in. [22]. In order to understand the difference between flat and general shell finite elements, the numerical solution of this example is analyzed, firstly, using the shell element and, secondly, using the plate element, both elements are available in the ADINA program.

General Shell Element Solution

The shell element available in ADINA library is a 4–32 node isoparametric element that can be employed to model thick and thin general shell structures. Either 5 or 6 degrees of freedom can be assigned at a shell element mid-surface node, which can be defined within the control menu bar selecting the degrees of freedom item [20]. Due to the slight curvature of the roof presented in Fig. 6.13, the shell finite elements will be almost coplanar. Thus, because of the zero diagonal elements associated

with the rotational degrees of freedom ϕ_3, the corresponding shell finite element model with six degrees of freedom per node leads to a global stiffness matrix that is singular or ill-conditioned. In fact, as suggested in the ADINA modeling guide, the best option passes to always specify five degrees of freedom at all shell mid-surface nodes, except for the following cases:

- Shell elements intersecting at an angle;
- Coupling of shell elements with other types of structural elements, such as isoparametric beams.
- Coupling of rigid links (see Chap. 8);
- Coupling of constraints or generalized constraints to the shell mid-surface nodes;
- Imposing rotational moments or boundary conditions at the node.

In this example the symmetry boundary conditions in Eqs. (6.115) and (6.116) are defined in the global coordinate system and, therefore, six degrees of freedom are associated with these two lines allowing there deletion. All the mid-surface nodes that are not on symmetry boundaries have rotations referenced to the $\mathbf{v}_1^k$, $\mathbf{v}_2^k$ directions (see Fig. 6.11). Figure 6.14 shows the shell finite element model of the roof for the case of using two cubic shell finite elements.

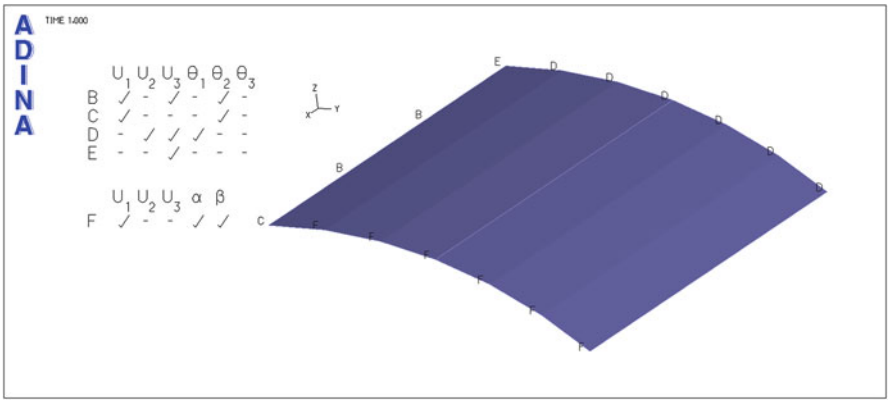

Fig. 6.14 Numerical model of the Scordelis-Lo cylindrical roof benchmark problem

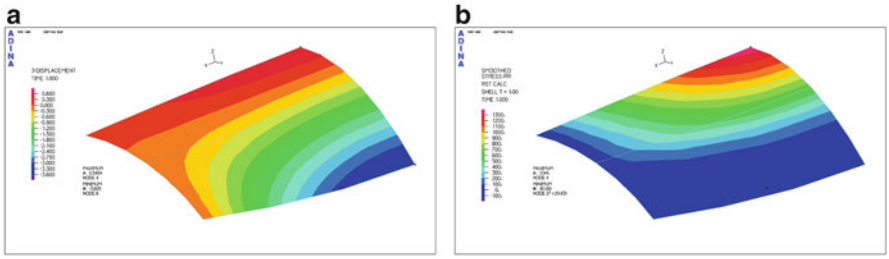

Fig. 6.15 Solutions of displacement and stresses for the Scordelis-Lo cylindrical roof benchmark problem

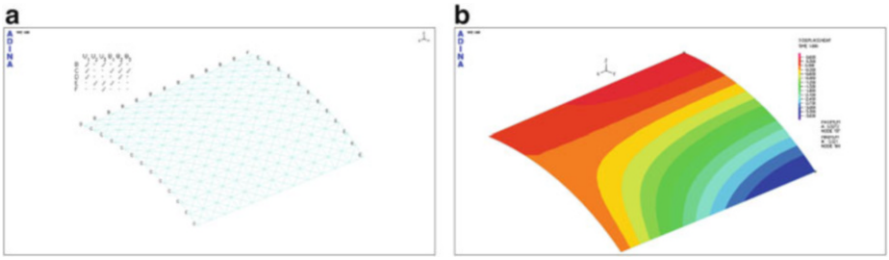

Fig. 6.16 Plate finite element model of the Scordelis-Lo cylindrical roof benchmark problem

The solution of the displacement field is showed in Fig. 6.15. The displacement of point B is of -3.605 in., which is very close to the quoted value. The local stress in r direction, σ_{rr}, in point C is of 1,344 psi. Note that only two cubic elements can be used to model this problem, resulting in good agreement with theoretical results for displacements.

Plate Element Solution

In order to verify the plate finite element of ADINA program when applied to a curved shell structure, the example of Fig. 6.13 is now modeled by a plate finite element and, as for the previous example, only one quarter of the structure needs to be modeled. The numerical model consist on a $12 \times 12 \times 4$ mesh of plate elements, see Fig. 6.16.

As shown in Fig. 6.16, although a large number of plate elements are used, the displacement solution for point B is still not as good as the solution obtained with only two isoparametric shell elements. One reason for that is the flatness of plate element, meaning that the cylindrical shell roof is approximated by straight segments. Another reason is that the membrane approximation, used in the plate element, is based on a constant strain triangle. Thus, the membrane forces are constant over each element, which limits the capability of the plate element to describe structures in which the membrane forces vary significantly.

6.6 Review Questions

1. If the plate were made of a composite material, how would the finite element equation be different?
2. What are the main differences between the thin and thick plate finite elements?
3. What are the main difference between flat and general shell elements?
4. What is the main difference between the soft and hard boundary conditions used in the elements based on Reissner-Mindlin plate theory? Why there is a need of using different boundary conditions on the solution of plates based on Kirchhoff and Reissner-Mindlin?

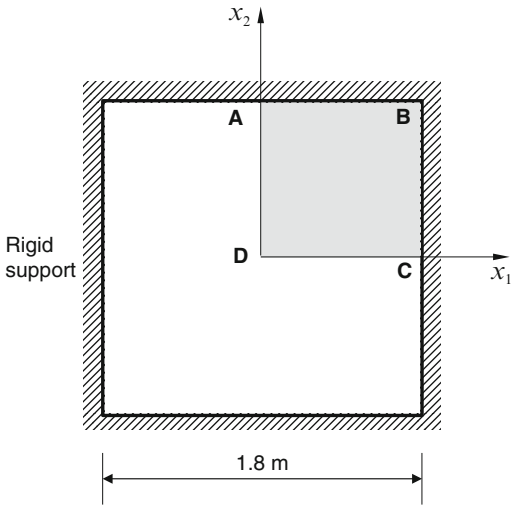

Fig. 6.17 Thin plate under an uniform pressure

5. A thin plate under a pressure load is shown in Fig. 6.17. Consider following data: pressure load of 1 KPa; Young's modulus of 210 GPa; Poisson's coefficient 0.3; plate thickness of 0.01 m. Compute the displacement at the plate center, using 12-node and 16-node shell elements. Compare the solution with the theoretical value given in [20].

References

1. Reddy JN (1993) Finite element method. Wiley, New York
2. Bathe K-J (1996) Finite element procedures. Prentice Hall, Englewood Cliffs
3. Zienkiewicz OC, Taylor RL (2000) The finite element method. Butterworth-Heinemann, Oxford
4. Liu GR, Quek SS (2003) The finite element method: a practical course. Butterworth-Heinemann, Oxford
5. Irons BM, Draper JK (1965) Inadequacy of nodal connections for analysis of plate bending. AIAA J 3(5):961
6. Zienkiewicz OC, Cheung YK (1964) The finite element method for analysis of elastic isotropic and orthotropic slabs. Proc Inst Civ Eng 28:471–488
7. Melosh RJ (1963) Structural analysis of solids. ASCE Struct J 4:205–223
8. Adini A (1961) Analysis of shell structures by the finite element method. University of California, Berkley
9. Melosh RJ (1963) Bases for the derivation of matrices for the direct stiffness method. AIAA J 1:1631–1637
10. Tocher JL, Kapur KK (1965) Discussion of 'Basis for derivation of matrices for the direct stiffness method'. AIAA J 3:1215–1216
11. Bogner FK, Fox RL, Schmidt LA Jr (1966) The generation of interelement compatible stiffness and mass matrices by the use of interpolation formulas. In: Proceedings of the conference on matrix methods in structural mechanics, WPAFB, Ohio, pp 397–444

12. Clough RW, Tocher JL (1966) Finite element stiffness matrices for the analysis of plate bending. In: First conference on matrix methods in structural mechanic, Air Force Institute of Technology, Dayton, pp 515–547
13. Dhatt G (1970) An efficient triangular shell element. AIAA J 8(11):2100–2102
14. Stricklin JA, Haisler WE, Von Riesemann WA (1971) Self-correcting initial value formulations in nonlinear structural mechanics. AIAA J 9:2066–2067
15. Batoz JL, Bathe K-J, Ho L-W (1980) A study of three-node triangular plate bending elements. Int J Numer Meth Engrg 15:1771–1812
16. Batoz JL (1982) An explicit formulation for an efficient triangular plate-bending element. Int J Numer Meth Engrg 18:1077–1089
17. Oñate E (1995) Cálculo de Estructuras por el Método de los Elementos Finitos. Ed. CIMNE
18. Reddy JN (1997) Mechanics of laminated composite plates and shells: theory and analysis. CRC Press, Boca Raton
19. Cantin G, Clough RW (1968) A curved, cylindrical shell, finite element. AIAA J 6:1057–1062
20. ADINA R & D I (2014) User's manual. R & D Inc., Boston
21. Scordelis AC, Lo KS (1964) Computer analysis of cylindrical shells. J Am Concr Inst 61:539–560
22. Simo JC, Fox DD, Rifai MS (1990) On a stress resultant geometrically exact shell model. Part III: computational aspects of the nonlinear theory. Comput Methods Appl Mech Eng 79:21–70

Chapter 7
Finite Element Method for 3D Solids

A three-dimensional (3D) solid element is the most general finite element because all the displacement variables are dependent in x_1, x_2 and x_3 coordinates. The formulation of 3D solids elements is straightforward, because it is basically an extension of 2D solids elements. All the techniques described in 2D solids can be utilized, except that all the variables are now functions of special coordinate.

7.1 Introduction

An example of a 3D solid structure under loading is shown in Fig. 7.1, where force vectors have an arbitrary direction in space. A three-dimensional solid can also have any arbitrary geometry, material properties and boundary conditions in space. As such, in a three-dimensional stress analysis there are altogether six possible stress components, three normal and three shear, that need to be taken into consideration. Typically, the 3D solid finite element shapes can be tetrahedron or hexahedron with either flat or curved surfaces. Even that the number of nodes in each solid finite element is different, each node of the finite element will have three translational degrees of freedom. Thus, the element deformation can be evaluated in all three directions in space. Since the 3D element is said to be the most general solid element, the truss, the beam, the plate, 2D solids and shell elements can all be considered special cases of the 3D solid elements. So, why is there a need to develop all the other elements? Why not just use the 3D element to model everything? [1]. Theoretically, yes, the 3D element can actually be used to model all kinds of structural components, including trusses, beams, plates, shells and so on. However, it can be very tedious in geometry creation and meshing. Furthermore, due to the coexistence of different dimensions, it is also most demanding on computer resources. Hence, if a structure can be simplified into a 1D (trusses, beams and frames) or 2D (2D solids and plates) structure, always do it and, use 3D solid

M.A. Neto et al., *Engineering Computation of Structures: The Finite Element Method*, DOI 10.1007/978-3-319-17710-6_7

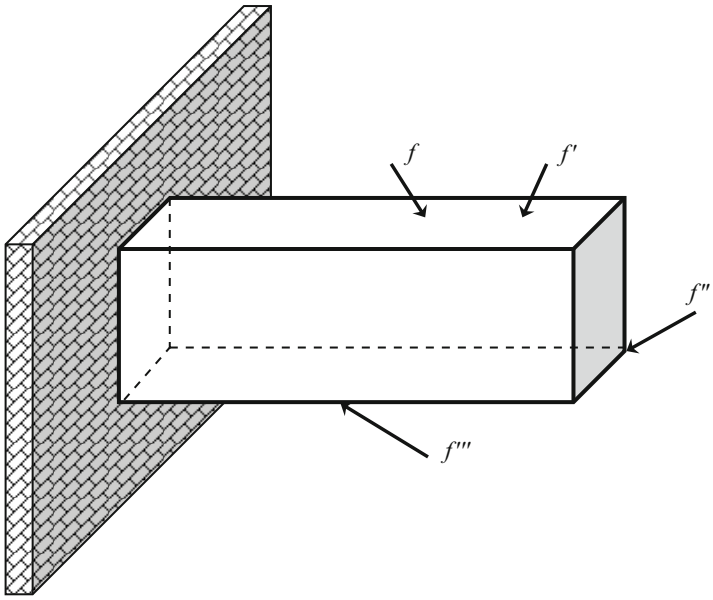

Fig. 7.1 Example of a three-dimensional structure under loading conditions

elements only when we have no other choices. The basic concepts, procedures and formulations for 3D solid elements can also be found in many existing books [2–4].

7.2 Tetrahedron Finite Element

The simplest two-dimensional continuum element is a triangle and, in three dimensions, its equivalent is a tetrahedron, which is an element with four nodal corners. In Fig. 7.2 is possible to see the discretization of the structural three-dimensional body presented on Fig. 7.1, whose domain is divided in a proper manner into a number of tetrahedron elements. This section will deal with the basic formulation of such an element.

7.2.1 Degrees of Freedom Identification

In a mesh of tetrahedron elements, each element has four nodes and six straight edges. Consider now the tetrahedron in the Fig. 7.3, each node has three degrees of freedom, the three displacements (u_1, u_2, u_3) in the directions of the three coordinates x_1, x_2 and x_3, making a total of 12 element degrees of freedom.

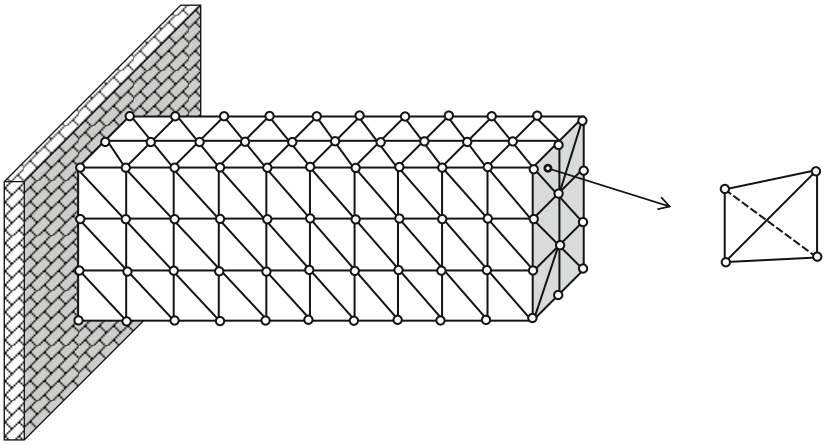

Fig. 7.2 Three-dimensional structure divided into four-node tetrahedron elements

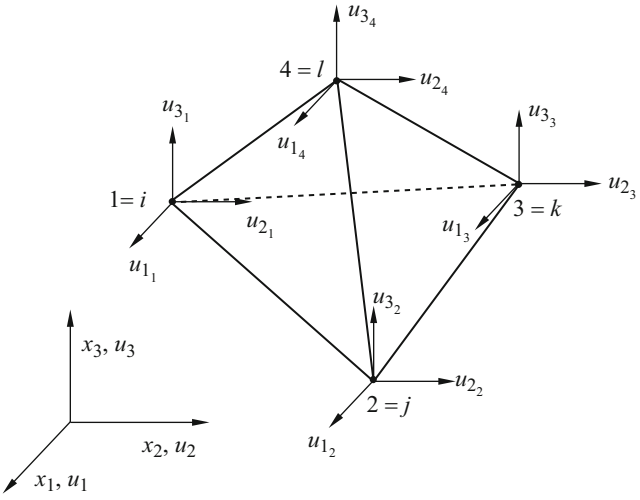

Fig. 7.3 A tetrahedron finite element

The vector of nodal displacements is arranged in the following order:

$$\mathbf{u} = \left[\mathbf{u}_1 \ \mathbf{u}_2 \ \mathbf{u}_3 \ \mathbf{u}_4 \right]^T \tag{7.1}$$

with

$$\mathbf{u}_i = \left[u_{1_i}, \ u_{2_i}, \ u_{3_i} \right]^T \tag{7.2}$$

7.2.2 FE Approximation of the Displacement

Each displacement field $\tilde{u}_i; (i = 1, 2, 3)$ depend on the coordinates (x_1, x_2, x_3), and is interpolated by shape functions in the standard finite element form:

$$\tilde{\mathbf{u}}(x_1, x_2, x_3) = \mathbf{N}(x_1, x_2, x_3)\,\mathbf{u} \tag{7.3}$$

where the nodal displacement vector, $\mathbf{u}$, is defined in Eqs. (7.1) and (7.2) while the matrix of shape functions has the following form:

$$\mathbf{N} = \begin{bmatrix} N_1 & 0 & 0 & N_2 & 0 & 0 & N_3 & 0 & 0 & N_4 & 0 & 0 \\ 0 & N_1 & 0 & 0 & N_2 & 0 & 0 & N_3 & 0 & 0 & N_4 & 0 \\ 0 & 0 & N_1 & 0 & 0 & N_2 & 0 & 0 & N_3 & 0 & 0 & N_4 \end{bmatrix} \tag{7.4}$$

In the next section the shape functions for tetrahedron finite elements will be constructed.

7.2.3 Shape Functions

The procedure of determining the shape functions for triangular finite elements follows the standard procedure described in Sect. 2.3.3 of Chap. 2, by starting with an assumption of the displacements using polynomial basis functions with unknown constants. After which, these unknown constants are determined using the nodal displacements at the nodes of element.

Another alternative procedure and effective method for creating shape for tetrahedron elements is to use volume coordinates, which is a natural extension from the triangular coordinates for 2D solids. In fact, the use of the volume coordinates makes more convenient the shape function construction and the integration of element matrix. The volume coordinates for node 1 is defined as

$$\zeta_1 = \frac{V_{P234}}{V_{1234}} \tag{7.5}$$

where V_{p234} and V_{1234} are the volumes of the tetrahedrons P234 and P1234, respectively, presented in Fig. 7.4.

The volume coordinate for node 2–4 can also be defined in the same form, as

$$\zeta_2 = \frac{V_{P134}}{V_{1234}}; \zeta_3 = \frac{V_{P124}}{V_{1234}}; \zeta_4 = \frac{V_{P123}}{V_{1234}} \tag{7.6}$$

It can be easily confirmed that

$$\zeta_1 + \zeta_2 + \zeta_3 + \zeta_4 = 1 \tag{7.7}$$

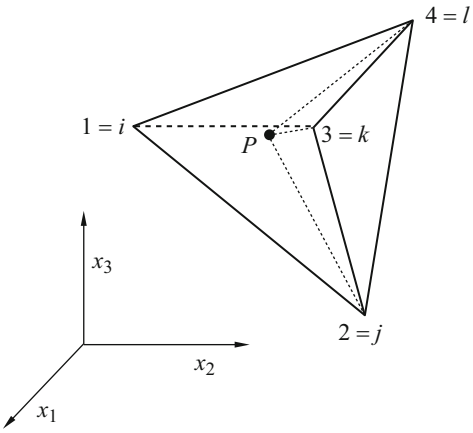

Fig. 7.4 Volume coordinates for tetrahedron element

Since

$$V_{P234} + V_{P134} + V_{P124} + V_{P123} = V_{1234} \tag{7.8}$$

It can also be easily confirmed that

$$\zeta_i = \begin{cases} 1 & \text{at home node } i \\ 0 & \text{at remote nodes } jkl \end{cases} \tag{7.9}$$

This means, that the use of these coordinates leads to the shape functions. So, the relationship among the volume coordinates and the Cartesian coordinates can be easily derived as

$$\begin{aligned} x_1 &= \zeta_1 x_1^1 + \zeta_2 x_1^2 + \zeta_3 x_1^3 + \zeta_4 x_1^4 \\ x_2 &= \zeta_1 x_2^1 + \zeta_2 x_2^2 + \zeta_3 x_2^3 + \zeta_4 x_2^4 \\ x_3 &= \zeta_1 x_3^1 + \zeta_2 x_3^2 + \zeta_3 x_3^3 + \zeta_4 x_3^4 \end{aligned} \tag{7.10}$$

The isoparametric representation of a tetrahedron can be obtained if Eqs. (7.7) and (7.10) are expressed as a single matrix equation, as follows:

$$\begin{bmatrix} 1 \\ x_1 \\ x_2 \\ x_3 \end{bmatrix} = \begin{bmatrix} 1 & 1 & 1 & 1 \\ x_1^1 & x_1^2 & x_1^3 & x_1^4 \\ x_2^1 & x_2^2 & x_2^3 & x_2^4 \\ x_3^1 & x_3^2 & x_3^3 & x_3^4 \end{bmatrix} \begin{bmatrix} \zeta_1 \\ \zeta_2 \\ \zeta_3 \\ \zeta_4 \end{bmatrix} \tag{7.11}$$

The inversion of Eq. (7.11) can be expressed as

$$\begin{bmatrix} \zeta_1 \\ \zeta_2 \\ \zeta_3 \\ \zeta_4 \end{bmatrix} = \frac{1}{6V} \begin{bmatrix} a_1 & b_1 & c_1 & d_1 \\ a_2 & b_2 & c_2 & d_2 \\ a_3 & b_3 & c_3 & d_3 \\ a_4 & b_4 & c_4 & d_4 \end{bmatrix} \tag{7.12}$$

Where

$$\begin{aligned} a_i &= \begin{vmatrix} x_1^j & x_2^j & x_3^j \\ x_1^k & x_2^k & x_3^k \\ x_1^l & x_2^l & x_3^l \end{vmatrix}; \quad b_i = -\begin{vmatrix} 1 & x_2^j & x_3^j \\ 1 & x_2^k & x_3^k \\ 1 & x_2^l & x_3^l \end{vmatrix} \\ c_i &= -\begin{vmatrix} x_2^j & 1 & x_3^j \\ x_2^k & 1 & x_3^k \\ x_2^l & 1 & x_3^l \end{vmatrix}; d_1 = -\begin{vmatrix} x_2^j & x_3^j & 1 \\ x_2^k & x_3^k & 1 \\ x_2^l & x_3^l & 1 \end{vmatrix} \end{aligned} \tag{7.13}$$

In which the subscript i varies from 1 to 4, and j, k and l are determined by a sequential permutation. For instance, if $i = 1$, then $j = 2, k = 3, l = 4$ and when $i = 2$, then $j = 3, k = 4, l = 1$. The volume of the tetrahedron element can be defined as

$$V = \frac{1}{6} \times \begin{vmatrix} 1 & x_1^i & x_2^i & x_3^i \\ 1 & x_1^j & x_2^j & x_3^j \\ 1 & x_1^k & x_2^k & x_3^k \\ 1 & x_1^l & x_2^l & x_3^l \end{vmatrix} \tag{7.14}$$

The properties presented at Eqs. (7.6), (7.7), (7.8) and (7.9) show that ζ_i can be used to define the shape functions of a four-node tetrahedron element, i.e.

$$N_i = \zeta_i = \frac{1}{6V}(a_i + b_i x_1 + c_i x_2 + d_i x_3) \tag{7.15}$$

Because Eq. (7.15) is a linear function of x_i $(i = 1, 2, 3)$, the four-node tetrahedron finite element is also a linear finite element.

7.2.4 FE Approximation of Strain

The strains can now be obtained by substituting Eq. (7.3) into Eq. (1.4):

$$\boldsymbol{\varepsilon} = \mathbf{L}\tilde{\mathbf{u}} = \mathbf{LNu} = \mathbf{Bu} \tag{7.16}$$

where the strain matrix is given by

$$\mathbf{B} = \mathbf{L}\mathbf{N} = \begin{bmatrix} \partial/\partial x_1 & 0 & 0 \\ 0 & \partial/\partial x_2 & 0 \\ 0 & 0 & \partial/\partial x_3 \\ 0 & \partial/\partial x_3 & \partial/\partial x_2 \\ \partial/\partial x_3 & 0 & \partial/\partial x_1 \\ \partial/\partial x_2 & \partial/\partial x_1 & 0 \end{bmatrix} \mathbf{N} \tag{7.17}$$

Using Eq. (7.4) and computing the derivatives of Eq. (7.15), is possible to write the strain matrix as

$$\mathbf{B} = \frac{1}{2V} \begin{bmatrix} b_1 & 0 & 0 & b_2 & 0 & 0 & b_3 & 0 & 0 & b_4 & 0 & 0 \\ 0 & c_1 & 0 & 0 & c_2 & 0 & 0 & c_3 & 0 & 0 & c_4 & 0 \\ 0 & 0 & d_1 & 0 & 0 & d_2 & 0 & 0 & d_3 & 0 & 0 & d_4 \\ c_1 & b_1 & 0 & c_2 & b_2 & 0 & c_3 & b_3 & 0 & c_4 & b_4 & 0 \\ 0 & d_1 & c_1 & 0 & d_2 & c_2 & 0 & d_3 & c_2 & 0 & d_4 & c_2 \\ d_1 & 0 & b_1 & d_2 & 0 & b_2 & d_3 & 0 & b_3 & d_4 & 0 & b_4 \end{bmatrix} \tag{7.18}$$

From Eq. (7.18) it can be seen that the strain matrix for a linear tetrahedron finite element is a constant matrix and, therefore, so it will be the stress. Hence, the linear tetrahedron elements are referred as a constant strain or constant stress finite elements.

7.2.5 Element Matrices

The stiffness matrix for 3D solid elements can be obtained by subsisting Eq. (7.18) into Eq. (2.49) and, because the strain matrix is constant, the element matrix stiffness matrix is defined as

$$\mathbf{k} = \int_{\Omega} \mathbf{B}^T \mathbf{c} \mathbf{B} \, d\Omega = V \mathbf{B}^T \mathbf{c} \mathbf{B} \tag{7.19}$$

In which the material constant matrix is given by Eq. (1.10).

The mass matrix can be obtained using Eq. (2.45) and Eq. (7.4), leading to

$$\mathbf{m} = \int_{\Omega} \rho \mathbf{N}^T \mathbf{N} \, d\Omega = \int_{\Omega} \rho \begin{bmatrix} \mathbf{N}_{11} & \mathbf{N}_{12} & \mathbf{N}_{13} & \mathbf{N}_{14} \\ \mathbf{N}_{21} & \mathbf{N}_{22} & \mathbf{N}_{23} & \mathbf{N}_{24} \\ \mathbf{N}_{31} & \mathbf{N}_{32} & \mathbf{N}_{33} & \mathbf{N}_{34} \\ \mathbf{N}_{41} & \mathbf{N}_{42} & \mathbf{N}_{43} & \mathbf{N}_{44} \end{bmatrix} d\Omega \tag{7.20}$$

where

$$\mathbf{N}_{ij} = \begin{bmatrix} N_i N_j & 0 & 0 \\ 0 & N_i N_j & 0 \\ 0 & 0 & N_i N_j \end{bmatrix} \tag{7.21}$$

The integral on Eq. (7.20) can be obtained using the formula of Eisenberg and Malvern [5].

$$\int_{\Omega} \zeta_1^m \zeta_2^n \zeta_3^p \zeta_4^q \, d\Omega = \frac{m!n!p!q!}{(m+n+p+q)!} 6V \tag{7.22}$$

Thus, Eq. (7.20) can be defined as

$$\mathbf{m} = \frac{\rho V}{20} \begin{bmatrix} 2 & 0 & 0 & 1 & 0 & 0 & 1 & 0 & 0 & 1 & 0 & 0 \\ & 2 & 0 & 0 & 1 & 0 & 0 & 1 & 0 & 0 & 1 & 0 \\ & & 2 & 0 & 0 & 1 & 0 & 0 & 1 & 0 & 0 & 1 \\ & & & 2 & 0 & 0 & 1 & 0 & 0 & 1 & 0 & 0 \\ & & & & 2 & 0 & 0 & 1 & 0 & 0 & 1 & 0 \\ & & & & & 2 & 0 & 0 & 1 & 0 & 0 & 1 \\ & & & & & & 2 & 0 & 0 & 1 & 0 & 0 \\ & sym. & & & & & & 2 & 0 & 0 & 1 & 0 \\ & & & & & & & & 2 & 0 & 0 & 1 \\ & & & & & & & & & 2 & 0 & 0 \\ & & & & & & & & & & 2 & 0 \\ & & & & & & & & & & & 2 \end{bmatrix} \tag{7.23}$$

The nodal force vector for 3D solid elements can be obtained using Eqs. (2.52) and (7.4). Assuming that the element is loaded by a distributed force $\mathbf{f}_s$ on the edge 2–3 of the element, the nodal force becomes

$$\mathbf{f} = \int_L \begin{bmatrix} 0 & 0 & 0 & N_2 & 0 & 0 & N_3 & 0 & 0 & 0 & 0 & 0 \\ 0 & 0 & 0 & 0 & N_2 & 0 & 0 & N_3 & 0 & 0 & 0 & 0 \\ 0 & 0 & 0 & 0 & 0 & N_2 & 0 & 0 & N_3 & 0 & 0 & 0 \end{bmatrix}^T \begin{bmatrix} f_{s_1} \\ f_{s_2} \\ f_{s_3} \end{bmatrix} dL \tag{7.24}$$

If the forces are uniformly distributed along the edge directions x_1, x_2 and x_3, then f_{s_1}, f_{s_2} and f_{s_3} are constants, and Eq. (7.24) can be rewritten as

$$\mathbf{f} = \frac{L}{2} \begin{bmatrix} 0 & 0 & 0 & f_{s_1} & f_{s_2} & f_{s_3} & f_{s_1} & f_{s_2} & f_{s_3} & 0 & 0 & 0 \end{bmatrix}^T \tag{7.25}$$

where L is the length of the edge 2–3 and, Eq. (7.25) implies that the distributed forces are equally divided and applied at the two edge nodes. A similar conclusion can be also applied to an eventually distributed surface forces applied on any face of the element and to an eventually distributed body force applied on the entire element volume.

7.3 Hexahedron Finite Element

Consider now that the structural three-dimensional body presented on Fig. 7.1 is divided in a proper manner into a number of hexahedron elements with eight nodes and six surfaces, as shown in Fig. 7.5. This hexahedron element has the eight nodes numbered in a counter-clockwise manner, as presented in Fig. 7.6. An hexahedron finite element with eight nodes has a total of 24 degrees of freedom, three degrees of freedom per node. The construction of shape functions can be facilitated if a natural coordinate system (ξ, η, ζ) is used. This natural coordinate system has the origin at the center of the transformed cube, as presented in Fig. 7.6.

Because, this element has also an isoparametric formulation, the coordinate mapping is performed in a similar way as for plate/shell elements in Chap. 6. The shape functions are used to interpolate the coordinates, of any point at the element, from the nodal coordinates, i.e.

$$x_1 = \sum_{i=1}^{8} N_i(\xi, \eta, \zeta)\, x_1^i; x_2 = \sum_{i=1}^{8} N_i(\xi, \eta, \zeta)\, x_2^i; x_3 = \sum_{i=1}^{8} N_i(\xi, \eta, \zeta)\, x_3^i \tag{7.26}$$

Where N_i are the shape functions of a hexahedron finite element.

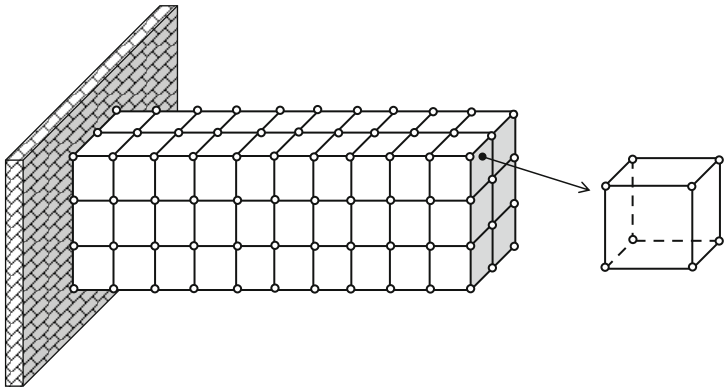

Fig. 7.5 Three-dimensional structure divided into eight-node hexahedron elements

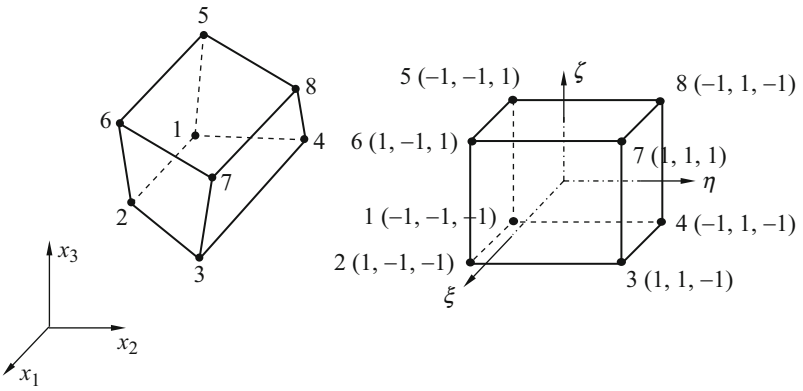

Fig. 7.6 Eight-node hexahedron element and the coordinate systems

7.3.1 FE Approximation of the Displacement

Each displacement field $\tilde{u}_i$; $(i = 1, 2, 3)$ will be a function of coordinates (x_1, x_2, x_3), and is interpolated by shape functions in the standard finite element form:

$$\tilde{\mathbf{u}}(x_1, x_2, x_3) = \mathbf{N}(x_1, x_2, x_3)\,\mathbf{u} \tag{7.27}$$

where the nodal displacement vector, $\mathbf{u}$, is defined in Eqs. (7.1) and (7.2) while the matrix of shape functions has the following form:

$$\mathbf{N} = \begin{bmatrix} \mathbf{N}_1 & \mathbf{N}_2 & \mathbf{N}_3 & \mathbf{N}_4 & \mathbf{N}_5 & \mathbf{N}_6 & \mathbf{N}_7 & \mathbf{N}_8 \end{bmatrix} \tag{7.28}$$

In which each sub-matrix, $\mathbf{N}_i$, is given as

$$\mathbf{N}_i = \begin{bmatrix} N_i & 0 & 0 \\ 0 & N_i & 0 \\ 0 & 0 & N_i \end{bmatrix} \tag{7.29}$$

And the nodal displacement vector is given by

$$\mathbf{u} = \begin{bmatrix} \mathbf{u}_1 & \mathbf{u}_2 & \mathbf{u}_3 & \mathbf{u}_4 & \mathbf{u}_5 & \mathbf{u}_6 & \mathbf{u}_7 & \mathbf{u}_8 \end{bmatrix}^T \tag{7.30}$$

In which each sub-vector $\mathbf{u}_i$ is given as

$$\mathbf{u}_i = \begin{bmatrix} u_{i_i} \\ u_{2_i} \\ u_{3_i} \end{bmatrix} \tag{7.31}$$

In the next section the shape functions for hexahedron finite element will be constructed.

7.3.2 Shape Functions

For the hexahedron presented in Fig. 7.6, the shape functions are defined in the local natural coordinate system as

$$\begin{aligned} N_1 &= \frac{1}{8}(1-\xi)\ (1-\eta)\ (1-\zeta)\,; N_2 = \frac{1}{8}(1+\xi)\ (1-\eta)\ (1-\zeta) \\ N_3 &= \frac{1}{8}(1+\xi)\ (1+\eta)\ (1-\zeta)\,; N_4 = \frac{1}{8}(1-\xi)\ (1+\eta)\ (1-\zeta) \\ N_5 &= \frac{1}{8}(1-\xi)\ (1-\eta)\ (1+\zeta)\,; N_6 = \frac{1}{8}(1+\xi)\ (1-\eta)\ (1+\zeta) \\ N_7 &= \frac{1}{8}(1+\xi)\ (1+\eta)\ (1+\zeta)\,; N_8 = \frac{1}{8}(1-\xi)\ (1+\eta)\ (1+\zeta) \end{aligned} \tag{7.32}$$

Or in a more compact way, as

$$N_i = \frac{1}{8}(1+\xi\xi_i)\ (1+\eta\eta_i)\ (1+\zeta\zeta_i) \tag{7.33}$$

where (ξ_i, η_i, ζ_i) denotes the natural coordinates of node i.

In Eq. (7.33) it can be seen that the shape functions vary linearly in the ξ, η and ζ directions and, therefore, often are called tri-linear functions. Moreover, from Eq. (7.33), it is very easy to verify that the shape functions possess the delta function property. In addition, since all these shape functions can be formed from the set of the following eight basis functions:

$$1, \xi, \eta, \zeta, \xi\eta, \xi\zeta, \zeta\eta, \xi\eta\zeta \tag{7.34}$$

That contain both constant and linear basis function, these shape functions can expect to possess both of the unity property as well as the linear reproduction property.

7.3.3 FE Approximation of Strain

The strains can now be obtained by substituting Eq. (7.27) into Eq. (1.4):

$$\boldsymbol{\varepsilon} = \mathbf{L}\tilde{\mathbf{u}} = \mathbf{L}\mathbf{N}\mathbf{u} = \mathbf{B}\mathbf{u} \tag{7.35}$$

where the strain matrix is given by

$$\mathbf{B} = \left[\mathbf{B}_1\ \mathbf{B}_2\ \mathbf{B}_3\ \mathbf{B}_4\ \mathbf{B}_5\ \mathbf{B}_6\ \mathbf{B}_7\ \mathbf{B}_8\right] \tag{7.36}$$

with

$$\mathbf{B}_i = \mathbf{L}\mathbf{N}_i = \begin{bmatrix} \partial N_i/\partial x_1 & 0 & 0 \\ 0 & \partial N_i/\partial x_2 & 0 \\ 0 & 0 & \partial N_i/\partial x_3 \\ 0 & \partial N_i/\partial x_3 & \partial N_i/\partial x_2 \\ \partial N_i/\partial x_3 & 0 & \partial N_i/\partial x_1 \\ \partial N_i/\partial x_2 & \partial N_i/\partial x_1 & 0 \end{bmatrix} \tag{7.37}$$

Because the shape functions are defined in terms of natural coordinates ξ, η and ζ, to obtain their derivatives with respect to x_1, x_2 and x_3 in Eq. (7.37), the chain rule of partial differentiation needs to be used, as

$$\begin{aligned} \frac{\partial N_i}{\partial \xi} &= \frac{\partial N_i}{\partial x_1}\frac{\partial x_1}{\partial \xi} + \frac{\partial N_i}{\partial x_2}\frac{\partial x_2}{\partial \xi} + \frac{\partial N_i}{\partial x_3}\frac{\partial x_3}{\partial \xi} \\ \frac{\partial N_i}{\partial \eta} &= \frac{\partial N_i}{\partial x_1}\frac{\partial x_1}{\partial \eta} + \frac{\partial N_i}{\partial x_2}\frac{\partial x_2}{\partial \eta} + \frac{\partial N_i}{\partial x_3}\frac{\partial x_3}{\partial \eta} \\ \frac{\partial N_i}{\partial \zeta} &= \frac{\partial N_i}{\partial x_1}\frac{\partial x_1}{\partial \zeta} + \frac{\partial N_i}{\partial x_2}\frac{\partial x_2}{\partial \zeta} + \frac{\partial N_i}{\partial x_3}\frac{\partial x_3}{\partial \zeta} \end{aligned} \tag{7.38}$$

Which can be defined in a matrix form as

$$\begin{bmatrix} \partial N_i/\partial \xi \\ \partial N_i/\partial \eta \\ \partial N_i/\partial \zeta \end{bmatrix} = \mathbf{J} \begin{bmatrix} \partial N_i/\partial x_1 \\ \partial N_i/\partial x_2 \\ \partial N_i/\partial x_3 \end{bmatrix} \tag{7.39}$$

Where $\mathbf{J}$ is the Jacobian matrix defined by

$$\mathbf{J} = \begin{bmatrix} \partial x_1/\partial \xi & \partial x_2/\partial \xi & \partial x_3/\partial \xi \\ \partial x_1/\partial \eta & \partial x_2/\partial \eta & \partial x_3/\partial \eta \\ \partial x_1/\partial \zeta & \partial x_2/\partial \zeta & \partial x_3/\partial \zeta \end{bmatrix} \tag{7.40}$$

Note that because the coordinates x_1, x_2 and x_3 of any point within the finite element are interpolated by the shape functions from the nodal coordinates, is possible to use Eq. (7.26) into Eq. (7.40), which gives

$$\mathbf{J} = \begin{bmatrix} \frac{\partial N_1}{\partial \xi} & \frac{\partial N_2}{\partial \xi} & \frac{\partial N_3}{\partial \xi} & \frac{\partial N_4}{\partial \xi} & \frac{\partial N_5}{\partial \xi} & \frac{\partial N_6}{\partial \xi} & \frac{\partial N_7}{\partial \xi} & \frac{\partial N_8}{\partial \xi} \\ \frac{\partial N_1}{\partial \eta} & \frac{\partial N_2}{\partial \eta} & \frac{\partial N_3}{\partial \eta} & \frac{\partial N_4}{\partial \eta} & \frac{\partial N_5}{\partial \eta} & \frac{\partial N_6}{\partial \eta} & \frac{\partial N_7}{\partial \eta} & \frac{\partial N_8}{\partial \eta} \\ \frac{\partial N_1}{\partial \zeta} & \frac{\partial N_2}{\partial \zeta} & \frac{\partial N_3}{\partial \zeta} & \frac{\partial N_4}{\partial \zeta} & \frac{\partial N_5}{\partial \zeta} & \frac{\partial N_6}{\partial \zeta} & \frac{\partial N_7}{\partial \zeta} & \frac{\partial N_8}{\partial \zeta} \end{bmatrix} \begin{bmatrix} x_1^1 & x_2^1 & x_3^1 \\ x_1^2 & x_2^2 & x_3^2 \\ x_1^3 & x_2^3 & x_3^3 \\ x_1^4 & x_2^4 & x_3^4 \\ x_1^5 & x_2^5 & x_3^5 \\ x_1^6 & x_2^6 & x_3^6 \\ x_1^7 & x_2^7 & x_3^7 \\ x_1^8 & x_2^8 & x_3^8 \end{bmatrix} \tag{7.41}$$

and Eq. (7.39) can be re-written as

$$\begin{bmatrix} \partial N_i/\partial x_1 \\ \partial N_i/\partial x_2 \\ \partial N_i/\partial x_3 \end{bmatrix} = \mathbf{J}^{-1} \begin{bmatrix} \partial N_i/\partial \xi \\ \partial N_i/\partial \eta \\ \partial N_i/\partial \zeta \end{bmatrix} \tag{7.42}$$

The relation in Eq. (7.42) can be used to compute the strain matrix in Eq. (7.37), in which all the derivatives of the shape functions with respect to x_1, x_2 and x_3 can be computed as

$$\begin{aligned} &\frac{\partial N_i}{\partial x_j} = J_{j1}^{-1} \frac{\partial N_i\,(\xi,\eta,\zeta)}{\partial \xi} + J_{j2}^{-1} \frac{\partial N_i\,(\xi,\eta,\zeta)}{\partial \eta} + J_3^{-1} \frac{\partial N_i\,(\xi,\eta,\zeta)}{\partial \zeta} \\ &(i = 1,\ldots,8; j = 1,2,3) \end{aligned} \tag{7.43}$$

From Eqs. (7.43) and (7.32) it can be seen that the strain matrix for an eight-node hexahedron finite element (trilinear) is no longer a constant matrix and, therefore, so will not be the stress.

7.3.4 Element Matrices

The definition of the strain matrix, **B**, allow to compute the stiffness matrix for 3D solid elements, by substituting **B** into Eq. (2.49), i.e.

$$\mathbf{k} = \int_{\Omega} \mathbf{B}^T \mathbf{c}\, \mathbf{B}\; d\Omega = \int_{-1}^{+1}\int_{-1}^{+1}\int_{-1}^{+1} \mathbf{B}^T \mathbf{c}\, \mathbf{B}\, |\mathbf{J}|\; d\xi\; d\eta\; d\zeta \tag{7.44}$$

where $|\mathbf{J}|$ denotes the determinant of Jacobean matrix and **c** is given by Eq. (1.10). Because the strain matrix is dependent on the natural coordinates ξ, η and ζ, the evaluation of Eq. (7.44) can be very difficult. Therefore, the triple integration of Eq. (7.44) can be performed using numerical integration schemes, namely the Gauss integration scheme discussed in Sect. 5.4.4. For the case of three-dimensional integrations, the Gauss integration is sampled in three directions, as follows:

$$I = \int_{-1}^{+1}\int_{-1}^{+1}\int_{-1}^{+1} f\,(\xi,\eta,\zeta)\; d\xi\; d\eta\; d\zeta = \sum_{i=1}^{n}\sum_{j=1}^{m}\sum_{k=1}^{l} w_i w_j w_k f\left(\xi_i, \eta_j, \zeta_k\right) \tag{7.45}$$

The mass matrix for the hexahedron element can be obtained by substituting the shape matrix, Eq. (7.28), into Eq. (2.45), as

$$\mathbf{m} = \int_{\Omega} \rho \mathbf{N}^T \mathbf{N}\; d\Omega = \int_{-1}^{+1}\int_{-1}^{+1}\int_{-1}^{+1} \rho \mathbf{N}^T \mathbf{N}\, |\mathbf{J}|\; d\xi\; d\eta\; d\zeta \tag{7.46}$$

In Eq. (7.46), the triple integral can also be carried out using Gauss integration. If the hexahedron is rectangular with dimensions of $a \times b \times c$ the determinate of the Jacobian matrix is simply given by [1]

$$|\mathbf{J}| = abc = \Omega \tag{7.47}$$

and the mass matrix can be explicitly obtained as

$$\mathbf{m} = \begin{bmatrix} \mathbf{m}_{11} & \mathbf{m}_{12} & \mathbf{m}_{13} & \mathbf{m}_{14} & \mathbf{m}_{15} & \mathbf{m}_{16} & \mathbf{m}_{17} & \mathbf{m}_{18} \\ & \mathbf{m}_{22} & \mathbf{m}_{23} & \mathbf{m}_{24} & \mathbf{m}_{25} & \mathbf{m}_{26} & \mathbf{m}_{27} & \mathbf{m}_{28} \\ & & \mathbf{m}_{33} & \mathbf{m}_{34} & \mathbf{m}_{35} & \mathbf{m}_{36} & \mathbf{m}_{37} & \mathbf{m}_{38} \\ & & & \mathbf{m}_{44} & \mathbf{m}_{45} & \mathbf{m}_{46} & \mathbf{m}_{47} & \mathbf{m}_{48} \\ & & & & \mathbf{m}_{55} & \mathbf{m}_{56} & \mathbf{m}_{57} & \mathbf{m}_{58} \\ & \textit{Sym.} & & & & \mathbf{m}_{66} & \mathbf{m}_{67} & \mathbf{m}_{68} \\ & & & & & & \mathbf{m}_{77} & \mathbf{m}_{78} \\ & & & & & & & \mathbf{m}_{88} \end{bmatrix} \tag{7.48}$$

where

$$\begin{aligned} \mathbf{m}_{ij} &= \int_{-1}^{+1}\int_{-1}^{+1}\int_{-1}^{+1} \rho abc \mathbf{N}_i \mathbf{N}_j d\xi d\eta d\zeta \\ &= \rho abc \int_{-1}^{+1}\int_{-1}^{+1}\int_{-1}^{+1} \begin{bmatrix} N_i & 0 & 0 \\ 0 & N_i & 0 \\ 0 & 0 & N_i \end{bmatrix} \begin{bmatrix} N_j & 0 & 0 \\ 0 & N_j & 0 \\ 0 & 0 & N_j \end{bmatrix} d\xi d\eta d\zeta \\ &\quad - \rho abc \int_{-1}^{+1}\int_{-1}^{+1}\int_{-1}^{+1} \begin{bmatrix} N_i N_j & 0 & 0 \\ 0 & N_i N_j & 0 \\ 0 & 0 & N_i N_j \end{bmatrix} d\xi d\eta d\zeta \end{aligned} \tag{7.49}$$

or

$$\mathbf{m}_{ij} = \begin{bmatrix} m_{ij} & 0 & 0 \\ 0 & m_{ij} & 0 \\ 0 & 0 & m_{ij} \end{bmatrix} \tag{7.50}$$

In which

$$m_{ij} = \rho abc \int_{-1}^{+1}\int_{-1}^{+1}\int_{-1}^{+1} N_i N_j \; d\xi d\eta d\zeta \tag{7.51}$$

All the components of mass matrix can be easily computed if shape functions in Eq. (7.33) are used.

The nodal force vector for a rectangular hexahedron finite element can be obtained using Eqs. (2.52), (7.28) and (7.29). Assuming that the element is loaded by a distributed force $\mathbf{f}_s$ on the edge 2–3 of the element, the nodal force becomes

$$\mathbf{f} = \int_L \begin{bmatrix} \mathbf{0} \\ \mathbf{N}_2 \\ \mathbf{N}_3 \\ \mathbf{0} \\ \mathbf{0} \\ \mathbf{0} \\ \mathbf{0} \\ \mathbf{0} \end{bmatrix} \begin{bmatrix} f_{s_1} \\ f_{s_2} \\ f_{s_3} \end{bmatrix} dl \tag{7.52}$$

If the forces are uniformly distributed along the edge directions x_1, x_2 and x_3, then f_{s_1}, f_{s_2} and f_{s_3} are constants, and Eq. (7.52) can be rewritten as

$$\mathbf{f} = \frac{L}{2}\left[0\ 0\ 0\ f_{s_1}\ f_{s_2}\ f_{s_3}\ f_{s_1}\ f_{s_2}\ f_{s_3}\ 0\ 0\ 0\ 0\ 0\ 0\ 0\ 0\ 0\ 0\ 0\ 0\ 0\ 0\right]^T \tag{7.53}$$

where L is the length of edge 2–3. Eq. (7.53) implies that the distributed forces are equally divided and applied at the two end nodes of edge 2–3.

7.4 Higher Order Elements

7.4.1 Tetrahedron Elements

Higher order tetrahedron elements can be constructed from linear tetrahedron element by adding additional nodes at the edges and faces of element, such as the 10-node tetrahedron element presented in Fig. 7.7 that is a quadratic element. Compared with the linear tetrahedron finite element developed previously, six additional nodes are added at the middle of the edges of the element.

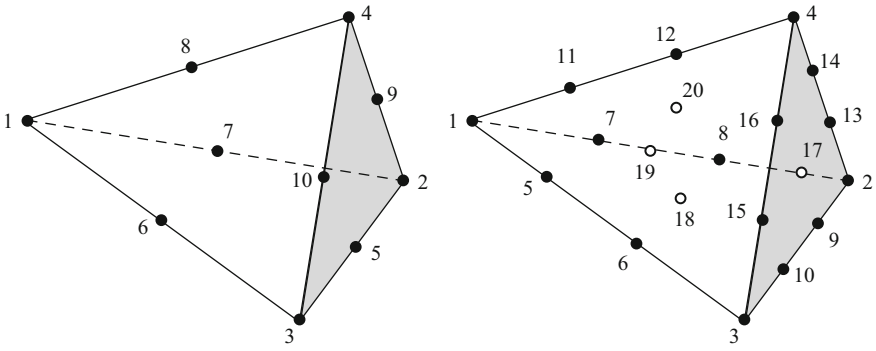

Fig. 7.7 Higher order 3D tetrahedron elements: (**a**) 10-node tetrahedron element; (**b**) 20-node tetrahedron element

The shape functions for a quadratic tetrahedron element can be defined in volume coordinates as [1]

$$\begin{aligned} &N_i = (2\zeta_i - 1)\,\zeta_i;\ i = 1, 2, 3, 4 \\ &N_5 = 4\zeta_2\zeta_3;\ N_6 = 4\zeta_1\zeta_3 \\ &N_7 = 4\zeta_1\zeta_2;\ N_8 = 4\zeta_1\zeta_4 \\ &N_9 = 4\zeta_2\zeta_4;\ N_{10} = 4\zeta_3\zeta_4 \end{aligned} \tag{7.54}$$

where ζ_i is the i volume coordinate, which is coincident with the shape function for the linear tetrahedron elements given by Eq. (7.15).

The 20-node tetrahedron element is a cubic element. Compared with the linear tetrahedron element developed earlier, two additional nodes are added evenly on each edge of the element, and four-node central-face nodes are added at geometry center of each triangular surface of the element. The approximation of a 20-node tetrahedron can be based on a complete polynomial up to third order. The shape functions for this cubic tetrahedron finite element in the volume coordinate are given as follows:

$$\begin{aligned} &N_i = \frac{1}{2}(3\zeta_i - 1)\ (3\zeta_i - 2)\,\zeta_i \ \textit{for corner nodes}\ i = 1, 2, 3, 4 \\ &\left.\begin{aligned} N_5 &= \frac{9}{2}(3\zeta_1 - 1)\,\zeta_1\zeta_3;\ \ N_{11} = \frac{9}{2}(3\zeta_1 - 1)\,\zeta_1\zeta_4 \\ N_6 &= \frac{9}{2}(3\zeta_3 - 1)\,\zeta_1\zeta_3;\ \ N_{12} = \frac{9}{2}(3\zeta_4 - 1)\,\zeta_1\zeta_4 \\ N_7 &= \frac{9}{2}(3\zeta_1 - 1)\,\zeta_1\zeta_2;\ \ N_{13} = \frac{9}{2}(3\zeta_2 - 1)\,\zeta_2\zeta_4 \\ N_8 &= \frac{9}{2}(3\zeta_2 - 1)\,\zeta_1\zeta_2;\ \ N_{14} = \frac{9}{2}(3\zeta_4 - 1)\,\zeta_2\zeta_4 \\ N_9 &= \frac{9}{2}(3\zeta_2 - 1)\,\zeta_2\zeta_3;\ \ N_{15} = \frac{9}{2}(3\zeta_4 - 1)\,\zeta_2\zeta_4 \\ N_{10} &= \frac{9}{2}(3\zeta_3 - 1)\,\zeta_2\zeta_3;\ \ N_{16} = \frac{9}{2}(3\zeta_4 - 1)\,\zeta_3\zeta_4 \end{aligned}\right\} \textit{for edge nodes} \\ &\left.\begin{aligned} N_{17} &= 27\zeta_2\zeta_3\zeta_4 \\ N_{18} &= 27\zeta_1\zeta_2\zeta_3 \\ N_{19} &= 27\zeta_1\zeta_3\zeta_4 \\ N_{20} &= 27\zeta_1\zeta_2\zeta_4 \end{aligned}\right\} \textit{for centre surface nodes} \end{aligned} \tag{7.55}$$

7.4.2 Brick Elements

Lagrange Type Elements

A Lagrange type brick element can be developed using the concept described in the development of 2D rectangular elements in Chap. 5. Figure 7.8 shows

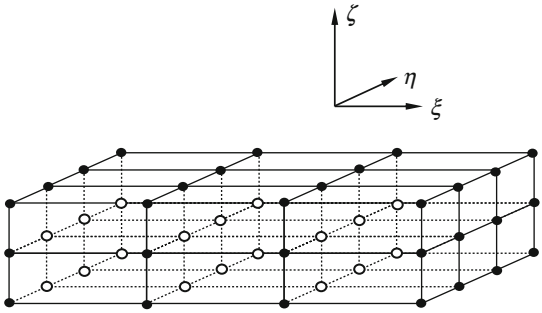

Fig. 7.8 Brick finite element of arbitrary high order

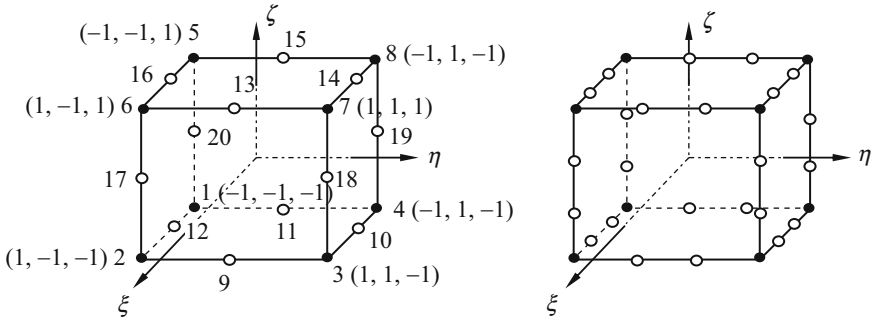

Fig. 7.9 High order 3D serendipity elements: 20-node quadratic element; 32-node cubic element

a brick finite element of arbitrary high order, with a number of nodes $(n+1)\quad(m+1)\quad(p+1)$. The element is defined in natural coordinates over the domain $(-1 \leq (\xi, \eta, \zeta) \leq +1)$. Due to the regularity of the nodal distribution along the ξ, η and ζ directions, the shape function of the element can be simply obtained by multiplying one-dimensional shape functions with respect to the and ζ directions using the Lagrange functions defined in Eq. (3.51) as

$$N_i = N_I^{1D} N_J^{1D} N_K^{1D} = l_I^n(\xi)\, l_J^m(\eta)\, l_K^p(\eta) \tag{7.56}$$

Due to the delta function property of the 1D shape functions given in Eq. (3.52), it is easy to confirm that the N_i defined by Eq. (7.56) also has the delta function property. Meanwhile, due to the presence of interior nodes the Lagrange type elements are not widely used.

Serendipity Type Elements

A Lagrange type brick element without interior nodes is called Serendipity type element. A Serendipity type of brick elements may be created using the concept described in the development of 2D rectangular elements in Chap. 5.

Figure 7.9 shows a 20-node and 32-node serendipity finite elements. The 20-nodal element is a tri-quadratic element with 8 corner nodes and 12 mid-side nodes.

The shape functions in the natural coordinates for the quadratic brick element are given as follows [1]:

$$\begin{aligned}
N_j &= \tfrac{1}{8}\left(1+\xi_j\xi\right)\ \left(1+\eta_j\eta\right)\ \left(1+\zeta_j\zeta\right)\ \left(\xi_j\xi+\eta_j\eta+\zeta_j\zeta-2\right)\\
&\quad \textit{for corner nodes } j=1,\ldots,8\\
N_j &= \tfrac{1}{4}\left(1-\xi^2\right)\ \left(1+\eta_j\eta\right)\ \left(1+\zeta_j\zeta\right)\\
&\quad \textit{for mid}-\textit{sides nodes } j=10,12,14,16\\
N_j &= \tfrac{1}{4}\left(1+\xi_j\xi\right)\ \left(1-\eta^2\right)\ \left(1+\zeta_j\zeta\right)\\
&\quad \textit{for mid}-\textit{sides nodes } j=9,11,13,15\\
N_j &= \tfrac{1}{4}\left(1+\xi_j\xi\right)\ \left(1+\eta_j\eta\right)\ \left(1-\zeta^2\right)\\
&\quad \textit{for mid}-\textit{sides nodes } j=17,18,19,20
\end{aligned} \tag{7.57}$$

where (ξ_j, η_j, ζ_j) are the natural coordinates of node j. It is very easy to observe that the shape functions have the delta function property. The shape function is constructed by simple inspections, making use of the shape properties. For example, for corner node 2, where $\xi_2 = 1, \eta_2 = -1,\ \zeta_2 = -1$, the shape function N_2 it only vanish at remote nodes if passes the following four planes:

$$\begin{aligned}
&1+\xi=0 \Rightarrow \textit{vanishes at nodes } 1,4,5,8,11,15,19,20\\
&\eta-1=0 \Rightarrow \textit{vanishes at nodes } 3,4,7,8,10,14,18,19\\
&\zeta-1=0 \Rightarrow \textit{vanishes at nodes } 5,6,7,8,13,14,15,16\\
&\xi-\eta-\zeta-2=0 \Rightarrow \textit{vanishes at nodes } 9,12,7
\end{aligned} \tag{7.58}$$

So, the shape N_2 can then be immediately written as

$$N_2 = C\,(1+\xi)\ (1-\eta)\ (1-\zeta)\ (\xi-\eta-\zeta-2) \tag{7.59}$$

where C is a constant to be determined using the condition that it has to be unity at node 2, which gives

$$C = \frac{1}{(1+1)\ (1-(-1))\ (1-(-1))\ (-1\,(-1)-(-1)-2)} = \frac{1}{8} \tag{7.60}$$

and, finally, is possible to write

$$N_2 = \frac{1}{8}\,(1+\xi_2\xi)\ (1+\eta_2\eta)\ (1+\zeta_2\zeta)\ (\xi_2\xi+\eta_2\eta+\zeta_2\zeta-2) \tag{7.61}$$

That is coincident with first Eq. at Eq. (7.57) for $j = 2$.

Shape functions at all other nodes can be constructed using a similar procedure. Moreover, following the similar procedure, the shape functions for the 32-node tri-cubic element can be written as

$$
\begin{aligned}
&N_j = \tfrac{1}{64}\left(1+\xi_j\xi\right)\left(1+\eta_j\eta\right)\left(1+\zeta_j\zeta\right)\left(9\xi^2+9\eta^2+9\zeta^2-19\right)\\
&\quad \textit{for corner nodes } j=1,\ldots,8\\
&N_j = \tfrac{9}{64}\left(1-\xi^2\right)\left(1+9\xi_j\xi\right)\left(1+\eta_j\eta\right)\left(1+\zeta_j\zeta\right) \textit{ for side nodes with}\\
&\quad \xi_j=\pm\tfrac{1}{3};\ \eta_j=\pm1;\zeta_j=\pm1\\
&N_j = \tfrac{9}{64}\left(1+\xi_j\xi\right)\left(1-\eta^2\right)\left(1+9\eta_j\eta\right)\left(1+\zeta_j\zeta\right) \textit{ for side nodes with}\\
&\quad \xi_j=\pm1;\ \eta_j=\pm\tfrac{1}{3};\zeta_j=\pm1\\
&N_j = \tfrac{9}{64}\left(1+\xi_j\xi\right)\left(1+\eta_j\eta\right)\left(1-\zeta^2\right)\left(1+9\zeta_j\zeta\right) \textit{ for side nodes with}\\
&\quad \xi_j=\pm1;\ \eta_j=\pm1;\zeta_j=\pm\tfrac{1}{3}
\end{aligned}
\tag{7.62}
$$

7.5 Discussion Example

In this example a simple beam structure subjected to an end moment is analyzed. The problem consists of a rectangular beam with the dimensions shown in Fig. 7.10, the material is homogeneous and isotropic with $E = 210$ GPa and $\upsilon = 0.3$.

In order to understand the difference of degrees of freedom between 2D-Beam and 3D-Solid numerical models, the solution of this example is analyzed, firstly, using the 2D-Beam finite element and, secondly, using 3D-Solid finite elements. Nevertheless, a deep exact analytical solution can be obtained from the strong formulation of a beam structure, namely from the governing Eq. (1.155), of Chap. 1. Since the beam is free of body forces, the equation can now be written as

$$EI\frac{\partial^4 w}{\partial \bar{x}_1^4} = 0 \tag{7.63}$$

The general solution of Eq. (7.63) can be obtained very easily after four integrations, as

$$w(\bar{x}) = c_0 + c_1\bar{x} + c_2\bar{x}^2 + c_3\bar{x}^3 \tag{7.64}$$

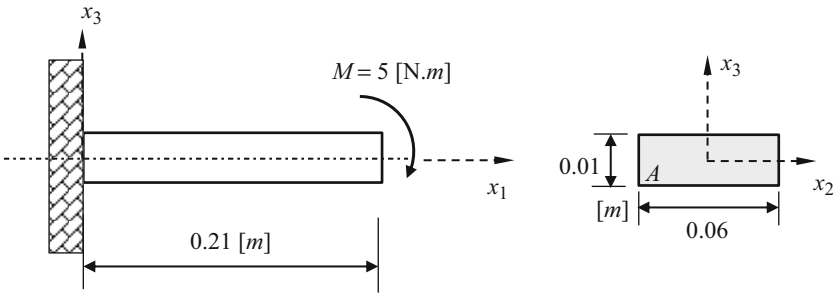

Fig. 7.10 Beam structure loaded by an ending moment

where c_i $(i = 0, 1, 2, 3)$ are unknown constants that can be determined by imposing the boundary conditions. Since the displacement and the rotation at the clamped end are known, the boundary conditions are

$$w(\bar{x} = 0) = 0 \tag{7.65}$$

$$\left.\frac{\partial w}{\partial \bar{x}}\right|_{\bar{x}=0} = 0 \tag{7.66}$$

and, therefore, Eq. (7.65) leads to $c_0 = 0$, while Eq. (7.66) leads to $c_1 = 0$. To compute c_2 and c_3 is necessary to use the natural boundary condition. The first natural boundary condition is related with the transverse load and second one is related with bending moment at the free end of beam, those can be write as

$$\left.\frac{\partial}{\partial \bar{x}}\left(-EI\frac{\partial^2 w}{\partial \bar{x}^2}\right)\right|_{\bar{x}=0.21} = 0 \Rightarrow c_3 = 0 \tag{7.67}$$

$$\left.EI\frac{\partial^2 w}{\partial \bar{x}^2}\right|_{\bar{x}=0.21} = 5 \Rightarrow c_2 = -5 \tag{7.68}$$

Substituting c_i $(i = 0, 1, 2, 3)$ into Eq. (7.64), the solution of the displacement of the beam is written as

$$w(\bar{x}) = -\frac{2\bar{x}^2}{2EI} \tag{7.69}$$

and the displacement at the free end is given by

$$w(\bar{x} = 0.21) = -\frac{5 \times 0.21^2}{2EI} = -1.05 \times 10^{-4} m \tag{7.70}$$

Moreover, the rotation of the cross-section at the free end is given by

$$\phi_2|_{\bar{x}=0.21} = -\left.\frac{\partial w}{\partial \bar{x}}\right|_{\bar{x}=0.21} = \left.\left(\frac{5\bar{x}}{EI}\right)\right|_{\bar{x}=0.21} = 1.00 \times 10^{-3} rad \tag{7.71}$$

The stress σ_{xx} at the free end can be obtained using Eq. (7.69) into Eqs. (1.111) and (1.113), leading to

$$\sigma_{xx} = E\varepsilon_{xx} = E\left(-z\frac{d^2 w}{d\bar{x}^2}\right) = \frac{5z}{I} \tag{7.72}$$

2D-Beam Element Solution

To get the 2D-Beam solution, firstly it is necessary setting up the 1D geometrical of the beam, meaning that the geometry of the straight line representing the beam neutral axis can be used. Since the 2D-Beam finite element has one rotational

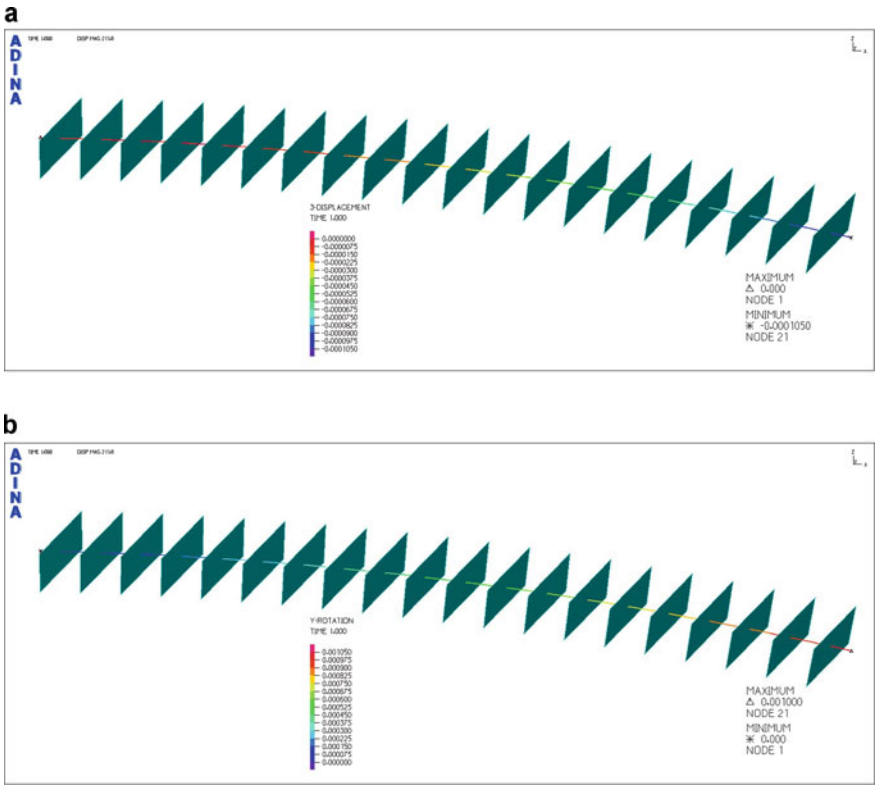

Fig. 7.11 Numerical solution of the clamped beam: (**a**) displacement solution; (**b**) rotational solution

degrees of freedom per node, the external moment can be directly applied in the geometric point that is located at the free end of beam. The solution of the displacement and rotations fields are showed in Fig. 7.11**.** These values are coincident with exact values.

3D-Solid Element Solution

To use the 3D-Solid finite element on modelling the beam structure subjected to an end moment, it is necessary setting up the 3D geometrical of the beam, meaning that the geometry of a straight line representing the beam neutral axis can no longer be used. Figure 7.12 shows the 3D beam geometry with boundary conditions. Because the rotational degrees of freedom are not included on a 3D-Solid element, the rotational movement of the beam cross section at the clamped end, can no longer be constrained. Another discussion point that is associated with the lack of rotational degrees of freedoms in the 3D-solid elements, is the following: how to apply the external bending moment? The solution is to replace the bending moment by a simple couple. A couple is a pair of forces, equal in magnitude, oppositely directed,

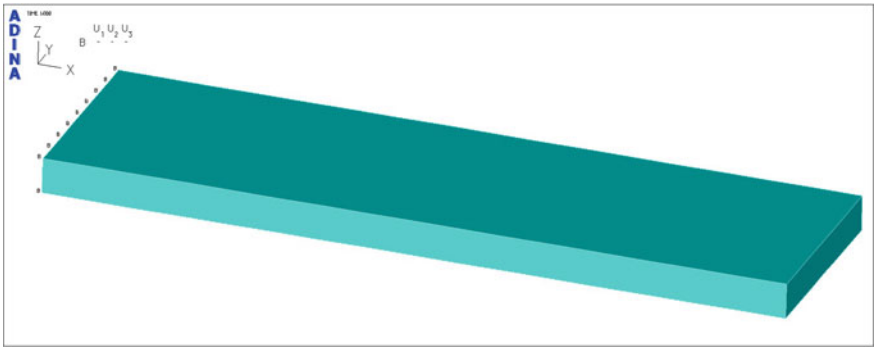

Fig. 7.12 Tridimensional geometry of beam structure with boundary conditions

and displaced by perpendicular distance or moment. If the two forces are P and − P, then the magnitude of the torque is given by $M = P \times d$, where d is the perpendicular distance between the two forces, the arm of the couple. Using $d = 0.01$ and $M = 5$ at the previous formula, we get the magnitude of P, i.e. 500 N. The external force is applied considering two different scenarios: **a** the two opposite forces are applied in two opposite points; **b** the two opposite forces are distributed over the two opposite top widths. Figure 7.13 shows both loading scenarios.

The numerical model consist on a $16 \times 8 \times 1$ mesh of 8-node hexahedron elements, and the results of z-displacement for scenario **a** is of $-0.001035\,m$ and for scenario **b** is of $-0.001042\,m$. The maximum z-displacement of **b** scenario compares better with the exact solution than that obtained for the **a** scenario, but the difference between both values is not significant. Moreover, if higher order hexahedron elements were used, a better solution will be computed.

Figure 7.14 shows the stress σ_{xx} distribution computed by ADINA in both loading scenarios. These values can be compared with the exact solution given by Eq. (7.72) when z = 0.005, which gives 5 MPa.

From Figure 7.14 it can be seen that loading scenario **b** leads to high levels of stress concentration on the neighborhood of the point at which the concentrated load is applied, the maximum stress σ_{xx} on the model is of 24.23 MPa. But at a sufficiently large distance from this point, the maximum stress is coincident to that one of loading scenario **a** [6]. Despite the extra effort in the geometry and mesh modelling of a 3D model, the advantage is quite visible in this example, the analyst can have access to the stress distribution in any arbitrary plane in the complete model.

Although a 3D-Solid finite element doesn't has rotational degrees of freedom, is possible to estimate the rotation of cross section at the free end. For that, one can take into account the x-displacement at the free end. Hence, using the Reissner-Mindlin assumption, the rotation of the beam cross section, in the loading scenario **a**, is given as

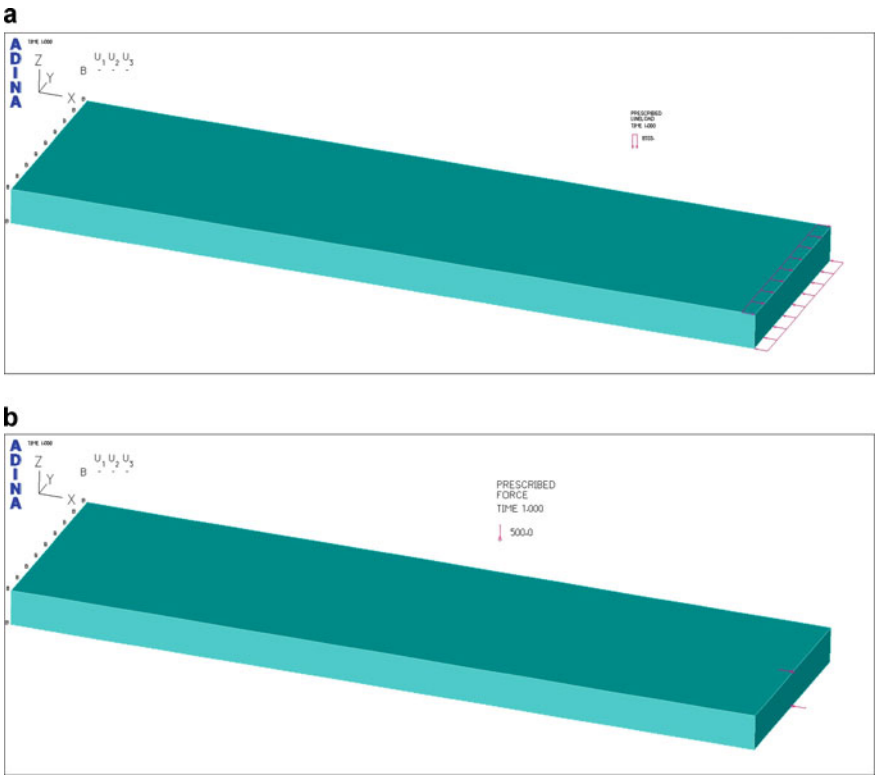

Fig. 7.13 Tridimensional geometry of beam structure and loading scenarios: (**a**) two opposite forces are distributed over the two opposite top widths; (**b**) two opposite forces are applied in two opposite points

$$\phi_2|_{0.21} = artg\left(\frac{u|_{0.21}}{0.005}\right) = artg\left(\frac{4.667 \times 10^{-6}}{0.005}\right) = 0.000933\ rad \tag{7.73}$$

and, in the loading scenario **b**, is given as

$$\phi_2|_{0.21} = artg\left(\frac{u|_{0.21}}{0.005}\right) = artg\left(\frac{6 \times 10^{-6}}{0.005}\right) = 0.0012\ rad \tag{7.74}$$

The value given in Eq. (7.74) is computed in the point at which the concentrated load is applied. Nevertheless, for a node placed far enough of this point, the rotation of the beam cross section is of 0.000935 rad.

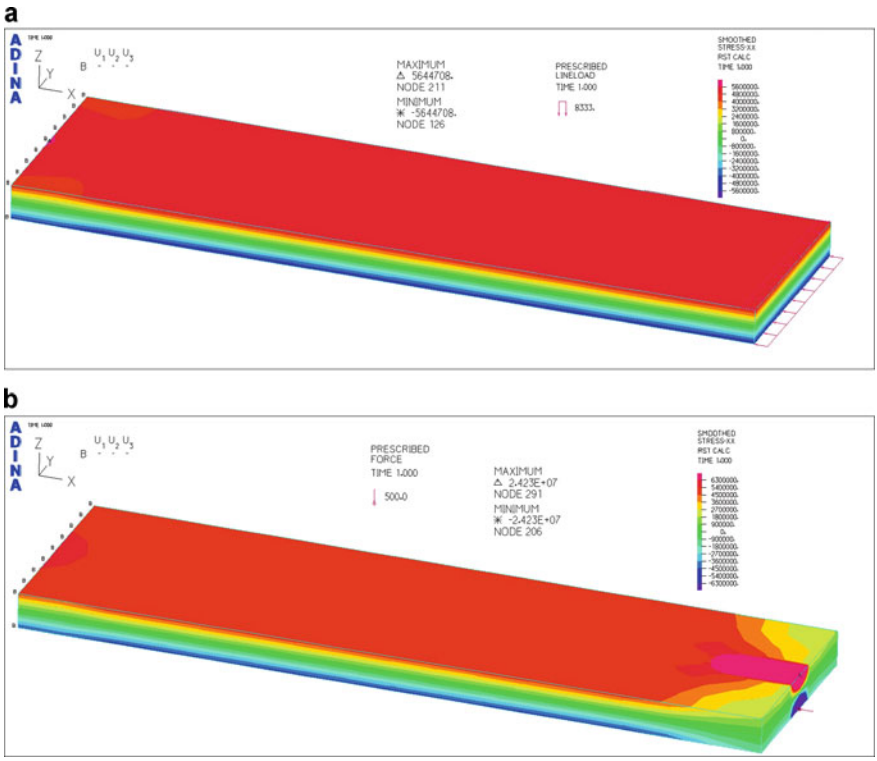

Fig. 7.14 Stress σ_{xx} distribution for cases in which: (**a**) two opposite forces are distributed over the two opposite top widths; (**b**) two opposite forces are applied in two opposite points

7.6 Case Study: Stress Analysis of a Dental Bridge

A dental bridge usually consists of a false tooth or teeth suspended between two supports. The bridge support can be natural teeth, implants or a natural tooth and an implant. Support elements have a height above the soft tissue, and the bridge is cemented in the support elements as one unit. Figure 7.15 illustrates how this is done. While this works well for one missing tooth, or possibly two adjacent missing teeth, it can be inadequate for replacing multiple missing teeth, because long-span bridges may put too much stress on the adjacent teeth. A dental implant consists of a root form that is screwed in the jawbone and then a prosthetic screw is screwed in the implant and then a false crown is attached to that abutment, as is shown in the Fig. 7.15.

Because of the recent growing interest in aesthetics and metal allergies, metal-free restorations have become common treatments. In particular, all-ceramic crowns and fixed partial dentures (FPDs) using zirconia have spread rapidly, and zirconia has been widely used in frameworks of crowns and FPDs due to its unique

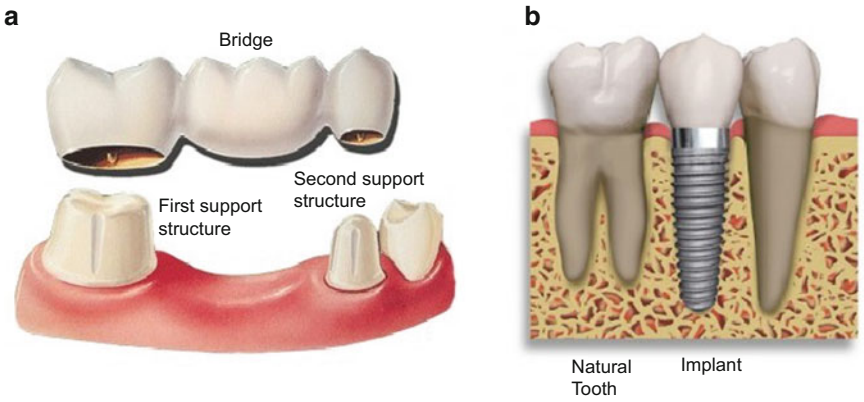

Fig. 7.15 (**a**) Dental bridge components; (**b**) dental implant [7]

mechanical properties [8, 9]. FPDs using zirconia are assumed to improve the rigidity of the bridge and allow them to reduce the distortion under functional loads [10].

In all ceramic fixed partial dentures the connector area is a common fracture location. The survival time of fixed partial dentures may be improved by altering the connector design in regions of maximum tension [11]. Study of such stress distribution is a very active research and, in this case study, an example of modelling a zirconia bridge with 4 teeth (12, 11, 21 and 22- FDI) by the finite element method is used to access the stress distribution.

Meshing

Because the 3D modelling of any structure is generally more complex than the 1D or 2D modelling, in this case, the geometry of the ceramic bridge was scanned optically by the principle of triangulation and, afterwards, the geometrical model of the bridge was imported into ADINA. Figure 7.16 shows a schematic representation of all dental bridge components that were used in the modelling process. The adhesive cement is, generally, a resin with a very small thickness (0.15 mm) and, because the glass ionomer and the resin modified glass ionomer cements had better bonding strength than zinc phosphate and polycarboxylate, the resin based cements are the gold standard for bonding fibre posts owing to their high bonding strength [12]. The first and second supports shown in Fig. 7.16, intend to represent dental implants that can be used to teeth replacement. Hence, in this case study, the bridge was fixed with acrylic resin to duplicate titanium implants, which were fixed at the model base in a region 11 mm below the bridges base.

The meshing process can have a strong effect on the numerical results, thus the quality of mesh has to be prosecuted during a convergence study. The 3D mesh of dental bridge components is shown in Fig. 7.17. The numerical model is divided into three element groups, allowing the analyst to distinguish among

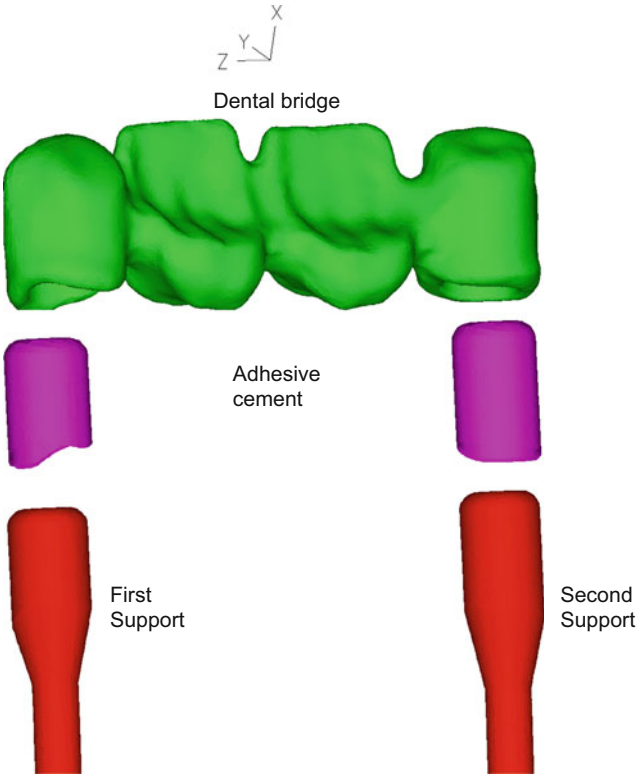

Fig. 7.16 Schematic representation of dental bridge components

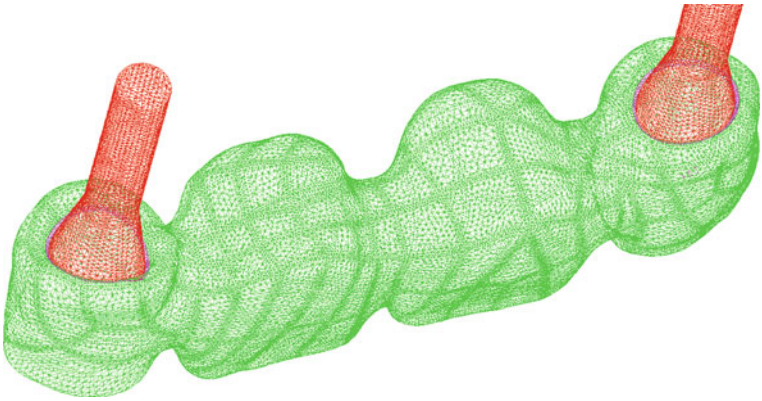

Fig. 7.17 3D mesh of dental bridge components

Table 7.1 Mechanical properties of dental bridge components

Material	Young modulus [GPa]	Poisson's coefficient
Zirconia	210	0.27
Glass ionomer	12	0.3
Titanium	110	0.3

them more conveniently. This division allows also that each element group may has associated different mechanical properties. The mesh can be generated with the help of automatic mesh generators able of treating the relatively complex shape of a dental bridge. Due to the non-convex geometry of the dental bridge, some mesh generators may not be able to mesh it with hexahedron elements. So, the solution shown in Fig. 7.17, is the one that more mesh generators are able to achieve, i.e. the solution that end up with tetrahedron elements.

Material Properties

In this case study, an anterior zirconia dental bridge is cemented over two implants. Therefore, the dental bridge finite model will be considered with the mechanical properties of Zirconia and the finite element model of implants will be modelled using the mechanical properties of titanium. The finite element model of the adhesive cement is represented by a volume with a thickness of 0.15 mm and the mechanical properties of Glass ionomer [9]. As mentioned before, this is an example in which is convenient dividing the model into three element group. In all element groups it is assumed that the materials have isotropic properties, which are listed in Table 7.1.

Loading and Boundary Conditions

Boundary conditions for static analysis are prescribed at the nodes placed in a region 11 mm below the bridges base. The model is constrained in such away that the three nodal degrees of freedom of each node placed on the external surfaces in the region 11 mm below the bridge are restrained. The bridge-adhesive and adhesive-implant interfaces are assumed to be completely bonded without any loosening. For the static analysis a resultant load of 200 N is applied [13]. The load area is located at the middle point of the bridge on the imaginary line that passes through the incisal edge. The direction of the resultant load makes an inclination angle of 130° with the bridge plan, as shown in Fig. 7.18.

Results and Discussion

Running the problem in ADINA, we are able to get the displacement and stress distributions of all dental bridge components. Figure 7.19 shows the displacement distribution obtained in all components, while Fig. 7.20 shows the stress (von-Mises) distribution over the zirconia dental bridge only. From the stress distribution, one can observe that the area that is under higher level of stress is coincident with the loading area, but as in the case of discussion example of Sect. 7.4, this stress level should not be considered for the analysis of the dental bridge behavior. Nevertheless, remaining on the lingual side of the bridge, the higher level of stress

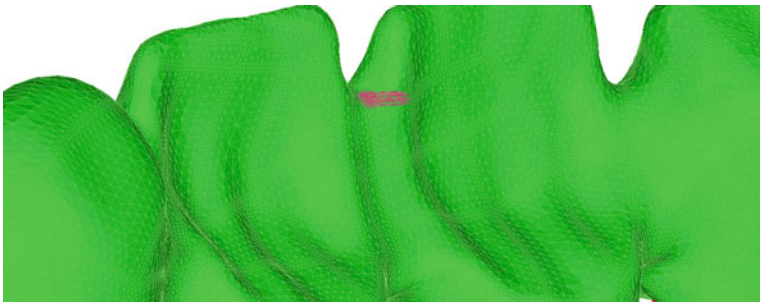

Fig. 7.18 Perspective view of the bridge loading

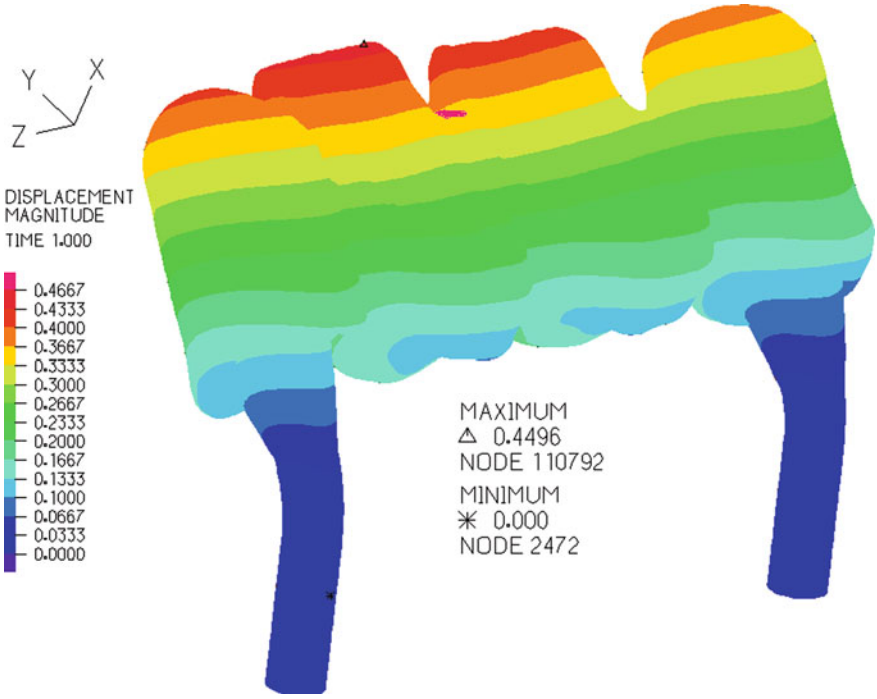

Fig. 7.19 Distribution of the displacement magnitude over the dental bridge

is located at the middle connector just below the loading area and its value is about 300 MPa. Figure 7.21 shows the stress distribution on the buccal side of dental bridge, showing a von-Mises stress of about 315 MPa. From this figure is also possible to conclude that the left side connector is under higher level of stress than the right side connector. The difference of stress on both connector is clearly affected by the connector area, being the connector with a smaller area the one who shows higher stress level.

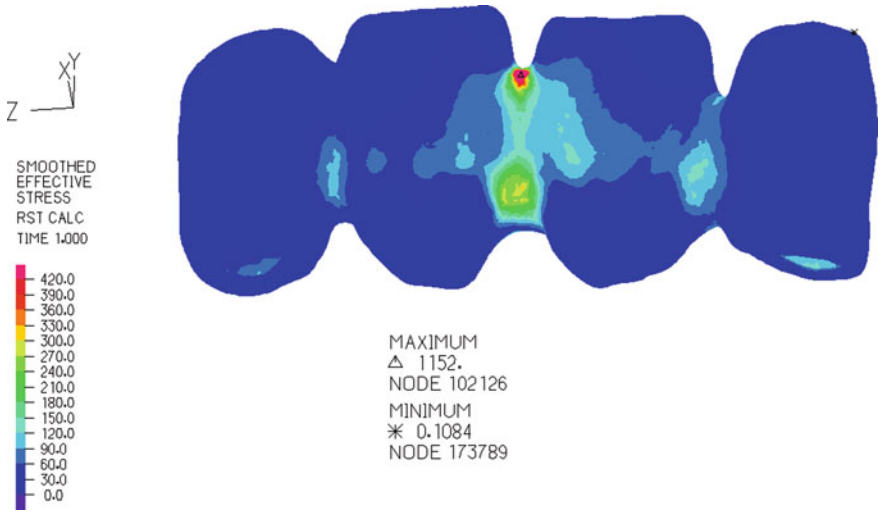

Fig. 7.20 Stress, von-Mises, distribution in the lingual side of dental bridge

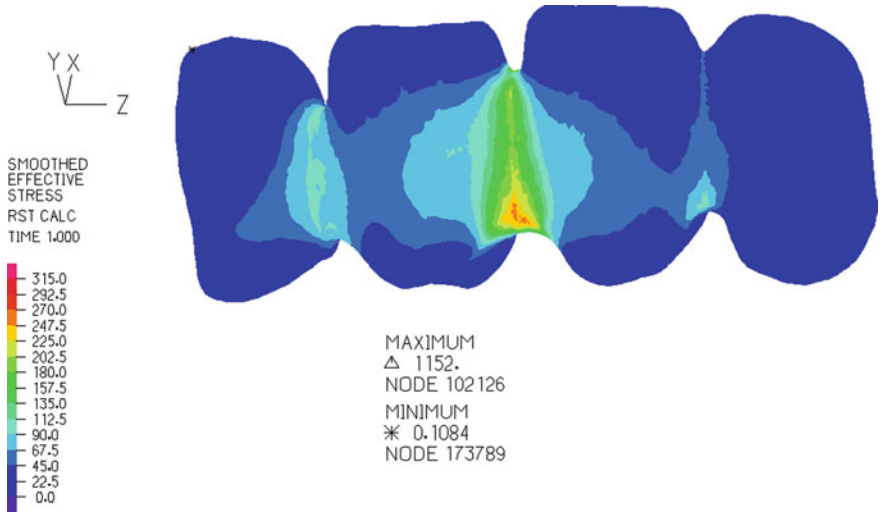

Fig. 7.21 Stress, von-Mises, distribution in the buccal side of dental bridge

Although the number of clinical studies that supports zirconia's performance potential has been growing, the primary issues noted in such studies are related with chipping, wear, and fracture of the veneering ceramics, and fracture that can occur in the most vulnerable part of the connector [14]. The veneering ceramics exhibit some compositional and microstructural differences comparatively to those

used for lithia disilicate-reinforced glass–ceramic, but are manufactured to identical international standards in terms of mechanical properties. So, based on clinical observations, the question arises: whether zirconia veneers are more susceptible to chipping than LDRGC veneers? Answering at this question may comprise the dental bridge model presented here. In fact, Wakabayashi et al. [15] reported that the thickness ratio of the core to the veneer is the dominant factor that controls the failure initiation site in bilayered ceramic disks with a relatively strong core and weak ceramic veneer. So, further research on this issue comprise the generation of dental bridge model that should include ceramic veneer geometry. Nevertheless, because this is a case study that was selected to show some daily practical capabilities of 3D-solid numerical models, further developments are no longer presented.

7.7 Review Questions

1. How many components of the stress tensor is possible to evaluate from a numerical analysis in which 3D-Solid elements are used?
2. What is the difference on the strain approximation when 4-node tetrahedron elements and 8-node hexahedron elements are used?
3. How many Gauss points should be selected for evaluating mass and stiffness matrices for four-node tetrahedron elements?
4. How many Gauss points should be selected for evaluating mass and stiffness matrices for eight-node tetrahedron elements?
5. A simple beam structure is under an end tip load as shown in Fig. 7.22. Consider the following data: Young's modulus of 210 GPa; Poisson's coefficient 0.3. Compute the displacement at the free end plate and the maximum normal stress, using 4-node and 8-node 3D-solid elements. Compare solutions with the theoretical values.

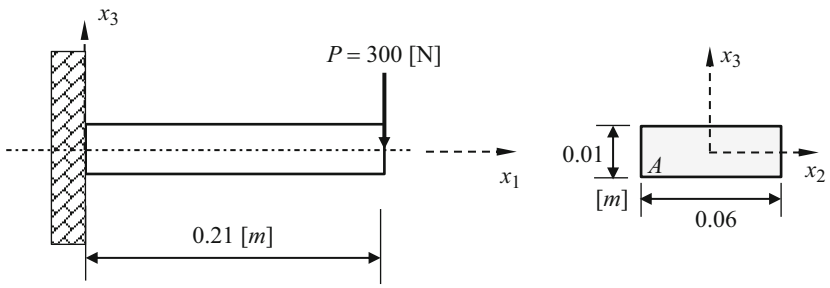

Fig. 7.22 Cantilever beam

References

1. Liu GR, Quek SS (2003) The finite element method: a practical course. Butterworth-Heinemann, Oxford
2. Bathe K-J (1996) Finite element procedures. Hall Prentice, Englewood Cliffs
3. Oñate E (1995) Cálculo de Estructuras por el Método de los Elementos Finitos. Ed. CIMNE
4. Zienkiewicz OC, Taylor RL (2000) The finite element method. Butterworth-Heinemann, Oxford
5. Eisenberg MA, Malvern LE (1973) On finite element integration in natural coordinates. Int J Numer Method Eng 7:574–575
6. Love AEH (1927) A treatise on the mathematical theory of elasticity. Cambridge University Press, London
7. (2015) http://lakeforestdentalarts.com/northshore/chicago-partial-dentures.html
8. Onodera K, Sato T, Nomoto S, Miho O, Yotsuya M (2011) Effect of connector design on fracture resistance of zirconia all-ceramic fixed partial dentures. Bull Tokyo Dent Coll 52(2):61–67
9. Nemoto R, Nozaki K, Fukui Y, Yamashita K, Miura H (2013) Effect of framework design on the surface strain of zirconia fixed partial dentures. Dent Mater J 32(2):289–295
10. Kou W, Kou S, Liu H, Sjögren G (2007) Numerical modeling of the fracture process in a three-unit all-ceramic fixed partial denture. Dent Mater 23(8):1042–1049. doi:10.1016/j.dental.2006.06.039
11. Rezaei SMM, Heidarifar H, Arezodar FF, Azary A, Mokhtarykhoee S (2011) Influence of connector width on the stress distribution of posterior bridges under loading. J Dent (Tehran, Iran) 8(2):67–74
12. Romeed SA, Dunne SM (2013) Stress analysis of different post-luting systems: a three-dimensional finite element analysis. Aust Dent J 58(1):82–88. doi:10.1111/adj.12030
13. Kermanshah H, Bitaraf T, Geramy A (2012) Finite element analysis of IPS Empress II ceramic bridge reinforced by Zirconia Bar. J Dent (Tehran, Iran) 9(4):196–203
14. Lin J, Shinya A, Gomi H, Shinya A (2012) Finite element analysis to compare stress distribution of connector of Lithia disilicate-reinforced glass-ceramic and zirconia-based fixed partial denture. Odontol/Soc Nippon Dent Uni 100(1):96–99. doi:10.1007/s10266-011-0025-2
15. Wakabayashi N, Anusavice KJ (2000) Crack initiation modes in bilayered alumina/porcelain disks as a function of core/veneer thickness ratio and supporting substrate stiffness. J Dent Res 79(6):1398–1404

Chapter 8
Advanced FEM Modelling

This chapter presents a discussion on some modelling techniques for the stress analyses of solids and structures. Mesh symmetry, rigid elements and constraint equations, mesh compatibility, modelling of offsets, supports and connections between elements with different mathematical bases are all covered. Advanced modelling of laminated composite materials are also presented.

8.1 Geometry Modelling

Actually, structural components can have a very complex geometry and the analyst should decide, whenever possible, on how can reduce a complex geometry to a controllable one. In this process, the analyst must decide in what kind of finite element should be used in the numerical model: tridimensional (3D), bidimensional (2D solids, plates or shells) or unidimensional (1D truss, 1D beam) finite elements? The answer to this question requires a good understanding of the mechanics of the problem. Thus, often, the easier answer is to think in 3D elements, since this kind of element can be used for modeling the generality of structures. However, for structures with a complex geometry, it can be extremely expensive if only 3D elements are used within the domain. In fact, the generality of complex structures have on its geometry several ranges of dimensions and, therefore, the mesh is often a combination of different type of elements created to take advantage of that geometrical feature. The analyst should analyze the problem in hands, examining the geometry of the problem domain, and try to make use of 2D and 1D elements for areas or parts of the structure that satisfy the assumptions that lead to the formulation of 2D or 1D elements [1]. This process is very important, because the use of 2D and 1D elements can drastically reduce the number of DOFs.

In Fig. 8.1, is possible to see that the modeling of the geometry of a part, in which 3D elements are used, has the same geometrical shape of the original

M.A. Neto et al., *Engineering Computation of Structures: The Finite Element Method*, DOI 10.1007/978-3-319-17710-6_8

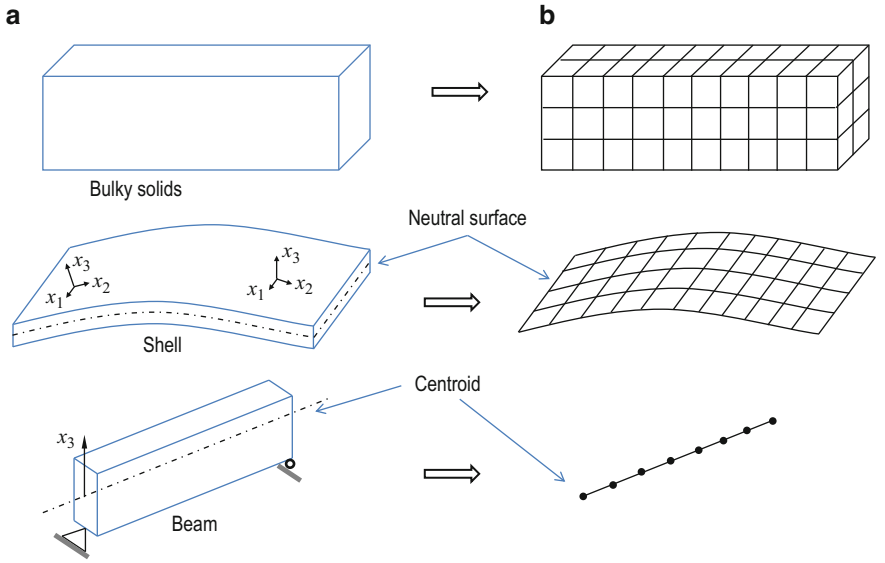

Fig. 8.1 Geometry modeling: (**a**) physical model of the structural component; (**b**) geometry created in the numerical model [1]

structure. Nevertheless, the geometrical modeling of parts of a component in which 2D elements are used needs only the geometric creation of its neutral surface, whereas for parts where 1D elements are used, needs only the geometric creation of its neutral axes. Thus, theoretically, an additional advantage of using 2D or 1D element is that the task of creating geometry can be drastically diminished.

The quantity and the quality of information that is required for the result is another important factor, when it comes to the creation of the problem domain. For instance, if critical results are expected for specific areas, the analysts should give a detailed modelling of the geometry of these areas. Nowadays, many structures are designed using Computer Aided Design (CAD) packages. Therefore, the geometry of such structures is already created electronically. Moreover, most commercial preprocessors of FEM software packages can read certain formats of CAD files. So, making use of these files can reduce the effort in creating the geometry of the structure, but it requires a certain amount of effort to modify the CAD geometry to be suitable for FEM meshing [1].

8.2 Meshing

Finite element mesh generation can be performed by package codes such as Cubit, Fluent, Patran, Adina and etc. these and others mesh generation codes are specially suitable to create initial meshes on complicated geometries arising from assemblies

of mechanical parts such as those found in automobiles, nuclear reactors, and even particle accelerators [2]. For instance, in the automobile industry a common application of finite element method is that of crash simulations involving non-linear computational mechanics [3]. Thus, over the years, automotive engineers have devised certain mesh quality metrics that are used to automatically detect defective meshes [4]. The metrics measure such things as whether or not an individual element within a mesh is inverted, has excessively small or large angles, poor shape, and other undesirable properties. So, in this section, we will give an overview on what may contribute to mesh quality and how it is measured. An interesting point of view of what, exactly, is mesh quality is given by Knupp: Some would say it is a little bit like pornography in that one knows it when one sees it, but can't define it ahead of time [2]. With a more precise definition, Knupp says: Mesh quality concerns the characteristics of a mesh that permit a particular numerical simulation to be efficiently performed, with fidelity to the underlying physics, and with the accuracy required for the problem.

8.2.1 Mesh Density

To minimize the problem DOFs, often, the mesh is created using different density of elements in its several areas, such that a finer mesh is applied in the areas of interest, namely expected zones of stress concentration, re-entrant corners, holes; slots; notches; or cracks. Figure 8.2 shows an example of a finite element mesh with mesh density transition. In this example the gear tooth is meshed with a finer density, in which is located the contact area, and the region at the center of the gear is meshed with a relatively coarse mesh, because this region is not so critical.

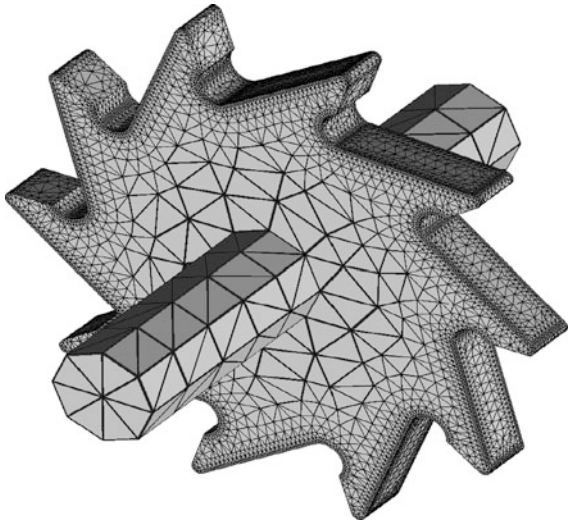

Fig. 8.2 Finite element mesh of a gear

Pre-processors of FEM packages can control the mesh density by using the called mesh density parameters: line, surface, volume subdivisions; the mesh seeds are created before meshing and, after the geometry creation.

8.2.2 Element Distorsion

Since the very early days of finite element research is well known that a distorted finite element is much less accurate than a finite element of regular shape (e.g. a quadrilateral element as compared to a rectangular element). Nevertheless, it is not always possible to create regular shaped elements, especially for cases in which an irregular geometry needs to be meshed. Irregular or distorted elements are acceptable in FEM, but there are limitations, and it is necessary to control the degree of element distortion in the process of mesh generation [1]. The distortion of a finite element is measured against its basic shape, i.e. quadrilateral are measured against square, triangle elements are measured against isosceles triangle, hexahedron elements are measured against Cube and tetrahedron elements are measured against isosceles tetrahedron. In this context, five possible forms of element distortions are listed as follows [5]:

- Aspect ratio: distortion related with the elongation of element, describes the proportional relationship between its width and its height, see Fig. 8.3a.
- Angular distortion: when the angle between edges approaches either 0 degrees and 180 degrees (skew or taper geometry), see Fig. 8.3b. angular distortions occur frequently in practice and are usually unavoidable. For instance, they are present in the transition regions from coarse to finer meshes, next to complicated geometrical boundaries, in meshes generated by automatic mesh generators and, in meshes created by adaptative algorithms.
- Curvature distortion: the straight edges of the element are distorted into curves when matching the nodes to the geometric points, see Fig. 8.3c. In practice, curved-edge distortions occur also very frequently when modeling curved boundary, the edges of the elements that form the boundary have to be curved.
- Volumetric distortion: is the distortion measured by the determinant of the Jacobean matrix and is used to calculating the element stiffness matrix. The Jacobean matrix allows transferring the irregular shape of the element within the physical coordinate system into a regular one in the non-dimensional natural coordinate system. For concave elements there are areas outside the elements that will be transformed into an internal area in the natural coordinate system, see the shadowed area in Fig. 8.4. The element volume integration for the shadowed area based on the natural coordinate system will thus result in a negative value.
- Mid-node position distortion: can occur with higher order elements. Mid nodes should be placed as close as possible to the middle of the element edge. The limit for mid-node displacement away from the middle edge of the element is a quarter of the element edge, as shown in Fig. 8.4b.

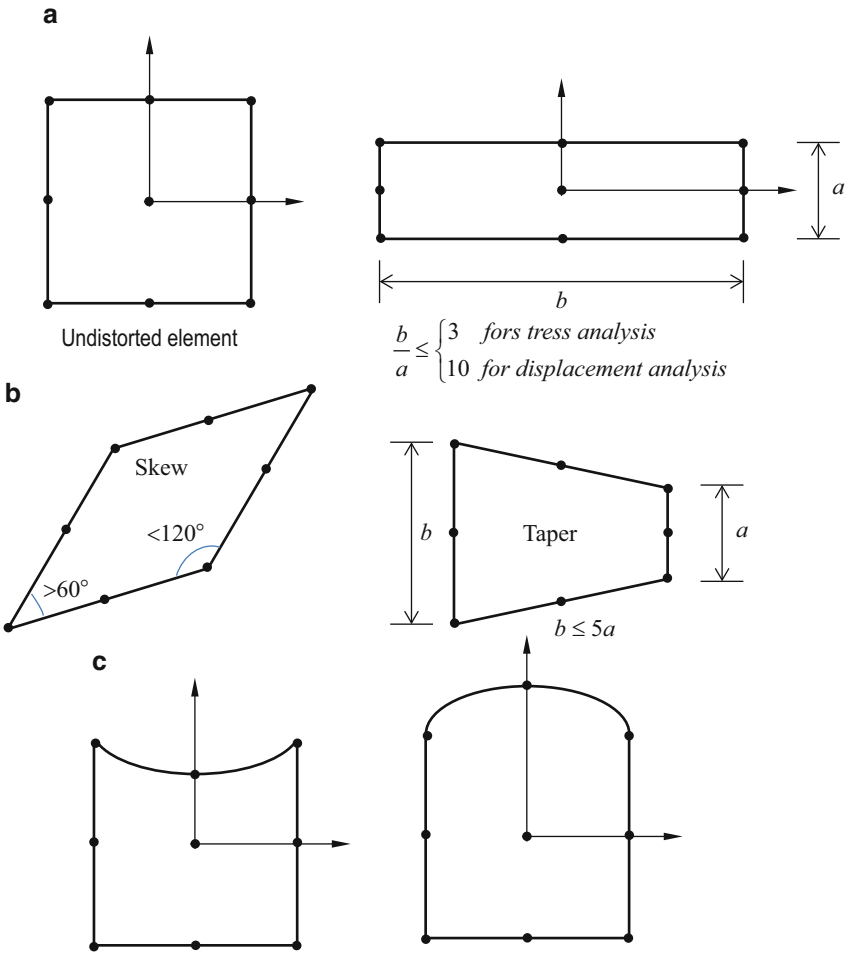

Fig. 8.3 Classification of element distortion: (**a**) aspect ratio; (**b**) angular distortion; (**c**) curvature distortion [1]

Some of the FEM preprocessors have a tool for analyzing the element distortion rate for the created mesh. Moreover, some of FEM packages allow to define limit values to the several distortion classifications and the numerical simulations can only run if these values are not exceed.

8.3 Mesh Compatibility

The finite element method makes use of the assumption of displacement admissibility, which demands continuity of the displacement field in the entire problem domain, and a mesh is said compatible if displacements are continuous

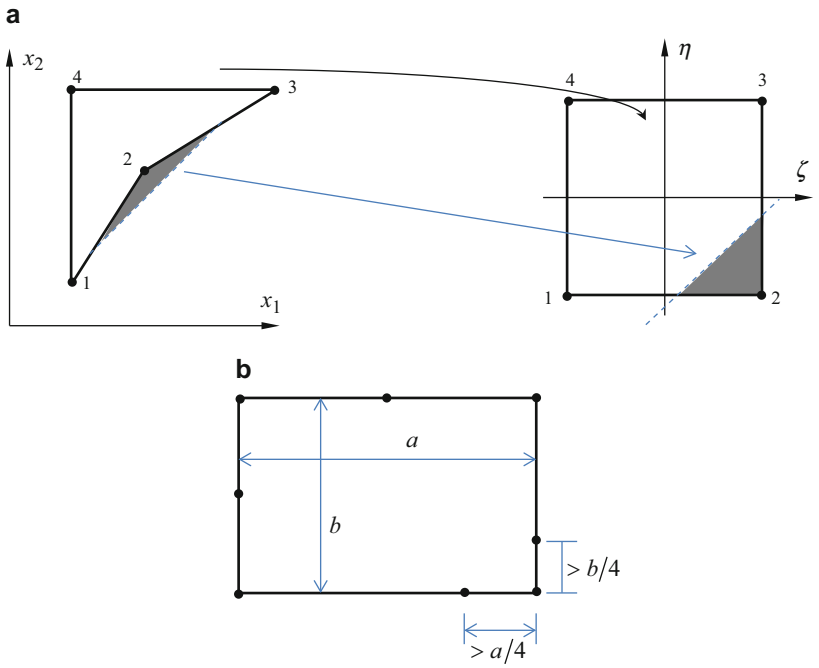

Fig. 8.4 Classification of element distortion: (**a**) Mapping between the physical coordinate and the natural coordinate for volumetric distorted elements; (**b**) limits for the mid-node displacing away from the middle edge of the element [1]

along all the edges of all elements. The use of different types of elements in the same mesh or improper connection of elements can result in an incompatible mesh [1].

8.3.1 Compatibility in the Order of Elements

Generally, high-order elements have a higher number of nodes per element than low-order elements. Thus, mesh incompatibility issues can appear in meshes comprised of different element types, for instance when a quadratic element is joined with one or more linear elements, as shown in Fig. 8.5, an incompatibility due to the difference in the orders of shape functions used appears.

The eight-node element in Fig. 8.5 has quadratic shape functions, which implies that the displacement along the edge follows a quadratic function. On the other hand, the four-node linear element in the same Fig. 8.5 has linear shape function, which result in a linear displacement along each element edge. The combination of both elements within a mesh could result in the two combinations presented in Fig. 8.5a, b. For the case shown in Fig. 8.5a, the displacement of nodes 1 and

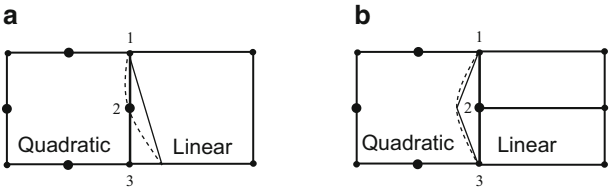

Fig. 8.5 Incompatible mesh caused by different shape functions along a common edge of the quadratic and linear elements: (**a**) a quadratic element connected to a one linear element; (**b**) a quadratic element connected to two linear elements [1, 6]

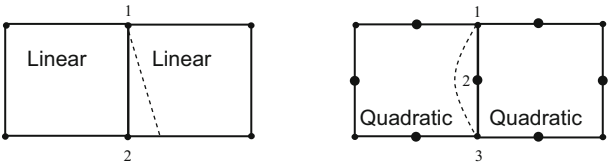

Fig. 8.6 Use of elements of the same type with complete edge-to-edge connection automatically ensures mesh compatibility [1, 6]

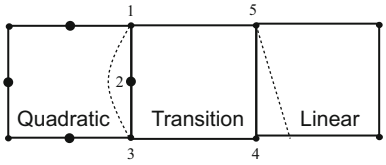

Fig. 8.7 Transition element used to connect quadratic and linear elements, assuring mesh compatibility, in the edge of nodes 1, 2 and 3 the displacement field varies quadratically while along the edge of nodes 4 and 5 varies linearly [1]

3 for the quadratic and the linear element is the same, but displacement of the edges between nodes 1 and 3 will be different [1]. A possible discrepancy in the displacement field along this edge is shown by the dotted lines in Fig. 8.5a. For the case shown in Fig. 8.5b, the incompatible of nodes 1, 2 and 3 for the quadratic element and two linear elements is the same, but displacement of the edges between nodes 1 and 2 and nodes 2 and 3 will be different.

This type of mesh incompatibility can be solved using only one type of element throughout the entire domain. In this case, a complete compatibility is naturally satisfied, see Fig. 8.6. Nevertheless, if for some reason elements of different orders needed to be used, the mesh compatibility can be guaranteed using transition elements. An example of transition elements is shown in Fig. 8.7, which is a five-node element. This element can be obtained from one linear element by adding one additional node along one side, resulting in a quadratic variation of the displacement along this edge, while preserving the linear behavior in the other three

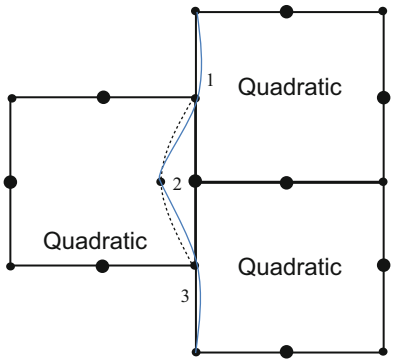

Fig. 8.8 Incompatible mesh caused by sliding element along a common edge [6]

edges. An alternative method that assures the mesh compatibility is based in the use of multipoint constraints (MPC) equations. Nevertheless, this method is more complicated and requires the ability to create constraint equations.

8.3.2 Sliding Incompatibility

The mesh sliding incompatibility is illustrated in Fig. 8.8. This case of incompatibility is the outcome of connecting nodes with different nature: middle-edge and corner nodes. The finite element developers knows that one of major difficulties in the development of finite elements is associated with the continuity requirements, namely the slope inter-element compatibility, see Sect. 6.2.1. Thus, the majority of finite elements meet the requirement of displacement inter-element continuity, while ignoring the complete slope inter-element continuity.

In Fig. 8.8 is possible to see that although the order of the shape functions of these connected elements is the same, the sliding of the left finite element along the edges of the other two right elements can result in incompatible deformation modes of edges comprised between nodes 1 and 2. The dashed line has a different slope than the blue line. The method for fixing the problem of the mesh incompatibility of sliding elements is to make sure that there are no sliding elements in the mesh. Most mesh generators are designed not to produce such an element mesh. However, care needs to be taken in the process of creating a mesh manually [1].

8.4 Mesh Symmetry

A great number of structures and objects show some degree or level of symmetry. Objects such as drinks can exhibit axial symmetry, and even huge structures such as the Eiffel Tower in Paris exhibits mirror symmetry [1]. So, an experienced finite element analyst should be able to take advantage of all structural symmetries during

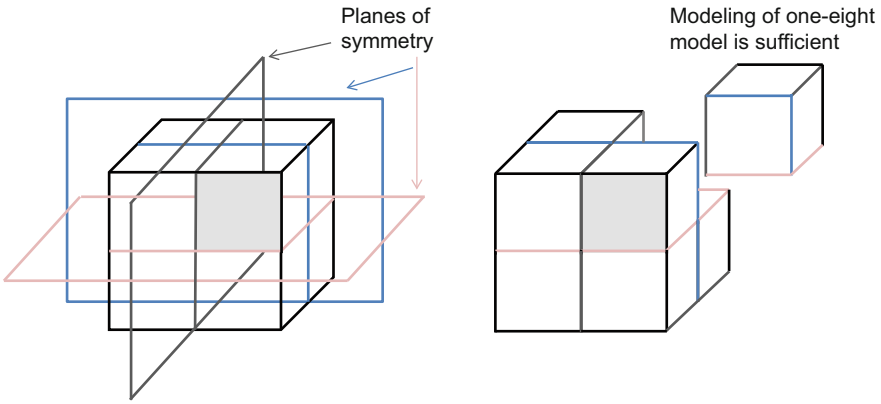

Fig. 8.9 Geometrical model of a cubic block

the modeling process. In fact, because of symmetry properties of some structures the analyst can reduce the total number of degrees of freedom of the system and, therefore, the CPU time used to solve the problem. Moreover, because only a part of the structural model is required during modeling, the time expended by the analyst to create the model is also reduced.

8.4.1 Plane Symmetry

Plane symmetry can also be called mirror symmetry if the symmetry is about a particular plane; moreover, the majority of CAD programs use the term mirror symmetry instead of plane symmetry. The position of the mirror is called the plane of symmetry. A structure is said symmetric if there is symmetry of geometry, support conditions and of material properties. The majority of structures shows only one plane of symmetry, while others are symmetric with respect to multiple planes. An example of these structures is the cubic block presented in Fig. 8.9, the cube geometry has three planes of symmetry and the simplest geometric model is just one-eight of the cube.

The structure presented in Fig. 8.10 is symmetric with respect the axis and, therefore, the right half of the domain can be modeled with imposing the following boundary condition on the line located over the symmetric axis

$$u_1 = 0 \tag{8.1}$$

Loading conditions on a symmetrical structure are of main importance to classify the problem as symmetrical, anti-symmetrical or neither. The loading is considered symmetric if loads can also be reflected off a particular plane, as for the loading in Figs. 8.10 and 8.11. Moreover, because in Fig. 8.11 the support conditions are

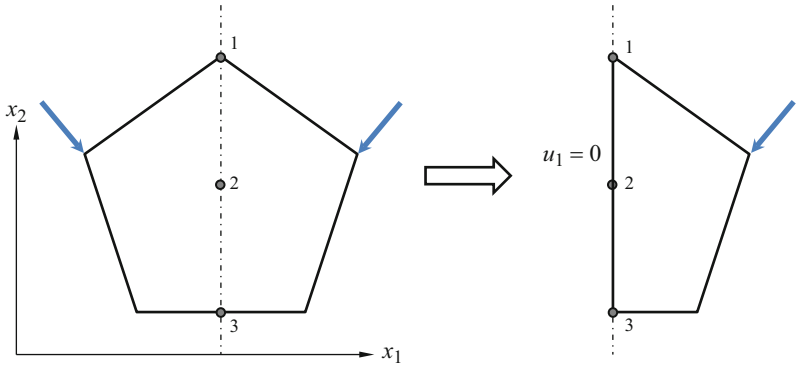

Fig. 8.10 2D solid with an axis of symmetry: the x1 axe. One half of the geometric model is modeled on the right hand side of the figure, imposing symmetric boundary conditions in the line containing the points 1, 2 and 3

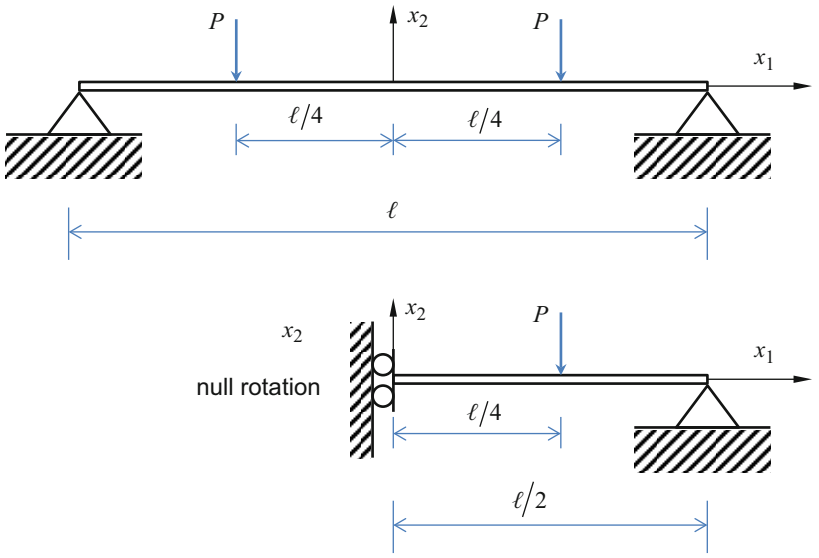

Fig. 8.11 Symmetric beam structure

also symmetric with respect to the axis x_2, the problem is said symmetric, which means that the analysis of half of the whole structure using the symmetric boundary conditions would yield as complete a solution as that of the full model with at least less than a quarter of the effort.

If the structure is symmetric but the loading is anti-symmetric, the problem is said to be anti-symmetric. The problem presented in Fig. 8.11 can be transformed into an anti-symmetric problem using loads on opposite directions. In that case,

modeling half of the structure must be accomplished with anti-symmetric boundary conditions, i.e. the rotation is free and the displacement is zero on the plane of structure symmetry.

When deciding the boundary conditions to the structural plane of symmetry, the following two general rules can be used:

If the problem is symmetric

- There are no translational displacement components normal to the plane of symmetry;
- There are no rotational displacement components with respect to the axes that are parallel to the plane of symmetry.

If the problem is anti- symmetric

- There are no translational displacement components parallel to the plane of symmetry;
- There are no rotational displacement components with respect to the axis that is normal to the plane of symmetry.

8.4.2 Axial Symmetry

A solid or structure is said to have axial symmetry when the solid can be generated by rotating a planar shape about an axis. The stress distribution in an axisymmetric structure is three-dimensional and could be calculated using a 3D solid finite element idealization. However, such a solid can be modelled by simply using special types of 2 or 1D element, called axisymmetric elements. In this way it is possible to take advantage of the axisymmetric geometry of the structure and, depending on the exact loading applied, reduce the modelling and computational efforts. When the load is independent of the angle θ, it is also called axisymmetric. Problems in which both the geometry and load are axisymmetric are named axisymmetric problems. The important characteristic of these axisymmetric problems is that all quantities, be they stress, displacement, strain, or anything else associated with the problem, must be independent of the circumferential variable θ.

Using symmetry conditions, the two components of the displacement field in the section of the body along the axis of symmetry, which define the planar shape of revolution, define completely the state of strain and, therefore, the state of stress. Such a cross-section is presented in Fig. 8.12.

If r and x_3 denote respectively the radial and axial coordinates of a point, with u and v being the corresponding displacements, it can readily be seen that precisely the same displacement functions as those used in Chap. 5 can be used to define the displacements within the finite element [7]. In plane stress or strain problems, the stress or strain components normal to the coordinate plane are not involved, due to zero values of either the stress or the strain. However, in the

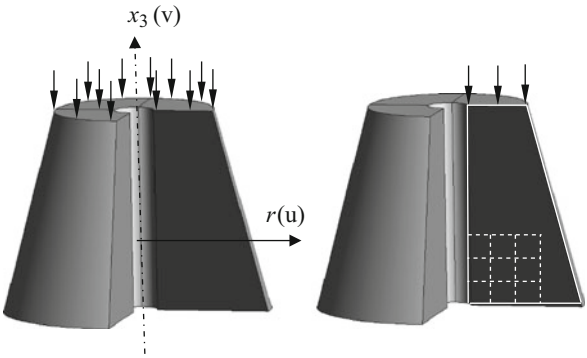

Fig. 8.12 Axial symmetry of a 3D structure, which can be modelled using 2D axisymmetric elements

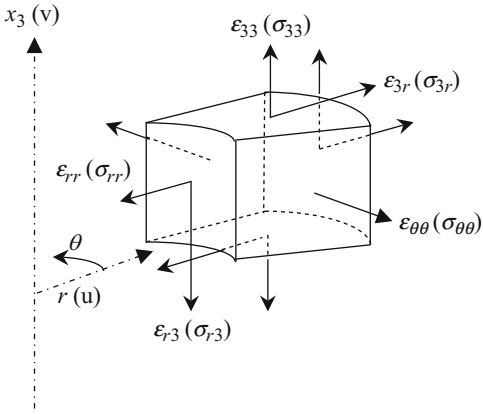

Fig. 8.13 Stress and strain components for an axisymmetrical problem

axisymmetrical situation any radial displacement automatically induces a strain in the circumferential direction, and as the stresses in this direction are certainly non-zero, fourth component of strain and of the associated stress has to be considered. Thus, four components of strain have now to be considered, Fig. 8.13 illustrates and defines these strains and the associated stresses.

8.5 Constraint Equations

In the modelling of beams, plates and shells, the finite element models are defined using the corresponding neutral geometric surface of the structure, as shown in Fig. 8.1. In many applications, stiffened plates are often reinforced by beam-like structures and beams are loaded by off-centroidal forces or linked to others off-centered beams, as shown in Fig. 8.14.

For elements that are not collinear or coplanar, there will be a distance of offset between the nodes in the finite element model. Figure 8.14b and d show typical cases of beams with different thickness joined. For the case of Fig. 8.14b a proper

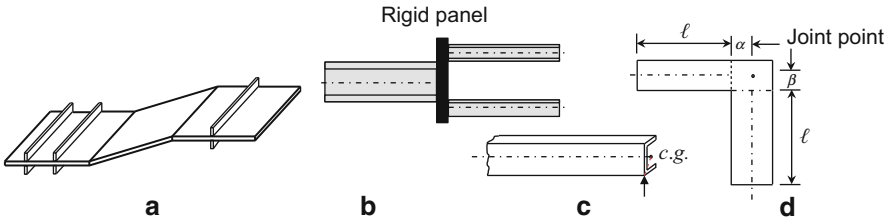

Fig. 8.14 Plate and beams with offset linkages

finite element technique may be needed to model accurately the actual connected situation. In the case of Fig. 8.14d, however, there are two offsets α and β at the corner. In such cases, if the offsets are too small compared to the length of the beam ℓ, we can often ignore it, and the connection is simply modelled by extending the corner nodes to the joint. If the offsets are too large, it has to be treated using proper modelling techniques. Whether offsets should be modelled depends upon the engineering judgment [1]. A rough guideline shown below can be followed:

- If $\ell > 100 \times \alpha$, the offset can be safely ignored;
- If $5 \times \alpha < \ell < 100 \times \alpha$, the offset needs to be modelled;
- If $\ell < 5 \times \alpha$, the ordinary beam, plate and shell elements should not be used.

For the cases where the offset needs to be modelled, there are three methods that can be used: very stiff element; rigid element and constraint equations. Note that constraint equations are only used if the rigid element is not available in the software package or if, being available, the rigid elements doesn't are suitable for the recommend design. The methodologies that making use of very stiff elements are based on the application on an artificial element with very high stiffness (high Young's modulus, large second moment of inertia or large cross-sectional area). Generally, this is done by increasing the Young's modulus by a factor of about 10^6. This method is very simple and convenient to use, but because can leads to a large difference in stiffness among the elements, is not recommended. Alternatively, is possible to use rigid elements or rigid links. Rigid links are special constraint equations, which can be established automatically by the program between two nodes, a master node and a slave node. As the nodes displace due to deformation, the slave node is constrained to translate and rotate such that the distance between the master node and the slave node remains constant, and that the rotations at the slave node are the same as the corresponding rotations at the master node [8].

8.5.1 Creation of Constraint Equations

The main idea of using constraint equations is ensuring that the relative displacement between two nodes is according the connection between them. This happens for cases in which the finite element analysis of a structure involves the mixing

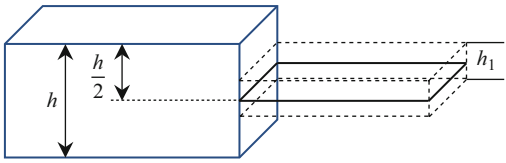

Fig. 8.15 Solid and plate linkages

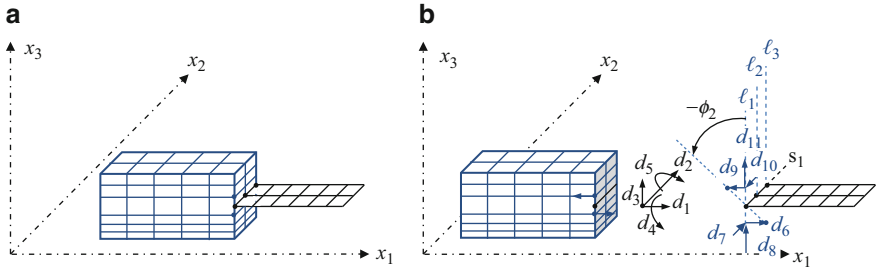

Fig. 8.16 Solid and plate linkages

elements of different type. For instance, assume that the connection between 3D solid elements and shell elements presented in Fig. 8.15 is necessary. Because solid elements provide stiffness in only the three displacement directions and a shell element provide also the stiffness for two rotations, solid and shell elements are incompatible. So, to connect the two dissimilar elements together, is necessary create constraint equations to account for the rotational degrees of freedom defined in the shell element.

First, we consider the connection among shell and solid finite elements in the way shown in Fig. 8.16a. A node in a solid element has three DOFs: translational displacement components u, v and w; whereas a node in a shell element has five (or six) DOFs: three translational displacement components u, v and w; and two rotational DOF. The nodes at the interface (white nodes) are not shared among 3D solid and shell elements, which means that continuity of translational displacements can only by ensured if mesh compatibility on the displacement interface is assured. For that, let assume that the first edge of 3D solid element is coincident with the edge 7–3 of the hexahedron presented in Fig. 7.6. So, along this edge, the displacements can be interpolated as

$$\begin{aligned} d_{x_1} &= N_3 d_6 + N_7 d_9 \\ d_{x_2} &= N_3 d_7 + N_7 d_{10} \\ d_{x_3} &= N_3 d_8 + N_7 d_{11} \end{aligned} \tag{8.2}$$

and the displacement at the white node can be obtained substituting the coordinates ($\xi = 1,\ \eta = 1,\ \zeta = 0$) in shape functions, as

$$
\begin{aligned}
d_1 &= d_{x_1}\,(\xi = 1,\ \eta = 1,\ \zeta = 0) = \frac{d_6 + d_9}{2} \\
d_2 &= d_{x_2}\,(\xi = 1,\ \eta = 1,\ \zeta = 0) = \frac{d_7 + d_{10}}{2} \\
d_3 &= d_{x_3}\,(\xi = 1,\ \eta = 1,\ \zeta = 0) = \frac{d_8 + d_{11}}{2}
\end{aligned}
\tag{8.3}
$$

Constraint equations on the form of Eq. (8.3) can also be used to solve mesh incompatibilities of type presented in Fig. 8.7.

Nevertheless, the rotational DOFs of shell nodes are still free. Therefore, the shell can rotate freely with respect to the solid structure and the continuity of the rotational movement between both structures is not assured. This is because the shell rotational movement cannot be transmitted onto the node of a 3D solid element, simply because it does not account for the rotational DOF. An effective method to fix the rotation of the shell structure on the 3D solid mesh is to use constraint equations to create a rotational connection between the two types of elements. The detailed process is given as follows. First, assume that there is a very thin rigid welded joint, assuring the connection between the shell and the solid, as shown in Fig. 8.16b. This welded joint connects three nodes together, one in the shell and two on the solid. These three nodes have to move together with the rigid welded. Thus, following classical or Reissner-Mindlin plate theories assumption, which states that the transverse normal of the plate remains straight during deformation, the constraint equations are given as:

$$
\begin{aligned}
d_4 &= \phi_1 = \frac{d_7 - d_{10}}{h_1} \\
d_5 &= -\phi_2 = \frac{d_9 - d_6}{h_1}
\end{aligned}
\tag{8.4}
$$

In which small values of rotations are assumed, meaning that $\sin\phi_2 \approx \phi_2$ and $\sin\phi_1 \approx \phi_1$.

In many practical application some portions of a structure are best modeled with shell elements and others with solids. A very simple example that can be used to study this kind of approaches is a cantilever beam loaded at the tip as presented in Fig. 8.17a.

A $0.2032 \times 0.0254 \times 0.00635\ \text{mm}^3$ (l × b × h) aluminum beam is used to investigate different interfaces connections. The beam Young's modulus is of 68.9475 GPa and the Poisson ratio is of 0.3. The load at the tip is of 266.89 N and acts in the x_3 direction. The theoretical solutions for bending deflection and stress can be provided by beam theory, which not includes end effects and assumes that plane sections remain plane after bending. However, the solutions obtained with models presented at Fig. 8.17b, c and d include end effects. The finite element model in Fig. 8.17b contains implicitly 3D-Solid hexahedrons with 8 and 20 nodes, which are denoted by acronyms H8 and H20, respectively, while the finite element model in Fig. 8.17c

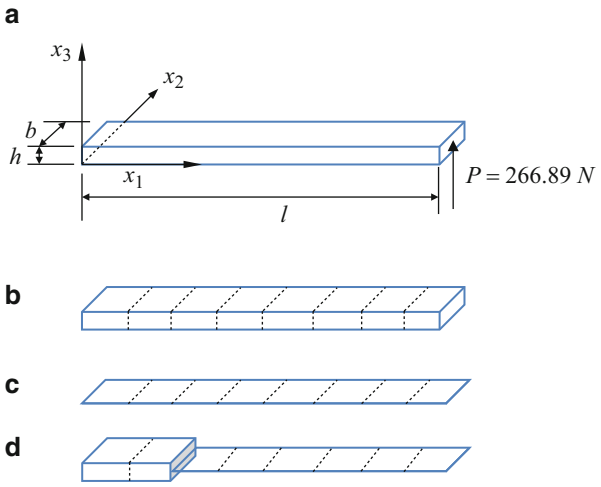

Fig. 8.17 Cantilever beam loaded at the tip: (**a**) geometrical dimensions; (**b**) 3D-solid finite model; (**c**) shell finite model; (**d**) finite model using 3D-solid and shell elements

contains implicitly Shell elements with 4 and 8 nodes, which acronyms are Q4 and Q8, respectively. Figure 8.17d shows the numerical model using interfaces: H8Q4 that is the interfacing model of 8-node Hexa and 4-node shell elements; H20Q8 is the interfacing model of 20-node Hexa and 8-node shell elements. In all numerical models, the load is distributed over the beam tip element face.

Figure 8.18a show the linear numerical solutions (Beam, Q4 and H8) for the variation of the displacement along the beam span. The worst solution was obtained by the H8 numerical model, because of geometrical dimensions and of bending solicitation of the beam. Nevertheless, increasing the mesh density of this numerical model may leads to an improvement of the solution presented in Fig. 8.18a.

The solution of the H8Q4 model is closer to the beam solution than the H8 solution, but is not as closer as the Q4 solution. This behavior can be explained by the use of constraint Eq. (8.4), this equation states that the rotational degrees of freedom of shell interface nodes are dependent on the displacement of the solid interface nodes and, because the displacement solution of the H8 is stiffer than the theoretical one, the rotational degrees of freedom of the shell interface nodes are under approximated, as shown in Fig. 8.19a, b. The solution of H20Q8 model is very close to the beam and Q8 solutions and, as can be seen in Fig. 8.19c, in this case the rotational degrees of freedom of the shell interface nodes are better approximated from the displacement of the solid interface nodes. The effect of different interfaces connection in the normal stress is shown on Fig. 8.20, in which is possible to seen that both interfaces have perturbation of stress continuity in the interface nodes, being higher for the case of H8Q4 model.

Figure 8.21 shows a finite element model created with shell and 3D-Solid finite elements, the difference between this model and the H8Q4 model is related with the position of the solid part. The solutions of this model, denoted by Q4H8, are presented in Fig. 8.22.

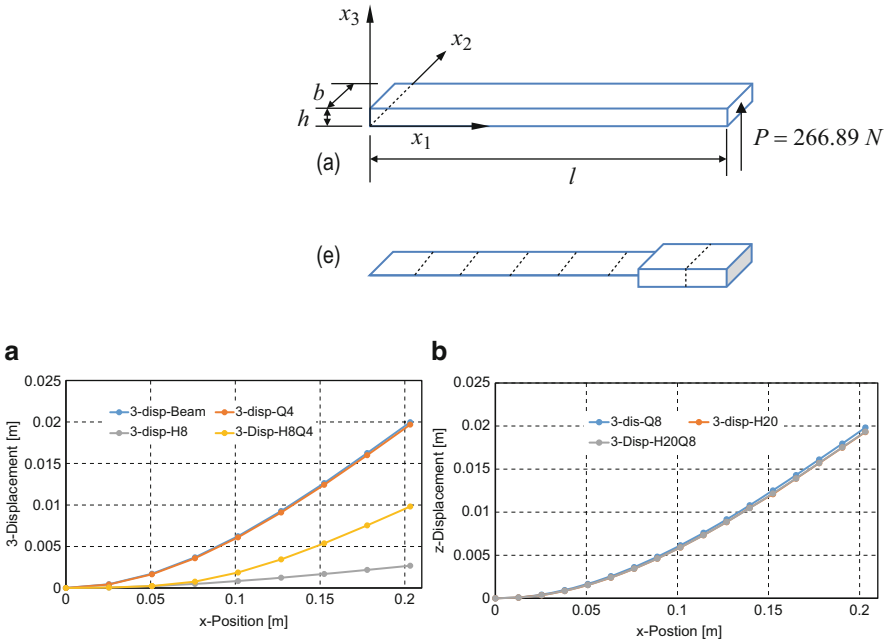

Fig. 8.18 Variation of x_3 displacement along the beam span: (**a**) linear numerical models; (**b**) quadratic numerical models

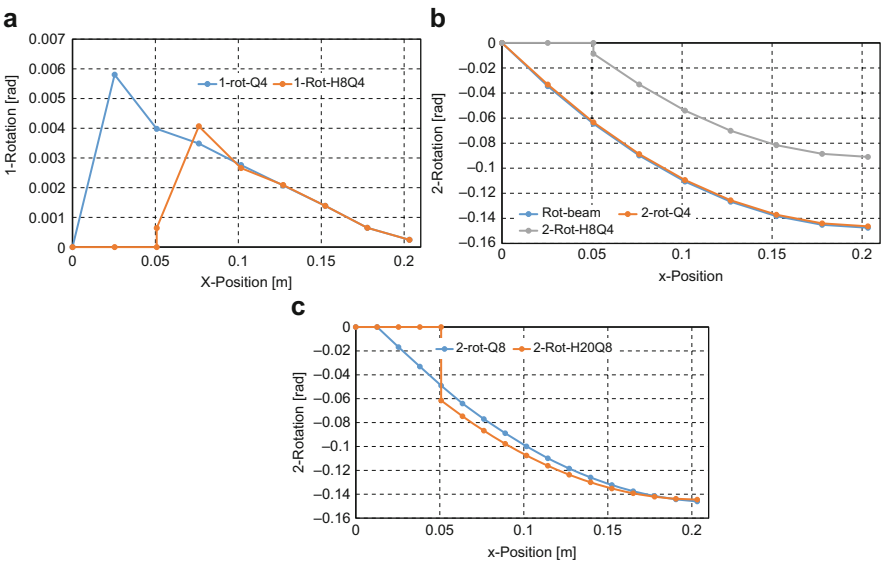

Fig. 8.19 Variation of rotational degrees of freedom along the beam span: (**a**) rotation about axis x1 in linear models; (**b**) rotation about axis x2 in linear models; (**c**) rotation about axis x2 in quadratic models

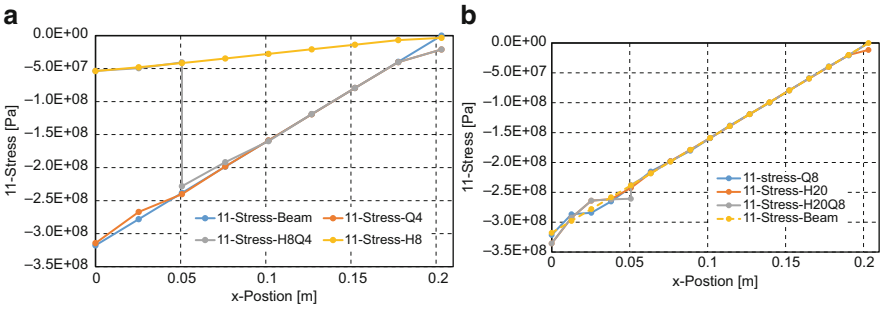

Fig. 8.20 Variation of normal stress, σ_{11}, along the beam span: (**a**) in linear models; (**b**) in quadratic models

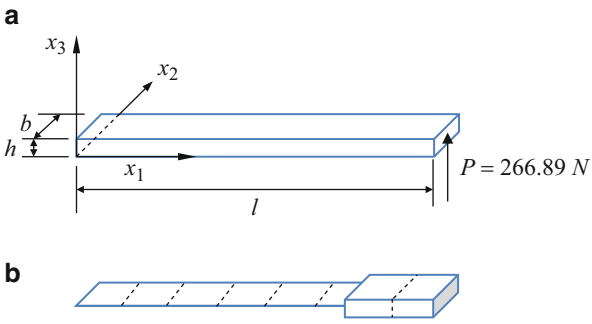

Fig. 8.21 (**a**) Cantilever beam load at the tip; (**b**) finite element model using shell and 3D-solid elements

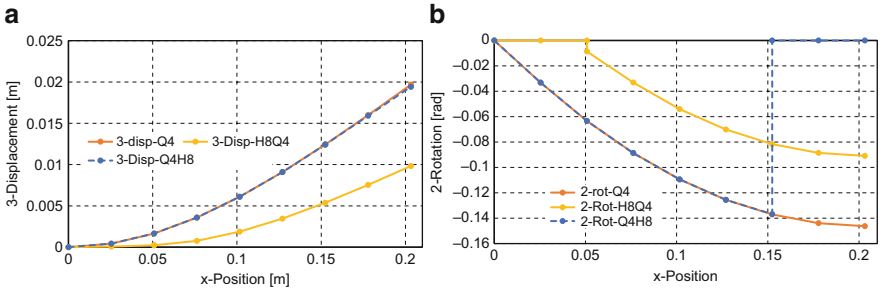

Fig. 8.22 Cantilever beam results: (**a**) Variation of x3 displacement along the beam span; (**b**) rotation about axis x2 in linear models

Figure 8.22 shows that changing the location of the solid part may leads to a better approximation of displacements and rotational degrees of freedom. This behavior can be justified with the different effect of Eq. (8.4) on the shell structure: in the H8Q4 model Eq. (8.4) seems to be a rigid boundary condition to the shell structure, while in the Q4H8 model the Eq. (8.4) represents a load condition to the shell structure. So, in this second situation, the forces from solids elements are well

introduced as moments and forces into shell elements, while in the H8Q4 model the shell structure is over-constrained. Hence, a finite element analyst is faced with simplification issues that can be used to save computational time, however, the simplification itself could be very time consuming and, eventually, an additional source of errors. So, knowledge, experience and engineering judgment are very important in the finite element modelling of a system.

8.6 Material Modelling

Materials modelling is as vast as the types of existing materials. For decades, emphasis has been placed on structural (metals, polymers, composites, etc.) and geotechnical (soils and rocks) classical materials. Behavior prediction of such materials subjected to a given load (mechanical or thermal) in process operations or stress – strain/heat transfer analysis has constituted the bulk of numerical approaches available in the literature. The existing solution approaches are comprehensive and provide accurate results for most classical materials subjected to strain paths of reasonable complexity [9].

In the framework of finite element formulation, material modelling issues allow that a finite element can be used to the response prediction of problems in which specific constitutive descriptions are necessary. In fact, finite element equations contain displacement and strain-displacement matrices plus the material constitutive matrix. Displacement matrices are related with the mathematical models that can be used to summarize the displacement field of a physical problem, while strain-displacement matrices arise naturally from the kinematic analysis of a deformable body, in which the displacements of the material particles are assumed to be much smaller than any relevant dimension of the body, and the stress may be described as a mobilized internal material reaction which resists any tendency towards deformation. But, the stress and strain tensors are insufficient for description of the mechanical behavior of deformable bodies [10]. Body deformations depend on the applied forces and the force-displacement or the stress-deformation relationship depends on the material of the body. Therefore, to complete the specification of the mechanical behavior of a body we require additional equations. These equations are called the constitutive equations and serve to distinguish one material from another [10]. The main purpose of this section is to present some fundamental aspects related to the use of material laws in linear finite element analysis.

8.6.1 Generalized Hooke's Law

It has been found experimentally that for most solid materials, the measured strains are proportionally to the applied forces, as long as the load does not exceed the elastic limit. This experimental observation can be stated as follows: the stress

components at any point in the body are a linear function of the strain components [10]. This statement tracks the generalized Hooke's law and is only valid for linear elastic materials. Hence, the generalized Hooke's law allows relating the nine components of stress to the nine components of strain as [11]

$$\sigma_{ij} = c_{ijkl}\varepsilon_{kl};\ \ i,j,k,l = 1,2,3 \tag{8.5}$$

Where σ_{ij} are the components of the second order tensor known as the Cauchy stress tensor, ε_{kl} are the infinitesimal components of another second order tensor known as strain tensor and c_{ijkl} is a fourth order tensor known as the stiffness tensor and its individual components are the material coefficients. The nine equations presented at Eq. (8.5) contains a total of 81 material coefficients. However, as explained in Sect. 1.1.2, the state of stress of a point is completely defined with the knowledge of only six stress components, σ_{ij}. Moreover, due to the symmetry of both stress and strain tensors, the state of stress is often written in the form of Eq. (1.9). The reduction in the number of material coefficients can be explained as follows: the σ_{ji} stress components can be obtained as

$$\sigma_{ji} = c_{jikl}\varepsilon_{kl};\ \ i,j,k,l = 1,2,3 \tag{8.6}$$

Subtracting Eqs. (8.6) and (8.5) leads to

$$\sigma_{ij} - \sigma_{ji} = \left(c_{ijkl} - c_{jikl}\right)\varepsilon_{kl} = 0 \Rightarrow c_{ijkl} = c_{jikl} \tag{8.7}$$

and, because the strain components are also symmetric, Eq. (8.5) can be written as

$$\sigma_{ij} = c_{ijlk}\varepsilon_{lk};\ \ i,j,k,l = 1,2,3 \tag{8.8}$$

Subtracting Eq. (8.8) from Eq. (8.5), the equation obtained is defined as

$$\sigma_{ij} - \sigma_{ij} = \left(c_{ijkl} - c_{ijlk}\right)\varepsilon_{kl} = 0 \Rightarrow c_{ijkl} = c_{ijlk} \tag{8.9}$$

Hence, because both $c_{ijkl} = c_{jikl}$ and $c_{ijkl} = c_{ijlk}$ relations are true, there are only 36 independent elastic coefficients and the generalized form of Hooke's law may thus be written as

$$\begin{cases} \sigma_{11} = c_{11}\varepsilon_{11} + c_{12}\varepsilon_{22} + c_{13}\varepsilon_{33} + c_{14}\gamma_{23} + c_{15}\gamma_{13} + c_{16}\gamma_{12} \\ \sigma_{22} = c_{21}\varepsilon_{11} + c_{22}\varepsilon_{22} + c_{23}\varepsilon_{33} + c_{24}\gamma_{23} + c_{25}\gamma_{13} + c_{26}\gamma_{12} \\ \sigma_{33} = c_{31}\varepsilon_{11} + c_{32}\varepsilon_{22} + c_{33}\varepsilon_{33} + c_{34}\gamma_{23} + c_{35}\gamma_{13} + c_{36}\gamma_{12} \\ \sigma_{23} = c_{41}\varepsilon_{11} + c_{42}\varepsilon_{22} + c_{43}\varepsilon_{33} + c_{44}\gamma_{23} + c_{45}\gamma_{13} + c_{46}\gamma_{12} \\ \sigma_{13} = c_{51}\varepsilon_{11} + c_{52}\varepsilon_{22} + c_{53}\varepsilon_{33} + c_{54}\gamma_{23} + c_{55}\gamma_{13} + c_{56}\gamma_{12} \\ \sigma_{12} = c_{61}\varepsilon_{11} + c_{62}\varepsilon_{22} + c_{63}\varepsilon_{33} + c_{64}\gamma_{23} + c_{65}\gamma_{13} + c_{66}\gamma_{12} \end{cases} \tag{8.10}$$

Nevertheless, as shown in Eq. (1.9), the number of independent material coefficients can be further reduced. So, let U_0 be the strain energy per unit of volume that represent the work done by internal stress and is given as [10]

$$dU_0 = \boldsymbol{\sigma}^T d\boldsymbol{\varepsilon} \tag{8.11}$$

with the property that

$$\boldsymbol{\sigma} = \left(\frac{\partial U_0}{\partial \boldsymbol{\varepsilon}}\right)^T; \ \sigma_{ij} = \frac{\partial U_0}{\partial \varepsilon_{ij}}, \ \ i,j = 1,2,3 \tag{8.12}$$

Using Eq. (8.10) into Eq. (8.11) is possible to conclude that the strain energy per unit of volume is a quadratic function of strain, meaning that its second order derivative with respect the strain components should be constant.

Equations (8.10) and (8.12) yield

$$\begin{cases} \sigma_{11} = \dfrac{\partial U_0}{\partial \varepsilon_{11}} = c_{11}\varepsilon_{11} + c_{12}\varepsilon_{22} + c_{13}\varepsilon_{33} + c_{14}\gamma_{23} + c_{15}\gamma_{13} + c_{16}\gamma_{12} \\ \sigma_{22} = \dfrac{\partial U_0}{\partial \varepsilon_{22}} = c_{21}\varepsilon_{11} + c_{22}\varepsilon_{22} + c_{23}\varepsilon_{33} + c_{24}\gamma_{23} + c_{25}\gamma_{13} + c_{26}\gamma_{12} \\ \sigma_{33} = \dfrac{\partial U_0}{\partial \varepsilon_{33}} = c_{31}\varepsilon_{11} + c_{32}\varepsilon_{22} + c_{33}\varepsilon_{33} + c_{34}\gamma_{23} + c_{35}\gamma_{13} + c_{36}\gamma_{12} \\ \sigma_{23} = \dfrac{\partial U_0}{\partial \gamma_{23}} = c_{41}\varepsilon_{11} + c_{42}\varepsilon_{22} + c_{43}\varepsilon_{33} + c_{44}\gamma_{23} + c_{45}\gamma_{13} + c_{46}\gamma_{12} \\ \sigma_{13} = \dfrac{\partial U_0}{\partial \gamma_{13}} = c_{51}\varepsilon_{11} + c_{52}\varepsilon_{22} + c_{53}\varepsilon_{33} + c_{54}\gamma_{23} + c_{55}\gamma_{13} + c_{56}\gamma_{12} \\ \sigma_{12} = \dfrac{\partial U_0}{\partial \gamma_{12}} = c_{61}\varepsilon_{11} + c_{62}\varepsilon_{22} + c_{63}\varepsilon_{33} + c_{64}\gamma_{23} + c_{65}\gamma_{13} + c_{66}\gamma_{12} \end{cases} \tag{8.13}$$

So, the differentiation of Eq. (8.13) yields

$$\begin{cases} \dfrac{\partial \sigma_{22}}{\partial \varepsilon_{11}} = \dfrac{\partial^2 U_0}{\partial \varepsilon_{11}\partial \varepsilon_{22}} = c_{21} = \dfrac{\partial \sigma_{11}}{\partial \varepsilon_{22}} = \dfrac{\partial^2 U_0}{\partial \varepsilon_{22}\partial \varepsilon_{11}} = c_{12} \\ \dfrac{\partial \sigma_{33}}{\partial \varepsilon_{11}} = \dfrac{\partial^2 U_0}{\partial \varepsilon_{11}\partial \varepsilon_{33}} = c_{31} = \dfrac{\partial \sigma_{11}}{\partial \varepsilon_{33}} = \dfrac{\partial^2 U_0}{\partial \varepsilon_{33}\partial \varepsilon_{11}} = c_{13} \\ \qquad\qquad\qquad\qquad \vdots \\ \dfrac{\partial \sigma_{12}}{\partial \varepsilon_{11}} = \dfrac{\partial^2 U_0}{\partial \varepsilon_{11}\partial \gamma_{12}} = c_{61} = \dfrac{\partial \sigma_{11}}{\partial \gamma_{12}} = \dfrac{\partial^2 U_0}{\partial \gamma_{12}\partial \varepsilon_{11}} = c_{16} \end{cases} \tag{8.14}$$

That is $c_{ij} = c_{ji}$, which shows that the matrix of elastic coefficients is symmetric and, therefore, there are only 21 independent elastic coefficients for a general anisotropic linearly elastic material.

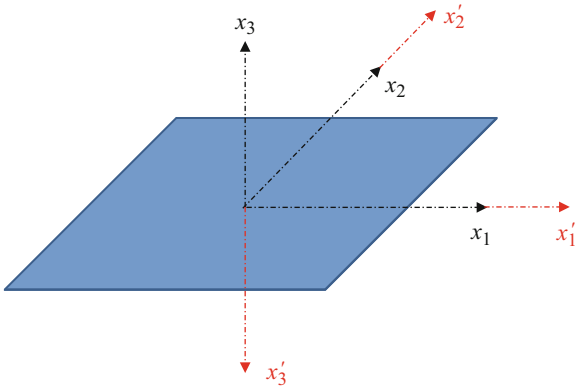

Fig. 8.23 Material symmetry about plane x_1x_2

8.6.2 Material Symmetry

In some kind of structural materials there are special kinds of material symmetry for which elastic coefficients may remain invariant under a coordinate transformation. For instance, consider that an anisotropic material has only one plane of material symmetry. A material with one plane of material symmetry is called a monoclinic material.

Let consider the x_1x_2 plane as the plane of material symmetry. This case is illustrated in Fig. 8.23, and can be given by the following transformation:

$$x_1' = x_1;\ x_2' = x_2;\ x_3' = -x_3 \tag{8.15}$$

that gives the following transformation matrix

$$\mathbf{A} = \begin{bmatrix} 1 & 0 & 0 \\ 0 & 1 & 0 \\ 0 & 0 & -1 \end{bmatrix} \tag{8.16}$$

and the transformed stress and strain tensors $\boldsymbol{\sigma}'$ and $\boldsymbol{\varepsilon}'$ are given, respectively, as

$$\begin{aligned} \boldsymbol{\sigma}' &= \mathbf{A}^{\mathbf{T}}\boldsymbol{\sigma}\ \mathbf{A} \\ \boldsymbol{\varepsilon}' &= \mathbf{A}^{\mathbf{T}}\boldsymbol{\varepsilon}\ \mathbf{A} \end{aligned} \tag{8.17}$$

Which yields

$$\begin{bmatrix} \sigma_{11}' & \sigma_{12}' & \sigma_{13}' \\ & \sigma_{22}' & \sigma_{23}' \\ Sym & & \sigma_{33}' \end{bmatrix} = \begin{bmatrix} \sigma_{11} & \sigma_{12} & -\sigma_{13} \\ & \sigma_{22} & -\sigma_{23} \\ Sym & & \sigma_{33} \end{bmatrix} \tag{8.18}$$

$$\begin{bmatrix} \varepsilon'_{11} & \varepsilon'_{12} & \varepsilon'_{13} \\ & \varepsilon'_{22} & \varepsilon'_{23} \\ Sym & & \varepsilon'_{33} \end{bmatrix} = \begin{bmatrix} \varepsilon_{11} & \varepsilon_{12} & -\varepsilon_{13} \\ & \varepsilon_{22} & -\varepsilon_{23} \\ Sym & & \varepsilon_{33} \end{bmatrix} \tag{8.19}$$

Now, using the constitutive law, on both coordinate systems, and comparing the stress in Eq. (8.18) as

$$\begin{aligned} \sigma_{11} = \sigma'_{11} \iff & c_{11}\varepsilon_{11} + c_{12}\varepsilon_{22} + c_{13}\varepsilon_{33} + c_{14}\gamma_{23} + c_{15}\gamma_{13} + c_{16}\gamma_{12} \\ & = c'_{11}\varepsilon'_{11} + c'_{12}\varepsilon'_{22} + c'_{13}\varepsilon'_{33} + c'_{14}\gamma'_{23} + c'_{15}\gamma'_{13} + c'_{16}\gamma'_{12} \end{aligned} \tag{8.20}$$

using the relations from Eq. (8.19), the above equation reduce to

$$c_{14}\gamma_{23} + c_{15}\gamma_{13} = c'_{14}\gamma'_{23} + c'_{15}\gamma'_{13} \iff c_{14}2\varepsilon_{23} + c_{15}2\varepsilon_{13} = -c'_{14}2\varepsilon_{23} - c'_{15}2\varepsilon_{13} \tag{8.21}$$

Noting that $c'_{ij} = c_{ij}$, Eq. (8.21) can only be true when $c_{14} = c_{15} = 0$. Similarly, the following relations are also true:

$$\begin{aligned} \sigma_{22} = \sigma'_{22} &\Rightarrow c_{24} = c_{25} = 0 \\ \sigma_{33} = \sigma'_{33} &\Rightarrow c_{34} = c_{35} = 0 \\ \sigma_{12} = \sigma'_{12} &\Rightarrow c_{64} = c_{65} = 0 \end{aligned} \tag{8.22}$$

Therefore, for a monoclinic material the number of independent constants reduce to 13, and if the plane of symmetry is the x_1x_2, the stiffness matrix is given as

$$\mathbf{c} = \begin{bmatrix} c_{11} & c_{12} & c_{13} & 0 & 0 & c_{16} \\ & c_{22} & c_{23} & 0 & 0 & c_{26} \\ & & c_{33} & 0 & 0 & c_{36} \\ & sym & & c_{44} & c_{45} & 0 \\ & & & & c_{55} & 0 \\ & & & & & c_{66} \end{bmatrix} \tag{8.23}$$

Let assume that the material under consideration has one more plane of material symmetry. This case is illustrated in Fig. 8.24, in which the additional plane of symmetry is defined along x_2x_3 axes, and can be given by the following transformation:

$$x'_1 = -x_1;\ x'_2 = x_2;\ x'_3 = -x_3 \tag{8.24}$$

which gives the following transformation matrix

$$\mathbf{A} = \begin{bmatrix} -1 & 0 & 0 \\ 0 & 1 & 0 \\ 0 & 0 & -1 \end{bmatrix} \tag{8.25}$$

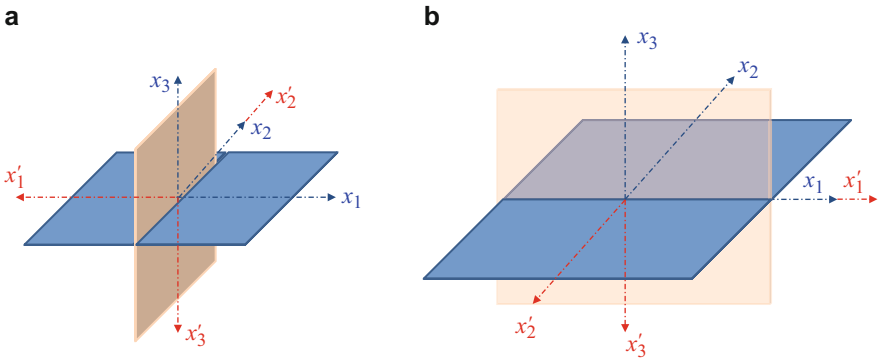

Fig. 8.24 Material symmetry: (**a**) about planes x_1x_2 and x_2x_3; (**b**) about planes x_1x_2 and x_1x_3

and the transformed stress and strain tensors $\boldsymbol{\sigma}'$ and $\boldsymbol{\varepsilon}'$ are given, respectively, as

$$\begin{bmatrix} \sigma'_{11} & \sigma'_{12} & \sigma'_{13} \\ & \sigma'_{22} & \sigma'_{23} \\ Sym & & \sigma'_{33} \end{bmatrix} = \begin{bmatrix} \sigma_{11} & -\sigma_{12} & \sigma_{13} \\ & \sigma_{22} & -\sigma_{23} \\ Sym & & \sigma_{33} \end{bmatrix} \tag{8.26}$$

$$\begin{bmatrix} \varepsilon'_{11} & \varepsilon'_{12} & \varepsilon'_{13} \\ & \varepsilon'_{22} & \varepsilon'_{23} \\ Sym & & \varepsilon'_{33} \end{bmatrix} = \begin{bmatrix} \varepsilon_{11} & -\varepsilon_{12} & \varepsilon_{13} \\ & \varepsilon_{22} & -\varepsilon_{23} \\ Sym & & \varepsilon_{33} \end{bmatrix} \tag{8.27}$$

Now, using the stiffness matrix given in Eq. (8.23) and comparing the components of stress tensors of Eq. (8.26), is possible to write

$$\begin{aligned} \sigma_{11} = \sigma'_{11} \iff & c_{11}\varepsilon_{11} + c_{12}\varepsilon_{22} + c_{13}\varepsilon_{33} + c_{16}\gamma_{12} \\ & = c'_{11}\varepsilon'_{11} + c'_{12}\varepsilon'_{22} + c'_{13}\varepsilon'_{33} + c'_{16}\gamma'_{12} \end{aligned} \tag{8.28}$$

Which holds true when $c_{16} = 0$. Following a similar procedure is possible to conclude that

$$\begin{aligned} \sigma_{22} = \sigma'_{22} &\Rightarrow c_{26} = 0 \\ \sigma_{33} = \sigma'_{33} &\Rightarrow c_{36} = 0 \\ \sigma_{13} = \sigma'_{13} &\Rightarrow c_{45} = 0 \end{aligned} \tag{8.29}$$

Thus, the number of independent constants reduces to nine and the elastic coefficient matrix reduced to:

$$\mathbf{c} = \begin{bmatrix} c_{11} & c_{12} & c_{13} & 0 & 0 & 0 \\ & c_{22} & c_{23} & 0 & 0 & 0 \\ & & c_{33} & 0 & 0 & 0 \\ & sym & & c_{44} & 0 & 0 \\ & & & & c_{55} & 0 \\ & & & & & c_{66} \end{bmatrix} \tag{8.30}$$

Alternately, if the second plane of material symmetry is selected along the axes x_1x_3, as shown in Fig. 8.24b, then the transformation is as following:

$$x_1' = x_1;\ x_2' = -x_2;\ x_3' = -x_3 \tag{8.31}$$

Leading to the following transformation matrix

$$\mathbf{A} = \begin{bmatrix} 1 & 0 & 0 \\ 0 & -1 & 0 \\ 0 & 0 & -1 \end{bmatrix} \tag{8.32}$$

and the transformed stress and strain tensors $\boldsymbol{\sigma}'$ and $\boldsymbol{\varepsilon}'$ are now given, respectively, as

$$\begin{bmatrix} \sigma_{11}' & \sigma_{12}' & \sigma_{13}' \\ & \sigma_{22}' & \sigma_{23}' \\ Sym & & \sigma_{33}' \end{bmatrix} = \begin{bmatrix} \sigma_{11} & -\sigma_{12} & -\sigma_{13} \\ & \sigma_{22} & \sigma_{23} \\ Sym & & \sigma_{33} \end{bmatrix} \tag{8.33}$$

$$\begin{bmatrix} \varepsilon_{11}' & \varepsilon_{12}' & \varepsilon_{13}' \\ & \varepsilon_{22}' & \varepsilon_{23}' \\ Sym & & \varepsilon_{33}' \end{bmatrix} = \begin{bmatrix} \varepsilon_{11} & -\varepsilon_{12} & -\varepsilon_{13} \\ & \varepsilon_{22} & \varepsilon_{23} \\ Sym & & \varepsilon_{33} \end{bmatrix} \tag{8.34}$$

Now using the same procedure as this used previously it will be possible to show that the reduced stiffness matrix has also the form of Eq. (8.30).

When a material has (any) two orthogonal planes of material symmetry is called an orthotropic material. In fact, is possible to understand that when two orthogonal planes are planes of material symmetry, a third mutually orthogonal plane is also a plane of material symmetry, and Eq. (8.30) remains true for this case also. Note that unidirectional fibrous composites are an example of orthotropic materials. A unidirectional fibrous lamina with the principal material directions is shown in Fig. 8.25. The direction 1 is along the fiber, directions 2 and 3 are perpendicular to the direction 1, and they are mutually perpendicular to each other. The direction 3 is along the thickness of lamina.

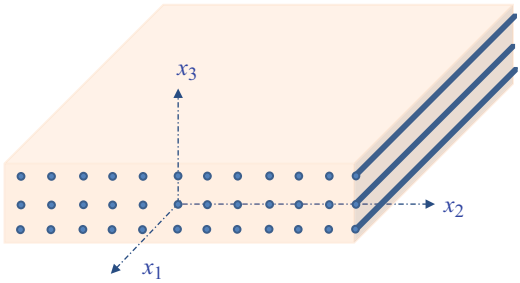

Fig. 8.25 unidirectional lamina with principal material axe directions

The stiffness matrix components of Eq. (8.30) are not directly measured from laboratory tests. The quantities that can be measured by laboratory testing are engineering or material constants like Young's modulus, shear modulus and Poisson's ratio. Thus, the orthotropic material properties of a lamina are obtained either by theoretical approach or by laboratory testing [11]. The relationship between engineering constants and the stiffness matrix components is not straight forward. Therefore, this relationship will be developed based on the relationship between engineering constants and the compliance matrix components.

The compliance matrix gives the strain-stress relationships of a linear elastic material and can be obtained from the reverse form of Eq. (8.5) leading to

$$\varepsilon_{ij} = s_{ijkl}\,\sigma_{kl} \tag{8.35}$$

or in an extended form as

$$\begin{bmatrix} \varepsilon_{11} \\ \varepsilon_{22} \\ \varepsilon_{33} \\ 2\varepsilon_{23} \\ 2\varepsilon_{13} \\ 2\varepsilon_{12} \end{bmatrix} = \begin{bmatrix} s_{11} & s_{12} & s_{13} & 0 & 0 & 0 \\ s_{21} & s_{22} & s_{23} & 0 & 0 & 0 \\ s_{31} & s_{32} & s_{33} & 0 & 0 & 0 \\ 0 & 0 & 0 & s_{44} & 0 & 0 \\ 0 & 0 & 0 & 0 & s_{55} & 0 \\ 0 & 0 & 0 & 0 & 0 & s_{66} \end{bmatrix} \begin{bmatrix} \sigma_{11} \\ \sigma_{22} \\ \sigma_{33} \\ \sigma_{23} \\ \sigma_{13} \\ \sigma_{12} \end{bmatrix} \tag{8.36}$$

all components of compliance matrix are obtained from the engineering constants, which can be defined as

$$E_k = \frac{\sigma_{kk}}{\varepsilon_{kk}^{(kk)}};\ k = 1, 2, 3 \tag{8.37}$$

$$G_{ij} = \frac{\sigma_{ij}}{2\varepsilon_{ij}^{(ij)}};\ i \neq j \tag{8.38}$$

$$\upsilon_{mn} = -\frac{\varepsilon_{nn}^{(mm)}}{\varepsilon_{mm}^{(mm)}};\ m \neq n \tag{8.39}$$

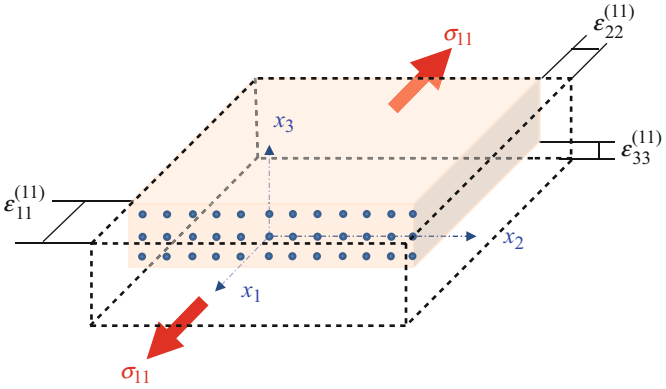

Fig. 8.26 Experiments for extracting Young's modulus and Poisson's ratios υ_{12} and υ_{13}

Equation (8.37) defines the Young's modulus in 1, 2 and 3 directions, in which E_k relates the normal stress and the extension strain on the face with the normal vector, when the applied load is in the direction x_k. Shear modulus are defined in Eq. (8.38), G_{ij} relates the in-plane shear stress and the in-plane shear strain acting in the plane $x_i x_j$, it should be noted that $G_{ij} = G_{ji}$. In Eq. (8.39), the term υ_{mn} represent the Poisson's ratio and it is defined as the ratio between extension strain in the direction perpendicular to the direction of applied stress and the extension strain in the direction of applied stress. It should be noted that, in general, $\upsilon_{mn} \neq \upsilon_{nm}$.

In order to evaluate the quantities in Eqs. (8.37), (8.38), and (8.39) is possible to make laboratory tests. For instance, assume that lamina specimens are subjected to a sequence of four experiments:

Experiment 1 *the lamina is loaded in traction along the fibrous direction, as shown in Fig. 8.26, and the strains along the three principal directions are recorded as the load is varied.*

Young modulus E_1 can be obtained as the slope of the axial stress (σ_{11}) versus axial strain ($\varepsilon_{11}^{(11)}$) curve, while Poisson's ratios are given as

$$\upsilon_{12} = -\frac{\varepsilon_{11}^{(11)}}{\varepsilon_{22}^{(11)}};\ \upsilon_{13} = -\frac{\varepsilon_{11}^{(11)}}{\varepsilon_{33}^{(11)}} \tag{8.40}$$

Due to the definition of elasticity modulus and the definitions in Eq. (8.40) is possible to write

$$\varepsilon_{11}^{(11)} = s_{11}\sigma_{11} \Rightarrow\ s_{11} = \frac{\varepsilon_{11}^{(11)}}{\sigma_{11}} = \frac{1}{E_1} \tag{8.41}$$

$$\varepsilon_{nn}^{(11)} = s_{n1}\sigma_{11} \Rightarrow s_{n1} = \frac{\varepsilon_{nn}^{(11)}}{\sigma_{11}} = \frac{\varepsilon_{nn}^{(11)}}{E_1\varepsilon_{11}^{(11)}} = -\frac{\upsilon_{1n}}{E_1};\ \ n = 2, 3 \tag{8.42}$$

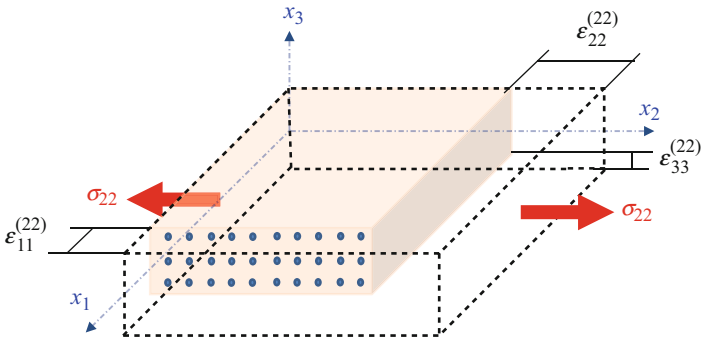

Fig. 8.27 Experiments for extracting Young's modulus E_2 and Poisson's ratios υ_{21} and υ_{23}

Experiment 2 *the lamina is loaded in traction along direction* x_2*, as shown in Fig. 8.27, and the strains along the three principal directions are recorded as the load is varied. Young modulus* E_2 *can be obtained as the slope of the axial stress* (σ_{22}) *versus axial strain* ($\varepsilon_{22}^{(22)}$) *curve, while Poisson's ratios are given as*

$$\upsilon_{21} = -\frac{\varepsilon_{11}^{(22)}}{\varepsilon_{22}^{(22)}};\ \upsilon_{23} = -\frac{\varepsilon_{33}^{(22)}}{\varepsilon_{22}^{(22)}} \tag{8.43}$$

Once more, using the definition of elasticity modulus and the information in Eq. (8.43) is possible to write

$$\varepsilon_{22}^{(22)} = s_{22}\sigma_{22} \Rightarrow\ s_{22} = \frac{\varepsilon_{22}^{(22)}}{\sigma_{22}} = \frac{1}{E_2} \tag{8.44}$$

$$\varepsilon_{nn}^{(22)} = s_{n2}\sigma_{22} \Rightarrow s_{n2} = \frac{\varepsilon_{nn}^{(22)}}{\sigma_{22}} = \frac{\varepsilon_{nn}^{(22)}}{E_2\varepsilon_{22}^{(22)}} = -\frac{\upsilon_{2n}}{E_2};\ \ n = 1, 3 \tag{8.45}$$

Experiment 3 *the lamina is loaded in traction along direction* x_3*, and the strains along the three principal directions are recorded as the load is varied. Young modulus* E_3 *can be obtained as the slope of the axial stress* (σ_{33}) *versus axial strain* ($\varepsilon_{33}^{(33)}$) *curve, while Poisson's ratios are given as*

$$\upsilon_{31} = -\frac{\varepsilon_{11}^{(33)}}{\varepsilon_{33}^{(33)}};\ \upsilon_{32} = -\frac{\varepsilon_{22}^{(33)}}{\varepsilon_{33}^{(22)}} \tag{8.46}$$

and using the definition of elasticity modulus and the information in Eq. (8.46) is possible to write

$$\varepsilon_{33}^{(33)} = s_{33}\sigma_{33} \Rightarrow\ s_{33} = \frac{\varepsilon_{33}^{(33)}}{\sigma_{33}} = \frac{1}{E_3} \tag{8.47}$$

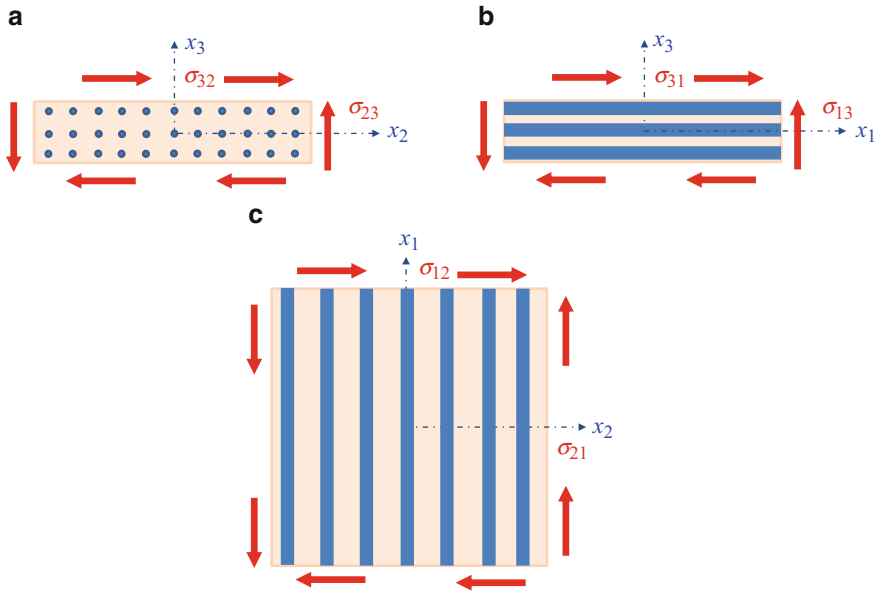

Fig. 8.28 Experimental tests: (**a**) for extracting shear modulus G_{23};. (**b**) for extracting shear modulus; (**c**) for extracting shear modulus G_{21}

$$\varepsilon_{nn}^{(33)} = s_{n3}\sigma_{33} \Rightarrow s_{n3} = \frac{\varepsilon_{nn}^{(33)}}{\sigma_{33}} = \frac{\varepsilon_{nn}^{(33)}}{E_3\varepsilon_{33}^{(33)}} = -\frac{\upsilon_{3n}}{E_3};\quad n = 1,2 \tag{8.48}$$

Experiment 4 *the lamina is loaded in shear within plane* x_2x_3*, as shown in Fig.* 8.28*a, and the slope of the in-plane shear stress* (σ_{23}) *versus angular strain* ($2\varepsilon_{23}^{(23)}$) *curve gives the shear modulus* G_{23}*, and is possible to write*

$$2\varepsilon_{23}^{(23)} = s_{44}\sigma_{23} \Rightarrow\ s_{44} = \frac{2\varepsilon_{23}^{(23)}}{\sigma_{23}} = \frac{\gamma_{23}^{(23)}}{\sigma_{23}} = \frac{1}{G_{23}} \tag{8.49}$$

and in a similar way, is also possible to load the lamina by shear within planes x_1x_3 and x_1x_2 to get shear modulus G_{31} and G_{21}, respectively, as shown in Fig. 8.28b, c. The slope of the in-plane shear stress versus angular strain curves gives the shear modulus as

$$2\varepsilon_{13}^{(13)} = s_{55}\sigma_{13} \Rightarrow\ s_{55} = \frac{2\varepsilon_{13}^{(13)}}{\sigma_{13}} = \frac{\gamma_{13}^{(13)}}{\sigma_{13}} = \frac{1}{G_{13}} \tag{8.50}$$

$$2\varepsilon_{21}^{(21)} = s_{66}\sigma_{21} \Rightarrow\ s_{66} = \frac{2\varepsilon_{21}^{(21)}}{\sigma_{21}} = \frac{\gamma_{21}^{(21)}}{\sigma_{21}} = \frac{1}{G_{21}} \tag{8.51}$$

After all these experiments is possible to write the compliance matrix in the form:

$$\mathbf{s} = \begin{bmatrix} \frac{1}{E_1} & -\frac{\upsilon_{21}}{E_2} & -\frac{\upsilon_{31}}{E_3} & 0 & 0 & 0 \\ -\frac{\upsilon_{12}}{E_1} & \frac{1}{E_2} & -\frac{\upsilon_{32}}{E_3} & 0 & 0 & 0 \\ -\frac{\upsilon_{13}}{E_1} & -\frac{\upsilon_{23}}{E_2} & \frac{1}{E_3} & 0 & 0 & 0 \\ 0 & 0 & 0 & \frac{1}{G_{23}} & 0 & 0 \\ 0 & 0 & 0 & 0 & \frac{1}{G_{13}} & 0 \\ 0 & 0 & 0 & 0 & 0 & \frac{1}{G_{12}} \end{bmatrix} \tag{8.52}$$

And, from elementary linear algebra, it is known that the inverse of a symmetric matrix is also a symmetric matrix. Then, because the stiffness matrix is symmetric and the compliance matrix is the inverse of stiffness matrix, the compliance matrix has to be symmetric also. Thus, Eq. (8.52) and the symmetry property of compliance matrix allows deriving more useful relations. For instance, form the comparison of components s_{ij} and s_{ji}, the following relations are given

$$\frac{\upsilon_{21}}{E_2} = \frac{\upsilon_{12}}{E_1}; \ \frac{\upsilon_{31}}{E_3} = \frac{\upsilon_{13}}{E_1}; \ \frac{\upsilon_{23}}{E_2} = \frac{\upsilon_{32}}{E_3}; \tag{8.53}$$

Or in a compact form

$$\frac{\upsilon_{ij}}{E_i} = \frac{\upsilon_{ji}}{E_j}; \ \mathrm{i,j} = 1,2,3; \ \ (\text{no sum over i and j}) \tag{8.54}$$

The stiffness matrix can be obtained using Eq. (8.52) into Eq. (8.36) and inverting the resulted equation, the stiffness matrix of an orthotropic material will be defined as

$$\mathbf{c} = \begin{bmatrix} \frac{E_1(1-\upsilon_{23}\upsilon_{32})}{\Delta} & \frac{E_1(\upsilon_{21}+\upsilon_{23}\upsilon_{31})}{\Delta} & \frac{E_1(\upsilon_{31}+\upsilon_{21}\upsilon_{32})}{\Delta} & 0 & 0 & 0 \\ \frac{E_2(\upsilon_{12}+\upsilon_{32}\upsilon_{13})}{\Delta} & \frac{E_2(1-\upsilon_{13}\upsilon_{31})}{\Delta} & \frac{E_2(\upsilon_{32}+\upsilon_{12}\upsilon_{31})}{\Delta} & 0 & 0 & 0 \\ \frac{E_3(\upsilon_{13}+\upsilon_{12}\upsilon_{23})}{\Delta} & \frac{E_3(\upsilon_{23}+\upsilon_{13}\upsilon_{21})}{\Delta} & \frac{E_3(1-\upsilon_{12}\upsilon_{21})}{\Delta} & 0 & 0 & 0 \\ 0 & 0 & 0 & G_{23} & 0 & 0 \\ 0 & 0 & 0 & 0 & G_{13} & 0 \\ 0 & 0 & 0 & 0 & 0 & G_{12} \end{bmatrix};$$

$$\Delta = 1 - (\upsilon_{12}\upsilon_{21} + \upsilon_{13}\upsilon_{31} + \upsilon_{23}\upsilon_{32} + \upsilon_{13}\upsilon_{21}\upsilon_{32} + \upsilon_{12}\upsilon_{23}\upsilon_{31}) \tag{8.55}$$

Using the relations on Eq. (8.53) into the second equation of Eq. (8.55), is possible to write Δ as

$$\Delta = 1 - (\upsilon_{12}\upsilon_{21} + \upsilon_{13}\upsilon_{31} + \upsilon_{23}\upsilon_{32} + 2\upsilon_{13}\upsilon_{21}\upsilon_{32}) \tag{8.56}$$

A special class of orthotropic materials is those that have isotropy in one plane, for instance the x_2x_3 plane, meaning that in this plane the material has the same material properties on both directions and, therefore, the following relations are true

$$E_2 = E_3;\ \upsilon_{13} = \upsilon_{12};\ \upsilon_{31} = \upsilon_{21};\ \upsilon_{23} = \upsilon_{32};\ G_{13} = G_{12}\ \textit{and}\ G_{23} = \frac{E_2}{2\,(1+\upsilon_{23})} \tag{8.57}$$

Substituting the relations of Eq. (8.57) into Eq. (8.52), yields

$$\mathbf{s} = \begin{bmatrix} \frac{1}{E_1} & -\frac{\upsilon_{12}}{E_1} & -\frac{\upsilon_{12}}{E_1} & 0 & 0 & 0 \\ -\frac{\upsilon_{12}}{E_1} & \frac{1}{E_2} & -\frac{\upsilon_{23}}{E_2} & 0 & 0 & 0 \\ -\frac{\upsilon_{12}}{E_1} & -\frac{\upsilon_{23}}{E_2} & \frac{1}{E_2} & 0 & 0 & 0 \\ 0 & 0 & 0 & \frac{1}{G_{23}} & 0 & 0 \\ 0 & 0 & 0 & 0 & \frac{1}{G_{12}} & 0 \\ 0 & 0 & 0 & 0 & 0 & \frac{1}{G_{12}} \end{bmatrix} \tag{8.58}$$

Equation (8.58) defines the compliance matrix for the called transverse isotropic materials, and they are described by five independent elastic constants, instead of nine for fully orthotropic. The stiffness matrix for transverse isotropic materials can be found from the inverse of the compliance matrix.

Is well known that for isotropic materials there are constraints on material constants, namely Young's modulus and shear modulus should be always positive and the Poisson's ratio should not be larger than half. If these constraints are violated then, for certain load conditions, the strain energy may be non-positive and the evolution of material is not thermodynamically inadmissible [12]. The requirement of positive definiteness of strain energy for isotropic material is also valid for the case of orthotropic materials. Thus, the work done by all stress components must be positive and, this condition, requires that both compliance and stiffness matrices must be positive definite. The physical meaning of these requirements can be clarify if we assume that each component of stress field is applied isolated, then is possible to find the corresponding strain component from the corresponding diagonal entry

of compliance matrix and, therefore, for the strain energy to be positive definite is necessary that the diagonal entries of the compliance matrix must be positive, yielding

$$\mathrm{E}_1, \mathrm{E}_2, \mathrm{E}_3, \mathrm{G}_{23}, \mathrm{G}_{13}, \mathrm{G}_{12} > 0 \tag{8.59}$$

To assure the positive definiteness of stiffness matrix, is possible to consider states of deformation that include only one strain component at a time and find the corresponding stress, using the corresponding diagonal entry of the stiffness matrix. Hence, to assure that the strain energy produced by each one of this stress components is positive definite, is necessary to assure the following conditions

$$(1\text{-}\upsilon_{23}\upsilon_{32}),\ (1\text{-}\upsilon_{13}\upsilon_{31}),(1\text{-}\upsilon_{12}\upsilon_{21}) > 0 \tag{8.60}$$

$$\Delta = 1 - (\upsilon_{12}\upsilon_{21} + \upsilon_{13}\upsilon_{31} + \upsilon_{23}\upsilon_{32} + 2\upsilon_{13}\upsilon_{21}\upsilon_{32}) > 0 \tag{8.61}$$

If relations on Eq. (8.53) are used into Eq. (8.60), the Eq. (8.60) can be further rewritten as

$$\begin{aligned} |\upsilon_{12}| &< \left(\frac{\mathrm{E}_1}{\mathrm{E}_2}\right)^{1/2} \quad |\upsilon_{21}| < \left(\frac{\mathrm{E}_2}{\mathrm{E}_1}\right)^{1/2} \\ |\upsilon_{13}| &< \left(\frac{\mathrm{E}_1}{\mathrm{E}_3}\right)^{1/2} \quad |\upsilon_{31}| < \left(\frac{\mathrm{E}_3}{\mathrm{E}_1}\right)^{1/2} \\ |\upsilon_{23}| &< \left(\frac{\mathrm{E}_2}{\mathrm{E}_3}\right)^{1/2} \quad |\upsilon_{32}| < \left(\frac{\mathrm{E}_3}{\mathrm{E}_2}\right)^{1/2} \end{aligned} \tag{8.62}$$

The conditions on Eq. (8.62) estimate that Poisson's coefficients must be smaller than ratios of Young's modulus of the lamina. Since E_1, generally, is much greater than the other two Young's modulus, Eq. (8.62) justifies that Poisson's ratio greater than unity is feasible for an orthotropic lamina.

Using relations on Eq. (8.53) into Eq. (8.61) and rewriting the resulted equation, is possible to obtain the following relation

$$\begin{aligned} \upsilon_{13}\upsilon_{21}\upsilon_{32} &< \frac{1 - \upsilon_{12}\upsilon_{21} - \upsilon_{13}\upsilon_{31} - \upsilon_{23}\upsilon_{32}}{2} \\ \upsilon_{13}\upsilon_{21}\upsilon_{32} &< \frac{1 - (\upsilon_{21})^2\left(\frac{E_1}{E_2}\right) - (\upsilon_{13})^2\left(\frac{E_3}{E_1}\right) - (\upsilon_{32})^2\left(\frac{E_3}{E_1}\right)}{2} \end{aligned} \tag{8.63}$$

Because the terms inside the brackets are all positive, the right-hand-side of Eq. (8.63) is always smaller than 1/2, and is possible to write

$$\upsilon_{13}\upsilon_{21}\upsilon_{32} < \frac{1}{2} \tag{8.64}$$

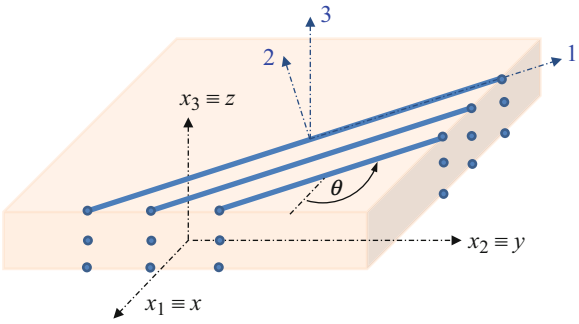

Fig. 8.29 Principal material directions and reference coordinate system of a unidirectional lamina

Equation (8.64) shows that the three Poisson's ratios can't have all large positive values and that their product must be smaller than 1/2.

8.6.3 Stress and Strain Transformations

Often we may want to describe the behavior of a structure with reference to more than one set of axes. For instance, the analysis of an airplane can be done using different loading axes for wings and fuselage or the analysis of fibrous composite materials in which the principal material directions may not be parallel to the directions of a reference axis system. Nevertheless, it must be clear that if we change the axis system in which some physical information (stress or strain) is described does not change the physical quantity, only its description. Thus the stress state and the strain state do not change, we just describe them differently. In order to introduce this description it should be noted that the stress and strain states are described by second order tensors and, therefore, they follow tensor transformation rules.

In this section two different coordinate systems are used and, therefore, the two following nations are defined: subscripts 123 denote quantities described in principal material directions; while subscripts xyz denote the corresponding quantity in reference coordinate system. Figure 8.29 shows the orientations of both coordinate systems. The fibers assumed their orientation by a simple rotation of the principal material axes about the 3 axis. The orientation angle θ is considered positive when the fibers rotate counterclockwise from the $+$x towards the $+$y. Transformation of stress and strain tensors, between both coordinate systems, follows the transformation rules of second order tensors described in Eq. (8.17), in which is necessary to define the transformation matrix between both coordinate systems, and for that, it is necessary the knowledgment of direction cosines of this axes transformation, which are given below in Table 8.1. In Eq. (8.17), the primed stress components denote the component in 123 coordinate system.

Using the relation in Eq. (8.17), transformation matrix of Table 8.1 and the stress symmetry, is possible to obtain each component of stress in the coordinate system of principal material directions as

Table 8.1 Direction cosines for the axes transformation

From/	Direction cosines		
To	1	2	3
x	$a_{11} = \cos\theta$	$a_{12} = \cos(90° + \theta)$	$a_{13} = \cos(90°)$
y	$a_{21} = \cos(90°–\theta)$	$a_{22} = \cos(\theta)$	$a_{23} = \cos(90°)$
z	$a_{31} = \cos(90°)$	$a_{32} = \cos(90°)$	$a_{33} = \cos(0°)$

$$\begin{aligned}\sigma_{11} = {} & a_{11}a_{11}\sigma_{xx} + a_{21}a_{21}\sigma_{yy} + a_{31}a_{31}\sigma_{zz} \\ & + 2a_{31}a_{31}\sigma_{yz} + 2a_{31}a_{11}\sigma_{xz} + 2a_{21}a_{11}\sigma_{xy}\end{aligned} \tag{8.65}$$

and using the information on Table 8.1 yields

$$\sigma_{11} = \cos^2\theta\,\sigma_{xx} + \sin^2\theta\,\sigma_{yy} + 2\cos\theta\,\sin\theta\,\sigma_{xy} \tag{8.66}$$

The remaining stress components can also be obtained in a similar way, and the final relation may be written using the pseudo-vector form of stress tensor as

$$\overline{\boldsymbol{\sigma}} = \mathbf{T}_\sigma \boldsymbol{\sigma} \tag{8.67}$$

where $\overline{\boldsymbol{\sigma}}$ represents the pseudo-vector of stress components in the principal material direction axes, $\boldsymbol{\sigma}$ is the pseudo-vector of stress components in the reference coordinate system and $\mathbf{T}_\sigma$ is the newly defined transformation matrix given as [13]

$$\mathbf{T}_\sigma = \begin{bmatrix} m^2 & n^2 & 0 & 0 & 0 & 2mn \\ n^2 & m^2 & 0 & 0 & 0 & -2mn \\ 0 & 0 & 1 & 0 & 0 & 0 \\ 0 & 0 & 0 & m & -n & 0 \\ 0 & 0 & 0 & n & m & 0 \\ -mn & mn & 0 & 0 & 0 & m^2\text{-}n^2 \end{bmatrix} \tag{8.68}$$

where $m = \cos\theta$ and $n = \sin\theta$. Because $\mathbf{T}_\sigma$ is not a symmetric matrix, the inverted relation of Eq. (8.67) is written as

$$\boldsymbol{\sigma} = \mathbf{R}_\sigma \overline{\boldsymbol{\sigma}} \tag{8.69}$$

$\mathbf{R}_\sigma$ is a transformation matrix that can be obtained from matrix $\mathbf{T}_\sigma$ replacing θ with $-\theta$.

In a similar way, is possible to transform the strain components between the two coordinate systems. Strains are also represented by a second order tensor, hence the second equation in transformation Eq. (8.17) is applied to the strain tensor and using the strain symmetry is possible to write

$$\begin{aligned}\varepsilon_{12} = {} & a_{11}a_{12}\varepsilon_{xx} + a_{21}a_{22}\varepsilon_{yy} + a_{31}a_{32}\varepsilon_{zz} \\ & \left(a_{21}a_{32} + a_{31}a_{22}\right)\varepsilon_{yz} + \left(a_{32}a_{11} + a_{31}a_{12}\right)\varepsilon_{xz} \\ & + \left(a_{22}a_{11} + a_{21}a_{12}\right)\varepsilon_{xy}\end{aligned} \tag{8.70}$$

Substituting the direction cosines and rearranging, yields

$$\varepsilon_{12} = -\sin\theta\ \cos\theta\ \varepsilon_{xx} + \sin\theta\ \cos\theta\ \varepsilon_{yy} + \left(\cos^2\theta - \sin^2\theta\right)\varepsilon_{xy} \tag{8.71}$$

And because the shear strains are half of the engineering shear strains, i.e.

$$\gamma_{12} = 2\varepsilon_{12}\ \textit{and}\ \gamma_{xy} = 2\varepsilon_{xy} \tag{8.72}$$

Equation (8.71) assumes the following form

$$2\varepsilon_{12} = -2\sin\theta\ \cos\theta\ \varepsilon_{xx} + 2\sin\theta\ \cos\theta\ \varepsilon_{yy} + \left(\cos^2\theta - \sin^2\theta\right)2\varepsilon_{xy} \tag{8.73}$$

and if m = cos θ and n = sin θ are used in previous equation, a simplified form is written as

$$2\varepsilon_{12} = -2\mathrm{mn}\ \varepsilon_{xx} + 2\mathrm{mn}\ \varepsilon_{yy} + \left(\mathrm{m}^2 - \mathrm{n}^2\right)2\varepsilon_{xy} \tag{8.74}$$

Each of one of the other five strain terms can also be obtained in a similar way, and the final relation may be written using the pseudo-vector form of strain tensor as

$$\bar{\boldsymbol{\varepsilon}} = \mathbf{T}_{\varepsilon}\boldsymbol{\varepsilon} \tag{8.75}$$

where $\bar{\boldsymbol{\varepsilon}}$ represents the pseudo-vector of strain components in the principal material direction axes $\boldsymbol{\varepsilon}$ is the pseudo-vector of stress components in the reference coordinate system and $\mathbf{T}_{\varepsilon}$ is the newly defined transformation matrix given as [13]

$$\mathbf{T}_{\varepsilon} = \begin{bmatrix} \mathrm{m}^2 & \mathrm{n}^2 & 0 & 0 & 0 & \mathrm{mn} \\ \mathrm{n}^2 & \mathrm{m}^2 & 0 & 0 & 0 & -\mathrm{mn} \\ 0 & 0 & 1 & 0 & 0 & 0 \\ 0 & 0 & 0 & \mathrm{m} & -\mathrm{n} & 0 \\ 0 & 0 & 0 & \mathrm{n} & \mathrm{m} & 0 \\ -2\mathrm{mn} & 2\mathrm{mn} & 0 & 0 & 0 & \mathrm{m}^2\text{-}\mathrm{n}^2 \end{bmatrix} \tag{8.76}$$

The matrix $\mathbf{T}_{\varepsilon}$ is the transpose of the matrix $\mathbf{R}_{\sigma}$ in Eq. (8.69) and, therefore, Eq. (8.75) can also be represented as

$$\bar{\boldsymbol{\varepsilon}} = \mathbf{R}_{\sigma}^{T}\boldsymbol{\varepsilon} \tag{8.77}$$

In a similar form, the inverse relation is given by

$$\boldsymbol{\varepsilon} = \mathbf{T}_{\sigma}^{T}\overline{\boldsymbol{\varepsilon}} \tag{8.78}$$

8.6.4 Transformation of Stiffness and Compliance Matrices

The transformation of stress and strain components between the material and global coordinate systems have been discussed in the previous section, but it is also required to relate the stress components with strain components in the global coordinate system. For that, it is necessary to transform the stiffness and compliance matrices components from the material coordinate system to the global coordinate system.

To obtain these transformations, let the stress-strain relations given in Eq. (8.5) be used in the stress transformation described by Eq. (8.69), and written as

$$\boldsymbol{\sigma} = \mathbf{R}_{\sigma}\overline{\boldsymbol{\sigma}} = \mathbf{R}_{\sigma}\overline{\mathbf{c}}\,\overline{\boldsymbol{\varepsilon}} \tag{8.79}$$

now, substituting Eq. (8.77) into Eq. (8.79) yields to

$$\boldsymbol{\sigma} = \mathbf{R}_{\sigma}\overline{\mathbf{c}}\,\overline{\boldsymbol{\varepsilon}} = \mathbf{R}_{\sigma}\overline{\mathbf{c}}\,\mathbf{R}_{\sigma}^{T}\boldsymbol{\varepsilon} = \mathbf{c}\,\boldsymbol{\varepsilon} \tag{8.80}$$

Where the transformed stiffness matrix $\mathbf{c}$ is defined as

$$\mathbf{c} = \mathbf{R}_{\sigma}\overline{\mathbf{c}}\,\mathbf{R}_{\sigma}^{T} \tag{8.81}$$

and, the material stiffness matrix in Eq. (8.81) is defined in the laminate (global) coordinate system as

$$\mathbf{c} = \begin{bmatrix} c_{11} & c_{12} & c_{13} & 0 & 0 & c_{16} \\ & c_{22} & c_{23} & 0 & 0 & c_{26} \\ & & c_{33} & 0 & 0 & c_{36} \\ & sym & & c_{44} & c_{45} & 0 \\ & & & & c_{55} & 0 \\ & & & & & c_{66} \end{bmatrix} \tag{8.82}$$

Where the c_{ij} components are expressed in the global coordinate system and are directly dependents on the layer orientation of the orthotropic material.

In order to relate the compliance coefficients in both coordinate systems, Eq. (8.35) is used in Eq. (8.78) yielding

$$\boldsymbol{\varepsilon} = \mathbf{T}_{\sigma}^{T}\overline{\boldsymbol{\varepsilon}} = \mathbf{T}_{\sigma}^{T}\overline{\mathbf{s}}\,\overline{\boldsymbol{\sigma}} \tag{8.83}$$

and substituting Eq. (8.67) in the latter equation leads to

$$\boldsymbol{\varepsilon} = \mathbf{T}_{\sigma}^{T}\bar{\mathbf{s}}\,\bar{\boldsymbol{\sigma}} = \mathbf{T}_{\sigma}^{T}\bar{\mathbf{s}}\,\mathbf{T}_{\sigma}\boldsymbol{\sigma} = \mathbf{s}\,\boldsymbol{\sigma} \tag{8.84}$$

The quantity $\mathbf{s} = \mathbf{T}_{\sigma}^{T}\bar{\mathbf{s}}\,\mathbf{T}_{\sigma}$ contains the transformed compliance coefficients referred to the laminate coordinate system.

8.6.5 *Reduced Form of Stiffness and Compliance Matrices for an Orthotropic Lamina*

Equation (8.36) is written in the most general case. However, most laminates are thin and experience a planar state of stress, i.e., the transverse stresses $\overline{\sigma}_{33}$, $\overline{\sigma}_{13}$ and $\overline{\sigma}_{23}$ are negligible. Nevertheless, when fibers that provide the strength are in the x_1x_2 plane, the fiber-reinforced composite laminates are much weaker in the transverse direction. Therefore, even when the transverse stresses are small, when compared to the values of in-plane stresses, they still can induce failures of the laminates in these transverse directions. Consequently, transverse stresses are not always neglected in the laminate analyses. By neglecting the transverse normal strain and by including the transverse shear stress, the strain stress relations given by Eq. (8.36) reduces to

$$\begin{bmatrix} \overline{\varepsilon}_{11} \\ \overline{\varepsilon}_{22} \\ 2\overline{\varepsilon}_{23} \\ 2\overline{\varepsilon}_{13} \\ 2\overline{\varepsilon}_{12} \end{bmatrix} = \begin{bmatrix} \overline{s}_{11} & \overline{s}_{12} & 0 & 0 & 0 \\ \overline{s}_{12} & \overline{s}_{22} & 0 & 0 & 0 \\ 0 & 0 & \overline{s}_{44} & 0 & 0 \\ 0 & 0 & 0 & \overline{s}_{55} & 0 \\ 0 & 0 & 0 & 0 & \overline{s}_{66} \end{bmatrix} \begin{bmatrix} \overline{\sigma}_{11} \\ \overline{\sigma}_{22} \\ \overline{\sigma}_{23} \\ \overline{\sigma}_{13} \\ \overline{\sigma}_{12} \end{bmatrix} \tag{8.85}$$

Where the components of the reduced compliance in Eq. (8.85) are those in Eq. (8.52) by removing the third row and third column.

Equation (8.85) is written in a reverse form to obtain the stress-strain relations, as

$$\begin{bmatrix} \overline{\sigma}_{11} \\ \overline{\sigma}_{22} \\ \overline{\sigma}_{23} \\ \overline{\sigma}_{13} \\ \overline{\sigma}_{12} \end{bmatrix} = \begin{bmatrix} \overline{c}_{11} & \overline{c}_{12} & 0 & 0 & 0 \\ \overline{c}_{12} & \overline{c}_{22} & 0 & 0 & 0 \\ 0 & 0 & \overline{c}_{44} & 0 & 0 \\ 0 & 0 & 0 & \overline{c}_{55} & 0 \\ 0 & 0 & 0 & 0 & \overline{c}_{66} \end{bmatrix} \begin{bmatrix} \overline{\varepsilon}_{11} \\ \overline{\varepsilon}_{22} \\ 2\overline{\varepsilon}_{23} \\ 2\overline{\varepsilon}_{13} \\ 2\overline{\varepsilon}_{12} \end{bmatrix} \tag{8.86}$$

Where the reduced stiffness coefficients are now given by

$$\begin{aligned} &\bar{c}_{11} = \frac{E_1}{\Delta};\ \bar{c}_{22} = \frac{E_2}{\Delta};\ \bar{c}_{44} = G_{23} \\ &\bar{c}_{55} = G_{13};\ \bar{c}_{66} = G_{12} \\ &\bar{c}_{12} = \frac{E_2\upsilon_{12}}{\Delta};\ \Delta = 1 - \upsilon_{12}\upsilon_{21} \end{aligned} \tag{8.87}$$

Equation (8.86) is the constitutive equation of an orthotropic lamina written in its material coordinate system. For the conditions defined, the stress-strain relations expressed in the laminate coordinate system are

$$\begin{bmatrix} \sigma_{11} \\ \sigma_{22} \\ \sigma_{23} \\ \sigma_{13} \\ \sigma_{12} \end{bmatrix} = \begin{bmatrix} c_{11} & c_{12} & 0 & 0 & c_{16} \\ c_{12} & c_{22} & 0 & 0 & c_{26} \\ 0 & 0 & c_{44} & c_{45} & 0 \\ 0 & 0 & c_{54} & c_{55} & 0 \\ c_{61} & c_{62} & 0 & 0 & c_{66} \end{bmatrix} \begin{bmatrix} \varepsilon_{11} \\ \varepsilon_{22} \\ 2\varepsilon_{23} \\ 2\varepsilon_{13} \\ 2\varepsilon_{12} \end{bmatrix} \tag{8.88}$$

or in a compact form

$$\boldsymbol{\sigma}_p = \mathbf{c}_p \, \boldsymbol{\varepsilon}_p \tag{8.89}$$

where $\boldsymbol{\sigma}_p = \left[\sigma_{11} \; \sigma_{22} \; \sigma_{23} \; \sigma_{13} \; \sigma_{12} \right]^T$ is the stress pseudo-vector, $\boldsymbol{\varepsilon}_p = \left[\varepsilon_{11} \; \varepsilon_{22} \; 2\varepsilon_{23} \; 2\varepsilon_{13} \; 2\varepsilon_{12} \right]^T$ is the deformation pseudo-vector and $\mathbf{c}_p$ is the matrix of the reduced stiffness coefficients, defined in the laminated coordinate system given as

$$\mathbf{c}_p = \mathbf{R}_p \, \bar{\mathbf{c}}_p \, \mathbf{R}_p^T \tag{8.90}$$

Matrix $\bar{\mathbf{c}}_p$ is the reduced stiffness defined in Eq. (8.86) and matrix $\mathbf{R}_p$ is obtained from the transformation matrix in the right hand side of Eq. (8.69) by removing the third row and third column.

8.6.6 Finite Element Matrices for Laminated Plates

In preceding chapters we presented some of the tools needed for understanding elastic response of small volume of fiber-reinforced material assuming that the fibers and the matrix material were smeared into one equivalent homogeneous material. Nevertheless, fiber-reinforced materials are most frequently applied in the form of multiple layers of material to form a laminate. Each layer is thin and may have different fiber orientation, and in some cases, not all the layers are of the same material [13]. Actually, two laminates may involve the same number of layers and the same set of fiber angles, but the two laminates can be different and most certainly can exhibit entirely different behavior due to the arrangement of the layers [13]. Figure 8.30, shows two laminates with the same number of layers and the same set of angles, but different arrangement of layers.

The first step on the discussion of laminates is to have a method for describing the laminate, especially the fiber orientation of each layer. The fiber angle of the several layers is identified by specifying the fiber angle θ of each layer relatively to global +x. The specification starts with layer 1, which is the layer at the most

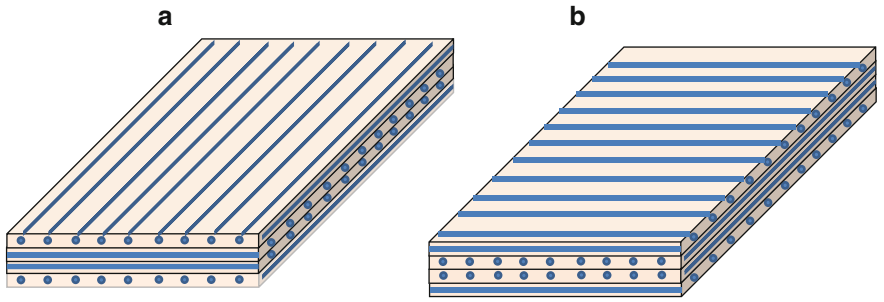

Fig. 8.30 Stacking sequence of laminates: (**a**) [90/0]s laminate; (**b**) [0/90]s

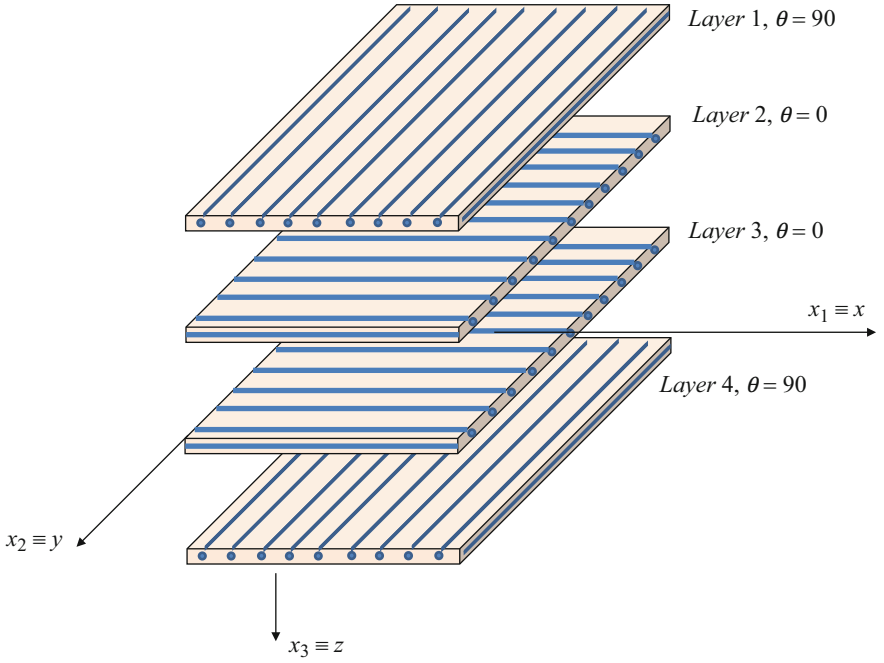

Fig. 8.31 Stacking sequence of laminate [90/0]s

negative z location. For instance the laminate in Fig. 8.30a is a [90/0/0/90] laminate, while the laminate in Fig. 8.30b is a [0/90/90/0]. Where, in each case, the global +x is aligned as showed in Fig. 8.31.

Additionally, to the method used to describe the fiber orientation of each layer, it is also necessary to establish a coordinate system for specifying locations through the thickness of the laminate. Figure 8.32 shows a global coordinate system and a general laminate, in which the total number of layers is of *nl*.

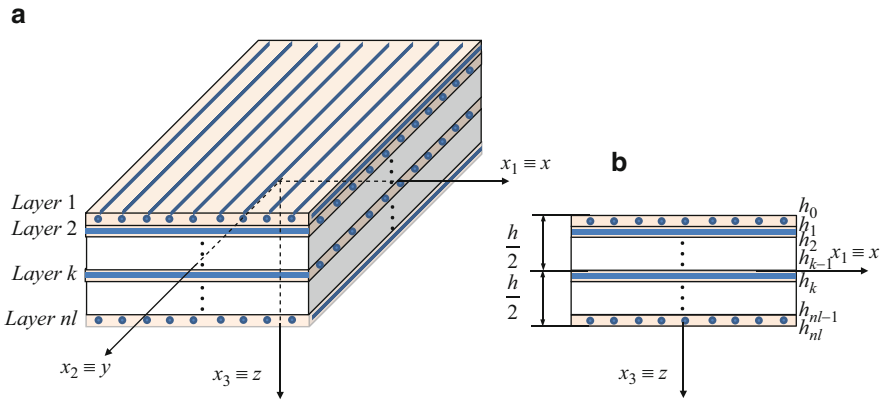

Fig. 8.32 Coordinate system and layer numbering for a typical laminated plate

The laminate thickness is denoted by h, and the k individual layer is located between the point $x_3 = h_{k-1}$ and $x_3 = h_k$, as shown in Fig. 8.32. If the laminates shown in Fig. 8.30 have layers with the same thickness, then both laminates are called symmetric. A laminate is said symmetric when the material, angle and thickness are located symmetrically with respect to the reference surface.

In order to describe the finite element matrices of laminated plates, let assume that flat shell finite elements of Sect. 6.4.1 are used. Thus, following Eq. (6.77), the element stiffness matrix for layer k can be formulated by combining sub-matrices as follows

$$\left(\mathbf{k}_{ij}^{s}\right)_k = \left(\begin{bmatrix} \mathbf{k}_{ij}^{m} & \mathbf{k}_{ij}^{mb} & 0 \\ \mathbf{k}_{ji}^{bm} & \mathbf{k}_{ij}^{b} + \mathbf{k}_{ij}^{s} & 0 \\ 0 & 0 & 0 \end{bmatrix} \right)_k ; \ (i,j = 1,\ldots,4) \tag{8.91}$$

Where $(\mathbf{k}_{ij}^{m})_k$ is the membrane stiffness sub-matrix, given by

$$\left(\mathbf{k}_{ij}^{m}\right)_k = \int_A (\mathbf{B}_{m_i})^T (\mathbf{D}_m)_k \mathbf{B}_{m_j} dA \tag{8.92}$$

and $\mathbf{B}_{m_i}$ is the membrane strain sub-matrix associated with node i, which is described in Eq. (5.71), and $(\mathbf{D}_m)_k$ is the sub-matrix that relates resultant membrane forces to membrane strains defined as

$$(\mathbf{D}_m)_k = \begin{bmatrix} c_{11} & c_{12} & c_{16} \\ c_{21} & c_{22} & c_{26} \\ c_{61} & c_{62} & c_{66} \end{bmatrix}_k (h_k - h_{k-1}) \tag{8.93}$$

In Eq. (8.91), $(\mathbf{k}_{ij}^{b})_k$ is the bending stiffness sub-matrix, given by

$$\left(\mathbf{k}_{ij}^{b}\right)_k = \int_A (\mathbf{B}_{b_i})^T (\mathbf{D}_b)_k \mathbf{B}_{b_j} dA \tag{8.94}$$

and $\mathbf{B}_{b_i}$ is the bending strain sub-matrix associated with node i, which is described in Eq. (6.56), and $(\mathbf{D}_b)_k$ is the sub-matrix that relates generalized moments to generalized curvatures and is defined as

$$(\mathbf{D}_b)_k = \begin{bmatrix} c_{11} & c_{12} & c_{16} \\ c_{21} & c_{22} & c_{26} \\ c_{61} & c_{62} & c_{66} \end{bmatrix}_k \left(h_k^2 - h_{k-1}^2\right) \tag{8.95}$$

In Eq. (8.91), $(\mathbf{k}_{ij}^{s})_k$ is the shear stiffness sub-matrix, given by

$$\left(\mathbf{k}_{ij}^{s}\right)_k = \int_A (\mathbf{B}_{s_i})^T (\mathbf{D}_s)_k \mathbf{B}_{s_j} dA \tag{8.96}$$

and $\mathbf{B}_{s_i}$ is the shear strain sub-matrix associated with node i, which is described in Eq. (6.59), and $(\mathbf{D}_s)_k$ is the sub-matrix that relates resultant transverse shear forces to shear strains and is defined as

$$(\mathbf{D}_s)_k = k \begin{bmatrix} c_{44} & c_{45} \\ c_{45} & c_{55} \end{bmatrix}_k (h_k - h_{k-1}) \tag{8.97}$$

In Eq. (8.91), $\left(\mathbf{k}_{ij}^{mb}\right)_k = \left(\mathbf{k}_{ji}^{bm}\right)_k^T$ is the coupling membrane-bending stiffness sub-matrix, given by

$$\left(\mathbf{k}_{ij}^{mb}\right)_k = \int_A (\mathbf{B}_{m_i})^T (\mathbf{D}_{mb})_k \mathbf{B}_{b_j} dA \tag{8.98}$$

and $(\mathbf{D}_{mb})_k$ is the sub-matrix that relates resultant membrane forces to generalized curvatures and is defined as

$$(\mathbf{D}_{mb})_k = \begin{bmatrix} c_{11} & c_{12} & c_{16} \\ c_{21} & c_{22} & c_{26} \\ c_{61} & c_{62} & c_{66} \end{bmatrix}_k \frac{1}{3}\left(h_k^3 - h_{k-1}^3\right) \tag{8.99}$$

As each layer may have different properties, the elasticity matrices must be evaluated by a summation carried out all over the thickness. Therefore, equivalent single layer theories produce an equivalent stiffness matrix, which is a weighted sum

of the individual layer stiffness through the thickness. Thus, the element stiffness matrix for the laminate can be formulated as

$$\mathbf{k}_{ij}^{s} = \sum_{k=1}^{nl} \left(\mathbf{k}_{ij}^{s}\right)_{k} \tag{8.100}$$

Where *nl* is the layer numbers of the laminate.

8.6.7 Force and Moment Resultants for Laminated Plates

Integrating the stress through the laminate thickness the resultant forces and moments acting in the laminate are obtained. Hence, the resultant membrane forces are

$$\mathbf{N}_{m} = \begin{bmatrix} N_{11} \\ N_{22} \\ N_{12} \end{bmatrix} = \sum_{k=1}^{nl} \int_{h_{k-1}}^{h_k} \begin{bmatrix} \sigma_{11} \\ \sigma_{22} \\ \sigma_{12} \end{bmatrix} dx_3 \tag{8.101}$$

The resultant bending moments are

$$\mathbf{M} = \begin{bmatrix} M_{11} \\ M_{22} \\ M_{12} \end{bmatrix} = \sum_{k=1}^{nl} \int_{h_{k-1}}^{h_k} \begin{bmatrix} \sigma_{11} \\ \sigma_{22} \\ \sigma_{12} \end{bmatrix} x_3 \, dx_3 \tag{8.102}$$

While the resultant shear forces are written as

$$\mathbf{N}_{s} = \begin{bmatrix} N_{23} \\ N_{13} \end{bmatrix} = \sum_{k=1}^{nl} \int_{h_{k-1}}^{h_k} \begin{bmatrix} \sigma_{23} \\ \sigma_{13} \end{bmatrix} dx_3 \tag{8.103}$$

Since in the Reissner-Mindlin plate theory, the transverse shear strains are constant through the laminate thickness, it follows that the transverse shear stresses also have a constant distribution through the laminate thickness. However, in plates the transverse shear stress varies at least quadratically through the layer thickness. This discrepancy between the two states of stress is often corrected in computing the transverse shear force resultants by multiplying the integrals in Eq. (8.103) by a parameter k, called shear correction coefficient, as

$$\mathbf{N}_{s} = \begin{bmatrix} N_{23} \\ N_{13} \end{bmatrix} = k \sum_{k=1}^{nl} \int_{h_{k-1}}^{h_k} \begin{bmatrix} \sigma_{23} \\ \sigma_{13} \end{bmatrix} dx_3 \tag{8.104}$$

The factor k is computed such that the strain energy due to the transverse shear stresses equals the strain energy due to the true transverse shear stresses predicted by the three-dimensional elasticity theory. A parameter value $k = 5/6$ has been extensively used for the case of homogeneous rectangular beams and plates made of isotropic materials. However, the shear correction factor for a general laminate depends on the lamina properties and on the lamination schemes.

Using relations (8.89), (5.14), (6.53) and (6.57) into Eqs. (8.101), (8.102) and (8.104) and integrating through the laminated thickness the constitutive relations can be written in a compact form as

$$\begin{bmatrix} \mathbf{N}_m \\ \mathbf{M} \\ \mathbf{N}_s \end{bmatrix} = \begin{bmatrix} \mathbf{D}_m & \mathbf{D}_{mb} & \mathbf{0} \\ \mathbf{D}_{mb} & \mathbf{D}_b & \mathbf{0} \\ \mathbf{0} & \mathbf{0} & \mathbf{D}_s \end{bmatrix} \begin{bmatrix} \boldsymbol{\varepsilon}_m \\ \boldsymbol{\chi} \\ \boldsymbol{\varepsilon}_s \end{bmatrix} \tag{8.105}$$

where $\boldsymbol{\varepsilon}_m$ is the vector of membrane strains defined by Eq. (5.14), $\boldsymbol{\chi}$ is the vector of bending curvatures described in Eq. (6.53) and $\boldsymbol{\varepsilon}_s$ contain the shear strains described in Eq. (6.57). The matrix on the right-hand-side of Eq. (8.105) is called laminate stiffness matrix, and defines a relationship between the stress resultants, applied to the laminate, and the reference surface strains and curvatures. Sub-matrices $\mathbf{D}_m$, $\mathbf{D}_b$, $\mathbf{D}_s$ and $\mathbf{D}_{mb}$ are evaluated performing a summation carried out all over the thickness of Eqs. (8.93), (8.95), (8.97) and (8.99), respectively. Often laminates are classified according their stacking arrangement and this kind of classification have some effects on the form of laminate stiffness matrix. For instance, for symmetric laminates the matrix $\mathbf{D}_{mb}$ is zero, which means that there is no coupling between extension and bending load.

8.6.8 *Laminated Composite Cylindrical Roof Loaded Under Its Own Weight*

Laminated composite plate structures find numerous applications in aerospace, military and automotive industries. The role of transverse shear is very important in composites, as the material is weak in shear due to its low shear modulus compared to extensional rigidity [14]. Hence, the effect of transverse shear deformation on deflection and stresses of laminated composite panels must be accounted for, especially in plates with side-to-thickness ratios of 10 or smaller.

Discussion example of Sect. 6.5 is now analyzed assuming that the shell is laminated of a composite material. The boundary conditions are those presented in Fig. 6.13 of Sect. 6.5. The material properties are [15]

$$\mathrm{E}_1 = 25\,\mathrm{E}_2;\ \mathrm{E}_3 = \mathrm{E}_2;\ G_{12} = G_{13} = 0.5\mathrm{E}_2;\ \upsilon_{12} = \upsilon_{13} = 0.25 \tag{8.106}$$

Table 8.2 Maximum transverse deflections of a laminated cylindrical shell roof

Layers	R/h	$\overline{w}$ [15]	$\overline{w}$ [ADINA]
2	20	12.1529	12.120
	50	5.4211	5.414
	100	3.1191	3.116
10	20	8.7239	8.695
	50	3.1358	3.130
	100	1.8877	1.887

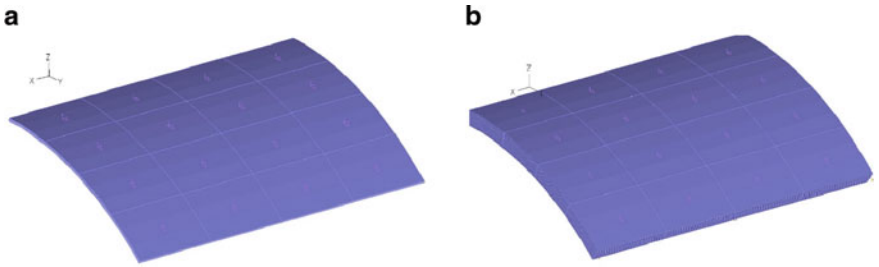

Fig. 8.33 Composite laminates with ten layers and radius-to-thickness ratio of: (**a**) 100; (**b**) 20

This problem is solved using the ADINA program, and because in ADINA the Poisson's ratio is defined differently from the standard convention, the Poisson's ratio in Eq. (8.106) is modified using the following relation [8]

$$\upsilon_{ij}^{ADINA} = \frac{E_j}{E_i}\upsilon_{ij} \tag{8.107}$$

The composite shell solution quoted for the vertical displacement at the center of the free edge, point B in Fig. 6.13, for two layers and ten-layer antisymmetric cross-ply [0/90/0/90/...] laminated shells and for different radius-to-thickness ratio are presented in Table 8.2 [15]. In the ADINA program the load is applied considering a mass proportional load, so in order to assure that the composite shell is always loaded under the same conditions, i.e. under its own weight, the density ρ is always of 0.208333 [lb/in^3]. The vertical displacement presented at Table 8.2 is normalized using the following dimensionless relation

$$\overline{w} = 10\, w_B \frac{E_1 h^2}{\rho R^4} \tag{8.108}$$

The solutions are obtained modelling one quarter of the structure and a mesh density of 4×4 using the 16 node isoparametric shell element. The thickness of the shell that has a radius-to-thickness ratio of 20 is about five times higher than the thickness of the shell that has the radius-to-thickness ratio of 100. In order to see the thickness difference between both laminates, Fig. 8.33 shows both laminated shells for the case of ten layers.

In Fig. 8.33 is also possible to visualize the principal material direction associated to the top layer, a triad is plotted within each finite element showing the direction of

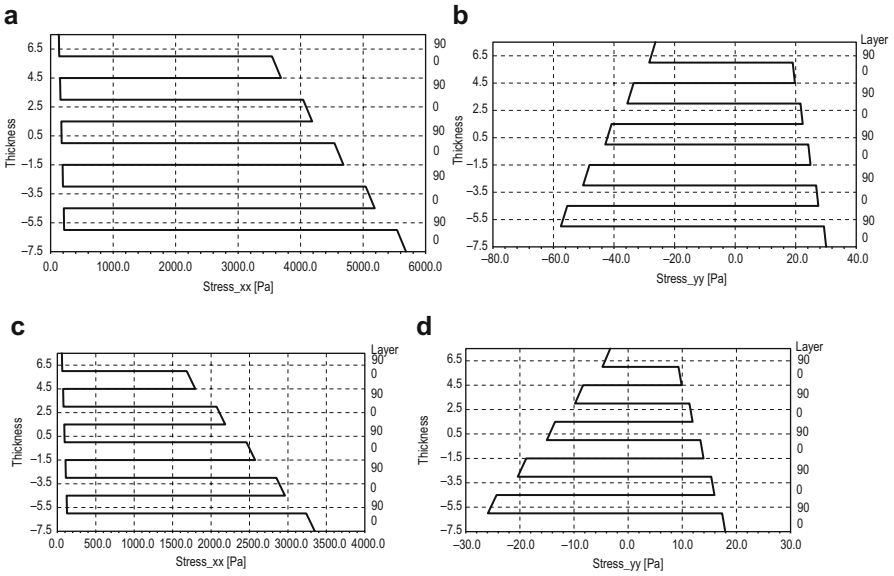

Fig. 8.34 Stress distribution through the thickness: (**a**) and (**b**) laminated with R/h = 100; (**c**) and (**d**) laminated with R/h = 20

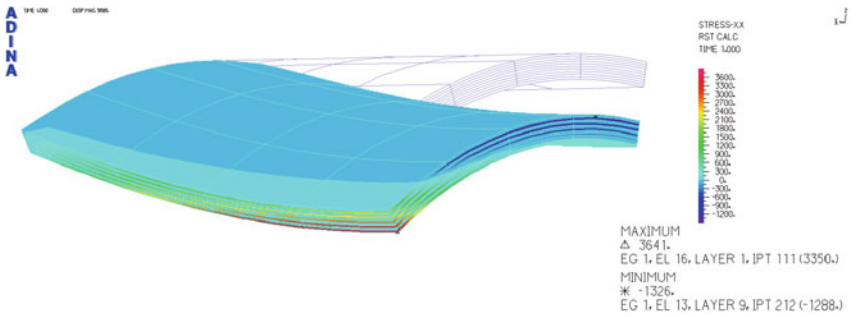

Fig. 8.35 Stress distribution through the thickness of laminated with R/h = 20

the principal material coordinate system. Normal stresses distribution through the thickness in point B are presented in Fig. 8.34. Is clear that 0° layer carries the most axial stress, i.e. stress parallel to the axis of cylinder, while the 90° layer carries the most circumferential stress. Since the thickness of a cylinder, or a structure, greatly determines its weight, and this roof is loaded by its own weight, we could think that a thicker roof will show higher levels of stress, but Fig. 8.34 does not confirm this effect. Nevertheless, that can be explained with the improvement of bending stiffness of a thick cylinder.

The distribution of axial stress through the thickness of the laminated roof with the R/h = 20 ratio is shown in Fig. 8.35.

References

1. Liu GR, Quek SS (2003) The finite element method: a practical course. Butterworth-Heinemann, Burlington
2. Knupp PM (2007) Remarks on mesh quality. Paper presented at the 45th AIAA aerospace sciences meeting and exhibit, Reno, 7–10 Jan 2007
3. Sousa L, Veríssimo P, Ambrósio J (2008) Development of generic multibody road vehicle models for crashworthiness. Multibody Sys Dyn 19(1–2):133–158. doi:10.1007/s11044-007-9093-z
4. Robinson J (1987) CRE method of element testing and the Jacobian shape parameters. Eng Comput 4(2):113–118. doi:10.1108/eb023689
5. Lee N-S, Bathe K-J (1993) Effects of element distortions on the performance of isoparametric elements. Int J Numer Methods Eng 36(20):3553–3576. doi:10.1002/nme.1620362009
6. Bathe K-J (1996) Finite element procedures. Prentice Hall
7. Zienkiewicz OC, Taylor RL (2000) The finite element method. Butterworth-Heinemann, R&D Inc. Boston, MA, USA
8. ADINA R & D I (2014) User's manal. R&D Inc., Boston
9. Vaz M, de Souza Neto EA, Munoz-Rojas PA (2011) Advanced computational materials modeling: from classical to multi-scale techniques. Wiley
10. Shabana AA (2005) Dynamics of multibody systems. Cambridge University Press, Cambridge
11. Reddy JN (1997) Mechanics of laminated composite plates and shells: theory and analysis. CRC Press, Boca Raton
12. Bunsell AR, Renard J (2005) Fundamentals of fibre reinforced composite materials. Taylor & Francis, Bristol
13. Hyer MW (1998) Stress analysis of fiber-reinforced composite materials. Mechanical engineering. WCB/McGraw-Hill, Boston
14. Reddy B, Reddy A, Kumar J, Reddy K (2012) Bending analysis of laminated composite plates using finite element method. Int J Eng Sci Technol 4(2):177–190
15. Reddy JN (2003) Mechanics of laminated composites plates and shells: theory and analysis. CRC Press, Boca Reton

Index

M.A. Neto et al., *Engineering Computation of Structures: The Finite Element Method*, DOI 10.1007/978-3-319-17710-6